

Rachel C. Evans
Peter Douglas
Hugh D. Burrows *Editors*

Applied Photochemistry

 Springer

Applied Photochemistry

Rachel C. Evans · Peter Douglas
Hugh D. Burrows
Editors

Applied Photochemistry

 Springer

Editors

Rachel C. Evans
School of Chemistry, Trinity College
The University of Dublin
Dublin
Ireland

Hugh D. Burrows
Department of Chemistry
University of Coimbra
Coimbra
Portugal

Peter Douglas
Chemistry Group, College of Engineering
Swansea University
Swansea
UK

ISBN 978-90-481-3829-6 ISBN 978-90-481-3830-2 (eBook)
DOI 10.1007/978-90-481-3830-2
Springer Dordrecht Heidelberg New York London

Library of Congress Control Number: 2013931951

© Springer Science+Business Media Dordrecht 2013

This work is subject to copyright. All rights are reserved by the Publisher, whether the whole or part of the material is concerned, specifically the rights of translation, reprinting, reuse of illustrations, recitation, broadcasting, reproduction on microfilms or in any other physical way, and transmission or information storage and retrieval, electronic adaptation, computer software, or by similar or dissimilar methodology now known or hereafter developed. Exempted from this legal reservation are brief excerpts in connection with reviews or scholarly analysis or material supplied specifically for the purpose of being entered and executed on a computer system, for exclusive use by the purchaser of the work. Duplication of this publication or parts thereof is permitted only under the provisions of the Copyright Law of the Publisher's location, in its current version, and permission for use must always be obtained from Springer. Permissions for use may be obtained through RightsLink at the Copyright Clearance Center. Violations are liable to prosecution under the respective Copyright Law. The use of general descriptive names, registered names, trademarks, service marks, etc. in this publication does not imply, even in the absence of a specific statement, that such names are exempt from the relevant protective laws and regulations and therefore free for general use.

While the advice and information in this book are believed to be true and accurate at the date of publication, neither the authors nor the editors nor the publisher can accept any legal responsibility for any errors or omissions that may be made. The publisher makes no warranty, express or implied, with respect to the material contained herein.

Printed on acid-free paper

Springer is part of Springer Science+Business Media (www.springer.com)

Preface

Photochemistry is a mature science. We now have a fairly detailed understanding of the physical and chemical pathways involving production and deactivation of excited states and photochemistry is currently used in a broad range of applications ranging from transistor chip production using photolithography, through advanced synthetic methodologies, sensing, and imaging, to clinical use in the phototherapy of jaundice and photodynamic therapy of cancer. In addition, sunlight is the only fully sustainable energy source that is capable of meeting all the earth's requirements for the foreseeable future, and photochemistry plays a crucial role in the interconversion of solar energy into electricity or chemical fuels. However, although a number of excellent books are available on the scientific aspects of photochemistry, and individual monographs are available on specific applications, there is a lack of a general text on the applications of photochemistry. Our aim with *Applied Photochemistry* is to remedy this with contributions from specialists involved in applications of photochemistry in the key areas of chemistry, physics, medicine and engineering. We feel that this book will be useful for students and researchers in chemical, physical, biological, environmental and atmospheric sciences, as well as those in engineering and biomedical research, who are interested in applying photochemistry to their work. The chapters are self-contained, so the text can either be read as a whole or individual chapters can be used to rapidly obtain information on specific areas. Topics are treated in sufficient depth, with references to appropriate current literature, to lead the reader to discover the state of the art in each topic.

The first Chapter provides a comprehensive background on the foundations of photochemistry, which will be useful for non-specialists. [Chapters 2](#) and [3](#) cover the most important aspects of organic and inorganic photochemistry, from both synthetic and mechanistic viewpoints. Applications in materials science are discussed in [Chap. 4](#), and range from colorants, pigments and dyes through light emitters for use in illumination and displays to photochromic materials. [Chapter 5](#) presents a comprehensive description of the main photochemical processes occurring in the atmosphere, including those leading to air pollution. Water and waste pollution are discussed in [Chap. 6](#) from the viewpoint of direct and catalytic photochemical processes which can be used for treatment and remediation. The

conversion of sunlight into electrical energy through photovoltaic systems or chemical fuels by mimicking the water splitting and carbon dioxide reduction of photosynthesis is treated in detail in [Chap. 7](#). Many of the processes involved in biomedical applications of photochemistry involve free radicals and reactive oxygen species, and [Chap. 8](#) discusses these and provides a description of the experimental methods used for their study. Medical aspects of photochemistry are treated in [Chap. 9](#) and [10](#) in terms of the application of light in various clinical treatments in the area of photomedicine, including the important topic of photodynamic therapy, and the way that photochemical diagnostics are proving valuable in a wide variety of clinical assays. [Chapter 10](#) also shows the important role of photochemistry in the developing area of nanomedicine. [Chapter 11](#) provides a detailed description of photochemical processes in imaging, describing the historical development of ‘silver halide’ and other photographic processes and extending these to non-silver photographic and electrophotographic processes. Optical sensors and probes are discussed in [Chap. 12](#) in terms of the fundamental principles behind optical sensing, the different types of optical probes available and the way to design appropriate devices for studying single or multiple analytes. [Chapter 13](#) shows the important roles that photoactive polymers and photolithography play in the fabrication of advanced semiconductor devices. The last two chapters describe the basic instrumentation, equipment and requirements necessary for setting up a laboratory dedicated to photochemical research and the experimental methods involved in the characterisation of excited states.

We are indebted to all of the authors for their excellent contributions to this volume. We would also like to acknowledge our many teachers, colleagues, co-workers and students for their efforts in showing that the interaction of light with molecules is of both great academic interest and very real practical application. Finally, we would like to thank Ilaria Tassistro and Sonja Ojo from the Springer UK Chemistry Editorial Team for their patience and support.

Rachel C. Evans
Peter Douglas
Hugh D. Burrows

Contents

1	Foundations of Photochemistry: A Background on the Interaction Between Light and Molecules	1
	Peter Douglas, Hugh D. Burrows and Rachel C. Evans	
2	Photochemical Synthesis	89
	Valentina Dichiarante and Angelo Albini	
3	Inorganic Photochemistry	105
	Julia A. Weinstein	
4	Photochemical Materials: Absorbers, Emitters, Displays, Sensitisers, Acceptors, Traps and Photochromics	149
	Matthew L. Davies, Peter Douglas, Rachel C. Evans and Hugh D. Burrows	
5	Atmospheric Photochemistry	217
	Rod S. Mason	
6	Photodegradation of Pesticides and Photocatalysis in the Treatment of Water and Waste	247
	M. Emília Azenha, Andreia Romeiro and Mohamed Sarakha	
7	Solar Energy Conversion	267
	Luis G. Arnaut, Monica Barroso and Carlos Serpa	
8	Radiolytic and Photolytic Production of Free Radicals and Reactive Oxygen Species: Interactions with Antioxidants and Biomolecules	305
	Ruth Edge	

9	Photomedicine	331
	Marina K. Kuimova and David Phillips	
10	Photochemistry in Medical Diagnostics	349
	Huw D. Summers	
11	Photochemical Imaging	363
	Gareth B. Evans, Michael B. Ledger and Henry H. Adam	
12	Optical Sensors and Probes	403
	Rachel C. Evans and Peter Douglas	
13	Photochemistry in Electronics	435
	Owen J. Guy, Gregory Burwell, Ambroise Castaing and Kelly-Ann D. Walker	
14	The Photochemical Laboratory	467
	Peter Douglas, Rachel C. Evans and Hugh D. Burrows	
15	Experimental Techniques for Excited State Characterisation	533
	J. Sérgio Seixas de Melo, João Pina, Fernando B. Dias and António L. Maçanita	
	Index	587

Contributors

Henry H. Adam Kodak Ltd Research Laboratory (retired), London, UK, e-mail: harry.adam@btinternet.com

Angelo Albini Dipartimento di Chimica, Università di Pavia, v. Taramelli 10, 27100 Pavia, Italy, e-mail: angelo.albini@unipv.it

Luis G. Arnaut Department of Chemistry, University of Coimbra, Coimbra, Portugal, e-mail: lgarnaut@ci.uc.pt

M. Emília Azenha Departamento de Química da Faculdade de Ciências e Tecnologia da, Universidade de Coimbra, Coimbra, Portugal, e-mail: mezenha@ci.uc.pt

Monica Barroso Department of Chemistry, University of Coimbra, Coimbra, Portugal; Department of Chemistry, Imperial College London, London SW7 2AZ, UK, e-mail: m.barroso@imperial.ac.uk

Hugh D. Burrows Department of Chemistry, University of Coimbra, Coimbra, Portugal, e-mail: burrows@ci.uc.pt

Gregory Burwell College of Engineering, Swansea University, Singleton Park, Swansea SA3 8PP, UK, e-mail: G.Burwell.436734@swansea.ac.uk

Ambroise Castaing College of Engineering, Swansea University, Singleton Park, Swansea SA3 8PP, UK, e-mail: A.Castaing@swansea.ac.uk

Matthew L. Davies School of Chemistry, Bangor University, Gwynedd LL57 2UW, UK, e-mail: m.davies@bangor.ac.uk

Fernando B. Dias Department of Physics, Durham University, Durham DH1 3LE, UK, e-mail: f.m.b.dias@durham.ac.uk

Valentina Dichiarante Service de Bioénergétique Biologie Structurale et Mécanismes (SB2SM), CEA, iBiTec-S, 91191 Gif-sur-Yvette, France

Peter Douglas Chemistry Group, College of Engineering, Swansea University, Swansea, UK, e-mail: P.Douglas@swansea.ac.uk

Ruth Edge Dalton Cumbrian Facility, The University of Manchester, Westlakes Science and Technology Park, Moor Row, Cumbria CA24 3HA, UK, e-mail: ruth.edge@manchester.ac.uk

Gareth B. Evans Kodak Ltd Research Laboratory (retired), London, UK, e-mail: gareth@evansgb.plus.com

Rachel C. Evans School of Chemistry, Trinity College Dublin, Dublin 2, Ireland, e-mail: raevans@tcd.ie

Owen J. Guy College of Engineering, Swansea University, Singleton Park, Swansea SA3 8PP, UK, e-mail: o.j.guy@swansea.ac.uk

Marina K. Kuimova Chemistry Department, Imperial College London, Exhibition Road, London SW7 2AZ, UK, e-mail: m.kuimova@imperial.ac.uk

Michael B. Ledger Kodak Ltd Research Laboratory (retired), London, UK, e-mail: mbledger@yahoo.co.uk

António L. Maçanita Centro de Química Estrutural, Instituto Superior Técnico (IST), Lisbon, Portugal

Rod S. Mason Physical Science Solutions Ltd, 28 Fernhill Close, Blackpill, Swansea SA3 5BX, UK; School of Medicine, Institute of Mass Spectrometry, Swansea University, Singleton Park, Swansea SA2 8PP, UK, e-mail: rods_mason@googlemail.com

David Phillips Department of Chemistry, Imperial College London, London SW7 2AZ, UK, e-mail: d.phillips@imperial.ac.uk

João Pina Department of Chemistry, University of Coimbra, Coimbra, Portugal, e-mail: jpina@qui.uc.pt

Andreia Romeiro Departamento de Química da Faculdade de Ciências e Tecnologia da, Universidade de Coimbra, Coimbra, Portugal, e-mail: aromeiro@ci.uc.pt

Mohamed Sarakha Université Blaise Pascal U.F.R. Sciences et Technologies Laboratoire de Photochimie Moléculaire, 24 avenue des Landais, 80026-63171 Aubière Cedex, France, e-mail: mohamedsarakha@univ-bpclermont.fr

J. Sérgio Seixas de Melo Department of Chemistry, University of Coimbra, Coimbra, Portugal, e-mail: sseixas@ci.uc.pt

Carlos Serpa Department of Chemistry, University of Coimbra, Coimbra, Portugal, e-mail: serpasoa@ci.uc.pt

Huw D. Summers Centre for Nanohealth, Swansea University, Singleton Park, Swansea SA2 8PP, UK, e-mail: h.d.summers@swansea.ac.uk

Kelly-Ann D. Walker College of Engineering, Swansea University, Singleton Park, Swansea SA3 8PP, UK, e-mail: K.D.Walker@swansea.ac.uk

Julia A. Weinstein Department of Chemistry, University of Sheffield, Sheffield S3 7HF, UK, e-mail: Julia.Weinstein@sheffield.ac.uk

Acronyms and Abbreviations

0D	Zero-dimension(al)
1D	One-dimension(al)
2D	Two-dimension(al)
3D	Three-dimension(al)
A	Adenine
AC	Alternating current
ACS	American Chemical Society
AE	Appearance energy for dissociative photoionisation
AFM	Atomic force microscopy
AIBN	2,2'-azobis(2-methylpropionitrile)
ALA	Aminolevulinic acid
ANN	Artificial neural networks
AMD	Age-related macular degeneration
AO	Acridine orange <i>or</i> Atomic orbital
AOP	Advanced oxidation process
aq.	Aqueous
A–T	Adenine–thymine nucleotide pair
Atm	Atmosphere (unit of pressure)
ATR	Attenuated total reflection
BAC	Bacterial artificial chromosome
BAF	Boronic acid containing fluorophore
BDE	Bond dissociation energy
BHJ	Bulk heterojunction
Bipy	2,2'-bipyridyl
B&W	Black and white
C	Cytosine
CAB	Cellulose acetate butyrate
CAR	Carotenoid
CB	Conduction band
CCD	Charge coupled device
CCP	Cationic conjugated polymer

CFC	Chlorofluorocarbon
CFL	Compact fluorescence lamp
C-G	Cytosine-guanine nucleotide pair
CIE	Commission International de l'Éclairage
CMOS	Complementary metal oxide semiconductor
CP	Conjugated polymer
CPC	Compound parabolic collector
CPE	Conjugated polyelectrolyte
CRT	Cathode ray tube
CT	Charge transfer
CV	Crystal violet <i>or</i> Cyclic voltammetry
CW	Continuous wave
CYPMPO	5- (2, 2-dimethyl-1, 3-propoxycyclophosphoryl)-5-methyl-1-pyrroline- <i>N</i> -oxide
DAB	1,2-Diazabutadiene
DABCO	1,4-diazabicyclo[2.2.2]octane
DAPI	4',6-Diamidino-2-phenylindole
DC	Direct current
Dcbpy	4,4-dicarboxy-2,2-bipyridine
DEPMPO	5-(Diethoxyphosphoryl)-5-methyl-1-pyrroline- <i>N</i> -oxide
DFT	Density functional theory
DIR	Development inhibitor releasing
div.	Division
DMF	Dimethylformamide
DMSO	Dimethyl sulfoxide
DNA	Deoxyribonucleic acid
DNBP	2-(2',4'-dinitrobenzyl)pyridine
DOS	Density of states
DPPC	Dipalmitoylphosphatidylcholine
Dppe	Diphenylphosphinoethane
DSSC	Dye-sensitised solar cells
EBL	Electron beam lithography
EC	Ethyl cellulose
EIA	Enzyme immunoassay
ELISA	Enzyme-linked immunosorbant assay
EMI	Electromagnetic interference
EMR	Electromagnetic radiation
EPA	Diethyl ether: isopentane: ethanol
EPR	Electron paramagnetic resonance
ESD	Electrostatic dispersive
ESR	Electron spin resonance
EUV	Extreme ultraviolet
EUVL	Extreme ultraviolet lithography
EXAFS	Extended X-ray absorption fine structure
<i>fac</i>	Facial

FC	Frank–Condon
Fc/Fc ⁺	Ferrocene/ferrocenium redox couple
FCS	Fluorescence correlation spectroscopy
FLIM	Fluorescence lifetime imaging
FISH	Fluorescence in situ hybridisation
FITC	Fluorescein isothiocyanate
FF	Fill factor
FRET	Förster resonance energy transfer
FT	Fourier transform
FTO	Fluorine doped tin oxide
G	Guanine
GC	Gas chromatography
HER	Hydrogen evolution reaction
HID	High intensity discharge
HOMO	Highest occupied molecular orbital
HPLC	High performance liquid chromatography
HPTS	Hydroxypyrene trisulfonate
Hr	Hour
HSQ	Hydrogen silsesquioxane
ICT	Intramolecular charge transfer
IDA	Indicator displacement assay
IE	Ionisation energy
IL	Intra-ligand
ILCT	Intra-ligand charge transfer
IP	Ionisation potential
IPA	Isopropyl alcohol
IPCE	Incident photon-to-current conversion efficiency
IR	Infrared
ISC	Intersystem crossing
IT	Information technology
ITO	Indium-doped tin oxide
<i>J–V</i>	Current–voltage
KE	Kinetic energy
L	Ligand
LC	Ligand-centred
LCD	Liquid crystal display
LDA	Linear discriminant analysis
LED	Light-emitting diode
LEP	Light-emitting polymer
LF	Ligand field
LHE	Light harvesting efficiency
LLCT	Ligand-to-ligand charge transfer
LMCT	Ligand-to-metal charge transfer
LTE	Local thermal equilibrium
LUMO	Lowest unoccupied molecular orbital

MB	Methylene blue
MC	Metal-centred
MCP	Multi-channel plate
MEF	Metal-enhanced fluorescence
MEH-PPV	Poly[2-methoxy-5-(2-ethyl-hexyloxy)-1,4-phenylenevinylene]
MEMS	Micro-electro mechanical systems
<i>mer</i>	Meridional
MIKB	Methyl isobutyl ketone
MLC	Metal-ligand complex
MLCT	Metal-to-ligand charge transfer
MO	Molecular orbital
MOS	Metal oxide semiconductor
MPS-PPV	Poly[5-methoxy-2-(3-sulfopropoxy)-1,4-phenylenevinylene]
MRI	Magnetic resonance imaging
MV	Methyl viologen
NA	<i>N</i> -allyl- <i>N</i> -methylaniline <i>or</i> Numerical aperture
NAPD	Nicotinamide adenine dinucleotide phosphate
NBD	Nitrobenzoxadiazole
ND	Neutral density
Nd:YAG	Neodymium-doped yttrium aluminum garnet
NHE	Normal hydrogen electrode
NIL	Nanoimprint lithography
NIR	Near-infrared
NMR	Nuclear magnetic resonance
OEC	Oxygen-evolving complex
OEG	Oligo(ethyl glycol)
OER	Oxygen evolution reaction
OFET	Organic field effect transistor
OLED	Organic light-emitting diode
OMC	Octylmethoxycinnamate
OPV	Oligo(<i>p</i> -phenylene vinylene) <i>or</i> Organic photovoltaic
Ormosil	Organically modified silane
PAN	Peroxyacetylnitrate
PANI	Poly(aniline)
Pc	Phthalocyanine
PC	Photocatalytic
PCA	Principal component analysis
PCBM	[6,6]-phenyl-C61-butyric acid methyl ester
PDMS	Poly(dimethylsiloxane)
PDP	Plasma display panel
PDT	Photodynamic therapy
PE	Potential energy
PEC	Photoelectrochemical
PEDOT	Poly(3,4-ethylenedioxythiophene)
PET	Photoinduced electron transfer

PF	Poly(fluorene)
PFO	Poly(9,9'-dioctylfluorene)
PLED	Polymer light-emitting diode
PMMA	Poly(methyl methacrylate)
PMT	Photomultiplier tube
PNA	Protein nucleic acid
PNI	<i>N</i> -(1,10-phenanthroline)-4-(1-piperidinylnaphthalene-1,8-dicarboximide
POM	Polyoxometalate
ppb	Parts per billion
ppm	Parts per million
PPP	Poly(<i>p</i> -phenylene)
ppt	Parts per trillion
PPV	Poly(<i>p</i> -phenylenevinylene)
PS	Photosystem
PSC	Polar stratospheric ice cloud
PSP	Pressure sensitive paint
PT	Poly(thiophene)
PtOEP	Platinum octaethylporphyrin
PUFA	Polyunsaturated fatty acid
PUVA	Psoralen ultraviolet-A irradiation
PV	Photovoltaic
PVA	Poly(vinyl alcohol)
PVC	Poly(vinyl chloride)
P3HT	Poly(3-hexylthiophene-2,5-diyl)
P3OT	Poly(3-octylthiophene-2,5-diyl)
QD	Quantum dot
RET	Resonance energy transfer
RI	Refractive index
RIE	Reactive ion etching
RNA	Ribonucleic acid
ROS	Reactive oxygen species
rpm	Revolutions per minute
rR	Resonance Raman
r.t.	Room temperature
SAM	Self-assembled monolayers
SBLCT	Sigma bond to ligand charge transfer
sc	Supercritical
SEM	Scanning electron microscopy
SFIL	Step and flash imprint lithography
SNOM	Scanning near-field optical microscopy
SOD	Superoxide dismutase
SPR	Surface plasmon resonance
S _N 1	Unimolecular nucleophilic substitution
S _{RN} 1	Unimolecular radical-nucleophilic aromatic substitution

S/N	Signal-to-noise ratio
SHE	Standard hydrogen electrode
SNOM	Scanning near-field optical microscopy
STED	Stimulated depletion emission spectroscopy
T	Thymine
TA	Transient absorption
TCSPC	Time-correlated single photon counting
<i>t</i> -Boc	<i>N</i> - <i>tert</i> -butoxycarbonyl
TD-DFT	Time-dependent density functional theory
TEMPO	2,2,6,6-Tetramethyl-1-piperidinyloxy
TFT	Thin film transistor
THF	Tetrahydrofuran
T-2DIR	Transient two-dimensional infrared spectroscopy
TMAH	Tetramethyl ammonium hydroxide
TMPyP	5,10,15,20-Tetrakis(1-methyl-4-pyridinio)porphyrin tetra(<i>p</i> -toluenesulfonate)
TNT	Trinitrotoluene
TPE	Two-photon excitation
TPP	Tetraphenylporphyrin
TRIR	Time-resolve infrared
USD	US dollars
UV	Ultraviolet
UV/Vis	Ultraviolet/Visible
VB	Valence band
WOLED	White organic light-emitting diode
XANES	X-ray absorption near edge spectrum
XPS	X-ray photoelectron spectroscopy
XLCT	Halide to ligand charge transfer
YO	Oxazole yellow
YOYO	Dimer of oxazole yellow

Symbols

Fundamental Constants

Symbol	Name	Value
c	Velocity of an electromagnetic wave in a vacuum	$2.99792 \times 10^8 \text{ m s}^{-1}$
e	Elementary charge	$1.60219 \times 10^{-19} \text{ C}$
h	Planck constant	$6.626068 \times 10^{-34} \text{ J s}$
\hbar	Reduced Planck constant ($h/2\pi$)	$1.0546 \times 10^{-27} \text{ J s}$
k_B	Boltzmann constant	$1.3806503 \times 10^{-23} \text{ J K}^{-1}$
k_e	Coulomb constant	$8.987551 \times 10^9 \text{ N m}^2 \text{ C}^{-2}$
m_e	Mass of an electron	$9.109\ 382\ 15(45) \times 10^{-31} \text{ kg}$
R	Molar gas constant	$8.314472 \text{ J K}^{-1} \text{ mol}^{-1}$
N_A	Avogadro constant	$6.02214129(27) \times 10^{23} \text{ mol}^{-1}$
ϵ_0	Permittivity of free space	$8.85418782 \times 10^{-12} \text{ J}^{-1} \text{ C}^2 \text{ m}^{-1}$
e	Mathematical constant	2.71828182846
π	Mathematical constant	3.14159265359

Light, Waves, Optics

Symbol	Name
c	Velocity of an electromagnetic wave in a vacuum
d	Diffraction limit
$h\nu$	Photon
n	Refractive index
ρ	Photon flux
R	Reflectivity
λ	Wavelength
θ_c	Critical angle of incidence
ν	Frequency
$\tilde{\nu}$	Wavenumber
ω	Angular velocity

Spectroscopic and Photochemical

Symbol	Name
a	Pre-exponential factor in multi component decay
A, Abs	Absorbance
A_{21}, B_{12}, B_{21}	Einstein coefficients
E_S, T	Energy; singlet, triplet
$E_{\nu\max}$	Energy of fluorescence maximum
$\Delta E(S_1-T_1)$	Singlet-triplet energy gap
$f(R)$	Kubelka-Munk function
I	Intensity
I_{abs}	Absorbed intensity
I_{em}	Emitted intensity
I_{inc}	Incident intensity
I_0	Incident intensity
I_{RA}	Intensity of Raman scattering
I_{RS}	Intensity of Rayleigh scattering
I_{ss}	Integrated intensity across a decay curve
I_{ss}	Intensity of steady-state absorption
$I(t)$	Intensity at time t
I_z	Incident radiation at altitude z
k	Extinction coefficient in Kubelka-Munk equation
OD	Optical density (another name for absorbance, A)
ΔOD	Change in optical density
r	Fluorescence anisotropy
s	Scattering coefficient
$S_{0,1,2,\dots}$	Singlet state
$T_{1,2,\dots}$	Triplet state
T	Transmittance
v	Vibrational level
$\epsilon, \epsilon_S, \epsilon_T$	Molar absorption coefficient, for singlet, for triplet
λ_x	Wavelength of property x
λ_{abs}	Absorption wavelength, wavelength of maximum absorption
λ_{em}	Emission wavelength, wavelength of maximum emission
λ_{max}	The wavelength where the property under discussion is a maximum
λ_{RA}	Wavelength of Raman scattering
λ_{RS}	Wavelength of Rayleigh scattering
$\tilde{\nu} \text{ cm}^{-1}$	Wavenumber-frequency of EMR expressed as $1/\lambda$ with λ in cm —also used as an expression for energy of EMR
ΔS	Change in electron spin

General Physical, Instrumental

Symbol	Name
A	Acceleration
c	Concentration
$c(t)$	Concentration at time t
D, d	Diameter
E	Energy
E_{hv}	Energy of photon
f	Correction factor, fraction
F	Force
g	Acceleration due to gravity
G	In radiation chemistry, the number of excited intermediates produced per 100 eV of absorbed energy
KE	Kinetic energy
m	Mass
m	Molar mass
$M, \Delta M$	In atmospheric chemistry, mass of air, change in mass of air
n_z	Molecular density of reacting gas at altitude z
N_n, m, \dots	Number in state n, m, \dots
p	Partial pressure
P	Pressure
PE	Potential energy
q	Charge
R, r	Radius
$S_{\text{min, max}}$	Instrument response; minimum; maximum
S/N	Signal-to-noise ratio
t	Time
T	Temperature
V	Velocity
V	Volume
z	Altitude
ϵ	Dielectric constant
η	Viscosity
σ_λ	Absorption cross-section
θ	Angle, azimuthal angle of the sun
χ^2	Chi-squared (statistical 'goodness of fit' parameter)

Atomic and Molecular Properties, Quantum Numbers, Orbitals

Symbol	Name
A	Atomic mass number
AE	Appearance energy
$d_{\text{H-H}}$	Molecular bond length for hydrogen
$D_{\text{H-H}}$	Bond dissociation energy for hydrogen
$d(z^2)$	A specific one of the five d orbitals; the 'dee zed squared' orbital
e^-	Electron
e_g	Orbital symmetry label
I	Nuclear spin quantum number
IE	Ionisation energy
J	Rotational energy state
l	Orbital angular momentum (spin) quantum number
L	Angular momentum
L	Total orbital angular momentum
L	Sum of van der Waals radii
m_l	Orbital magnetic quantum number
m_n	Mass of nucleus
m_s	Spin quantum number
n	Principal quantum number
n	Non-bonding orbital
N	Neutron number
S	Total electron spin angular momentum
s, p, d, f	Atomic orbital labels, a following superscript gives number of electrons in these orbitals e.g. f^{14}
t_{2g}	Orbital symmetry label
Z	Atomic number
λ_{thresh}	Wavelength of photodissociation threshold
μ_e	Reduced mass of electron
μ_g, μ_e	Dipole moment of ground state, excited state
$\hat{\mu}$	Dipole moment operator
σ, π, δ	Orbital symmetry labels, superscript * indicates antibonding orbital
Ψ	Wavefunction
$ M_{12} $	Transition dipole moment
*	Excited-state or antibonding orbital

Rates, Rate constants, Lifetimes and Quantum Yields

Symbol	Name
J	Rate of reaction
J_{abs}	Rate of absorption (excited-state formation)
J_{AD}	Spectral overlap integral of a donor and acceptor
J_{total}	Rate of excited-state deactivation by all intramolecular deactivation pathways
$k_{1,2,\dots}$	Rate constant for process, 1,2,.....
k_{a}	Bimolecular association rate constant
k_{d}	Rate constant for dissociation
k_{DEX}	Rate constant for Dexter energy transfer
k_{diff}	Rate constant for diffusion-controlled reactions
k_{F}	Rate constant for fluorescence
k_{FRET}	Rate constant for Förster resonance energy transfer (FRET)
k_{IC}	Rate constant for internal conversion
k_{isc}	Rate constant for intersystem crossing
k_{NR}	Rate constant for non-radiative decay
k_{obs}	Observed decay rate constant
k_{PC}	Rate constant for a photochemical process (in competition with vibrational relaxation)
k_{q}	Bimolecular quenching rate constant
k_{rad}	Radiative rate constant
k_{SV}	Stern–Volmer constant
k_{v}	Rate constant for vibrational relaxation
R_{abs}	Rate of absorption of photons
R_{DA}	Donor–acceptor separation
R_0	Förster distance
R_z	Rate of reaction at z
κ^2	Dipole orientation parameter
ϕ_x	Quantum yield of process x
ϕ_{D}	Quantum yield of donor emission
ϕ_{em}	Quantum yield of emission
ϕ_{F}	Quantum yield of fluorescence
ϕ_{L}	Quantum yield of luminescence
ϕ_{IC}	Quantum yield of internal conversion
ϕ_{ISC}	Quantum yield of intersystem crossing
$\phi_{\text{P}}, \phi_{\text{Ph}}$	Quantum yield of phosphorescence
ϕ_{T}	Quantum yield of triplet state formation
ϕ_{v}	Quantum yield of vibrational relaxation
ϕ_{Δ}	Quantum yield of singlet oxygen production
τ	Lifetime
${}^x\tau$	Excited-state lifetime of state x ($x = 1$ for a singlet state, $x = 3$ for a triplet state etc.)
${}^x\tau_0$	Radiative lifetime of state x ($x = 1$ for a singlet state, $x = 3$ for a triplet state etc.)
τ_{chem}	Chemical lifetime—the lifetime of a chemical species in the atmosphere
τ_{D}	Donor lifetime
τ_{res}	Residence time in atmospheric chemistry
τ_{P}	Phosphorescence lifetime
$\tau_{\text{S,T}}$	Lifetime of singlet state, triplet state

Chemical Species, Structures, Equilibria, Concentrations

Symbol	Name
A	Acceptor
A	Analyte
aq	In aqueous medium, hydrated (usually as subscript)
A, B	Two different chemical groups
<i>cp</i>	Compound
D	Donor
D	Dye
D _{4h}	Symmetry label
<i>e</i> ⁻	Electron
<i>e</i> _{cb} ⁻	Conduction band electron
<i>fac, mer</i>	Facial or meridional isomers of octahedral complexes
<i>h</i> ⁺	Hole
<i>i</i> -	Iso
<i>K</i>	Equilibrium constant
<i>K</i> _d	Dissociation constant
<i>K</i> _a	Acid dissociation constant
L	Ligand
M	Metal
M	Molar
<i>M</i>	Molecular segment
<i>n</i> -	Normal, i.e. a linear chain
<i>p</i> -	Para isomer
<i>P</i>	Probe; <i>P</i> _B , <i>P</i> _F : probe bound, probe free
<i>pK</i> _a	-log ₁₀ <i>K</i> _a
<i>pK</i> _{sp}	-log ₁₀ <i>K</i> _{sp} where <i>K</i> _{sp} is the solubility product
ppm, ppb, ppt	Concentration as: parts per million; billion; trillion
Q	Quencher
R	Substituent group
<i>R, ref</i>	Reference
S	Sensitiser, solute
Sens	Sensitiser
SA	Sample
<i>t</i> -	Tertiary
v/v	Concentration as volume to volume
X	Chemical group (usually a halide)
Δ, Λ	Two optical isomers in octahedral complexes
<i>η</i> ⁵	In organometallic chemistry, signifies cyclopentadiene rings bonded through all 5 carbon atoms
•	Unpaired electron, i.e. radical species

Electrochemical, Photoelectric, Thermodynamic and Semiconductor

Symbol	Name
D	Diffusion coefficient
E_g	Semiconductor band gap energy
E°	Standard electrode potential
E^7	Electrode potential at pH 7
FC	Frank–Condon factor
G	Gibbs free energy
ΔG°	Change in standard Gibbs free energy
ΔG_{PET}	Change in Gibbs free energy for photoelectron transfer
P_{max}	Maximum cell power
Fc^+/Fc	Ferrocenium/ferrocene couple
H^2	Electronic coupling factor
J	Current
J_{sc}	Short circuit current
k_{inj}	Rate constant for charge injection by thermal state
k_{inj}^*	Rate constant for charge injection by hot states
k_{rec}	Rate constant for charge recombination
k_T	Rate constant for thermal relaxation
k_{th}	Rate constant for exciton thermalisation
L	Exciton diffusion length
V_{oc}	Open circuit voltage
V	Voltage
Δ	‘Change in’: (final–initial)
ΔH	Change in enthalpy
η_{coll}	Electron collection efficiency
η_{DSSC}	Dye-sensitised solar cell efficiency
η_{inj}	Electron injection efficiency

Units

Symbol	Name
A	Amp
Å	Angstrom (10^{-10} m)
atm	atmosphere
cd	candela
°C	degree centigrade
E	Einstein
eV	electron volt
g	gram
h	hour
Hz	Hertz
J	Joule
K	degree Kelvin
lm	lumen
m	metre
mol	mole
s	second
V	Volt
W	Watt
Ω	Ohm

Prefixes

Symbol	Name	Factor
a	atto	10^{-18}
f	femto	10^{-15}
p	pico	10^{-12}
n	nano	10^{-9}
μ	micro	10^{-6}
m	milli	10^{-3}
c	centi	10^{-2}
d	deci	10^{-1}
k	kilo	10^3
M	mega	10^6
G	giga	10^9
T	tera	10^{12}
P	peta	10^{15}

Chapter 1

Foundations of Photochemistry: A Background on the Interaction Between Light and Molecules

Peter Douglas, Hugh D. Burrows and Rachel C. Evans

Abstract This chapter gives an introduction to the key ideas which underpin photochemistry: the nature of electromagnetic radiation, the nature of matter, and the way the two interact. After a discussion of ultraviolet and visible electromagnetic radiation and its interaction with the optical properties of materials, an account is given of the fundamental properties of the four components involved in photochemistry, the protons, neutrons and electrons which make up atoms, and the photon. The ideas of wave mechanics and its application to atomic structure are introduced in a non-mathematical way, with atomic orbitals described in terms of quantum numbers, energies, degeneracies, shapes and symmetries. The role of electron spin in governing orbital occupancy is discussed, along with the structure of many-electron atoms and the use of term symbols to identify the various spin, orbital, and total angular momenta of atomic states. The use of atomic orbitals as constructs for molecular orbitals and molecular bonding is described. Term symbols for small molecules are illustrated briefly using O₂, which is particularly important in photochemistry, as an example. The concepts of a Highest Occupied Molecular Orbital (HOMO) and Lowest Unoccupied Molecular Orbital (LUMO) are introduced, and the importance of these orbitals in photochemistry is explained. Bonding in conjugated systems, metals and semiconductors is described. The link between energy levels and electrochemical redox potentials is made. The various

P. Douglas (✉)
Chemistry Group, College of Engineering, Swansea University,
Swansea, UK
e-mail: P.Douglas@swansea.ac.uk

R. C. Evans
School of Chemistry and CRANN, Trinity College Dublin, Dublin 2, Ireland
e-mail: raevans@tcd.ie

H. D. Burrows
Department of Chemistry, University of Coimbra, Coimbra, Portugal
e-mail: burrows@ci.uc.pt

energy states in atoms molecules and solids, and the way energy is distributed within these energy levels according to the Boltzmann equation, are described. Timescales for various physical and photochemical processes are given. The interaction of electronic energy states with ultraviolet and visible light is discussed in terms of absorption, emission and stimulated emission, using the Einstein *A* and *B* coefficients, transition probabilities, and absorption coefficients. The absorption process and the various selection rules which control the efficiency of absorption, and emission, are described, as are the common types of electronic transitions. Absorption in gas, solution, and solid phases, and the effect of aggregation on absorption in solution, are discussed. Unimolecular radiative and non-radiative excited state deactivation processes are discussed in terms of the Jablonski diagram, and the ideas of, competition between decay routes, and quantum yield, are introduced. Bimolecular interactions, quenching and energy transfer are described, with Förster Resonance Energy Transfer (FRET) and Dexter energy transfer discussed in some detail, and the analysis of bimolecular quenching kinetics using the Stern–Volmer equation is given. The chapter finishes with brief discussions of excimers, exciplexes, delayed fluorescence and proton transfer.

1.1 Introduction

If you are reading this in paper form, you can see the text because light scattered by the surface of the page is focused by the optics of your eye onto light-sensitive cells in your retina. The light will be from either the Sun or some ‘artificial’ light source, probably a tungsten bulb or fluorescent lamp, perhaps a light-emitting diode (LED) or a flat panel electroluminescent display. The page is bright white, because the inhomogeneous surface scatters all wavelengths of white light with high efficiency; also, in part, because it contains an optical brightener, which absorbs any near ultraviolet (UV) light and re-emits it as blue light—under UV excitation the white page will glow blue. The print is black because the pigment absorbs all visible light with high efficiency; any regions of colour arise because the pigments there absorb some wavelengths of white light more efficiently than others, those wavelengths which are not absorbed are reflected into your eye. The lens in your eye bends the light to focus it onto your retina. The retina contains light-sensitive cells, or *photoreceptors*, in which a pigment, 11-*cis*-retinal, held in a protein chain, undergoes a chemical transformation, a *cis*–*trans* isomerisation, when it absorbs a photon of light (Fig. 1.1). The pigment is chemically bound to a protein, *opsin*, through a weak Schiff’s base linkage, and this transformation distorts the shape of the protein, initiating a cascade of chemical events in the cell which results in the generation of an electrical signal to other cells. These compare the colour and intensity across your field of view, sending a signal to the brain. You can see colour because you have three different types of light-sensitive cell, called

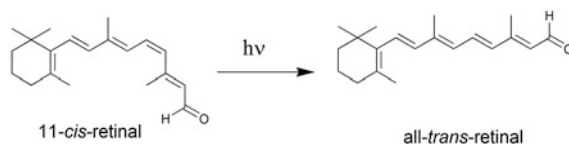


Fig. 1.1 In the first step of vision, light-sensitive cells in the eye are activated when light induces the isomerisation of the pigment 11-*cis* retinal to all-*trans* retinal

cone cells, which respond differently to different regions of the visible spectrum, roughly speaking the red, green, and blue. Cone cells all use 11-*cis*-retinal, but wavelength selectivity is introduced by a difference in the structure of the protein holding the pigment which changes the protein conformation around 11-*cis*-retinal and, hence, its absorption spectrum. In these steps of the visual process there is an interaction between electromagnetic radiation (light) and matter. It is this interaction that is the subject of this book.

Photochemistry deals with the chemical changes in chemical species: atoms, molecules, polymers, semiconductors, crystals etc., which are brought about as a consequence of absorption of electromagnetic radiation (EMR) in the wavelength range *ca.* 200–2000 nm. The range 200–400 nm is the readily accessible ultra-violet region, *ca.* 400–800 nm is the visible (Vis) spectrum, and *ca.* 800–2000 nm is the near-infrared (NIR). The range is bounded below 200 nm by the vacuum ultraviolet, where oxygen, nitrogen and water vapour absorb, and above 2000 nm by the mid-infrared. The region 315–400 nm is commonly termed UV-A, 280–315 nm UV-B and 200–280 nm UV-C [1]. The lower limit of the UV-A region corresponds to the cut-off of transmission by glass, while the UV-B range is approximately the limit of sunlight on a clear day reaching the Earth's surface. Absorption bands are frequently seen in the NIR region due to overtone vibrational transitions. For example, water shows overtone bands at 836, 970, 1200, 1470 and 1900 nm [2]. Chemical changes are those involving the rearrangement of electrons and nuclei in chemical structures. If we include transient as well as permanent changes in electronic structure and the positions of nuclei, then the absorption of light, the subsequent processes occurring in the transient species formed, as well as those electronic changes immediately following absorption, are included in this definition of photochemistry.

The most important chemical effect of the absorption of light is the transition of an electron from an orbital in the normal, ground, energy state of the atom or molecule, into a higher energy orbital to produce an electronically excited-state. The understanding of the nature of the energy states of electrons and of their effects on the structures of excited-states is central to photochemistry. As a consequence of the redistribution of electron density, bond lengths, bond orders and bond angles in excited-states may be significantly different from their corresponding ground-states, such that they can be considered as chemically distinct species. In addition, by their very nature, excited-states are highly energetic, and they must lose their excess energy *via* a variety of intra and intermolecular processes, which operate over time

scales ranging from femtoseconds ($1 \text{ fs} = 10^{-15} \text{ s}$) to hours. For example, the loss of excess vibrational energy of large polyatomic molecules in the liquid phase can occur within tens of femtoseconds [3], while the lifetime of the lowest excited-state of He atoms (the $^3\text{S}_1$ state) is over 2 h [4]. Although the radiative lifetime of the lowest excited-state of singlet molecular oxygen in the gas phase at low pressures is over an hour [5], it is reduced by 9–10 orders of magnitude by solvent interactions in solution. Studying these deactivation processes makes up another important area, frequently described as *photophysics*. Because of both their excess energy and the differences in electron distribution, the chemistry of excited-states can be very different from that of the same molecule in the ground-state, and the chemical behaviour and reactions of excited-states, and the consequences and practical applications of excited-state reactions are also fundamental to photochemistry.

In applied photochemistry we are interested in studying these interactions because of their useful or damaging consequences. But before dealing with photochemistry, we first need some understanding of the structure and properties of matter and electromagnetic radiation.

1.2 Matter and Electromagnetic Radiation: Particles and Waves

In physics at the end of nineteenth century, the world was seen as being of two mutually exclusive entities: particles and waves. Matter was particulate. All electromagnetic radiations: ultraviolet, visible, infrared, and radio waves, were seen as electromagnetic waves which travelled in a vacuum at the same speed, but which differed in wavelength and frequency. The nature of the atom was a mystery, but spectroscopy and other experiments gave hints of an inner atomic structure incorporating a regular pattern of energy levels. In the first third of the twentieth century there was a revolution in theoretical chemical physics, largely driven by the need to understand atomic and molecular structure. The result was ‘*quantum*’ or ‘*wave*’ *mechanics*, a theory that removes the distinction between waves and particles, and views both matter and electromagnetic radiation in essentially the same way.

The characteristics of particles are: mass, momentum, localisation of position in time and space, and fixed trajectories under the action of forces as described by Newton’s laws of motion. These characteristics are those of matter in our everyday macroscopic world.

The characteristics of electromagnetic waves are: wavelength, frequency, extension in time and space, interference, diffraction, refraction, and polarisation. These are, perhaps, less immediately apparent in our everyday life, although polarised sunglasses, interference colours of oil films on water and soap bubbles, or the interference fringes around raindrops on spectacles when looking at street lamps on a rainy evening, are everyday manifestations of the wave properties of light. We will treat these characteristics descriptively—more quantitative accounts can be found elsewhere [6].

1.2.1 Physics of Electromagnetic Waves

An electromagnetic wave is a periodic disturbance in the electric and magnetic environment; it is a simultaneous oscillation of the *electric* and *magnetic fields*. The electric and magnetic fields can be treated as vectors, whose direction of oscillation are at right angles to one another and at right angles to the direction of propagation of the wave (*i.e.* it is a *transverse* wave, Fig. 1.2). As the wave passes a given point in space, a free moving charged particle will experience an oscillatory force and will itself oscillate with the same frequency as the wave. A similar everyday example is the way that a cork floating on water bobs up and down as a wave passes, and just as we can make a water wave by holding the cork and making it oscillate up and down, an oscillating charged particle, such as an electron, will also generate an electromagnetic wave.

Photochemistry deals with the interaction of electromagnetic waves of visible and UV wavelength with the electrons in chemical structures. These interactions are predominantly through the effect of the *electric field* on *electric dipoles*—structures in which there is a separation of positive and negative charge, such as atoms and molecules. These are termed *electric dipole interactions*, or, when they result in a change of state, *electric dipole transitions*. Such transitions are the most important processes involved in production of electronic excited-states. The

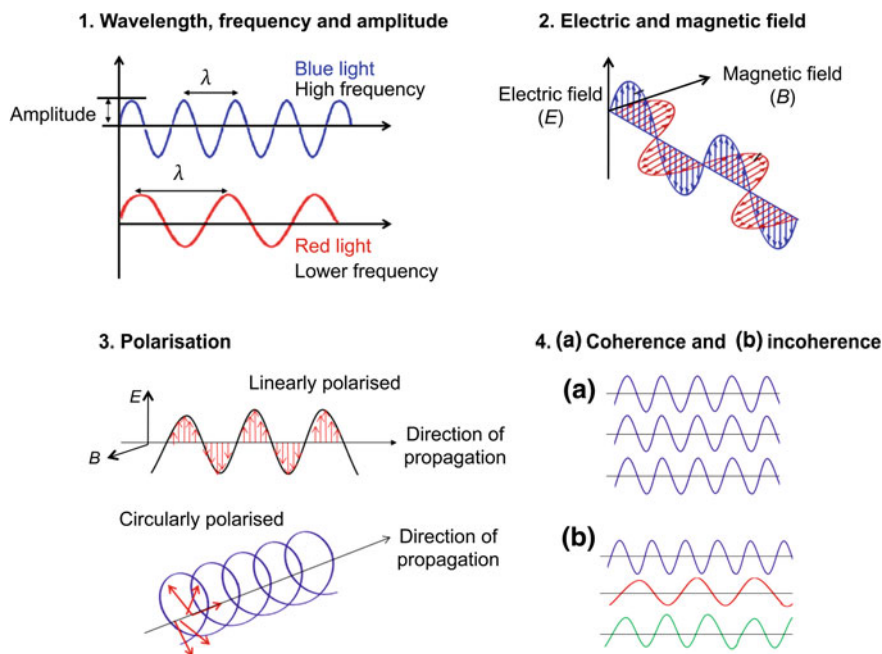


Fig. 1.2 The key properties of electromagnetic radiation

magnetic field of an electromagnetic wave will, however, also interact with *magnetic dipoles*, leading to *magnetic dipole transitions*; it is this magnetic interaction that gives spin spectroscopies such as *Electron Spin Resonance* (ESR) and *Nuclear Magnetic Resonance* (NMR) spectroscopy. Magnetic dipole interactions may also be important in photochemistry, particularly in systems having unpaired electrons. In addition, higher order, e.g. *quadrupolar*, interactions can be important for some chemical species.

The key properties of electromagnetic waves are: velocity (V), wavelength (λ), frequency (ν), amplitude, polarisation, intensity and coherence. These are illustrated in Fig. 1.2. The relationship between the first three is given by: $V = \lambda\nu$. Polarisation can be either linear, or circular, and linear polarised light can be represented as the sum of two equal amplitude, circularly polarised waves moving clockwise and anticlockwise in phase. The intensity of the wave is proportional to the square of the amplitude.

Many light sources, such as the Sun or typical domestic lighting, are polychromatic, *i.e.* many wavelengths are present. For detailed scientific studies and many technological applications it is advantageous to use a monochromatic beam, which has radiation of a single wavelength (and frequency). A typical example is the red diode laser used as a bar code reader in a shop or as a laser pointer. In practice, even laser sources are not completely monochromatic, but cover a very small but finite range of wavelengths (the *bandwidth*). Lasers demonstrate another important property of light, *coherence*. Standard illumination sources, such as room lighting, involve an incoherent beam in which the waves are moving in random phases with respect to one another. In a coherent light beam, such as that generated by lasers, all waves are moving in phase with respect to each another (Fig. 1.2). This has important optical implications since coherent light can be both focused down to a very narrow beam so it is possible to obtain a very narrow spot in which high light intensities are present [7], and also transmitted as a beam over long distances with little divergence. The combination of laser light of appropriate wavelength (typically in the near IR) and fibre optic cables has been one of the main factors contributing to high speed, high density data transmission, such as in international telecommunications and broad band internet. The development of new laser sources, amplifiers and detectors is an important current area of interest in applied photophysics (see Chap. 14).

It is, perhaps, convenient at this stage to distinguish between two related, but distinct terms. *Optics* refers to “that branch of physical science concerned with vision and certain phenomenon of electromagnetic radiation in the wavelength range extending from the vacuum ultraviolet... to the far infrared” [8]. This is part of the more general area of *photonics*, which involves both generating and utilising photons of radiant energy. For more details see any standard textbook on the subject [9].

1.2.2 Wave–Matter Interactions

1.2.2.1 Refractive Index, Refraction and Dispersion

The velocity, V , of an electromagnetic wave in a vacuum is normally given the symbol c (2.99792×10^8 m s⁻¹). The thickness of a typical sheet of paper is around 0.1 mm, and light takes about 3×10^{-13} s (300 fs) to pass from one side to the other. According to the special theory of relativity, c is the maximum speed at which energy can be propagated. In all other media the wave velocity is less than this. The relationship between the two is the *refractive index*, RI (often given the symbol n), of the medium, which is given by:

$$\text{RI} = c/V_{(\text{medium})} \quad (1.1)$$

where $V_{(\text{medium})}$ is the wave velocity in the medium.

The refractive index is a measure of the degree of interaction between the wave and the medium. If the electrons in the medium are easily perturbed by the wave, *i.e.* if the medium has a high *polarisability*, the interaction is strong and the RI high. This depends upon the wavelength, chemical structure, phase (*i.e.* whether the material is solid, liquid or gas) and temperature.

When moving between two different transparent media the wavelength of the wave is reduced in proportion to the velocity, but its frequency remains constant. If the refractive index is wavelength dependent, a polychromatic wave is dispersed as it travels through the medium. Dispersion causes a separation of wavelengths as the radiation moves; thus a pulse of white light is broadened, and separated spatially in wavelength, as it travels through a dispersing medium.

If a wave is incident on an interface between media of varying refractive indices, the direction of propagation is altered, and the wave is ‘bent’, or refracted, by the interface. The angle between incident (θ_1) and refracted (θ_2) rays is given by *Snell’s law*:

$$\sin\theta_1/\sin\theta_2 = V_1/V_2 = n_1/n_2 \quad (1.2)$$

where n_1 and n_2 are the refractive indices of the media at either side of the interface, as illustrated in Fig. 1.3.

It is this behaviour that allows the focusing and movement of beams of light by the curved surfaces of lenses. If one of the media is dispersive then the degree of bending is wavelength dependent, and white light is dispersed into its various colours by a prism.

1.2.2.2 Transmission and Reflection

Light incident on an interface between media of different RI will be subject to either transmission or reflection at the interface. If the interface is flat, such as a

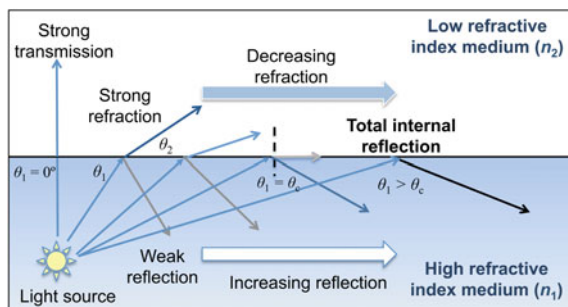


Fig. 1.3 The refraction and/or reflection of light at an interface depend on the refractive indices of the surrounding media. As the angle of incidence (θ_1) of the wave impinging on the surface normal increases from 0° to larger angles, the refracted ray becomes dimmer (the degree of refraction decreases) and the reflected ray becomes brighter (the degree of reflection increases). For a flat, polished surface the angle of incidence equals the angle of reflection. When the angle of incidence approaches the critical angle, θ_c , the refracted ray can no longer be observed. For $\theta_1 > \theta_c$, the light is said to be ‘totally internally reflected’

polished surface, the light is reflected at an angle equal to that of the incident beam; the surface acts as a mirror, a *speculum*, and the phenomenon is termed *specular reflection*. The fraction of reflected light increases with the difference in RI between the media and also with the angle of incidence, such that for a very shallow angle of incidence, almost any interface is a good mirror (see Fig. 1.3). Anti-reflection coatings employ thin layers of media of intermediate RI for enhanced transmission.

If the interface is totally irregular, such as a finely ground powder, the light is reflected more diffusely as *diffuse reflectance*. Reflection spectroscopy, particularly diffuse reflectance, is a widely used technique for studying solids and surfaces. The reflected light is collected in an integrating sphere, or some similar optical arrangement, and there is usually the facility to collect or reject the specularly or diffusely reflected components. Diffuse reflectance spectroscopy is discussed in more detail in [Chap. 14](#).

As a coloured material is ground from bulk to a powder, the fraction of light which is reflected from the surface increases and less light penetrates into the bulk material where selective absorption causes colour. Thus the intensity of the colour of a material decreases as it is ground; intensely blue copper sulfate crystals can be ground to a white powder.

It is possible to create materials with either multi-layered structures, continuously varying mixes of materials, or nanostructures, such that RI varies continuously across an interfacial region rather than at a definite optical interface. These materials, analogies of which are found in nature, offer enhanced optical properties for a number of applications, such as reduced glare from liquid crystal display (LCD) computer monitors and televisions and improved signal-to-noise ratio in photodetectors.

1.2.2.3 Total Internal Reflection and the Evanescent Wave

When light passes from a medium of high RI to one of low RI there is a critical angle of incidence, θ_c , depending upon the RIs of the media, above which all light is reflected back into the medium of high RI. Thus, as illustrated in Fig. 1.3, all light incident at an angle greater than the critical angle is *totally internally reflected*. This phenomenon is used in fibre optic cables in which light can be transmitted along the cable without serious loss in intensity because it is trapped within it by total internal reflection. It is also responsible for loss of emission efficiency from flat surface displays and lamps. Total internal reflection is also found, and used to advantage, in some natural structures. It is responsible, for example, for the sparkle of cut diamonds or the mirror like appearance of the water surface seen when you are swimming under water. Although light incident at greater than the critical angle is totally internally reflected, the wave itself penetrates for some fraction of a wavelength into the outer medium; this is the *evanescent wave*. The evanescent wave can interact with any substance adsorbed to or pressed close to the interface, and this forms the basis of evanescent wave, or *Attenuated Total Reflection* (ATR), spectroscopy. Here, the spectroscopic monitoring beam is contained within an optical fibre, or transparent crystal and the material to be studied is adsorbed or pressed against the fibre or crystal; the technique is now very widely used, particularly in infrared spectroscopy. Another important application for a variety of devices is *evanescent wave coupling*, where evanescent waves can be transmitted from one medium to another if appropriate conditions are met. Evanescent wave coupling is a hot topic of research in the field of nanophotonics [8], with promising results being obtained in areas such as wireless power transfer.

1.2.3 Wave–Wave Interactions

1.2.3.1 Interference

When two or more waves overlap the amplitudes at any position are the sum of the amplitudes of the individual waves. *Constructive interference* occurs when the waves reinforce each other, *destructive interference* when they cancel each other out (Fig. 1.4). The effect resulted in one of the most important experiments in optics carried out by Thomas Young at the beginning of the nineteenth Century, where he passed sunlight through two slits in an opaque material, and observed distinct fringes due to interference. This experiment established the wave nature of light. A modification was subsequently used by Michelson and Morley in a classic experiment [10], which showed that light did not need any medium for transmission. This experiment failed to achieve the original objective of these researchers, but instead laid part of the basis from which the special theory of relativity was developed.

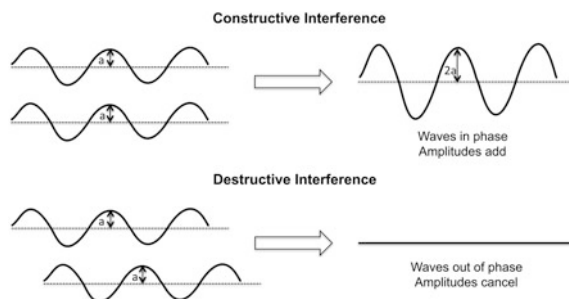


Fig. 1.4 Constructive and destructive interference of two identical waves. In constructive interference, the two waves reinforce each other to produce a wave with twice the amplitude. However, in destructive interference, the two waves are 180° out of phase, and the amplitudes exactly cancel out

1.2.3.2 Diffraction

Diffraction occurs when light waves pass through small openings, around obstacles, or are incident upon a sharp edge. When light passes through a small aperture an interference pattern is observed, rather than a spot of light and a sharp shadow. The light wave spreads in various directions beyond the aperture and into regions where shadows would be expected if the wave travelled in straight lines. Even though matter seems to be involved in these examples, diffraction is actually a wave–wave interaction with interference between waves made apparent by the blocking of some light paths by opaque objects.

Diffraction is crucially important in optics, since light cannot be focused to a smaller size than the diffraction limit, first defined by the German physicist Ernst Abbe as:

$$d = \lambda / (2n \sin \theta) \quad (1.3)$$

where d is the *diffraction limit* (*i.e.* the finest spatial resolution that can be resolved), and λ is the wavelength of a light beam, travelling through a medium of refractive index, n , and converging to a spot with angle θ . The denominator ($n \sin \theta$) is called the *numerical aperture* (NA) and can reach ~ 1.4 with modern optics, such that the diffraction limit is roughly given by $\lambda/2$. Thus, the diffraction limit is in the order of 200–400 nm for wavelengths in the visible spectral region (400–800 nm).

This limits the spatial resolution of optical devices and the size of patterning produced by techniques such as photolithography. A pair of objects separated by a distance smaller than the diffraction limit cannot be resolved into two separate images. The resolution of an ordinary optical microscope is improved by increasing the RI of the medium between the lens and object (*i.e.* using an *oil objective lens*) and/or using short wavelengths of light.

There are also now a number of techniques in optical microscopy, which do manage, with certain systems, to overcome the diffraction limit [11], such as

Scanning Near-field Optical Microscopy (SNOM) and *Stimulated Depletion Emission Microscopy* (STED) and these are discussed more fully in [Chap. 14](#).

1.2.3.3 Standing Waves: Localised Waves and Energy Levels

If a wave is constrained within a fixed volume of space, only certain waveforms, known as *standing waves*, are stable; for all but these certain wavelengths, interference of the wave within the volume prevents formation of a stable wave. This phenomenon is most obvious in stringed musical instruments where the length of the string determines which vibrations are allowed.

The *boundary condition* for a light wave trapped between two mirrors (similarly, a wave on a string), at a separation, L , is that at the surface of the mirrors (the fixed ends of the string) the wave displacement is zero (*i.e.* there is no movement of the string). These positions of zero displacement are termed *nodes*. Under these conditions, the only wavelengths that are stable over time are given by:

$$\lambda = 2L/n \quad (1.4)$$

or, in terms of frequency:

$$\nu = nc/2L \quad (1.5)$$

where n is an integer (not to be confused with the use of n for refractive index). All other wavelengths are destroyed by interference. Thus, constraining a wave in space by introducing boundary conditions naturally generates a system of fixed wavelengths, frequencies and energies; the properties of the waves are not continuously variable but are *quantised* as a consequence of the boundary conditions and we call n a *quantum number*. The value of n is not continuous but limited to discrete values. For a light wave between two mirrors, or a wave on a string, n can be any positive integer, but for some other types of waves and boundary conditions the quantum number can be half integral, positive or negative, zero, and in some cases, the quantum number itself is restricted to only certain integral or half integral values, or zero. When first encountered, quantum numbers can seem to be mysterious things, but they arise naturally from waves constrained in space. Also, since the value of the quantum number(s) fixes all the properties of the given wave, the quantum number itself can be used as a label to describe the wave, or any property of the wave such as energy, succinctly.

The waves, and relative energies for $n = 1, 2, 3, 4$ are shown in [Fig. 1.5](#). Note that in addition to the nodes at the ends of the wave, the wave shapes themselves can generate nodes at various points on the wave; in this case the number of these internal nodes is given by $n-1$. The actual wave shape (vibration of a string) is not limited to only one of these *fundamental mode* vibrations, and it may be much more complex; but all vibrations, however complex, can be represented by the addition or subtraction, that is, a superposition or linear combination, of different fundamental modes. By the reverse process, any complex waveform can be

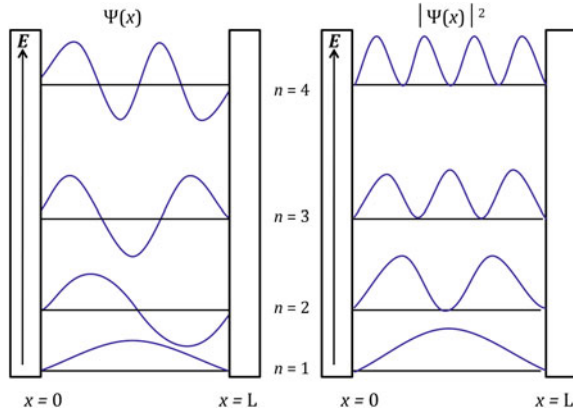


Fig. 1.5 The first four stable waveforms for a trapped light wave. As n increases, the number of places where the wave exhibits zero displacement (*nodes*) also increases. $\Psi(x)$ is the *wavefunction*—see Sect. 1.4.2.2 and Ref. [6]. $|\Psi(x)|^2$ describes the probability of finding the particle (*i.e.* the light wave, or *photon*) in space. When n is small, the particle has a higher probability of being at the centre, than it does of being near the edges, but as n gets large, the particle has an approximately equal probability of being anywhere between $x = 0$ and $x = L$. For particle waves, such as electron waves, the trapped wave in one dimension (1D) is often referred to as a *particle in a 1D box*, or *particle on a string*

resolved into a summation of fundamental modes. This process, known as *Fourier Transformation* (FT), is widely used in the analysis of complex waves, and forms the basis of Fourier Transform spectroscopy.

1.2.3.4 Wave Pulses

While an infinitely long sine wave (Fig. 1.2) is the common representation of an electromagnetic wave, it is possible to generate pulses of electromagnetic radiation that last for no more than a few tens of femtoseconds (fs) and which are therefore only a few hundred microns (μm) in length. This has important implications in photonics.

1.2.4 Physics of Particles

1.2.4.1 Mass, Acceleration, Velocity, Momentum, Angular Momentum, Kinetic and Potential Energy

Mass is a familiar concept. The behaviour of objects with mass under the influence of forces and when in collision is the subject of Newton's laws of motion. If an otherwise free object of mass, m , is acted upon by a constant force, F , then that object undergoes a constant acceleration, a , in the direction of the force, where $F = ma$. If

the force is removed, the object does not stop but continues moving with constant velocity, V . Force and velocity are vector quantities; they have direction as well as magnitude. An important property of a moving mass is *linear momentum*, p , where $p = mV$. The kinetic energy, KE , of a moving body is given by $\frac{1}{2}mV^2$.

Rotating objects also have *angular momentum*. Consider an object of mass, m , revolving in a circle of radius r . The rotation can be described by an angular velocity, ω , in units of radians s^{-1} (2π radians = 360° , so the time taken for one complete revolution is $\omega/2\pi$). The object has a linear velocity, V , at a tangent to the circumference of the circle, (to see this, imagine the direction the object would fly off if the force of attraction to the centre was suddenly removed) and has angular momentum, L , given by, $L = r \times mV$. The length of the arc moved by the object in 1 s is V , and since the circumference of a circle is $2\pi r$ then the change in angle per second, *i.e.* the angular velocity, ω , is given by V/r radians s^{-1} . Thus the angular momentum expressed in terms of angular velocity, is:

$$L = \omega mr^2 \quad (1.6)$$

where the angular momentum vector L is normal to the plane of the circle. Since the object can revolve clockwise or counter clockwise, L can point up or down.

A body spinning on its axis also has angular momentum, and thus a spinning body which is also revolving about a point has two types of angular momentum: the angular momentum due to its spinning, and the angular momentum due to its rotation about a point. These momenta can combine to reinforce each other, *i.e.* both vectors can point up or down, or they can oppose one another with one pointing up and one pointing down. The angular momenta of electrons in atoms and molecules, and restrictions on how these can combine, and can change upon absorption of light, is very important in photochemistry.

1.2.4.2 Universal Conservation Laws

Angular momentum, linear momentum and energy are all subject to universal conservation laws such that in any interaction the total angular momentum, total linear momentum, and total energy, before and after the event, remain unchanged.

1.2.5 The Link Between Waves and Particles

The link between the classical wave property of wavelength, λ , and the classical particle property of momentum, p , is given by the *de Broglie equation*:

$$\lambda = h/p. \quad (1.7)$$

In describing the behaviour of waves and particles, any wave must also be viewed as being made up of particles each with momentum h/λ , and any moving particle must also be viewed as a wave of wavelength h/p .

1.2.5.1 Particle Waves

The size of Planck's constant, h , determines the broad boundary of mass at which either the wave or particle properties of an object dominate in our experience of it. The wavelengths of some everyday objects, moving atoms and fundamental particles are shown in Table 1.1. The wavelength of a heavy particle moving at moderate speed is very short, while that for a particle of very small mass is relatively long. If the wavelength of an object is very small, then wave behaviour is not observable and our experience of that object is as a particle. If the wavelength is significant, then wave properties are apparent and our experience of that object is predominantly as a wave. In our everyday world macroscopic particles do not exhibit measurable wave properties. In the atomic and molecular world, neutrons, protons, nuclei, and, most importantly for photochemistry, electrons do.

The wave property of electrons is shown directly in electron diffraction, and the electron microscope. As described earlier the resolution of a microscope is determined by the wavelength of the analysing wave. In an electron microscope the resolution is controlled by the acceleration given to the electrons, since, from the de Broglie relationship, high velocity electrons have shorter wavelengths than low velocity electrons. The wave properties of neutrons are apparent in neutron

Table 1.1 The wavelengths of some everyday objects, moving atoms and fundamental particles

Particle	Mass/g	Velocity/m s ⁻¹	Wavelength/pm
London Routemaster bus	7.4×10^6	13	6.9×10^{-27}
Fastest kicked football	430	60	2.5×10^{-23}
Fast bowled cricket ball	160	25	1.66×10^{-22}
^a 22-rifle bullet	1.9	320	1.1×10^{-21}
Housefly	12×10^{-3}	2	2.8×10^{-17}
^a α -particle from radium	6.6×10^{-24}	1.51×10^7	6.6×10^{-3}
100-volt α -particle	6.6×10^{-24}	6.9×10^4	1.5
100-volt proton	1.67×10^{-24}	1.38×10^5	2.9
10,000-volt electron	9.1×10^{-28}	5.9×10^7	12
^a H ₂ molecule at 200 °C	3.3×10^{-24}	2.4×10^3	82
100-volt electron	9.1×10^{-28}	5.9×10^6	120
1-volt electron	9.1×10^{-28}	5.9×10^5	1200

Notes The wavelength of green light is about 500,000 pm; a 1 V electron has the same energy as a 1240 nm photon; an atom is typically a few hundred pm in diameter; the potential energy of an outer electron in an atom is a few eV and the wavelength of such an electron is comparable to an atomic diameter

^a From Ref. [12]

diffraction and scattering experiments, while wave properties of atoms are seen in atomic beam experiments.

Although directly observable quantum mechanical effects, such as interference and diffraction, cannot be measured for everyday macroscopic objects, these objects are made up of the nuclei and electrons of atoms, and since quantum mechanical properties control the interactions between these small units, they also control the bulk properties of matter. The structures of bulk matter itself, and all interactions between matter and radiation, arise from the quantum mechanical behaviour of the smaller units from which it is composed.

1.2.5.2 Photons and Photon Energy

A *photon* is a discrete packet (or *quantum*) of electromagnetic radiation. Photons are always in motion, and each individual photon carries momentum and, since it is travelling at the speed of light, relativistic energy. For EMR in a vacuum, $c = \lambda\nu$. Replacing λ by c/ν in the de Broglie relationship gives:

$$c/\nu = h/cm \quad \text{i.e.} \quad mc^2 = h\nu \quad (1.8)$$

where mc^2 is the *relativistic energy*. Thus, the energy of a photon is $h\nu$, the relativistic mass is $h\nu/c^2$, and the linear momentum is h/λ .

For long wavelength, low momentum radiation, e.g. radio waves, it is the wave properties which dominate in our experience (although this is due in part also to the fact that radio waves are most often of interest because of their interaction with electrons in bulk metals and gases, where *quantisation* is not such an obvious property). For short wavelength, high energy, high momentum waves, e.g. γ -rays, particle properties are more apparent—we speak of γ -rays and X-rays ‘knocking out’ electrons from atoms.

The particle property of EMR waves is shown directly in the *photoelectric effect*, and the scattering of γ -rays by electrons, known as *Compton scattering*.

1.3 The Building Blocks of Photochemistry: The Proton, Neutron, Electron and Photon

1.3.1 Fundamental Properties

The fundamental properties of the four particles involved in photochemical transformations, the proton, neutron and electron which make up the atom, and the photon, are given in Table 1.2.

Table 1.2 Fundamental properties of the four particles involved in photochemical transformations

	Proton	Neutron	Electron	Photon
Mass (kg)	$1.672621777(74) \times 10^{-27}$	$1.674927351(74) \times 10^{-27}$	$9.10938291(40) \times 10^{-31}$	0
Electric charge (C)	$1.602176565(35) \times 10^{-19}$	0	$-1.602176565(35) \times 10^{-19}$	0
Spin quantum number	$\frac{1}{2}$	$\frac{1}{2}$	$\frac{1}{2}$	1

1.3.1.1 Mass

The masses of the proton and neutron are similar but not identical. The mass of the electron is much smaller, 1/1840, that of the proton. Although the photon has zero rest mass, it is always moving at the speed of light and has relativistic mass.

1.3.1.2 Electric Charge

The electron and proton carry equal but opposite charge, while both the neutron and photon have zero charge. Charged particles interact through the *electrostatic*, or *Coulombic force* (after the French physicist Charles-Augustin de Coulomb, who in 1785 first published the law that describes how charged bodies interact) [13]. The force between two bodies of charges q_1 and q_2 separated by a distance, r , in a medium of *relative permittivity* (also called *dielectric constant*), ϵ , is given by:

$$F = k_e q_1 q_2 / \epsilon r^2 \quad (1.9)$$

where k_e is the *Coulomb constant*. (k_e is also written as $1/(4\pi\epsilon_0)$ where the constant, ϵ_0 , is the *permittivity of free space*.) The force depends on the product of the two charges and is inversely proportional to the distance between them—the force increases rapidly as the bodies approach one another. When the two charges are of the same sign the force is positive, corresponding to repulsion; when different, it is negative, corresponding to attraction.

The electrostatic energy of two charges at distance r , when the reference zero energy is when they are at infinite separation, is given by:

$$E = k_e q_1 q_2 / \epsilon r. \quad (1.10)$$

The energy of two opposite charges at any finite distance r is negative and increases (becomes more positive) as they are pulled apart, until it is zero at $r = \infty$; the energy of two bodies with the same sign charges increases as they are pushed together. The *relative permittivity* is an important property of the medium, since it determines the strength of charge interactions. The forces and energy between two charged bodies in hexane, a *non-polar solvent*, with $\epsilon \sim 1.9$, are forty times stronger than those in water, a *polar solvent*, with $\epsilon \sim 80$. This difference is an important factor in influencing the chemistry in those media.

It is the electrostatic force of attraction between the negatively-charged electron and positively-charged nucleus that leads to the formation of stable atoms and molecules.

We are so familiar with the idea that charge only occurs in units of the fundamental charge we do not usually speak of it as being quantised.

1.3.1.3 Spin

The *spin* of fundamental particles and the *spin quantum number* are not familiar everyday concepts. Spin is a property of fundamental particles, and also groups of fundamental particles, such as atomic nuclei. Spin has no true counterpart in the macroscopic world. It was introduced as an additional property of electrons to account for the fine detail in atomic emission spectra. This detail could be rationalised if it was assumed the electron had an intrinsic magnetic moment, as if it behaved in some ways like a tiny bar magnet. The term *spin* was chosen for this electron property by analogy with a spinning charged body, which will generate a magnetic moment. But this cannot be taken literally; while the electron magnetic moment is a measurable property, the electron does not behave as if it were a spinning charged body, even though this might sometimes be a useful picture. Although spin was originally introduced rather arbitrarily, Dirac showed that electron spin arises naturally when quantum mechanics and relativity are combined.

The electron, neutron, proton and photon have intrinsic quantised, non-zero, angular momentum, in the same way that they have intrinsic mass, and electrons and protons have intrinsic quantised charge. The magnitude of this intrinsic *spin angular momentum* is described by the spin quantum number, s , through the following equation:

$$\text{Spin angular momentum} = [s(s + 1)]^{1/2} \cdot h/2\pi \quad (1.11)$$

where h is Planck's constant. The value $h/2\pi$ occurs so regularly in quantum mechanics that it is given its own symbol, \hbar , pronounced "h cross" or "h bar", sometimes called the reduced Planck constant, and sometimes the angular momentum unit (amu) (the units of h are the same as those of angular momentum).

Not only is the absolute spin angular momentum of a particle quantised in this way, but also the direction in which the spin vector can point, *i.e.* the amount of spin angular momentum along any specified axis. If we do keep the analogy of a spinning body, a child's spinning top for example; in our macroscopic world we can make such a top spin at any speed and point it in any direction we desire with respect to an axis, the vertical axis for example. In the quantum world the 'fundamental particle top' can only spin at one fixed speed and it is also only allowed to point at certain angles to the vertical. For a spin $\frac{1}{2}$ particle, such as an electron or proton, the spin angular momentum can be aligned with a reference direction in only one of two specified ways, to give a spin angular momentum component of

either $+\frac{1}{2}$ or $-\frac{1}{2} \hbar$ along the reference axis. These two arrangements are colloquially known as “spin up” and “spin down” (often represented by arrows pointing up, \uparrow , or down, \downarrow), and identified more formally by the quantum number, m_s , which for electrons can take values of $+\frac{1}{2}$ or $-\frac{1}{2}$.

The interaction of the spin angular momentum of the electron with an external magnetic field is the basis of ESR spectroscopy, while the interaction of the spin of the proton with an external magnetic field gives proton NMR spectroscopy (^1H NMR) and *Magnetic Resonance Imaging* (MRI).

For the photon, the spin quantum number also generates two spin angular momentum components, $+1$ and -1 , corresponding to left- and right-handed circularly polarised light. (As will be discussed later the general number of orientations of spin angular momentum is given by $2S + 1$ and we might then expect three possible spin angular momentum components for the photon, *i.e.* $+1$, 0 , -1 ; however relativistic quantum theory forbids the $m_s = 0$ component for particles travelling at the speed of light, leaving $m_s = +1$ (left circularly polarised), and -1 (right circularly polarised).

1.3.1.4 Fermions and Bosons

Particles with half-integral spin interact with one another differently to those with integral spin, most notably in the way they fill available energy levels. Particles with half-integral spin are called *fermions* because their distribution among energy levels follows *Fermi-Dirac statistics* in which at most only two particles can occupy any given energy level. Particles with integral spin are called *bosons* because their distribution among energy levels is governed by *Bose-Einstein statistics*, where any number of particles can occupy the same energy level. It is the half-integral spin of electrons, their *fermionic* nature, as much as anything, which, through its influence on atomic structure, defines the nature of bulk matter.

1.3.1.5 Movement and Energy of an Electron in an Electric Field: the Electron Volt

When an electron is placed in an external electric field an electric force will act on it, the electron will accelerate, and its kinetic energy will change. The energy gained by an electron when it moves through a potential difference of 1 Volt makes a useful unit of energy: the *electron volt*, eV. $1 \text{ eV} = 1.60219 \times 10^{-19} \text{ J}$ (the energy of a photon of 1240 nm wavelength is 1 eV; a photon of 620 nm is 2 eV and one of 413 nm is 3 eV). The relationship between electron volts and some other commonly used energy units, along with some comparative energy outputs, are given in Table 1.3.

Table 1.3 The relationship between common energy units and some comparative energies

Relationships between energy units	Comparative energies/J	
1 eV = 1.986×10^{-19} J = 96.486 kJ mol ⁻¹ = 8065.5 cm ⁻¹	Big Bang	10 ⁶⁸
	Sun's radiation for 1 year	10 ³⁴
	Volcanic eruption	10 ¹⁹
1 cal = 4.184 J = 23.060 kcal mol ⁻¹	<i>Tsar Bomba</i> hydrogen bomb	10 ¹⁷
	Largest man made nuclear explosion	
1 W = 1 J s ⁻¹	Largest planned man made conventional explosion (4.8 kton ammonium nitrate fuel oil)	10 ¹³
	Lightning flash	10 ¹⁰
	Combustion of 3 L diesel	10 ⁸
	Kinetic energy of Formula One racing car	10 ⁶
	Burning 2 sugar cubes (~ 6 g)	10 ⁵
	Muzzle energy of 0.44 pistol	10 ³
	Lifting 1 kg 1 metre	10
	Human heart beat	1
	Tapping a keyboard key	10 ⁻²
	Kinetic energy of a housefly	10 ⁻⁵
	1 grain of sand falling 1 cm	10 ⁻⁹
	Photon of visible light	10 ⁻¹⁸ –10 ⁻¹⁹
	An electron moved through 1 V	10 ⁻¹⁹
	Molecular vibration	10 ⁻²⁰
	Spin flipping an electron	10 ⁻²⁴
	BBC radio 4 longwave 'photon'	10 ⁻²⁸

1.4 The Structure of the Atom

1.4.1 The Atomic Nucleus: Protons, Neutrons, Nuclear Spin

The nuclei of the atoms of the chemical elements are composed of neutrons and protons. Every nucleus of any given element has the same number of protons and this number, the *atomic number*, usually given the symbol Z , is different from that of any other element. In the 'natural' elements, Z ranges from hydrogen with one proton to uranium with 92. 'Artificial' elements with up to 116 protons have, so far, been prepared in nuclear reactors, although the distinction between natural and artificial elements is, of course, arbitrary. In addition to protons, the nuclei of all elements other than hydrogen (^1H) contain neutrons.

For electrical neutrality, the atom must have the same number of electrons as protons. However, the number of neutrons in an atom of an element can vary, and variation in the number of neutrons gives rise to *isotopes*. The number of neutrons is the *neutron number*, usually given the symbol N . The sum of the neutrons and protons is the *atomic mass number*, symbol A . The atomic nucleus is very small, with a diameter of *ca.* 10^{-15} m, and the protons and neutrons are held together in

this very small volume by the strong nuclear force. This is a very strong, but short range (*ca.* fm range), attractive force between proton–proton, proton–neutron, and neutron–neutron, which is independent of electric charge. As the atomic number increases, charge repulsion between protons increases also, and the number of neutrons required for a stable nucleus, in which the strong force between all particles is greater than the electrostatic repulsion between protons, increases. Thus, the neutron to proton ratio for the elements increases rapidly with Z . But this nucleus stabilisation by neutrons is limited in effect, and above an atomic number of 83 (Bi) all nuclides are unstable to radioactive decay (^{209}Bi , $Z = 83$, is the heaviest stable nucleus).

The way the spins of the protons and neutrons in the nucleus combine can lead to nuclei with spin quantum numbers (I), varying from 0 to 6, and isotopes of the same element can have, and usually do have, different spin quantum numbers. Isotopic nuclear spin is important in NMR. For example, ^{12}C has $I = 0$ and ^{13}C has $I = \frac{1}{2}$, so that NMR spectroscopy is not possible with ^{12}C nuclei but is possible with ^{13}C . Fortunately for chemists the natural carbon isotopes include $\sim 1\%$ ^{13}C , and ^{13}C NMR is a very important tool in chemical structure elucidation [14]. Nuclear spin can also have subtle effects in other spectroscopies [15], and nuclear mass is important in molecular vibrational and rotational spectroscopies.

There is an electrostatic force of attraction between electrons and the nucleus and for atoms with more than one electron, there is also electrostatic repulsion between electrons. Since the electron mass is much smaller than that of the nucleus, the centre of mass of an electron–nucleus system lies much more closely to the nucleus than the electron. The force of attraction between a nucleus and electron acts on both bodies equally, and since $F = ma$, the electron is accelerated much more by this attraction than the nucleus. This gives us a simple atomic model: a very small, yet relatively massive, slow moving positively-charged nucleus around which there are relatively light, rapidly moving, negatively-charged electrons, all held together by electrostatic forces. These electrostatic forces, nucleus–electron and electron–electron, control the momentum, and also, through the de Broglie relationship, the wavelength of an electron as it moves around the nucleus. So between them, the nature of the electrostatic force and the mass of the electron determine the shapes of the stable electron waves in atoms.

1.4.2 Electron Waves in Atoms: Atomic Orbitals

1.4.2.1 Electron Waves

The physical boundaries of a musical instrument, the length of a string or column of air, or the area of a drum, restrict the possible shapes and frequencies, and hence energies, of the sound waves the instrument can produce. In a similar way the ‘boundaries’ of a molecule created by the electrostatic forces between electrons

and nuclei restrict the shapes and energies of the electron waves within the molecule. In a musical instrument the different wave shapes and energies give rise to the fixed frequencies of the fundamental and overtones generated by the instrument. In chemical structures, the restriction of possible wave shapes and energies controls the behaviour of electrons, and hence chemical properties. The mathematics for an electron in a chemical structure is more complex than a wave on a string or in a column of air, but the principle is the same; the combination of constraints and boundary conditions, naturally limits the properties of the electron waves in atoms and molecules to discrete, fixed, 'quantised', values. The shapes of the waves are limited, and the important properties of: electron wave energy, absolute electron wave orbital angular momentum, and orientation of the electron wave orbital angular momentum, are also naturally quantised.

The answer to the question of what stable electron waves are allowed in any chemical structure is given by the *time-independent Schrödinger wave equation* for that structure. (The time-independent wave equation is used to obtain the stable electron waves around atoms and other chemical structures, and the *time-dependent wave equation* is used for calculations of electron waves as they undergo 'transitions' from one wave into another). The Schrödinger equation is not derivable directly from any previous equations; it combines ideas of wave and particle behaviour that were previously considered mutually exclusive. This combination of particle and wave properties can be illustrated by discussion of the equation for the hydrogen atom.

1.4.2.2 The Hydrogen Atom

The particles. The hydrogen atom is made up of only two particles, the proton and electron. The mathematics of the relative movement of two particles is such that we can reduce the problem to only one moving particle of reduced mass moving around the centre of gravity of the pair. Because of the difference in masses of the proton and electron, it is convenient to identify the electron as the moving particle (with the reduced mass, μ_e , given by $\mu_e = (m_e m_n)/(m_e + m_n)$, where m_e and m_n are the mass of an electron and the nucleus, respectively). The difference in mass and reduced mass of the electron is less than 0.1 %, and the centre of gravity of the atom lies very close to the centre of the proton, so that, for all but detailed calculations, we can keep the simple model of an electron moving around a proton. The energy of the negatively charged electron moving around the positively-charged proton is made up of two parts: (1) the potential energy, which is the electrostatic energy of the electron associated with its position with regard to the nucleus, PE ; and (2) the kinetic energy, KE , due to its velocity. The sum of the two is the total energy of the system, *i.e.* $E_{total} = PE + \frac{1}{2}mV^2$. As the electron moves about the nucleus there is a constant interchange between these two types of energy: the potential energy is greatest when the electron is furthest from the nucleus and is moving slowly, and the kinetic energy is greatest when the electron

is moving rapidly, close to the nucleus. Conservation of energy requires their sum, the total energy, to be constant.

The waves. The wave equations for two charged particles moving with respect to one another can be obtained exactly. In Schrödinger's equation the wavelength of the electron at any point and time is given by its momentum ($p = mv$) using the de Broglie equation $\lambda = h/p$. The electron is constantly changing velocity as it moves around the proton so the wavelength of the electron wave varies as it moves. Only some electron waves will 'fit' and be stable to interference as they oscillate. The energy of the electron wave, *i.e.* the sum of the potential and kinetic energy, is equated with the frequency of the oscillation of the wave by $E = hv$.

The mathematics of the Schrödinger wave equation determines which electron energies give waves that are stable to destructive interference. It also gives the shapes and angular momenta of the waves. As for all waves that are constrained in space, only certain waves are stable, only certain electron waves can fit within the atom and these waves have fixed energies. The electron can only have one of these fixed energies and no other; the electron energy is quantised, The electron energy is not continuously variable unless the electron escapes from the constraints of the atom itself, *i.e.* it is ionised and becomes a free moving electron.

Just as there are a number of waves which will fit on the string of a musical instrument—the fundamental and the overtones, there are a number of solutions to the Schrödinger wave equation for an atom, each one a different electron wave shape with a different energy. Each solution is called a *wavefunction*, given the symbol Ψ . The wavefunction gives the amplitude of the electron wave as a function of the position of the electron around the nucleus when in that electron wave. (The wavefunction for a wave on a string gives the amplitude of the displacement of the string, as a function of position on the string as in Fig. 1.5). The amplitude can be positive or negative, *i.e.* the sign of the wavefunction can vary in different regions of the wave. This property of sign or *phase* is critically important when electron waves overlap in space. If both waves have the same sign then the waves interfere constructively in that region of space, when the waves are of opposite sign they interfere destructively. It is this wave interference that is responsible for the formation of chemical bonds between atoms.

In atoms, these three dimensional electron waves are referred to as *atomic orbitals* (AO's); in molecules, they are *molecular orbitals* (MO's). In hydrogen, the solutions of the Schrödinger equation give a series of orbitals, which are characterised by three properties, each with an associated *quantum number*:

1. Energy (quantum number n).
2. Orbital angular momentum (quantum number l). Like orbital energy this is quantised and can only take fixed values. The orbital angular momentum controls the shape and symmetry of the wave.
3. Orientation of the orbital angular momentum (quantum number m_l). The orientation of the waves is limited to those in which the angular momentum along any chosen axis is quantised in integral units.

n is the *principal quantum number* and can only take integral values 1, 2, 3, ... etc. For a single electron atom, such as hydrogen, it defines the energy of the wave; as n increases, the energy of the wave increases and the wave moves further away from the nucleus. The value of n determines the total number of *nodal surfaces* (surfaces where the amplitude of the wave function is zero, and across which the wave function changes sign) in the wave; the number of such surfaces is given by $n-1$ (see also Fig. 1.5 where the number of nodes is also given by $n-1$). The value of n also controls the possible values that the total orbital angular momentum quantum number, l , can take. All orbitals of the same n make up the n shell.

The *orbital angular momentum quantum number*, l , defines the total angular momentum of the orbital. l defines the shape (symmetry) of the wave. As n increases the orbitals can have more angular momentum, *i.e.* the greater the value of n , the more shapes are available (Fig. 1.6). l can take values of $l = 1, 2, 3 \dots (n-1)$. Atomic

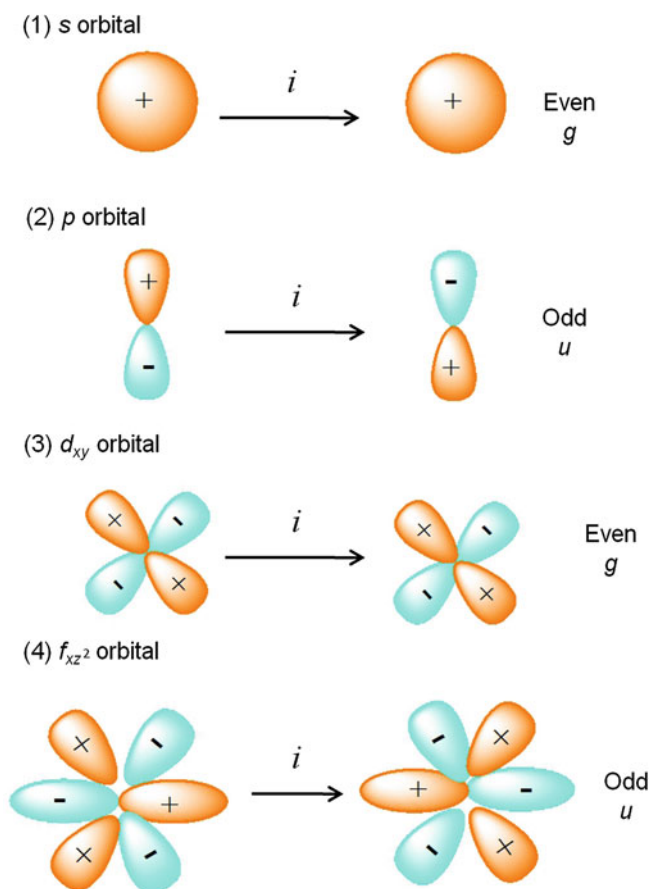


Fig. 1.6 Parity and the effect of inversion on the sign of the wavefunctions for some s , p , d and f orbitals

orbitals are usually described by a letter associated with each l value. When $l = 0$ the orbital is an s orbital, when $l = 1$ it is a p orbital, when $l = 2$ it is a d orbital, and when $l = 3$ it is an f orbital (these letters arise from spectroscopic studies of emission lines which were classified as: *sharp* (s), *principal* (p), *diffuse* (d), and *fundamental* (f)). Orbitals with $l > 3$ (g orbitals etc.) are not important in general chemistry or photochemistry, but are very important in atoms excited close to their dissociation limit, so-called *Rydberg atoms*.

The angular momentum of each orbital is given by:

$$\text{orbital angular momentum} = [l(l + 1)]^{1/2} \cdot h/2\pi. \quad (1.12)$$

l determines the number of nodal planes which go through the nucleus. If $l = 0$ or is even (2, 4...), then the orbitals are symmetric with respect to inversion through the nucleus, *i.e.* the sign of the wavefunction at any point is the same at the corresponding point across the nucleus. For $l = \text{odd number}$ (1, 3...), the orbitals are anti-symmetric with respect to inversion, *i.e.* the sign of the wavefunction changes across the nucleus. This is of particular relevance when the molecules have a centre of symmetry and these properties are sometimes described as *parity*; the orbitals which are symmetric by inversion have even (symmetric) parity, while those which are asymmetric have odd (anti-symmetric) parity. The German terms *gerade*, g , (even) and *ungerade*, u , (odd) are also commonly used. Figure 1.6 shows the parity of some s , p , d and f orbitals in a centrosymmetric system.

The *orbital magnetic quantum number*, m_l , specifies the orientation of the orbital in space and the magnitude of the orbital angular momentum component along any specified axis. Orbitals with the same n and l , but different m_l , are all equal in energy in the absence of a magnetic field, (orbitals of the same energy are described as *degenerate*), but, because their magnetic moments point in different directions, they align with slightly different energies in the presence of an applied magnetic field. The values of m_l are limited by the value of l to: $m_l = l, (l-1), \dots, -l$.

The orbital description of the electron can then be given as either a series of the three quantum numbers, n, l, m_l , or, more usually, the principal quantum number, n , followed by the letter corresponding to the angular momentum quantum number, l , *i.e.* s, p, d or f . Grouped by principal quantum number, the atomic orbitals for the first four n shells are:

$$\begin{aligned} &1s(n = 1, l = 0); \\ &2s(n = 2, l = 0), 2p(n = 2, l = 1); \\ &3s(n = 3, l = 0), 3p(n = 3, l = 1), 3d(n = 3, l = 2); \\ &4s(n = 4, l = 0), 4p(n = 4, l = 1), 4d(n = 4, l = 2), 4f(n = 4, l = 3). \end{aligned}$$

While the electron wavefunction can be used to obtain the energy and other properties of the electron, the question arises, in quantum mechanics generally, as to what the wavefunction itself “means”. This has been, and still is, the subject of much debate and there is currently intense research activity into using attosecond spectroscopy to probe atomic wavefunctions [16]. The most useful interpretation of the wavefunction for chemistry is that due to Born, who, by analogy to a light wave, where the intensity is proportional to the square of the amplitude, suggested

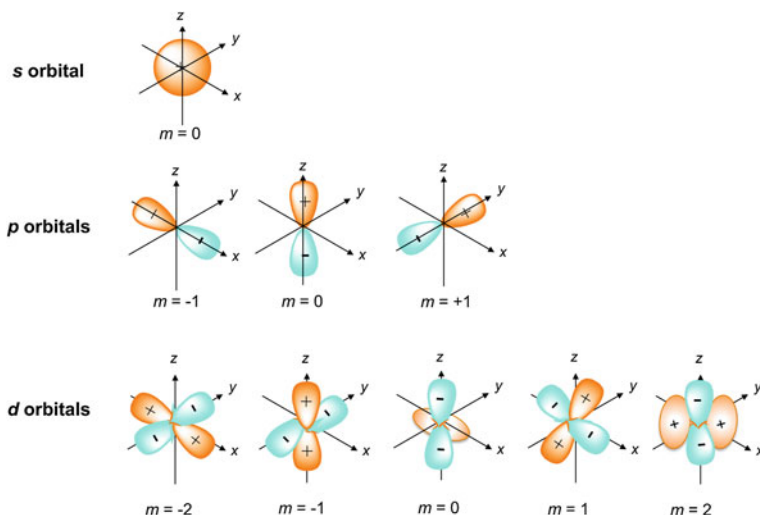


Fig. 1.7 Three-dimensional shapes of the s , p and d atomic orbitals for the hydrogen atom. The “+” and “-” signs represent the sign of the electron wavefunction in that region of space

that the *square of the amplitude of the wavefunction in a small volume of space gives the probability of finding the electron there*. Thus, the square of the wavefunction can be used to calculate electron density maps and surfaces.

Figure 1.7 summarises the atomic orbitals for the hydrogen atom, and shows their three dimensional shape using the usual chemist’s representation where the outer surface is all at the same electron density, *i.e.* they are isoelectronic density plots, such that the probability of finding the electron in the volume drawn is some fixed value—usually 95 or 90 %. The orbitals are often marked with the sign of the wavefunction in that region of space (not to be confused with ionic charges), or regions of different sign are shown in two different colours.

The lines in the emission and absorption spectra of the atoms correspond to the electronic transitions as electrons move from one orbital to another. The energy of the photon emitted, or absorbed, corresponds to the difference in energies of the electron in the two orbitals involved. The yellow/orange glow of sodium lamps or street lights corresponds to the photons emitted as excited sodium atoms with the outermost electron in the $4p$ orbital fall down to the ground atomic state in which it is in the $3s$ orbital.

The Schrödinger equation (more precisely the refined version incorporating both relativity and quantum electrodynamics), and those obtained from it, describe the physical and chemical features of the hydrogen atom with an accuracy limited only by the precision to which the fundamental constants required are known. Unfortunately, the hydrogen atom is the only chemical structure for which the Schrödinger equation can be solved exactly; everything else requires approximation. For small atoms and very small molecules the approximations can be very good, but for any

structure of much complexity, and that means most interesting structures, they are not good enough to allow the calculation of many important chemical properties to a useful level of accuracy. Because of this, chemistry and photochemistry remain essentially experimental subjects. Theory is, however, invaluable in our understanding of the underlying phenomena.

1.4.2.3 Multi-Electron Atoms

For multi-electron atoms the Schrödinger equation cannot be solved analytically, so methods involving approximations, of varying degrees of sophistication, are used instead. The first approximation is that the wave equation for the whole system is made up of individual wave equations for each electron, and each electron is in an orbital of a form modelled on those of the hydrogen atom. For purposes of calculation and modelling, sophisticated approximations such as *Slater orbitals* or *Gaussian orbitals* are used. However, because orbital symmetry is often of paramount importance when combining orbitals to give molecular structures, the simple orbital shapes and symmetries given in Fig. 1.7 provide an excellent basis for the understanding and visualisation of chemical bonding and chemical structures. Also, usually we are only concerned with the electrons in the highest energy, outer, or *valence*, orbitals of an atom. Electrons in lower energy orbitals, the core orbitals, are held closely to the nucleus and are not generally involved in chemical or photochemical transformations.

The first question for multi-electron atoms is: “how are the electrons placed in the orbitals of different energies?” In the absence of any other information, we might expect that in the state of lowest energy all of the electrons in the atom would be in the lowest orbital, although we would also be aware that putting electrons together in the same region of space will result in some increase in overall energy due to electrostatic repulsion.

However, we have not yet incorporated electron spin into our atomic model. The alignment of the electron spin angular momentum along any axis can only be such to give a resultant spin angular momentum along the axis of either $= +\frac{1}{2}\hbar$ or $-\frac{1}{2}\hbar$. We can describe which of these two spin states an electron adopts using the additional quantum number, m_s , which can take values of $+\frac{1}{2}$ or $-\frac{1}{2}$. Thus, the complete description of the electron in an atom requires four quantum numbers: n , l , m_l , and m_s . It is a general property of electrons (and all fermions), expressed in the *Pauli Exclusion Principle*, that no two can have the same four quantum numbers. Thus, it is possible to place two, *but only two*, electrons in the same n , l , m_l state and when they are so placed they must have electron spins arranged in opposing directions, *i.e.* one with $m_s = +\frac{1}{2}$ and one with $m_s = -\frac{1}{2}$. If we use an arrow to indicate the electron spin direction, up or down, when two electrons are in the same orbital the electron spins are arranged thus, $\uparrow\downarrow$.

So the first two electrons can go into the $1s$ orbital, but with two electrons the orbital is full and the next electron must go into the next highest orbital, the

2s. Putting electrons together in the same orbital raises the energy of both electrons due to electron–electron repulsion, the total increase in energy this causes is called the *electron pairing energy*. Therefore, when filling orbitals of equal energy, *i.e.* degenerate orbitals, such as the three *p* orbitals, the electrons go into the individual orbitals singly at first (*Hund's rule*). Also, for two different singly occupied orbitals the arrangement in which the two electron spins are parallel, $\uparrow\uparrow$, is lower in energy than that in which they are opposed, $\uparrow\downarrow$, because in the parallel spin arrangement the electrons tend to spend more time apart in space. So when electrons go singly into different orbitals the arrangement with spins parallel is lower in energy than that with spins opposed. The magnitude of the separation between these spin opposed and spin-paired energy states (sometimes referred to as the *exchange energy integral*) is determined by the spatial overlap of the two orbitals, *i.e.* how likely the two electrons are to occupy the same region of space. If the orbitals have little overlap in space this energy difference is small. We will see later how the same ideas apply to molecules and are important in their excited state behaviour.

The arrangement of electrons is thus governed by four factors: the energy of the orbitals, an orbital occupancy of at most two electrons spin paired per orbital, the magnitude of the electron–electron repulsion spin pairing energy, and the direction of the spin angular momenta of the electrons. Using these ideas, and a few refinements in the relative energy of *s*, *p*, *d* and *f* orbitals in many electron-atoms, the electronic structure of all atoms can be understood [17].

1.4.2.4 Size of Atoms and Molecules Compared to Wavelength of Light

Atoms are not hard incompressible spheres and so the definition of their size is somewhat arbitrary. A variety of atomic sizes can be measured from intermolecular distances, or liquid or solid volumes, and can also be calculated from the Schrödinger equation. In the lowest electronic state, atomic diameters are of the order of one hundred to a few hundred pm. The Schrödinger equation shows, that for the H atom, the orbital radii increase in proportion to n^2 , so if an electron is promoted into a higher energy orbital the size of the electronically excited atom will be significantly larger than the ground state. (In terms of our analogy of waves in boxes, the atomic energy levels corresponding to different principal quantum number *n*, are not so much the different energy levels arising from waves in a box of fixed size, which would increase in energy separation as *n* increases as shown in Fig. 1.5, but rather the different energy levels corresponding to waves in boxes of different size which decrease in energy separation as the box size increases.) The importance of atomic/molecular size for the interaction between UV/Vis photons and chemical species is that, since the wavelength of UV/Vis radiation is one thousand times larger than an atomic diameter then, even for a large or excited-state atom, or molecule, the wavelength of a UV/Vis photon is big enough that the electromagnetic field of the photon acts on all electrons and nuclei in the atom/molecule with, to a very good approximation, the same phase. (Although the fact

that the electromagnetic phase is not exactly the same across an atom or molecule is one reason why nominally *forbidden transitions* (see Sect. 1.12.1) are allowed to some degree.)

1.4.3 Description of Atomic Electronic States: Term Symbols, Spin Multiplicity, Angular Momenta, Spin Orbit Coupling and the Heavy Atom Effect

Depending upon the precise electronic arrangement, the various combinations of electron spin and orbital angular momentum can lead to atomic energy levels of different spin, orbital and total angular momenta. *Term symbols* are a useful shorthand representation of the angular momenta of these individual atomic states. The values which need to be represented are: the total electron spin angular momentum, described by the quantum number S ; the total orbital angular momentum, described by the quantum number L ; and the total angular momentum resulting from the combination of L and S , described by the quantum number J .

The term symbol gives these three angular momenta in the following form:

$$\text{multiplicity, i.e. } (2S+1) \text{ corresponding letter for } L \text{ (i.e. S, P, D, F)} \text{ } J_{\text{value, or values}} \quad (1.13)$$

using ‘upright’ font for the letter to help distinguish it from the italic quantum number(s).

The first superscript does not give S directly but rather the *spin multiplicity*, the number of possible values of electron spin momentum along a specific axis, which is $2S + 1$. Thus if $S = 0$, (all electrons spin paired), there is only one arrangement; the total spin is zero and therefore also zero along the axis, and the state is called a *singlet*. For $S = \frac{1}{2}$ (one unpaired electron), there are two arrangements, the total spin is $[\frac{1}{2}(\frac{1}{2} + 1)]^{1/2}\hbar$ and this can point up or down the axis to give values $+\frac{1}{2}\hbar$ and $-\frac{1}{2}\hbar$ along the axis, and the state is a *doublet*. For $S = 1$ (two unpaired electrons), there are three arrangements, the total spin is $[1(1 + 1)]^{1/2}\hbar$ and this can point up, to give spin $+1\hbar$ along the axis, point down to give $-1\hbar$, or point at $0\hbar$ along the axis (i.e. at 90° to the axis), and the state is a *triplet*. A schematic diagram showing the formation of singlet and triplet states from the spin momenta of two electrons is shown in Fig. 1.8.

As a simple example, an atom with only one unpaired electron, consider a ground state sodium atom (11 electrons). This has a full $n = 1$ shell, a full $n = 2$ shell and the single outermost electron in a $n = 3$ s -orbital, i.e. $l = 0$. The full shells have zero spin and angular momenta and therefore do not contribute to the term symbol, which, since $S = \frac{1}{2}$ and $L = 0$, is $^2S_{1/2}$ (read as: doublet S one half). If the electron is excited into an $n = 3$ p -orbital, then since $S = \frac{1}{2}$, $L = 1$ the spin and angular momenta can reinforce or oppose each other giving $J = \frac{3}{2}$ or $\frac{1}{2}$ to give two term symbols $^2P_{3/2}$ and $^2P_{1/2}$ (read as: doublet P three halves, doublet P one half); see Fig. 1.8 for a diagram of this case). These two *levels* with $J = \frac{3}{2}$

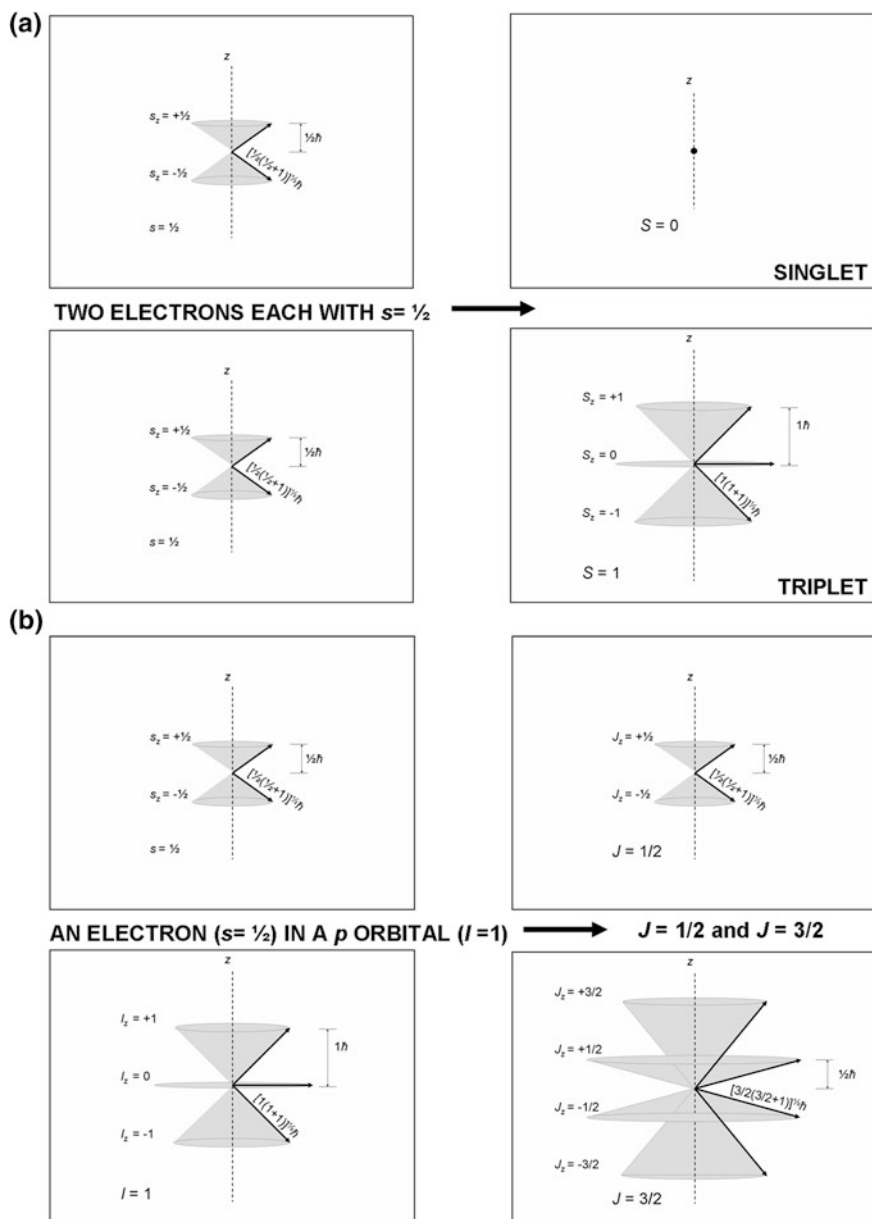


Fig. 1.8 Combining spin–spin, and spin-orbital, angular momenta. **a** The resultant total electron spin angular momentum and spin orientations arising from the combination of electron spin from two electrons, each $s = \frac{1}{2}$, which gives a singlet ($S = 0$, *i.e.* no resultant spin) and a triplet state ($S = 1$). The triplet state is triply degenerate because the spin angular momentum vector can point so as to have three values along the z -axis. **b** The resultant total angular momentum and orientations from the combination of the spin of one electron, $s = \frac{1}{2}$, and orbital angular momentum from a p orbital ($l = 1$) which gives rise to $J = \frac{1}{2}$ and $J = \frac{3}{2}$

and $J = 1/2$ differ slightly in energy, and close examination of the yellow/orange line at 589 nm produced by sodium atoms in a flame, or a sodium street lamp, shows that it is in fact made up of two lines very close together, one at 589.76 nm and one at 589.16 nm, corresponding to the transition from the two ${}^2P_{3/2,1/2}$ levels to the single ${}^2S_{1/2}$ ground state.

Consider now a magnesium atom (12 electrons). In the ground state it has a full $n = 1$ shell, a full $n = 2$ shell and the two ‘outermost electrons’ are in an $n = 3$ s -orbital, *i.e.* $l = 0$. By the *Pauli exclusion principle*, the two electrons in the $n = 3$ s -orbital must be spin paired and so $S = 0$, $L = 0$ and the term symbol is 1S_0 (read: singlet S nought). The atom can be excited by promoting one of the $n = 3$ s -electrons to an $n = 3$ p -orbital, for which $l = 1$. There are now two electrons in different orbitals and these are not restricted by the Pauli exclusion principle. If they are spin paired $S = 0$, $L = 1$ and the term symbol is 1P_1 , (singlet P one) if they are not spin paired but spin parallel, then $S = 1$, $L = 1$, and the term symbols are 3P_2 (triplet P two), 3P_1 (triplet P one), and 3P_0 (triplet P nought). The triplet states are of lower energy than the singlet due to the spin-pairing energy of the singlet.

Most molecules have a ground state with electrons paired, *i.e.* a *singlet ground state*, and just like the Mg atom, promotion of an electron to a higher orbital leads to two possible spin states, *i.e.* *singlet* and *triplet* states. For virtually all organic systems and many (but far from all) inorganic ones, the singlet and triplet spin states are the only ones which are relevant for photochemical processes. Note that the three levels of a triplet state are *degenerate* (*i.e.* they have the same energy) under normal conditions, but have different energies in a magnetic field. We can obtain information on the properties of triplet states by studying them in a magnetic field (*magnetic field effects*).

In general, spin- and orbital- angular momenta for atoms can be combined in one of two ways, depending upon the strength of coupling between the spin and orbital angular momenta for the electrons in the atom. Where the coupling between spin and orbital momenta is *weak* (the most important case) *Russell–Saunders coupling* is used. Due to weak coupling, spin and orbital angular momenta are first of all treated separately, *i.e.* all the electron spin momenta are combined together to give S , all the orbital angular momenta are combined to give L and these are then combined to give J . *Strong* coupling between spin and orbital momenta, gives *jj coupling*, in which the individual electron spin and orbital angular momenta combine first, to give an electron overall angular momentum, j , for each electron, and these j momenta combine to give the total overall angular momentum of the atom, J . The strength of *spin–orbit coupling* increases rapidly with atomic number, depending as it does on Z^n , (where $n \geq 4$); thus Russell–Saunders coupling is found for light and moderate Z atoms, while *jj* coupling is found for the heavier atoms of the Periodic Table. A strong spin-orbit coupling is evident in the relatively easy interchange of spin angular momenta and orbital angular momenta, known as the *heavy atom effect*. The heavy atom effect mixes electron spin and electron orbital angular momenta. For atoms, and molecules composed of atoms, which have weak spin orbit coupling, *i.e.* those of low or medium atomic number, electron spin angular momenta and orbital momenta can be considered distinct and

the rules for changes in spin and orbital momenta operate independently; we might say the electron spin and orbital angular momentum quantum numbers are ‘good quantum numbers’. For heavy atoms, and molecules containing heavy atoms, the rules governing changes in spin and orbital angular momenta cannot be separated and for these we say the electron spin and orbital angular momentum quantum numbers are ‘poor quantum numbers’.

The majority of atoms making up chemical structures are ‘light’ rather than ‘heavy’, and Russell–Saunders coupling is appropriate for most (but far from all) of them. This separation of spin and orbital angular momenta means that in these cases optical transitions take place with no change in electron spin, giving the most useful *spin selection rule*, $\Delta S = 0$, *i.e.* singlet \leftrightarrow triplet transitions are forbidden. However, *heavy atom effects* have important consequences in photochemistry, since spin–orbit coupling allows nominally *spin forbidden processes* such as phosphorescence, which is a triplet to singlet transition, for which $\Delta S \neq 0$.

1.5 Chemical Bonding and Molecular Orbitals

Bonding is usually considered in terms of three extreme types: ionic bonding, covalent bonding and metallic bonding.

1.5.1 Ionic Bonding

In ionic bonding there is a transfer of one or more electrons from one species to another. The ‘bonding’ is then due only to electrostatic attraction between the two ions, which cluster together in the form of a very large *lattice*. A common example is table salt where the chemical structure is a lattice of Na^+ and Cl^- ions held together by the electrostatic forces of attraction between positive and negative charges. For a purely ionic bond we need only deal with the atomic orbitals of the two ions formed by adding (anion) or taking away (cation) electrons to or from the atoms involved. Although, it is possible that one or both of the ionic species are themselves made up of a number of atoms covalently bonded.

1.5.2 Covalent Bonding

In covalent bonding, electrons are shared between atoms. A useful approximation in estimating the solution to the Schrödinger equation for molecular species is the assumption that the *molecular orbitals* (MOs) are some combination of the *atomic orbitals* (AOs) of the atoms involved. Where the atomic orbitals, *i.e.* the electron waves, overlap between atoms with constructive interference, the build-up of

electron density gives a *bonding orbital* of lower energy than either of the two component atomic orbitals; where the orbitals overlap destructively between atoms the decrease in electron density gives an *antibonding orbital* of higher energy than either of the two component atomic orbitals. In addition, we may have orbitals that are largely localised on one of the atoms such that there is no net interaction between the two atoms, *i.e.* a *non-bonding* interaction. Thus, the combination of any AOs on neighbouring atoms can be: bonding, antibonding, or non-bonding, depending upon whether the *overlap integral*, the integral of the product of the two atomic functions over space, is positive (bonding), negative (antibonding) or zero (non-bonding). Consideration of the process shows that it is the symmetry properties of the orbitals that determine which of these interactions are possible. For any combination of the signs of the orbitals which give a bonding interaction there is also an opposite arrangement giving an antibonding interaction, so there is always a pair of bonding and antibonding orbitals if the overlap integral is non-zero.

Although we have limited this discussion to molecular orbitals formed from the combination of only two atomic orbitals, more orbitals can be involved, their inclusion in the process being determined by their symmetry and energy. Figure 1.9 shows some molecular orbitals formed from combinations of *s* and *p* orbitals. The important symmetry considerations for molecular orbitals are those concerning the internuclear axis. If the combination of the atomic orbitals is in the direction of the axis joining the nuclei of the two atoms we term this a *sigma* (σ) orbital. Figure 1.9 shows how the combination of two *s* orbitals leads to a bonding σ orbital and an antibonding σ^* orbital (antibonding orbitals are indicated by the superscript *). The σ orbital has no nodal planes between the nuclei, while the σ^* antibonding orbital has one nodal plane. A plot of the potential energy as a function of the internuclear distance, the *potential energy curve* for the ground state hydrogen molecule is given in Fig. 1.10. The minimum on the curve shows both the molecular bond length ($d_{\text{H-H}}$) and the bond dissociation energy ($D_{\text{H-H}}$). Sigma orbitals are also formed with *p*, *d*, and to a lesser extent, *f*, orbitals. With *f* orbitals, as these are spatially closer to the nuclei and somewhat protected by the outer *s*, *p* and *d* orbitals, the degree of bonding is more limited. This has important consequences in photochemistry and spectroscopy, since these *f* orbitals have characteristics more typical of atomic orbitals. This is particularly true for the lanthanide (III) ions, where very sharp transitions involving the *4f* orbitals are observed in UV/Vis absorption and photoluminescence spectra. These have applications in areas such as phosphors, lasers and photoluminescence probes (see Chaps. 4 and 12). A second type of bonding involves combination of *p* or *d* orbitals in which the internuclear axis is in a nodal plane. This is termed a *pi* (π)-bond. When describing molecular orbitals we use Greek letters to represent similar symmetry properties to those represented by Roman letters in atomic systems; thus the *s*, *p*, and *d* orbitals in atoms become Σ , Π and δ orbitals in molecules. Similarly, for electronic states (which are the descriptions of the various multi-electron combinations) the S, P, D states in atoms become Σ , π and Δ states in molecules. There are the same number of antibonding π^* orbitals as π orbitals.

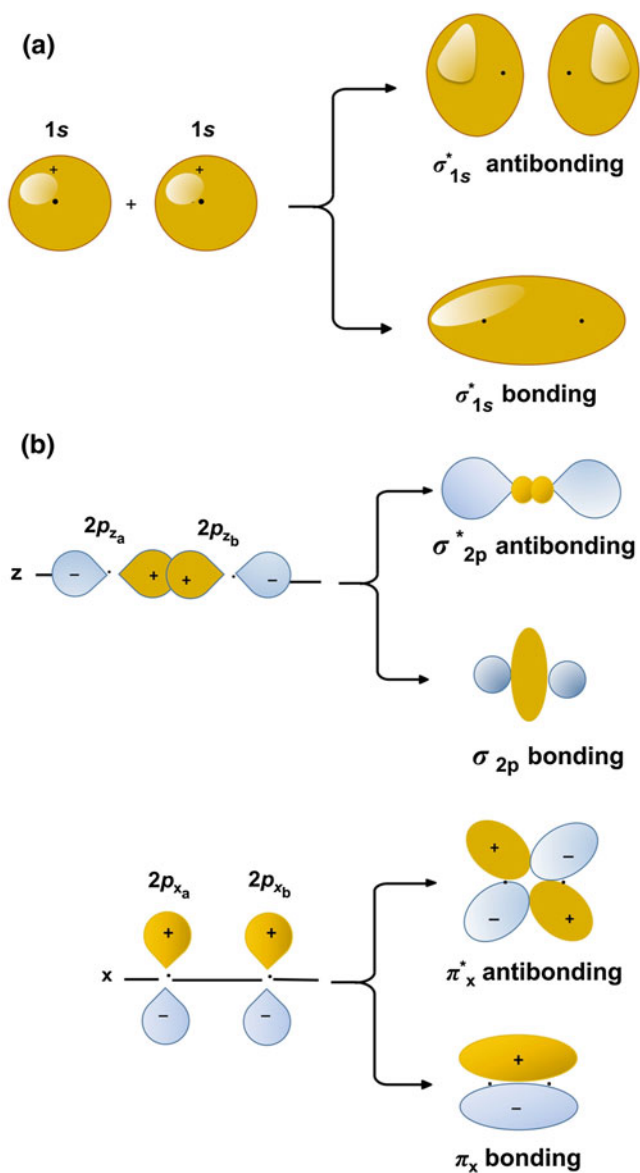
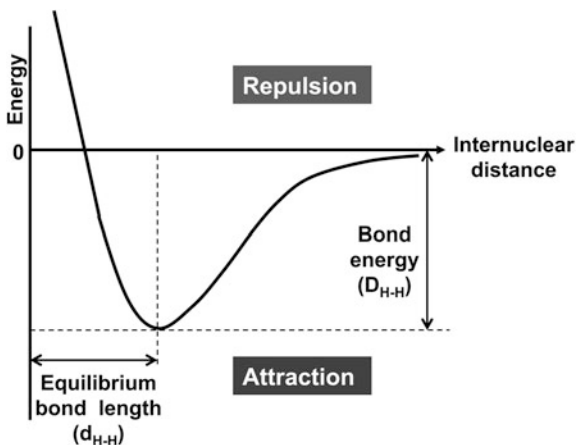


Fig. 1.9 Formation of sigma bonding (σ) and antibonding (σ^*) molecular orbitals (MOs) from combination of s and p atomic orbitals (AOs) and of pi bonding (π) and antibonding (π^*) MOs for combination of p AOs

Fig. 1.10 Potential energy curve for the combination of two atoms to form a diatomic molecule, such as H_2



1.5.3 Orbital Hybridisation

The above ideas hold rigorously when only two atoms are involved (*diatomic molecules*), but in *polyatomic molecules*, where three or more atoms are present, the shapes of the molecules determined experimentally do not correspond to the orientation of the atomic orbitals. For example, water has two hydrogen and one oxygen atom in a bent arrangement with an H-O-H bond angle of 104° . However, in the simplest description, the central oxygen atom only has the $2p$ orbitals available for bonding and these are at 90° . There is a convenient concept, *hybridisation* (or mixing) of atomic orbitals, which, even though there are serious theoretical criticisms of the concept [15], provides a useful way of visualising the formation of molecules. The shapes of molecules are known from experiment, and if we could solve the Schrödinger equation for molecules to the required level of precision the result would be an energy minimum in keeping with the experimental data. Hybridisation is a simple method to visualise the spatial result of a complete Schrödinger analysis, using simple MOs without too much additional complexity. Given the difficulty of the problem, the relatively small energy differences involved, and the approximations used in MO theory, it is not surprising that a model which gives a good representation of the spatial arrangement of atoms might not necessarily give a good representation of other molecular properties [18]. With the simplest molecular hydrides of oxygen (water, H_2O), nitrogen (ammonia, NH_3) and carbon (methane, CH_4), we assume that we mix the three $2p$ orbitals with the one $2s$ orbital on the central atom to give four sp^3 hybrid orbitals which are oriented tetrahedrally. These can then combine with the hydrogen $1s$ orbitals to give two (H_2O), three (NH_3) or four (CH_4) sigma bonds. The other orbitals in water and ammonia which are not involved in bonding will contain *lone pairs* of electrons and be non-bonding. Hybridisation and bonding for methane is shown in Fig. 1.11 and the redirected tetrahedral bond angle (109.28°) is observed experimentally. The bond angles in ammonia and water are slightly less due to the effect of the lone pair

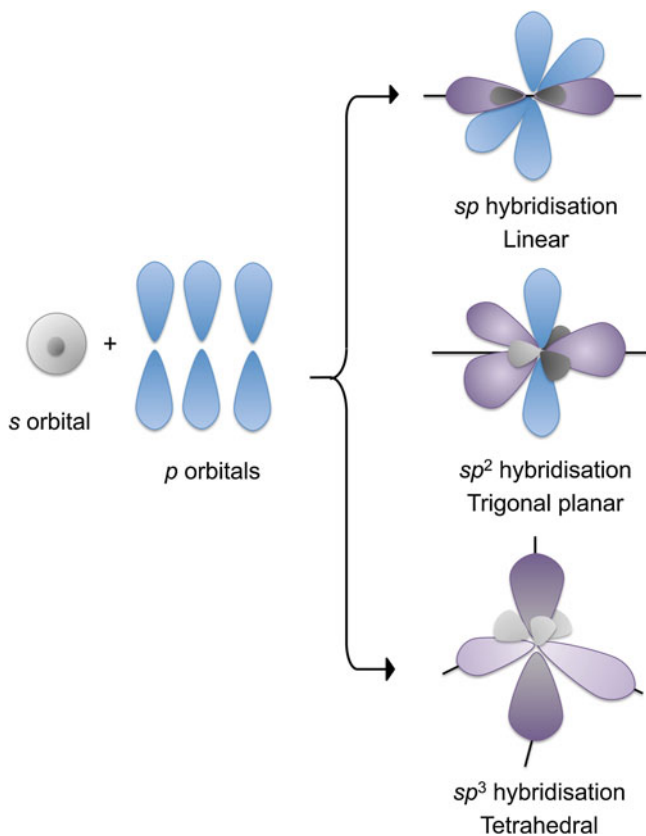


Fig. 1.11 Results of hybridisation of s and p atomic orbitals. Hybridisation in methane is sp^3 with four equivalent orbitals in a tetrahedral arrangement

non-bonding electrons which take up rather more space than a bond. Other forms of hybridisation are possible. For example, with carbon we can use one $2s$ and two $2p$ orbitals to give sp^2 hybridisation or one $2s$ and one $2p$ orbital to give sp hybridisation. These hybrid orbitals can then form σ bonds, while the remaining $2p$ orbitals can participate in π bonding with other atoms.

1.5.4 Electronic Occupation of Molecular Orbitals

Electron filling of MOs follows the same rules as described for AOs: lowest energy orbitals first, with spins in parallel arrangements for degenerate orbitals, and consideration of the spin-pairing energy for any decision about whether an electron goes into a low energy orbital requiring spin-pairing or into a completely empty higher energy orbital.

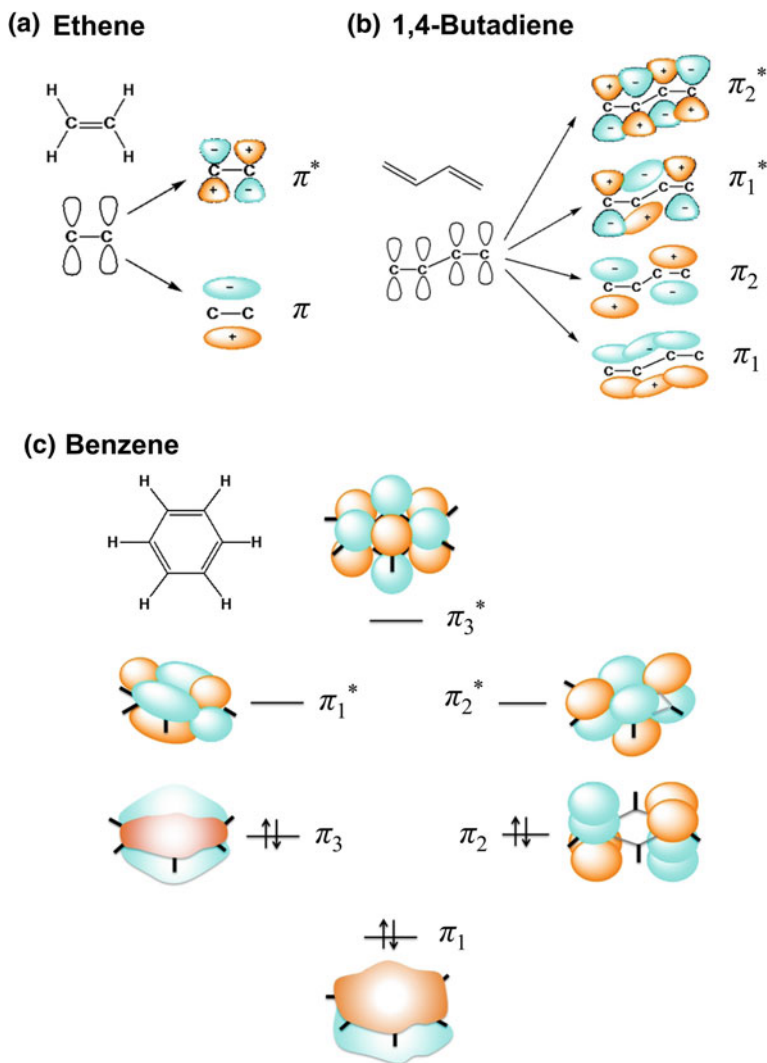


Fig. 1.12 Pi (π) molecular orbitals in ethene, butadiene and benzene

The number of bonds, the *bond order*, between atoms is given by:

$$\text{Bond order} = (\text{number of bonding electrons} - \text{number of antibonding electrons})/2. \quad (1.14)$$

So, if when two atoms, X and Y, interact, the number of electrons in bonding and antibonding orbitals is equal, then no bond is formed; if there is one more bonding orbital filled than antibonding orbitals the bond order is 1, to give a single

bond, *i.e.* X–Y; when two more bonding than antibonding orbitals are filled, the bond order is 2, *i.e.* a double bond X=Y; and when three, a triple bond is formed, X≡Y.

1.5.5 Conjugation and Extended Electron Orbitals

The overlap of AOs localised between neighbouring atoms gives rise to a localised electron bond in which the electron wavefunction is determined by the electrostatic attraction of only a few atoms, and the location of the electron is constrained to within a relatively small volume around those atoms. Orbital overlap across a number of atoms in a molecule leads to a different situation, one in which the MOs extending across many atoms. The term for this behaviour is *conjugation*. Consider the organic molecules ethene and butadiene (Fig. 1.12). In ethene, each carbon atom forms three σ bonds, one with the other carbon and one with each of the hydrogen atoms. The remaining $2p$ orbitals on the two carbon atoms then form a π bond. In butadiene, the terminal CH₂ groups and two CH groups have sp^2 hybrid orbitals forming three σ bonds. We now have $2p$ orbitals on each of the four carbon atoms which can form four π bonds. As shown in Fig. 1.12, the combination of the orbitals depends on the signs of the wavefunctions and will lead, in order of increasing energy, to two bonding (π_1 , π_2) and two antibonding (π_2^* , π_1^*) orbitals. There are four electrons to go into these orbitals, and these will fill the two bonding orbitals. Although the bond order between the middle two carbon atoms is less than that for the end ones, the π electrons are now delocalised over the whole molecule.

Since the energy gaps between orbitals in conjugated structures lie in the UV and visible spectral regions, and increasing conjugation decreases the energy separation between the orbitals and, hence, increases the absorption wavelength, conjugated structures make up many of the structures of interest to the photochemist. The orange colour of many plants and vegetables, such as carrots, is due to the presence of the highly conjugated polyolefin β -carotene (see Chap. 4). A particularly important case of conjugated systems is observed with certain planar cyclic systems, such as benzene, which have $4n + 2$ electrons in p orbitals. This provides increased delocalisation in the π orbitals and the systems are termed *aromatic* (Fig. 1.12c).

1.5.6 Symmetry, Angular Momentum and Term Symbols for Small Molecules

The symmetry labels and term symbols for small molecules are discussed in detail in Ref. [14]. Here we illustrate the approach using H₂ and O₂ as examples.

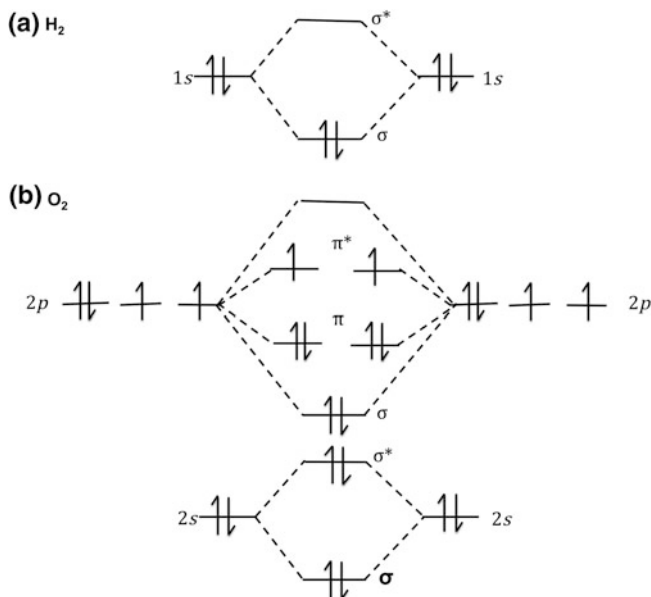


Fig. 1.13 Electron correlation diagrams and ground state molecular orbital occupation for **a** hydrogen (H_2) and **b** oxygen (O_2) molecules. For oxygen, the $1s$ orbitals are so low in energy, *i.e.* so tightly held by their respective nuclei, that they do not contribute significantly to bonding

Figure 1.13 shows the filling with electrons of the molecular orbitals for the ground state of the molecules H_2 and O_2 . In H_2 , the two electrons enter the lower energy σ molecular orbital. To do this they must have opposite spins so the overall spin is zero, the spin multiplicity, $(2S + 1)$, is one, and it is a *singlet* state. The bond order is 1. The molecule has no node along the internuclear axis and, in orbital terms, we say it has Σ symmetry. With centrosymmetric molecules we can also indicate two other properties, the *parity*, discussed earlier, which is the effect of inversion in a plane of symmetry. The sign of the wavefunction is unchanged by this and we represent it with the symbol g . In addition, H_2 also has *planes* of symmetry. The symmetry operation associated with a plane is reflection, and if the sign of the wavefunction is unchanged by this operation we give it the symbol $+$, if it changes we represent it by a minus ($-$) sign. The electronic ground state of the H_2 molecule is represented $^1\Sigma_g^+$.

We will now consider the O_2 molecule, which, in both ground and excited states, is of major importance in photochemistry (e.g. see [Chaps. 8, 9](#) and [15](#)). The electronic configuration of the oxygen atom is $1s^2, 2s^2, 2p^4$. The $1s^2$ electrons are too tightly held to the nucleus to be involved in bonding and they remain as essentially atomic orbitals. Since we have the same number of bonding and antibonding electrons when molecular orbitals are formed from the $2s$ orbitals, their net contribution to the bonding is zero. So, for bonding purposes, we only need to consider the combinations of the $2p$ orbitals. The pair of p orbitals along

the internuclear axis (let us say p_z) overlap strongly to give σ and σ^* orbitals, while each of the other pair of p orbitals, p_x and p_y , overlap less strongly and give two degenerate π , and π^* orbitals. Introducing the electrons into the molecular orbitals (Fig. 1.13), in the same way that we did with atoms, we arrive at the important results that molecular oxygen has a bond order of 2, and that there are two unpaired electrons in the π^* orbital. With two unpaired electrons the spin multiplicity of the lowest energy state, the *ground state* of oxygen is given by $(2S + 1)$, *i.e.* 3, it is a *triplet* state. The orbital component has electron density along the internuclear axis, and has Σ symmetry. O_2 has both a centre and a plane of symmetry. We showed in Fig. 1.6 the effect of inversion across the centre of symmetry and reflection in the plane of symmetry on the signs of the wavefunctions. The sign is unchanged on inversion but changes on reflection. The ground state is, thus, represented ${}^3\Sigma_g^-$. The lowest excited state has the two highest energy electrons spin-paired in the same π^* antibonding orbital, and therefore has $S = 0$. This highly reactive species is termed *singlet oxygen*, and is represented ${}^1\Delta_g$. There is also a higher ${}^1\Sigma_g^+$ excited state. The triplet character of ground state oxygen means that it will be reactive with other species containing unpaired electrons, most notably in photochemistry with other triplet states. The term *oxidation* historically is derived from reactions with oxygen, although its meaning now is much broader.

1.5.7 Spectroscopic Nomenclature for More Complex Molecules

For polyatomic molecules, although we can always show the spin multiplicity, it is no longer practical to give a complete orbital description. The degree of information we can present will depend on the symmetry of the molecule. For small, symmetrical non-linear molecules, it is possible to describe the electronic states using the effect of symmetry operations on the sign of the wavefunction [19]. The electronic states are classified using the symmetry labels A, B, E and T, with appropriate subscripts. These are obtained using *Group Theory*. We will not go into detailed treatment of symmetry here. Appropriate treatments are given elsewhere [20]. However, we will consider the nomenclature for the electronic states of the important case of the aromatic molecule benzene. This has a fairly high symmetry and is said to belong to the *point group* D_{6h} . A set of the possible electronic states can be obtained from the so-called *character tables* given by Group Theory for this symmetry. A number of electronic states are possible. However, for reasons we will see shortly, only the ground-state and the lowest electronic excited-states are of interest in photochemistry. The wavefunction in the ground-state is fully symmetric in all operations and is termed A_1 . It has a spin multiplicity of one (*i.e.* it is a singlet state), and has even parity. The full description of this state is ${}^1A_{1g}$. The lowest excited singlet state is classified ${}^1B_{2u}$.

Benzene absorbs UV light around 256 nm due to an electronic transition between these two states, which we indicate as a ${}^1A_{1g} \rightarrow {}^1B_{2u}$ transition. A good experiment describing this is given elsewhere [21]. (Note: Photochemists tend to describe the transition with the ground state first and the excited state second. Spectroscopists often use the reverse order.)

With more complex molecules, it is not normally possible to indicate any symmetry elements of the orbitals involved, and normally it is only possible to describe these in terms of the total spin angular momentum. Typically, organic molecules have a spin-paired singlet ground state, represented S_0 . They will have a series of excited singlet (S_1, S_2, \dots, S_n) and triplet (T_1, T_2, \dots, T_n) excited states, represented in order of increasing energy. However, for spectroscopic transitions it may be possible to indicate the nature of the orbitals involved. For the above case of benzene, the lowest energy transition is between a bonding π orbital and an antibonding π^* orbital, and can be represented as a $\pi \rightarrow \pi^*$ transition. The corresponding lowest excited state is described as a ${}^1(\pi, \pi^*)$ state.

1.5.8 HOMOs and LUMOs

The π molecular orbitals for butadiene and benzene are shown in Fig. 1.12. In both cases, the orbitals are separated into π and π^* orbitals of increasing energy. In the molecular ground state, all the electrons are in the bonding π orbitals. For chemistry and photochemistry, the two most important orbitals are the **H**ighest energy **O**ccupied **M**olecular **O**rbital (HOMO; π_2 for butadiene, π_2 and π_3 for benzene) and the **L**owest energy **U**noccupied **M**olecular **O**rbital (LUMO, π_1^* for butadiene, π_1^* and π_2^* for benzene). Changes in the occupancy of these orbitals are the lowest energy electronic processes possible: if an electron is added to a molecule it goes into the LUMO, if an electron is removed it is removed from the HOMO, the lowest electronic transition is from HOMO to LUMO, and even if higher energy photons cause higher energy transitions, excited-state molecules usually relax very quickly to the first excited-state, *i.e.* that corresponding to the HOMO \rightarrow LUMO transition. For some molecules, HOMO-1 and LUMO + 1 may also be important if higher excited-states play some role in the molecular photochemistry.

1.5.9 Molecular Excitons in Crystals and Large Systems with Extended Conjugation

Two or more molecules close together can interact, leading to splitting of their electronic states to produce delocalised electron systems. If these are in solid crystals, the electronically excited states can be considered as chargeless *quasi-*

particles, termed *excitons*, which are considered to involve the separation of an electron from a positively charged *hole*. These electron–hole pairs are capable of migration over long distances [22]. In many inorganic systems, these are relatively weakly bound, are delocalised over a large volume of the system, and are termed *Wannier* (or *Wannier-Mott*) excitons. They are conventionally treated within a semiconductor band model, as will be discussed in the next section. In other systems, such as alkyl halide crystals or crystalline aromatic molecules, the binding is much stronger, the exciton is more localised and is termed a *Frenkel* exciton. This is particularly relevant for aromatic and other highly conjugated systems and has important spectroscopic and photophysical consequences. There is a third type, which is likely to be of particular importance for systems such as conjugated polymers, where the electron and hole are separated by a distance similar to the size of a molecule. These are termed *charge-transfer excitons*. The theory of exciton interactions in organic molecular crystals was developed in particular by Davydov [23], and applied by Kasha for molecular dimers and polymers with various geometrical arrangements of chromophoric groups [24]. The concept of molecular excitons is important for treating electronic processes in organic crystals, dye aggregates, conjugated polymers, etc. Electronic energy migration in these systems can be treated in terms of exciton migration, either by hopping from one site to another or rapid dissipation through delocalised bands.

1.5.10 Metallic Bonding

Wannier excitons correspond to a delocalisation of electrons (and holes) over a solid structure. This corresponds to the model used in metals and semiconductors. The picturesque view of metallic bonding is “*a regular array of ions in a sea of electrons*”. If many AOs are involved in creating MOs that extend across a great many atoms, then a *band structure* is formed, in which there are two bands of electron energy levels, one bonding, one antibonding, each made up of many closely spaced energy levels, as shown in Fig. 1.14. Within a band there is a *pseudo-continuum* of energy levels. If the band is partially filled or overlaps with an empty band, electrons have access to many unoccupied levels, which are very close together in energy (*i.e.* they have a *high density of states*), and can freely move between these states. This accounts for the electrical conductivity of metals and their metallic lustre. Metals are normally reflective across a wide range of wavelengths because photons in the visible region penetrate deeply into the strongly coupled band containing the conducting electrons and are typically reflected. There are some important materials in which the electronic structure allows transmission/reflection of certain frequencies and the metals are coloured, such as copper and gold [25]. With certain conductors and semiconductors the appropriate absorption/reflection is in the infrared and these transmit light in the visible region. An important example is indium tin oxide (ITO) which is often used as a transparent electrode material for a variety of optoelectronic devices including

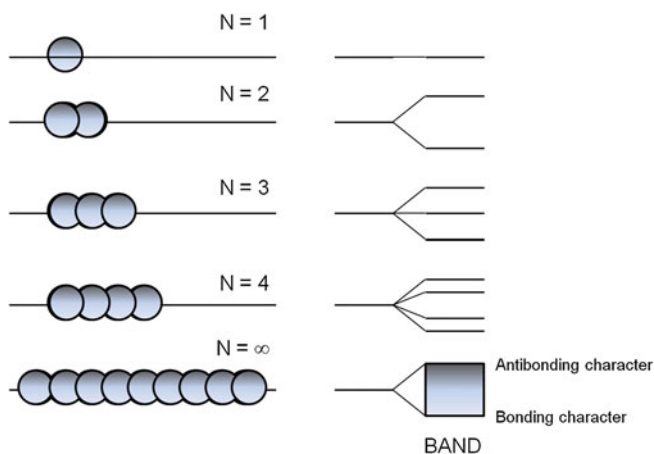


Fig. 1.14 The formation of an energy band of orbitals as a result of adding N metal atoms to a one-dimensional chain. The band contains a *pseudo*-continuum of energy levels, which exhibit bonding character at the bottom of the band and antibonding character at the top of the band

dye sensitised solar cells (see [Chap. 7](#)). If the energy of a photon is high enough it is possible to eject an electron completely from a metal. The energy required to do this is termed the *work function*. This *photoelectric effect* can be used to detect photons, and alloys of the alkali metals, which have relatively low work functions, are used in the most important photodetector—the photomultiplier tube (PMT) (see [Chap. 14](#)). Photomultipliers can be used to detect photons right across the spectrum from the vacuum UV out to the NIR, but beyond this photons are of too low an energy to overcome the work function of the alloy and different detectors must be used.

1.5.11 Electronic Energy Band Structures in Semiconductors

The ideas of electronic energy bands are also useful in describing electron behaviour in semiconductors. In a semiconductor, energy levels are also band structures, but in this case a low energy filled *valence band* is separated from a higher energy, nominally empty, *conduction band*, by an energy gap termed the semiconductor *bandgap*. If the bandgap is small enough, thermal excitation can promote an electron from the valence band to the conduction band, where it is free to move among the otherwise empty conduction band orbitals, thus giving the structure some limited electrical conductivity. Excitation from the valence to conduction bands can also be caused by absorption of a photon. This photoexcitation process, and the photochemistry resulting from formation of a mobile electron (e^-) and the mobile hole (h^+), left in the valence band, are the dominant

features of semiconductor photochemistry for photocatalysis (see [Chap. 6](#)). And electron injection into the semiconductor conduction band is a key step in dye-sensitised solar cells ([Chap. 7](#)).

1.5.12 Electronic Energy and Structures in Conjugated Polymers

The earliest studies on conjugated polymers were concerned principally with their electrical conductivity as organic semiconductors and this was conveniently treated in terms of a one-electron semiconductor band model [26]. However, it was found that this description did not explain many of the spectroscopic and excited-state properties of these systems [27, 28] and excited-states in conjugated polymers are now normally described within a molecular exciton model [29]. An important result is that, because of strong electron–hole binding, there are well defined and energetically well-separated excited singlet and triplet states [30]. Excitons in conjugated polymers may either be localised on a single chain (*in-trachain excitons*) or the electron and hole can be on different chains (*interchain excitons*) [31]. Interchain excitons are particularly important for energy migration within conjugated polymer thin films in optoelectronic devices.

1.6 Excited-State Energies, Electron Transfer, Oxidation, Reduction, Ionisation and Redox Potentials

Much of chemistry involves the transfer of electrons from one compound to another. The addition of an electron is a *reduction* process, and the removal of an electron, *oxidation*. The energy required for reduction or oxidation of a material is determined by the energy of the HOMO or LUMO. A molecule is easy to reduce if it has a low energy LUMO; it is easy to oxidise if it has a high energy HOMO. In order to compare the energetics of these processes it is convenient to use the energy of some particular electron state as a point of reference.

For gas phase processes the ‘natural’ reference energy is that of the stationary ‘*free electron*’ in a vacuum. This is often used as the zero reference energy for atomic orbital energies, and since all orbital energies are lower than that of the free electron orbital energies, then on this scale they all have negative values. The energy of the HOMO relative to complete loss of the electron is termed the *ionisation potential* (IP), and can be determined experimentally. For atoms, this is typically carried out by measuring the electrical potential needed to induce ionisation. For molecules, this is normally carried out in the gas phase by photoelectron spectroscopy [32]. For example, in *X-ray Photoelectron Spectroscopy* (XPS), the sample is bombarded with a monochromatic beam of X-rays, and the

Table 1.4 Ionisation energies (potentials) of some atoms and molecules in the gas phase

System	Ionisation energy/eV
H	13.60 ^a
Li	5.39 ^a
Na	5.14 ^a
Mg	7.65 ^{a,b}
Al	5.99 ^{a,b}
Ca	6.11 ^{a,b}
Ammonia	10.16 (adiabatic), 10.85 (vertical) ^{c,d}
Triethylamine	7.50 (adiabatic), 8.08 (vertical) ^{c,d}
N,N-Dimethylaniline	7.12 (adiabatic), 7.37 (vertical) ^{c,d}
Carbazole	7.57 (adiabatic) ^c
Ferrocene	6.86 (vertical) ^c
Tetraphenylporphyrin, free base	6.39 (vertical) ^c
Tetrathiafulvene	6.70 (adiabatic), 6.92 (vertical) ^{c,d}

^a Taken from Ref. [33]

^b First ionisation energy

^c Taken from Ref. [34]

^d The vertical ionisation energy is the energy required to form the positive ion with the same geometry as the ground state molecule. In the adiabatic ionisation energy, the positive ion is formed in its thermally-relaxed vibrational ground state (see Fig. 1.23)

ejected electrons are collected at an appropriate detector. The photoelectron spectrum relates the number of electrons ejected as a function of the energy carried by each electron. This gives a measure of the binding energies of all the core-level electrons in the molecule. The ionisation potentials are normally given in eV. Some values for typical metal atoms and organic molecules are given in Table 1.4.

In condensed phases (solutions and solids), electrochemical measurements are a relatively easy way to measure the potential energy difference between two electron states. Electrochemical methods use volts (V) as the scale of potential energy. A potential difference of 1 V is equivalent to an energy separation of electron energy levels of 96.5 kJ mol⁻¹. A convenient electrochemical reference point is the energy of an electron on a platinum electrode dipping into an acidic aqueous solution in which the proton concentration is 1 mol dm⁻³ (more precisely of *unit activity*) at equilibrium with an atmosphere of hydrogen gas at a pressure of 1 atmosphere at a temperature of 298 K. This is the *Standard Hydrogen Electrode* (SHE), sometimes called the *Normal Hydrogen Electrode* (NHE). Direct electrochemical comparison of the potential energy of an electron state against the zero of the SHE is obtained by the measurement of the potential difference, in volts, between the electron state of interest and the SHE. This gives the potential energy of the electron state of interest, its *redox potential*, directly. Conventionally, electrode potentials are given for the reduction half-reaction, *i.e.*



Table 1.5 Standard reduction potentials (E_0) for ground and excited states of some electrochemical couples in aqueous solution

Couple	Ground state E_0/V (vs SHE)	Lowest excited state E_0/V (vs SHE)
$[\text{Ru}(\text{bpy})_3]^{3+/2+}$ ^a	+1.26	-0.86 ^b
$[\text{Ru}(\text{bpy})_3]^{2+/+}$	-1.28	+0.84 ^b
$\text{UO}_2^{2+/+}$	+0.163	+2.60 ^c

^a bpy is 2,2'-bipyridyl

^b From Ref. [39]

^c From Ref. [40]

Older literature sometimes represents the oxidation potentials for the reverse reaction. These are related simply by changing the sign. Table 1.5 shows the standard reduction potentials for the ground and excited states of some commonly investigated electrochemical couples in aqueous solution.

Experimentally, the SHE is not very convenient but there are other reference electrodes, and a variety of reliable methods which can be used to measure or estimate the redox potential of electron energy states in many chemical species. In addition, various attempts have been made to obtain 'absolute' standard hydrogen electrode potentials. Various different definitions have been provided, but one of the most common is to define this *vs* a free electron at rest in vacuum. A value of -4.44 ± 0.02 V has been recommended for the absolute electrode potential of the standard hydrogen electrode in water at 25 °C. This has been calculated from a detailed thermodynamical analysis of the various processes involved [35]. This value can be added to standard electrode potentials of any electrochemical couple to calculate the absolute potential. Data are also available for the absolute electrode potential of the SHE in a variety of organic solvents. However, it is frequently more convenient in this case to determine oxidation and reduction potentials by the method of cyclic voltammetry (CV) using a known reference couple [36]. The ferrocene/ferrocinium (Fc/Fc^+) couple is often chosen as the reference since this is relatively unaffected by environment effects [37]. Absolute energy level values can be calculated from the electrochemical results using an appropriate energy for the Fc/Fc^+ couple [38].

Using a combination of electrochemical and spectroscopic measurements, MO calculations and other methods, energy level diagrams, such as the one shown for benzene in Fig. 1.15, have been obtained for many chemical species. Even for species where precise measurements are not available, such diagrams illustrate the theoretical relationship between electrochemical and spectroscopic measurements and the MOs of the species of interest. Note that, because of the high energy electron in the LUMO and the electron vacancy in the HOMO, the excited-state is simultaneously both a better reductant and a better oxidant than the ground-state by an energy corresponding to the excitation energy.

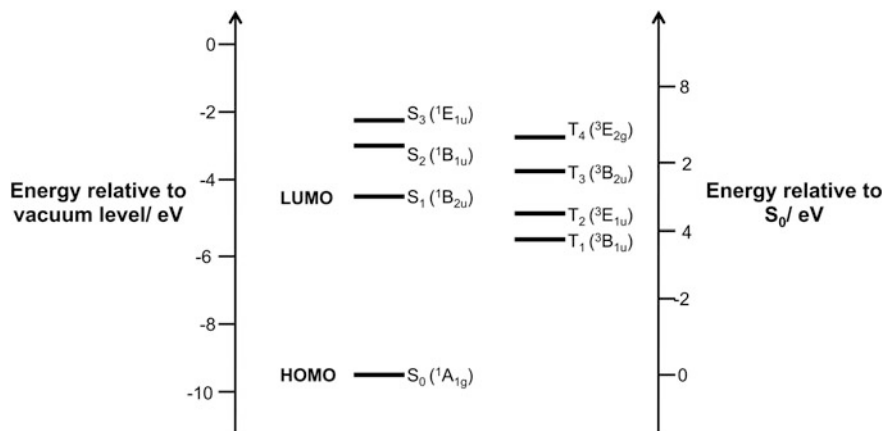


Fig. 1.15 Electronic energy levels of singlet and triplet states of benzene, with “absolute” values relative to the vacuum level (the Fermi limit) obtained from photoelectron spectra and relative values (with reference to the ground state) obtained experimentally from UV/Vis absorption and photoluminescence spectra. The absolute values are based on Koopmans’ theorem [41], that the energy of the highest occupied molecular orbital (HOMO) is the first vertical ionisation energy of a molecule. The energy of the HOMO level is obtained from the vertical ionisation energy of benzene in Ref. [42] and the energies of the excited states are from Ref. [43]. Assignment of the symmetry of the S₂ (¹B_{1u}) state is from Ref. [44]

1.7 Molecular Energies: Vibrations and Rotations

The formation of chemical species more complex than atoms introduces two new types of energy into the system—*vibrational* and *rotational*. In the same way that the moving electron has a wave associated with it, the solutions of which are obtained by the Schrödinger equation, the moving nuclei in vibrations, and rotations of the whole molecule in space, also have waves associated with them, and the wavefunctions for these motions can also be obtained using the Schrödinger wave equation. As in the case of the electron constrained within the atom, the time-independent solutions for vibrations and rotations allows only certain stable waves, of fixed, quantised energies, giving rise to discrete vibrational and rotational energy states associated with each electronic energy level. Electronic spectra of molecules often show features arising from simultaneous electronic, vibrational, and for gas phase samples, rotational transitions.

The potential energy (PE) of multi-atomic species varies with intermolecular distances. Fig. 1.16 shows the generic one-dimensional PE curve for a diatomic molecule. A triatomic molecule would require a two-dimensional surface, and polyatomics a multi-dimensional surface; but the key features can be illustrated by reference to the diatomic PE curve. Vibrational energy spacings are in the order of 100–4000 cm⁻¹, much smaller than electronic energy spacings, and transitions between vibrational levels can be induced by IR and NIR photons. Strong bonds

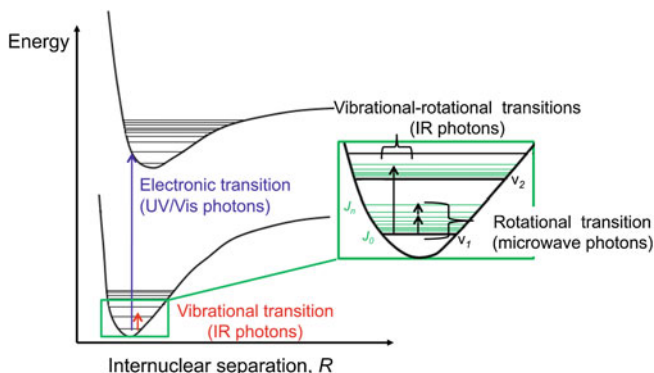


Fig. 1.16 A one-dimensional potential energy curve for a diatomic molecule, indicating possible electronic, vibrational, vibrational–rotational and rotational transitions

involving hydrogen, e.g. O–H, N–H, C–H, give high energy, high frequency vibrations ($\sim 4000\text{--}3000\text{ cm}^{-1}$), strong/moderate bonds between moderately heavy atoms, e.g. C–C, C = O, give rise to moderate frequency vibrations ($\sim 2000\text{--}1000\text{ cm}^{-1}$), and bonds between heavy atoms, e.g. metal–ligand; C-halogen; I_2 ; give low frequency vibrations of a few hundred cm^{-1} . Molecular vibrations are very important in photochemistry for two main reasons. Firstly, because of the perturbing effects molecular distortions have on the symmetry of chemical structures, which allow processes that may not, in an otherwise rigidly symmetrical system, be expected to occur. Secondly, vibrations are a route for rapid deactivation of energy both internally within the molecule, and externally to the surrounding, such that in solution and solid phases energy can be transferred from the system of interest to surrounding molecules within the timescale of molecular vibrations, *i.e.* picoseconds (10^{-12} s) or less. Rotational energy spacings are much smaller than vibrational energy spacings, in the range $\sim 20\text{--}200\text{ cm}^{-1}$, and transitions between rotational energy levels are caused by microwave photons. Rotational energy is generally less important in condensed phase photochemistry, since in solution and solid phases contact with neighbouring molecules dampens or completely stops free rotation so the energy levels are either not quantised or non-existent.

1.8 Energy Levels in Atoms, Molecules and Crystal Lattices

Due to the difference in masses of electrons and nuclei it is possible, and very convenient, to consider as a very good approximation, the energy of the electron to be separate from the energy of nuclear motions, *i.e.* vibrations and rotations. Furthermore, it is also possible to treat vibrations and rotations separately. Thus, we can consider the energy of a molecule to be made up of the sum of distinct

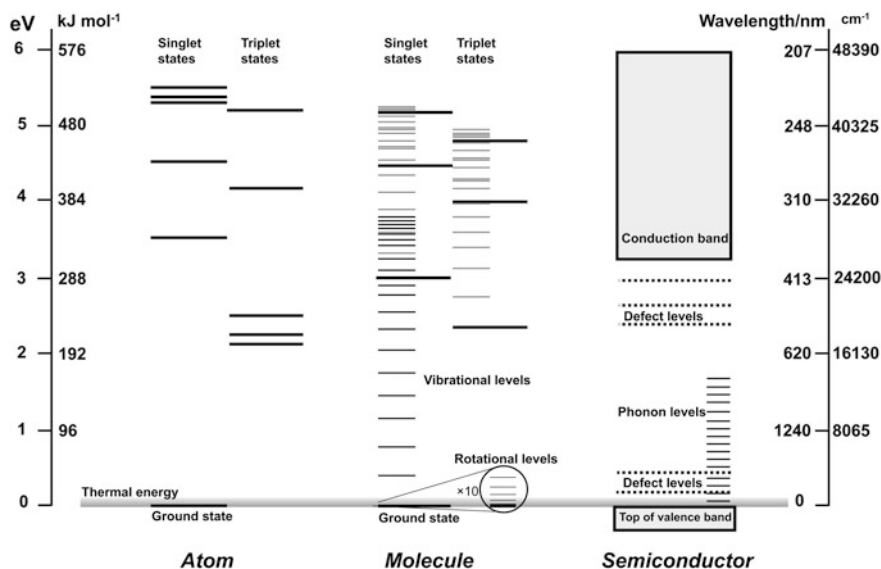


Fig. 1.17 Schematic energy levels in atoms, molecules and semiconductors. The atom, which for simplicity is taken to be a spin paired, *i.e.* a singlet, ground state, has only electronic energy levels (*long dark lines*) which get closer together as their energy increases. The molecule, also taken to be a singlet ground state, has: electronic levels (*long dark lines*); vibrational levels (*shorter lines*); and rotational levels, which are so close together they require magnification $\times 10$ to be shown separately on the diagram. Ground-state vibrational levels are in *black* and, for clarity, those for higher energy electronic states are in *dark grey*. Molecular electronic energy levels get closer together as their energy increases, as do vibrational energy levels, but rotational energy levels increase in separation with energy. Note the relatively *high density of states* above the first excited singlet state, which increases further as energy increases. The semiconductor has: valence and conduction bands; intermediate ‘defect’ energy levels, which may be due to deliberate doping, crystal defects, or impurities; and *phonon* energy levels which correspond to a wide variety of low energy and high energy lattice vibrations (for clarity, phonon levels are shown only for intermediate energies between valence and conduction band). Thermal energy at room temperature is shown by the *horizontal graded grey band*

types of energy behaving independently, *i.e.* we can treat the electronic, vibrational, and rotational energies of a molecule separately and then sum them for the total molecular energy. This is the *Born–Oppenheimer approximation*. For solids, vibrations of the crystal lattice as a whole (*phonons*), or the electronic waves of the “free” electrons in a metal (*plasmons*) are other important modes of energy.

For all of these different types of energy, the energy levels are quantised, but the spacings of the energy levels vary considerably from energy type to energy type. Fig. 1.17 shows the relative spacings of energy levels in atoms, molecules and semiconductors. The energy levels of electronic states are those most widely separated, followed by vibrational, rotational, spin, and translational energy. The energy level spacings for molecular translational energy in typical sample volumes, even at very low temperatures, are so small that they can be considered a

continuum, so that *translational*, or *thermal*, energy differs from the other energy types in that *experimentally* it does not appear quantised. Because of this, it is often considered separately from the other types of energy, perhaps not mentioned specifically but always recognised as being there.

In some cases, a number of energy states which are equal in energy are available, *i.e.* which are *degenerate*. For example, the triply degenerate $l = 1$ atomic state. This is important when considering how energy levels are populated. Degeneracy arises from the symmetry properties of the wavefunctions of the states, and can sometimes be recognised from the symmetry of the chemical species in question.

The lowest energy level possible is referred to as the *ground state*: we say a molecule is in its *ground electronic state*, or if dealing with vibrational energy, in its *ground vibrational state*. The lowest possible energy state is that adopted at 0 K, when the molecule has its *zero point energy*.

Although the approximation that the total energy of the molecule can be assigned to these different types of energy and that they can be considered independently, is generally sufficiently accurate for most applications, the different energy levels are not totally independent, and molecular properties such as *bond lengths* and *moments of inertia* depend on electronic and vibrational energy states. The nuclear geometries of electronic excited-states differ from the ground-state, as do their vibrational and rotational energy levels. As a molecule increases in vibrational energy the average nuclear separation increases, the moment of inertia along that bond decreases and rotational energy levels become closer together.

1.9 Collections of Atoms and Molecules: Ensembles and Distributions

The discussion so far has focused on individual atoms and molecules, but most often we deal with the average behaviour of a very large number of molecules. Even when we select an individual molecule for study, or record an event from an individual molecule, such as the emission of a photon from an excited state in the method of single photon counting, that molecule is usually only one from an enormous collection of molecules. Every single event is due to a change in an individual molecule, but the sum of all these single events, which is the usually observable result, reflects the distribution of properties, most notably energy, in all of the molecules in the sample under study. The behaviour of large numbers of chemical species is described by *thermodynamics* and *statistical mechanics*.

Each individual atom or molecule is, at any time, in a particular energy state, but even within a microscopic sample at any temperature much above 0 K, there is a distribution of states within the sample. The sample as a whole, the *ensemble*, will have a specific total energy, and the average molecular energy is calculated by dividing this energy by the number of molecules present. However, most

molecules will not have exactly this average energy, rather there will be a distribution of energies, with some molecules more energetic than the average and some less. Over time, the energy state of any individual molecule will vary, sometimes it will be higher than the average, at other times, lower, but the ‘time-averaged’ energy for any individual molecule will be the average energy of the ensemble. The way energy is distributed among inter-converting energy states at equilibrium is given by the *Boltzmann distribution equation*:

$$\frac{N_i}{N_j} = \exp^{-(E_i - E_j)/k_B T} \quad (1.16)$$

where N_i/N_j gives the ratio of the number of particles in states i and j , with energies E_i and E_j , k_B is the *Boltzmann constant* and T is the temperature (in Kelvin). The Boltzmann constant is related to the *molar gas constant*, R , by $R = N_A k_B$, where N_A is *Avogadro’s constant*.

The Boltzmann distribution links the concept of temperature, which is a property of ensembles of matter, *i.e.* matter in bulk, with the relative populations of the different energy states in the components of that ensemble. The equation shows that in an ensemble of interconverting states at equilibrium:

1. states of equal energy are populated equally;
2. the difference in populations between two states is determined by the energy difference between the state and the temperature; the difference increases with both an increase in the difference in energy and a decrease in temperature;
3. as the temperature is lowered, the relative populations of any two states of different energy shifts towards the lower state, such that at 0 K all of the ensemble are in their lowest state;
4. at ∞ K every state is populated equally;
5. at any experimentally available temperature, higher energy states are less populated than lower energy states;
6. the temperature at which the population of two different energy state becomes essentially equal depends upon the energy gap between the states. States differing by a small energy, e.g. nuclear spin states, will be almost (but not quite) equally populated even at room temperature, while temperatures of thousands of degrees are required before states separated by a large energy difference, e.g. atomic electronic states, have comparable populations.

Applying the Boltzmann equation to a typical molecule at room temperature shows the following. All of the molecules are in the ground electronic state. Almost all molecules are also in the ground vibrational state, although if the molecule has big atoms in relatively weak bonds, e.g. I_2 , then the first few vibrational levels will be significantly populated. If the molecule is in the gas phase, where rotational states are important, only a few of the molecules are in the lowest rotational state, with most in higher rotational states; energetically the lowest state, $J = 0$, is the most highly populated, singly-degenerate state, but each rotational state is $2J + 1$, degenerate and this, combined with the small energy

spacing for rotational levels, gives a spread of populated rotational states, generally peaking, depending upon energy spacing, around $J \sim 5-50$.

1.10 Equilibrium, Change and the Timescales of Physical and Chemical Processes

The Boltzmann equation is only valid for interconverting energy states at equilibrium. Not all states interconvert, or exchange energy efficiently. A mechanism is required for exchanges of energy. Much of photophysics deals with the interconversion of energy between electronic, vibrational, rotational, and thermal states. Almost the whole of chemistry deals with the nature of the non-interconverting energy states of kinetically stable chemical structures, together with the mechanisms by which the kinetic stability inhibiting energy exchange can be removed to allow ‘chemical reactions’ to proceed. A chemical reaction, by which reactants change structure to products to give a new, kinetically stable, equilibrium mixture, is a process which allows the interconversion of chemical energy between previously kinetically stable chemical structures. In gases and liquids, thermal and vibrational energy (rotational energy also), and for high temperature gases electronic energy, are exchanged by molecular collisions. Typical timescales for various chemical and photochemical processes are given in Fig. 1.18.

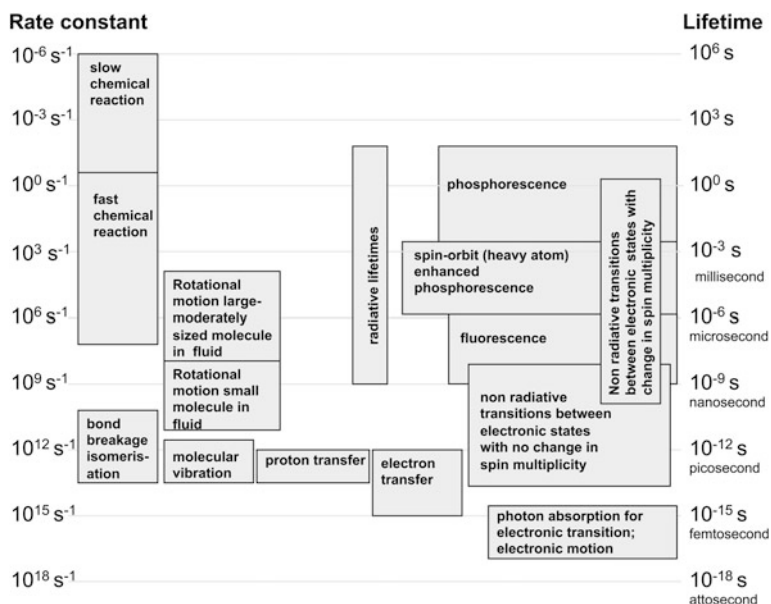


Fig. 1.18 Typical timescales for various chemical and photochemical processes

1.11 Interaction Between Electromagnetic Radiation and Atoms or Molecules: Two-state Systems and the Einstein Coefficients

When electromagnetic radiation and atomic or molecular systems interact, there are three distinct processes which are relevant to photochemistry: *absorption*, *stimulated emission* and *spontaneous emission*. These were treated theoretically by Einstein and are shown diagrammatically for a system involving two states, 1 and 2, in Fig. 1.19.

In *absorption*, a photon interacts with the system in a low energy state, 1, and transforms it into a higher energy state, 2. This corresponds to a second-order kinetic process with rate:

$$dN_1/dt = -B_{12}N_1\rho \quad (1.17)$$

where N_1 is the concentration of molecules in state 1, ρ is the density of photons (*photon flux*) and B_{12} is a proportionality constant. There will be a corresponding process with molecules in state 2, with rate:

$$dN_2/dt = -B_{21}N_2\rho. \quad (1.18)$$

This is termed *stimulated emission*, and is responsible for *lasing* (see Sect. 14.4.2.4). According to microscopic reversibility:

$$B_{21} = B_{12} \quad (1.19)$$

such that the rate of stimulated emission is $B_{12}N_2\rho$. Under thermal equilibrium, the Boltzmann distribution shows that $N_1 \gg N_2$, such that stimulated emission is not important. However, it will become important if a population *inversion* can be achieved where $N_2 > N_1$ (See Sect. 14.4.2.4).

Since stimulated emission normally has a relatively low probability and the Boltzmann equilibrium must be maintained, the theory of radiation requires a further process for conversion of state 2 to state 1. This is termed *spontaneous emission*. This is the normal emission processes of *fluorescence* and

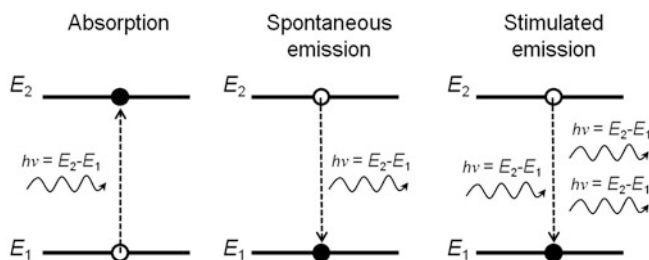


Fig. 1.19 The processes of absorption, spontaneous emission and stimulated emission observed upon interaction of electromagnetic radiation with atoms or molecules

phosphorescence. In fluorescence, spontaneous emission of light occurs within a few ~ 10 – 100 nanoseconds after formation of the excited state, whereas, in contrast, spontaneous emission by phosphorescence may persist for much longer timescales, typically of the order of milliseconds to seconds. Fluorescence and phosphorescence are discussed in more detail in Sect. 1.13.3.

Spontaneous emission is a random process, such that for a statistical ensemble of molecules it will follow first-order kinetics with the rate law:

$$dN_2/dt = A_{21}N_2. \quad (1.20)$$

The proportionality constants B_{12} ($= B_{21}$) and A_{21} are termed the *Einstein coefficients*. They are related by:

$$A_{21} = (8\pi h\nu_{12}^3/c^3)B_{12} \quad (1.21)$$

where ν_{12} is the frequency of the radiation corresponding to the transition between states 1 and 2, c is the velocity of light and h is Planck's constant. This equation is sometimes termed the “ ν^3 law”. As will be discussed later, both B_{12} and A_{21} can be related to experimental properties for the absorption and emission of light.

1.12 The Absorption of Light

The absorption of light is governed by two conservation laws: the conservation of energy and the conservation of angular momentum. The energy in a monochromatic light beam behaves like a collection of small packets, or *quanta*, of energy, in particle terms *photons*, each of energy equal to $h\nu$. Each photon also carries an equal and fixed amount of spin angular momentum. In a polychromatic beam, each photon of different wavelength carries a different amount of energy but each photon still carries the same amount of spin angular momentum. As a consequence of absorption, all of the photon energy and all of the photon spin angular momentum is transferred into the new electronic state of the absorbing structure.

Transitions in which a single photon is absorbed by a single absorbing unit, e.g. a molecule or atom, are by far the most common. It is possible, by the use of high intensity radiation from a laser, to have transitions in which more than one photon is absorbed simultaneously.

1.12.1 Single Photon Transitions

The requirements for absorption of electromagnetic radiation can be considered as twofold: a photon energy which matches the energy gap between two states; and a mechanism for coupling between the EMR and the transition between the two states involved.

The energy match is given by:

$$E_2 - E_1 = \Delta E = h\nu = hc/\lambda \quad (1.22)$$

where E_1 is the energy of the lower energy state, E_2 the energy of the higher energy state, ΔE is the difference in energy between the two states, h is Planck's constant, c the speed of light, and ν and λ the frequency and wavelength of the absorbed light. If this energy-matching criterion is not met, then photons of this particular energy cannot be absorbed, and the material will transmit, reflect, or scatter them.

The absorption process involves three waves: the two electronic waves of the two energy states, plus the EMR wave of the incident light. A detailed understanding of the coupling mechanism between these requires quantum mechanics, but the essence of the question, in mechanistic terms, is, "How efficiently can the incident photon wave perturb the positions and momenta of the electron in the lower state wave such that it can be pushed into positions and momenta corresponding to the higher energy wave?"

The mechanism of interaction is *via* the oscillatory force an electromagnetic wave exerts on the dipole formed between the nucleus and an electron. For a 'picture' of the process it is easiest to consider the case of the hydrogen atom. At any time there is an instantaneous dipole between the electron and nucleus. The wavelength of visible light is many times bigger than the atomic diameter, and as the wave passes, both the electron and nucleus experience essentially the same magnitude of electromagnetic oscillatory force, but, as they are oppositely charged, the force acts on the two ends of the dipole, the nucleus and electron, in opposite directions. This electromagnetic force causes an oscillation in the dipole, and perturbs the electron wavefunction. If this perturbation is of the right frequency, the electron can be pushed from positions and momenta characteristic of the lower state to those characteristic of the higher state; the electron wavefunction is then that corresponding to the higher state rather than the lower state, energy is absorbed and the transition made. If the perturbation cannot shift the electron from the lower to the upper orbital, the electron remains in the lower orbital, no energy is absorbed, although the oscillating electric field caused by the perturbed electron oscillation can result in a scattered photon of the same frequency as the incident radiation. (This latter process gives rise to *Rayleigh scattering*, scattering of light at the same frequency of incident light, which occurs when any inhomogeneous material is irradiated.)

In a similar way that the calculation of orbital overlap for the formation of MOs depends on the integral of two wavefunctions, the transition probability is also calculated from an integration involving two wavefunctions; this time those corresponding to the lower and upper states. But an additional term, to identify the effect of the electromagnetic radiation in coupling these two states together is required, this is the *dipole moment operator*, $\hat{\mu}$, which for a single electron is $-er$, where $-e$ is the charge on an electron and r is position relative to the nucleus, *i.e.* the vector position along x , y , z axes with the nucleus at zero. The "allowedness"

of an electric dipole absorption from E_1 to E_2 , is calculated from the *transition dipole moment*, M_{12} (i.e. the electric dipole moment associated with the transition between the two states):

$$M_{12} = \int \Psi_1 \hat{\mu} \Psi_2 d\tau \quad (1.23)$$

where Ψ_1 and Ψ_2 are the wavefunctions for the electronic ground and excited states, 1 and 2, respectively, and the integral is across all space ($\int \dots d\tau$). M_{12} is a vector, and the transition probability for absorption is given by the *square of the magnitude of the transition dipole moment*, i.e. $|M_{12}|^2$ (the vertical bars indicate it is the magnitude of the vector, i.e. its length, which is squared, rather than squaring the vector itself).

If the overall integral is large, then there is a high probability that an incident photon will be absorbed, the transition takes place, and the molecule is excited into the higher energy state, 2. If the integral is small, then there is a low probability of absorption. If the integral is zero, there will be no absorption at all. From equation (1.23) the two wavefunctions must have some overlap in space, but also the symmetry of the wavefunctions, when combined with the symmetry properties of the dipole moment operator, must be such as to give a non-zero resultant integral. A consideration of those cases, where, for reasons of wavefunction symmetry, the integral is zero, leads to what are called *selection rules*.

1.12.1.1 The Parity Selection Rule: Atomic Transitions and Electron Orbital Angular Momentum

For an atom the dipole moment operator has inversion symmetry across the nucleus; therefore the absorption integral is zero if both the electron wavefunctions are of the same parity, but non-zero if they are of different parity. Thus an $s \rightarrow s$ orbital transition is '*forbidden*', but $s \rightarrow p$ orbital transition is '*allowed*'. This is the *Laporte selection rule* (also known as the *parity selection rule*), perhaps the most commonly observed consequence of which is the low intensities of $d-d$ transitions in transition metal complexes. By itself, the parity selection rule would suggest that an $s \rightarrow f$ transition is allowed. However, consideration of conservation of angular momentum, restricts changes to those transitions in which $\Delta l = \pm 1$. (The possibilities of an increase or decrease in l arise because of the vector nature of momenta, which can oppose or reinforce one another).

Although the strongest interaction between electromagnetic radiation and chemical structures is *via* the dipole interaction, there are weaker multipole and magnetic interactions which may become important in certain circumstances, notably when considering $f-f$ transitions in lanthanide (III) ions.

1.12.1.2 The Spin Selection Rule: Atomic Transitions and Spin–Orbit Coupling

The spin-angular momentum of an absorbed photon can be incorporated into an absorbing atom as electron orbital angular momentum, *i.e.* a difference of ± 1 in the l quantum number for atomic transitions. However, there is no electric-dipole mechanism for the direct conversion of photon spin angular momentum into a change in electron spin angular momentum. (ESR spectroscopy has its origin in the interaction of the magnetic, rather than electric, field of the incident radiation). Thus, the general electron spin selection rule is $\Delta S = 0$ and absorption takes place with no change in electron spin angular momentum, so that, notably, transitions between singlet and triplet states are *spin-forbidden*.

However, as discussed in Sect. 1.4.3, atoms with high Z , *i.e.* ‘heavy atoms’, can have electron spin angular momentum and electron orbital angular momentum ‘coupled’, such that, in optical transitions of heavy atoms, a change in electron spin angular momentum, an electron ‘spin flip’, can be coupled to a change in orbital angular momentum while total angular momentum is conserved. Thus, when all three types of angular momentum involved in absorption: photon, electron spin, and electron orbital angular momentum, can be coupled together, absorptions for which $\Delta S = \pm 1$ can become allowed. For example, the $n = 6$ ${}^3P_1 \rightarrow {}^1S_0$ transition of the Hg atom is very strongly allowed, even though it is a triplet–singlet transition for which $\Delta S \neq 0$.

1.12.1.3 Selection Rules and Light Absorption in Molecules

The probabilities of absorption by structures larger than an atom are determined in essentially the same way. For diatomic and linear polyatomic molecules the *orbital momentum selection rule* becomes $\Delta A = 0, \pm 1$, where A is the symbol for *molecular* total orbital angular momentum. For systems with appropriate symmetry, the rules are $g \leftrightarrow u$, $+$ \leftrightarrow $+$, $- \leftrightarrow -$. For non-linear polyatomic molecules which have some symmetry, the selection rule for orbital angular momentum can be given in terms of symmetry properties [45]. For centrosymmetric systems, the rule $g \leftrightarrow u$ still holds. In addition, the allowed transitions can be related to the symmetry properties of a particular point group. For example, benzene has D_{6h} symmetry, and electric dipole transitions are symmetry forbidden from the A_1 ground state to B_1 , B_2 or other A_1 states (see Fig. 1.15) [46]. However, the symmetry arguments only hold for completely rigid structures. In practice, vibrations can act to distort molecular structures sufficiently to allow some absorption for transitions, which would be ‘forbidden’ if only the symmetry of the electronic wavefunctions were to be considered. These transitions are usually much weaker than fully allowed ones. For example, the lowest energy (longest wavelength) absorption band in benzene corresponds to the symmetry forbidden ${}^1A_{1g} \rightarrow {}^1B_{2u}$ transition (see Fig. 1.15). Although this transition is forbidden for pure electronic states, the structure of benzene is distorted from that of a pure

hexagon because of interaction with the various vibrational modes. This is termed *vibronic coupling* (*vibrational* + *electronic*). This reduces the symmetry and the selection rule is partially relaxed. Nevertheless this band, which is seen around 256 nm, is 30 times weaker than the second band at 203 nm and 200 times weaker than the third absorption band at 183 nm [21].

The spin selection rule, $\Delta S = 0$, also applies to molecules, and transitions between, for example, molecular singlet and triplet states are *spin-forbidden*. However, in the presence of heavy atoms, either in the molecular structure itself, or in the solvent, the rule may be relaxed enough for singlet to triplet absorptions to be detected, although usually they are still weak absorption bands.

1.12.1.4 Selection Rules for Vibrational Transitions, Rotational Transitions, and Raman Scattering

The vibrational transitions of a molecule can be probed directly using infrared spectroscopy and are subject to the gross selection rule that *for a change in a vibrational state brought about by the absorption or emission of a photon, there must be an accompanying change in the dipole moment of the molecule*. Homonuclear diatomics are an important group of molecules which do not absorb IR radiation because of this selection rule.

Pure rotational spectra can be observed in the gas phase; however the *selection rule for rotational transitions requires the molecule to have a permanent electric dipole*. Homonuclear diatomics are, again, an important group of molecules which do not show microwave absorption because of this selection rule.

Although these selection rules limit IR and microwave absorption, electronic transitions can be, and usually are, simultaneously accompanied by both vibrational and rotational transitions, and for an electronic transition there is no restriction on the associated change in vibrational state. Vibrational transitions accompanying an electronic transition are called vibronic transitions. In high resolution gas phase work, these, along with their accompanying rotational transitions give rise to what is called an *electronic band system*. In solution the vibrational structure is usually not well resolved, but there is often some structure, a *vibrational progression*, corresponding to transitions into a number of electronic levels in the upper electronic state (see Fig. 1.20).

Raman spectroscopy is a complementary technique used to probe vibrational and rotational modes. It is based on the inelastic scattering of light. Upon irradiation of a sample with a monochromatic light source (typically a laser), some of the incident photons collide with the molecules and lose energy to vibrational/rotational modes, and will emerge from the sample with lower energy (*Stokes radiation*); other photons may gain energy from vibrationally *hot* states and will emerge with a higher energy (*anti-Stokes radiation*); finally some photons will be directly scattered without a change in frequency (*Rayleigh radiation*). The observed energy ‘losses’ or ‘gains’ provide information about the vibrational and rotational states of molecules. The gross selection rule for *rotational Raman*

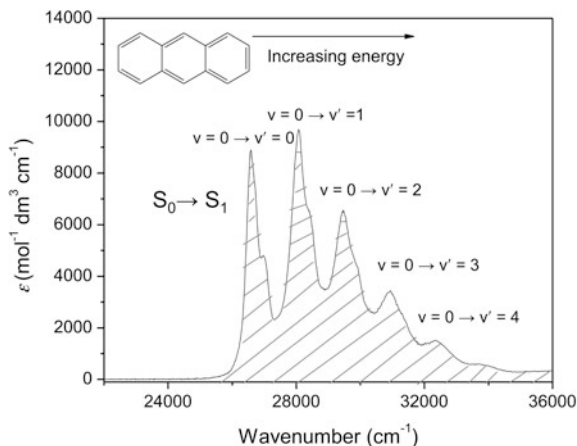


Fig. 1.20 UV/Vis absorption spectrum of anthracene in cyclohexane for the $S_0 \rightarrow S_1$ transition. The vibrational progression in the absorption spectrum corresponds to transitions to excited-state vibrations. The hatched area under the peak corresponds to the integrated absorption coefficient (IAC) as defined in Eq. 1.26

transitions is that the molecule must be anisotropically polarisable, while for *vibrational Raman transitions* the polarisability should change as the molecule vibrates.

1.12.1.5 Absorbance, Transmittance, Molar Absorption (Extinction) Coefficient, Beer–Lambert Law and Deviations from Beer–Lambert Law

For a parallel monochromatic radiation beam, where the proportion of radiation absorbed by a substance is independent of the intensity of the incident irradiation, *i.e.* the probability of absorption is linearly dependent on incident intensity, which is the usual case for single photon transitions, each successive layer of thickness dx absorbs an equal fraction $-dI/I$ of radiant intensity I , and integration across a finite thickness, x , with an initial irradiation intensity I_0 gives:

$$\ln(I_0/I_t) = bx \quad (1.24)$$

where I_t is the transmitted intensity and b is a constant dependent upon the sample. This is Lambert's law. Beer showed that b is proportional to concentration (strictly limited to low concentrations), and, as is most commonly the case, using \log_{10} , this gives:

$$\log_{10}(I_0/I_t) = \log_{10}(I_0/(I_0 - I_{\text{abs}})) = \epsilon cx \quad (1.25)$$

Table 1.6 Typical values of molar absorption coefficients (ϵ) for some electronic transitions in organic molecules and metal complexes

Species	Transition type	$\epsilon/\text{mol}^{-1} \text{ dm}^3 \text{ cm}^{-1}$
Highly conjugated organic molecules	Spin-allowed $\pi \rightarrow \pi^*$	10^4 – 10^5
Small aromatic compounds	Spin-allowed, symmetry forbidden lowest energy $\pi \rightarrow \pi^*$	200–500
Carbonyl compounds	Spin-allowed $n \rightarrow \pi^*$	10–50
Metal complexes	Spin- and Laporte-allowed charge transfer	10^4 – 10^5
Tetrahedral metal complexes	Spin-allowed, partially Laporte-forbidden $d \rightarrow d$	10^2 – 10^3
Octahedral and square planar metal complexes	Spin-allowed, Laporte-forbidden $d \rightarrow d$	1–10
All systems	Spin forbidden ^a	10^{-5} – 10^{-3}

^a These values increase with systems containing high atomic number atoms due to increased spin–orbit coupling

where I_{abs} is the absorbed intensity, ϵ is the molar absorption (formerly called *extinction*) coefficient, and c is the concentration of absorbing material. If c is given in mol dm^{-3} , ϵ is the *decadic molar absorption coefficient* (although usually the term decadic is omitted); x , the *pathlength*, is usually given in cm (a 1 cm pathlength cell being the most commonly used in solution phase experimental photochemistry; note pathlength is often given the symbol l), so the units of ϵ are usually $\text{mol}^{-1} \text{ dm}^3 \text{ cm}^{-1}$. ϵ is wavelength dependent. $\log_{10}(I_0/I_t)$ is called *absorbance*, or *optical density* (usually given the symbol A , Abs, or OD), and it varies linearly with concentration and path length. For a solution made up of a mixture of absorbers, i , the total absorbance at a given wavelength is the sum of the absorbances of the individual components at that wavelength, *i.e.* $A_{\text{total}} = x \sum \epsilon_i c_i$.

If a transition is forbidden by the spin-selection rule, the molar absorption coefficient is typically 10^{-5} – $10^{-3} \text{ mol}^{-1} \text{ dm}^3 \text{ cm}^{-1}$, irrespective of whether the transition is Laporte- or vibrationally-allowed. If a transition is spin-allowed but parity forbidden, ϵ is typically of the order of 10^0 – $10^3 \text{ mol}^{-1} \text{ dm}^3 \text{ cm}^{-1}$. If the transition is both spin- and Laporte-allowed, ϵ is large (10^3 – $10^5 \text{ mol}^{-1} \text{ dm}^3 \text{ cm}^{-1}$) and the absorption is said to be “fully-allowed”. Typical values for “allowed” and “forbidden” transitions in some common organic and inorganic complexes are given in Table 1.6.

Apparent deviations from the Beer–Lambert law arise mainly because of instrumental factors such as: stray light, sample fluorescence, and use of a wide radiation bandwidth. Real deviations arise because of high concentrations which introduce solute–solute interactions and changes in ϵ with solution refractive index, and concentration dependent chemical equilibria.

1.12.1.6 The Strength or Probability of Absorption

We saw earlier that the probability of electric dipole absorption is related to the transition dipole moment. However, there are a variety of terms commonly used to describe the strength or probability of absorption. The ‘allowedness’ or ‘forbiddenness’ of the transition, and *oscillator strength*, f , are useful ideas where the relative, rather than absolute value, of the strength of coupling is required. These terms are factors used to describe how likely absorption is by reference to the ‘ideal oscillator’ of a free electron where the transition is ‘fully allowed’ and both the ‘allowedness’ and oscillator strength are unity.

The molar absorption (extinction) coefficient, Einstein coefficient and absorption cross-section are commonly used measures of transition probability. The first three are used for atomic and molecular species in the gas or solution phase, while the latter is commonly used in solid-state studies. These are absolute measures of absorption probability and are ultimately derived from the transition dipole moment, and are therefore all related. They can be measured experimentally from the absorption spectrum and can, in some cases, be calculated using molecular orbital theory programs. (Note that generally MO calculations will give the oscillator strength for any ‘forbidden’ transition as zero).

The method of calculation of these parameters from the absorption spectrum is illustrated in Fig. 1.20, where the spectrum is plotted as ϵ vs wavenumber ($\tilde{\nu}$ in units of cm^{-1}), instead of the conventional wavelength units [47]. The integrated absorption coefficient, (IAC), is the area of the absorption peak, which is given by:

$$IAC = \int_0^{\infty} \epsilon(\tilde{\nu}) d\tilde{\nu}. \quad (1.26)$$

The IAC is proportional to the square of the transition dipole moment, *i.e.* $|M_{12}|^2$. The related oscillator strength, f , of the transition is given by:

$$f = 4.33 \times 10^{-9} \int_0^{\infty} \epsilon(\tilde{\nu}) d\tilde{\nu}. \quad (1.27)$$

The maximum value of f for a fully-allowed transition is 1 and it is a unitless quantity.

The IAC is also related to the B_{12} Einstein coefficient for spontaneous absorption by:

$$IAC = \int_0^{\infty} \epsilon(\tilde{\nu}) d\tilde{\nu} = B_{12} h \tilde{\nu} N_A / \ln 10 \quad (1.28)$$

where N_A is Avogadro's number, and the term $\ln 10$ arises from the use of the *decadic* molar absorption coefficient, *i.e.* one based on \log_{10} . Finally, the Einstein coefficient for spontaneous emission, A_{21} , can be related to B_{12} by:

$$B_{12} = A_{21}/(8\pi hc\tilde{\nu}^3) \quad (1.29)$$

and, thus to the IAC by:

$$A_{21} = \frac{8\pi c\tilde{\nu}^2 \ln 10(\text{IAC})}{N_A}. \quad (1.30)$$

1.12.1.7 Types of Transitions

While bearing in mind the limitations of our approximations to the Schrödinger equation for complex molecules, it is still often found that transitions arise predominantly from the movement of an electron from one molecular or atomic orbital to another. The nature of the transition is then described by the two orbitals involved; the most common types of transition are given below.

1. **Transitions between orbitals localised on atoms;** e.g. $d-d$ transitions of transition metal salts, $f-f$ transitions of lanthanide ions. Such *metal-centred* (MC) transitions are ubiquitous in transition metal and lanthanide complexes. They are relatively weak because they are symmetry (Laporte) forbidden. Although they may not be the important transitions for any particular application of transition metal photochemistry, they will almost always be present. These are the transitions that give many transition metal salts their characteristic colour and are found in some gemstones and minerals. For example, the red colour in ruby is due to the $d-d$ transitions in chromium (III) present at certain sites in an aluminium oxide (*corundum*) crystal.
2. **Transitions between atomic orbitals in mixed oxidation state transition metal complexes.** These transitions can be relatively strong and are known as *metal to metal charge transfer* (MMCT) transitions. Two common examples are those involving the $\text{Fe}^{2+}/\text{Fe}^{3+}$ centres in the pigment prussian blue and the $\text{Fe}^{2+}/\text{Ti}^{4+}$ ions in sapphire.
3. **Transitions between ligand and metal orbitals in transition metal complexes.** These are called *metal to ligand*, and *ligand to metal charge transfer* (MLCT and LMCT) transitions, respectively. These can be fully-allowed transitions and are usually the source of colour in intensely coloured transition metal complexes, e.g. the LMCT transitions in chromate, CrO_4^{2-} , and permanganate, MnO_4^- ions, and the intense absorptions in ferroin (tris(phenanthroline) iron(II)) and tris(2,2'-bipyridyl)ruthenium(II) (see [Chap. 4](#)).
4. **Transitions between molecular orbitals in organic compounds:** e.g. polyaromatics, organic dyes, biological colorants such as chlorophylls and carotenes (see [Chap. 4](#)). The lowest energy transitions are those between the HOMO and

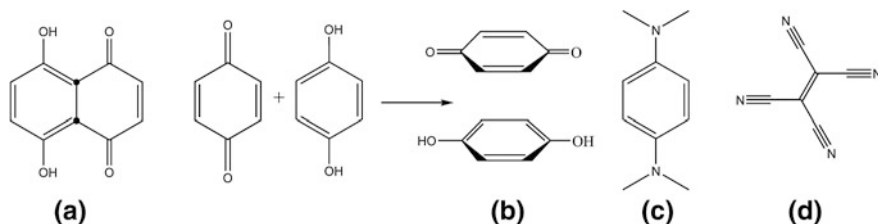


Fig. 1.21 Structures of some organic molecules that show charge transfer: **a** naphthazarin; **b** quinhydrone (a complex between quinone and 1,4-dihydroxybenzene); **c** TMPD (electron donor) and **d** TCNE (electron acceptor)

LUMO. The two most important types of transitions in organic molecules are $n \rightarrow \pi^*$ and $\pi \rightarrow \pi^*$ transitions; $\sigma \rightarrow \pi^*$ and $\sigma \rightarrow \sigma^*$ transitions; are usually of such high energy that they occur in the vacuum UV region. Most molecules are not of particularly high symmetry and for these, $\pi \rightarrow \pi^*$ transitions are generally highly allowed and have high molar absorption coefficients. For those molecules which do have high symmetry, some $\pi \rightarrow \pi^*$ transitions may be symmetry forbidden and show significantly reduced molar absorption coefficients (e.g. some transitions of pyrene). Pure $n \rightarrow \pi^*$ transitions are symmetry forbidden when the n orbital has σ symmetry, such as carbonyls; but vibrations are effective in reducing the degree of forbiddenness; and a phenomenon known as *intensity borrowing*, by which the intensity of a forbidden transition lying close to an allowed transition can be increased, allows many $n \rightarrow \pi^*$ transitions to have significant molar absorption coefficients. (The need to introduce the concept of ‘intensity borrowing’ is an example of the failure of the simple MO approach to match the solutions of the Schrödinger equation for complex systems.) For many organic molecules containing heteroatoms, such as O and N, $n \rightarrow \pi^*$ and $\pi \rightarrow \pi^*$ transitions are energetically close and in some cases the relative positions of the absorptions can be reversed in solvents of differing polarity. In certain cases, transitions can take place between electron rich and electron poor regions in complex organic molecules. These *charge transfer* transitions usually have very high molar absorption coefficients and are responsible for many of the intense colours found in typical organic dyes (see Chap. 4), such as naphthazarin (Fig. 1.21a).

- 5. Transitions between the valence and conduction bands in semiconductors.** These are the origin of colour in semiconductor pigments and quantum dots. In addition to colour from bandgap transitions, introduction of dopants or impurities into semiconductors leads to localised energy levels on the dopant or impurity atoms/molecules (so-called *colour centres*) and transitions between these levels and those of the semiconductor conduction and valence bands become possible; the colour in blue and yellow diamonds arises from these types of transitions.
- 6. Transitions between electronic energy levels in imperfect crystals.** The colours of some minerals and semi-precious gems, notably: *Cairngorms* or *smoky quartz* where colour comes from defects in the quartz lattice caused by

radiation from nearby radioactive minerals, and blue topaz where similar defects are introduced into otherwise colourless stones deliberately in the laboratory.

7. **Transitions of the hydrated electron.** One of the effects of radiation on aqueous systems is the ejection of electrons, which are then hydrated by surrounding water molecules. The blue colour of the hydrated electron arises because of transitions between the electronic energy levels of the electron held in the potential well created by these water molecules. Similar intense colours due to solvated electrons are seen upon dissolving sodium or other alkali metals in liquid ammonia or aliphatic amines.
8. **Charge transfer transitions between molecules in association.** Here, the transition occurs between the molecules themselves, with an electron transferred from one molecule to the other. The various colours observed with molecular iodine (I_2) with aromatic molecules are due to charge-transfer [48]. Intermolecular charge transfer is also responsible for the yellow colour in *quinhydrone*, a complex formed between quinone and 1,4-dihydroxybenzene (Fig. 1.21b). Naphthazarin can be considered as an intramolecular equivalent of quinhydrone. Organic charge transfer complexes having strong absorption bands can also be readily formed between aromatic molecules and strong electron donors, such as *N,N,N',N'*-tetramethyl-*p*-phenylenediamine (TMPD or *Wurster's blue*), Fig. 1.21c or acceptors, such as tetracyanoethylene ((TCNE), Fig. 1.21d).

1.12.2 Absorption Spectra

1.12.2.1 Absorption Spectra in the Gas Phase

Atoms lack vibrational and rotational energy levels. Low pressure atomic gases show absorption lines which are extremely narrow, limited in width by *Doppler broadening* due to the range of molecular velocities in a thermally equilibrated gas. (The Doppler effect is a change in absorption/emission frequency due to relative motion of the absorber/emitter and the source/detector. The reader will almost certainly have experienced the effect while standing at a railway station as a non-stopping train passes sounding its horn. The sound of the horn shifts from a high frequency to low frequency tone as it first approaches and then leaves the station). At high pressures and temperatures interatomic interactions, *i.e.* collisions, and the perturbing effects of neighbouring molecules, also cause lines to broaden.

For molecular species, gas-phase absorption spectra show a series of electronic transitions upon which vibrational and rotational structure are superimposed. For simple molecules in the gas phase this structure is simple enough for individual electronic-vibrational-rotational transitions to be seen, particularly at low temperatures where only the very lowest vibrational and rotational energy states are

populated in the ground state. However, for molecules of any complexity there are many vibrational levels, and since rotational energy spacings decrease with molecular mass [14] rotational levels are much closer together, so that even in the gas phase, where molecules are isolated from one another, the absorption spectrum can become so complex that it resembles more a series of overlapping bands than groups of discrete lines.

1.12.2.2 Absorption Spectra in Solution

Absorption bands in solution are less structured and broader than those in the gas phase. In solution, molecular rotation is hindered through collision with solvent molecules such that rotational quantisation is lost and solvent–solute interactions broaden vibrational bands further. The magnitude of the latter effect depends on the strength of the solute–solvent interaction and it is therefore most pronounced in polar solvents, so that spectra in a non-polar solvent such as hexane will generally show more distinct vibrational structure than those recorded in a more polar solvent such as acetone or an alcohol. While molecular absorption bands in solution may be very broad, there is almost always some electronic/vibrational structure and usually a number of electronic absorption bands can be identified.

1.12.2.3 Absorption Spectra in Solution: Effect of Aggregation

Consider the relatively simple case of two aromatic molecules. If they are close enough, they may interact, or *couple*, leading to splitting of the excited-state into two levels [49]. The effect of this coupling depends upon the way the *transition dipole moments* of the two molecules are arranged. If they are parallel, the transition to the upper excited state becomes more probable, and this leads to a *blue* or *hypsochromic shift* in the absorption spectrum. If, in contrast, the transition dipoles are in a head-to-tail arrangement, the transition to the lower excited state becomes more probable, and there is a *red* or *bathochromic shift* in the absorption spectrum. (There are corresponding shifts in the fluorescence spectra and changes in the emission quantum yield.) A third possibility is that the transition dipoles are arranged in an oblique fashion. In this case the absorption band is split into two. These cases are shown in Fig. 1.22. Similar behaviour exists with larger aggregates. For historical reasons, if the shift is to longer wavelengths, these are termed *J-aggregates*. (After the scientist Edwin Jelley, who observed the effect with photographic dyes [50]. It was also reported independently by G. Scheibe [51].) *J*-aggregates frequently have very sharp absorption bands and show considerable potential in various functional dye systems [52]. The aggregates where there is a shift to shorter wavelengths are termed *H-aggregates* (after the *hypsochromic* or blue shift in the spectrum).

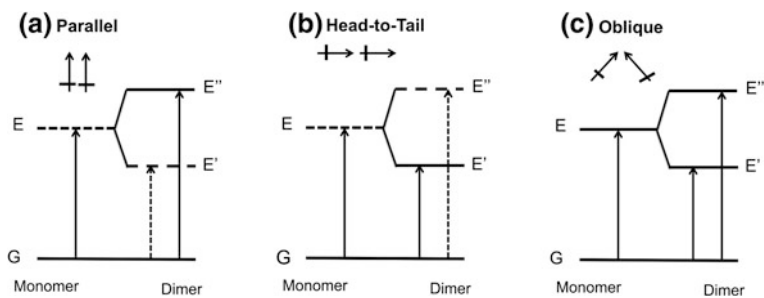


Fig. 1.22 Schematic exciton splitting and absorption probabilities for molecular dimers with different orientations of their transition dipole moments. Adapted from Ref. [49]

1.12.2.4 Absorption in the Solid-State

We need to distinguish absorption of: (1) isolated species held in a solid inert matrix; (2) solids in which all the molecules are those of the absorbing materials; (3) solids in which there is a mixture of components; and (4) semiconductor solids. In the first case, the electronic component of the absorption is usually similar to that in solution, but specific intermolecular interactions may enhance or reduce specific vibrational features. In the second and third cases, if the electronic orbitals remain localised on individual atoms/molecules then solid-state molecular absorption is generally similar to that in solution. However, if the close proximity of neighbouring molecules leads to overlapping molecular orbitals then ‘new’ transitions such as intermolecular charge transfer bands become possible. In addition, as discussed above there may be aggregation of chromophores, which will lead to red-shifts (*J-aggregates*) or blue shifts (*H-aggregates*).

The fourth case, semiconductor absorption, is different because here we are dealing with the transition between two bands only—valence and conduction. Semiconductor absorption is characterised by a cut-off wavelength at around the semiconductor band-gap, above which there is no absorption and below which absorption is highly efficient. The absorption profile around the band-gap wavelength may correspond to a sharp or shallow transition between no absorption and maximum absorption, depending on temperature and *impurities* or *dopants*. Dopant energy levels can act as electron–hole recombination sites, which may or may not be emissive, and they can also introduce new energy levels, which may become involved in absorption and emission. Blue and yellow diamonds are spectacular examples of this. In the former case, boron generates *acceptor* energy levels at just 0.4 eV above the valence band, giving rise to absorption in the IR and long wavelength region, which gives a blue cast to the stone, whereas nitrogen in the stone generates *donor* levels 4 eV below the conduction band, resulting in UV absorptions which tail out in the visible blue spectral region and hence give a yellow cast to the diamond [53].

The relationship between electron momentum in conduction and valence bands of semiconductors determines the coupling between the two states and the

radiation field, and hence the probability of optical absorption and emission. This behaviour, which arises from the conservation of momentum, is similar to the way the relationship between the molecular spin of two states in a molecular transition can give rise to spin-allowed and spin-forbidden optical transitions. Semiconductors in which electron wave momentum in conduction and valence bands match are termed *direct band-gap* semiconductors. These have strongly-allowed optical transitions, *i.e.* high absorption coefficients, they are highly coloured if the band gap lies in the visible, with relatively short radiative rate constants and thus short-lived excited states, which can be highly emissive following excitation. When momenta in conduction and valence bands do not match, the semiconductor is termed an *indirect band-gap* semiconductor. For these, optical transitions are forbidden, absorption coefficients are low, they have relatively long radiative lifetimes and therefore potentially long-lived excited states, and deactivation after excitation is not usually emissive. CdS, which is both a highly effective colorant and an emissive semiconductor used to make *quantum dots* (see [Chap. 4](#)), is a typical direct band-gap semiconductor, whereas silicon is a low absorbing indirect band gap semiconductor which, as a consequence, needs to be used in relatively thick sheets (tens of μm) in solar cells for effective absorption of solar radiation.

1.12.2.5 Temperature Effects on Absorption

The effect of reducing the temperature of molecules on absorption spectra is two-fold. Firstly, it shifts the population of those states in thermal equilibrium, *e.g.* vibrational and rotational states, and states in which a range of energies may be possible, by, for example, molecular torsion or interactions with solvent or neighbouring molecules, towards the lower energy levels. Secondly, and as a consequence of the first, the transfer of population from higher energy states to low energy states narrows the energy range of levels which are populated, and from which absorption can occur. This generally leads to a narrowing of absorption bands, and an increase in structure in the bands.

Lowering the temperature also reduces the rate of any process requiring activation energy, such as molecular motion and many equilibration processes, and it also increases solvent viscosity, which makes molecular collisions less frequent. A note of caution is required because a change in temperature can also shift the position of chemical equilibria, and, as it decreases solubility, it might also cause aggregation or precipitation of the solutes under study.

1.12.3 Multi-Photon Absorption

In a multi-photon process two, or more, low energy photons, are used rather than one high energy photon. This can be a great experimental advantage in areas such as biology and medicine if the medium absorbs strongly at the normal single

excitation wavelength. For example, blood absorbs strongly at wavelengths shorter than 630 nm. However, it is possible to excite chromophores within this region by two-photon excitation. Two 700 nm photons can be absorbed simultaneously to excite a molecule at 350 nm. This can be useful for both fluorescence microscopy and various types of phototherapy. It is possible to have simultaneous absorption of two photons of the same or different wavelengths to produce excited states of molecules. The energy is the sum of that of the two photons. This is a *non-linear* optical process [54], the probability of which depends both on the square of the light intensity and on properties of the molecules, such as the two-photon cross section.

1.12.4 Other Methods of Excitation

The creation of an excited-state requires energy and this energy can be supplied in various ways. For example, electrical discharge gives us electroluminescent materials. Excited-states may also be produced in chemical or biochemical processes. Interaction between high energy radiation and materials leads to ionisation, and in certain cases the subsequent charge recombination can lead to excited state formation and if the materials are light emitters, this leads to *radioluminescence*. Finally, certain solid materials may have trapped charges, which on heating may recombine, leading to excited state formation and *thermoluminescence*. These methods of excitation are discussed in more detail in [Chap. 4](#).

1.12.5 Consequences of Absorption/Excitation

The effect of absorption is to take an absorbing unit from one electronic state—usually the ground-state—into a higher electronic state. For normal experimental conditions, with an ensemble of absorbers, all with somewhat different energies, the absorption process selectively excites those ground-states for which absorption is most efficient. In a mixture of chemical species this selectivity, usually obtained by choice of excitation wavelength, is often used to excite only one of the chemical species present. If a suitably narrow excitation bandwidth is used, it is even possible to excite specific isotopes in gas-phase isotopic mixtures, as in laser isotope separation. Selectivity can also be introduced by use of polarised excitation light, such that only absorbing species with transition moments along the polarisation axis are excited. Selective excitation has, as a necessary corollary, selective depletion of the ground-state. Thus, it is possible to remove a detectable fraction of ground-state molecules of a particular energy, and/or polarisation, in a process termed *hole-burning*; the value of hole-burning experiments is in the study of the bulk relaxation back to the equilibrium distribution of states, from which information on molecular motion and energy exchange can be gleaned.

It is unusual for the equilibrium nuclear arrangement in an excited-state to be exactly the same as that for the ground-state. Excitation of bonding electrons into anti- or non-bonding orbitals means a reduction in bond order of the excited-state compared to the ground-state, and an associated lengthening of one or more bonds; excitation of antibonding electrons into bonding or non-bonding orbitals has the opposite effect; while excitation of non-bonding electrons generally has a lesser effect, depending on the higher energy orbital populated. The absorption and emission of a photon occurs on the timescale of femtoseconds, while the timescale for nuclear movement, vibrations and rotations is *ca.* 100–1000 times longer. Therefore absorption and emission occur while the nuclear arrangement is fixed and, since the molecular coordinates cannot change in such a short transition time, these are ‘*vertical transitions*’ on potential energy diagrams, which often initially generate vibrationally excited states. However, unless very short lived, the excited-state has enough time to explore the various energetically available nuclear configurations, *i.e.* molecular rotations, torsions, vibrations etc. within the molecule in the excited-state. Furthermore, unless the molecule is isolated, neighbouring molecules, solvent molecules etc. will also respond to the electronic change in the absorbing molecule. So that, within a short time of excitation the excited-state and surroundings relax to a new *pseudo*-equilibrium nuclear arrangement, and it is usually from this thermally relaxed excited-state that subsequent photochemical and photophysical processes occur. These changes in molecular arrangement, and the spectroscopic consequences are shown in Fig. 1.23.

A common situation found in condensed phases under illumination is for all levels, except electronic levels, to be thermally equilibrated. Thus, under constant illumination, the sample is a mixture of thermally/vibrationally-equilibrated ground-state(s) with a very small, non-Boltzmann population of the excited electronic state, but which is itself thermally and vibrationally Boltzmann distributed. So the situation is similar to two non-equilibrated chemical species each of which is thermally equilibrated: a thermally equilibrated ground-state, and a thermally equilibrated high energy excited-state.

The electronic configuration/distribution is different in the excited-state compared to the ground-state and therefore the chemical nature of the excited electronic state is also different. This leads to differences in chemical reactivity, redox activity, charge distribution, pK_a equilibria, and in semiconductors and conjugated polymers particularly, electron and energy mobility.

1.13 Deactivation of Excited States

1.13.1 Deactivation Pathways: The Jablonski Diagram

A summary of the possible deactivation routes for typical organic and inorganic molecules, semiconductors, and atoms in crystal matrices is shown in Fig. 1.24. Such diagrams are often referred to as *Jablonski diagrams* after the Polish

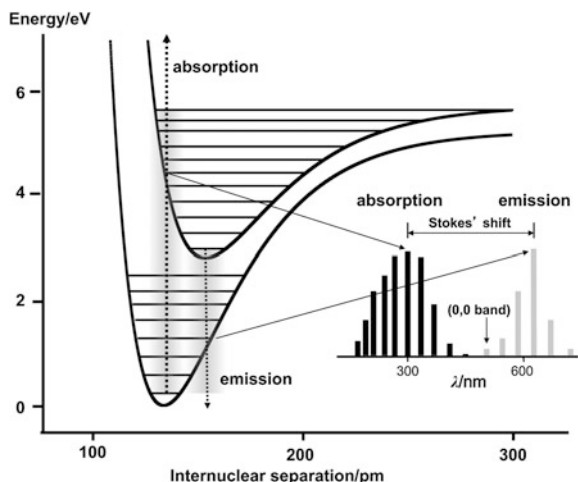


Fig. 1.23 Influence of changes in equilibrium nuclear geometry on absorption and emission. In this extreme example the excited state has a significantly longer bond length than the ground state. Absorption occurs from the first vibration level of the ground state, across the range of nuclear coordinates represented by the vertical transitions in the *grey band*. In the excited-state these nuclear coordinates correspond to a compressed bond, so absorption is into highly vibrationally excited levels of the excited state. These quickly relax to the lowest vibrational level of the excited state. Emission occurs from the first vibration level of the ground state, across the range of nuclear coordinates represented by the vertical transitions in the *grey band*. In the ground state these nuclear coordinates correspond to a stretched bond, so emission is into vibrationally excited levels of the ground state. As a consequence, the emission spectrum is at lower energy, longer wavelength, than the absorption spectrum. This difference in energy is called the *Stokes shift*. The closer the ground and excited state geometries, the smaller the Stokes shift. The vibrational spacing in the absorption spectrum corresponds to excited-state vibrations; that in emission corresponds to ground state vibrations. The 0,0 band corresponds to the electronic transition when both states are in their lowest vibrational energy

physicist Aleksander Jabłoński. The Jablonski diagram shows the electronic states and their relative energies, which are typically singlet (S_0, S_1, \dots, S_n) and triplet (T_1, T_2, \dots) electronic states of increasing energy for most organic molecules. The vibrational levels associated with each electronic state are also shown and are denoted as $v = 1, 2$ etc. For simplicity, only the excited-state primary relaxation pathways are illustrated here—a more detailed Jablonski diagram may be found in Fig. (15.1). An important distinction is made between processes involving radiative deactivation, *i.e.* emission, and those which are radiationless. Radiative transitions are shown as straight vertical arrows, while non-radiative transitions are represented by wavy horizontal, *i.e.* isoenergetic, arrows. Note, that neither absorption nor radiative relaxation are restricted to transitions to the lowest vibrational level of an electronic energy state, so that both ground and excited states may be populated as vibrationally ‘hot’ states from radiative transitions.

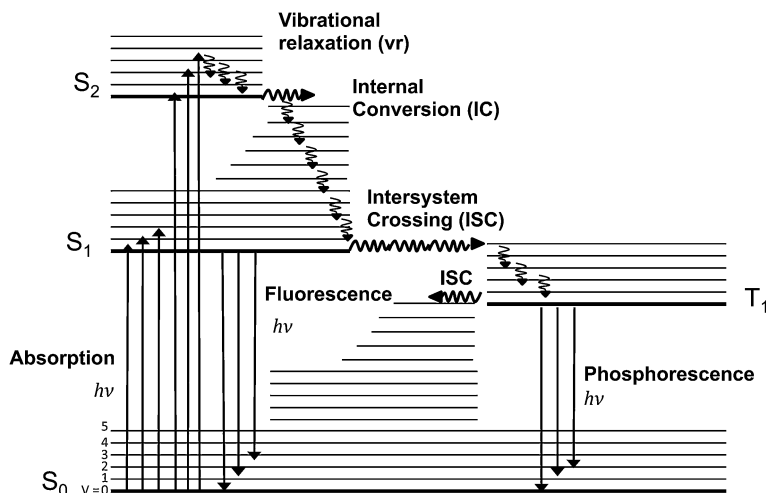


Fig. 1.24 Simple Jablonski diagram illustrating the primary deactivation processes occurring upon excitation

1.13.2 Radiative Decay Processes: Stimulated Emission, Fluorescence and Phosphorescence

Radiative decay is the inverse of absorption and requires coupling of the two states *via* either an incident photon, which results in *stimulated emission*, or the constantly fluctuating radiation field, which results in *spontaneous emission*. The radiative lifetime is also the inverse of the Einstein A coefficient. This can be calculated from the integrated molar absorption coefficient in the absorption spectrum using the *Strickler–Berg relationship* [55].

The transition probabilities for both stimulated and spontaneous emission are linked to the transition probability for absorption, such that a transition that is highly allowed in absorption will be highly allowed in emission, and one forbidden in absorption will be forbidden in emission. The transition probability for stimulated emission is exactly the same as that for absorption, and the ratio of the rates of absorption and stimulated emission is given simply by the ratio of the ground and excited state populations. Thus, for electronic transitions for systems in thermal equilibrium at room temperature, absorption dominates; at a high enough temperature to give essentially equal populations (see Boltzmann Eq. 1.16) the rates of absorption and stimulated emission will be approximately equal, although absorption is always slightly more probable than stimulated emission; and for those non-equilibrium cases, where the population of the higher state exceeds that of the lower, which is the condition of a population inversion, stimulated emission will dominate and the system will lase (see Sect. 14.4.2.4).

The transition probability for spontaneous emission shows that the rate of spontaneous emission depends linearly on the oscillator strength for the absorption

and the cube of the emission frequency (Eqs. 1.21 and 1.30). Thus, spontaneous emission is a much faster process for high frequency transitions than low frequency transitions, all other things being equal. Also, because of the spin selection rule, oscillator strengths for radiative transitions between states of the same spin multiplicity, *i.e.* fluorescence, are much higher than those for radiative transitions between states of different spin multiplicity, *i.e.* phosphorescence, and therefore radiative rates are much higher for fluorescence than phosphorescence.

Fluorescence lifetimes for strongly absorbing transitions in the visible are typically a few ns; those for symmetry-forbidden fluorescence transitions, such as found with symmetrical polyaromatics can be hundreds of ns. Radiative lifetimes for phosphorescence, in the absence of any heavy-atom relaxation of the spin selection rule, can be as long as many minutes, while systems with some relaxation of the rule typically show phosphorescence radiative lifetimes of microseconds (μs) to milliseconds (ms).

Direct semiconductors have strongly allowed optical transitions, with relatively short radiative rate constants and thus short-lived excited states, which can be highly emissive following excitation. For indirect semiconductors optical transitions are forbidden, absorption coefficients are low, they have relatively long radiative lifetimes and therefore potentially long-lived excited states, and deactivation after excitation is not usually emissive.

1.13.3 Non-Radiative Processes

All non-radiative electronic processes are isoenergetic transitions to another electronic state, which may or may not be the ground state. This other state may be localised on the same molecule, or on molecules produced by unimolecular chemical reaction from the excited-state; or the process may involve interaction with states on another system which acts as a quencher of the excited-state, e.g. by energy transfer or bimolecular reaction. (The resultant electronic state(s) may themselves deactivate non-radiatively or radiatively, e.g. the phosphorescence from a triplet state formed from a higher singlet, emission from *excimers* and *exciplexes* formed from ground-state excited state interaction (see Sect. 1.13.5.5), or emission from quencher states produced by energy transfer or chemical reaction.)

1.13.3.1 Internal Non-Radiative Processes

In an isolated molecule, non-radiative processes are not a deactivation of energy, but rather a redistribution of energy within the molecule to give a more probable distribution within the rotational, vibrational and electronic energy levels available; a distribution which, for any individual molecule, will itself be constantly changing, as nuclei and electrons move within the molecular framework. For energy to be lost non-radiatively, there must be a mechanism for loss of energy to

other molecules or the surroundings. In gas and solution phases this is usually *via* collisions, in the solid-state it is to thermal/vibrational states of the solid material. In solution, the frequency of collision with solute is of the order of picoseconds, and therefore thermal equilibration of vibrational states, *i.e.* the relaxation of non-Boltzmann high-energy vibrational states, *vibrational relaxation*, is usually faster than all but the fastest photophysical processes (see Chaps. 3 and 15 for examples where it is not). Hence, population of a higher vibrational level of an electronic state is almost immediately followed by rapid deactivation ($\sim 10^{-14}$ – 10^{-11} s) to the lowest vibrational level of that state. In gases at moderate pressures, collision frequencies are of the order of ns–ps, but at low temperature and low pressures collisional deactivation in gases can be very much slower than photophysical processes.

1.13.3.2 Internal Conversion, Intersystem Crossing and Vibrational Relaxation

Internal conversion (IC) is the transition to a state of the same spin multiplicity, while *intersystem crossing* (ISC) is the transition to a state of different spin multiplicity; in both cases the transition is often to high vibrational levels of the final state. Internal conversion and intersystem crossing are normally immediately followed by vibrational relaxation (vr) to the lowest vibrational level of the new electronic state. IC is usually very fast from S_n to S_1 , and from T_n to T_1 , and this along with fast vibrational relaxation is the basis of *Kasha's rule*—that emission occurs from the lowest excited-state of a given multiplicity [56]. Conservation of angular momentum requires a mechanism to exchange the electron spin angular momentum for orbital angular momentum during intersystem crossing. Overlap of the vibrational wavefunctions of any two electronic states decreases rapidly as the energy difference between the zero point vibrational levels of the states increases. Because of this, the rate of non-radiative processes decreases rapidly as the energy gap between the two electronic states increases. This means that non-radiative processes are fastest between states which are close in energy, and slowest between states which are very different in energy. This effect of the energy gap between states on the rate of non-radiative processes is called the 'energy gap law'.

1.13.3.3 Unimolecular Chemical Reactions

Ionisation, *dissociation* and *isomerisation* are the three unimolecular reactions possible following absorption. Ionisation requires excitation with enough energy for electron ejection (electron transfer also leads to ion formation but this is a different process where an electron is transferred to another molecule).

Bond breaking in the excited-state can result in dissociation and isomerisation. Dissociation is quite common for small molecules, where breaking a single bond is

sufficient to break the molecule. For example, hydrogen peroxide on photolysis can *photodissociate* to form two hydroxyl radicals:



For larger molecules held together by a network of bonds, and where transitions are more delocalised, photodissociation is less likely, but isomerisation, made achievable by bond breakage, is possible, e.g. breakage of one bond in a double bond can lead to *cis-trans* isomerisation, such as the *cis-trans* isomerisation of retinal in the photochemical step in vision (Fig. 1.1). Breakage of a single bond in ring structures can lead to ring opening, as in the spiropyran photochromics, which are discussed in detail in Chap. 4.

1.13.4 Competition Between Decay Routes and Quantum Yield

All deactivation processes are competitive, so the rate constant for decay of the excited state, k_{obs} , (the *observed* decay rate constant) is given by the sum of rates for all deactivation processes, *i.e.* if all decay routes are first order process:

$$k_{\text{obs}} = \sum k_{\text{deactivation}} \quad (1.32)$$

The *quantum yield* of a process, event or reaction x , ϕ_x , relates the rate of photon absorption with the rate of any process of interest, and by integration of these over time, also gives the ratio of the total number of events of interest to the total number of photons absorbed, *i.e.*

$$\phi_x = \frac{(\text{total number of processes, events or reaction, } x)}{(\text{total number of photons absorbed})} \quad (1.33)$$

According to the *Stark-Einstein law*, ϕ_x should be equal to unity or less. However, if secondary processes occur, ϕ_x can sometime be greater than 1. Under continuous illumination, a steady-state will be reached, such that the rate of excited-state formation, J_{abs} , will be equal to the rate of deactivation by all intramolecular processes, J_{total} , *i.e.*

$$J_{\text{abs}} = J_{\text{total}} \quad (1.34)$$

If we consider the vibrationally-relaxed S_1 excited-state in Fig. 1.24 as an example, the competing intramolecular photophysical process that can lead to its relaxation are fluorescence, internal conversion and intersystem crossing, and J_{total} is given by:

$$J_{\text{total}} = -d[\text{S}_1]/dt = (k_{\text{F}} + k_{\text{IC}} + k_{\text{ISC}})[\text{S}_1] = k_{\text{total}}[\text{S}_1] \quad (1.35)$$

where k_F , k_{IC} , k_{ISC} are the first-order rate constants for fluorescence, internal conversion and intersystem crossing, respectively. Solution of Eq. 1.35 gives:

$$[S_1]_t = [S_1]_0 \exp(-t/{}^1\tau) \quad (1.36)$$

where $[S_1]_0$ and $[S_1]_t$ are the concentration of excited S_1 states at time $t = 0$ (*i.e.* immediately after excitation) and time t following excitation, respectively and ${}^1\tau$ is the *excited-state lifetime*. Time-resolved fluorescence is a convenient technique by which the lifetime of the excited-state may be measured (see Chaps. 14 and 15 for experimental details). Note that ${}^1\tau$ is the excited singlet-state lifetime in the presence of *all* intramolecular deactivation pathways, *i.e.*

$${}^1\tau = 1/(k_F + k_{IC} + k_{ISC}) = 1/k_{\text{total}}. \quad (1.37)$$

In the absence of radiationless decay, the *radiative lifetime* ${}^1\tau_0$ is given by:

$${}^1\tau_0 = 1/k_F. \quad (1.38)$$

The *fluorescence quantum yield*, ϕ_F , of a material will often determine its suitability for a given application, for example ϕ_F should be high for display technology (Chap. 4) but low for solar cells (Chap. 7). The experimental determination of ϕ_F (and other quantum yields) is discussed in Chap. 15. From Eqs. 1.33 and 1.34, ϕ_F is given by:

$$\phi_F = J_F/J_{\text{abs}} = J_F/J_{\text{total}} \quad (1.39)$$

where J_F is the rate of fluorescence. This may be rewritten as:

$$\phi_F = k_F[S_1]/k_{\text{total}}[S_1] = k_F/k_{\text{total}}. \quad (1.40)$$

Since $k_F = 1/{}^1\tau_0$ and $k_{\text{total}} = 1/{}^1\tau$:

$$\phi_F = {}^1\tau/{}^1\tau_0. \quad (1.41)$$

1.13.5 Bimolecular Interactions, Quenching and Energy Transfer

So far we have only considered the *intramolecular* processes which may lead to the deactivation of an excited state. *Intermolecular* excited-state relaxation is also possible. Any molecule or substance which upon interaction with an excited-state leads to an increase in the rate of relaxation is known as a *quencher*. The quencher may either be the same chemical species as the excited-state itself (*self-quenching*) or a different one.

1.13.5.1 The Nature of the Quenching Processes

The first distinction comes between *short range quenching*, where overlap of the orbitals of the quencher and excited-state molecule of interest is required, and *long range quenching*, where there is a through space coupling between the deactivating transition of the excited-state being quenched and an excitation transition on the quencher molecule. Quenching can also be classified by whether or not a chemical change is caused; if there is, it is *chemical quenching*, if not, it is *physical quenching*.

1.13.5.2 Long range dipole–dipole quenching: Förster Resonance Energy Transfer (FRET)

Energy can be exchanged between molecules at a significant intermolecular separation by a process in which the transition dipole moments on the two molecules couple through space. This was first observed by Franck and Cario between excited mercury and thallium atoms in the gas phase [57], and subsequently studied for molecules in condensed phases by Förster [58, 59]. The process is commonly termed *Förster Resonance Energy Transfer* (FRET). It involves dipole–dipole coupling between electronic energy donor and acceptor, as represented schematically in Fig. 1.25. The rate constant, k_{FRET} , can be calculated from the spectral properties of the donor and acceptor, their separation, and their relative orientations:

$$k_{\text{FRET}} = K_{\text{FRET}} \phi_{\text{D}} J_{\text{AD}} \kappa^2 / n^4 \tau_{\text{D}} R_{\text{DA}}^6. \quad (1.42)$$

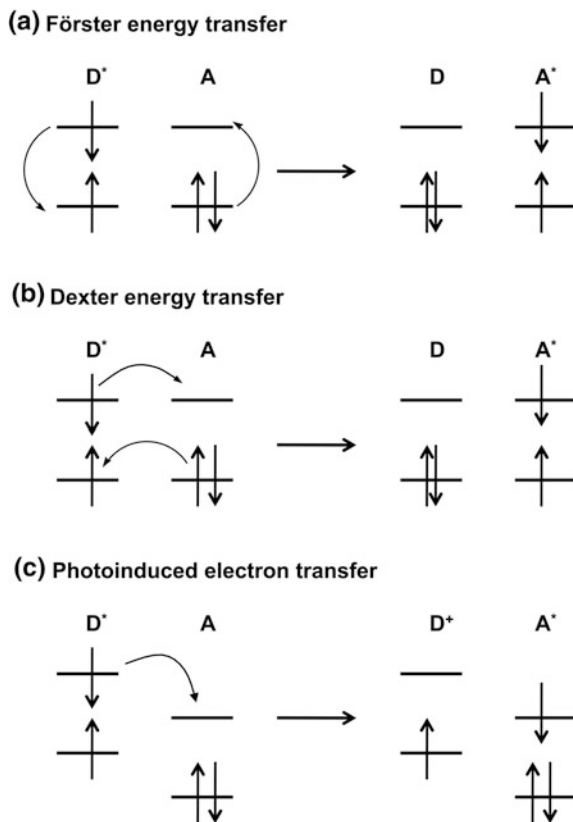
Here, K_{FRET} is a collection of various constants, ϕ_{D} is the donor emission quantum yield; J_{AD} is the overlap integral between the emission spectrum of the donor and the absorption spectrum of the acceptor; κ^2 is the dipole orientation factor, which depends upon the relative orientations of donor and acceptor; n is the refractive index of the medium; τ_{D} the observed donor lifetime (note that $\phi_{\text{D}}/\tau_{\text{D}}$ is the radiative rate constant of the donor) and R_{DA} is the donor acceptor separation.

The efficiency of FRET is often represented by the Förster distance (R_0), which is that separation at which the rate of FRET is equal to all other decay rates of the donor, *i.e.* when 50 % of the initial excitation energy will be transferred to the acceptor. The rate constant for FRET at any separation R is then given by:

$$k_{\text{FRET}} = (1/\tau_{\text{D}})(R_0/R)^6. \quad (1.43)$$

Energy transfer is an isoenergetic process, hence the requirement for donor emission and acceptor absorption band overlap. J_{AD} is calculated from the area of the overlap of the emission spectrum, normalised to an area of 1 and plotted in frequency (usually cm^{-1}) rather than wavelength, with the absorption spectrum, plotted in terms of ϵ vs frequency. In addition, FRET is most commonly encountered when both transitions are highly allowed, *e.g.* in singlet–singlet energy transfer these conditions are met by a high donor radiative decay rate

Fig. 1.25 Orbital comparison of long- and short-range quenching of an excited state (D^*) and a ground state acceptor (A) by **a** Förster energy transfer (long-range), **b** Dexter energy transfer (short-range) and **c** photoinduced electron transfer (short range)



constant, and large J_{AD} arising from a high acceptor ϵ . However, it is possible for the donor transition to be forbidden and FRET to still be *efficient*, even if not *fast*, provided the long lifetime of the donor is sufficient to compensate for the reduction in the rate of FRET; thus triplet–singlet FRET is possible. Singlet–triplet and triplet–triplet FRET are so slow that they are unimportant processes. Table 1.7 gives FRET distances for typical donor–acceptor pairs of molecules. FRET is characterised by a reduction in both the donor emission quantum yield and donor lifetime. However, if donor–acceptor distances are fixed, but not equal, then each different donor–acceptor distance must be considered a different population for kinetic analysis.

1.13.5.3 Short Range Quenching: Static and Dynamic Quenching, Perturbation, Electron Transfer and Dexter Quenching

In these processes the two molecules must be at (or able to approach each other to) the relatively short distances required for orbital overlap. This requires approach to

Table 1.7 Förster energy transfer distances for some typical donor–acceptor pairs

Donor	Acceptor	R_0/nm
Anthracene	Rhodamine 6G	2.51 ^a
Benzene	1,3,5-triphenylbenzene	1.93 ^b
Biphenyl	Naphthalene	1.09 ^b
Biphenyl	2-Phenylnaphthalene	2.81 ^b
Indole	Rose Bengal	2.65 ^a
Naphthalene	Quinine sulfate	2.50 ^a
Naphthalene	Rhodamine 6G	2.44 ^a
Pyrene	Uranine (fluorescein)	3.00 ^a
p-Terphenyl	1,4-bis(5-phenyloxazol-2-yl) benzene (POPOP) ^c	4.21 ^b

Data taken from Ref. [60]. The structures and photophysical data for many of these molecules can be found in [Chap. 4](#)

^a In ethanol solution

^b In cyclohexane solution

^c 1,4-bis(5-phenyloxazol-2-yl) benzene

typically $\sim 200\text{--}500$ pm. If close approach is obtained by molecular diffusion, or energy or exciton migration, then the lifetime of the excited-state, concentration of quencher, and diffusion rate, are key parameters in determining the efficiency of quenching. Thus the much longer lifetime of the triplet-state compared to singlet-state means that collisional triplet quenching can be very effective in typical non-viscous solvents even at low ($\sim 10^{-6}$ mol dm⁻³) quencher concentrations, whereas diffusional collisional quenching of singlets in typical non-viscous solvents requires quencher concentrations of $\sim 10^{-2}$ mol dm⁻³.

The second-order rate constant for diffusion-controlled reactions, k_{diff} , depends on the viscosity (η , in mPa s) according to the Smoluchowski equation:

$$k_{\text{diff}} = 8RT/3\eta. \quad (1.44)$$

The diffusion-controlled rate constant in water ($\eta = 0.890$ mPa s) is 7.4×10^9 mol⁻¹ dm s⁻¹; values in a variety of solvents are given in the literature [34]. This equation is valid for reaction between neutral species of the same size. The effect of charge and size is discussed in standard textbooks on chemical kinetics [61]. Diffusional quenching is often termed *dynamic quenching* because it involves movement. The effect of dynamic quenching is a reduction in both the quantum yields of competing processes, such as emission from the donor, and the lifetime of the donor excited-state.

If close approach is obtained by a random distribution of quenchers in a fixed matrix then the excited-state lifetime is somewhat less important. The rate depends on orbital overlap, and this decreases exponentially with distance, so only those donors with a neighbouring acceptor will be quenched, and these quenched very quickly, while those without a neighbouring quencher will remain unquenched. This leads to the condition of *static quenching* in which the quantum yields of competing processes, such as emission from the donor, are reduced by very fast

quenching of a certain fraction of donors, but the lifetime of the unquenched donor remains the same as in the absence of quencher.

Three mechanisms of short range quenching can be identified: perturbation, electron transfer, and energy transfer.

Perturbation quenching. Here, orbital overlap allows some property of the quencher molecule to be shared with the donor excited-state. Heavy-atom quenching and paramagnetic quenching are of this type. In heavy-atom quenching orbital overlap with a heavy atom quencher introduces an element of spin-orbit coupling into the orbitals of the excited-state donor and provides a mechanism for deactivation *via* otherwise spin-forbidden routes, notably intersystem crossing. Paramagnetic quenching is similar, but here the quencher is a paramagnetic ion and it is the unpaired spins on the quencher which introduce otherwise spin-forbidden deactivation routes.

Electron transfer quenching. Here, orbital overlap allows transfer of an electron between the two molecules. As discussed earlier a molecule in an excited state is simultaneously a better oxidant and reductant than the ground-state, and a quencher with a HOMO or LUMO at the correct energy, which can overlap with either the HOMO or LUMO of the excited-state will act as an electron transfer quencher (see Fig. 1.25). The requirement for electron transfer quenching is overlap of two orbitals, one from each participant. Transfer is most rapid, and quenching most efficient, for those cases in which there is little nuclear rearrangement required in moving from neutral to oxidised/reduced species. The theory of rates of ground state electron transfer reactions has been comprehensively developed notably by Rudolph Marcus [62], and similar considerations apply to excited-state electron transfer. A detailed description is given in Chap. 15 of Ref. [61].

Collisional energy transfer quenching. In this case, simultaneous exchange of two electrons occurs, requiring overlap of two pairs of orbitals, and orbital overlap criteria are more demanding than for electron transfer quenching [63] (Fig. 1.25):



The process is often referred to as Dexter energy transfer, after David L. Dexter who, following on from earlier work by Förster, developed a detailed quantitative description of the various coupling mechanisms involved in electronic energy transfer [64]. The relevant equation in its simplest form is:

$$k_{\text{DEX}} = K_{\text{DEX}} J \exp(-2R_{\text{DA}}/L) \quad (1.46)$$

The key term is usually the exponential in which R_{DA} is the mean distance between the donor and acceptor, and L is the sum of their van der Waals radii, so the rate constant decreases exponentially with increasing D-A separation and Dexter energy transfer is only efficient when A and D are close. k_{DEX} cannot, generally, be so easily related to spectral features as is possible for Förster energy transfer, and K_{DEX} is a constant which usually has to be determined experimentally. Note that there are no constraints on the ‘allowedness’ of either D or A

transitions, all that is required is energy conservation (*i.e.* an isoenergetic energy transfer) and overall spin conservation, so transitions to and from all multiplicities are possible: singlet–singlet, singlet–triplet, triplet–singlet, and triplet–triplet, and other combinations of D and A multiplicities, are all possible. J_{DEX} is termed the *normalised spectral overlap integral* (*cf.* J_{AD} for FRET) and corresponds to the overlap of the emission spectrum of the donor and absorption spectrum of the acceptor, given in cm^{-1} , with *both* normalised to an area of 1. The term spectral overlap may seem something of a misnomer when describing Dexter energy transfer, since the process is possible between species for which spectral data for the transition(s) is impossible to obtain, such as highly forbidden $S \leftrightarrow T$ transitions where neither absorption nor emission can be detected. The importance of the spectral overlap term, however, is that it gives an estimate of the probability of *energy matching* for the transitions on D and A. Where spectral data are not available, estimation of the transition energies for transitions on A and D can be used to assess whether energy transfer will occur or not. Generally, the relatively high *density of states* for molecules means that energy matching is not limiting for molecular energy transfer where the change in electronic energy on A is lower than that on D. For atoms, which have a low density of states, energy matching can limit k_{DEX} , although for atoms in solids, energy matching can be enhanced if the electronic transition is coupled with lattice phonon transitions, the solid effectively generating higher densities of states than are present in isolated atoms.

It is important to note that the Dexter and Förster models involve a number of simplifications, in particular in treating the systems as involving point dipoles. More recent theoretical studies have concentrated on overcoming these limitations [65, 66].

1.13.5.4 Quantification of the Quenching Process: The Stern–Volmer Relationship

Quenching, by any of the mechanisms outlined above, will also compete with the various intramolecular photophysical relaxation routes that deactivate the excited-state. The presence of quenching, therefore, will lead to a reduction in the luminescence intensity (fluorescence or phosphorescence), which is related to the quencher concentration [Q] by the Stern–Volmer equation [67]:

$$\frac{I^0}{I} = 1 + k_{\text{SV}}[\text{Q}] \quad (1.47)$$

where I^0 and I are the luminescence intensity (at a given wavelength) in the absence and presence of the quencher at concentration [Q], respectively and k_{SV} is the *Stern–Volmer constant*. For *dynamic* quenching, k_{SV} is related to the bimolecular quenching rate constant, k_{q} , and the excited-state lifetime: $k_{\text{SV}} = k_{\text{q}}\tau$.

For dynamic quenching, the Stern–Volmer relationship may also be described in terms of the excited-state lifetime:

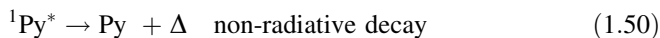
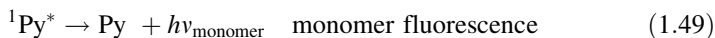
$$\frac{{}^1\tau^0}{1\tau} = \frac{I^0}{I} = 1 + k_{SV}[Q] \quad (1.48)$$

where ${}^1\tau^0$ is the excited-state lifetime in the absence of the quencher (note this is not usually the same as the radiative lifetime). For dynamic quenching, the *Stern–Volmer plot* of I^0/I (or ${}^1\tau^0/1\tau$) against $[Q]$ is linear with a slope k_{SV} and an intercept of 1. (Note: eq. 1.48 is also true for dynamic quenching of triplet states, *i.e.* ${}^3\tau^0/{}^3\tau$). Steady-state and time-resolved luminescence measurements should yield identical Stern–Volmer plots for dynamic quenching (within experimental error). The relationship between the intensity and the quencher concentration provides a convenient method of accurately determining the quencher concentration (for a pre-calibrated system) by measuring the luminescence intensity. Luminescence quenching is therefore often exploited to develop optical sensors and probes, which are discussed in more detail in [Chap. 12](#).

Static quenching will also lead to a decrease in the luminescence intensity and is described by Eq. 1.47. In this instance, k_{SV} may be considered to be an indicator of the extent of the lumophore–quencher interaction, and often fits Eq. 1.47 especially at low to moderate quenching efficiencies. As described above, static quenching leads to very fast luminescence quenching of only a certain fraction of donors, and the lifetime of the unquenched donor is unchanged. Since ${}^1\tau^0/1\tau = 1$ for static quenching, Eq. 1.48 does not hold, and therefore combined steady-state and time-resolved luminescence experiments can be used to provide insight into the quenching mechanism. It is very common, however, that the observed quenching will arise from a combination of both static and dynamic mechanisms.

1.13.5.5 Excimers and Exciplexes

In addition to the above processes, it is possible to form new transient species by reaction between an atom or molecule in the excited state and another in the ground state. Studies of pyrene (Py) showed that in dilute solutions only a single structured band in the 350–450 nm region was observed (Fig. 1.26). However, at high concentrations, a new, unstructured band was seen around 460–470 nm in addition to the structured short range emission [68]. There were no corresponding changes in the absorption spectrum. This was attributed to the formation of dimers, which were later termed *excimers* (**EXC**ited state **diMERS**) [69]. The general scheme for excimer formation and decay in the pyrene excited singlet state is:



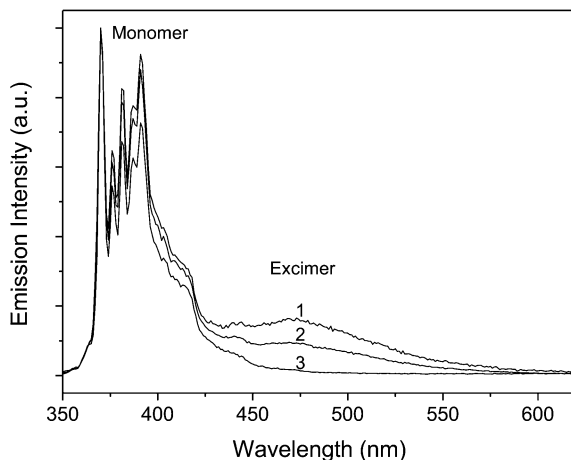
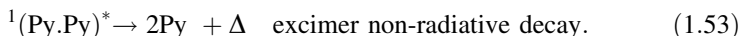
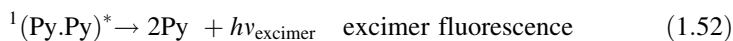


Fig. 1.26 The effect of concentration on the emission spectrum of pyrene in air-equilibrated ethanol for $\lambda_{\text{exc}} = 330$ nm. The spectra are normalised to the 372 nm peak and the concentrations are: (1) 1×10^{-3} mol dm $^{-3}$; (2) 1×10^{-4} mol dm $^{-3}$; (3) 1×10^{-5} mol dm $^{-3}$. In dilute solution, a structured emission band between 350 and 450 nm is observed, which is assigned to the pyrene monomer. As the pyrene concentration is increased, a broad emission band between 425 and 550 nm emerges, which is attributed to emission from the pyrene excimer. The monomer to excimer ratio is dependent on both pyrene concentration and the excited state lifetime, which is reduced here due to oxygen quenching. Degassing of the solution to remove oxygen would result in an increase in the relative intensity of the excimer emission band

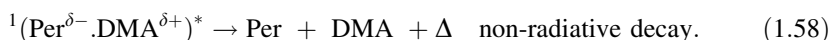
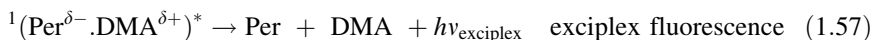
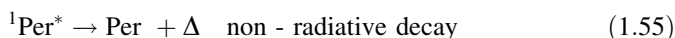
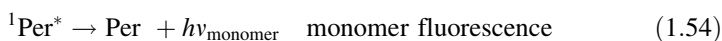


Detailed kinetic analysis of excimer formation has been carried out, in particular by Birks [70] and is discussed in more detail in [Chap. 15](#). Excimer formation is not restricted to pyrene, and is relatively common among aromatic hydrocarbons. It is also observed in other systems, and was detected with helium two decades before its observation in aromatic molecules [71]. The electronic configuration of the *noble gas* (Group 18) elements precludes their formation of stable ground state dimers. However, excimer formation is possible. As described earlier, stimulated emission normally requires a population inversion, where more molecules are present in an upper energy state than in a lower energy one, and because the ground state in noble gas dimers is dissociative, these systems show excellent conditions for stimulated emission and lasing. Noble gas lasers are particularly valuable for emission in the deep ultraviolet, and have been developed for xenon (172 and 175 nm), krypton (146 nm) and argon (126 nm).

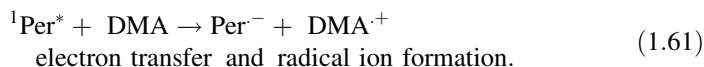
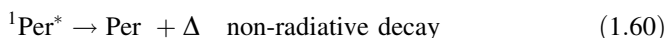
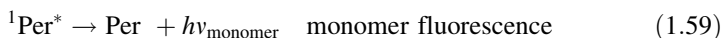
Extensive studies were also carried out in the 1950s and 1960s on mixed excimers involving two different molecules forming excited state complexes. During this period, Weller, who had collaborated extensively with Förster, noted

an excimer type emission when dimethylaniline (DMA) was added to solutions of the aromatic hydrocarbon perylene (Per) in non-polar solvents [72]. However, the properties differed significantly from that of a mixed excimer, and in polar solvents (such as acetonitrile), no emission was observed, but flash photolysis experiments revealed production of the perylene radical anion and dimethylaniline radical cation [73]. (The experimental technique of flash photolysis is described in more detail in Chaps. 8, 14 and 15). The formation of these charged species in polar solvents suggested that the complex formed in non-polar solvents must possess a considerable charge transfer character. Similar findings were obtained independently by a number of other groups, notably that of Mataga [74]. The species formed in non-polar solvents is termed an *exciplex* (**EXC**ited state charge transfer **COMPLEX**), and plays an important role in many excited state processes. The general scheme for interaction between excited perylene and dimethylaniline in non-polar and polar solvents is given below:

Non-Polar Solvents



Polar solvents

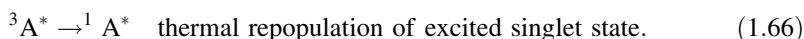
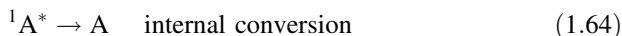
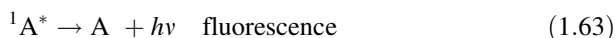
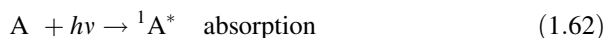


It is possible to have excited states in which electron donor and acceptor groups are present within the same molecule, if the donor and acceptor groups are orthogonal [75]. These so called twisted intramolecular charge transfer (TICT) states may be relevant in excited processes of these highly polar species.

1.13.5.6 Delayed Fluorescence

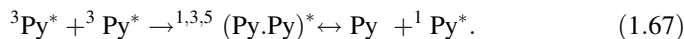
Fluorescence typically has luminescence lifetimes in the ns range, whereas phosphorescence has lifetimes of ms, seconds or even longer. However, sometimes luminescence is observed with a spectrum identical to that of fluorescence, but

with much longer lifetime. This is due to *delayed fluorescence*, in which a molecule excited to its singlet state forms its triplet state through intersystem crossing, but these can then repopulate the singlet state. The lifetime of this emission is, therefore, determined by that of the triplet state [76]. Two distinct mechanisms are involved. In *E-type* delayed fluorescence (named after the dye *eosin*), the energy separation between the lowest singlet and triplet states is small (of the order of the thermal energy $k_B T$). Photoexcitation initially produces the singlet state, which can undergo normal fluorescence ($\phi_F \sim 0.19$ for eosin), form the triplet state ($\phi_T \sim 0.71$), or decay by internal conversion. However, since the energy between the triplet state and lowest singlet state (*i.e.*, the *singlet–triplet splitting*) is small, thermal energy is sufficient to repopulate the singlet excited state, which can then decay by delayed fluorescence. The scheme for E-type delayed fluorescence is given below:



The decay of E-type delayed fluorescence will depend upon the triplet state lifetime, but thermal repopulation indicates that the probability of this type of delayed fluorescence will increase with increasing temperature. The temperature dependence therefore gives an excellent method for confirming this mechanism. E-type delayed fluorescence is observed in various dye molecules and is also seen with fullerenes, such as C_{70} [77].

A second mechanism of delayed fluorescence was first observed with pyrene (Py), and is, hence, termed *P-type* delayed fluorescence. In this case, the interaction between two molecules in their excited triplet state can lead to an excited singlet state [78] as indicated below:



The reaction is termed *triplet–triplet annihilation* (it is similar to the formation of singlet oxygen by ground state triplet oxygen quenching of triplet states—see Chap. 15). The singlet excited state can then decay by fluorescence, but with the lifetime determined by that of the triplet state. This mechanism requires having a sufficiently high concentration of triplet states, which depends upon the excitation light intensity (I). Normally, the intensity of P-type delayed fluorescence is proportional to I^2 . This process is important in laser-induced excitation of fluorescence in solution, and is also observed in organic crystals [79], where efficient exciton

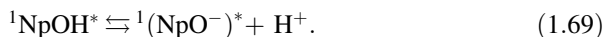
energy migration is possible. Both intrachain and interchain triplet–triplet annihilation and delayed fluorescence are also possible with conjugated polymers [80], and may be used to increase efficiencies of fluorescence emission in organic light-emitting diodes. An interesting case is seen with dilute solutions of conjugated polymers where more than one triplet state can be produced by pulse radiolysis-energy transfer on an isolated conjugated polymer chain, and triplet–triplet annihilation and delayed fluorescence are observed [81]. (The pulse radiolysis technique is described further in [Chap. 8](#)).

1.13.5.7 Excited-State Proton Transfer

Excited-states are chemically distinct species from the corresponding ground-states and if there are ionisable groups present, the corresponding acid–base dissociation coefficients (pK_a values) may be very different in ground- and excited-states. A classic example is seen with the fluorescence of 2-naphthol (NpOH) [82]. The ground-state pK_a in aqueous media is 9.47 [83], and the absorption spectrum shows a change in the pH region 9–10 due to the acid–base dissociation:



In acidic solution, the fluorescence spectrum shows a band at 350 nm, corresponding to the NpOH fluorescence, while in strongly basic solution, a blue fluorescence is seen around 425 nm corresponding to the emission from the NpO^- anion. However, in neutral solution, where the compound is present entirely as the neutral NpOH species in the ground state, emission from both species is observed. This is a consequence of acid–base dissociation in the excited state, which has a much lower pK_a than the ground state due to a different electronic distribution.



The pK_a values of excited states can be determined experimentally if the protonation–deprotonation equilibria are established during their lifetimes. In addition, they can be estimated using a thermodynamic cycle, the *Förster cycle* [84]. In the case of 2-naphthol, the excited state ($pK_a^* 2.6$) is a stronger acid than the ground state ($pK_a 9.47$), whereas for 1-naphthoic acid, the excited singlet state ($pK_a^* 7.7$) is a weaker acid than the ground state ($pK_a 3.7$). Differences are also observed between pK_a values of ground states and lowest triplet states. However, these tend to be more modest.

Reversible intramolecular proton transfer is an important deactivation route for many dyes and sunscreens (see [Chap. 4](#)) and is probably responsible for their high photostability.

1.14 Concluding Remarks

In this chapter we have introduced some of the basic concepts of photochemistry. We have shown some of the possible effects resulting from absorption of photons by molecules. While photochemistry is a mature science there are still constant new and exciting developments, both recently found and waiting to be discovered. It remains a very active area of research in both fundamental science and across diverse areas of applications from medicine to sustainable energy. The following chapters explore these in more depth.

References

1. Braslavsky SE (2007) Glossary of terms used in photochemistry 3rd edition (IUPAC recommendations 2006). *Pure Appl Chem* 79:293–465
2. <http://www.lsbu.ac.uk/water/vibrat.html>. Accessed 8 Sept 2012
3. Elsaesser T, Kaiser W (1991) Vibrational and vibronic relaxation of large polyatomic molecules in liquids. *Ann Rev Phys Chem* 42:83–107
4. Hodgman SS, Dall RG, Byron LJ, Baldwin KGH, Buckman SJ, Truscott AG et al (2009) Metastable helium: a new determination of the longest atomic excited-state lifetime. *Phys Rev Lett* 103:053002
5. Newman SM, Lane IC, Orr-Ewing AJ, Newnam DA, Ballard J et al (1999) Integrated absorption intensity and Einstein coefficients for the O₂ a ¹Δ_g- X ³Σ_g-(0,0) transition: A comparison of cavity ringdown and high resolution Fourier transform spectroscopy with a long-path absorption cell. *J Chem Phys* 110:10749–10757
6. Atkins P, de Paula J, Friedman R (2009) *Quanta, matter and change: a molecular approach to physical chemistry*. Oxford University Press, Oxford
7. Dorn R, Quabis S, Leuchs G (2003) Sharper focus for a radially polarized light beam. *Phys Rev Lett* 91:233901–233904
8. *The photonics dictionary* (2009) Book 4, 45th edn. Laurin Publishing Co, Pittsfield
9. Smith FG, King TA (2000) *Optics and photonics. An introduction*. John Wiley, Chichester
10. Michelson AA, Morley EW (1887) On the relative motion of the earth and the luminiferous ether. *Am J Sci* 34:333–345
11. Hell SW (2007) Far-field optical nanoscopy. *Science* 316:1153–1158
12. Moore WJ et al (1972) *Physical chemistry*. Longman, London
13. Moore AD (ed) (1983) *Electrostatics and its applications*. John Wiley, New York Chapter 1
14. Banwell C, McCash E (1994) *Fundamentals of molecular spectroscopy*, 4th edn. McGraw-Hill
15. Hollas JM (2004) *Modern spectroscopy*, 4th edn. Wiley, Chichester
16. Wörner HJ, Niikura H, Bertrand JB, Corkum PB, Villeneuve DM (2009) Observation of electronic structure minima in high-harmonic generation. *Phys Rev Lett* 102:103901
17. Housecroft CE, Sharpe AG (2001) *Inorganic chemistry*. Prentice Hall, Harlow, pp 16–25
18. Pritchard HO (2012) We need to update the teaching of valence theory. *J Chem Ed* 89:301–303
19. Sandorfy C (1964) *Electronic spectra and quantum chemistry*. Prentice-Hall, Englewood Cliffs
20. Harris DC, Bertolucci MD (1989) *Symmetry and spectroscopy: an introduction to vibrational and electronic spectroscopy*. Dover, New York
21. Campbell MK (1980) The ¹A_{1g} → ¹B_{2u} transition of benzene. *J Chem Ed* 57:756–758

22. Pope M, Swenberg CE (1999) *Electronic processes in organic crystals and polymers*. Oxford University Press, Oxford
23. Davydov AS (1971) *Theory of molecular excitons*. Plenum, New York
24. Kasha M, Rawls HR, El-Bayoumi MA (1965) The exciton model in molecular spectroscopy. *Pure Appl Chem* 11:371–392
25. Guerrero AH, Fasoli HJ, Costa JL (1999) Why gold and copper are coloured but silver is not. *J Chem Ed* 76:200
26. Heeger AJ, Kivelson S, Schrieffer JR, Su WP (1988) Solitons in conducting polymers. *Rev Mod Phys* 60:781–850
27. Rauscher U, Bässler H, Bradley DDC, Hennecke M (1990) Exciton versus band description of the absorption and luminescence spectra in poly(p-phenylenevinylene). *Phys Rev B* 42:9830–9836
28. Sariciftci NS (ed) (1998) *Primary photoexcitations in conjugated polymers: molecular exciton versus semiconductor band model*. World Scientific, Singapore
29. Schweitzer B, Bässler H (2000) Excitons in conjugated polymers. *Synth Met* 109:1–6
30. Köhler A, Bässler H (2011) What controls triplet exciton transfer in organic semiconductors? *J Mater Chem* 21:4003–4011
31. Schwartz BJ (2003) Conjugated polymers as molecular materials: How chain conformation and film morphology influence energy transfer and interchain interactions. *Ann Rev Phys Chem* 54:141–172
32. Ebsworth EAV, Rankin DWH, Cradock S (1991) *Structural methods in inorganic chemistry*, 2nd edn. Blackwell Scientific Publications, Oxford
33. Moore CE (1970) *Analyses of optical spectra*. Office of Standard Reference Data, NSRDS-NBS 34. National Bureau of Standards, Washington, DC
34. Montalti M, Credi A, Prodi L, Gandolfi MT (2006) *Handbook of photochemistry*, 3rd edn. CRC Press, Boca Raton
35. Trasetti S (1986) The absolute electrode potential—an explanatory note. *Pure Appl Chem* 58:955–966
36. Brett CMA, Brett AMO (1993) *Electrochemistry: principles, methods, and applications*. Oxford University Press, Oxford
37. Connelly NG, Geiger WE (1996) Chemical redox agents for organometallic chemistry. *Chem Rev* 96:877–910
38. Cardona CM, Li W, Kaifer AE, Stockdale D, Bazan GC et al (2011) Electrochemical considerations for determining absolute frontier orbital energy levels of conjugated polymers for solar cell applications. *Adv Mater* 23:2367–2371
39. Kalyanasundaram K (1982) Photophysics, photochemistry and solar energy conversion with tris(bipyridyl)ruthenium(II) and its analogues. *Coord Chem Rev* 46:159–244
40. Burrows HD, Azenha ME, Monteiro CJP (2008) Homogeneous photocatalysis. In: Figueiredo JL, Pereira MM, Faria J (eds) *Catalysis from theory to application*. Coimbra University Press, Coimbra
41. Koopman T (1934) Über die Zuordnung von Wellenfunktionen und Eigenwerten zu den einzelnen Elektronen eines Atoms. *Physica* 1:104–113
42. Ramsey BG (1977) A comparison of the role of charge transfer hyperconjugation, inductive and field interactions in substituted methyl and silyl substituent effects in benzene π vertical ionization energies. *J Organomet Chem* 135:307–319
43. Doering JP (1977) Electronic energy levels of benzene below 7 eV. *J Chem Phys* 67:4065–4070
44. Palmer MH, Walker IC (1989) The electronic states of benzene and the azines. 1 The parent compound benzene. Correlation of vacuum UV and electron scattering data with ab initio calculations. *Chem Phys* 133:113–121
45. Orchin M, Jaffe HH (1971) *Symmetry, orbitals and spectra*. Wiley, New York
46. Wayne RP (1988) *Principles and applications of photochemistry*. Oxford University Press, Oxford
47. Sturm JE (1990) Grid of expressions related to the Einstein coefficients. *J Chem Ed* 67:32–33

48. Benesi HA, Hildebrand JH (1949) A spectrophotometric investigation of the interaction of iodine with aromatic hydrocarbons. *J Am Chem Soc* 71:2703–2707
49. Kasha M (1963) Energy transfer mechanisms and the molecular exciton model for molecular aggregation. *Radiat Res* 20:55–71
50. Jelley EE (1936) Spectral absorbance and fluorescence of dyes in the molecular state. *Nature* 138:1009–1010
51. Scheibe G (1937) Über die Veränderlichkeit der Absorptionsspektren in Lösungen und die Nebenvalenzen als ihre Ursache. *Angew Chem* 50:212–219
52. Würthner F, Kaiser TE, Saha-Möllner CR (2011) J-aggregates: from serendipitous discovery to supramolecular engineering of functional dye molecules. *Angew Chem Int Ed* 50:3376–3410
53. Tilley R (2011) *Colour and the optical properties of materials*, 2nd edn. Wiley, Chichester
54. Prasad PN, Williams DJ (1990) *Introduction to nonlinear optical effects in molecules and polymers*. Wiley, New York
55. Strickler SJ, Berg RA (1962) Relationship between absorption intensity and fluorescence lifetime of molecules. *J Chem Phys* 37:814–822
56. Kasha M (1950) Characterization of electronic transitions in complex molecules. *Disc Faraday Soc* 9:4–19
57. Cario G, Franck J (1923) On sensitized fluorescence of gases. *Z Phys* 17:202–212
58. Förster T (1948) Zwischenmolekulare energiewanderung und fluoreszenz. *Ann Phys* 2:55–75
59. Förster T (1959) Transfer mechanisms of electronic excitation. *Disc Faraday Soc* 27:7–17
60. Berlman IB (1973) *Energy transfer parameters of aromatic compounds*. Academic Press, New York
61. Arnaut L, Formosinho S, Burrows H (2007) *Chemical kinetics: from molecular structures to chemical reactivity*. Elsevier, Amsterdam, pp 229–235
62. Marcus RA, Sutin N (1985) Electron transfers in chemistry and biology. *Biochim Biophys Acta* 811:265–322
63. Piotrowiak P (2001) Relationship between electron and electronic excitation transfer. In: Balzani V (ed) *Electron transfer in chemistry*, vol 1. Wiley-VCH, Weinheim
64. Dexter DL (1953) A theory of sensitized luminescence in solids. *J Chem Phys* 21:836–850
65. Saini S, Srivivas G, Bagchi M (2009) Distance and orientation dependence of excitation energy transfer: From molecular systems to metal nanoparticles. *J Phys Chem B* 113:1817–1832
66. Hwang I, Scholes GD (2011) Electronic energy transfer and quantum-coherence in π -conjugated polymers. *Chem Mater* 23:610–620
67. Stern O, Volmer M (1919) Über die Abklingzeit der Fluoreszenz. *Physikalische Zeitschrift* 20:183–188
68. Förster T, Kasper K (1954) Ein Konzentrationsumschlag der Fluoreszenz. *Z Phys Chem Neue Folge* 1:275–277
69. Stevens B, Hutton E (1960) Radiative lifetime of the pyrene dimer and possible role of excited dimers in energy transfer processes. *Nature* 186:1045–1046
70. Birks JB (1970) Excimer fluorescence of aromatic compounds. *Prog React Kinetics* 5:181–272
71. Hopfield JJ (1930) Absorption and emission spectra in the region $\lambda = 600$ –1100. *Phys Rev* 35:1133–1134
72. Leonhardt H, Weller A (1963) Elektronenübertragungsreaktionen des angeregten Perylens. *Ber Buns Phys Chem* 67:791–795
73. Knibb H, Rehm D, Weller A (1968) Intermediates and kinetics of fluorescence quenching by electron transfer. *Ber Buns Phys Chem* 72:257–263
74. Mataga N, Chosrojan H, Taniguchi S (2005) Ultrafast charge transfer in excited electronic states and investigation into fundamental problems of exciplex chemistry: our early studies and recent developments. *J Photochem Photobiol C* 6:37–79
75. Grabowski ZR, Dobkowski J (1983) Twisted intramolecular charge transfer (TICT) excited states: energy and molecular structure. *Pure Appl Chem* 55:245–252

76. Parker CA (1964) Phosphorescence and delayed fluorescence from solutions. *Adv Photochem* 2:305–383
77. Berberan Santos MN, Garcia JMM (1996) Unusually strong delayed fluorescence of C70. *J Am Chem Soc* 118:9391–9394
78. Birks JB (1967) Quintet state of pyrene excimer. *Phys Lett A* 24:479
79. Misra TN (1973) Delayed fluorescence of organic mixed crystals—temperature independent delayed fluorescence in biphenyl host. *J Chem Phys* 58:1235–1242
80. Monkman A, Rothe C, King S, Dias F (2008) Polyfluorene photophysics. *Adv Polym Sci* 212:187–225
81. Monkman AP, Burrows HD, Hamblett I, Navaratnam S (2001) Intrachain triplet–triplet annihilation and delayed fluorescence in soluble conjugated polymers. *Chem Phys Lett* 340:467–472
82. Förster TH (1950) Die pH Abhängigkeit der Fluoreszenz von Naphthalinderivaten. *Z Electrochem* 54:531–535
83. Ireland JF, Wyatt PAH (1976) Acid-base properties of electronically excited states of organic molecules. *Adv Photochem* 12:131–221
84. Weller A (1961) Fast reactions of excited molecules. *Prog React Kinet* 1:187–214

Chapter 2

Photochemical Synthesis

Valentina Dichiarante and Angelo Albini

Abstract Photochemical reactions are generally easily carried out, at least in laboratory scale, and require no expensive apparatus. Some general reactions, e.g. the cycloaddition of enones to alkenes and various oxygenations have been extensively investigated and represent an excellent choice for preparative applications. Many other possibilities are known—and a few are presented below. This suggests that photochemical steps should be considered more often in synthetic planning.

2.1 Role of Photochemistry in Synthesis

Of all the diverse applications of photochemistry, the most *chemical* one, that is chemical *synthesis* has been actively investigated for over a century, but has probably still much to reveal with future development [1]. In fact, photochemical synthesis is less widely used than it may be. This may appear surprising since chemical synthesis is actually based on the generation of high-energy intermediates for forming new bonds and electronic excitation offers a wonderful opportunity by activating molecules in a controlled way. Unfortunately, practitioners of organic synthesis sometimes feel that photochemical reactions are interesting from the mechanistic point of view, but ill-suited for preparative purposes because they

V. Dichiarante

CEA, iBiTec-S, Service de Bioénergétique Biologie Structurale et Mécanismes (SB2SM),
91191 Gif-sur-Yvette, France

A. Albini (✉)

Dipartimento di Chimica, Università di Pavia, v. Taramelli 10 27100 Pavia, Italy
e-mail: angelo.albini@unipv.it

require expensive instruments, tend to give mixtures and at any rate their course is difficult to rationalise.

Some of the known photochemical reactions may appear appealing, but also 'unexpected'. As a matter of fact, even a scientist such as Georg Büchi, who played a major role in the relaunch of organic photochemistry after World War II and rediscovered the photochemical carbonyl + alkene cycloaddition that now bears his name along with that of the original discoverer, Emanuele Paternò, was not convinced of the viability of the photochemical approach in synthesis. In an interview he declared that "...*useful applications were not forthcoming...*" from that side and he felt that "...*the course of the transformations could rarely be predicted, thus robbing the investigator of the pleasure derived from designing new reactions*" [2]. Several decades later, it is still felt that it is not always simple to teach this topic. As it has been recently expressed, sometimes this seems to involve a "*somewhat mysterious effect*" so that, "*by simply absorbing a UV/Vis photon, a molecule becomes something different, and in many cases behaves in a way completely opposite to that of its ground state*" [3].

In the opinion of the present contributors there are still many prejudices, but nowadays there is sufficient support, if not widespread application, in the literature for the important role that photochemistry can have in organic synthesis.

2.2 Carrying Out a Photochemical Synthesis

As a matter of fact, carrying out a preparative photochemical reaction is a simple and inexpensive procedure [4]. It is important that some precautions are taken, however, in order to avoid a disappointment. First of all, it must be checked that light is absorbed by the compound that is meant to. Thus, the lamp should have an emission spectrum (available from the maker) overlapping at least in part with the absorption of the reagent and not be hindered from reaching it. Thus, e.g. the walls of the vessel must be transparent to the wavelength used, as must the solvent. The correct choice of the lamps also helps to minimise expenses. Low pressure mercury arcs emitting at 254 nm (or, when phosphor-coated, in the near UV or the visible, being available for various wavelength ranges) are quite inexpensive and long-lived. Along with the slightly more expensive medium-pressure mercury lamps (125–400 W) these are fully sufficient for virtually all of the photochemical syntheses in the scale of some grams. The emission spectra for low and medium pressure Hg lamps may be found in [Chap. 14](#) (Fig. 14.2).

Further precautions are that heating by the lamp (that is important with high pressure lamps or incandescent lamps emitting in the visible) is controlled and that the reaction is monitored by UV/Vis spectroscopy, besides as by the preferred analytical method. This is because it must be ascertained whether (one of) the photoproduct(s) absorb(s) competitively with the reagent; in that case the reaction may stop much before completion. Furthermore, the solutions should be not overly concentrated (this would cause a strongly decreasing absorption when proceeding

from the illuminated surface to the inner volume, a condition that tends to give 'dirty' reactions. However, circulating the solution to be irradiated around the lamp may give a significant advantage and an even better way is using a microreactor, an example of which is shown in [Chap. 14](#) ([Fig. 14.3](#)).

It is noteworthy that photochemical reactions are often little affected by the temperature and by small amounts of impurities (in both cases, because of the short lifetime of electronically excited states, which precludes reactions that have a sizeable activation energy or bimolecular reactions when the trap concentration is low). However, the above holds for excited states, not for ensuing intermediates, such as radicals or unstable species that often are the primary products in photochemical reactions and are usually quite sensitive to conditions. Furthermore, some impurities may specifically interact with the excited state at a very high (diffusion controlled, $\sim 1 \times 10^{10} \text{ mol}^{-1} \text{ dm}^3 \text{ s}^{-1}$) rate.

Typical examples are compounds having low lying triplets, which can function as acceptors in an energy transfer process and thus 'quench' the photoreaction (see [Chap. 1](#)). The most obvious case is oxygen for which the lowest-lying excited state is lower in energy with respect to practically all organic molecules and thus inhibits photoreactions, or at least most triplet states, while short-lived singlets are less affected. This makes it advisable that irradiations are carried out on a 'deaerated' solution (that is flushed for some minutes with an inert gas such as nitrogen or argon) at least in the initial tests, until the effect of oxygen has been established. On the other hand, this relative independence of the primary photochemical step on the temperature and on conditions is an advantage because it leaves more freedom for directing the chemistry of the following intermediates, e.g. radicals, thus making the photochemical method generally more versatile than thermal methods involving the same intermediate.

2.3 Photochemical Reactions

As for which reactions to do or to explore, it is certainly true that photochemical reactions have been much less applied than thermal ones, but a large number of these are perfectly known and, what is most important, have been rationalised by taking into account their electronic structure in the same way as it is customary to do for ground state reactions [5, 6]. Thus, as soon as the chromophore involved is identified, one may roughly predict the chemical behaviour. As an example, a $n \rightarrow \pi^*$ transition in a carbonyl group leaves a single electron in the n_{O} orbital, which makes such excited states quite similar to oxygen-centred radicals. Indeed, the chemistry observed is the same as that of alkoxy radicals and involves α -cleavage, hydrogen abstraction and electrophilic attack to π -bonds.

A brief survey of the general classes of photochemical reactions is given below. Some recent examples, in most of which a photochemical step is incorporated in a complex synthetic plan, are reported, in order to give at least a flavour of the (potential) role of photochemical synthesis.

2.3.1 Hydrocarbons

Non-conjugated alkenes do not absorb in the near UV, but polyenes or arylalkenes do and the absorption maximum progressively moves towards longer wavelengths and becomes more intense upon extending the conjugation. Furthermore, these derivatives have low-lying triplet states that can be populated by sensitizers (including those adventitiously present). $\pi\pi^*$ excited states are formed, where the double bond is broken. As a result, the molecules lose planarity and alkenes are most often characterised by efficient *E-Z* photoisomerism in the excited state, except when torsion is hindered by molecular constraint. A (mainly) one-way isomerisation can be obtained by exploiting the different absorption spectra of the two diastereoisomers—and thus by selective excitation, or by the appropriate choice of the sensitizer or by complexation [7].

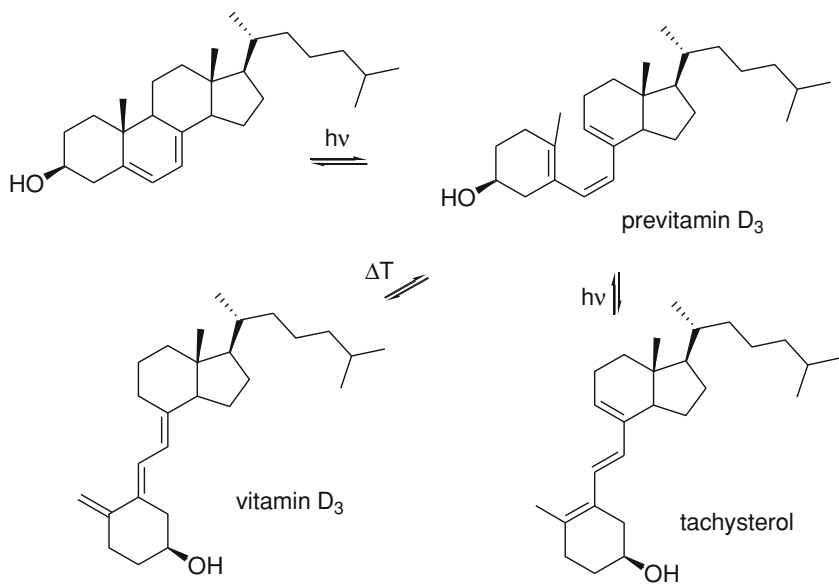
Geometrical isomerism is a general reaction, applying not only to C=C bonds, but also to carbon-heteroatom and heteroatom–heteroatom double bond, as in oximes, hydrazones and azo compounds.

With conjugated polyenes, electrocyclic reactions are generally observed. Due to the stereochemical control, these are often considered among the most representative photochemical reactions, although the occurrence of such processes in both directions means that mixtures are often obtained. A case of industrial importance is the synthesis of vitamin D. The competition between different π^6 electrocyclic reactions and sigmatropic hydrogen shift is shown in the scheme below for the case of the formation of a mixture of previtamin D₃ and tachysterol. The reaction has been recently enhanced by using a photomicroreactor combined with a thermal-microreactor. Heating converts the provitamin into the desired vitamin, and this causes a shift of the equilibrium towards the latter compound in the photoisomerisation of tachysterol to previtamin D₃ (see Scheme 2.1) [8].

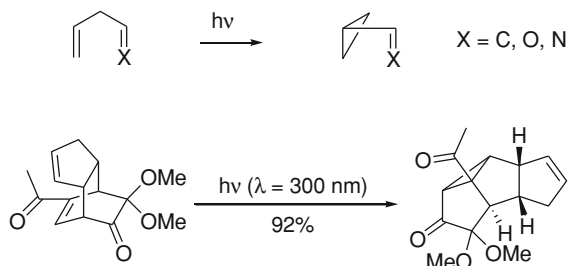
Not less useful is the photochemistry of non-conjugated dienes. Thus, 1,4-dienes undergo a typical photo-rearrangement to vinyl cyclopropanes, which may be a valid way for building a three-membered ring, particularly in a complex structure (this is known as the di- π -methane rearrangement, see Scheme 2.2). β,γ -Unsaturated ketones and imines rearrange in the same way to cyclopropylketones and imines respectively [9].

On the other hand, 1, ≥ 5 dienes undergo intramolecular 2+2 cycloaddition. Different modes are possible and mixtures may be obtained. However, at least when the relative arrangement of the two double bonds is fixed, either because freedom is restricted by the structure of the diene or because complexation by metal ions has been effected, the selectivity may be excellent (see Scheme 2.3) [10–12].

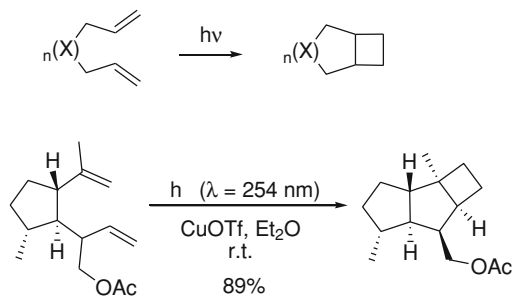
Aromatic compounds absorb strongly in the UV, with larger aromatic derivatives extending out to the visible. Extended conjugation and geometrical constraints make them less photoreactive than alkenes, or at least less efficiently reactive. However, the increased stability does not deter excited states from exhibiting their attitude for remarkable reactions. Among unimolecular processes, photo-rearrangements to polycyclic compounds, as in the benzene \rightarrow benzvalene



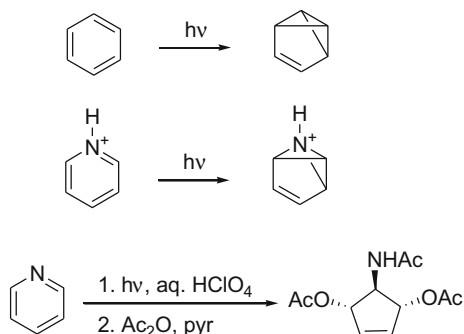
Scheme 2.1 Electrocyclic photoreactions and photoisomerization in the synthesis of vitamin D₃



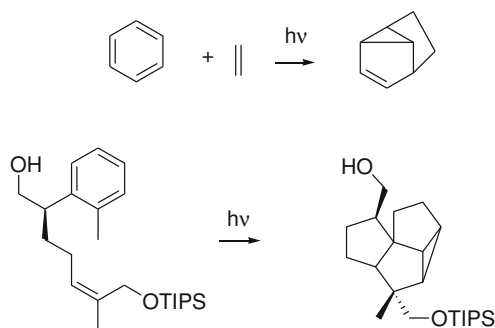
Scheme 2.2 (Oxa)-di- π -methane rearrangement



Scheme 2.3 [2+2] Olefin cycloaddition



Scheme 2.4 Benzene to benzvalene rearrangement and aza analogue



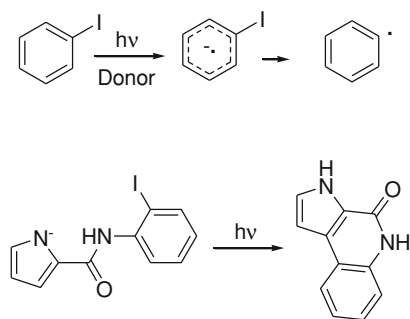
Scheme 2.5 *Meta* benzene-olefin cycloaddition

case (see Scheme 2.4), are well known. This is synthetically useful with heteroaromatics, in particular pyridine or rather pyridinium salts, where the three-membered ring undergoes nucleophilic opening [13, 14].

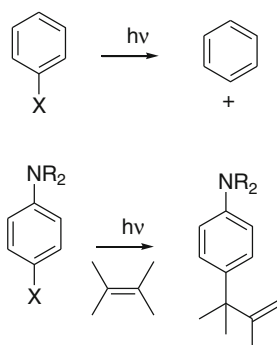
Remarkable also is the related case of the *meta* benzene-alkene cycloaddition. Here again, mixtures are formed, but at least when the alkene moiety is tethered to the benzene ring and a preferred conformation exists, regio-selective processes have been found where several new stereocenters are formed in a single step and in a rigorously controlled way—and thus are synthetically highly valued (see Scheme 2.5) [15].

In the field of (hetero)aromatic photochemistry substitution reactions are also quite useful. The two most useful classes are the $S_{RN}1$ reaction [16] and S_N1 reaction [17], involving respectively the aromatic radical anion and the aryl cation as the key intermediates. In the former case, (generally photoinduced) electron transfer generates the radical anion of an aryl halide. With less strongly bonded derivatives (usually iodides) the intermediate cleaves to an aryl radical that gives the new product *via* a chain process (see Scheme 2.6).

Aryl cations, on the other hand, are the typical example of ground state intermediates that cannot be generated thermally, whereas these are smoothly accessed photochemically by irradiation of phenyl chlorides and fluorides, or at least of the



Scheme 2.6 The photo $S_{RN}1$ reaction



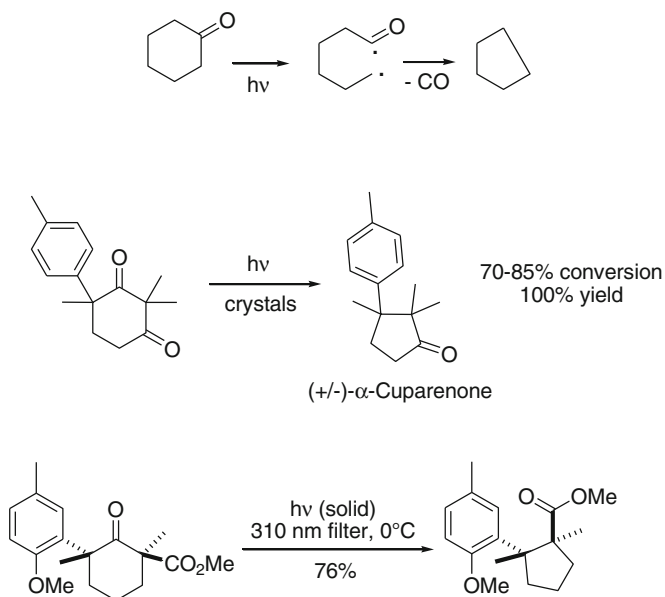
Scheme 2.7 The photoarylation of alkenes *via* $S_{N}1$

electron-donating substituted types, in polar solvents (see Scheme 2.7). The reaction has been applied for the arylation of alkenes, alkynes, benzenes and heterocycles, offering a metal-free alternative to catalysed reactions largely used in synthesis.

2.3.2 Ketones and Related Chromophores

The lowest-lying excited state of ketones most often corresponds to a $n_{\text{O}} \rightarrow \pi^*_{\text{C=O}}$ transition. The maximum of this band is around 280 nm with simple aldehydes or ketones and is shifted to the red for conjugated or aryl derivatives. As hinted above, the unpaired electron on the n_{O} orbital gives to these states electrophilic properties similar to those of alkoxy radicals, and indeed the observed chemistry is similar in the two cases. Typical reactions are α -fragmentation, inter- or intramolecular (from the easily accessible γ position) hydrogen abstraction and attack of alkenes (finally resulting in a formal 2+2 cycloaddition to give an oxetane, the Paternò-Büchi reaction).

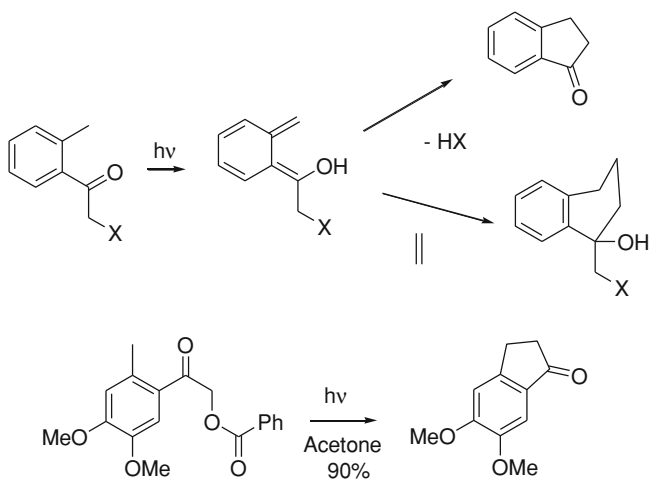
Fragmentation has given synthetically useful results particularly in the solid state for α -(poly)substituted ketones, where both α -bonds are cleaved and the



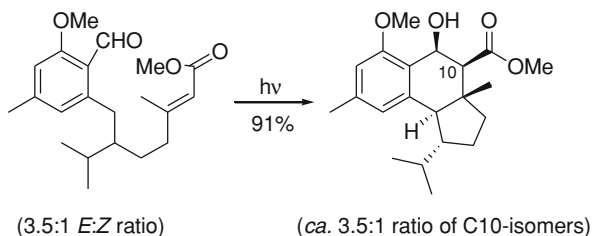
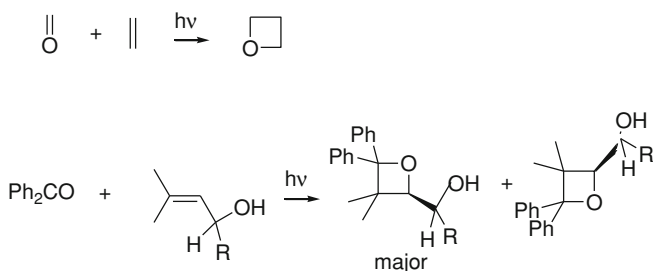
Scheme 2.8 Decarbonylation reactions

recombination of the adjacently formed radical centres is more easily controlled leading to the chemo- and stereoselective photo-decarbonylation reactions (see Scheme 2.8) [18, 19].

When conformationally favored, intramolecular hydrogen abstraction is very effective. This reaction has been observed in *o*-methylbenzophenone and related

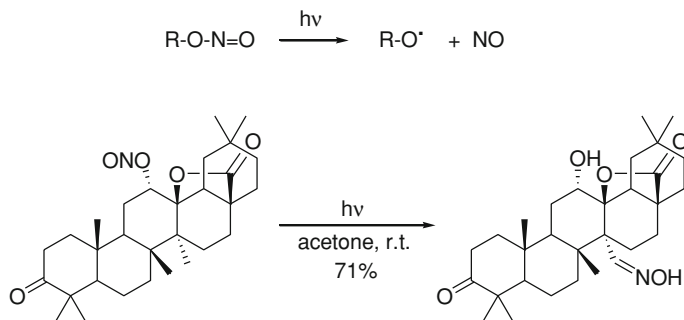


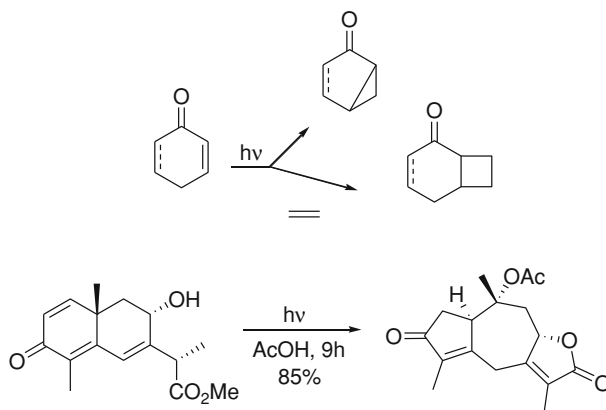
Scheme 2.9 Enolisation and fragmentation

**Scheme 2.10** Enolisation and [4+2] cycloaddition**Scheme 2.11** Synthesis of oxetanes

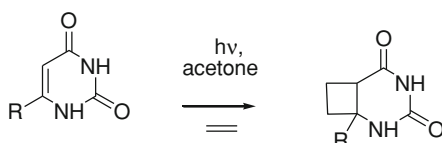
compounds and has been frequently used for producing the enol form of the starting material, and thus access to the high reactivity of such a group. In a typical application, this is trapped by an alkene, whether intra- or intermolecularly, leading to a 4+2 cycloaddition regenerating aromaticity [20]. In the presence of a suitable leaving group, an elimination reaction can also take place (see Schemes 2.9, 2.10) [21]. The photocycloaddition to alkenes, a regioselective but not stereospecific reaction, offers a useful entry to oxetanes (see Scheme 2.11) [22].

The nitro group has an electronic structure similar to the carbonyl and likewise a $n\pi^*$ lowest state that again shows radicalic properties (hydrogen abstraction). Interesting is the case of nitrites that generally undergo easy homolytic cleavage of

**Scheme 2.12** Photolysis of a nitrite



Scheme 2.13 Enones rearrangement



Scheme 2.14 Intermolecular enone cycloaddition

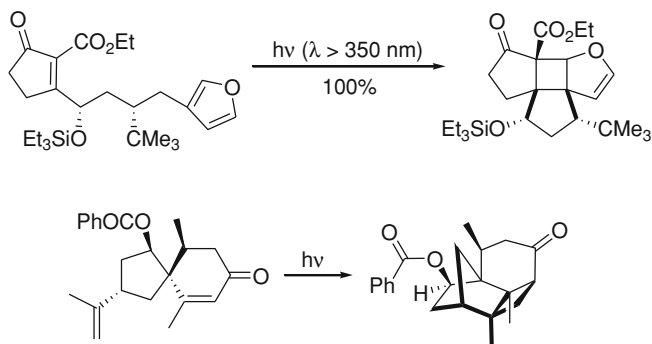
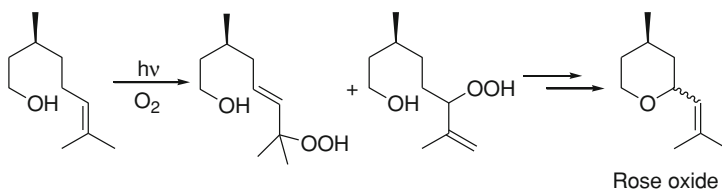
the N–O bond. This is often followed by intramolecular hydrogen abstraction by the alkoxy radical and addition of NO molecule leading to function exchange (Barton reaction) (see Scheme 2.12) [23].

As one would expect, conjugated ketones are mostly poor hydrogen abstractors. This is a fortunate circumstance, because it leaves room for a variety of reactions that are quite useful from the preparative point of view. These include rearrangements [24], addition reactions and 2+2 cycloaddition with alkenes. An example of rearrangement of a cross-conjugated cyclohexadienone is shown above. This gives a cyclopropylcyclopentenone that opens up in the reaction medium (see Scheme 2.13).

As for the synthesis of acylcyclobutanes by cycloaddition, this is often a very efficient process and is one of the most largely used synthetic procedures in organic photochemistry. An example is the addition of uracil to alkenes (see Scheme 2.14) [25]. The intramolecular version is most often used and gives excellent results (see Scheme 2.15) [26, 27].

2.3.3 Oxidations

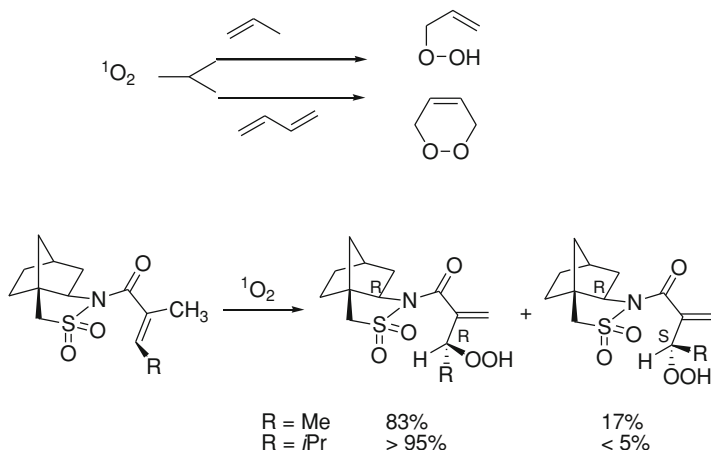
Along with the cycloaddition of enones, photooxidation is probably the most consistently used photochemical reaction for synthetic purposes. This is also one

**Scheme 2.15** Intramolecular enone cycloaddition**Scheme 2.16** Synthesis of rose oxide

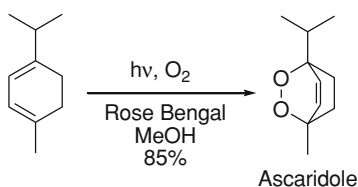
of the few that have found application in an industrial context, notably in the case of rose oxide. This fragrance is produced in Germany in a considerable yearly tonnage, making recourse to photochemistry in one of the first steps. This involves the oxidation of citronellol in the presence of a sensitizer (Rose Bengal) using molecular oxygen (see Scheme 2.16). The thus generated excited (singlet) oxygen is a highly electrophilic species that attacks alkenes in a very mild process [28]. The resulting hydroperoxides are then reduced to the alcohols, which then are transformed into the corresponding cyclic ethers.

Oxygenation *via* singlet oxygen is often convenient [29] and occurs according to two processes; the ene (Schenck) reaction to give allylhydroperoxides with alkenes [30] and the cycloadditions with dienes to give 1,2-dihydrodioxins (see Scheme 2.17) as in the case of the synthesis of ascaridole (see Scheme 2.18). The cycloaddition occurs effectively also with electron-donating substituted aromatics (e.g. phenols and naphthols, see Scheme 2.19) [31] or multi-ring aromatics (quite effectively with anthracenes and higher homologues, see Scheme 2.20) [32].

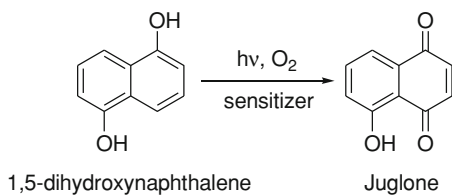
The addition of oxygen to furans to form ozonides and hydroxyfuranones (Scheme 2.21) has been largely exploited in view of the ensuing easy elaboration of these versatile intermediates [33–35].



Scheme 2.17 Modes of reaction of singlet oxygen



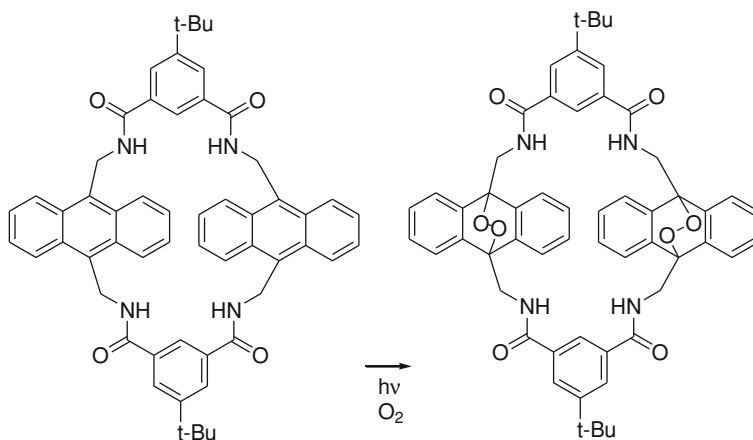
Scheme 2.18 Synthesis of ascaridole



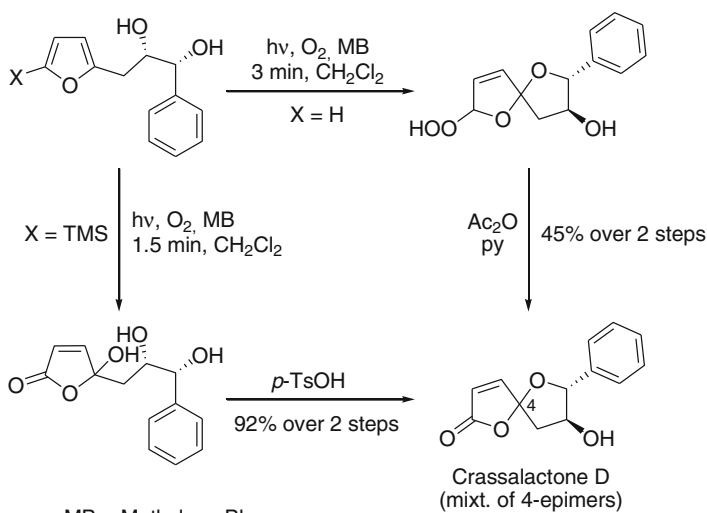
Scheme 2.19 Oxygenation of naphthol

2.3.4 Miscellaneous

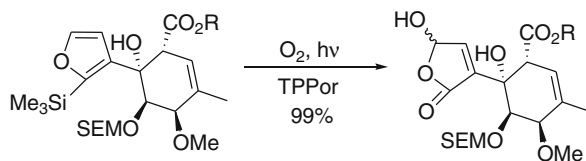
There are many more preparatively useful classes of photochemical reactions that could be addressed in this short presentation. Perhaps, one should at least mention halogenation, sulfonation and sulfochlorination that have large industrial significance for the preparation of surfactants. As an example, the sodium salts of secondary alkanesulfonamidoacetic acid were synthesised using *n*-alkanesulfonyl



Scheme 2.20 Oxygenation at the anthracene ring



MB = Methylene Blue

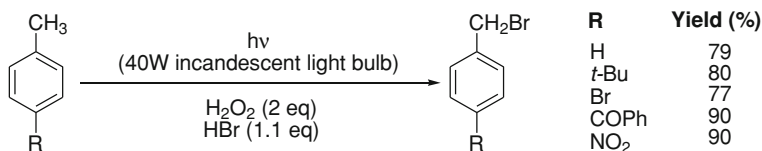


R = $(\text{CH}_2)_2\text{SiMe}_3$

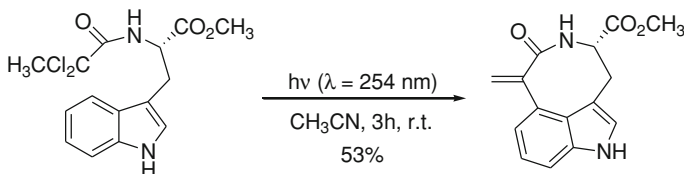
SEM = trimethylsilyloxyethyl

TPPor = 5,10,15,20-tetraphenyl-21*H*,23*H*-porphine

Scheme 2.21 Oxygenation of furans



Scheme 2.22 Photoinduced halogenation



Scheme 2.23 An example of *N*-chloroacetamide cyclisation

chlorides as starting materials. These surfactants, having the formula $R-SO_2-NH-CH_2-COONa$, with $R=C_{12}$, C_{14} , C_{16} and C_{18} derived from the corresponding *n*-alkylsulfonyl chlorides obtained by photochemical sulfochlorination of the alkanes under visible light using sulfuryl chloride [36]:



Photochemical halogenations may also be convenient on the laboratory scale. As an example, benzylic bromination is conveniently carried by using HBr/H_2O_2 under irradiation with a common incandescent lamp (see Scheme 2.22)[37]. Apropos halides, it may be added that fragmentation of the carbon-halogen bond has been considered above for aromatic derivatives, but is useful also for aliphatic derivatives. A typical example is the photocyclisation of *N*-phenyl chloroacetamides and *N*-arylalkyl chloroacetamides (see Scheme 2.23)[38].

2.4 Conclusions

The variety of chemical reactions reported above is impressive. Most of them hardly have a simple thermal alternative. When it is further considered that these reactions are usually more easily carried out than many modern synthetic reactions, it may be concluded that the role of photochemistry in chemical synthesis is bound to further develop.

References

1. White JD (1979). <http://www.orgsyn.org/obits/buchi.pdf>. Accessed 20 June 2012
2. Albini A (2010) Photosciences: a look into the future. *Photochem Photobiol Sci* 9:1533–1534
3. Griesbeck AJ (2009) Photochemistry of organic compounds. *Angew Chemie Int Ed* 48:4671–4672
4. Albini A, Fagnoni M (eds) (2010) Handbook of preparative photochemistry. Wiley, Weinheim
5. Turro NJ, Ramamurthy V, Scaiano JC (2010) Modern molecular photochemistry of organic molecules. University Science Books, Herndon
6. Klàn P, Wirz J (2009) Photochemistry of organic compounds. From principles to practice. Wiley, Hoboken
7. Saito H, Sivaguru J, Jockusch S et al (2007) Controlled diastereoselectivity at the alkene-geometry through selective encapsulation: *E-Z* photoisomerization of oxazolidinone-functionalized enecarbamates within hydrophobic *nano*-cavities. *Chem Commun* 43:819–821
8. Fuse S, Tanabe N, Yoshida M et al (2010) Continuous-flow synthesis of Vitamin D₃. *Chem Commun* 46:8722–8724
9. Yen CF, Liao CC (2002) Concise and efficient total synthesis of *Lycopodium* alkaloid Magellanine. *Angew Chemie Int Ed* 41:4090–4093
10. Bach T, Spiegel A (2002) Stereoselective total synthesis of the tricyclic sesquiterpene (\pm)-Kelsoene by an intramolecular Cu(I)-catalyzed [2+2]-photocycloaddition reaction. *Synlett*: 1305–1307
11. Shipe WD, Sorensen EJ (2002) A convergent synthesis of the tricyclic architecture of the Guanacastepenes featuring a selective ring fragmentation. *Org Lett* 4:2063–2066
12. Sarkar N, Nayek A, Ghosh S (2004) Copper(I)-catalyzed intramolecular asymmetric [2+2] photocycloaddition. Synthesis of both enantiomers of cyclobutane derivatives. *Org Lett* 6:1903–1905
13. Zou J, Mariano PS (2008) The synthetic potential of pyridinium salt photochemistry. *Photochem Photobiol Sci* 7:393–404
14. Zhao Z, Song L, Mariano PS (2005) A concise sequential photochemical-metathesis approach for the synthesis of (+)-Castanospermine and possible Uniflorine-A stereoisomers. *Tetrahedron* 61:8888–8894
15. Gaich T, Mulzer J (2010) From Silphinenes to Penifulvins: a biomimetic approach to Penifulvins B and C. *Org Lett* 12:272–275
16. Vaillard VA, Budén ME, Martín SE et al (2009) Synthesis of novel fused azaheterocycles by photostimulated intramolecular S_{RN}1 reactions with nitrogen nucleophiles. *Tetrahedron Lett* 50:3829–3832
17. Fagnoni M, Albini A (2005) Arylation reactions. The S_N1 path via phenyl cation as an alternative to metal catalysis. *Acc Chem Res* 38:713–721
18. Ng D, Yang Z, Garcia-Garibay MA (2004) Total synthesis of (\pm)-Herbertenolide by stereospecific formation of vicinal quaternary centers in a crystalline ketone. *Org Lett* 6:645–647
19. Natarajan A, Ng D, Yang Z et al (2007) Parallel syntheses of (+)- and (–)- α -Cuparenone by radical combination in crystalline solids. *Angew Chem Int Ed* 46:6485–6487
20. Nicolaou KC, Gray DLF, Tae J (2003) Total synthesis of Hamigerans and analogues thereof. Photochemical generation and Diels-Alder trapping of hydroxy-*o*-quinodimethanes. *J Am Chem Soc* 126:613–627
21. Pospíšil T, Veetil AT, Antony LAP et al (2008) Photochemical synthesis of substituted indan-1-ones related to Donepezil. *Photochem Photobiol Sci* 7:625–632
22. Abe M, Terazawa M, Nozaki K, Masuyama A, Hayashi T (2006) Notable temperature effect on the stereoselectivity in the photochemical [2+2] cycloaddition reaction (Paternò-Büchi reaction) of 2,3-dihydrofuran-3-ol derivatives with benzophenone. *Tetrahedron Lett* 46:2527–2530

23. Sugimoto A, Sumino Y, Takagi M et al (2006) The Barton reaction using a microreactor and black light. Continuous-flow synthesis of a key steroid intermediate for an endothelin receptor antagonist. *Tetrahedron Lett* 47:6197–6200
24. Blay G, Barges V, Cardona L et al (2000) Stereoselective synthesis of 7,11-guaian-8,12-olides from Santonin. Synthesis of Podoandin and (+)-Zedolactone A. *J Org Chem* 65:6703–6707
25. Roy O, Faure S, Aitken DJ (2006) A solution to the component instability problem in the preparation of peptides containing C2-substituted cis-cyclobutane β -aminoacids: synthesis of a stable rhodopeptin analogue. *Tetrahedron Lett* 47:5981–5984
26. Crimmins MT, Pace JM, Nantermet PG et al (2000) The total synthesis of (\pm)-Ginkgolide B. *J Am Chem Soc* 122:8453–8463
27. Srikrishna A, Ramasastry SSV (2006) Enantiospecific first total synthesis of (+)-2 β -hydroxysolanascone, the aglycone of the phytoalexin isolated from flue-cured tobacco leaves. *Tetrahedron Lett* 47:335–339
28. Wootton RCR, Fortt R, de Mello AJ (2002) A microfabricated nanoreactor for safe, continuous generation and use of singlet oxygen. *Org Process Res Dev* 6:187–189
29. Clennan EL, Pace A (2005) Advances in singlet oxygen chemistry. *Tetrahedron* 61:6665–6691
30. Adam W, Bosio SG, Turro NJ (2002) Highly diastereoselective dioxetane formation in the photooxygenation of enecarbamates with an oxazolidinone chiral auxiliary: steric control in the [2+2] cycloaddition of singlet oxygen through conformational alignment. *J Am Chem Soc* 124:8814–8815
31. Coyle EE, Joyce K, Nolan K, Oelgemöller M (2010) Green photochemistry: the use of microemulsions as green media in photooxygenation reactions. *Green Chem* 12:1544–1547
32. Gassensmith JJ, Baumes JM, Eberhard J et al (2009) Cycloaddition to an anthracene-derived macrocyclic receptor with supramolecular control of regioselectivity. *Chem Commun* 45:2517–2519
33. Montagnon T, Tofi M, Vassilikogiannakis G (2008) Using singlet oxygen to synthesize polyoxygenated natural products from furans. *Acc Chem Res* 41:1001–1011
34. Bailey S, Helliwell M, Teerawutgulrag A et al (2005) A total synthesis of Milbemycin G: approaches to the C(1)-C(10)-fragment and completion of the synthesis. *Org Biomol Chem* 3:3654–6477
35. Pavlakos E, Georgiou T, Tofi M et al (2009) γ -Spiroketal γ -lactones from 2-(γ -hydroxyalkyl)furans: syntheses of *epi*-pyrenolides D and crassalactone D. *Org Lett* 11:4556–4559
36. Mousli R, Tazerouti A (2011) Synthesis and some surface properties of glycine-based surfactants. *J Surfact Deterg* 14:65–72
37. Podgoršek A, Stavber S, Zupan M et al (2009) Environmentally benign electrophilic and radical bromination ‘on water’: H₂O₂-HBr system versus *N*-bromosuccinimide. *Tetrahedron* 65:4429–4439
38. Feldman KS, Ngermmeesri P (2005) Dragmacidin E synthesis studies. Preparation of a model heptacyclic core structure. *Org Lett* 7:5449–5451

Chapter 3

Inorganic Photochemistry

Julia A. Weinstein

Abstract The fascinating field of inorganic photochemistry is extremely diverse. This chapter discusses some general principles governing light-induced properties of metal-containing molecular compounds. The great variety of excited states of different nature—far greater than those available in organic compounds—accessible in metal-containing species is discussed, and linked to various photochemical transformations. The emphasis is placed on the diversity and open-end possibilities to use wavelength-dependent reactivity of such species for creating a variety of products. Modern methods for the interrogation of excited states on ever faster time scales are briefly outlined. Recent technological advances open up exciting prospects of modulating the outcome of photochemical reactions by altering the earliest photo-events. It is clear that inorganic photochemistry will continue to play a central role in light-driven applications.

3.1 Introduction

The general principles of the interaction of light with metal-containing compounds described in this chapter follow the same general rules as those already introduced in [Chap. 1](#).

There are several important features which distinguish photophysical and photochemical properties of metal-containing compounds from those of organic molecules.

J. A. Weinstein (✉)

Department of Chemistry, University of Sheffield, Sheffield S3 7HF, UK
e-mail: Julia.Weinstein@sheffield.ac.uk

1. Metal-containing species offer a much greater diversity of types of excited state compared to organic molecules because of the participation of metal orbitals in addition to ligand orbitals.
2. A manifold of several excited states of different origin close in energy to one another is an intrinsic feature of metal-containing species. Due to their different origin and often different spatial localization, internal conversion between these states is not always efficient. This intriguing property results in several excited states being independently emissive and/or reactive, thus violating one of the main rules developed for organic photochemistry, *viz.* Kasha's rule [1] (Chap. 1). This feature gives rise to exciting phenomena such as multiple emission, or excited state branching, where the nature of the products and their yields depend on the excitation wavelength, such that a control of photochemical pathways is in principle possible.
3. The energy of the lowest optically accessible excited state frequently lies in the visible spectral range, enabling photochemical transformations to be accomplished with visible light.
4. The presence of the heavy metal atom induces strong spin-orbit coupling, considerably relaxing the spin selection rule and resulting in fast or ultrafast intersystem crossing. Thus long-lived, low-energy triplet excited states are readily accessible, enabling many applications.
5. The almost modular structure of transition metal complexes—Ligand₁-Metal-Ligand₂—brings about synthetic versatility inaccessible with organic compounds. It is possible to adjust the periphery of a complex to meet a particular requirement—tuning the energy of the lowest electronic transition, controlling solubility, adding functional groups required for attachment to surfaces, etc.—whilst maintaining both the immediate coordination sphere of a metal complex and the nature of the lowest excited state.

The photophysics, photochemistry and applications of transition metal complexes are the subjects of several comprehensive books [2–5] and recent reviews [6–9]. Hence, we will only briefly present the basic aspects of this broad field. We

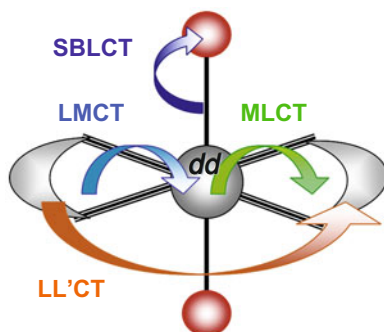


Fig. 3.1 Main types of excited state in transition metal complexes

start from the description and classification of different types of electronic excited state which can be potentially formed in metal-containing species (Fig. 3.1), and follow with some examples of reactions for each type of the excited state.

3.2 The Two Timescales

The photochemistry and photophysics of metal-containing compounds can occur in two very different time domains: ‘ultrafast’ (from a non-equilibrated excited state), and ‘slow’, from thermally-equilibrated excited states. The distinction is not often clear, but it is important to note that a thermally equilibrated excited state has reached Boltzmann distribution, and is usually considered to be in the lowest vibrational level on the corresponding potential energy surface. Such excited states can possess a very long lifetime, from nanoseconds to milliseconds or even longer. They can be regarded as independent species—a higher energy ‘isomer’ of the ground state—whose reactivity can be described by equilibrium thermodynamics and transition state theory.

In contrast, ‘ultrafast’ photochemistry frequently occurs from a non-equilibrated, higher lying and/or vibrationally ‘hot’ excited states, in which the reaction takes place from a vibrational level higher than the zero level of the relevant electronic excited state. This phenomenon is partly due to the fact that Frank–Condon (FC) electronic excited states are usually formed vibrationally ‘hot’, due to the relative displacement of the potential energy surface of the excited state with respect to that of the ground state. Energy dissipation from the FC state leading to the population of the zero vibrational level of the final electronic state involves three main processes: vibrational relaxation, intramolecular vibrational energy redistribution, and transfer of energy to the solvent. The overall process usually takes from several picoseconds if organic groups are involved, to several tens of picoseconds if the coupling between the group in question and the rest of the molecule is weak, as is often the case with, for example, metal carbonyls. An example of an ultrafast process originating from a non-relaxed excited state is intersystem crossing in metal complexes, in which the heavy atom effect facilitates spin–orbit coupling, leading to the rates of intersystem crossing (ISC) being on the scale of tens/hundreds of femtoseconds—orders of magnitude faster than in organic molecules. More generally, examples include ‘predissociation’ [1] or any ultrafast photodissociation, which occur on a timescale faster than relaxation to the zero vibrational level of the lowest excited state. Of course processes occurring on different photochemical time scales are closely interrelated—the formation and reactions of vibrationally relaxed electronically excited states follows from the ultrafast steps. A special type of non-equilibrated excited state process is when a chemical reaction occurs from a non-zero vibrational level of the *ground* electronic state—this type of reactivity is sometimes termed *infrared photochemistry*.

The distinction between ‘non-relaxed’ and ‘relaxed, equilibrium’ photochemistry has been acknowledged for a long time [10]. However, only recently with the

advent of ultrafast methods has it become possible to directly follow the processes involving vibrationally ‘hot’ excited states in real time [11]. Here, we define the *ultrafast* scale in condensed media as that from femtoseconds to the completion of vibrational relaxation, *i.e.* tens to hundreds of picoseconds. From the point of view of experimental observations, vibrational relaxation is accompanied by a shift of the absorption bands in the electronic transient absorption (TA) spectrum. The process is considerably more evident in the transient infrared spectra, where vibrational cooling from *e.g.* $\nu' = 1$ to $\nu' = 0$ is accompanied by a disappearance of the absorption due to $\nu'_1 \rightarrow \nu'_2$ (or transitions involving higher vibrational levels) and an increase in the intensity of the absorption band due to $\nu'_0 \rightarrow \nu'_1$. A narrowing of the transient IR bands is also observed in the course of vibrational relaxation. An emerging method for study of vibrational relaxation is transient two-dimensional infrared spectroscopy (T-2DIR) which allows direct insight into the dynamics of vibrational energy redistribution in the interrogated system [12, 13]. T-2DIR also has the power to resolve coupling between individual vibrational modes in the excited state(s), as well as coupling between intermolecular and solvent vibrational modes accompanying a particular excited state reaction, thus providing a new insight into reaction mechanisms in photochemistry.

In order to obtain a complete picture of the excited states of a metal complex, a combination of time-resolved spectroscopic techniques are typically used. Transient electronic spectroscopy is the most common tool to follow dynamics of the excited states. In this type of transient spectroscopy, the probe pulse usually is in the UV/Vis part of the spectrum. However, the electronic absorption spectra of excited states are generally very broad and not always distinct. Therefore, if multiple excited states are formed, electronic spectroscopy is best combined with time-resolved vibrational spectroscopy. Time-resolved vibrational spectroscopy (TRVS) provides a powerful and complementary method to resolve a manifold of close-lying excited states because it probes molecular structure. TRVS is also invaluable for elucidating the dynamics of vibrationally hot electronic states which are frequently formed upon initial photo-excitation and play a key role in the ultrafast intramolecular energy redistribution. The frequently used types of TRVS are time-resolved infrared (TRIR) [9], and time-resolved Raman methods. TRIR uses UV/Vis excitation and probe/detection in the mid-IR range of the spectrum, typically from 1200 up to 2500 cm^{-1} . It was initially applicable mainly to molecules bearing strong IR-reporters such as C=O, or C \equiv C, or C \equiv N [14]. Major developments in detector sensitivity have made it possible to investigate much weaker IR bands, essentially covering the entire molecular framework. Changes in the *energy* of the infrared bands of a metal complex in the excited state, if compared to the ground state, indicate changes of electron density distribution, and assists in assignment of the nature of the excited states involved. Changes in the relative *intensity* of the IR bands between ground and excited electronic states can yield further structural information.

The combined use of spectroelectrochemical and time-resolved IR methods, which illustrates the value of complementary methods used in parallel, is illustrated in Fig. 3.2, for a Pt(II) diimine complex Pt(bpyam)Cl₂, bpyam = 4,4'-{C(O)NEt₂}₂-2,2'-bipyridine [15]. The bottom panel in Fig. 3.2 demonstrates the

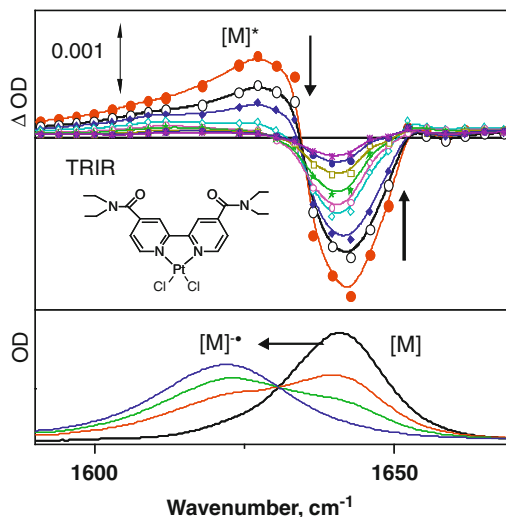


Fig. 3.2 *Bottom panel:* ground state FTIR spectrum (*black*) and a series of spectra obtained in the course of electrochemical reduction. *Top panel:* a series of TRIR spectra of Pt(bpyam)Cl₂ in CH₂Cl₂, recorded at 1, 2, 3, 5, 7, 10, 15, 20 and 25 ps time delays after initial excitation with a 400 nm, ~150 fs laser pulse [15]

19 cm⁻¹ shift to lower energy of the $\nu(\text{CO})$ of the neutral molecule upon electrochemical reduction to [Pt(bpyam)Cl₂]^{-•}. This species, according to density functional theory (DFT) calculations, should be represented as [Pt(bpyam^{-•})Cl₂] following a ligand-centred reduction, with an excess of electron density on the π^* orbital which is largely -C=O localised. On the other hand, upon promotion to the excited state, the ground-state $\nu(\text{CO})$ is transiently shifted to lower energy by about the same amount such that it almost coincides with $\nu(\text{CO})$ of [Pt(bpyam)Cl₂]^{-•}. Thus, the TRIR behaviour is consistent with the Pt → bpyam metal-to-ligand charge transfer (MLCT) nature of the lowest excited state, in which the same $\nu(\text{CO})$ π^* antibonding orbital is populated.

Another type of TRVS, time-resolved resonance Raman spectroscopy, highlights vibrations coupled to a particular electronic transition in the excited state, assisting in assignment of the nature of the frontier orbitals [16, 17].

Apart from optical methods already mentioned above a plethora of other methods for characterising excited states exist, including application of X-rays for direct structural interrogation of transient species. Time-resolved X-ray diffraction and X-ray absorption spectroscopy [X-ray absorption near edge structure (XANES), and the extended X-ray absorption fine structure (EXAFS)] allow unprecedented insight into both dynamics and structure of short-lived excited states [18–22]. Another interesting aspect of modern inorganic photochemistry is the use of various reaction media such as low-temperature matrices to trap reactive intermediates, supercritical fluids [23] or ionic liquids [24] to encourage reaction conditions not accessible in conventional solvents.

Inorganic photochemistry embraces all modern methods, rapidly developing with the increasing technological advances in excitation sources and detectors, which make accessible detection and measurement of ever faster processes, and ever more elusive reaction intermediates and excited states.

3.3 Classification of Excited States in Transition Metal Complexes

The photoreactivity of an excited state depends largely on its energy, lifetime, and the nature of the orbitals involved. It is therefore important to provide classification of the most common types of excited state in metal-containing species.

3.3.1 *Intra-Ligand Excited States (IL)*

Most intra-ligand (also called ligand-centred) transitions will remain upon coordination of the ligand to the metal centre, although their energies may be somewhat perturbed, and the rates of intersystem crossing (hence emission lifetimes and yields) may be strongly affected by the metal centre due to the heavy atom effect. Examples of IL transitions include $\pi \rightarrow \pi^*$ or $n \rightarrow \pi^*$ transitions. Examples of coordination compounds whose lowest excited states are ligand-centred include metalloporphyrins as well as some metal complexes such as $[\text{Rh}(\text{bpy})_3]^{3+}$ or $[\text{Zn}(\text{terpy})_2]^{2+}$ in which the metal centre is redox inactive.

Given the focus of this chapter on metal complexes, we concentrate below on those types of electronic transitions which either involve directly, or are affected by, the metal centre. These involve metal-centred transitions such as *dd* or *ff*; charge-transfer metal/ligand transitions (metal-to-ligand or ligand-to-metal), and transitions between different ligands which can only occur because they are anchored to the same metal ion.

3.3.2 *Metal-Centred Excited States: dd*

According to ligand field (LF) theory, the energy of the MC (LF) state depends on the ligand and on the metal centre (Fig. 3.3) [25].

For a given ligand, the ligand field splitting increases with the increase of the number of electrons of the central atom, thus following the trend 1st row transition metals < 2nd row transition metals < 3rd row transition metals, and therefore the energy of the LF transitions follow the same trend. The important consequences for photophysics and photoreactivity are that LF states are much more often lowest

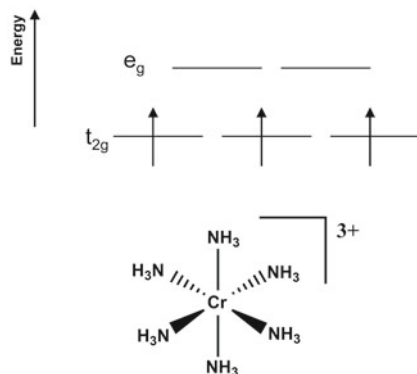


Fig. 3.3 An example of a Cr(III) complex

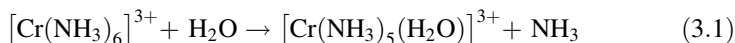
in energy in complexes of 1st and 2nd transition metal complexes, and frequently determine their photoreactivity. A typical example, which we will discuss in detail below, is ligand dissociation, initiated by a ligand field transition corresponding to electron density shift from a metal-ligand non-bonding to a metal-ligand antibonding orbital. A classical example is photosubstitution of the ligands in Cr(III) complexes in aqueous solutions [2].

3.3.2.1 Reactivity of dd States: Octahedral Cr^{3+} (d^3)

The electronic configuration of Cr(III) complexes is d^3 (${}^4A_{2g}$ in octahedral symmetry). The lowest excited state in these complexes is frequently a dd -state (${}^4T_{2g}$), formed as a result of a $t_{2g} \rightarrow e_g$ transition with no spin change [25]. This $d \rightarrow d$ transition corresponds to a transition from a non-bonding to an antibonding metal-ligand orbital, hence the metal-ligand bonding is weaker in the excited state, promoting photodissociation and photosubstitution of the ligands.

Octahedral Cr(III) complexes undergo ligand photosubstitution reactions through a variety of mechanisms:

Photoaquation reactions:

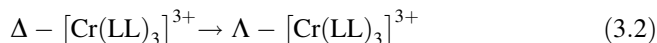


Photolabilisation reactions:

Photolabilisation of the ligand (*i.e.* ligand loss) is believed to be the first step in the light-induced water substitution in the hexa-aqua complex $[\text{Cr}(\text{H}_2\text{O})_6]^{3+}$. For instance, photolysis of $[\text{Cr}(\text{H}_2\text{O})_6]^{3+}$ in the wavelength range 400–575 nm in the presence of Cl^- or SCN^- ions lead to a substitution of the water molecule by halogen or pseudohalogen. The quantum yield of this reaction is extremely low—in the order of 10^{-4} . Such low efficiency corresponds well with the very short lifetime of the excited state, of the order of several picoseconds.

Photoracemisation reactions:

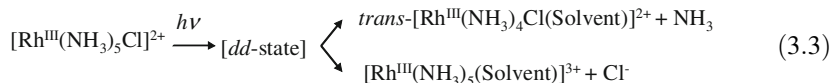
Octahedral complexes of three chelating bidentate ligands, LL, can exist as two optical isomers, Δ and Λ . Due to weaker metal-ligand bonding in the excited state, it is possible to induce racemisation photochemically:



These reactions have been studied for a variety of bidentate ligands, including 1,2-diaminoethane, pentane-2,4-dionate, and 1,10-phenanthroline. The quantum yield of the racemisation reaction is of the order of 1–2 % in each case, indicating similar pathways for all of those complexes [2].

3.3.2.2 Reactivity of *dd*-States: Rh(III) (d^6)

The electronic configuration of octahedral rhodium(III) complexes is low-spin d^6 . The lowest excited state in these complexes is a *dd*-state, formed as a result of a $t_{2g} \rightarrow e_g$ transition [26]. In contrast to the majority of other transition metal complexes, some Rh(III) complexes have a relatively large energy difference between the *dd*-state and higher lying states of different origin, such as a ligand-to-metal charge transfer (LMCT) state. Therefore the observed photochemistry, if it occurs from the lowest, equilibrated, state is exclusive to the *dd*-state—as confirmed by wavelength-independent photochemistry under excitation within the lowest absorption band manifold. Thus these complexes serve as an excellent model for the ligand field excited state chemistry of other complexes possessing the d^6 configuration. Their reactions involve largely ligand dissociation and ligand substitution processes.



3.3.2.3 Towards Long-Lived Excited States

Raising the energy of the *dd*-state

Another, indirect, influence of *dd*-states on photophysics and photoreactivity is through thermal population of a *dd*-state from a lower-lying excited state. The formation of *dd*-states is associated with the large structural distortions due to the Jahn-Teller effect [25]. Consequently, these states provide an efficient channel for non-radiative decay, leading to extremely short excited state lifetimes. For example, thermal population of *dd*-states is held to be responsible for the lack of emission and extremely short (sub-nanoseconds) excited state lifetimes for the lowest metal-to-ligand or ligand-to-ligand excited states (see below) in Pt(diimine)L₂ complexes (L = Hal, PhS⁻ or RO⁻).

Long-lived intra-ligand excited states

An alternative route to long-lived excited states in transition metal complexes is to populate an excited state localised on a pendant arm. For example, a switch from a very short lived MLCT state in $[\text{Pt}(\text{tpy})\text{Cl}]^+$ to a long-lived intra-pyrene excited state in $[(4'\text{-pyrene})\text{-tpy-Pt-Cl}]^+$, has been demonstrated: an electron-rich aryl substituent at the 4' position of the tpy ligand promotes the low-lying excited state with intra-ligand charge-transfer (ILCT) character, enhances the emission intensity, and extends the excited-state lifetime up to 64 μs in r.t. dichloromethane solution [35].

Another example is that of a Pt(II)-based dyad designed for photoinduced charge separation, $\text{Pt}(\text{phen-NDI})\text{Cl}_2$, featuring a naphthalene-1,8-dicarboxy-dii-mide electron acceptor (NDI) appended to the 1,10-phenanthroline (phen) moiety [36]. Here, an initial excitation producing $^1\text{MLCT}$ Pt-to-phen excited state is followed by ultrafast ISC into the corresponding $^3\text{MLCT}$ state, and formation of the charge-separated state $[\text{Cl}_2\text{-Pt}^{\text{II}}]^+(\text{phen})\text{-(NDI}^\bullet\text{)}$, which decays partially by reforming the ground state, and partially by populating a ^3NDI localised excited state which has a lifetime as long as 520 μs .

Yet another interesting instance of achieving a long lifetime—651 μs —of a charge-transfer excited state is a Re(I) complex $\text{Re}(\text{PNI-phen})(\text{CO})_3\text{Cl}$, where the PNI-phen is N-(1,10-phenanthroline)-4-(1-piperidinylnaphthalene-1,8-dicarboximide [37]. Introduction of the PNI-acceptor group increases the lifetime of the $^3\text{MLCT}$ excited state approximately 3000-fold in comparison to that of the model complex $[\text{Re}(\text{phen})(\text{CO})_3\text{Cl}]$. The effect was attributed to the thermal equilibration between the emissive $^3\text{MLCT}$ state and a long-lived triplet state of the ^3PNI chromophore, which is similar in energy. In this case, the long lifetime was attributed to a specific ‘reservoir effect’ between $^3\pi\pi^*$ and $^3\text{MLCT}$ states.

These examples demonstrate the wealth of excited states in metal chromophores and how subtle changes in structure can alter the nature of the lowest excited state and consequently the overall light-induced properties.

3.3.3 Metal-Centred Excited States: *ff*

Another type of MC transition is *ff*-transitions which occur in lanthanide and actinide complexes. In contrast to *dd*-transitions, much less relaxation of the Laporte selection rule is possible (see Chap. 1), with the result that the molar absorption coefficient for those transitions is typically less than 1–10 $\text{dm}^3 \text{mol}^{-1} \text{cm}^{-1}$. Excitingly, the strongly forbidden nature of the *ff*-transitions has a large positive effect on their photophysical properties—the emission emanating from *ff*-excited states is extremely long lived, which makes lanthanide complexes most attractive candidates for any emission-related applications, from sensing to imaging of live cells to pressure detectors and optoelectronics, of which the most well-known are the Nd:YAG laser and the phosphors used in ‘fluorescent’ lights and cathode-ray tube television screens [2]. The lability of the Ln/Ac metal–ligand bonds leads to a

wealth of thermal substitution reactions, and, consequently, photochemical ligand substitution is rarely studied. The main photochemical reactions of interest in the complexes of the lanthanide and actinide ions are photoredox reactions.

The photochemistry of lanthanide complexes typically concerns the ligands, and in most cases does not involve metal-centred redox process. The main exceptions are redox couples $\text{Eu}^{2+/3+}$, $\text{Yb}^{2+/3+}$ and $\text{Ce}^{3+/4+}$, in which the reactions are driven by increased stability of Ce^{4+} , Eu^{2+} , Yb^{2+} and due to the empty ($4f^0$) half-filled ($4f^7$) or filled ($4f^{14}$) electronic configurations respectively.

3.3.4 Charge Transfer Transitions

The charge transfer (CT) transitions discussed below are characterised by:

1. moderate to large molar absorption coefficients, from $\sim 10^2$ to $\sim 10^4 \text{ dm}^3 \text{ mol}^{-1} \text{ cm}^{-1}$;
2. the energy of the transition being dependent on the donor/acceptor properties of the ligands involved;
3. the corresponding absorption and emission bands do not show vibrational progression;
4. negative solvatochromism of the corresponding absorption band for the majority of CT transitions, whereby the energy of the transition decreases with the decrease in the polarity of the solvent [4].

3.3.4.1 Metal-to-Ligand Charge Transfer

This type of transitions is common when the metal centre has a relatively low oxidation potential, and a relatively low-lying vacant molecular orbital is localised on the electron-accepting ligand. Thus, the metal centre acts as an electron donor, and the ligand as an electron acceptor, to give a charge-transfer $\text{M}^{\bullet+}-\text{L}^{\bullet-}$ excited state with an oxidised metal centre and a reduced ligand. Typical examples include diimine complexes of transition metals, such as $\text{Ru}(\text{II})$, $\text{Re}(\text{I})$ or $\text{Pt}(\text{II})$.

The archetypal example of the compound which possesses an MLCT lowest excited state, formed as a result of a light-induced shift of electron density from the metal centre to the ligand, is the tris(bipyridyl) $\text{Ru}(\text{II})$ dication, $[\text{Ru}(\text{bpy})_3]^{2+}$. The structure and the schematic energy level diagram for this ion are given in Fig. 3.5.

The $[\text{Ru}(\text{bpy})_3]^{2+}$ dication efficiently absorbs light in the visible region ($\lambda_{\text{max}} = 452 \text{ nm}$, $\epsilon = 13,000 \text{ dm}^3 \text{ mol}^{-1} \text{ cm}^{-1}$ in acetonitrile), forming an $^1\text{MLCT}$ excited state. This process is followed by rapid intersystem crossing to the lowest triplet ($^3\text{MLCT}$) state, facilitated by strong spin-orbit coupling associated with the

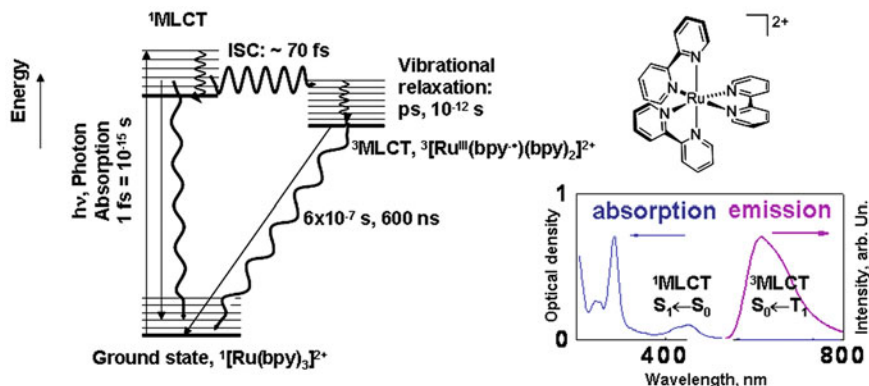


Fig. 3.5 Structure of the octahedral $[\text{Ru}(\text{bpy})_3]^{2+}$ ion, the corresponding energy level diagram showing the major processes and their time scales, and the absorption/emission spectra of $[\text{Ru}(\text{bpy})_3](\text{PF}_6)_2$ in hexane at r.t.

Ru-centre. The rate of intersystem crossing to the $^1\text{MLCT}$ state is of the order of hundreds of femtoseconds or even faster [38, 39]. As emission from the $^3\text{MLCT}$ excited state to the singlet ground state is spin-forbidden, it has a relatively long lifetime in deoxygenated solutions at r.t. (e.g. 630 ns in water) [40]. The relatively high emission quantum yield (2.8 % in aerated water) has led to its use as an emission standard.

The long lifetime of the $^3\text{MLCT}$ state, and the relative ease of its reduction and oxidation, make this complex a useful model for the studies of photoinduced electron transfer. As a result of such a favourable combination of photophysical properties, numerous artificial photosynthetic systems have been constructed based on this complex both as a chromophore and as an electron donor or acceptor in its excited state. Whilst the ion is photochemically inert at r.t., photolysis of its aqueous solution at 95 °C with 436 nm irradiation results in labilisation of 2,2'-bipyridine [40]. It was therefore proposed that a different, reactive excited state becomes accessible at higher temperatures. This upper state lies $\sim 3600 \text{ cm}^{-1}$ (0.44 eV) higher in energy than the lowest state, and is assigned to a dd -state, which gives rise to ligand substitution photochemistry.

A well-developed series of complexes with rich MLCT excited-state behaviour are Re(I)-diimine complexes. $[\text{Re}(\text{bpy})(\text{CO})_3\text{Cl}]$ was the first transition metal complex used as a catalyst for CO_2 reduction to CO, proposed by Lehn and Ziessel [41]. This series of complexes is particularly amenable to study of the excited state by time-resolved infrared spectroscopy. Formation of the $^3\text{MLCT}$ $\text{Re} \rightarrow \text{bpy}$ excited state leads to a reduction of the electron density on the metal centre. Consequently, $d \rightarrow \pi$ backbonding from Re d -orbitals to the antibonding π^* orbitals of CO ligands is reduced, resulting in an increase of the energy of the stretching vibrations, $\nu(\text{CO})$, by several tens of wavenumbers in the excited state if

compared to the ground state. This large effect allowed the researchers to follow the dynamics of the charge transfer process by monitoring the rates of formation and decay of the transient bands in the infrared spectrum.

3.3.4.2 Ligand-to-Metal Charge Transfer

This type of transition occurs from an occupied, low-lying ligand-localised orbital to a vacant orbital of the metal centre. It is most common if the metal centre is highly oxidised, and the ligand is a strong electron donor (*i.e.* the exact converse of the situation which gives rise to MLCT excited states). A classical example is the permanganate anion MnO_4^- , in which an intense violet–purple color is due to an LMCT transition. Whilst MnO_4^- is formally a d -metal complex, no dd -transitions can take place in a fully oxidised Mn(VII) centre that has the d^0 configuration.

The uranyl ion, UO_2^{2+} , provides another example of an LMCT state, this time involving f -orbitals of the metal centre [42]. The LMCT excited state, which is the lowest excited state, is formed by electron transfer from a p -orbital of the uranyl oxygen atom to an empty $5f$ -orbital on the uranium centre, giving rise to intense absorption at *ca.* 420 nm. An intriguing property of the UO_2^{2+} is its phosphorescence that emanates from the lowest triplet state with a potential quantum yield of 100 % in the solid state. The chemistry and photochemistry of the uranyl cation has seen a recent renaissance, largely inspired by its relevance to nuclear waste monitoring and processing. A variety of luminescent adducts have been developed (Fig. 3.6, left) [43], which can potentially be used for emission sensing in the environment and/or in extraction and reprocessing conditions.

An LMCT is also the lowest transition of some Mo-dithiolene complexes which are used as components in various magnetic and conducting materials and in chemical analogues of the catalytic centres of molybdenum oxo-transferase enzymes such as sulfite oxidase and DMSO reductase [44]. Also, many Mo-dithiolene complexes, including $[(\text{Cp})_2\text{Mo}(\text{dithiolene})]$ compounds (Fig. 3.6, right), possess not one but several dithiolene-Mo LMCT transitions close in energy to one another due to the presence of several closely-spaced and energetically accessible vacant d -orbitals on the Mo centre [45].

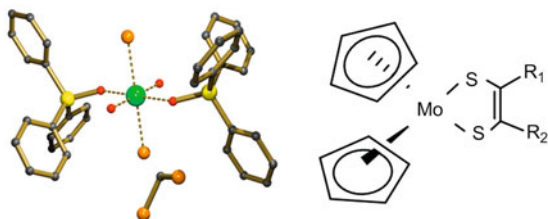


Fig. 3.6 Examples of compounds with a lowest energy LMCT excited state. *Left*– UO_2 -adducts $\text{trans-UO}_2\text{Cl}_2(\text{OAsPh}_3)_2$ [43], *right*– $\text{Mo}(\text{Cp})_2(\text{dithiolene})$ [45]

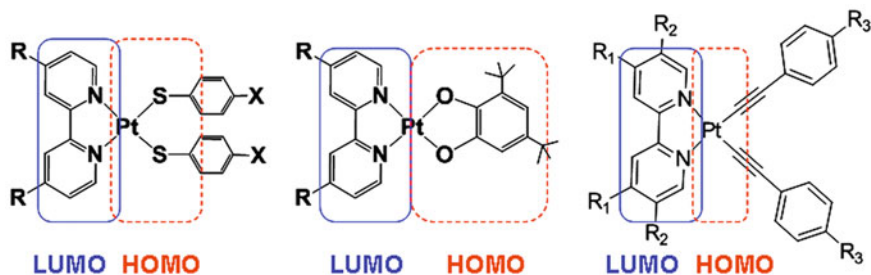


Fig. 3.7 Different types of charge-transfer transitions in Pt(II) diimine complexes bearing thiolate, catecholate, or acetylide donor ligands

3.3.4.3 Ligand-to-Ligand Charge Transfer

This type of electronic transition occurs if one of the ligands has a high-lying occupied orbital, and another has a low-lying vacant orbital, such that one is a good electron donor and the other a good electron acceptor. In most cases the orbitals involved cannot be classified as ‘pure’ ligand-localised orbitals, but have some degree of metal character. Thus the usual notation is not LLCT, but $ML'/LLCT$ for this type of transition, which is a more correct reflection of the orbital composition. Of course the transition probability depends on an overlap between the orbitals involved, and hence metal d -orbital contribution in both the highest occupied molecular orbital (HOMO) and the lowest unoccupied molecular orbital (LUMO) increase significantly the extinction coefficient of such electronic transitions.

Pt(diimine)(dithiolate) [46], Pt(diimine)(thiolate)₂ or Pt(diimine)(catecholate) complexes (Fig. 3.7) are typical examples of the compounds possessing lowest electronic transition of mainly LLCT nature, from thiolate/catecholate (HOMO) to diimine π^* (LUMO). The absorption maxima, emission maxima and oxidation potential of these compounds dramatically depend on the donor ligand. For example, the oxidation peak potential for Pt(2,2'-bipyridine)(4-X-C₆H₄-S)₂ compounds changes from +0.58 V for X = NO₂, to -0.23 V for X = NMe₂ (vs Fc⁺/Fc in THF), whereas the 1st reduction potential is almost not affected. Such a strong influence of the thiolate ligand on the oxidation potential of the complex clearly indicates its significant participation in the HOMO [47]. However, even in this case there is a considerable contribution of Pt d -orbitals in both the HOMO and the LUMO, and thus the excited state is a combination of MLCT/LLCT, denoted {charge-transfer-to-diimine}, or $ML'/LLCT$ lowest excited state.

The extent of the contribution of the Pt d -orbitals to the frontier orbitals can be directly assessed by electron paramagnetic resonance (EPR) (spectro) electrochemical experiments as demonstrated in Fig. 3.8. These experiments are only possible for those compounds in which the redox process in question is chemically and electrochemically reversible. For example, the EPR studies on the radical anions revealed ~10 % contribution of Pt(II) orbitals in the LUMO of Pt(4,4'-X₂-2,2'-bipyridine)Cl₂ systems [48]. Likewise, 12 % Pt $d(z^2)$ contribution in the

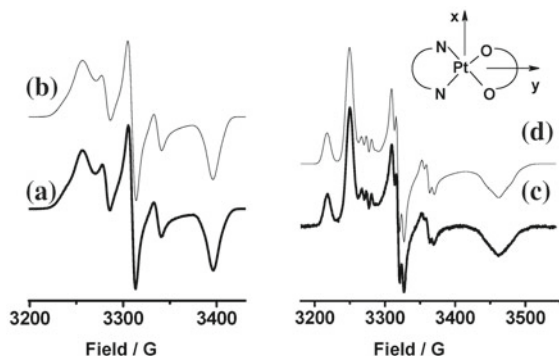


Fig. 3.8 Pt^(Bubpy)(^{Bucat}) radical-cation (*left*) and anion (*right*). Experimental **a** and simulated **b** EPR spectra of radical-cation in CH₂Cl₂ containing 0.4 M [Bu₄N][PF₆] at 77 K. Experimental **c** and simulated **d** EPR spectra of 1 the radical-anion in DMF containing 0.2 M [Bu₄N][PF₆] at 77 K. Copyright © American Chemical Society 2008 [49]

HOMO was determined by modelling the EPR spectra of the radical-cation of the complex [Pt(2,9-Ph₂-1,10-phenanthroline)(catecholate)], and of related compounds [49]. Participation of metal-based orbitals in the HOMO and the LUMO is significant for photophysical properties—it leads to higher molar absorption coefficients ($\sim 10^3 \text{ dm}^3 \text{ mol}^{-1} \text{ cm}^{-1}$) than for a transition which is purely LLCT in nature, such as the one observed in the analogous tetrahedral Zn(diimine)(SAr)₂ complexes where the LLCT is ‘pure’ with $\epsilon \sim 200 \text{ dm}^3 \text{ mol}^{-1} \text{ cm}^{-1}$ [50].

The solvatochromic behaviour of the absorption spectra of complexes of this type illustrated in Fig. 3.9 is a further proof of the charge-transfer nature of the lowest electronic transition. Differently to thiolate or catecholate complexes, the lowest excited state in the bis-acetylide complexes Pt(diimine)(C≡C-R)₂ (R = 4-X-C₆H₄-) mentioned above is a charge-transfer from the largely Pt based HOMO to the Pt/diimine-based LUMO. Consequently, the effect of electron donating properties of the acetylide ligand has much lesser influence on the redox and optical properties of the complexes [29, 30, 51] if compared to thiolate ligands.

3.3.4.4 Sigma-Bond-to-Ligand Charge Transfer

Another type of CT transition is that resulting in sigma-bond-to-ligand charge transfer states, also known as σ - π^* states. Those involve an occupied orbital located on a sigma-bond between the metal centre and a ligand, and a vacant orbital located on the ligand. Examples of compounds with a SBLCT excited state are the metal–metal bonded compounds [M(SnR₃)₂(CO)₂(α -diimine)] (M=Ru, Os; R=Me, Ph) [52, 53] (Fig. 3.10). The SBLCT transition is accompanied by a shift of electron density from the σ (Sn–M–Sn) bonding orbital to the α -diimine-ligand. Consequently, the SBLCT excited states often undergo a photo-induced M–Sn

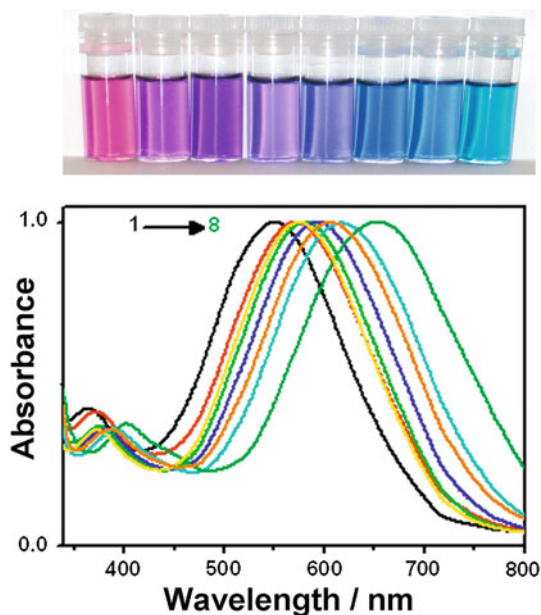


Fig. 3.9 The LLCT lowest absorption band, and its solvatochromism, for Pt(bpy)(3,5-di-^tBu-catecholate). Normalised absorption spectra recorded in solvents of different polarity: 1 methanol, 2 ethanol, 3 CH₃CN, 4 DMSO, 5 DMF, 6 acetone, 7 CH₂Cl₂, and 8 CHCl₃. Adapted with permission from Ref. [15]. Copyright 2010 American Chemical Society

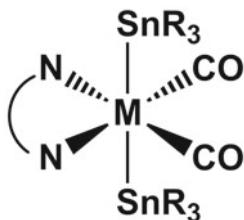


Fig. 3.10 Sigma-bond-to-ligand charge transfer is exemplified in [M(SnR₃)₂(CO)₂(diimine)] (M = Ru, Os; R = Me, Ph)

bond homolysis at room temperature and provide an example of dissociative photochemistry, which in turn opens up routes to new compounds.

The selected examples above demonstrate the wealth of excited states in metal chromophores and how subtle changes in structure can alter the nature of the lowest excited state and consequently the overall light-induced properties.

3.3.5 Tuning the Nature of the Lowest Excited State by the Nature of the Ligand

The presence of a manifold of close in energy low-lying excited states of different origin is an intrinsic feature of transition metal complexes. This feature opens up exciting possibilities to tune their photophysical properties as well as their photoactivity by modifying the ligand(s).

A series of octahedral complexes $[\text{Re}^{\text{I}}\text{X}(\text{CO})_3(\text{bpy})]$ ($\text{X} = \text{halide}$) and related Ru(II) complexes provide an illustration of this idea. The lowest excited state in $[\text{Re}(\text{Cl})(\text{CO})_3(\text{bpy})]$ is of primarily $\text{Re} \rightarrow \text{bpy}$ MLCT character, although the HOMO has some Cl^- contribution. Upon replacement of Cl^- with Br^- , and further with I^- , the HOMO gains an increasingly larger contribution from the halide anion, and the lowest excited state gradually becomes a halide(X) \rightarrow ligand ($\text{bpy} \pi^*$) charge-transfer (XLCT) [54]. A similar trend is observed for the nature of the lowest excited state in complexes $[\text{RuX}(\text{Me})(\text{CO})_2(\text{diimine})]$ (diimine = bpy; R-DAB: *N,N*-di-*R*-1,4-diaza-1,3-butadiene) along the sequence $\text{X} = \text{Cl}, \text{Br}, \text{I}$.

These complexes also demonstrate a change in the excited state character between a Frank-Condon (vibrationally 'hot') electronically excited state and the vibrationally relaxed, lowest excited state. Resonance Raman (rR) spectra show that the vibrationally hot Franck-Condon states of $[\text{RuI}(\text{Me})(\text{CO})_2(i\text{Pr-DAB})]$ have virtually pure XLCT character [55]. However, the TRIR data indicate that thermally equilibrated, vibrationally-relaxed excited state has a mixed MLCT-XLCT character [6]. Hence, combining the results from resonance Raman and TRIR data allows one to obtain insight into charge redistribution processes in the excited state on a very short timescale.

The nature of the lowest excited state in Pt(II) diimine complexes $\text{Pt}(\text{diimine})\text{X}_2$ can also be tuned by the nature of the ligands—and is shifted from largely $\text{Pt} \rightarrow \text{bpy}$ MLCT (for $\text{X} = \text{Cl}$), to a ML'/LLCT excited state for $\text{X} = \text{ArS}^-$.

The diversity of excited state types and how they can be tuned by the nature of the ligand is also very well illustrated by metal-metal and metal-alkyl bonded diimine complexes of Re, Ru, Pt and Os. The photochemistry and photophysics of those complexes varies dramatically with the change of the ligands, as the nature of the lowest excited state changes from a long lived SBLCT state in $\text{Ru}(\text{SnPh}_3)_2(\text{CO})(i\text{Pr-DAB})$ (DAB = 1,2-diazabutadiene) which has a strong Ru-Sn bond, to dissociative in $\text{Pt}(\text{alkyl})_2(\text{diimine})$, to very reactive SBLCT-ones in the case of $\text{Re}(\text{SnR}_3)(\text{CO})_3(\text{diimine})$ (with formation of radicals) or triangular clusters such as $\text{Os}_3(\text{CO})_{10}(\text{diimine})$ (which generates biradicals and zwitterions). We will return to some of those examples later in the Chapter.

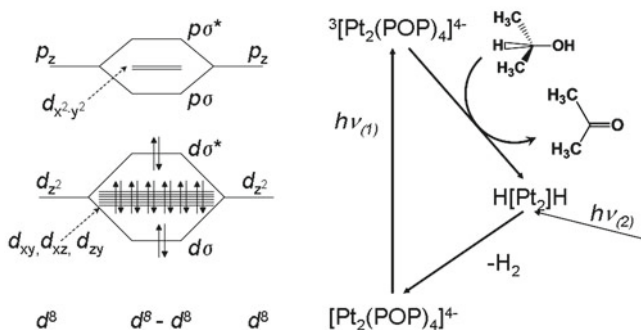


Fig. 3.11 *Left* molecular orbital diagram of $[\text{Pt}_2(\text{P}_2\text{O}_5\text{H}_2)_4]^{4-}$; *Right* Dehydrogenation of isopropanol to acetone using $[\text{Pt}_2(\text{P}_2\text{O}_5\text{H}_2)_4]^{4-}$ as a photocatalyst, based on the description in [6]

3.3.6 Some Dimetallic Species

The excited states of dinuclear d^8 – d^8 platinum, rhodium, and iridium complexes with a variety of bridging ligands exhibit unusually diverse reactivity. These types of compound in their lowest triplet state engage in oxidative and reductive electron transfer reactions, and exciplex formation [56]. They can also engage in atom transfer reactions: *i.e.* they can abstract hydrogen atoms from a wide range of substrates as well as halogen atoms from alkyl and aryl halides.

The most widely documented diplatinum(II) complex is $[\text{Pt}_2(\text{P}_2\text{O}_5\text{H}_2)_4]^{4-}$, which contains bridging (P,P-bonded) diphosphito ligands (Figs. 3.11, 3.12). Photophysical studies confirm that the properties of the photoactive excited state are a manifestation of d^8 – d^8 metal–metal interactions [57].

Excited-state atom transfer: Halogens and H

The triplet state of $^3[\text{Pt}_2(\text{POP})_4]$ is quenched by halogen atom transfer reagents such as alkyl and aryl halides. It also reacts with hydrogen-atom donors—alcohols, Bu_3SnH , Et_3SiH , or H_3PO_3 [57]. The first example of C–H bond cleavage by $[\text{Pt}_2(\text{P}_2\text{O}_5\text{H}_2)_4]^{4-}$ was the photochemical conversion of isopropyl alcohol to acetone and hydrogen (Fig. 3.11). The first step is hydrogen atom abstraction of the methine hydrogen, yielding the radical pair $\{[\text{Pt}_2(\text{P}_2\text{O}_5\text{H}_2)_4]^{4-}\text{-H}\}^\bullet$ and $(\text{CH}_3)_2\text{COH}^\bullet$. This photoinduced reaction is a two-electron process, is catalytic in $[\text{Pt}_2(\text{P}_2\text{O}_5\text{H}_2)_4]^{4-}$, and has been shown to occur *via* a triplet excited state (Fig. 3.11).

There is no formal metal–metal bond in the ground electronic state of these bimetallic compounds. However, light absorption promotes an electron from the antibonding $d\sigma^*$ to the bonding $p\sigma$ (p_z -derived) orbitals, creating a partial (formal order of one) metal–metal bond in the excited state [56]. This transient bonding determines the photophysical and photochemical properties of these complexes. The ultrafast intersystem crossing in the initially formed $^1d(\sigma^*)p(\sigma)$ state yields a corresponding triplet state, which, after thermal equilibration, persists for microseconds.

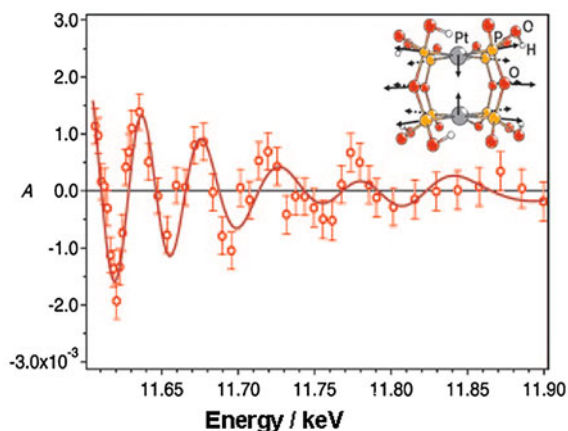


Fig. 3.12 Photoinduced structural changes in $[\text{Pt}_2(\text{P}_2\text{O}_5\text{H}_2)_4]^{4-}$ in solution obtained from EXAFS studies. Transient data (circles) and best fit (solid line) were obtained with the following parameters: a Pt–Pt contraction of 0.31(5) Å, a Pt–ligand elongation of 0.010(6) Å, zero energy shift, and 7 % excitation yield. The error bars represent the standard error of the measurement. Red circles oxygen, orange circles P, grey circles Pt, small white circles H atoms. Adapted with permission from Ref. [59]. Copyright 2009, John Wiley & Sons

Since the reactivity is largely occurring from this lowest triplet state, it is important to directly determine its structure. Recently, a large contraction of the Pt...Pt bond in the triplet excited state of $[\text{Pt}_2(\text{P}_2\text{O}_5\text{H}_2)_4]^{4-}$ has been confirmed directly by time-resolved X-ray diffraction [58] and pico-nanosecond X-ray absorption [59] spectroscopy (Fig. 3.12) and DFT calculations [60]. The results suggest that the strengthening of the Pt–Pt interaction is accompanied by a weakening of the ligand coordination bonds, resulting in an elongation of the platinum–ligand bonds, as schematically shown in the inset in Fig. 3.12.

3.3.7 Multiple Metal–Metal bonds

Another type of excited state arising in multinuclear metal systems is the $\delta\delta^*$ excited state [61–64]. This occurs in quadruply-bonded dinuclear complexes, such as $[\text{Re}_2\text{Cl}_8]^{2-}$ or $[\text{M}_2\text{X}_4(\text{PR}_3)_4]$ where M=Mo or W. In contrast to $[\text{Pt}_2(\text{P}_2\text{O}_5\text{H}_2)_4]^{4-}$ described above, this type of compound possesses a strong—quadruple—bond between two metal centres in the ground electronic state, with the overall electronic configuration of $\sigma^2\pi^4\delta^2$. This bonding is weakened by a promotion of electron density to the antibonding, δ^* , orbital in its lowest $\delta \rightarrow \delta^*$ electronic excited state. An interesting feature of these compounds is that in the initially studied, phosphate-supported M_2 -systems the singlet $^1\delta \rightarrow \delta^*$ excited state is longer lived than its triplet counterpart, $^3\delta \rightarrow \delta^*$. The reason for this

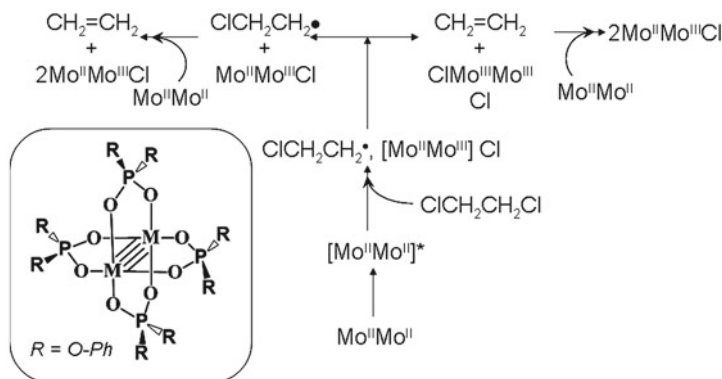


Fig. 3.13 Proposed mechanism of the photochemical reduction of 1,2-dichloroethane by $\text{Mo}_2(\text{O}_2\text{P}(\text{OC}_6\text{H}_5)_2)_4$, adapted from [64]

behaviour is two-fold: firstly, the $S_1 - T_1$ splitting is very large, and secondly, the $T_1 - S_0$ splitting is relatively small, as manifested by the emission occurring in the NIR range of the spectrum. The small $T_1 - S_0$ splitting promotes non-radiative deactivation due to higher density of overlapping vibrational states, which can be described in terms of the energy gap law (Chap. 1) [65].

The presence of two metal centres opens up the possibility to study electronic coupling, and for multielectron photoredox processes to take place, whilst relatively long lifetimes of the excited states (see below) makes possible bimolecular reactions in solution. Accordingly, quadruply-bonded di-Re complexes have been reported to engage in bimolecular electron-transfer reactions, whereas the di-Mo and di-W complexes participate in oxidative addition and two-electron redox reactions. For example, UV irradiation of phosphate-supported M_2 dinuclear complexes under acidic conditions leads to one- or two-electron oxidation of the metal–metal core accompanied by production of H_2 gas by reduction of two protons.

A further example of multielectron photooxidation is that of $[\text{Mo}_2\{\text{PO}_2(\text{OC}_6\text{H}_5)_2\}_4]$ (Fig. 3.13). The lowest energy absorption maximum in this compound occurs at 515 nm in dichloroethane ($\epsilon = 156 \text{ dm}^3 \text{ mol}^{-1} \text{ cm}^{-1}$) and corresponds to the formation of a ${}^1\delta \rightarrow \delta^*$ excited state, whose lifetime of 68 ns is sufficiently long to engage in bimolecular reactions in solution at r.t. Irradiation of this compound with visible light ($> 500 \text{ nm}$) in 1,2-dichloroethane led to formation of ethene, whilst the two Cl atoms from a solvent molecule undergo oxidative addition to the two Mo centres. The maximum quantum yield (0.040) for this reaction is observed upon irradiation at 510 nm, confirming that the reactivity originates from the ${}^1\delta \rightarrow \delta^*$ state whose absorption maximum is in this region [64].

These M_2 complexes offer ample opportunities for tuning their photophysical and photochemical properties by the change of the metal and the supporting ligands. This property is well illustrated by the quadruply bonded dicarboxylates of $\text{M}=\text{Mo}$ or W , $[\text{M}_2(\text{O}_2\text{CR})_4]$, in which the $[\text{M}_2(\text{O}_2\text{CR})_4]$ core has a paddle-

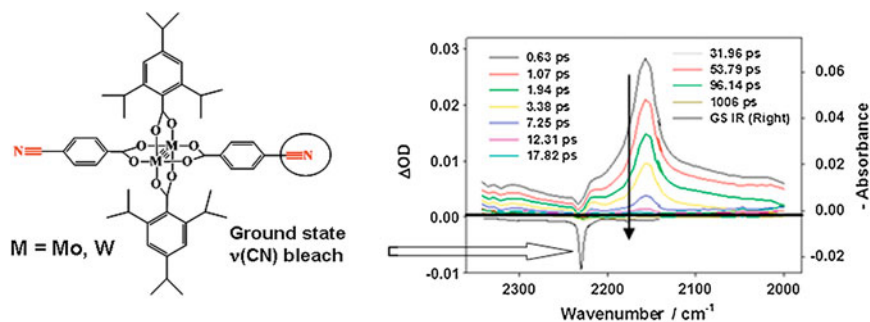


Fig. 3.14 Ultrafast time resolved infrared spectroscopy of a Mo_2 -system supported by carboxylate-type ligands (*left*) in THF at r.t. The spectra are interpreted as a delocalised $^1\text{MLCT}$ excited state at early times, which fully decays into $^3\delta\delta^*$ excited state (lifetime < 10 ns), not detectable in this experiment. Reprinted with permission from Ref. [67]. Copyright © 2011 the National Academy of Sciences

wheel arrangement and local D_{4h} symmetry [66]. In contrast to the phosphinate-supported dinuclear systems described above, these carboxylate-supported systems possess a low-energy $^1\text{MLCT}$ transition due to the low-lying π^* orbital of the carboxylate unit, $\{\sigma(\text{M}_2) \rightarrow \pi^*(\text{CO}_2)\}$. The energy of this transition can be tuned across the entire visible and NIR region of the spectrum, from 400 nm to 1000 nm, by changing the metal (Mo vs W) and involving different conjugated R-groups. Thus interplay between singlet and triplet MLCT and $\delta \rightarrow \delta^*$ excited states is possible. These M_2 complexes frequently exhibit dual emission, demonstrating the presence of several weakly interacting excited states. The fluorescence from these compounds is typically solvent-dependent, pointing towards a charge-transfer nature of the emitting state, *i.e.* $^1\text{MLCT}$. On the contrary, phosphorescence from the majority of Mo_2 -containing compounds is solvent independent, and is also relatively unaffected by the nature of the carboxylate ligand. It occurs at ~ 1100 nm and possess a long emission lifetime of 10–100 μs ; this indicates that the emitting, lowest triplet state for Mo_2 -carboxylate-supported compounds is a $^3(\delta \rightarrow \delta^*)$ one, associated with the MoMo bond. Therefore there is the possibility to change the relative order of MLCT vs $\delta \rightarrow \delta^*$ excited states by changing the design of the compound and thus controlling the reactivity [66–68].

An important question with respect to the structure and the nature of the reactive excited state(s) in such species is whether it is a localised or a delocalised state(s), and what is the time scale of the intersystem crossing?

These questions have been recently addressed using ultrafast time-resolved infrared spectroscopy (Fig 3.14), on the example of *trans*- $\text{M}_2(\text{TiPB})_2(\text{O}_2\text{CC}_6\text{H}_4-4\text{-CN})_2$, where TiPB is 2,4,6-triisopropyl benzoate, which has an IR-reporting CN group. Figure 3.14 shows an example of the TRIR spectra for $\text{M}=\text{Mo}$. The bleach of the stretching vibration $\nu(\text{CN})$ in the ground state, at 2239 cm^{-1} is clearly seen. Notably, the IR bands in the excited state are much broader, and more intense than

that of the ground state. Such behavior is indicative of the large delocalisation in the excited state [66, 67].

Thus, the TRIR studies indicated that in *trans*-M₂(TiPB)₂(O₂CC₆H₄-4-CN)₂ the S₁ state is delocalised over a *trans* pair of carboxylate ligands, and is ¹MLCT in nature for both Mo and W complexes. The lowest triplet excited state in the W₂-compounds was assigned as ³MLCT [67]. In contrast, in the Mo₂ analogue the long-lived triplet states (~50 μs) is ³δ → δ* in nature. This excited state is not detectable by TRIR as it results in no significant changes in the CN stretching vibrations, but is detectable with transient absorption studies.

These differences in the nature of the lowest excited state arise from the balance between the relative orbital energies of the M₂(δ) or M₂(δ*) and the ligand π* orbitals, as well as the magnitudes of the orbital overlap. Such differences in the nature and the degree of delocalisation between singlet and triplet excited states, fine-tuned by ligand design in a set of structurally similar M₂ compounds, demonstrates the breadth of excited states and associated potential reactivity in quadruply-bonded complexes.

One practical application lies in molecular photonics, where incorporation of the M₂ units into conjugated oligomers and polymers could allow for the optical properties and conductivity to be modulated by the properties of the M₂ unit [68].

3.4 Dissociative Photochemistry

The majority of ligand-dissociation reactions are thought to occur on the ultrafast time scale. A relatively rare case of a ‘slow’ ligand dissociation from a relaxed excited state takes place in some amino complexes of Rh(III) and Ir(III), or in Co(II) polycyano complexes. In these complexes, the lowest ligand-field (*dd*) state is formed upon t_{2g} → e_g excitation, and undergoes ligand dissociation and consequent ligand substitution reaction on a nanosecond time scale.

3.4.1 Ligand loss: Dissociation of CO in Metal Carbonyls

Metal carbonyl complexes provide an important advantage for large-scale chemical synthesis due to the high efficiency of the carbonyl ligands’ dissociation under photo-excitation, or at elevated temperatures. Accordingly, metal carbonyl compounds have been extensively used as catalysts in organic syntheses and in catalytic industrial processes [69]. Moreover, recently metal carbonyl complexes have been incorporated into photochromic materials, with applications such as logic gates, information storage or optical switches in mind [7].

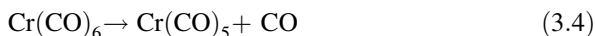
The photochemistry of classic examples of transition metal carbonyls—such as Cr(CO)₆, W(CO)₆ or Fe(CO)₅—demonstrates the diversity of reaction pathways and potential products. The labilisation of CO and replacement by another ligand

is the most common photoreaction of mononuclear metal carbonyls $M(\text{CO})_x$ [70]. Detailed spectroscopic studies of the photoreaction intermediates in low temperature matrices [71], and early studies in solutions [72] have shown that in most cases the first step in this reaction is monomolecular dissociation. The dissociation product can be easily solvated by an even weakly coordinating solvent, which can be replaced should a ‘trapping ligand’—a stronger coordinating moiety—be present in solution, thus forming a new compound.

$\text{Ni}(\text{CO})_4$ —the first metal carbonyl compound, discovered in 1890 [73]—and $\text{Fe}(\text{CO})_5$, which was discovered the following year, are the two most studied metal carbonyl compounds [74]. In particular, the photochemistry of $\text{Fe}(\text{CO})_5$ has been extensively studied due to its widespread use in industrial processes as a cheap and reactive compound utilised in a variety of applications, from polymerisation to metallurgy. Consequently, there has been great interest in the mechanisms of reactions, and especially the initial photochemical processes, occurring in $\text{Fe}(\text{CO})_5$ upon irradiation under ambient conditions [75]. Initially, such photochemical studies were only possible in low temperature matrices, in which reactive intermediates would be ‘trapped’ and interrogated by infrared spectroscopy. Several key intermediates such as $^3\text{Fe}(\text{CO})_4$ and $\text{Fe}(\text{CO})_3$ have been identified.

The development of ultrafast methods has allowed the study of the photochemistry of $\text{Fe}(\text{CO})_5$ in solutions at r.t. The photochemical mechanisms thus became accessible, and, for example, the elusive species $\text{Fe}(\text{CO})_3$ and the conversion between $\{^3\text{Fe}(\text{CO})_4\}$ and $\{^1\text{Fe}(\text{CO})_4(\text{solvent})\}$ has been observed in heptane solution and in supercritical (sc) fluids, such as scCH_4 or scXe [76].

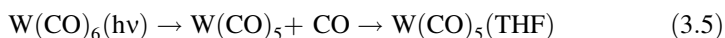
Another classic example of a ligand loss reaction is the ultrafast [77] dissociation of CO from $\text{Cr}(\text{CO})_6$, with the formation of the pentacarbonyl $\text{Cr}(\text{CO})_5$, which occurs with a lifetime of less than 100 fs:



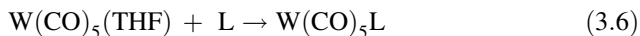
$\text{Cr}(\text{CO})_5$ is only observable in the gas phase at reduced pressure; this $16e^-$ species is extremely reactive and engages in an assortment of processes to complete its coordination sphere—dimerisation yielding dimetallic species, or ligand coordination, leading to a variety of products in the gas and liquid phase.

The nature of the dissociative excited state is still being discussed. For instance, for $\text{Cr}(\text{CO})_6$, the dissociative excited state was initially believed to be a *dd*-state; however, calculations by DFT and TD-DFT methods indicated that the lowest excited state may have a Cr-to-CO MLCT character.

In a similar fashion, photolysis of $\text{W}(\text{CO})_6$ leads to CO loss, and the resulting species $\text{W}(\text{CO})_5$ persists in weakly coordinating solvents such as heptane. However, addition of a coordinating solvent such as THF to the heptane leads to fast (diffusion-controlled) formation of the corresponding THF complex:



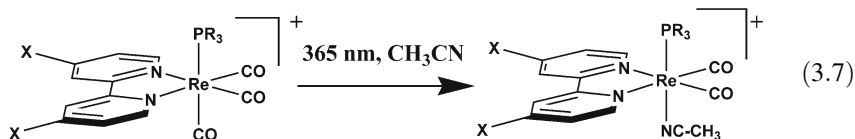
If the reaction is performed in THF, but in the presence of an even stronger coordinating ligand L, such as pyridine, THF may also be replaced:



For instance, photolysis of $\text{W}(\text{CO})_6$ in benzene and cyclohexane in the presence of $\text{L} = \text{py}$ or CH_3CN occurs with a quantum yield of 0.7, which is independent of the excitation wavelength in the range from 254 to 366 nm, and also independent of the concentration of the coordinating ligand L [78]. These early observations pointed towards a dissociative mechanism of photosubstitution, in accordance with the subsequently established ultrafast nature of the CO-dissociation.

Monosubstituted metal carbonyls $\text{M}(\text{CO})_5\text{L}$ can react with another coordinating ligand L^1 via two principal dissociative pathways: initial CO loss and subsequent formation of $[\text{M}(\text{CO})_4\text{LL}^1]$, or initial loss of the ligand L followed by formation of $\text{M}(\text{CO})_5\text{L}^1$. The balance between the two pathways is determined by the nature of the ligand L . For example, for $\text{M} = \text{W}$, when L is a nitrogen-donor ligand such as acetonitrile or pyridine, the lack of back-donation from the ligand to $\text{M}-\text{CO}$ bond increases the bond strength (as is also reflected in the $\nu(\text{CO})$ values), making the $\text{M}-\text{CO}$ bond dissociation unfavourable and thus encouraging the L -loss pathway. If $\text{L} = \text{phosphine}$, the L -loss and the CO -loss pathways have similar quantum yields of 0.3 [79]. This type of reaction is the gateway to a very wide range of organometallic compounds.

Other metal carbonyls—for example those of Ru or Re —are less photolabile, however, in some cases CO dissociation can also occur. For example, irradiation at 365 nm of *fac*- $[\text{Re}(\text{X}_2\text{bpy})(\text{CO})_3(\text{PR}_3)]^+$ leads to photoinduced CO loss and its replacement with the coordinated solvent molecule, CH_3CN :



Metal carbonyls are capable of photoactivating small molecules, such as N_2 , H_2 , or alkanes. In this context, studies of high pressure reactions in polyethylene films have demonstrated the versatility of the photochemistry of $\text{Fe}(\text{CO})_5$, in which one of the CO-ligands could be photochemically replaced by N_2 or H_2 , whilst the thermal reaction of $\text{Fe}(\text{CO})_4(\text{N}_2)$ with H_2 demonstrated the higher stability of the H_2 -complex (Fig. 3.15) [80].

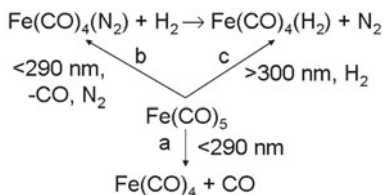


Fig. 3.15 Photochemical ligand substitution in $\text{Fe}(\text{CO})_5$ [80]

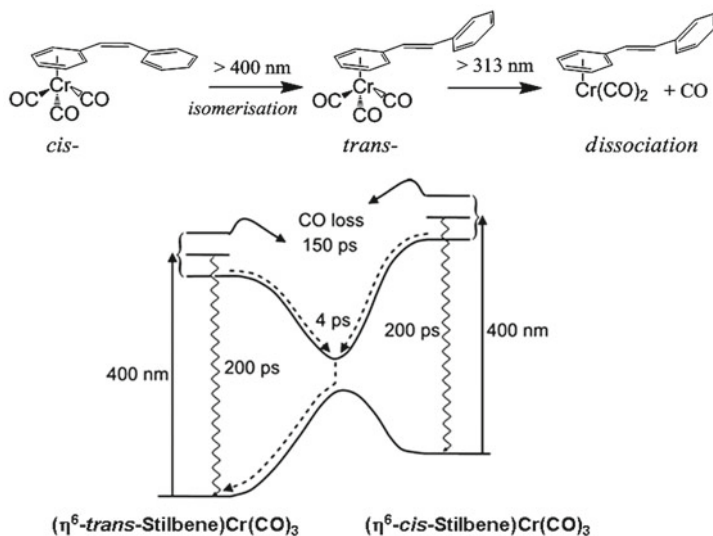


Fig. 3.16 Wavelength-dependent photochemical transformations in a Cr carbonyl complex. Reprinted with permission from Ref. [86]. Copyright 2007, American Chemical Society

For binuclear metal carbonyls, $\text{M}_2(\text{CO})_{2X}$, the photophysics and photoreactivity are strongly affected by the presence of a metal–metal bond and of a bridging carbonyl ligand. The CO-dissociation is still of course possible, however, a M–M bond cleavage is also taking place, producing $17e^-$ species:



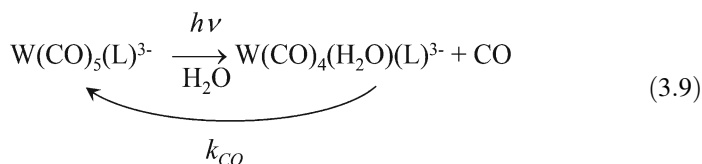
The ratio of the products is usually wavelength-dependent. Their subsequent reactions will be determined by the coordinating ability of the solvent, and by other species present in solution, all of which will compete with recombination and reformation of the starting material.

For example, in the photochemistry of $\text{Mn}_2(\text{CO})_{10}$ the balance between initial formation of $^*\text{Mn}(\text{CO})_5$ (by cleavage of the Mn–Mn bond) and $\text{Mn}_2(\text{CO})_9$ (by dissociation of CO) is wavelength dependent. Irradiation with 355 nm light populates selectively the lowest $\sigma \rightarrow \sigma^*$ transition, leading to the Mn–Mn bond cleavage and the ratio between the two pathways being 0.74. On the other hand, irradiation with 266 nm light populates a metal-to-CO π^* antibonding orbital, leading to CO dissociation, and the ratio of the two pathways becomes 0.21, with formation of $\text{Mn}_2(\text{CO})_9$ dominating [81]. It is interesting to note the potential for photochemically selective reactions: for example, selective CO loss has been achieved in mixed dinuclear species, e.g. $\text{MnRe}(\text{CO})_{10}$, studied using matrix isolation and time-resolved infrared spectroscopy [82].

Photoinduced CO loss frequently competes with other possible photochemical pathways. The example of $\text{Cr}(\text{stilbene})(\text{CO})_3$ photochemistry demonstrates

wavelength-dependent photo-transformations (Fig. 3.16). Irradiation with >400 nm light leads to photoisomerisation *via* population of an intermediate MLCT excited state. On the other hand, irradiation with 313 nm light leads to CO loss, *via* an MC-state, and formation of a solvent adduct.

Apart from fundamental interest in photochemistry of metal carbonyls, there is considerable interest in therapeutic applications of carbon monoxide release to physiological targets [83]. A photo-activated ‘pro-drug’ which would release CO only upon irradiation would be a good option for CO delivery. One of the challenges for such applications is to create water soluble complexes. A photoactivated carbon monoxide releasing moiety, $[\text{W}(\text{CO})_5(\text{L})]^{3-}$ has been designed, which is an air-stable, water-soluble tungsten(0) carbonyl complex of the trianionic ligand $\text{L} = \text{tris}(\text{sulphonatophenyl})\text{phosphine}$. Near-UV photolysis of this compound in an aqueous buffer solution leads to release of a single CO molecule with high quantum yield (Eq. 3.9). Furthermore, in aerated media, additional CO is slowly released from the $[\text{W}(\text{CO})_4(\text{H}_2\text{O})(\text{L})]^{3-}$ photoproduct owing to autoxidation of the tungsten centre. Thus this water-soluble complex serves as a carbon monoxide releasing moiety both in the primary photochemical reaction and in the secondary reactions of the initially formed photoproduct [83].



The carbonyl complex salt $\text{Na}_3[\text{W}(\text{CO})_5(\text{L})]$ is very stable in aerated aqueous media unless subjected to photolysis. Under irradiation, this compound demonstrates high photolability, leading to the release of approximately one CO. Nuclear magnetic resonance (NMR) data confirm that phosphine photolabilisation is at most a minor pathway ($<5\%$), making $\text{Na}_3[\text{W}(\text{CO})_5(\text{L})]$ an effective photoactivated carbon monoxide releasing moiety for possible pharmaceutical applications [83].

3.4.2 Ligand Loss: NO

Many transition metal nitrosyl complexes release NO upon photolysis. For example, NO release was observed from $\text{Mo}(\text{CO})(\text{NO})(\text{dppe})(\text{dte})$, where $\text{dte} = \text{S}_2\text{CNMe}_2$, and $\text{dppe} = \text{diphenyl-phosphino-ethane}$. The lowest energy absorption band of this compound, at 520 nm, has been assigned to a LLCT ($\text{dte} \rightarrow \text{NO}^*$) transition. Photolysis into the low energy side of this band ($\lambda_{\text{irr}} = 546$ nm) in benzene solutions results in loss of NO ($\phi = 0.0018$) [84].

This state decays to the ground state with lifetimes of <42 and 430 ps without isomerisation, indicating that the ^3IL state can not be populated [87].

Another well-studied example of *cis-trans* isomerisation is that of azobenzene and derivatives (Fig. 3.17c). Similarly to the stilbenes described above, an attachment of the azobenzene derivative as a ligand to the transition metal centre allows photoisomerisation of azobenzene by using lower energy light than is needed for the free ligand.

Photoisomerisation on a metal centre can alter emission properties of the complexes, or even result in an on/off emission switch, and accordingly this type of reactions has been explored for sensing applications [88].

It is important to reiterate that the timescales of many of the processes discussed above are ultrafast—picoseconds or even sub-picoseconds—and therefore these reactions occur from a non-equilibrated, vibrationally hot electronic excited state(s).

3.4.4 Photoinduced Linkage Isomerism

Thermally activated linkage isomerism in solution has been known since the time of the pioneering work of Alfred Werner (Nobel prize in Chemistry, 1913). Recognition of *photoinduced* linkage isomerism came only a few decades ago, and since then a very large number of transition metal complexes have been shown to undergo this inner-sphere photoreaction. Ligands susceptible to this process are *ambidentate*, *i.e.* they have the potential to coordinate in more than one way. Examples of ligands engaging in linkage isomerism include: nitrosyl ligand $-\text{NO}$ coordinating *via* either the N or the O atoms; nitro-ligand with N *vs* O coordination, $-\text{SO}_2$ and dimethyl-sulfoxide (DMSO) ligands with S *vs* O atom coordination, isocyanate (N *vs* S donor), and some others. Linkage isomerism can be used as a synthetic tool to obtain a particular isomer in a pure form, but is also important technologically, in relation to potential photorefractive applications, including data storage and optical switching, as well as logic gates [89, 90].

Initially, this process was studied using low temperature methods, involving matrix isolation and IR spectroscopy, as the two linkage isomers would have very different IR spectra and frequently exhibit a change in the energy of the ligand stretching vibration of over 100 cm^{-1} upon isomerisation. For example, $\nu(\text{NO})$ in *cis*- $[\text{RuCl}(\text{en})_2\text{NO}]\text{Cl}_2$ shifts from 1901 to 1775 cm^{-1} between the two forms in which NO is coordinated *via* the N atom or the O atom [89].

In recent years, the investigation of photoinduced linkage isomerism has become intrinsically linked to the new method of photocrystallography [17]. Photocrystallography is a rapidly developing technique that enables the full three-dimensional structure of a molecule, in a crystalline environment, to be determined by X-ray crystallography when the molecule has been photoactivated into a short-lived excited state. Similarly, X-ray absorption (XAFS) can be used to provide structural details of excited state molecules in the solid state or in solution. In the

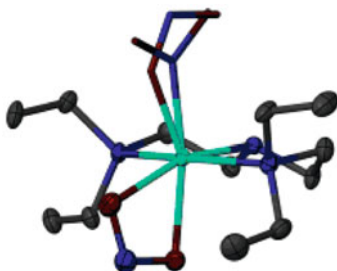


Fig. 3.18 Fully reversible nitro–nitrito linkage isomerism in a single crystal, in $-\text{NO}_2$ -containing complex of Ni(II), $[\text{Ni}(\text{Et}_4\text{dien})(\eta^2\text{-O,ON})(\eta^1\text{-NO}_2)]$. Ni turquoise, N blue, O red; $\text{Et}_4\text{dien} = N,N,N',N'$ -tetraethyldiethylenetriamine. Copyright © John Wiley & Sons 2011 [96]

solid state, photocrystallography has achieved the crystallographic characterisation of species with sub-microsecond lifetimes [18, 91, 92].

Amongst the examples above, linkage isomerism is particularly common in nitrosyl containing compounds—a recent review stated that out of over 100 nitrosyl coordination compounds studied, about 80 % showed evidence of N/O linkage isomerism [89]. Examples include $[\text{Ni}(\text{NO})(\eta^5\text{-Cp}^*)]$, a wide variety of Ru(II) complexes, e.g. *cis-trans*- $[\text{RuCl}(\text{en})_2\text{NO}]\text{Cl}_2$ or *trans*- $[\text{RuCl}(\text{NO})\text{Py}_4]\text{PF}_6$, and $\text{Mn}(\text{CO})(\text{NO})_3$.

Light-induced linkage isomerism has been documented in, for example, $\text{Na}_2[\text{Fe}(\text{CN})_5\text{NO}]$, upon excitation into the lowest absorption band assigned to a $\text{Fe}(d\pi) \rightarrow \text{NO}(\pi^*)$ MLCT transition [93]. The presence of two light-induced metastable states was indicated by Mossbauer spectroscopy, and their structural characterisation was performed in the late 1990s by photocrystallography [92]. Despite being a common occurrence, the linkage isomerism of nitrosyl compounds occurs only at low temperatures, and with very low yields, under the experimental conditions used.

Practical applications exploiting reversible switching between linkage isomers would require photostability, and 100 % reversible isomerisation at ambient temperature and pressure. The factors affecting the interconversion process have been the subject of intense study, and recent work [94] has shown that the excited state potential must possess a minimum close to the saddle point of the ground state energy surface between the ground and metastable states, or cross that surface, so that relaxation from the excited state into the metastable minima can occur. The first fully reversible single-crystal-to-single-crystal isomeric interconversion was observed in the nitrite complex $[\text{Ni}(\text{dppe})(\text{Cl})(\text{NO}_2)]$ at temperatures below 160 K [95]. A very recent example demonstrates fully reversible nitro–nitrito linkage isomerism in a single crystal, in an $-\text{NO}_2$ -containing complex of Ni(II), $[\text{Ni}(\text{Et}_4\text{dien})(\eta^2\text{-O,ON})(\eta^1\text{-NO}_2)]$ (Fig. 3.18). The N-bound NO_2 group in this complex has been shown to undergo reversible conversion into the O-bound nitrito linkage isomer under both thermal and photoactivation of a single crystal. Photocrystallographic studies were undertaken on the slow-cooled clean nitro- $(\eta^1\text{-NO}_2)$ isomer,

by irradiating the crystal *in situ* for a period of 1 h at 100 K. The subsequent X-ray data set showed that a photochemical linkage isomerisation reaction had occurred with 86 % of the crystal converted into the nitrito-(η^1 -ONO) isomer [96].

Linkage isomerism in sulfoxide complexes is also a rather frequent phenomenon [90]. Some metal sulfoxide complexes can exist in both S-bonded and O-bonded metastable states. The isomerisation can occur with high yields, at room temperature, and in solutions as well as in the solid state, as has been demonstrated for a wide variety of Ru(II) and Os(II) complexes. For example irradiation of $[\text{Ru}(\text{tpy})(\text{Me-pic})(\text{DMSO})]^+$, with 413 nm light (corresponding to the MLCT transition) yields sulfur \rightarrow oxygen (S/O) isomerisation of the DMSO ligand with a quantum yield of 0.79. Amongst many other examples are $[\text{Ru}(\text{bpy})(\text{tpy})(\text{DMSO})]^{2+}$ and $[\text{Ru}(\text{bpy})_2(\text{DMSO})_2]^{2+}$ in which the quantum yield of isomerisation varies considerably with changing from tpy to bpy ligands [90]. The S/O linkage isomerisation is believed to occur *via* temporary oxidation of Ru(II) to Ru(III); accordingly, it can be promoted either electrochemically, or photochemically *via* an MLCT state. Recent ultrafast optical spectroscopic studies are indicative of a $^3\text{MLCT}$ state being the key intermediate state in the isomerisation of Ru(II) complexes, whereas for $[\text{Os}(\text{bpy})_2(\text{DMSO})_2]^{2+}$ the transient absorption studies indicate that a higher-lying CT state is the intermediate state.

Linkage isomerism of DMSO in Ru(II) poly-pyridyl complexes has been used as a synthetic tool to access enantio-pure complexes such as $[\text{Ru}(\text{bpy})_2(\text{DMSO})\text{Cl}]^+$ [97]. The mechanism of the isomerisation and the nature of the excited states involved continue to be investigated by a variety of means, including picosecond transient absorption spectroscopy and modern crystallographic methods.

3.4.5 Photoinduced Isomerisation at the Metal Centre, Within the Coordination Sphere

Labilisation of the ligands can cause rearrangement of the positions of the ligands within the coordination sphere of a metal complex, without changing its composition. One of the first examples is the *cis-trans* isomerisation of $[\text{Ru}(\text{bpy})_2(\text{H}_2\text{O})_2]^{2+}$ (Fig. 3.19, left) under irradiation with visible light [98]. The quantum

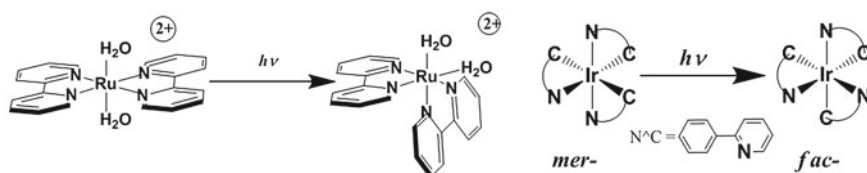


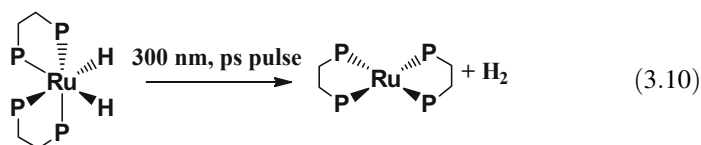
Fig. 3.19 Photoisomerisation in the coordination sphere. *Left:* *cis-trans* isomerisation of Ru(II) complex; *Right:* *mer/fac* isomerisation of an Ir(III) complex with three cyclometallating ligands, such as 2-phenyl-pyridine

yields for *cis-trans* and *trans-cis* isomerisations are wavelength-independent, suggesting that the process occurs from the lowest electronic excited state in each case.

Another possible type of coordination isomerisation is that observed for octahedral complexes of the type MA_3B_3 , or bearing three bidentate chelating ligands whose donor atoms are inequivalent. Such compounds can exist as facial (*fac*) or meridional (*mer*) isomers, and photoinduced transformation between the two is possible in some cases. Highly emissive complexes of Ir(III) with cyclometalating chelating ligands such as 2-phenylpyridine undergo such a transformation (Fig. 3.19, right). These compounds are highly luminescent, and are used in various light-related applications, from cell imaging to organic light-emitting diodes (OLEDs). A change from a *fac*- to *mer*- arrangement of the ligand set alters the photophysical properties of the complex (the *fac*-isomer is considerably more emissive) and as such this reaction is directly related to the performance and durability of the compounds in a particular application [99].

3.4.6 Reductive Elimination

Photochemical reductive elimination offers further examples of ultrafast light-induced reactions. Irradiation of *cis*-[Ru(dmpe)₂H₂] with 300 nm light in cyclohexane causes elimination of H₂, and rearrangement of the [Ru(dmpe)₂] ‘skeleton’ (dmpe—Me₂P—CH₂—CH₂—PMe₂) to the *trans* isomer. Interestingly, all of those processes were reported to be completed within the instrument response time of 16 ps [100].



3.4.7 Oxidative Addition

The conversion of alkanes into more useful products is one of the most important practical problems in chemistry. The insertion of metals into C–H bonds was first discovered by Chatt and Davidson in 1965 [101] for low-valent ruthenium complexes. Following the discovery of the photochemically induced insertion of a transition metal into alkane C–H bonds [102, 103], a large number of organometallic complexes have been shown to activate C–H bonds in alkanes. A typical example is the photochemical oxidative addition of alkanes to complexes such as Rh(Cp)(CO)₂. The reaction occurs *via* an initial loss of CO followed by σ -

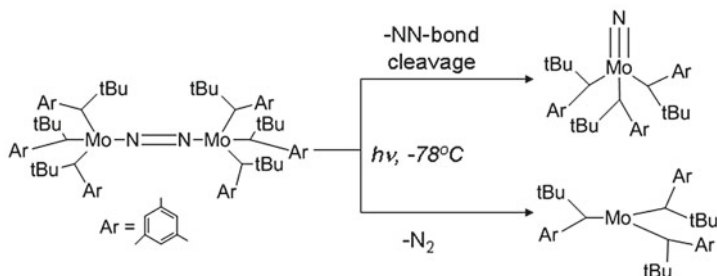
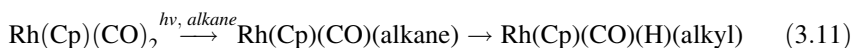


Fig. 3.20 Dinitrogen splitting with Mo complexes [105]

coordination of the alkane. A wide diversity of products can be obtained using this type of transformation.

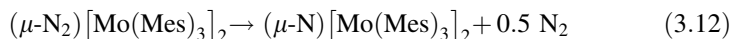


3.5 Photoactivation of Small Molecules with Transition Metal Complexes

3.5.1 Dinitrogen Splitting

Activation of the most stable molecule— N_2 —is another major challenge in chemistry. The difficulty originates from the extreme stability of the triply-bonded N_2 with the bond energy of the $\text{N}\equiv\text{N}$ bond being extremely high, 944 kJ mol^{-1} . A photochemical route to N_2 activation is an attractive option as it can potentially overcome this difficulty, providing the required energy through photoexcitation. Accordingly, photochemical studies of N_2 -bridged metal complexes with the aim of N_2 -splitting have been reported, although the number of such studies at present is very limited.

Photochemical NN bond cleavage has been realised in a linear, bimetallic Mo-mesityl complex ($\text{Mes} = 2,4,6\text{-Me}_3\text{C}_6\text{H}_2\text{-}$), which led to formation of a μ -nitride-product as well as dinitrogen [104]:



In a related example, a dimolybdenum N_2 -bridged complex was found to undergo competitive N_2 elimination and -NN-bond cleavage under photolysis into the lowest energy absorption band with 544 nm light. The presence of two different products (quantum yield = 0.05 with respect to the starting compound) was confirmed by a variety of methods including ^{15}N NMR spectroscopy and X-ray crystallography to isolate the product of N_2 -elimination (Fig. 3.20) [105].

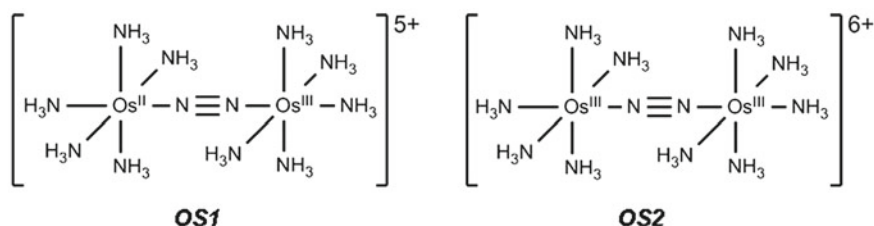
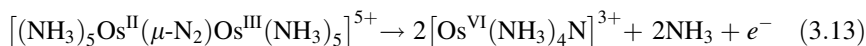


Fig. 3.21 Osmium complexes of dinitrogen [106]

In the examples above, the reactivity of the $-\text{N}=\text{N}-$ unit was exploited. A recent example discusses an N_2 -bridged Os dimer in which the $-\text{NN}-$ bridge largely preserves its triple bond character. It demonstrates how homoleptic N_2 -splitting can be achieved photochemically with the use of Os complexes, as well as how tuning of the nature of the lowest excited state can dramatically alter the photochemical properties and the nature of the reaction products [106].

The mixed-valence complex OS1 (Fig. 3.21), which contains Os(II) and Os(III) centres bridged by a dinitrogen ligand, exhibits two main bands in the absorption spectrum: 700 nm ($\epsilon = 4000 \text{ dm}^3 \text{ mol}^{-1} \text{ cm}^{-1}$) due to an intervalence $\text{Os}^{\text{II}} \rightarrow \text{Os}^{\text{III}}$ transition and 238 nm ($\epsilon = 41000 \text{ dm}^3 \text{ mol}^{-1} \text{ cm}^{-1}$) due to an MLCT transition $\text{Os}^{\text{II}}[d(\pi)] \rightarrow \text{N}_2(\pi^*)$.

Because of the different nature of those transitions, different photochemical products are formed depending on the excitation wavelength. Excitation into the inter-valence transition at 700 nm does not initiate any photoreactivity. However, irradiation with light $< 450 \text{ nm}$ populates an MLCT state, resulting in transient oxidation of the metal centre, reduction of the N_2 molecule, and dinitrogen splitting, with quantum yields 0.002 and 0.003 under 254 nm or 365 nm irradiation respectively.



Notably, compound OS1 is also an interesting example of a violation of Kasha's rule, *i.e.* the higher lying excited state does not simply convert quickly to the lower-lying one, but the two have independent and quite different reactivity (Fig. 3.21).

In sharp contrast with OS1, compound OS2 does not cleave dinitrogen. Instead, it evolves N_2 gas, and, whilst the compound is somewhat thermally unstable and slowly releases nitrogen even without irradiation, photolysis causes violent evolution of N_2 . The difference between the reactivity of OS1 and OS2 can be explained by differences in the energies of their MLCT states: the MLCT ($\text{Os}^{\text{III}} \rightarrow \text{N}_2$) is considerably higher in energy than $\text{Os}^{\text{II}} \rightarrow \text{N}_2$ MLCT, and is not accessible with light $> 230 \text{ nm}$. Instead, dd -states (ligand field, intra-Os) become the lowest energy excited states, and the corresponding dd -transition can initiate N_2 -elimination instead of N_2 -cleavage.

3.5.2 Solar Energy Conversion: Water Splitting and Reduction of CO₂

Owing to their strong light absorbing properties and diverse photoreactivity, many transition metal complexes have been utilised in research towards solar energy conversion—ranging from light-harvesting and efficient photoinduced charge separation, to dye-sensitised solar cells, and photovoltaics. Photocatalytic applications cover the whole spectrum of reactions, including H₂ production, water splitting, and CO₂ reduction towards value added products. There are exciting developments in this vibrant field [6, 7, 107] which are covered in more detail in Chap. 7.

3.6 Clusters

Many photoinduced reactions in organometallic chemistry start from organometallic clusters. The most widely used definition is that a cluster is a polynuclear complex consisting of three or more transition metal atoms, connected to one another by direct metal–metal bonds [108].

Cluster chemistry has been an area of intense interest over recent decades due to its relevance to the surface catalysis and interaction of small molecules with metal surfaces, their own catalytic capabilities, and a presence of multimetallic redox centres relevant to biological systems [109].

The clusters can be classified into two main types—so-called ‘naked’ clusters which do not have stabilising ligands, and those which do involve ligands. Clusters of main group elements typically carry hydride as a stabilising ligand. Most common stabilising ligands in transition metal clusters are CO, halides and pseudohalides, alkenes, and hydrides.

In general terms, based on the formal oxidation state of the metal and electron donating/accepting properties of the ligands, two main sub-categories of transition metal clusters can be identified:

1. Clusters of the group V–VII metals in high formal oxidation states, stabilised by π -donor ligands such as oxide, sulphide, or halides. Examples here include $[\text{Nb}_6\text{Cl}_{12}]^{4+}$, $[\text{W}_6\text{Br}_8]^{4+}$ and $[\text{Re}_3\text{Cl}_9]^{3+}$.
2. Clusters of transition metals in formal low oxidation states, stabilised by π -acceptor ligands, such as carbonyl or phosphine. Example include many clusters of Os, Mn, Re, Ru, or Fe.

Examples of the smallest clusters, consisting of only 3 metal atoms, are $[\text{Os}_3(\text{CO})_{12}]$ or $[\text{Ru}_3(\text{CO})_{12}]$. An increase in the number of metal atoms brings about a variety of geometries, such as tetrahedral $[\text{Co}_4(\text{CO})_{12}]$, octahedral $[\text{Rh}_6(\text{CO})_{16}]$, and proceed further to the large clusters, such as $[\text{Pt}_{24}(\text{CO})_{30}]^{n-}$ ($n = 0$ to 6).

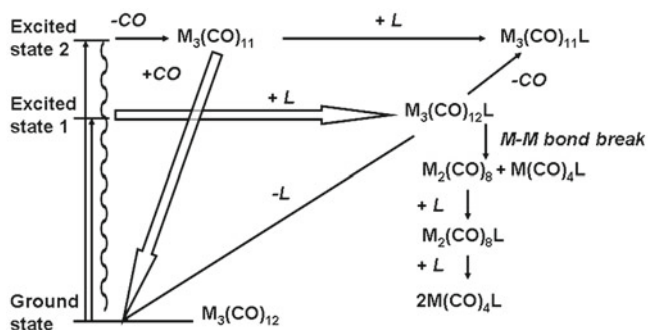


Fig. 3.22 Possible photoinitiated reactions of clusters $M_3(CO)_{12}$, $M = Fe(0), Os(0), Ru(0)$, in the presence of a coordinating ligand L [111]

The primary photochemical reactions of transition metal clusters include:

1. homoleptic metal–metal bond cleavage with the transient formation of a biradical;
2. heteroleptic metal–metal bond cleavage and formation of a zwitterion;
3. CO dissociation, frequently accompanied by a $-CO$ -bridge formation (the first direct observation of a CO-bridged primary photoproduct of $[Ru_3(CO)_{12}]$ was achieved by picosecond TRIR spectroscopy) [110].

Further reactions of these initially-formed transient species and the relative quantum yield of each pathway depend partly on the coordination ability of the solvent and the reagents, and partly on the nature of the metal involved (Fig. 3.22) [111].

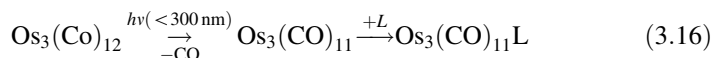
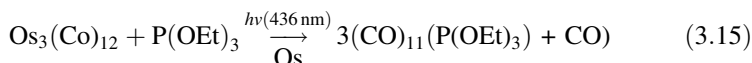
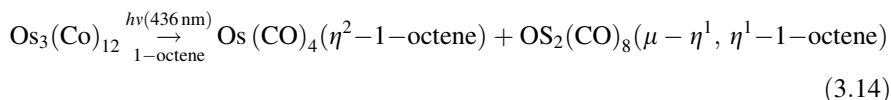
We will briefly consider the photochemistry of transition metal carbonyl clusters, which contain metal centres in low oxidation states and are stabilised by π -accepting CO ligands. Such transition metal carbonyl clusters are valuable synthetic precursors in both thermal and photochemical synthesis.

As discussed above, the primary process in monometallic carbonyl complexes is CO loss, whilst in dinuclear compounds, $M_2(CO)_{2X}$, there is a possibility of either CO loss, or $M-M$ bond dissociation. In molecular clusters, the photophysics and photoreactivity are significantly different from that of $M(CO)_X$ due to electronic delocalisation across the multi-metallic core.

3.6.1 Photochemistry of $[M_3(CO)_{12}]$ in Solution, $M = Fe, Ru, Os$

Some of the best known mixed-metal clusters are group VIII triangular clusters $[M_3(CO)_{12}]$ ($M = Fe, Ru, Os$) [111–113], where almost all possible metal combinations have been prepared [114, 115], and their bonding properties, electrochemistry and photochemistry have been studied in much detail [111–117].

The presence of several low-lying excited states in $[M_3(CO)_{12}]$ clusters gives rise to wavelength-dependent photochemistry, as exemplified for $M = Os$. Similarly to the binuclear species discussed above, excitation with light at wavelengths longer than 400 nm populates the lowest ($\sigma-\sigma^*$) excited state, and initiates M–M cleavage, resulting in photo-fragmentation and formation of a variety of mono- and dinuclear species— $M(CO)_5$, $M_2(CO)_3L$ and others. High-energy excitation, at wavelengths <350 nm, populates an antibonding, π^* M–CO orbital, initiating CO loss and subsequent substitution by coordinating ligands. The observation that the photoreactions under high energy excitation do not occur from the lowest excited state (*i.e.* Kasha's rule is not obeyed) once again indicates that CO loss is likely to occur on the ultrafast time-scale, from a vibrationally hot, non-equilibrated excited state.



3.6.2 α -Diimine-Containing Clusters

Replacement of two CO ligands with a diimine ligand to give $[Os_3(CO)_{10}(\text{diimine})]$ profoundly changes the photochemical properties compared to the parent cluster $[Os_3(CO)_{10}]$. The lowest excited state in a variety of those clusters has largely an MLCT (Os-to-diimine) character with some degree of π -delocalisation within the $[Os\text{-diimine}]$ moiety, as shown by resonance Raman spectroscopy. This transition gives rise to the absorption band in visible region of the spectrum.

These diimine clusters demonstrate solvent-dependent photochemistry (Fig. 3.23) [118]. Zwitterions $[^-Os(CO)_4-Os(CO)_4-Os^+(S)(CO)_2(\text{diimine})]$ are formed in coordinating solvents (S) such as acetonitrile, whilst irradiation in non-coordinating solvents such as toluene leads to homoleptic cleavage of the metal-meta bond and formation of biradicals $[^*Os(CO)_4-Os(CO)_4\{Os^+(CO)_2(\text{diimine})^{\bullet-}\}]$. The zwitterions are formed with quantum yields of ~ 0.01 , and have lifetimes of seconds in nitrile solvents, and even longer (minutes) in pyridine; they mainly regenerate the parent cluster when they collapse. The lifetimes of the biradicals are considerably shorter, and vary from 5 ns to 1 μ s, depending on the nature of the diimine ligand. In a minor reaction pathway, the biradicals can isomerise into a diimine-bridged Os-diimine-Os dimer. It is interesting to note that the photoproducts observed—biradical, zwitterions,

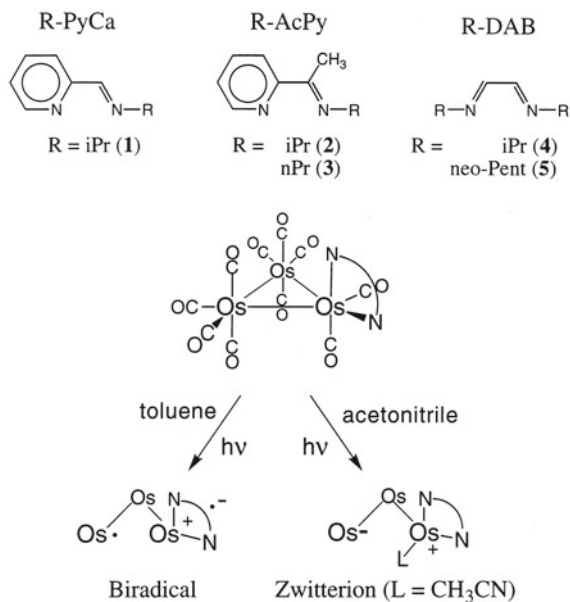


Fig. 3.23 Schematic structures of the Os₃(CO)₁₀(diimine) clusters, of their zwitterions and biradicals, and of the diimine ligands used: R-PyCa = pyridine-2-carbaldehyde *N*-alkylimine; R-AcPy = 2-acetylpyridine *N*-alkylimine; R-DAB = N,N'-dialkyl-1,4-diaza-1,3-butadiene. Copyright © American Chemical Society 1998 [121]

and diimine-bridged dimers—are similar to the binuclear, metal–metal bound complexes such as (CO)₅Mn–Mn(CO)₃(diimine), thus pointing towards homoleptic Os–Os bond breaking as a primary photoprocess. It was suggested that this reaction is most likely to occur from a reactive SBLCT state, populated as a result of surface crossing from an optically accessible MLCT state. Modification of the diimine ligand with redox-active groups, such as methyl viologen, allows for redox control of photoinduced charge-separation in this type of transition metal cluster [119].

Direct application of Ru₃(CO)₁₂ in photochemical synthesis has been described in detail [120]. Thermal reactions of this cluster in presence of two-electron donors L affords [Ru₃(CO)₉L₃]. The discovery in 1974 that irradiation of the cluster under those conditions produces mononuclear products instead of the substituted clusters initiated a wealth of research in Ru-clusters as precursors in photochemical synthesis [121]. Much research has been devoted to the preparation of mononuclear η²-olefin complexes, as well as alkyne complexes. For example, [Ru(CO)₃(PPh₃)₂] has been reported as an active catalyst for olefin polymerisation, and as such, many investigations have dealt with the reactivity of this compound. Other directions of research include formation of metallacycles, generation of new cluster species, and mixed transition metal/non-metal clusters.

3.7 Conclusions: What's Next for the Photochemistry of Metal Complexes?

Molecular inorganic photochemistry is extremely diverse. It lies at the very heart of many modern challenges—from fundamental understanding of reaction pathways with ever faster excitation sources, to applications in artificial photosynthesis and water splitting, radioisotopes separation, photocatalysis and photoelectrocatalysis. It involves all types of reaction occurring starting from the lowest, ground state, yet with the key difference that the reactions can only be initiated by light, and occur from much more energetic states.

It has long been acknowledged that the initial absorption of light creates a vibrationally hot, non-equilibrated excited state. However, only in the past decades has it become possible to follow the ultrafast events of vibrational energy dissipation and formation of thermally equilibrated excited states in real time. Thus the long expressed visionary ideas that photochemistry can be classified into ‘ultrafast’—occurring from a non-equilibrated state—and ‘slow’, occurring from a thermally-equilibrated but electronically excited state—has finally gained experimental support.

Perhaps the most exciting feature of inorganic photochemistry is the presence of a much greater diversity of electronic excited states available within the range of usual excitation sources than is the case for organic compounds. Since many of these excited states are of different origin, and do not necessarily relax rapidly to the lowest excited state, the opportunities arise to control the products by changing the wavelength and the energy per pulse of the excitation light in a way that is not possible for pure organic compounds. Extension of these principles towards multimetallic species with unusual bonding provides another means to access reactive intermediates and photochemical products.

Selective excitation of transitions of different types leads to formation of different products—switching between dissociation, substitution or isomerisation, or purely photophysical processes when no new products are formed. Moreover, coordination of organic chromophores as ligands to metal centres allows ligand-centred transformations—such as isomerisation—to be performed under visible instead of UV light.

The ‘modular’ structure of metal-containing compounds, for example, $\text{Ligand}_1\text{-M-Ligand}_2$, offer an opportunity to alter the periphery of the metal complex so that it can be tuned for a specific application—such as anchoring to semiconductor surfaces in heterogeneous catalysis or dye-sensitised solar cells (see [Chap. 7](#)), or coupling to biological entities (see [Chaps. 4, 9 and 10](#))—without altering significantly the orbital makeup and energy levels of the component parts, and hence the reaction pathways.

Bringing together the great diversity of excited states, the ultrafast means of initiating the transformations, the extremely sensitive modern means of detecting reactive intermediates, and novel theoretical methods to gain further insights into

electronic structure, dynamics and reactivity—the field of inorganic photochemistry will continue to make exciting contributions to fundamental and applied science.

References

1. Turro NJ, Ramamurthy V, Scaiano JC (2009) Principles of molecular photochemistry. University Science Books, California, p 495
2. Roundhill DM (1994) Photochemistry and photophysics of metal complexes. Plenum Press, New York
3. Balzani V, Venturi M, Credi A (2008) Molecular devices and machines, 2nd edn. Wiley-VCH, Weinheim
4. Solomon EI, Lever ABP (eds) (2006) Inorganic electronic structure and spectroscopy, 2nd edn. Wiley, New York
5. Horvath O, Stevenson KL (1993) Charge transfer photochemistry of coordination compounds. Wiley-VCH, New York, p 380
6. Vlcek A (2000) The life and times of excited states of organometallic and coordination compounds. *Coord Chem Rev* 200–202:933–977
7. Vos JG, Pryce MT (2010) Photoinduced rearrangements in transition metal compounds. *Coord Chem Rev* 254:2519–2532
8. Muro ML, Rachford AA, Wang X, Castellano FN (2009) Photophysics of platinum(II) acetylides. In: Lees A (ed) Photophysics of organometallics, series: topics in organometallic chemistry, vol 29, pp 159–191
9. Butler JM, George MW, Schoonover JR et al (2007) Application of transient infrared and near infrared spectroscopy to transition metal complex excited states and intermediates. *Coord Chem Rev* 251:492–514
10. Adamson AW, Fleischauer PD (eds) (1975) Concepts of inorganic photochemistry. John Wiley & Sons, New York
11. Elsaesser T, Kaiser W (1991) Vibrational and vibronic relaxation of large polyatomic molecules in liquids. *Annu Rev Phys Chem* 42:83–107
12. Hochstrasser RM (2007) Multidimensional ultrafast spectroscopy. *Proc Nat Acad Sci* 104:14190–14196
13. Hunt NT (2009) 2D-IR spectroscopy: ultrafast insights into biomolecule structure and function. *Chem Soc Rev* 38:1837–1848
14. Schoonover JR, Strouse GF (1998) Time-resolved vibrational spectroscopy of electronically excited inorganic complexes in solution. *Chem Rev* 98:1335–1355
15. Best J, Sazanovich IV, Adams H et al (2010) Structure and ultrafast dynamics of the charge-transfer excited state and redox activity of the ground state of mono- and binuclear platinum(II) diimine catecholates and bis-catecholates: A transient absorption, TRIR, DFT, and electrochemical study. *Inorg Chem* 49:10041–10056
16. Browne WR, McGarvey JJ (2007) The Raman effect and its application to electronic spectroscopies in metal-centered species: techniques and investigations in ground and excited states. *Coord Chem Rev* 251:454–473
17. Dyer RB, Woodruff WH (2007) Vibrational spectroscopy. In: Scott RA, Lukehart CM (eds) Applications of physical methods to inorganic and bioinorganic chemistry. John Wiley & Sons, Chichester
18. Coppens P (2011) Molecular excited-state structure by time-resolved pump probe X-ray diffraction. What is new and what are the prospects for further progress? *J Phys Chem Lett* 2:616–621

19. Coppens P, Gerlits O, Vorontsov II et al (2004) A very large Rh–Rh bond shortening on excitation of the $[\text{Rh}_2(1,8\text{-diisocyno-p-menthane})_4]^{2+}$ ion by time-resolved synchrotron X-ray diffraction. *Chem Comm* 2144–2145
20. Bressler C, Chergui M (2004) Ultrafast X-ray absorption spectroscopy. *Chem Rev* 104:1781–1812
21. Chergui M, Zewail AH (2009) Electron and X-Ray methods of ultrafast structural dynamics: advances and applications. *Chem Phys Chem* 10:28–43
22. Chen LX, Zhang X, Lockard JV et al (2010) Excited-state molecular structures captured by X-ray transient absorption spectroscopy: a decade and beyond. *Acta Cryst A* 66:240–251
23. Darr JA, Poliakoff M (1999) New directions in inorganic and metal-organic coordination chemistry in supercritical fluids. *Chem Rev* 99:495–541
24. Begel S, Heinemann FW, van Eldik R (2011) The classic “brown-ring” reaction in a new medium: Kinetics, mechanism, and spectroscopy of the reversible binding of nitric oxide to iron(II) in an ionic liquid. *Inorg Chem* 50:3946–3958
25. Cotton AF, Wilkinson G (1972) *Advanced inorganic chemistry*, 3rd edn. Wiley, New York, pp 555–620
26. Ford PC (1982) The ligand-field photosubstitution reactions of d^6 hexacoordinate metal complexes. *Coord Chem Rev* 44:61–82
27. Weinstein JA, Grills DC, Towrie M et al (2002) Picosecond time-resolved infrared spectroscopic investigation of excited state dynamics in a Pt(II) diimine chromophore. *Chem Comm* 382–383
28. Yam VWW, Wong KM, Zhu N (2002) Solvent-induced aggregation through metal center dot center dot metal/pi center dot center dot center dot pi interactions: large solvatochromism of luminescent organoplatinum(II) terpyridyl complexes. *J Am Chem Soc* 124:6506–6507
29. Chan CW, Cheng LK, Che CM (1994) Luminescent donor-acceptor platinum(II) complexes. *Coord Chem Rev* 132:87–97
30. Hissler M, Connick WB, Geiger DK et al (2000) Platinum diiminebis (acetylide) complexes: synthesis, characterization, and luminescence properties. *Inorg Chem* 39:447–457
31. Keller JM, Glusac KD, Danilov EO et al (2011) Negative polaron and triplet exciton diffusion in organometallic “molecular wires”. *J Am Chem Soc* 133:11289–11298
32. Lu W, Mi B-X, Chan MCW et al (2004) Light-emitting tridentate cyclometalated platinum(II) complexes containing sigma-alkynyl auxiliaries: Tuning of photo- and electrophosphorescence. *J Am Chem Soc* 126:4958–4971
33. Lu W, Chan MCW, Cheung KK et al (2001) Interactions in organometallic systems. Crystal structures and spectroscopic properties of luminescent mono-, bi-, and trinuclear trans-cyclometalated platinum(II) complexes derived from 2,6 diphenylpyridine. *Organometallics* 20:2477–2486
34. Williams JAG, Beeby A, Davies ES et al (2003) An alternative route to highly luminescent platinum(II) complexes: cyclometalation with $\text{N}^{\wedge}\text{C}^{\wedge}\text{N}$ -coordinating dipyritylbenzene ligands. *Inorg Chem* 42:8609–8611
35. Michalec JF, Bejune SA, McMillin DR (2000) Multiple ligand-based emissions from a platinum(II) terpyridine complex attached to pyrene. *Inorg Chem* 39:2708–2709
36. Sazanovich IV, Alamiry MAH, Best J et al (2008) Excited state dynamics of a Pt(II) diimine complex bearing a naphthalene-diimide electron acceptor. *Inorg Chem* 47:10432–10445
37. Yarnell JE, Deaton JC, McCusker CE et al (2011) Bidirectional “ping-pong” energy transfer and 3000-fold lifetime enhancement in a Re(I) charge transfer complex. *Inorg Chem* 50:7820–7830
38. Yeh AT, Shank CV, McCusker JK (2000) Ultrafast electron localization dynamics following photo-induced charge transfer. *Science* 289:935–938
39. Cannizzo A, van Mourik F, Gawelda W et al (2006) Broadband femtosecond fluorescence spectroscopy of $[\text{Ru}(\text{bpy})_3]^{2+}$. *Angew Chem Int Ed* 45:3174–3176

40. Van Houten J, Watts RJ (1976) Temperature dependence of photophysical and photochemical properties of tris(2,2'-bipyridyl)ruthenium ion in aqueous solution. *J Am Chem Soc* 98:4853–4858
41. Lehn JM, Ziessel R (1982) Photochemical generation of carbon-monoxide and hydrogen by reduction of carbon dioxide and water under visible light irradiation. *Proc Natl Acad Sci USA* 79:701–704
42. Burrows HD, Kemp TJ (1974) Photochemistry of uranyl-ion. *Chem Soc Rev* 3:139–165
43. Redmond MP, Cornet SM, Woodall SD et al (2011) Probing the local coordination environment and nuclearity of uranyl(VI) complexes in non-aqueous media by emission spectroscopy. *Dalton Trans* 40:3914–3926
44. Schwarz G (2005) Molybdenum cofactor biosynthesis and deficiency. *Cell Mol Life Sci* 62:2792–2810
45. Hsu JK, Bonangelino CJ, Kaiwar SP et al (1996) Direct conversion of alphasubstituted ketones to metallo-1,2-enedithiolates. *Inorg Chem* 35:4743–4751
46. Bevilacqua JM, Eisenberg R (1994) Synthesis and characterization of luminescent square-planar platinum(II) complexes containing dithiolate or dithiocarbamate ligands. *Inorg Chem* 33:2913–2923
47. Weinstein JA, Zheligovskaya NN, Mel'nikov MY et al (1998) Spectroscopic (UV/VIS, resonance Raman) and spectroelectrochemical study of platinum(II) complexes with 2,2'-bipyridine and aromatic thiolate ligands. *J Chem Soc Dalton Trans* 2459–2466
48. McInnes, EJM, Farley RD, Rowlands CC et al (1999) On the electronic structure of [Pt(4,4'-X₂-bipy)Cl₂](0/-/2-): an electrochemical and spectroscopic (UV/Vis, EPR, ENDOR) study. *J Chem Soc Dalton Trans* 4203–4208
49. Shavaleev NM, Davies ES, Adams H et al (2008) Platinum(II) diimine complexes with catecholate ligands bearing imide electron-acceptor groups: Synthesis, crystal structures (spectro) electrochemical and EPR studies, and electronic structure. *Inorg Chem* 47:1532–1547
50. Galin AM, Razskazovsky YV, Melnikov MY (1994) The photochemistry of mixed-ligand complexes (ArS)₂ZnPhen with the lowest ligand–ligand charge transfer excited state. *J Photochem Photobiol A: Chem* 78:113–117
51. Whittle CE, Weinstein JA, George MW, Schanze KS (2001) Photophysics of diimine platinum (II) bis-acetylide complexes. *Inorg Chem* 40:4053–4062
52. Aarnts MP, Wilms MP, Peelen K et al (1996) Bonding properties of a novel inorganometallic complex, Ru(SnPh₃)₂(CO)₂(iPr-DAB) (iPr-DAB = N, N'-diisopropyl-1,4-diaza-1,3-butadiene), and its stable radical-anion, studied by UVVis, IR, and EPR spectroscopy (spectro-)electrochemistry, and density functional calculations. *Inorg Chem* 35:5468–5477
53. van Slageren J, Hartl F, Stufkens DJ et al (2000) Changes in excited-state character of [M(L-1)(L-2)(CO)₂(alpha-diimine)] (M = Ru, Os) induced by variation of L-1 and L-2. *Coord Chem Rev* 208:309–320
54. Rossenaar BD, Stufkens DJ, Vlcek A Jr (1996) Halide-dependent change of the lowest-excited-state character from MLCT to XLCT for the complexes Re(X)(CO)₃(alpha-diimine) (X = Cl, Br, I; alpha-diimine equals bpy, iPr-PyCa, iPr-DAB) studied by resonance Raman, time-resolved absorption, and emission spectroscopy. *Inorg Chem* 35:2902–2909
55. Niewenhuis HA, Stufkens DJ, Oskam A (1994) Remarkable influence of X and R on the charge-transfer character (MLCT or XLCT) of the complexes [Ru(X)(R)(CO)₂(L)] (X = halide, CF₃SO₃ R = alkyl L = alpha-diimine)—a UV-VIS absorption and resonance Raman study. *Inorg Chem* 33:3212–3217
56. Pettijohn CN, Jochnowitz EB, Chuong B et al (1998) Luminescent excimers and exciplexes of Pt-II compounds. *Coord Chem Rev* 171:85–92
57. Roundhill DM, Gray HB, Che CM (1989) Pyrophosphito-bridged diplatinum chemistry. *Acc Chem Res* 22:55–61
58. Kim CD, Pillet S, Wu G et al (2002) Excited-state structure by time-resolved X-ray diffraction. *Acta Cryst A* 58(2):133–137

59. van der Veen RM, Milne C, El Nahhas A et al (2009) Structural determination of a photochemically active diplatinum molecule by time-resolved EXAFS spectroscopy. *Angew Chem Int Ed* 48:2711–2714
60. Novozhilova IV, Volkov AV, Coppens P (2003) Theoretical analysis of the triplet excited state of the $[\text{Pt}_2(\text{H}_2\text{P}_2\text{O}_5)_4]^{4-}$ ion and comparison with time resolved X-ray and spectroscopic results. *J Am Chem Soc* 125:1079–1087
61. Cotton FA, Murillo C, Walton RA (2005) Multiple bonds between metal atoms, 3rd edn. Springer Science, New York
62. Cotton FA, Nocera DG (2000) The whole story of the two-electron bond, with the delta bond as a paradigm. *Acc Chem Res* 33:483–490
63. Hopkins MD, Gray HB (1984) Nature of the emissive excited state of quadruply bonded $\text{Mo}_2\text{X}_4(\text{PMe}_3)_4$ complexes. *J Am Chem Soc* 106:2468–2469
64. Chang JJ, Nocera DG (1989) Oxidation photochemistry of dimolybdenum(II) diaryl phosphate promoted by visible-light. *Inorg Chem* 28:4311–4312
65. Caspar JV, Kober EM, Sullivan BP et al (1982) Application of the energy gap law to the decay of charge-transfer excited states. *J Am Chem Soc* 104:630–632
66. Alberding BG, Chisholm MH, Gustafson TL (2012) Detection of the singlet and triplet MM delta delta* states in quadruply bonded dimetal tetracarboxylates (M = Mo, W) by time-resolved infrared spectroscopy. *Inorg Chem* 51:491–498
67. Alberding BG, Chisholm MH, Gallucci JC et al (2011) Electron delocalization in the S-1 and T-1 metal-to-ligand charge transfer states of transsubstituted metal quadruply bonded complexes. *Proc Natl Acad Sci USA* 108:8152–8156
68. Chisholm MH (2012) Incorporating MM quadruple bonds into conjugated organic oligomers: syntheses and optoelectronic properties. *Macromol Chem Phys* 213:800–807
69. McQuillin FJ, Parker DG, Stephenson GR (1991) Transition metal organometallics for organic synthesis. Cambridge University Press, Cambridge
70. Geoffroy GL, Wrighton MS (1979) Organometallic photochemistry. Academic Press, New York
71. Turner JJ, Burdett JK, Perutz RN et al (1977) Matrix photochemistry of metal-carbonyls. *Pure Appl Chem* 49:271–285
72. Bonneau R, Kelly JM (1980) Flash photolysis of chromium hexacarbonyl in perfluorocarbon solvents—observation of a highly reactive chromium pentacarbonyl. *J Am Chem Soc* 102:1220–1221
73. Mond L, Langer C, Quincke F (1890) Action of carbon monoxide on nickel. *J Chem Soc Trans* 57:749–753
74. Long C (2010) Photophysics of CO loss from simple metal carbonyl complexes. In: Lees AJ (ed) Photophysics of organometallics. Topics in organometallic chemistry, vol 29, pp 37–71
75. Poliakoff M, Turner JJ (2001) The structure of $[\text{Fe}(\text{CO})_4]$ —an important new chapter in a long-running story. *Angew Chem Int Ed* 40:2809–2812
76. Portius P, Yang J, Grills DC et al (2004) Unraveling the photochemistry of $\text{Fe}(\text{CO})_5$ in solution. *J Am Chem Soc* 126:10713–10720
77. Lian T, Bromberg SE, Asplund MC et al (1996) Femtosecond infrared studies of the dissociation and dynamics of transition metal carbonyls in solution. *J Phys Chem* 100:11994–12001
78. Nasielski J, Colas A (1978) Primary process in photochemistry of group 6B metal hexacarbonyls 2. *Inorg Chem* 17:237–240
79. Dahlgren RM, Zink JI (1977) Ligand substitution photochemistry of monosubstituted derivatives of tungsten hexacarbonyl. *Inorg Chem* 16:3154–3161
80. Cooper AI, Poliakoff M (1993) High pressure reactions in polyethylene films. *Chem Phys Lett* 212:611–616
81. Kobayashi T, Yasufuku K, Iwai J et al (1985) Laser photolysis study of the photosubstitution in dimanganese and dirhenium decacarbonyls. *Coord Chem Rev* 64:1–19

82. Firth S, Hodges PM, Poliakoff M et al (1987) Selective loss of CO in the photochemistry of $\text{MnRe}(\text{CO})_{10}$ —a study using matrix isolation and time-resolved infrared spectroscopy. *J Organomet Chem* 331:347–355
83. Rimmer RD, Richter H, Ford PC (2010) A photochemical precursor for carbon monoxide release in aerated aqueous media. *Inorg Chem* 49:1180–1185
84. Kunkely H, Vogler A (2004) Ligand-to-ligand charge transfer in $\text{Mo}(\text{diphos})(\text{CO})(\text{NO})(\text{dtc})$ with $\text{diphos} = 1,2\text{-bis}(\text{diphenylphosphino})\text{ethane}$ and $\text{dtc}(-) = \text{dimethyldithiocarbamate}$. Spectroscopy and photochemistry. *Inorg Chem Commun* 7:767–769
85. Dattelbaum DM, Itokazu MK, Iha NYM et al (2003) Mechanism of metal-to-ligand charge transfer sensitization of olefin trans-to-cis isomerization in the $\text{fac-}[\text{Re}^{\text{I}}(\text{phen})(\text{CO})_3(1,2\text{-bpe})]^+$ cation. *J Phys Chem A* 107:4092–4095
86. Coleman A, Draper SM, Long C et al (2007) Photochemical cis-trans isomerization of $\text{cis-}(\text{eta}(6)\text{-}1,2\text{-diphenylethene})\text{Cr}(\text{CO})_3$ and the molecular structure of $\text{trans-}(\text{eta}(6)\text{-}1,2\text{-diphenylethene})\text{Cr}(\text{CO})_3$. *Organometallics* 26:4128–4134
87. Busby M, Hartl F, Matousek P et al (2008) Ultrafast excited state dynamics controlling photochemical isomerization of N-methyl-4-[trans-2-(4-pyridyl)ethenyl]pyridinium coordinated to a $\text{Re}(\text{CO})_3(2,2'\text{-bipyridine})$ chromophore. *Chem Eur J* 14:6912–6923
88. Patrocínio AOT, Iha NYM (2008) Photoswitches and luminescent rigidity sensors based on $\text{fac-}[\text{Re}(\text{CO})_3(\text{Me}_4\text{phen})(\text{L})]^+$. *Inorg Chem* 47:10851–10857
89. Bitterwolf TE (2006) Photochemical nitrosyl linkage isomerism/metastable states. *Coord Chem Rev* 250:1196–1207
90. Rack JJ (2009) Electron transfer triggered sulfoxide isomerization in ruthenium and osmium complexes. *Coord Chem Rev* 253:78–85
91. Srajer V, Teng TY, Ursby T et al (1996) Photolysis of the carbon monoxide complex of myoglobin: nanosecond time-resolved crystallography. *Science* 274:1726–1729
92. Carducci MD, Pressprich MR, Coppens P (1997) Diffraction studies of photoexcited crystals: metastable nitrosyl-linkage isomers of sodium nitroprusside. *J Am Chem Soc* 119:2669–2678
93. Manoharan PT, Gray HB (1966) Electronic structure of metal pentacyanonitrosyls. *Inorg Chem* 5:823–839
94. Schaniel D, Woike T (2009) Necessary conditions for the photogeneration of nitrosyl linkage isomers. *Phys Chem Chem Phys* 11:4391–4395
95. Warren MR, Brayshaw SK, Johnson AL et al (2009) Reversible 100% linkage isomerization in a single-crystal to single-crystal transformation: photocrystallographic identification of the metastable $[\text{Ni}(\text{dppe})(\eta^1\text{-ONO})\text{Cl}]$ isomer. *Angew Chem Int Ed* 48:5711–5714
96. Hatcher LE, Warren MR, Allan DR et al (2011) Metastable linkage isomerism in $[\text{Ni}(\text{Et}_4\text{dien})(\text{NO}_2)_2]$: a combined thermal and photocrystallographic structural investigation of a nitro/nitrito interconversion. *Angew Chem Int Ed* 50:8371–8374
97. Heseck D, Inoue Y, Ishida H et al (2000) The first asymmetric synthesis of chiral ruthenium tris(bipyridine) from racemic ruthenium bis(bipyridine) complexes. *Tetrahedron Lett* 41:2617–2620
98. Durham B, Wilson SR, Hodgson DJ et al (1980) Cis-trans photoisomerisation in $\text{Ru}(\text{bpy})_2(\text{OH}_2)_2^{2+}$ —crystal structure of $\text{trans-}[\text{Ru}(\text{bpy})_2(\text{OH}_2)(\text{OH})](\text{ClO}_4)_2$. *J Am Chem Soc* 102:600–607
99. Tamayo AB, Alleyne BD, Djurovich PI et al (2003) Synthesis and characterization of facial and meridional tris-cyclometalated iridium(III) complexes. *J Am Chem Soc* 125:7377–7387
100. Osman R, Perutz RN, Rooney AD et al (1994) Picosecond photolysis of a metal dihydride—rapid reductive elimination of dihydrogen from $\text{Ru}(\text{DMPE})_2\text{H}_2$ ($\text{DMPE} = (\text{CH}_3)_2\text{PCH}_2\text{CH}_2\text{P}(\text{CH}_3)_2$). *J Phys Chem* 98:3562–3563
101. Chatt J, Davidson JM (1965) The tautomerism of arene and ditertiary phosphine complexes of Ruthenium(0), and the preparation of new types of hydrido-complexes of ruthenium(II). *J Chem Soc* 843–855
102. Hoyano JK, Graham WAG (1982) Hydrogen-mediated photolysis of $(\eta^5\text{-C}_5\text{Me}_5)\text{Os}(\text{CO})_2\text{H}$. *J Am Chem Soc* 104:3723–3725

103. Janowicz AH, Bergman RC (1982) C–H activation in completely saturated hydrocarbons. *J Am Chem Soc* 104:352–354
104. Solari E, Da Silva C, Iacono B et al (2001) Photochemical activation of the NN bond in a dimolybdenum-dinitrogen complex: formation of a molybdenum nitride. *Angew Chem Int Ed* 40:3907–3909
105. Curley JJ, Cook TR, Reece SY et al (2008) Shining light on dinitrogen cleavage: structural features, redox chemistry, and photochemistry of the key intermediate bridging dinitrogen complex. *J Am Chem Soc* 130:9394–9405
106. Kunkely H, Vogler A (2010) Photolysis of aqueous $[(\text{NH}_3)_5\text{Os}(\text{N}_2)\text{Os}(\text{NH}_3)_5]^{5+}$: cleavage of dinitrogen by an intramolecular photoredox reaction. *Angew Chem Int Ed* 49:1591–1593
107. Archer S, Weinstein JA (2012) *Coord Chem Rev Charge-separated excited states in Platinum(II) chromophores: photophysics, formation, stabilization and utilization in solar energy conversion.* *Coord Chem Rev* 256:2530–2561
108. Johnson BFG (1980) In: Johnson BFG (ed) *Transition metal clusters.* Wiley, UK
109. Braunstein P, Oro LA, Raithby PR (eds) (1999) *Metal clusters in chemistry.* Wiley-VCH, Weinheim
110. Vergeer FW, Hartl F, Matousek P et al (2002) First direct observation of a CO-bridged primary photoproduct of $[\text{Ru}_3(\text{CO})_{12}]$ by picosecond time-resolved IR spectroscopy. *Chem Commun* 1220–1221
111. Ford PC (1990) Quantitative mechanistic studies of the photoreactions of trinuclear metal-carbonyl clusters of iron, ruthenium and osmium. *J Organomet Chem* 383:339–356
112. DiBenedetto JA, Ryba DW, Ford PC (1989) Reaction dynamics of photosubstitution intermediates of the tri-ruthenium cluster $\text{Ru}_3(\text{CO})_{12}$ as studied by flash photolysis with infrared detection. *Inorg Chem* 28:3503–3507
113. Bentsen JG, Wrighton MS (1987) Wavelength-dependent primary photoprocesses of $\text{Os}_3(\text{CO})_{12}$ in fluid solution and in rigid alkane glasses at low temperature: spectroscopic detection, characterization, and reactivity of coordinatively unsaturated $\text{Os}_3(\text{CO})_{11}$. *J Am Chem Soc* 109:4518–4530
114. Roberts DA, Geoffroy GL (1982) In *comprehensive organometallic chemistry*, vol 6. Pergamon, Oxford
115. Farrugia LJ (1995) In *comprehensive organometallic chemistry II*, vol 10. Pergamon, New York
116. Hunstock E, Mealli C, Calhorda MJ et al (1999) Molecular structures of $\text{M}_2(\text{CO})_9$ and $\text{M}_3(\text{CO})_{12}$ ($\text{M} = \text{Fe}, \text{Ru}, \text{Os}$): new theoretical insights. *Inorg Chem* 38:5053–5060
117. Nijhoff J, Hartl F, Stufkens DJ et al (1999) Light-induced insertion of a CO ligand into an Os–N bond of the clusters $\text{Os}_3(\text{CO})_{10}(\text{L})$, where L represents a potentially terdentate N, N'-chelating alpha-diimine. *Organometallics* 18:4380–4389
118. Nijhoff J, Bakker MJ, Hartl F et al (1998) Photochemistry of the triangular clusters $\text{Os}_3(\text{CO})_{10}(\text{alpha-diimine})$: Homolysis of an Os–Os bond and solvent dependent formation of biradicals and zwitterions. *Inorg Chem* 37:661–668
119. Vergeer FW, Kleverlaan CJ, Matousek P et al (2005) Redox control of light induced charge separation in a transition metal cluster: photochemistry of a methyl viologen-substituted $[\text{Os}_3(\text{CO})_{10}(\text{alpha-diimine})]$ cluster. *Inorg Chem* 44:1319–1331
120. Leadbeater NE (1995) The generation and reactivity of versatile ruthenium carbonyl organometallic intermediates by cluster photochemistry. *J Chem Soc Dalton Trans* 2923–2934
121. Johnson BFG, Lewis J, Twigg MV (1974) Photochemical reactions of $\text{Ru}_3(\text{CO})_{12}$ involving metal–metal bond fission. *J Organomet Chem* 67:C75–C76

Chapter 4

Photochemical Materials: Absorbers, Emitters, Displays, Sensitisers, Acceptors, Traps and Photochromics

Matthew L. Davies, Peter Douglas, Rachel C. Evans
and Hugh D. Burrows

Abstract In this chapter we discuss some of the typical materials used in photochemistry. We describe, in general terms, how their suitability for application as absorber, emitter, sensitiser, energy acceptor or quencher, depends on the energy states within the material and the routes of interconversion between these states, and also how suitability as a redox or chemical sensitiser/acceptor/trap is determined by specific chemical reactivities. We describe the application of photochemical principles to the design of light sources and displays, and describe the photochemical principles and applications of photochromics and molecular switches. A table giving the structures, characteristics, and uses, of a number of compounds widely used in photochemistry is provided at the end of the chapter.

4.1 Introduction

Whether a material will act as a *passive absorber*, an *emitter*, or *sensitiser*, depends, for the most part, on how excitation energy is deactivated in that material. If deactivation is *via* a fast non-radiative process, the material will act as a passive

M. L. Davies (✉)

School of Chemistry, Bangor University, Gwynedd LL57 2UW, UK
e-mail: m.davies@bangor.ac.uk

P. Douglas

Chemistry Group, College of Engineering, Swansea University, Swansea, UK
e-mail: P.Douglas@swansea.ac.uk

R. C. Evans

School of Chemistry, Trinity College Dublin, Dublin 2, Ireland

H. D. Burrows

Department of Chemistry, University of Coimbra, Coimbra, Portugal
e-mail: burrows@ci.uc.pt

absorber. If deactivation goes *via* an emissive excited-state, then the material may be a useful emitter. If deactivation proceeds *via* a relatively long lived excited-state, then the excited state may be useful as an energy transfer sensitiser, since the long lifetime may allow transfer of the excited-state energy to another species. If deactivation goes *via* a chemical reaction which leads to products of interest e.g. singlet oxygen, radicals, or redox active species (*i.e.* strong oxidants or reductants), then the material may be a useful photochemical sensitiser for these species.

Whether a material is useful as an *excited-state acceptor*, depends on the energy level of excited states within the material and the way those states deactivate once populated. A useful *redox* or *chemical acceptor/trap* will show efficient and specific reactions: redox traps will undergo a specific reduction or oxidation; singlet oxygen acceptors have specific reactions with singlet oxygen; and radical quenchers or traps have specific reactions with radicals.

In the following discussion, a number in bold indicates an entry for that compound in the table of commonly used compounds, their uses and properties, Table 4.1, found at the end of the chapter.

4.2 Passive Absorbers

The major uses of passive absorbers are as colorants and sunscreens, although in passive solar heaters the heat generated during excited-state deactivation is the important photo-product. Dyes and pigments are used as passive absorbers in established technologies such as: paints, plastics, textiles, paper, printing, imaging, and foodstuffs. In sunscreen formulations, UV absorption rather than visible absorption is required. High technology applications of passive absorption include: biochemical “stains” where not only colour intensity, but also selective binding to particular biochemical substrates, is required; recording dyes for optical storage in CDs and DVDs; and imaging and digital printing where a combination of the need for accurate colour reproduction, chemical and photochemical stability, and compatibility with printing processes, requires highly specialised dye design [1–3]. In the space available here we can give only a very brief account of what is commonly termed *colour chemistry*, but the interested reader is directed to references [1–3] which between them provide an excellent introduction and overview of this very important aspect of applied photochemistry.

Important characteristics for colorants are: intensity, brightness and stability. Relative costs mean that only colorants with high intensity absorptions are commonly used. This restricts the types of transition involved to: molecular charge transfer bands, $\pi-\pi^*$ bands, $n-\pi^*$ bands with a high degree of $\pi-\pi^*$ coupling, or direct bandgap semiconductor transitions. The brightness of a colorant depends primarily on absorption band width; narrow bands give bright colours. The absorption band width is influenced by the width of ground and excited state potential energy curves, how similar the molecular geometries in ground and excited state are, and also the presence of close or overlapping transitions.

Photostability/lightfastness is very important for all colorants; poor lightfastness causes loss of colour in imaging and printing, and leads to conservation problems for artwork and artefacts. Stability towards thermal degradation is important in colouring plastics which may be moulded at high temperatures, in colorants for outside structures, metalwork and cars, as well as for sublimable dyes. Stability towards hydrolysis is important in imaging, printing and artist's materials. Washfastness is a particularly important feature for textile dyes.

Colorants are used as *dyes* or *pigments*. *Dyes* are colouring materials which are *soluble* either in the medium in which they are incorporated, or, as the term is commonly used in textiles technology, in a dyeing solution applied to the medium in which they are incorporated. (Disperse 'dyes' are applied as a fine dispersion to synthetic textiles, but dissolve in the textile to give a 'solid solution'). *Pigments* are colouring materials which are *insoluble* in the medium in which they are incorporated. The principle applications of pigments are in paints, printing inks and plastics, although they are also used to colour cement, ceramics, concrete, cosmetics, glass, paper and rubber. Usually the application of pigments involves their incorporation into a liquid medium, a wet paint, or a molten thermoplastic material, by a dispersion process in which the pigment aggregates are broken down into very small primary particles or aggregates. When the medium solidifies, the individual pigment particles become fixed in the solid polymeric matrix. Apart from imparting colour, pigments also provide *opacity* by scattering light. The size and size distribution of the pigment particles is important in terms of both colour and opacity; particle sizes of $\sim 0.2\text{--}0.3\ \mu\text{m}$ are often used since these provide maximum opacity.

4.2.1 Inorganic Colorants

Most inorganic colouring materials are pigments. Surface treatments are often applied to inorganic pigments, e.g. coating with surfactants may improve ease of dispersion, while coating with inert inorganic oxides, such as silica, can give improved lightfastness and chemical stability. Among the most important inorganic pigments are titanium dioxide (white); carbon black; metal oxides e.g. iron and manganese (yellow, brown, red, black) and chromium (green); cadmium/zinc sulfides/selenides (yellow/orange/red); cobalt aluminate (cobalt blue); ultramarine blue; and Prussian blue. The origin of colour in these materials is varied.

TiO₂ (9.1) and Cd-Zn/S-Se (9.3–9.5) are semiconductors. TiO₂ has a band gap of 3.0–3.2 eV, *i.e.* it absorbs in the UV region. It is used as a white pigment because it has a very high refractive index, and therefore a high scattering efficiency and excellent opacity for all visible wavelengths. A surface coating is generally required to prevent photoreactions on the TiO₂ surface from damaging the dispersion medium, a phenomenon known in the paint industry as *chalking*. With a band gap of 1.6 eV CdSe absorbs all visible photons and therefore appears black; at 2.6 eV CdS absorbs blue photons and therefore appears yellow. Changing

the S/Se ratio shifts the band gap from 2.6 to 1.6 eV, taking the colour through the yellow-orange-red-black range. Replacement of Cd by Zn gives greenish-yellow tones.

In many oxide pigments the colour is due to ligand-metal charge transfer (LMCT) transitions (see Chap. 3). Natural iron oxide based pigments include: *yellow ochre*, *red haematite*, and the browns, *sienna* and *burnt sienna*; *umber* and *burnt umber* are iron oxide with manganese dioxide. Synthetic red iron oxides are anhydrous Fe_2O_3 , while synthetic yellow pigments are iron(III) oxide/hydroxides, $\text{FeO}(\text{OH})$, and black pigments are non-stoichiometric Fe(II)/Fe(III) oxides. They have excellent durability, high opacity, low cost, and low toxicity. Cr(III) oxide, which gives a dull green pigment with outstanding durability, is another important oxide pigment. Lead chromate pigments, which have now been almost completely replaced because of their toxicity, are important historically. Pure PbCrO_4 gives a rich yellow pigment, the colour of which originates from a charge transfer transition on the chromate CrO_4^{2-} ion; the role of lead is to make a highly insoluble pigment. Lemon shades are obtained by the addition of lead sulfate, while addition of molybdate gives orange red tones.

Cobalt blue is a cobalt aluminate, CoAl_2O_4 , with a spinel crystal structure in which Co atoms sit in a tetrahedral environment (the same coordination geometry which gives self-indicating silica gel a blue colour when dry—the pink colour when wet is due to cobalt in octahedral coordination). Here the colour originates from metal-centred $d-d$ transitions on Co(II). A blue/green analogue, CoCr_2O_4 , has Co in tetrahedral sites and Cr in octahedral sites in the crystal structure.

Ultramarines are complex sodium aluminosilicate structures, containing trapped sulfur anions, S^{2-} and S^{3-} , which absorb in the red spectral region, e.g. the S^{3-} anion has an absorption maximum, λ_{max} , at ~ 600 nm [4]. Originally from the mineral *lapis lazuli* (blue stone), brought to Europe from Afghanistan, where it is still mined today, and described as *ultramarine* (beyond the sea). It was very expensive, partly because of the source, but also due to difficulty in preparation, and in Western religious art it was often reserved for the mantle of the Virgin Mary [5]. Today, it is made synthetically as French ultramarine, after a synthetic route was discovered by Jean Baptiste Guimet in 1826.

Prussian blue is a mixed Fe(II)/Fe(III) complex polymeric species in which Fe(II) is octahedrally coordinated by C, and Fe(III) is octahedrally coordinated by N, to give a structure containing Fe(II)-C-N-Fe(III)-N-C-Fe(II)-linkages, in which the colour originates from electron transfer between the two metal oxidation states. It was discovered in 1704, and used in 'blueprints' and also in the cyanotype photographic process developed by Herschel (see Chap. 11). The cyanotype process is made possible by the photochemical reduction of Fe(III) citrate (or oxalate) to Fe(II), which reacts with ferricyanide present in the coating formulation to give Prussian blue. A similar photoreduction of Fe(III) oxalate to Fe(II) is used in the ferrioxalate actinometer (see Chap. 14).

4.2.2 Organic Colouring Materials

Here, pigments and dyes are both important. There is an enormous range of organic dyes available, and a number of classification methods have been used, but that based on the electronic nature of the transition is most relevant here [1].

Donor–acceptor colorants. These are by far the most important group of organic colorants, they include azo-, anthraquinone- and carbonyl-based dyes. Colour originates from transitions in which there is a significant shift in electron density from the donor to the acceptor parts of the molecule. Azo dyes account for over 50 % of all commercial dyes. There is a vast range available. They can contain multiple azo, ($-N=N-$), groups, but monoazo dyes are the most important (e.g. methyl orange **11.13**). These contain an electron donating group (often hydroxy or amine) and an electron accepting (often aryl) group on either side of the azo bond. The electronic transition occurs across the azo bridge from the electron donor to the electron acceptor group. These dyes cover the whole spectral range but yellows, oranges and reds are most important. Synthesis is relatively straightforward from cheap starting materials, so they are very cost effective. Azo dyes can also exhibit *cis–trans* photoisomerisation across the azo bond, which results in *photochromism* (see later), although this is not common in modern dyes. Addition of a hydroxy group adjacent to the azo bond generally improves light stability, since proton transfer between O and N atoms in the excited state can act as a rapid mechanism for loss of excitation energy. Metal complex azo dyes are also very common, with copper, cobalt and chromium being common metal ions used. The metal ion leads to improved lightfastness. There are probably a number of factors at play in this, e.g. reduction of electron density at the chromophore and therefore a reduction in ease of photooxidation, excited-state deactivation by low lying *d–d* levels, and steric protection of the chromophore. Metal dyes also show improved washfastness because of the larger size of the metal complex, and stronger fibre interactions. However metal complexes are generally duller colours than the parent azo due to their broader absorption bands, which result from additional overlapping *d–d* transitions and charge-transfer bands, and sometimes the presence of isomers with slightly different absorption spectra.

Anthraquinone dyes are the second most important group of organic colorants. The basic structure is 9,10-anthraquinone (**11.3**) but with electron donor groups in 1, 4, 5, and 8 positions. The absorption maximum can be shifted by choice of type and number of substituent. The historically important natural dye *alizarin* is 1,2-dihydroxyanthraquinone (**11.4**), originally obtained by extraction from the root of the madder plant. Hydrogen bonding from the carbonyl oxygen to an adjacent OH, or NH group is an important factor in light stability, since reversible proton transfer in the excited state can act as a rapid mechanism for loss of excitation energy (similar to putting a hydroxy group ortho to the azo group in azo dyes). It is possible to get the whole spectral range, but violets, blues and green are particularly important since these complement the yellow, oranges, and reds best obtained in azo dyes. Anthraquinone dyes have good brightness and fastness;

however they cost more than azo dyes because the molar absorption coefficient is lower and they are more expensive to make. They are not used much as pigments because pigment blues and green are best provided by phthalocyanines.

Indigo and 6,6-dibromoindigo (*tyrian purple*) (**11.11**) are two of the oldest known dyes [6]. Natural indigo is extracted from plants, indigo (*Indigofera tinctoria*) in the Far-East or woad (*Isatis tinctoria*) in Europe; tyrian purple is extracted from shellfish. In both cases the dyestuff itself is not present in the natural source but is generated by fermentation and/or air oxidation. Nowadays, only indigo is important commercially, and it is almost exclusively synthetic. It is used mainly for denim (*de-Nîmes*, where the thick cotton cloth was originally made), where fading without change of shade only, at points of textile stress and wear is a key fashion feature.

Polyenes. These are systems of extended conjugation in which the molecular orbitals extend over a large part of the molecule and the π - π^* transition does not result in a major shift in electron density from one part of the molecule to another. As the degree of conjugation increases, the spacing of electronic energy levels decreases, and λ_{\max} shifts to longer wavelengths. Phthalocyanines (**5.5**, **5.6**) are the most important synthetic commercial polyene colorants. Metallophthalocyanines (**5.6**) give brilliant intense blue/green colours of high stability. The intensity of colour is due to very high molar absorption coefficients, while the brilliance is due to very narrow absorption bands due to the rigidity of the molecular structure. They are most commonly used as pigments. They are too large to penetrate into many fibres, but can be used for polyester and as reactive dyes for cotton, where they are covalently bound onto the cotton surface. Naphthalocyanines have absorption maxima in the NIR which makes them interesting dyes for optical data storage and 'invisible' security printing. Carotenoids are important natural polyene colorants, and are used commercially in foodstuffs, the most important being β -carotene (**11.5**).

Cyanines, squaraines, rhodamines, xanthenes. Cyanines (**4.6**, **4.7**) are similar to polyenes, but with remarkably low energy transitions for such small molecules. This is because they have an odd number of atoms carrying p orbitals in the conjugated chain (polyenes have an even number), and the terminal N, rather than C, atoms results in two extra electrons per chain compared to polyene dyes. The resulting MO structure has a relatively high energy HOMO with significant non-bonding character, as opposed to the bonding HOMO of polyenes, and there is, therefore, a relatively low energy HOMO \rightarrow LUMO transition (see [Chap. 1](#)). These molecules give intense bright colours due to their high molar absorption coefficients and quite narrow absorption bands. The λ_{\max} is dependent upon chain length, and dyes absorbing from the blue to IR spectral regions are available. 'Hidden cyanines', in which the cyanine structure is not so obvious, e.g. phenolphthalein, rhodamines (**4.1**, **4.2**), squaraines (**11.19**, **11.20**) and other dyes such as methylene blue, (**11.12**) Nile blue (**11.15**) and triarylmethane dyes (**11.7**), and xanthenes (fluoresceins) (**4.3**–**4.5**), which can be considered oxygen analogues of cyanines, also give intense bright colours. Rigid structures such as rhodamines and fluoresceins are often highly fluorescent, whereas 'looser' structures like phenolphthalein are not. Dyes spanning the full spectral range can be made. Although historically important dyestuffs, particularly the triarylmethane dyes, cyanines and

hidden cyanines are not so chemically and photochemically stable as other dyes and so are not used as absorptive colorants, except in specialist applications such as biological ‘stains’ for microscopy, and as colorimetric pH indicators. The highly fluorescent variants e.g. rhodamines, are widely used as laser dyes, and also as biological stains and fluorescent markers. They are also used as fluorescent colorants, e.g. in artist’s inks, where the resultant brilliant colours are a product of both absorption and emission, but in this application their poor light stability is a significant disadvantage.

4.2.3 Sunscreens

Sunscreens are UV absorbing materials suspended in a cream or spray. The two main types of UV absorbers used are: (1) colloidal semiconductor particulates, notably ZnO (9.2) and silica- or alumina-coated TiO₂ (9.1), and (2) organic absorbers. Key photochemical requirements are high UV absorption with no visible absorption, (although scattering of visible light in opaque white sunscreens is acceptable), and high photostability with a complete lack of any photoreactions which may lead to phototoxicity. Chemical requirements are low toxicity, and compatibility with cream formulations. Ideally, excitation energy is rapidly lost as heat, and typical mechanisms for this in organic sunscreens are proton transfer in hydroxyl benzophenone (11.6) based sunscreens and molecular twisting in cinnamates (11.17).

4.3 Emitters

There are many type of emitters: gas phase atoms and ions; molecules in the gas, solution, or solid phase; metal ions as an integral part of a solid state lattice; energy traps or ‘activator’ sites, which may be a specific ion or site defect, in a semiconductor or other solid; conjugated polymers; semiconductors as either a solid, or as a colloidal dispersion in some other medium or solution; and hot metals. In all but the latter three cases emission is from a localised emitter, with both states involved in the transition localised in a small region of space, on an atom, ion, or molecule. However, for semiconductors, some emissive polymers, and hot metals, the states involved in the transition extend across a relatively large region of space and a large number of atoms.

The characteristics of the light emitted are determined by the following.

- (1) **The energy levels of the emitter in the medium used.** These determine the emission wavelength(s), and shape of the emission band(s). For semiconductors, and some emissive polymers (3.1–3.9), emission is a property of the whole material, and control of the size of the semiconductor particle or chain length of the polymer may be important, e.g. in semiconductor *quantum dots* (9.3–9.7).

For semiconductor materials on the macroscale the valence and conduction bands have band widths associated with the continuum of orbitals. However, on going from the macroscale to nanometre (nm) dimensions two effects occur due to the removal of atoms (and hence orbitals); firstly, the bands cease to be a continuum and individual orbitals, and hence quantised energy levels are observed (hence the term *quantum dot*); secondly, orbitals are removed from the edges of the valence and/or conduction bands, which increases the band gap. The size of the quantum dot dictates the absorption and emission characteristics; the smaller the quantum dot, the larger the band gap, and hence the more blue-shifted (shorter wavelength) the emission (Fig. 4.1) [7].

In metallic solids, the presence of a continuum of states means that there are many transitions possible, and so when heated, as in an electric tungsten filament bulb, these materials emit a continuous spectrum which is very different to the line or band emission of atomic or molecular species. Other hot solids, and hot high pressure gases, often emit a mix of line or bands on top of a continuum (see for example the spectrum of high pressure Hg or Xe lamps in Chap. 14).

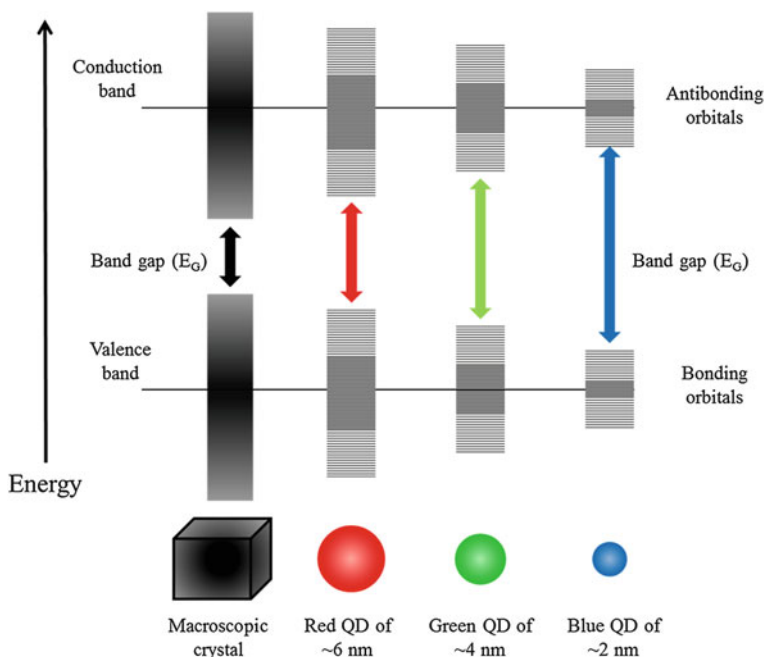


Fig. 4.1 Schematic representation of the effect of size on semiconductor properties, *i.e.* changes on going from the macro-scale (continuum of energy levels) to the nano-scale (quantised energy levels). The average energy position of the bands do not change (represented by the lines dissecting the relevant bands and orbitals) however, the band gap increases with decreasing size as extreme energy levels are removed. Figure adapted from Ref. [8]

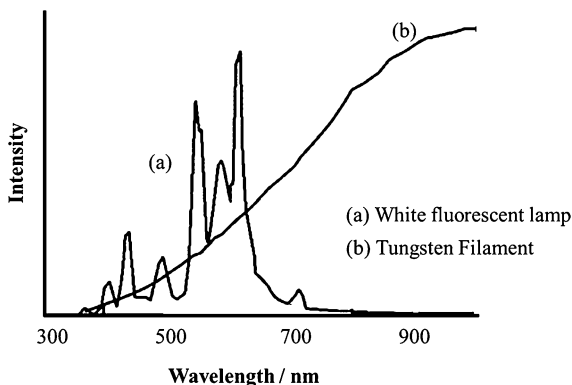
- (2) **The nature of the emissive transition.** Typically, allowed transitions, such as fluorescence or direct bandgap semiconductor emission, have radiative lifetimes between a few and a hundred ns. Forbidden transitions, such as molecular phosphorescence, have radiative lifetimes longer than μs , usually much longer.
- (3) **Competition with other deactivation routes for the excitation energy.** The competition between emission and other deactivation routes determines the emission quantum yield. Competing deactivation processes are important for almost all emitters, even those for which emission is a highly probable process; there are few emitters with an emission quantum yield approaching 1. Competing deactivating processes are particularly important for forbidden transitions, where radiative rates are relatively slow. Most reasonably efficient room temperature phosphorescent compounds are heavy metal complexes where the degree of forbiddenness is reduced by heavy-atom spin-orbit coupling, and the radiative lifetime is in the μs – ms range. Most organic molecules, which do not have such coupling, show phosphorescence only in a low temperature glass, with radiative lifetimes in the ms to tens of seconds range.
- (4) **The method of population of the emissive state.** If population is achieved directly from the initial excitation source, then as soon as that source is removed the emission intensity will decrease with a rate determined by the deactivation processes of the emissive state. However if the excited-state is populated by processes which occur after the initial excitation process, e.g. energy transfer, energy migration, exciton migration, or delayed fluorescence, then the emission intensity will decrease at a rate determined by both deactivation and population processes. In some cases, where the rate of population of the emissive state can be made very slow, e.g. by energy or exciton migration within a solid, very long lived *phosphors* (9.3) are possible.
- (5) **Population inversion.** If the emissive state can be formed such that a population inversion is obtained it may be possible to obtain laser emission (e.g. Nd^{III} ions (10.5) in the Nd/YAG laser, see Chap. 14).

Emitters can be classified in terms of those which emit in the gas phase, the solution phase, or the solid state, and also by mode of excitation, *i.e.* electroluminescence, thermoluminescence, chemiluminescence, radioluminescence and photoluminescence. We are most concerned with photoluminescent materials, but thermoluminescence and electroluminescence, in both gas and solid phases, are important technologies.

4.3.1 Solid State Thermoluminescence

The first commercial electric lamps of Edison and Swann involved *incandescence* produced by passing an electric current through a carbon filament. Modern incandescent lights use the same principle, but with the fragile carbon thread

Fig. 4.2 Emission spectra of: **a** 5000 K fluorescent lamp, **b** 2800 K tungsten filament lamp. Figure adapted from Ref. [10]



replaced by tungsten. The incandescent lamp has the advantage of good spectral output. Like the Sun, the broadband emission (Fig. 4.2) is, to a good approximation, that of a black body radiator [9]. However, although the cost of the incandescent lamp is low, the efficiency of energy conversion is limited (5–10 %) since most of the electrical energy used is lost as heat, and the lifetime of the lamps is limited. Although modest increases in efficiency are possible, there is a global tendency to phase out incandescent lamps for domestic use in favour of more energy efficient forms of lighting.

Other common incandescent emitters are the ‘glowbar’ used in IR spectroscopy which is also a good approximation to a black body emitter, and burning magnesium and the incandescent lanthanide oxides used in the mantles of gas lamps; for these emission is a combination of a broad band continuum with specific emission lines superimposed.

The measurement of *thermally-activated luminescence* from radiation-induced defects in minerals, particularly those in ceramics, is usually termed *thermoluminescence* when used in archeological dating, although the role of thermal excitation here is not the generation of emissive states but rather to allow defect relaxation, and concomitant emission, to occur. The general principle is as follows. When ceramics are fired, the high temperatures allow complete defect relaxation in the ceramic minerals, such that immediately after firing the thermoluminescence signal would be zero. Over time, natural radiation damage causes defect formation within the ceramic, and thus the intensity of thermoluminescence at any time after firing is related to the rate of defect formation and, the key archeological factor, the time since the firing.

4.3.2 Gas Phase Plasma Emission

All atoms and ions have some excited states which relax by emission in the UV/Vis spectral region. This forms the basis of atomic emission/fluorescence

spectroscopy. Excitation may be: thermal in a flame; electrical in an arc; or by radio- or microwave-frequency radiation. This produces a *plasma*, which leads to production of excited states of the atoms and molecules of the gas. These then emit light. Apart from its use in analysis *via* atomic emission spectrometry and flame photometry, and the generation of colours in fireworks and flares, thermal excitation is not widely used to generate gas phase excited-states. (The yellow/white emission of candle/spirit lamp and low air flow Bunsen flames is due to incandescent carbon particles rather than specific atom or molecular emission—these generate the blue component of the light of the flame.) However, electrically excited plasmas in *gas discharge* lamps give us many of our light sources. These have been known since the nineteenth century. Important gas discharge lamps used in experimental photochemistry are: (i) low, medium and high pressure mercury lamps which are excellent sources of UV radiation; (ii) the Xe arc lamp, which is widely used as an intense continuous or μs pulsed UV/vis source; (iii) Xe and Kr flash lamps which give UV/Vis emission with *ca.* μs pulse duration, (also used as photographic flashlamps); (iv) gas phase lasers; (v) the nitrogen and oxygen pulse spark lamps used in single photon counting; and (vi) the deuterium lamp which is used as a UV source in UV/Vis spectrophotometers and other instruments (see [Chap. 14](#) for further information on light sources).

Gas discharge lamps exhibit higher energy conversion efficiency than incandescent lamps and are widely used for general industrial and domestic illumination. They can be divided in terms of systems in which there is local thermal equilibrium (*LTE plasmas*) and those in which there is not (*non-LTE plasmas*) [[11](#)]. LTE plasmas, sometimes termed high intensity discharge (HID) lamps, operate at high gas pressures. A good example is the high-pressure sodium lamp, produced by adding sodium metal to the mercury lamp and used as an intense yellow light source for many outside applications, such as street lighting and freight yards. For these applications, the colour of the illumination is less important than the cost. An intense white HID lamp can be obtained by adding metal halide salts, and is frequently used in outdoor floodlighting. The most important non-LTE plasmas are low pressure mercury or sodium lamps. Gas discharge lamps have the disadvantage that the light is emitted in discrete lines rather than a broad band obtained through incandescence, as can be seen in the spectra of mercury lamps discussed in [Chap. 14](#) (see [Fig. 14.3](#)). In addition, in many cases, much of the light is in the UV (such as the 254 nm line in the mercury discharge lamp) and is not of itself useful for lighting, although it can be converted to visible light by a phosphor, e.g. the white phosphor coating on the inside of a fluorescent lamp.

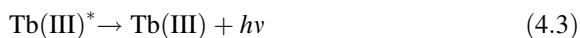
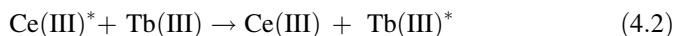
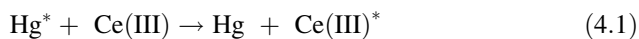
4.3.2.1 Fluorescent Lamps and Phosphors

During the early part of the twentieth century, considerable effort was made to convert the UV component of gas discharge lamps into broadband visible light through the use of solid state luminescent materials, commonly termed *phosphors*. Phosphors have been studied since the middle of the nineteenth century, and are,

typically, inorganic semiconductors, such as zinc sulfide (**9.3**), zinc silicate, or calcium tungstate [12, 13], frequently doped with other species. The first practical “fluorescent” lamps, invented in Germany in the 1920s and commercialised in the US in the following decade, involved low pressure mercury discharge lamps with the walls of the tube coated with appropriate phosphors. The same phosphors could be excited by high energy radiation, such as electron beams (cathode rays), and the search for new luminescent materials for fluorescent lamps has paralleled that for cathode ray tubes (CRTs) for television or other display applications. Much of the early research on phosphors was empirical [12]. However, by the middle of the twentieth century there was sufficient knowledge on electronic structure, luminescence spectra and photophysics of inorganic materials to apply a more rational approach to the design of phosphors. Luminescence of inorganic materials can be divided into that of localised centres, such as metal ions, and emission involving delocalised semiconductor bands [13]. In general, emission involving semiconductor bands will give a rather broad spectrum, while that from localised centres will involve sharp, well defined spectral lines. For display applications, it is often advantageous to have rather sharp spectra, such as is found with the f - f transitions of lanthanide ions (**10.1–10.6**). A major breakthrough in luminescent materials for CRTs came with the development of a good red phosphor involving europium(III) in yttrium vanadate (**10.1**) [14]. Full colour displays are obtained by combining emission from different coloured phosphors, typically red, green and blue (RGB) using the Commission Internationale de l’Éclairage (CIE) chromaticity diagram (Fig. 14.3) [15]. An entertaining account of the development of this diagram is given elsewhere [16].

Since the seminal work on europium(III) based phosphors, lanthanides have become some of the most important materials for both lighting and displays [17]. With the normal fluorescent lamps containing mercury vapour, electronic energy transfer is crucial for efficient conversion of UV into visible light. This can involve both Förster [18] and Dexter [19] mechanisms. As discussed in Chap. 1, the Förster mechanism involves dipole–dipole interactions which require good overlap between the emission spectrum of the energy donor and the absorption spectrum of the acceptor, while the Dexter mechanism involves electron exchange, and needs close proximity between the donor and acceptor. Frequently, cerium(III) is used as an intermediate in fluorescent lamps for good photochemical reasons. The electronic transitions in most lanthanide ions involve two f orbitals, and are very weak, since they are forbidden by the Laporte selection rule (Chap. 1). However, the electronic transitions in Ce(III) involve transition of an electron between $4f$ and $5d$ orbitals, which is allowed by both spin and Laporte selection rules. This gives the Ce(III) ion a good molar absorption coefficient, which favours energy transfer from excited mercury atoms. In addition, the lifetime of the Ce(III) fluorescence is short, which avoids problems of saturation of excited states at high light intensities. The consequence is that excited Ce(III) in the solid phosphor layer can transfer energy efficiently to neighbouring terbium(III) or other lanthanide ions. Although this discussion is an oversimplification, and there are many parts of the sensitisation mechanism that are still poorly understood, it does indicate some of

the photochemical ideas used in optimising the efficiency of fluorescent lamps. A schematic description of energy transfer from excited mercury atoms (Hg^*) to Tb(III) (**10.2**) *via* Ce(III) is given below.



In comparing the properties of different light sources, three parameters are commonly used. The first is the *luminous efficacy*, which is the response of the average eye to light over the visible spectral region (380–780 nm), and is measured in lumens (visible light) produced per watt of electrical power (lm/W). The second property, the *correlated colour temperature*, is a measure of the appearance of the light source and is given as the temperature of the black body which most closely represents the light source. The spectrum of sunlight depends upon altitude and time of day, but at noon typically has a correlated colour temperature of 5000–7500 K. Finally, the *colour-rendering index* is an indication of how accurately the light source can reproduce colours of objects compared with natural light (daylight), and is measured by comparison of the apparent colours of reference pigments using the light source and a black body standard [9].

A 35 W fluorescent lamp has a luminous efficacy of about 104 lm/W, compared with 16 lm/W for a 100 W incandescent lamp [20]. However, fluorescent lamps have a number of disadvantages. In particular, they need an electric ballast to produce the initial discharge in the mercury vapour, which requires a longer start-up than an incandescent lamp. This limits applications in areas, such as traffic lights, which need fairly rapid switching. In addition, white light is important for illumination, particularly for indoor applications, and although the phosphor in a fluorescent lamp can be developed to give a good spectral distribution, often by using a mixture of materials, there are always some lines present in the emission spectrum from the mercury lamp. This can influence the perceived appearance of colours. Most people will be familiar with the experience of buying clothes in a shop lit with fluorescent lighting and then finding the colour appears different in sunlight. This is because of differences in the emission of the light sources; spectra of typical incandescent and fluorescent lamps are compared in Fig. 4.2; the colour-rendering index is 100 for the incandescent lamp and 85 for the fluorescent one.

Fluorescent lamps have much higher luminous efficacy than incandescent ones. Although they are more expensive, their usable lifetimes are an order of magnitude longer. There are, thus, very real economic advantages of these systems, particularly the recently developed energy-saving compact fluorescent lamps (CFL), over tungsten filament lamps. However the majority of fluorescent lamps still use the toxic heavy metal mercury, although other gases are being tried. This has a long term environmental impact and has stimulated the development of other sources of lighting, in particular light-emitting diodes (LEDs).

4.3.3 Electroluminescence and Optoelectronic Displays

4.3.3.1 Cathode Ray Tubes (CRTs)

For much of the twentieth century, the dominant optoelectronic display device was the cathode ray tube, where an electron beam is scanned across a phosphor screen in a vacuum tube. Nowadays, conventional CRTs are being superseded in the display area by flat-panel displays for applications in television, laptop computers, mobile phones, etc. The main competitors in this area at the moment are liquid crystal displays (LCDs) [9, 21], plasma display panels (PDP) [22] and LEDs [23]. Plasma display panels generate a plasma discharge in a mixture of Xe and Ne to produce vacuum UV radiation. This is then used to excite a phosphor screen. This has the advantage that it is possible to prepare large area screens with high brightness [22]. The limitation is that it requires relatively high power consumption. Related technologies being developed for flat screen displays use field emission with a cold cathode and microcavity plasmas [22].

4.3.3.2 Liquid Crystal Displays (LCDs)

These are not, intrinsically, photochemical systems, however, they are optoelectronic systems, and backlighting is fundamental to both their functioning and overall energy efficiency. The most common LCDs involve an oriented twisted nematic phase of an organic material sandwiched between two optically transparent electrodes (typically indium tin oxide, ITO) [21]. This is illuminated by polarised light and the anisotropic liquid crystal changes the plane of polarisation. When observed through a second polariser, light is transmitted when this is parallel to the plane of polarisation or blocked when it is perpendicular. The orientation of the liquid crystal can be changed by application of an electrical potential. In displays this is used to switch between the light (transmitting) and dark (non-transmitting) states, with each pixel corresponding to a liquid crystal cell. A schematic of an LCD based on a typical twisted nematic liquid crystal is shown in Fig. 4.3. The initial monochrome liquid crystal displays were used in watches and calculators [21]. Full colour high definition LCDs are now common, and represent a multibillion pound sector of the display industry. Colour is achieved by dividing the pixels into three, with red, green and blue filters in separate layers. One of the early limitations was that the angle of vision of the displays was limited. This has been partially overcome by using thin film transistors (TFT) to address the cells in active matrix LCDs [21, 24], and has led to the high definition LCD screens currently in use for television, mobile phone and laptop applications. These displays have the advantage that they need very little power for switching. However, one limitation is that the need for backlighting increases the energy consumption, since light is lost on going through the polarisers and colour filters. The battery lifetime of laptop computers is frequently limited by energy usage by LCD backlights. More energy efficient

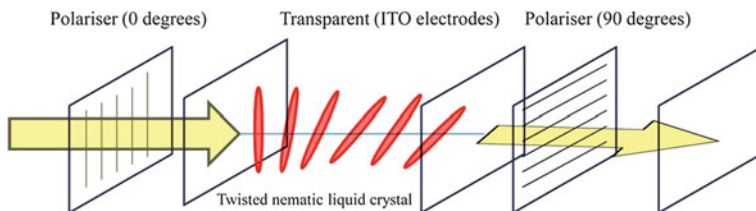


Fig. 4.3 Schematic diagram of one pixel of a twisted nematic liquid crystal display. Polarised light is twisted on passing through the twisted nematic liquid crystal. The orientation of this is changed by applying an electric field. Figure adapted from Ref. [166]

lighting systems, particularly involving light emitting diodes, are under development and are helping overcome this problem [25].

4.3.3.3 Electroluminescence: LEDs, OLEDs and PLEDs

LEDs. Electroluminescence is the emission of light from materials upon application of an electric field [24]. Although electroluminescence from carborundum (a form of amorphous silicon carbide) was first reported over a century ago [26], the development for practical applications in lighting and displays started in the early 1960s with the first report of a red light-emitting diode involving a GaAsP semiconductor [27]. The luminous efficacy of this early inorganic semiconductor LED was only 0.15 lm/W. The initial use focused on red indicator lights and low definition displays on calculators and watches. Since then the area has shown enormous developments in terms of luminous efficacy, available spectral output, intensity, cost and stability [25, 26], and high power LEDs, typically involving elements from Groups III (3) and V (15) of the Periodic Table, now occupy a major role as high-brightness visible light sources. The structure of a typical inorganic semiconductor LED is shown in Fig. 4.4a. Apart from their efficacy, which approaches that of fluorescent lamps, inorganic semiconductor LEDs have very fast switching times (ns), which makes them excellent candidates for technological applications in areas such as traffic signals and red car stop lights [25], and also pulsed sources for photochemical studies (see Chap. 14). A major advance for practical applications was the development of stable, intense blue LEDs based on wide band-gap nitride semiconductors, such as InGaN/AlGaN [28]. As well as expanding the spectral range of LEDs, which now extend into the UV, it has led to the development of high intensity white LEDs, with applications ranging from car headlights to solid state lighting for both domestic and industrial use [25, 26, 29, 30]. Various methods can be used to produce white semiconductor LEDs [25]. One involves combining red, green and blue LEDs. Although this gives high efficiency, and is used in backlighting for liquid crystal displays, the problem is matching the colours, particularly as they will age at different rates. Alternatives are to use a UV emitter to excite red, green and blue phosphors in a

similar fashion to their excitation in fluorescent lamps, or to use a blue LED to excite a yellow phosphor, such as YAG:Ce, mixing the blue with the yellow to give white light [25]. There is intense competition to develop good white LEDs using these ideas for solid state lighting [29, 30], and they are likely to shortly become one of the main sources of lighting. One problem which limits their unit cost is that it is only possible to prepare efficient inorganic semiconductor LEDs with a relatively small surface area. Lamps will typically require a number of these LEDs. As described in the next section, this problem can be overcome by replacing the inorganic semiconductors with organic ones.

OLEDs and PLEDs. Electroluminescence in aromatic molecules (**1.1–1.7**), such as single crystals of anthracene (**1.1**), has been known since the 1960s [21, 31]. However, very high voltages were needed to generate light emission. In 1987, Tang and Van Slyke at Eastman Kodak showed that it was possible to obtain efficient green light electroluminescence from an *organic light-emitting diode* (OLED) containing a thin, vacuum deposited film of tris(8-hydroxyquinoline)aluminium(III), Alq₃ (**6.1**) [51, 32]. The device had the metal complex sandwiched between an optically transparent ITO anode and a Mg:Ag cathode (Fig. 4.4b). The basic mechanism of electroluminescence in organic compounds [31] involves electron injection into the lowest unoccupied molecular orbital (LUMO) at the cathode and positive charge (*hole*) injection at the anode (Fig. 4.4c) to produce the

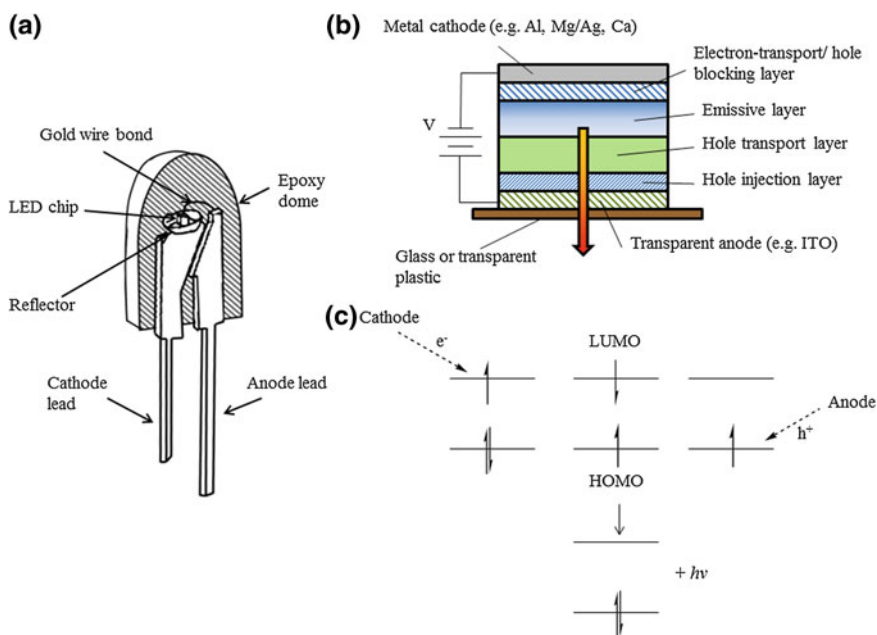


Fig. 4.4 **a** Structure of an inorganic semiconductor LED; **b** structure of an OLED; **c** charge injection and excited state formation in an OLED. Figure adapted from Ref. [167]

excited singlet state of Alq_3 , which then fluoresces. As expected from this mechanism the electroluminescence spectrum is very similar to the photoluminescence. Luminous efficacy of the initial device was 1.5 lm/W, but subsequent developments, in particular, using charge injection or blocking layers at the electrodes [23], led to rapid increases in efficiency of OLEDs, which are now major materials in the display area. One advantage for certain applications is that they can be prepared on flexible supports [31]. About 3 years after the first report of an OLED, Friend and coworkers at Cambridge showed that it is possible to use conjugated polymers (CPs) such as poly(*p*-phenylenevinylene) (**3.2**) as the light-emitting layer to give a *polymer light emitting diode* (PLED) [14, 33, 34]. This has the advantage in device preparation that these can be deposited from solution by using standard printing techniques, such as ink-jet printing, which makes them particularly suitable for preparation of large area displays. It is also feasible to perform large scale commercial production of displays through reel-to-reel printing methodologies. Structures of some commonly used conjugated polymers are shown in **3.1–3.9**. A more detailed description of conjugated polymers for electroluminescent applications is given elsewhere [35].

One limitation of electroluminescence in organic materials is that charge injection produces both singlet and triplet excited states. Statistically these will be produced in the ratio 1:3. Since only the singlet state is normally luminescent, this reduces the maximum efficiency possible from these devices to 25 %, although there are suggestions that for PLEDs it may be possible to have higher singlet:triplet ratios. Forrest and co-workers showed that it is possible to overcome this problem, and obtain increased luminescence efficiency, using room-temperature metal organic phosphorescent materials [45, 36]. The initial room temperature phosphor was a platinum porphyrin (**5.4**). Since then a wide range of other complexes [37, 38], in particular phenylpyridine complexes of iridium(III), have been developed (**6.6–6.8**). Both OLEDs and PLEDs are now on the market in high definition displays. The next step will be the use of both small molecule organics and conjugated polymers in white organic light emitting diodes (WOLEDs) for artificial lighting [37, 39]. These have the advantages of broad spectral output, giving good colour rendering indices, and good CIE coordinates (See [Chap. 14](#)). Key practical problems at the moment include light out-coupling efficiency, practical operating voltages and long-term operational stability. However, devices are now available with lifetimes greater than that of typical incandescent sources (≈ 1000 h), and the attractive design possibilities available with WOLEDs suggests that they will shortly make an important contribution to the technologies available for artificial lighting.

4.3.4 Radioluminescence

Radioluminescence is produced by the bombardment of a material with ionising radiation such as beta particles. One application is in tritium light sources, in

which gaseous tritium is encased in a glass tube lined with a phosphor, e.g. zinc sulfide (**9.3**). Since no electrical excitation source is required, tritium light sources are self-powered, and find application in emergency exit lighting and wristwatch illumination. The colour of the emitted luminescence depends on the phosphor. Radioluminescence is also used in scintillation counters to measure radiation levels. The scintillator consists of either an organic crystal, e.g. anthracene (**1.1**), or a mixture of lumophores (e.g. *p*-terphenyl, 2,5-diphenyloxazole) dispersed in an organic solvent or plastic film, that luminesces when struck by ionising radiation. A photomultiplier tube is used to quantify the emitted photons. Depending on the lumophore used, the emission may either be fluorescence, phosphorescence or delayed fluorescence. Scintillators are used in homeland security radiation detectors, medical diagnostics and high energy particle physics experiments.

4.3.5 Chemiluminescence

Chemiluminescence is the emission of light as the result of a chemical reaction. The classic example is luminol oxidation. When a basic solution of luminol (5-amino-2,3-dihydro-1,4-phthalazinedione) is mixed with hydrogen peroxide in the presence of a suitable catalyst (e.g. Cu^{2+} or ferricyanide), it becomes oxidised, forming an unstable peroxide radical in its excited state. The excited state radical relaxes radiatively emitting a blue glow. *Luminol* is used by forensic crime scene examiners to detect the presence of blood traces with a sensitivity at the parts per million (ppm) level, since the iron present in haemoglobin also catalyses this reaction. However, perhaps the most familiar application of chemiluminescence is in glow sticks. In this case, a chemical reaction is used to sensitise the emission from a lumophore. The glow stick contains a solution of a suitable fluorescent dye and diphenyl oxalate and a glass ampule containing hydrogen peroxide. When the glow stick is 'snapped', the glass ampule is broken, releasing the hydrogen peroxide which reacts with diphenyl oxalate forming a peroxyacid ester intermediate. This unstable intermediate decomposes spontaneously to carbon dioxide, releasing its excess energy and exciting the dye, which then relaxes by emitting a photon. The colour of the glow stick depends on the dye used.

A number of biological species, including fire flies, glow worms and marine organisms, emit light. This is termed *bioluminescence* and involves chemiluminescent reactions within the organism. Bioluminescence is a useful tool in genetic engineering and bioluminescence imaging can be used to study biological process *in vivo*.

4.3.6 *Photoluminescent Materials: Fluorescent and Phosphorescent Emitters*

4.3.6.1 Fluorescent Dyes and Pigments

Optical brighteners. These are used as additives in papers, plastics, fabrics, and fabric detergents, to convert the small fraction of sunlight which lies in the near UV into visible (usually blue) light. The photochemical requirements are: (i) efficient near UV absorption with no absorption tailing out into the visible, otherwise a yellow coloration will be produced; (ii) a high emission quantum yield in the blue spectral region; and (iii) high photochemical stability. Chemically, the compounds must adhere to the required substrate, and so optical brighteners with different chemical substituents may be required for cotton and nylon/silk fabrics. They must also be chemically and thermally stable. Triazole-stilbene derivatives are some of the most common optical brighteners (2.1–2.3). However, these tend to fade on long-term exposure to UV light, and when long-term stability is important non-stilbene compounds are favoured. Many optical brighteners are available from fine chemical suppliers, but relatively few are in the standard research chemical catalogues.

Fluorescent probes. Fluorescence probes are materials which indicate, by fluorescence, the presence of some specific chemical species or environment. There are two types: passive and active. Passive probes indicate the presence of the material of interest simply by physically or chemically binding to it. They thus indicate the presence of an analyte substrate by their own fluorescence (although this may also be altered by the presence of the analyte), the intensity of which can be used to determine the presence of the analyte either qualitatively or in some cases quantitatively. A typical use of such probes is in fluorescence microscopy, and there are a wide range of commercially available probes for this purpose (e.g. 4.3). Active probes undergo a photochemical change in the presence of the chemical or environmental feature to which they are sensitive. This results in a change in some emission property such as wavelength, intensity, polarisation, or lifetime (e.g. 1.4, 4.8). Optical probes are discussed in detail in Chap. 12.

Laser dyes. The role of a laser dye is to absorb the pump radiation efficiently, and convert this absorbed energy into an excited-state which can itself act as the upper state in a laser transition (see Chap. 14). Photo- and chemical stability are important, but the key photochemical features are: (i) absorption at the excitation wavelength; (ii) a lifetime sufficiently long to allow a population inversion to build, (although the lifetime required may be quite short, depending upon the duration of the pump pulse); and (iii) a low absorption at the lasing wavelength. In assessing and controlling the latter it is the absorption profile of the solution during the population inversion which is relevant, so it is the transient absorption as much as the ground state absorption which is important. Absorption due to long lived triplet states is a particular problem and so a very low triplet quantum yield is desirable. Triplet quenchers are sometimes used to reduce the lifetime and hence

quasi-steady-state concentration of triplets during the population inversion. There are now many laser dyes available which cover the full spectral range from the IR to the UV, and the best sources of up to date information are manufacturer's catalogues. However there are a few dye classes which are particularly useful as laser dyes, where the basic chemical skeleton is retained but changes in substituent are used to shift absorption and emission wavelengths, e.g. basic structures of **2.1**, **4.1**, **4.2**, **4.6**.

Emissive polymers. One of the major current areas of research is on emissive conjugated polymers (CPs) (**3.1–3.9**) due to their exceptional optical, electronic and mechanical properties [40]. Ionic conjugated polyelectrolytes (CPEs) tend to be highly sensitive to changes in their physical and chemical environment and, hence, one of their major potential uses is in biological and chemical sensors [41]. They have the advantage of high sensitivity with short luminescent lifetimes and the possibility of *amplified* fluorescence energy transfer or quenching processes (see [Chap. 12](#)) [42]. Recent research on the application of CPEs in biological and chemical sensors has led to a greater structural diversity and new synthetic protocols for their preparation [43]. Neutral CPs are also important technological materials, with applications in optoelectronic devices, such as PLEDs [34] and solar cells [44]. Part of the interest stems from the possibility of implementing solution-based deposition methods as part of the device fabrication process. Incorporation of ionic side groups increases solubility in polar organic solvents and water, which may allow more environmentally friendly manufacturing processes. Current interest in solar cells based on CPs stems from the promise of low cost fabrication. Research into cationic conjugated polymers (CCPs) has recently been mainly focussed on sequence specific DNA assays, designed by utilising the electrostatic interactions between cationic conjugated polymers and negatively charged DNA. These assays commonly exploit the ability of CCPs for efficient excitation energy transfer using, for example, protein nucleic acids (PNA) and Förster resonance energy transfer (FRET) to luminescent acceptors, such as fluorescein.

4.3.6.2 Phosphorescent Dyes and Materials

Phosphorescent molecular species in solution or matrices. Many organic molecules and dyes are phosphorescent in rigid low temperature glasses, where processes which might deactivate long lived triplet states are inhibited. Phosphorescent yields and lifetimes of many organic molecules, (and some inorganic complexes), are given in [45], quantum yields can be very high and triplet lifetimes can easily be up to a few tens of seconds at 77 K (the determination of these parameters is described in [Chap. 15](#)). However few organic molecules are phosphorescent at room temperature. Those commonly available organic compounds that, such as bromonaphthalene, usually carry heavy atom substituents, but even so they are usually only very weakly phosphorescent at room temperature. One particular group of organics which are strongly phosphorescent at room temperature are the thiocarbonyls (**11.21**). Although thiocarbonyls show an

interesting, rich, and unusual, photochemistry they are relatively photochemically and chemically unstable, which limits their uses.

A number of inorganic complexes show room temperature (and low temperature) phosphorescence, with two groups widely used as phosphorescent materials namely: Pt and Pd porphyrins (5.4), and Au (either in the monovalent or trivalent oxidation states), Ru(II), Rh(III) and Ir(III) complexes in which the metal is usually complexed by nitrogen, sulphur or heterocyclic rings (6.2–6.8). Further examples may be found in Ref. [38]. In these complexes the presence of the heavy transition metal gives those orbitals with some metal character spin-orbit coupling, which enhances both radiative and non-radiative singlet-triplet interconversion rates. The most important effect is a relative increase in the rate of the T_1 to S_0 radiative process; thus, while triplet quantum yields are much higher than those in organic molecules, emission lifetimes are much shorter, typically $\sim 1 \mu\text{s}$ –1 ms.

Delayed fluorescence. It is possible to generate relatively long lived fluorescence emission if there is a mechanism for repopulation of the singlet from the triplet. This is termed *delayed fluorescence*, and there are two common mechanisms.

- (1) Thermal repopulation, where the triplet level is close enough to the singlet level that the singlet state can be thermally populated from the triplet. Sometimes called *E-type* delayed fluorescence, after the compound *eosin* (4.4) which exhibits this behaviour. The lifetime of E-type delayed fluorescence is equal to the triplet lifetime. Other materials which exhibit E-type delayed fluorescence are palladium porphyrins (5.4) and thiocarbonyls (11.21).
- (2) *Triplet-triplet annihilation* in which two triplet states combine to give an excited singlet which generates fluorescence and a ground state singlet, called *P-type* delayed fluorescence after the molecule *pyrene* (1.4) which exhibits this behaviour. The lifetime of P-type delayed fluorescence is equal to one half that of the corresponding triplet.

Although named after the archetypical molecular examples, both types of delayed fluorescence are reasonably common. Delayed fluorescence is discussed in more detail in Chap. 1.

4.4 Sensitisers, Donors, Acceptors, Quenchers and Traps

Sensitisers are absorbing materials which can be used in photochemical processes in very specific ways; to make specific reactions occur, or force a specific reaction route by the generation of specific singlets, triplets, radicals or redox active chemicals *via* energy transfer, electron transfer, or radical reactions. When used as *donors* (D) in energy transfer reactions they can be used to generate singlets or triplets of *acceptor* (A) molecules which might not be available by direct excitation, or to generate acceptor triplet states without the need for direct excitation of the acceptor. Sensitisers can also be used to probe molecular arrangements and distributions since, if a sensitizer is expected to generate a specific product by reaction

with an acceptor, the presence or absence of sensitisation, as well as the efficiency of the process, can be used as a measure of either the proximity of the sensitiser and acceptor molecules, or the viscosity of the medium (see [Chap. 12](#)).

The term *acceptor* is used to describe: (1) a compound, or atom, which accepts energy from a higher energy donor in excited-state energy transfer, and which becomes, as a consequence, excited; or (2) a compound which reacts with an excited-state (or less frequently some other chemical species, notably singlet oxygen), to give a recognisable specific product. In both of these processes the acceptor undergoes a recognisable change, indicating its role in the reaction.

The term *quencher* is broader, and includes any material which acts to reduce emission, or the yield of a photochemical reaction, by interaction with an excited-state. This interaction may be physical, or chemical, and either reversible or irreversible, and nothing about the nature of the quenching process or any change in the state of the quencher is necessarily inferred.

The term *trap* has two uses. (1) In solid state chemistry a trap is a site, a part of the structure, into which energy, or an electron (or hole) can migrate, be trapped, and lost to the system. (2) The term trap is also used for chemical species which give specific, and usually measurable, reactions with species of interest, notably free radicals, *i.e.* free radical traps ([8.1–8.3](#)). Here, trap sense (2) is very similar to acceptor sense (2), but there is a subtle difference because of the different type of mobility free radicals and chemical species exhibit. Once formed, chemical species migrate by molecular diffusion. Free radicals also migrate by molecular diffusion but they also undergo transport and population growth through a series of propagation and branching reactions, and so the free radical itself is mobile, even though the molecular carrier itself is exchanged, in a similar way to the mobility of ‘energy’ in energy transfer migration in solids.

4.4.1 Excited State Sensitisers and Acceptors

For organic molecules, and most inorganic complexes, molecular singlet and triplet states are most important, and therefore singlet and triplet sensitisation are most commonly encountered. For some other groups of materials, notably those involving atomic transitions, such as gas phase atoms or lanthanide ions in solids or solution, sensitisation involving states of other spin multiplicities is important. In *singlet sensitisation* the required reaction is the transfer of singlet energy from the sensitiser, which is the donor, to another molecule, the acceptor. Any excited singlet state higher in energy than the acceptor singlet can thermodynamically act as a sensitiser, but as discussed in [Chap. 1](#), other conditions must be right for the energy transfer process. Energy transfer requires energy matching between donor and acceptor states. In practise, for molecules of moderate size the high density of states (DOS) means that almost any sensitiser of higher energy than the acceptor will act as a sensitiser by collisional or Dexter energy transfer, provided the donor and acceptor are, or can become, close enough within the donor lifetime. For Dexter

transfer involving states localised on atoms or ions, which do not have a high DOS, energy matching becomes a more stringent condition. For atomic states in a solid state lattice, energy matching can sometimes be promoted by coupling with the lattice vibrations (*phonons*). FRET involves coupling of molecular dipoles, and can occur over a much longer range because orbital overlap is not required. However, overlap of donor emission with an acceptor absorption band for an allowed transition is necessary for efficient energy transfer.

In general, the most effective singlet sensitiser will be those with long lifetimes, and as a consequence, high fluorescence quantum yields. The short lifetime of molecular singlet states means that for efficient Dexter singlet–singlet energy transfer the acceptor must be adjacent to the donor, or, if contact is diffusion controlled, the acceptor must be present at high concentration in a low viscosity medium.

Molecular triplet energy transfer is usually *via* Dexter energy transfer. However, because of the long lifetime of some triplets, FRET is also possible from a triplet donor to a singlet acceptor, where the long donor lifetime compensates for what must be, because the radiative transitions involves are spin forbidden, a slow energy transfer rate constant.

Generally, if the energy difference between D and A triplet states is greater than a few kJ mol^{-1} , energy transfer in solution will occur at every encounter between D and A and therefore the rate constant is close to the diffusion controlled value. However, if the molecular structure of one or both D and A is significantly different in the triplet state as compared to the ground state then the reaction requires major molecular structural reorganisation, and this can slow the energy transfer rate considerably. Balzani *et al.* have analysed the effect of structural rearrangement in a similar way to that used in the Marcus theory of electron transfer reactions [46].

For the determination of the triplet energy of an acceptor, a series of sensitiser with differing triplet energies and known transient difference spectrum are required; the experimental approach is described in [Chap. 15](#) which also gives triplet state properties for selected compounds ([Table 15.2](#)). The porphyrins ([5.1](#), [5.2](#)), phthalocyanines ([5.3](#), [5.5](#)) and naphthalocyanines ([5.7](#)) make a useful series of relatively low energy triplet sensitiser because of their structural similarity ([5](#)). Unfortunately only a few of these compounds are phosphorescent and therefore flash photolysis is required for direct kinetic studies of most triplet sensitisation.

Triplet sensitiser can generally be placed in one of three categories:

1. High to moderate energy polyaromatic and polyaromatic derivatives (such as [1.1–1.7](#)), or other organics, which are not phosphorescent at room temperature, but are often phosphorescent at 77 K. Most have triplet lifetimes of \sim ms duration and well-characterised triplet transient difference spectra. Many are commercially available.
2. The relatively low energy porphyrins ([5.1](#), [5.2](#)), phthalocyanines ([5.3](#), [5.5](#)), naphthalocyanines, and their metallated derivatives, some of which are phosphorescent at room temperature, but many of which are not phosphorescent at either room temperature or 77 K. Lifetimes are typically 100 μs to a few ms,

and most have well-characterised triplet transient difference spectra. Many are commercially available.

3. Moderate to low energy Au, Pt, Pd, Ir and Ru complexes which are phosphorescent at room temperatures with lifetimes typically 1–20 μs , some of which are commercially available (6.2, 6.6–6.8).

The use of triplet state acceptors has generally two roles. (1) Where the triplet state is to be removed and the transferred energy degraded as heat. Any passive absorber with lower triplet state energy than the donor will act in this way. Such a triplet state acceptor is also a photochemical *stabiliser*. (2) Where the triplet energy is to be trapped in a triplet state to be used for measurement or some specific function, e.g. energy transfer to an acceptor of known transient triplet absorption spectrum or emission. Here the acceptor triplet state photophysics and photochemistry must be known. Identification of energy transfer to such another known triplet state is often used as confirmatory evidence that a triplet state species is involved in the reaction under study.

Sensitisation is often used to generate electronic excited states in lanthanide (Ln) complexes and Ln-containing solid-state phosphors (e.g. 10.1–10.6). Ln-materials emit over the entire visible spectrum: red (Eu^{3+} , Pr^{3+} , Sm^{3+}), green (Tb^{3+} , Er^{3+}) and blue (Tm^{3+} , Ce^{3+}). They are therefore interesting for a wide variety of applications including solid-state lighting, lasers, and optical communications and storage. The optical transitions of Ln^{3+} ions take place predominantly within the $4f$ manifold, where the electrons are largely shielded from external crystal field effects by the filled $5s$ and $5p$ levels. Consequently, Ln^{3+} ions give rise to much narrower, atomic-like line absorption and emission spectra compared to organic small molecules or polymers. The Ln^{3+} electronic configuration gives rise to ground and excited states with a variety of multiplicities other than singlets and triplets (e.g. quartet, quintet etc.); consequently some ions are fluorescent ($\Delta S = 0$), others are phosphorescent ($\Delta S \neq 0$), and some are both.

However, f – f transitions are formally electric dipole forbidden by the Laporte selection rule, (a change in orbital angular momentum of ± 1 is required to accommodate the loss of photon spin upon absorption), although they are allowed by electric quadrupole, magnetic dipole and forced electric dipole mechanisms to some extent. Direct excitation of the Ln^{3+} ion is therefore not easily achieved, due to the low molar absorption coefficients associated with these transitions ($\epsilon \sim 5$ – $10 \text{ mol}^{-1} \text{ dm}^3 \text{ cm}^{-1}$). In Ln-complexes, indirect excitation *via* a sensitising ligand or *antenna* is used to overcome this limitation [46]. The sensitising ligand absorbs light, initially forming its excited singlet state. The excitation energy is transferred to the ligand's triplet state *via* intersystem crossing (the efficiency of this process being improved due to enhanced spin–orbit coupling induced by the heavy atom effect of the Ln^{3+} centre). Population of the Ln^{3+} excited emissive state is subsequently achieved through intramolecular energy transfer from the ligand triplet state. This process therefore requires that the ligand triplet state is higher in energy than the Ln^{3+} excited state being sensitised.

4.4.2 Singlet Oxygen Sensitisers, Quenchers and Acceptors

Most singlet oxygen sensitisers are triplet states. Singlet oxygen sensitisation is very similar to triplet sensitisation, except the spin state of the acceptor, ground-state oxygen, is a triplet, and the products are two singlets, *i.e.* singlet oxygen and the singlet ground state sensitiser [47, 48]. The energetic and spin conservation rules are the same as triplet energy transfer, but the spin statistics are different because the two reacting species are triplets. The spin angular momentum quantum number along any reference axis of each triplet state (*i.e.* the triplet sensitiser and ground state oxygen) can take one of three values; $-1, 0, +1$; thus when any two triplets combine in the encounter pair there are 3×3 possible combinations. $1/9^{\text{th}}$ of the encounters will give an overall singlet encounter pair, $3/9^{\text{th}}$ a triplet, and $5/9^{\text{th}}$ a quintet encounter pair. Of these three: only the singlet encounter pair can lead to two singlet state products; the triplet pair can, energetics allowing, give two electron transfer radical doublet states; while in the quintet case there are no spin-allowed energy transfer or electron transfer products possible, so that, in the absence of spin relaxation, the quintet encounter pair can only separate back into reactants. Thus singlet oxygen generation can be expected to occur with a maximum rate of around $1/9^{\text{th}}$ the encounter rate, and this is usually borne out experimentally.

Most species which generate a triplet state of significant lifetime and energy higher than that of singlet oxygen (94.3 kJ mol^{-1} , 0.98 eV , corresponding to a transition in the NIR at $\sim 1270 \text{ nm}$ —see Fig. 15.3) have the potential to be singlet oxygen sensitisers, since oxygen quenching of such triplet states generally goes predominantly *via* energy transfer (although electron transfer to give superoxide radical can be a significant, and interfering, reaction). For many such compounds the singlet oxygen yield in fluid air-equilibrated solution can be expected to be similar to the triplet yield. However the term *singlet oxygen sensitiser* is usually reserved for compounds which have: high triplet quantum yields; high oxygen quenching rate constants in which singlet oxygen predominates as the reaction product; reasonably high molar absorption coefficients and are thus efficient absorbers; low singlet oxygen quenching rates; and a well-characterised and quantified photochemistry. The measurement of the singlet oxygen yield is discussed in Chap. 15.

The role of a singlet oxygen quencher is usually just to remove singlet oxygen, often to inhibit singlet oxygen induced photodegradation. There are two main mechanisms by which this can be achieved.

- (1) Energy transfer into a low energy triplet acceptor in which molecule the triplet energy is rapidly degraded to heat; typical examples are Ni complexes (**11.10**).
- (2) Electron transfer into a molecule in the encounter complex followed by rapid reverse electron transfer before dissociation of the encounter complex. Typical examples of this type of quencher are hindered amines such as DABCO (**11.8**).

Quenching rate constants for triplet energy transfer quenchers are often faster than for electron transfer quenchers. However the requirement for a triplet state

lower than singlet oxygen invariably implies singlet state energies in the visible region, and thus singlet oxygen triplet energy acceptors are coloured to varying degrees. Apart from anything else this means they will also act as competitive absorbers in almost any mechanistic study. Amine electron transfer quenchers are usually colourless, often with longest wavelength absorptions in the mid UV.

The role of a singlet oxygen acceptor is usually to show evidence of singlet oxygen in mechanistic studies. The development of detectors for the direct detection of singlet oxygen emission (Chaps. 14, 15) has alleviated the need for indirect measurements where the singlet oxygen yield is reasonably high, but singlet oxygen acceptors are still useful especially when the singlet oxygen yield is so low as to be undetectable directly. Three common approaches are used.

- (1) Kinetic studies where the triplet state acceptor can be identified. A good example of this is shown by use of β -carotene (**11.6**). β -carotene itself has a very low quantum yield of triplet state formation by direct excitation, the triplet energy is lower than that of singlet oxygen and the triplet lifetime and transient absorption spectrum are known. Thus if the system under study allows the photochemical formation of singlet oxygen then this can be studied using ns laser flash photolysis by following the kinetics of energy transfer from singlet oxygen to β -carotene and formation of β -carotene triplet. β -carotene triplet will also be populated by energy transfer from any triplet state used in the initial formation of singlet oxygen but consideration of the kinetics shows that, because of the combination of rapid quenching of triplet state singlet oxygen sensitizers by oxygen in aerated solution and the relatively long lifetime of singlet oxygen, it is possible to separate out these two processes. Quenching of singlet oxygen by carotenoids is discussed in detail in Chap. 8.
- (2) Where the rate of loss of acceptor can be followed, either spectroscopically, or by chromatographic analysis such as GC or HPLC (in which case the specific involvement of singlet oxygen can often be confirmed by product analysis). Spectroscopic detection requires an acceptor of known absorption or emission characteristics. If ns laser flash photolysis is available then the kinetics of decay of the acceptor absorption or emission can be followed, and kinetic analysis can be used to confirm a singlet oxygen process. Diphenylisobenzofuran (**11.9**) and rubrene (**1.7**) have been widely used as singlet oxygen acceptors in these types of experiments, with reaction with singlet oxygen followed by either loss of absorption or of fluorescence.
- (3) Where the involvement of singlet oxygen can be identified by product analysis. Here the product from reaction between singlet oxygen and the acceptor gives rise to a stable molecular species which can be identified either spectroscopically or by chemical analysis such as GC or HPLC.

It is worth noting that the lifetime of singlet oxygen is highly dependent on solvent [49]. The lifetime is particularly short in solvents with OH bonds, which provide high frequency vibrations into which the electronic energy of singlet oxygen can be transferred, or in solvents, such as amines where electron transfer is possible, and it is particularly long in halogenated solvents which only have low

frequency vibrations. Due to the effect of OH oscillations in providing a quenching mechanism, the lifetime is also highly dependent upon solvent deuteration. Thus a comparison of rates or yields in H₂O and D₂O, or normal and deuterated alcohols, is a useful tool in helping unravel or identify a singlet oxygen mechanism.

4.4.3 Redox Sensitisers

An excited-state is simultaneously both a better oxidant and better reductant than the ground-state molecule. The difference in redox potentials between ground and excited-state is given, to a reasonable approximation, by the excited-state energy in eV. Redox sensitisers create charge transfer from an excited state. This can be either unimolecularly across a molecule or semiconductor, or bimolecularly *via* a process in which the excited-state undergoes a charge transfer reaction with the solvent, a redox quencher, or a semiconductor. The generated charge transfer products can then be used in further reactions. Photo-redox reactions lie at the heart of most photochemical process for solar energy conversion and redox sensitisation of solution phase reactions and electron injection into semiconductors have been widely studied with this application in mind. Although there has been a recent burst of interest in compounds which will inject electrons into semiconductor conduction bands because of their potential use in the dye sensitised solar cells (6.3–6.5, 11.19, 11.20) described in Chap. 7, the process has been of technological importance since the discovery of spectral sensitisation of silver halides in the late eighteen hundreds and the subsequent use of cyanines (e.g. 4.7) and other dyes as irreversible electron injection sensitisers in panchromatic photographic films (see Chap. 11). Photo-redox processes are also important in imaging science, semiconductor photocatalysis (see Chap. 6), and photo-redox based actinometers such as the ferrioxalate (see Chap. 14) and uranyl actinometers [45].

4.4.4 Radical Sensitisers, Quenchers and Traps

The products of redox sensitisation are usually radical ions. Neutral radicals can be generated unimolecularly by homolytic cleavage of an excited state molecule, or by bimolecular homolytic cleavage, the most common example of such being hydrogen abstraction from solvent. Energetically, electron transfer reactions become significantly less favourable as the polarity of the solvent is decreased, whereas the energetics of neutral radical reactions are relatively solvent independent. Photochemical radical initiation processes are important in gas, solution and solid-state radical reactions.

For aqueous phase studies, where, because of solvent polarity, radical ions are of most interest, the Ru(II)trisbipyridyl (6.2)/persulfate reaction pair [50] can be used. For organic solvents, benzophenone (11.5) in the presence of a hydrogen

abstractable solvent is a widely studied/used radical photoinitiator. Radical initiators are very important in photopolymerisations, and there are many commercially available photoinitiators (7.1–7.3). Where the molar absorption coefficient of the photo-produced radical is known, then flash photolysis allows a determination of the yield of subsequent radicals.

The essential feature of a radical quencher or trap is the availability of a radical state of low energy which is therefore relatively stable to further reaction. There are a wide range of radical quenchers available commercially as stabilisers, particularly polymer stabilisers. Electron spin resonance (ESR) is the obvious method of radical characterisation but some radical traps can be identified spectrophotometrically. Radical sensitisers, quenchers and traps are discussed in further detail in Chap. 8.

4.5 Photochromism and Molecular Switches

4.5.1 Chromism and Photochromism

Chromism is the reversible change in colour of certain materials upon application of external stimuli such as heat (*thermochromism*), light (*photochromism*), electrical current (*electrochromism*) or solvent polarity (*solvatochromism*) [24]. In this section we will concentrate on photochromism—light-induced colour changes. These have a variety of actual and potential applications, one of the most important of which is in photochromic ophthalmic lenses which darken in bright sunlight and become colourless in normal light. Photochromism involves a molecular system interconverting between two forms which have different absorption spectra. The process is reversible and the back reaction can either be induced by heat (designated *T-type*) or photochemically, using light of a different wavelength from the forward process, (*P-type*). The concept of photochromism is indicated schematically for a unimolecular process in Fig. 4.5, where light absorption by species A (normally absorbing in the UV) produces the longer wavelength absorbing species B through some photoinduced process; it is also possible to have bimolecular photochromic processes.

The first reports of photochromism in the scientific literature date back to the middle of the nineteenth century with the observation of bleaching of orange coloured solutions of tetracene in daylight and the regeneration of the coloured solution in the dark [51]. The reaction involves a photodimerisation [52]. The photochromic behavior of tetracene contrasts with that in Fig. 4.5, since the photoproducts absorb at shorter wavelengths than their precursor. This is termed *negative photochromism*. In addition, the forward reaction is a bimolecular process. A more common scenario is that the initial photochromic species absorbs in the UV and on photolysis produces a coloured photoproduct absorbing in the visible region of the spectrum (*positive photochromism*), and the process involves interconversion of a single molecule between two chemically distinct forms.

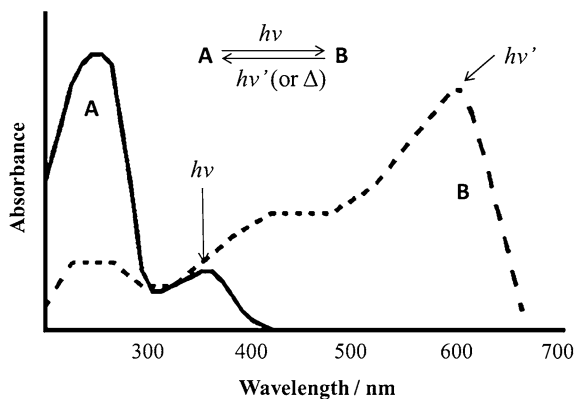
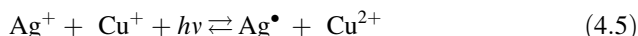
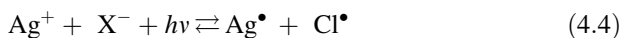


Fig. 4.5 Absorption spectra of a unimolecular two-state photochromic system. Figure adapted from Ref. [51]

The term photochromism is attributed to the distinguished Israeli scientist Yehuda Hirshberg [51, 53], who correctly identified the importance of chemical transformations in these systems. Some of the earlier literature used the term “phototropy” for the observed colour changes, suggesting that purely physical phenomena are involved [51]. However, it is now recognised that all important photochromic processes involve reversible chemical changes, and the term *phototropism* is reserved for the effect of light on the growth of plants, which may be directed either towards or away from the sun or other light sources [51]. Interest in photochromism in the early part of last century was rather limited [54], but was stimulated in the 1950s by the potential strategic importance of materials which could undergo reversible changes with light for various applications [55], including photochromic glasses which would darken rapidly following intense light pulses, such as those produced in nuclear explosions. These have been termed optical power-limiting substances [51]. Various reversible organic and inorganic photoprocesses were considered as possible systems for these applications, including formation of triplet excited states of aromatic molecules, isomerisations, electron and atom transfer. Subsequent developments concentrated on non-military uses, and the first serious practical application came with the development by Corning Glass in the U.S.A, of photochromic silicate glasses sensitised by silver halides, modulated by the presence of small amounts of copper(I) salts [55, 56]. The general reaction scheme can be summarised as:



The silver halide system is similar to that involved in the silver-based photographic process (see Chap. 11), but irreversible formation of photoproducts is inhibited by the fact that the silver halides are present as nanometre sized particles

dispersed in a non-conducting silicate matrix. This prevents the permanent photochemical reactions which take place in the photographic system to form the silver based latent images. Work on the silver halide glasses led to the development of the first viable photochromic lenses, which went on the market in the mid-1960s. The lenses have good optical properties, show excellent reversibility for their photochromic processes and reasonable darkening and bleaching times. However, the system involves silicate glass lenses, and in the following decade the ophthalmic market was moving towards plastic lenses [57]. While the silver halide system is excellent for silicate-based glasses, it is less suited for inclusion in the organic polymer systems used in plastic lenses. For this, organic photochromic systems involving thermal back reactions (T-type) are much more suitable [57, 58].

4.5.2 Organic Photochromic Systems

A variety of photochemical processes in organic molecules lead to photochromic changes, including pericyclic reactions, *cis-trans* (*E/Z*) isomerisations, intramolecular hydrogen transfer, photodissociation processes and electron transfer [51]. The area has been reviewed extensively [54, 59–62], and some typical examples of photochromic materials are given in Table 4.1 (12.1–12.6). The most important T-type ones for technical and industrial applications in areas such as ophthalmic lenses involve spiropyrans (12.1), spirooxazines (12.2) and naphthopyrans (chromenes, 12.3). In all three cases, light absorption leads to production of a coloured (merocyanine) form, where extended conjugation is achieved through ring opening. The absorption spectra of both the colourless and coloured forms can be modified by appropriate substitution of the aromatic rings. This allows colour tuning to produce the best properties for optical usage. There are a number of factors which need to be controlled, including the transmission (absorption) spectra of the coloured form, the light response, speed of recovery of the colourless form, the number of cycles the system can undergo and the long term stability of the system [51]. While the spiropyrans were some of the first systems to be studied, the spirooxazines show much lower fatigue on extended use [58], and the first commercial plastic photochromic lenses, which were introduced in the 1980s, involved an indolinospironaphthoxazine incorporated in a polycarbonate matrix [57]. More recently, the naphthopyrans have become the commercially most important class of photochromic materials for this type of application [58]. However, they still have some failings in terms of long term applications and there is considerable interest in the development of new photochromic materials involving these cyclisation/ring opening processes.

The way that the photochromic material is incorporated into the lenses is of importance for the commercial application of these materials. This can be achieved by injection-moulding in a thermoplastic or precursor monomer or resin system, surface coating, diffusion into lens surfaces (imbibition) or formation of

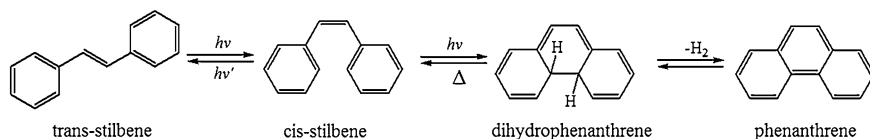


Fig. 4.6 *Cis–trans* isomerisation and cyclisation in stilbene

laminate structures, where a photochromic layer is placed between two halves of the lens structure [58].

Another important type of photochromic reaction involves *cis–trans* photoisomerisation [63]. With azobenzenes (**12.4**), the *trans* (*anti*) form has a strong absorption, attributed to a π,π^* transition in the near UV region and a weaker n,π^* band in the blue region of the spectrum. Upon photoexcitation with light of appropriate wavelengths (~ 340 nm for the unsubstituted derivative) the π,π^* band shifts to the blue and the longer wavelength n,π^* band increases in intensity due to formation of the *cis* (*syn*) form. Although photochromism will lead to a photo-stationary state, up to 90 % of the *cis* form can be produced. The reverse *cis–trans* reaction can take place either thermally or by irradiation with longer wavelength light [54, 63, 64]. This possibility of interconverting between two structures using light of different wavelengths is termed *photoswitching*. The *trans* isomer of azobenzene is planar but, due to steric hinderance, the *cis* form is bent. In addition to the colour change, this leads to changes in dipole moment, polarisability and, in the solid state, packing in crystal structures. This will also lead to modifications in the properties of the surrounding medium, which can enhance the applications of photochromic materials. For example, if azobenzenes (or other photochromic materials) are incorporated into a polymeric matrix their photochromic reaction can affect properties, such as shape, refractive index, phase, solubility and surface wettability [65]. This is termed a *photoresponsive system*. These have a number of important applications which are discussed later.

Reversible *trans–cis* isomerisations with alkenes (Fig. 4.6) are also relevant for photochromism and photoswitching. With the simple systems, normally only photoinduced processes are involved because of the high energy barrier between the two forms. These alkene-based photoswitches can be useful in molecular devices. With polyenes, both thermal and photochemical processes are possible, and these can be used as P-type and T-type photochromics. A rare, naturally occurring photochromic system involving *cis–trans* isomerisation process occurs with *bacteriorhodopsin*, which is found in halobacteria [66]. Its structure and photochemical processes are very similar to the visual pigment rhodopsin present in the retina of the eye. In both cases, the structure involves the polyolefin, retinal, linked to a protein through a Schiff's base (see Fig. 1.1). With bacteriorhodopsin, photochromism involves interconversion between the all-*trans* form absorbing at 570 nm and the 13-*cis* isomer absorbing around 410 nm. The system can be recycled many times without any signs of fatigue and shows excellent

long-term stability, which makes it a good candidate for use in optical memories and data processing.

With the *cis* isomer of diarylethenes, a second photochromic process can occur: photocyclisation [61, 67]. In the simplest case, *cis*-stilbene, the initially formed dihydrophenanthrene is rapidly oxidised to phenanthrene in an irreversible process (Fig. 4.6), making it unsuitable for photochromic applications. However, this can be overcome by replacing the phenyl rings by heterocyclic groups, such as thiophene (12.5). These diarylethenes are important P-type photochromic systems showing good thermal stability, resistance to fatigue, and are important as photo switches. Relatively large spectral shifts are seen between the shorter wavelength absorbing open structure and the long wavelength closed form. The spectral properties can be tuned by introducing substituents into the heterocyclic rings. The structural changes on ring closure affect properties such as fluorescence, refractive index, polarisability and electrical conductivity. A related P-type photochromic system involves the fulgides and fulgimides (12.6). Again, the photochromism involves a colourless open form, sometimes referred to as the *E*-form, and the product of photocyclisation, termed the *C*-form [68]. There is an additional photochemical pathway leading to the colourless *Z*-form. This competing process decreases the efficiency of the photochromic system, but can be minimised by appropriate design of the molecules.

While many other organic photochromic systems exist, the above are the most important types currently used for practical applications.

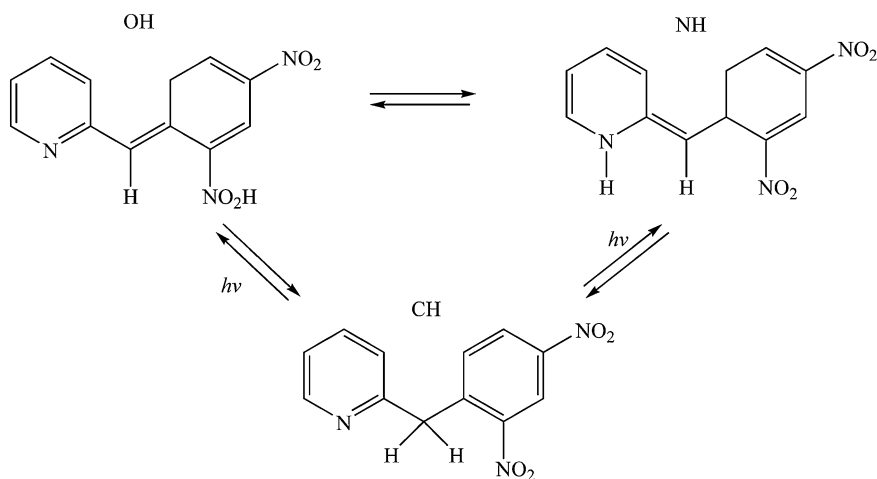


Fig. 4.7 Three photochromic forms produced from 2-(2',4'-dinitrobenzyl)pyridine (DNBP). Figure adapted from Ref. [69]

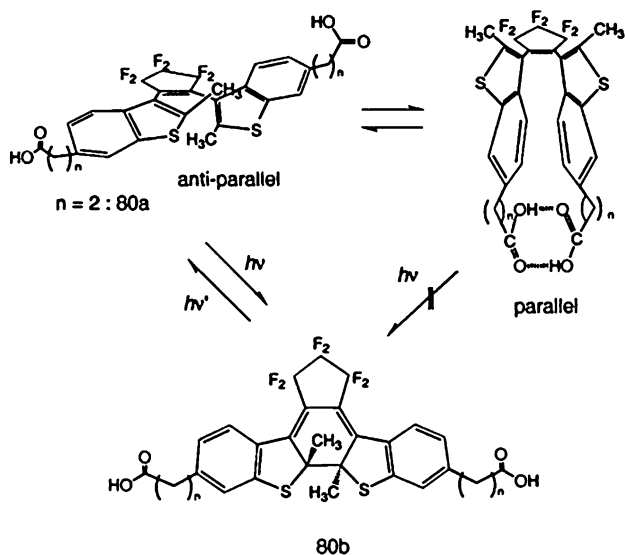


Fig. 4.8 Solvent gated photochromism in a diarylethylene. Reprinted with permission from Irie et al. [71]. Copyright (1992) American Chemical Society

4.5.3 Three State and Gated Photochromics and Two-Photon Systems

The previous section describes photochromic systems in which interconversion between two forms can be induced by absorption of light. However, more complex scenarios also exist and some have particular practical importance. With 2-(2',4'-dinitrobenzyl)pyridine (DNBP), photochromism involves phototautomerisation with hydrogen transfer [69, 70]. However, this can either be transferred to the pyridine nitrogen giving the blue NH form or to the oxygen of the nitro group to give the yellow OH form (Fig. 4.7). These can revert thermally or photochemically to the most stable colourless CH form.

For certain applications of photochromics, it is useful to be able to convert one or more of the forms reversibly into a stable non-photochromic structure. These systems are termed *gated photochromics* [51] and are of particular importance for optical data storage. Figure 4.8 shows an example of a gated photochromic involving diarylethenes [71]. According to the *Woodward-Hoffmann rules*, the photocyclisation is a conrotatory process and is only possible through the anti-parallel form. In hydrophobic solvents, such as cyclohexane, the parallel open form is stabilised by hydrogen bonding and cannot photocyclise. However, upon addition of a hydroxylic solvent, such as ethanol, or heating, the hydrogen bonds are broken leading to formation of the antiparallel open form which can undergo the photochromic reaction.

Chromism may also be induced by two separate external stimuli. This is termed *dual-mode photochromism* [51]. A particularly versatile example involves the flavylum system, the basic structure of anthocyanin dyes. With these, because of the complex acid–base behavior, interconversion between the various coloured species formed can be controlled by the dual application of light and pH changes [72]. It is possible in this way to have a pH gated photochromic system.

With photochromic systems, as with other areas of photochemistry, we are normally using monophotonic processes in which a molecule absorbs one photon. However, it is possible to have two-photon or multi-photon photochromic systems. These have certain attractive properties. Two possibilities exist [51]. In the first (sequential) case, a molecule absorbs one photon to form its excited state. This (or a subsequent species) may then absorb a second photon to give the product:



An example of this sequential two-photon photochromism has been reported with a naphthopyran derivative [73]. This has the advantage, when it is used for optical data storage, of non-destructive readout capacity.

In the second case, a molecule simultaneously absorbs two photons *via* a virtual level to produce the excited state, which is subsequently transformed into the photo-product:



Since it is only necessary that the sum of the energies of the two photons is sufficient to produce the excited state, the exciting light can be of longer wavelength than the absorption band of A. This means that NIR light can be used, minimising photochemical degradation. In addition, the probability of simultaneous interaction of two photons and one molecule is very low so an intense light source is necessary, typically a pulsed laser, and the effect can be limited optically to a small region of the sample. If the photochromic system is incorporated into a polymeric host this opens the possibility of achieving 3D data storage through focusing the laser at different points in the sample [74].

4.5.4 Some Applications of Photochromic Materials

By far the biggest application of photochromic systems is in ophthalmic lenses. These now normally involve T-type spiroxazine or naphthopyran photochromics in thermoplastic polymers. The lens colours under the UV component of sunlight, but not significantly under artificial light, which lacks this part of the spectrum. As the optimal systems involve neutral colours grey or brown, frequently mixtures of photochromics are used [75]. Design of commercial formulations is complicated

by the need for the various components to fade and undergo fatigue at the same rate, and there is currently considerable interest in the development of dyes which are intrinsically neutral in colour.

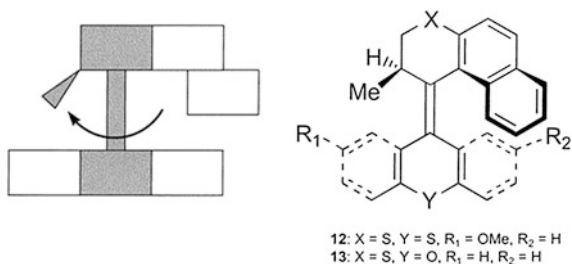
T-type photochromic thermoplastic systems are also finding non-ophthalmic specialty applications in areas such as colouring drinks bottles, toys (including dolls which develop suntans) and crash helmet visors for motorcyclists. Photochromic systems are also used in formulations for surface coatings, and have been used for security printing, such as in passports. In addition, they show potential for personal care use, such as in cosmetics and hair dyes. A good description of these applications is given in Ref. [58].

Interesting effects can be produced in textiles by using photochromic colorants. Because of stability problems in processing, these are often either incorporated into a polymer matrix inside textile fibres [76] or microcapsules containing the photochromic material are coated onto textile surfaces [77]. While products, such as T-shirts which change colour in sunlight, are available on the market, at present the development of this area is limited due to difficulties in obtaining cost-efficient, durable products [58].

Photochromic transformations in matrices such as polymers can lead to changes in the bulk properties of the matrix. Such photoresponsive systems can have various applications. We will indicate two of these. If a photochromic system, such as an azobenzene, is incorporated into a liquid crystalline polymer system, photoconversion can lead to changes in the ordering and orientation of the liquid crystalline mesophase [65]. This leads to changes in various physical properties, including the optical anisotropy, which can be used in display and other applications. A second case involves photo-responsive biomaterials [65]. Incorporation of photochromic molecules can be used in areas such as photo-regulation of biological properties, controlled drug release and photo-regulated membrane permeability.

The area of information technology (IT) has been based upon the electronic properties of semiconductors. Gordon Moore, one of the founders of Intel, published an article in 1965 which indicated that the capacity of computer processing will double about every 18 months [78]. This empirical law is still valid, but is reaching its limits, in particular because as electronic memories become smaller, they start to have problems of heating and cross-talk, and there is a need for development of new systems. Three characteristics are required for a memory, the ability to write, read and erase information. Optical (photonic) systems using photochromic materials can achieve these requirements while overcoming many of the problems of limitations of purely electronic systems, since the ultimate data density achievable is limited by the area which can be resolved, which depends upon light wavelength, as discussed in Chap. 1. Photonic systems also have the advantage that they can be multiplexed by using more than one property, e.g. wavelength, polarisation and phase, while memories can be further enhanced using 3D data storage through two-photon absorption [74, 79]. A further possibility is to obtain sub-diffraction limited systems through near-field optics [80]. Until recently, erasable memory systems have tended to use inorganic materials using magneto-optic effects or phase change for data recording. While these may have organic pigments to enhance spectral

Fig. 4.9 Schematic view and structure of a molecular motor. Reprinted with permission from Feringa [86]. Copyright (2001) American Chemical Society



properties [24], the IT industry had been wary of purely photonic organic systems because of doubts on long-term stability. However, a number of good, stable, low-fatigue photochromic systems have now been developed and show considerable promise for purely optical data storage. The desirable properties of photochromic systems for these applications are good thermal stabilities of the two photochromic forms, fast response, resistance to fatigue, high sensitivity and non-destructive read-out. The P-type photochromics, diarylethenes and fulgides [61, 67, 68, 81], fulfill many of these properties. One limitation of photochromic systems is that reading one photochromic form, either through absorption or emission spectra, can convert it back to the other form. However, as noted above, photochromism also leads to changes on other properties, such as the refractive index of the medium, and this can be used to address the system.

A somewhat different application of P-type photochromics is their use as ‘smart’ receptors in sensing cations, anions and biologically relevant systems [82]. This is based on photoinduced switching between two forms, only one of which is tailored to bind to the analyte through host–guest interactions. The possibility of switching between the two forms provides the attractive potential of reusing these sensors. A more detailed discussion of the general area of optical sensors and probes is given in [Chap. 12](#).

4.5.5 Photoswitches: Molecular Logic, Rotors and Machines

The ideas of molecular memories and data storage described in the previous section can be extended to molecular computing. IT systems are based on logic gates with specific input–output behavior. These typically involve binary systems, where the input can be 0 or 1, and the output is, equally, 0 or 1. Photochromic systems fulfill the requirements of such a two-state system, and have been used in molecular logic devices [83]. These can be extended to applications in more complex logic functions by using a second input, such as addition of a metal ion or a change in pH. Although the area is in its infancy, photochromic systems show excellent possibilities for application in molecular scale computing.

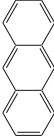

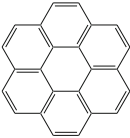

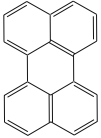
The distinguished physicist Richard Feynman in a famous talk to the American Physical Society entitled “There’s plenty of room at the bottom” [84] issued the

challenge that it should be possible to make machines out of molecules. In addition to the intellectual and synthetic challenges of designing and making such systems, they also have potential for applications as pumps and motors in a variety of chemical and biomedical applications. There is now considerable research activity devoted to the use of molecular switches to produce such molecular machines [81, 85–87]. The basic requirement of a molecular machine is that it should involve “*an assembly of a discrete number of molecular components (that is, a supra-molecular structure) designed to perform specific mechanical movements as a consequence of appropriate external stimuli*” [81]. Light is a particular valuable external stimulus [88], and, as shown in Fig. 4.6, photoswitching through *cis–trans* isomerisation does provide a possible basis for molecular rotor. However, for a true rotor it is necessary to have a unidirectional 360° rotation. This can be achieved by having a chiral photochromic system [86], as indicated in Fig. 4.9. This forms the basis for the development of true molecular motors and machines.

4.6 Conclusions

This chapter has discussed some of the most important and commonly encountered photochemical materials, whose properties and subsequent applications are primarily dependent on their absorption and emission characteristics. The most important factors are; (i) the available energy states of a given material and the routes of interconversion between these states and (ii) the excited state deactivation pathways. These factors dictate whether a material will act as a passive absorber, an emitter, or sensitiser. Absorbers, both organic and inorganic, find use in areas such as colorants, sunscreens, paints, pigments and dyes; high molar absorption coefficients are required to produce intense colours, while narrow absorption bands give rise to bright colours. For emitters, a high emission quantum yield in the required medium for the intended use is of obvious importance. The emission quantum yield is dependent on competition with other deactivation routes, while the emission wavelength (and therefore colour) and band structure depend on the relative energy levels of the emitter in any given medium. The emission lifetime is dependent on the probability of the radiative transition, i.e. whether it is ‘allowed’ (typically 10–100 ns) or ‘forbidden’ (μs or longer). The application of efficient emitters in light sources and display technology has been discussed. Excited state and radical sensitisers are useful for a variety of applications, including photodynamic therapy (e.g. singlet oxygen sensitisation, see Chap. 9) and photopolymerisation and device fabrication (see Chap. 13) and examples of the most commonly exploited sensitisation mechanisms have been provided. Photochromism and photochromic materials, including molecular switches, have also been discussed at length. For photochromic materials it is the absorption characteristics of both isomers that are most important for potential applications (change of colour, colourless to coloured or *vice versa*).

Table 4.1 A collection of data, structures, characteristics, uses and noteworthy properties of some commonly used photochemical materials

Compound	Structure	Specific uses	Physical, photophysical and noteworthy properties
1.1 Anthracene		An organic semiconductor. It is used as a scintillator for detectors of high energy photons electrons and alpha anthracene thermally or with UV irradiation below particles. Anthracene has the highest light output of all 300 nm. $\lambda_{\text{abs}} \sim 350\text{--}500$ nm; $E_S = 318$ kJ mol ⁻¹ ; $\phi_F = 0.3$; $\tau_S = 5.3$ ns; $E_T = 178$ kJ mol ⁻¹ ; $\phi_T = 0.71$; $\tau_T = 670$ μ s [45].	Photodimerises under UV light; the dimer reverts to for detectors of high energy photons electrons and alpha anthracene thermally or with UV irradiation below particles. Anthracene has the highest light output of all 300 nm. $\lambda_{\text{abs}} \sim 350\text{--}500$ nm; $E_S = 318$ kJ mol ⁻¹ ; $\phi_F = 0.3$; $\tau_S = 5.3$ ns; $E_T = 178$ kJ mol ⁻¹ ; $\phi_T = 0.71$; $\tau_T = 670$ μ s [45].
1.2 Tetracene		As a percent of anthracene light [89]. Anthracene is also a precursor to anthraquinone dyes.	
1.3 Coronene		An organic semiconductor used in organic field-effect transistors (OFETs) and as a dopant in OLEDs. A sublimed tetracene film was the first reported example of an OFET [90]. A light-emitting transistor made of a single tetracene crystal has been demonstrated [91].	An organic semiconductor used in organic field-effect transistors (OFETs) and as a dopant in OLEDs. A sublimed tetracene film was the first reported example of an OFET [90]. A light-emitting transistor made of a single tetracene crystal has been demonstrated [91].
1.4 Pyrene		An n-channel organic semiconductor. Emission intensity and number of bands is dependent on the solvent, as such easily detected long lived green phosphorescence in coronene can be used as a solvent probe. Coronene is a UV phosphor, and is used in charge-coupled devices (CCDs) in digital imaging; notably coronene-coated CCDs: are used on the Hubble Space Telescope.	An n-channel organic semiconductor. Emission intensity and number of bands is dependent on the solvent, as such easily detected long lived green phosphorescence in coronene can be used as a solvent probe. Coronene is a UV phosphor, and is used in charge-coupled devices (CCDs) in digital imaging; notably coronene-coated CCDs: are used on the Hubble Space Telescope.
1.5 Perylene		The fluorescence emission spectrum of pyrene is very sensitive to solvent polarity, and as such pyrene and its derivatives are useful polarity probes (cf. 1.3). Excimers are formed even at moderate concentrations, and this can be used as a probe of viscosity and molecular mobility [93].	The fluorescence emission spectrum of pyrene is very sensitive to solvent polarity, and as such pyrene and its derivatives are useful polarity probes (cf. 1.3). Excimers are formed even at moderate concentrations, and this can be used as a probe of viscosity and molecular mobility [93].
		Perylene, and substituted perylenes, are used as blue-emitting dopants in OLEDs. Perylene can be also used as a fluorescent lipid probe and is sensitive to fluorescence quenching by metal ions [94].	Perylene, and substituted perylenes, are used as blue-emitting dopants in OLEDs. Perylene can be also used as a fluorescent lipid probe and is sensitive to fluorescence quenching by metal ions [94].

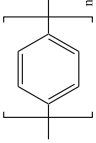
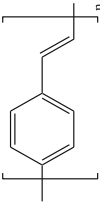
(continued)

Table 4.1 (continued)

Compound	Structure	Specific uses	Physical, photophysical and noteworthy properties
1.6 Fluorene		Named after its violet fluorescence, fluorene itself has few applications, but is a precursor to a number of important compounds, 2-Aminofluorene, 3,6-bis-(dimethylaminofluorene), and 2,7-dihydrofluorene are precursors to dyes. Polyfluorenes (3.6) are used in electroluminescent devices.	$E_S = 397 \text{ kJ mol}^{-1}$; $\phi_F = 0.68$; $\tau_S = 10 \text{ ns}$; $E_T = 282 \text{ kJ mol}^{-1}$; $\phi_T = 0.22$; $\tau_T = 150 \mu\text{s}$ [45].
1.7 Rubrene (5,6,11,12-tetraphenylnaphthalene)		An organic electronic material useful as a red dopant in OLEDs and as <i>p</i> -type organic semiconductors [95]. Reagent for chemiluminescence research. Singlet oxygen acceptor.	$\lambda_{em} = 550 \text{ nm}$; $E_S = 221 \text{ kJ mol}^{-1}$; $\phi_F = 0.98$; $\tau_S = 16.5 \text{ ns}$; $E_T = 110 \text{ kJ mol}^{-1}$; $\phi_T = 0.0092$; $\tau_T = 120 \mu\text{s}$ [45].
2. Stilbenes. Have the potential for photochemical isomerisation across the double bond, a reaction which has been widely studied. Addition of appropriate groups inhibits isomerisation and some substituted stilbenes have very high fluorescence yields. Stilbenes are commonly used as optical brighteners and laser dyes, and also find use as phosphors and scintillators.			
Compound	Structure	Specific uses	Physical, photophysical and noteworthy properties
2.1 Stilbene (1,2-diphenylethylene)		<i>Cis-trans</i> isomerisation possible (<i>trans</i> isomer shown). Used in manufacture of dyes and optical brighteners, and also as a phosphor and a scintillator.	$E_S = 358 \text{ kJ mol}^{-1}$; $\phi_F = 0.036$; $\tau_S = 0.075 \text{ ns}$. (data for <i>trans</i> -stilbene in a crystalline medium) [45].
2.2 4,4'-(diamino-2,2'-stilbenedisulfonic acid), (Fluorescent Brightener 28, Tinopal)		Fluorescent brightening agent for cellulose and polyamide fabrics, paper, detergents and soaps.	λ_{abs} range $\sim 340\text{--}370 \text{ nm}$; λ_{em} range $\sim 420\text{--}470 \text{ nm}$. Water soluble. High ϕ_F .
2.3 4,4'-Bis(2-benzoxazolyl)stilbene		Optical brightener for plastics.	λ_{abs} range $\sim 340\text{--}320 \text{ nm}$; λ_{em} range $\sim 420\text{--}470 \text{ nm}$; high ϕ_F .

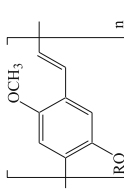
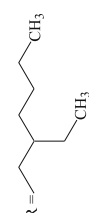
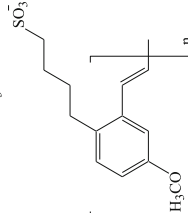
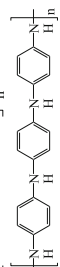
(continued)

Table 4.1 (continued)

Compound	Structure	Specific uses	Physical, photophysical and noteworthy properties
3.1 PPP (poly(p-phenylene))		<p>PPP was one of the first blue electroluminescent CPs to be reported, and blue LEDs can be made from PPP and its various derivatives [97].</p>	<p>Structurally simplest CP based on phenylene rings. PPP is insoluble and has poor conductivity but soluble PPPs can be synthesised [98, 99]. Substituted PPPs emit deep blue light with a significant portion of the emission in the near UV region; e.g. poly(2-decyloxy-1,4-phenylene) which exhibits both high photo- and electro-luminescence. $\lambda_{em} \sim 410$ nm.</p>
3.2 PPV (poly(p-phenylenevinylene))		<p>PPV was used as the emitter in the first PLED in 1990 [100]. PPV and PPV derivatives have also found wide use in electronic materials e.g. electrochemical sensors and integrated circuits. PPV is also used as an electron-donating material in organic photovoltaic solar cells [101]. Although PPV-based devices suffer from poor absorption and photodegradation, PPV and PPV derivatives (especially MEH-PPV, see below) find frequent application in research cells. Ladder-type PPV derivatives have been studied as blue emitters in OLEDs [102].</p>	<p>$\lambda_{abs} \sim 400\text{--}420$ nm (dependent on synthesis); band gap of ~ 2.5 eV. The yellow/green fluorescence of PPV has a structured emission band with λ_{em} 520 and 551 nm [103]. PPV has very low solubility in common organic solvents, and thus there has been a great deal of research on making soluble PPV derivatives (such as MEH-PPV and MPS-PPV, see below), see Ref. [104].</p>

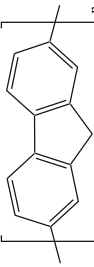
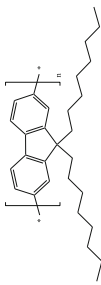
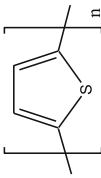
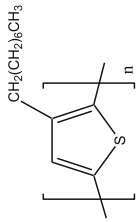
(continued)

Table 4.1 (continued)

Compound	Structure	Specific uses	Physical, photophysical and noteworthy properties
3.3 MEH-PPV (poly[2-methoxy-5-(2-ethylhexyloxy)-1,4-phenylenevinylene])	 	MEH-PPV is one of the most studied electroluminescent materials. It finds use as a CP in solar cells and carbon nanotube OLEDs [103, 104, 105]. Useful in producing bright and efficient white polymeric LEPs [106]. Although solid-state lasing has yet to be demonstrated in an organic LEP, MEH-PPV has been proven to be a promising laser dye due to its high fluorescence efficiency in solution [107].	Highly soluble in common organic solvents. Bright orange ($\lambda_{\text{abs}} \sim 490 \text{ nm}$) with red/orange emission ($\lambda_{\text{em}} \sim 560 \text{ nm}$). High ϕ_F in solution [103].
3.4 MPS-PPV (poly[5-methoxy-2-(3-sulfopropoxy)-1,4-phenylenevinylene])		MPS-PPV has found use in optoelectronic devices and LEDs [90, 108]. The highly charged backbone of MPS-PPV, with a charge density comparable to DNA, also makes it a model polymer for understanding the interactions and self-assembly properties of charged biopolymers.	Water-soluble. Blue absorber, green emitter ($\lambda_{\text{abs}} \sim 451 \text{ nm}$, $\lambda_{\text{em}} \sim 525 \text{ nm}$ in H_2O).
3.5 PANI (polyaniline)		p-type semiconductor, has been commercialised and is one of the most important conductive polymers. Potential uses include: antistatics, charge dissipation or electrostatic dispersive (ESD) coatings, electromagnetic interference (EMI) shielding, anti-corrosive coatings, hole injection layers [101], conducting layers, actuators, chemical vapour and solution based sensors, electrochromic coatings (for colour change windows, mirrors etc.), active electronic components such as for non-volatile memory. Photoluminescent conducting PANI can be useful as an electron mediator in biosensors [109].	Relatively cheap. Has three distinct oxidation states with different colours. High electrical conductivity. Amongst the family of conducting polymers and organic semiconductors, PANI is unique due to its ease of synthesis, environmental stability, and simple doping chemistry.

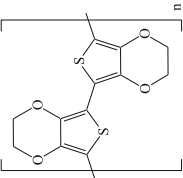
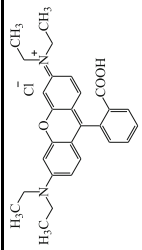
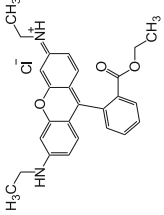
(continued)

Table 4.1 (continued)

Compound	Structure	Specific uses	Physical, photophysical and noteworthy properties
3.6 PF (polyfluorene)		PF derivatives are much investigated for use in OLEDs and polymer solar cells. PF derivatives are particularly useful because they contain a rigid biphenyl unit with large band gap and efficient blue emission, and substitution at the 9,9-positions in the 5-membered ring provides (e.g. 3.7) the possibility of improving the solubility and processing of polymers without significantly increasing the steric interactions in the polymer backbone [110].	PFs emit in the blue with high photo- and electroluminescence yields [111, 112]. They possess high charge carrier mobility, good processability, excellent thermal stability and high stability against oxidants. PFs are relatively wide band-gap materials and thus the emission colour can be tuned <i>via</i> energy transfer to smaller band-gap chromophores which can be incorporated into the polymer as co-monomers or substituents. With the right groups, PFs can be made which emit across the entire visible range with high efficiency and low operating voltage [113].
3.7 PFO (poly(9,9'-dioctylfluorene))		One of the most widely studied PF derivatives. It is a key blue emitter in OLEDs [103]. A two photon pumped PFO solid state laser has been reported [114]. Charged PFO based polymers have been used in the study of compaction of DNA with potential applications in DNA sensors [113, 114].	Solubility, photochemical and aggregation properties are very much dependent on chain length. λ_{abs} in the near UV and λ_{em} in the blue with $\phi_F \sim 0.5$ [103, 110].
3.8 PT (polythiophene)		Widely studied for a wide range of applications such as; FETs, solar cells, non-linear optics, resistors, batteries, diodes, electroluminescent devices, chemical sensors. Most potential applications arise due to the fact that PTs become highly conducting when doped to a metallic level. A fluorene substituted PT has achieved efficiencies of 7 % in polymer-fullerene solar cells [115].	Insoluble in common solvents but many soluble PT derivatives are available that are chemically and thermally stable and offer processing advantages such thin film casting and inkjet printing.
3.9 P3OT (poly(3-octylthiophene-2,5-diy))		P3OT is a conducting LEP that finds use in: OLED and PLED materials, FETs, and, probably most widely studied, polymer-based solar cells [116, 117]. Other alkyl substituted derivatives (particularly the regioregular 3-hexyl P3HT) are also widely used and are important materials for bulk heterojunction PV systems.	λ_{abs} range $\sim 380\text{--}620$ nm (max film = 506 nm); $\phi_L = 0.27$ in solution, CHCl_3 ; $\phi_L = 0.04$ as a film [103].

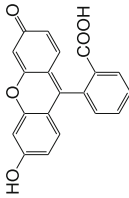
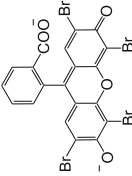
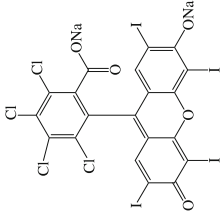
(continued)

Table 4.1 (continued)

Compound	Structure	Specific uses	Physical, photophysical and noteworthy properties
3.10 PEDOT (poly(3,4-ethylenedioxythiophene))		PEDOT is a widely used <i>p</i> -type semiconductor. Typical applications include: hole injection layers in OLEDs and LCD, antistatic coatings, electrically switchable windows, and polymer solar cells. In most of these applications, PEDOT–poly(styrenesulfonic acid) (PEDOT–PSS) copolymer is used because of improved solubility, film forming properties and stability [118].	Excellent transparency in the visible range, high conductivity, high stability, moderate band gap, low redox potential and good thermal stability [118]. A disadvantage is poor solubility which is partly circumvented by using copolymers e.g. PEDOT–PSS.
4. Rhodamines, cyanines and xanthenes. Three groups of widely used dyes. Most are highly fluorescent and widely used as: fluorophores; laser dyes; fluorescent labels in biotechnology; in fluorescence microscopy and flow cytometry; in fluorescence correlation spectroscopy and ELISA; they are also widely used in photochemical studies as singlet energy donors and/or acceptors. Heavy-atom substitution leads to a decrease in ϕ_F and increase in ϕ_T , and heavy-atom substituted xanthenes such as eosin and rose bengal are also used as triplet and singlet oxygen sensitizers. Some cyanines can also be used as electron transfer sensitizers, and are used as such in silver halide photography.			
Compound	Structure	Specific uses	Physical, photophysical and noteworthy properties
4.1 Rhodamine B		A common fluorophore and laser dye, used in fluorescence correlation spectroscopy and ELISA. Often used as a tracer dye to determine the rate and direction of flow and transport. A concentrated solution in glycerol is used as a quantum counter out to ~600 nm.	$\lambda_{\text{abs}} \sim 460\text{--}600$ nm; $\phi_F = 0.65$ in basic ethanol, 0.49 in ethanol. ϕ_T is temperature dependent [119, 20].
4.2 Rhodamine 6G		Widely used fluorophore and laser dye, readily pumped by the 532 nm harmonic from a Nd:YAG laser, or nitrogen laser [121, 122].	$\lambda_{\text{abs}} \sim 425\text{--}600$ nm; very high ϕ_F (0.95) [120]. Remarkably rhodamines it has a small Stokes' shift and its lasing range (555–585 nm) is close to its $\lambda_{\text{max}} \sim 530$ nm. Can be bought as: chloride, perchlorate, or tetrafluoroborate salts.

(continued)

Table 4.1 (continued)

Compound	Structure	Specific uses	Physical, photophysical and noteworthy properties
4.3 Fluorescein		Widely used fluorophore. Finds use in microscopy, as a laser dye in forensics and serology to detect latent blood stains, and in dye tracing. When substituted with reactive groups can be used to covalently label proteins. The excitation maximum (494 nm) is conveniently close to the spectral line of the argon-ion laser (488 nm) which makes fluorescein an important fluorophore for confocal scanning laser microscopy [123]. A common donor for FRET applications.	$\lambda_{\text{abs}} \sim 410\text{--}525$ nm; $\lambda_{\text{max}} = 494$ nm; $\lambda_{\text{em}} = 521$ nm (water); very high $\phi_F = 0.97$ in ethanol; $E_T = 197.5$ kJ mol ⁻¹ [124, 125]. High ϵ ; good water solubility. ϕ_F is pH dependent, decreasing with the decreasing pH. Relatively high rate of photo-bleaching which can limit applications.
4.4 Eosin		Eosin and its derivatives show weak room temperature phosphorescence and are particularly useful as phosphorescent probes for measuring the rotational properties of proteins and other biomolecules in solution and in membranes. Also useful for FRET studies and fluorescence recovery after photobleaching (FRAP) measurements of diffusion.	$\lambda_{\text{abs}} \sim 425\text{--}580$ nm; $\epsilon \sim 112,000$ mol ⁻¹ dm ³ cm ⁻¹ at 525 nm [125]. $\phi_T = 0.67$ in ethanol. Br, 'heavy atom' substituents reduce ϕ_F to typically only 10–20 % that of fluorescein and increase the triplet yield. Singlet oxygen sensitizer with $\phi_A \sim 0.57$.
4.5 Rose Bengal sodium salt		Rose bengal is used as a singlet oxygen sensitizer in photochemical synthesis. A form of rose bengal, PV-10, is currently undergoing clinical trials for melanoma and breast cancer. Also an active ingredient for the treatment of eczema and psoriasis; (drug known as PH-10 also currently in clinical trials). Used as a biological stain, e.g. to stain necrotic tissue and devitalised cells of the cornea and thereby identify damage to the eye.	$\lambda_{\text{abs}} \sim 455\text{--}615$ nm; high $\epsilon = 90,400$ mol ⁻¹ dm ³ cm ⁻¹ (EtOH); $\phi_F \sim 0.05\text{--}0.11$ (EtOH); $E_T = 175.7$ kJ mol ⁻¹ [124, 125]. I, 'heavy atom' substituents reduce ϕ_F and increase triplet yield compared to fluorescein or eosin.

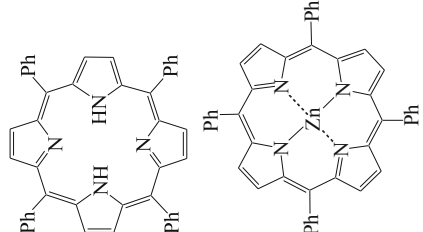
(continued)

Table 4.1 (continued)

Compound	Structure	Specific uses	Physical, photophysical and noteworthy properties
4.6 Cy3 and Cy5		<p>They are usually synthesised with reactive groups, R, on either one or both of the nitrogen atoms so that they can be chemically linked to nucleic acids or proteins. Used mainly for protein and nucleic acid labelling. Cy3 and Cy5 are commonly combined for 2 colour detection; Cy3 dyes fluoresce yellow-green while Cy5 dyes fluoresce red.</p>	<p>The effect of increasing cyanine dye chain length is illustrated by a comparison of absorption/emission wavelengths: Cy3 $\lambda_{\text{abs}} \sim 550$ nm, $\lambda_{\text{em}} \sim 570$ nm; Cy5 $\lambda_{\text{abs}} \sim 649$ nm, $\lambda_{\text{em}} \sim 650/670$ nm [126].</p>
4.7 Thiocarbocyanine		<p>Thiocarbocyanine and its derivatives are used in sensitising silver halide photographic emulsions. New applications of the dyes include use in LEDs. A great deal of research has been carried out on understanding the aggregation properties of cyanine dyes in solution [127].</p>	<p>Weak absorption in range $\sim 250\text{--}340$ nm; main λ_{abs} range $\sim 440\text{--}610$ nm; abs $\lambda_{\text{max}} = 559$ nm; λ_{em} range $\sim 555\text{--}700$ nm. Emission $\lambda_{\text{max}} = 625$ nm, 571 nm; $\phi_F = 0.05$ (EtOH). Readily aggregates in solution [127].</p>
4.8 TOTO-1		<p>Active fluorescent probe, widely used in fluorescence microscopy and flow cytometry for the study of nucleic acids [126].</p>	<p>Green emitter; cell-impermeable, high-affinity for nucleic acid; essentially non-fluorescent in the absence of nucleic acids; exhibits excitation/emission maxima $\sim 514/533$ nm when bound to nucleic acids. Sensitivity is sufficient for detecting single molecules of labelled nucleic acids [126].</p>

(continued)

Table 4.1 (continued)

<p>5. Porphyrins and Phthalocyanines. Porphyrins are highly conjugated rigid structures and as such tend to have very intense vibrationally-structured absorption bands in the visible region. Their properties can be readily modified by both ring substitution and metallation. Their well characterised fluorescence, moderate to high triplet yields, long-lived triplet states with well-known T-T absorption spectra, and the range of triplet energies available, make them useful singlet and triplet sensitisers and acceptors, and singlet oxygen sensitisers. They are also useful standard materials for both steady-state and time-resolved fluorescence and flash photolysis. Porphyrins have a characteristic sharp Soret band around 390–430 nm with very high absorption coefficients, and less intense Q bands in the visible. Phosphorescent Pt and Pd porphyrins are widely studied as oxygen sensors. The commercial uses of porphyrins and metalloporphyrins include: (i) photodynamic therapeutics such as Photofrin™ to fight viral infections and cancer; (ii) commercial oxidation catalysts to make fine chemicals; (iii) components of printing inks and toners; (iv) protective coatings. There have been several hundreds of patents issued in the past few years for the use of porphyrins in molecular electronics, catalysts, inks, and other new materials. Phthalocyanines are red-absorbing compounds with intense bands around 650–750 nm, a reasonable spectral window in the green/blue, and further absorption about 400 nm. Unsubstituted phthalocyanine, and metal phthalocyanines generally have quite poor solubility, but ring substitution can be used to increase solubility in either aqueous or organic solvents. Approximately 25 % of all artificial organic pigments are phthalocyanine derivatives.</p>	<p>Structure</p> 	<p>Specific uses</p> <p>Photosensitiser for the production of singlet oxygen [128]. TPP and its derivatives are related to the electron relay stations in the electron transport chain which form part of chlorophyll in plants. There are also various reduced forms of the cyclic tetrapyrrole ring structure, such as chlorins and bacteriochlorins, which are becoming increasingly important materials for a wide variety of photochemical applications.</p> <p>Photophysics of ZnTPP are well understood and it is often used as a 'model' metalloporphyrin to study other systems or as a reference compound. Derivatives have been used in dye sensitised solar cells (DSCs).</p>	<p>Physical, photophysical and noteworthy properties</p> <p>$\lambda_{\text{abs}} \sim 370\text{--}440$ nm and bands across 490–615 nm; high $\epsilon = 1.89 \times 10^4 \text{ mol}^{-1} \text{ dm}^3 \text{ cm}^{-1}$ at 515 nm (toluene); $\lambda_{\text{em}} \sim 615\text{--}770$ nm; $\phi_{\text{F}} = 0.11$ (toluene) [129]. High triplet yield, long lived (ms) triplet with well characterised T-T absorption spectrum. Dark purple solid that dissolves in nonpolar organic solvents such as chloroform and benzene, not soluble in water.</p> <p>$\lambda_{\text{abs}} \sim 385\text{--}450$ nm and two bands across $\sim 520\text{--}600$ nm; very high $\epsilon = 5.74 \times 10^5 \text{ mol}^{-1} \text{ dm}^3 \text{ cm}^{-1}$; $\lambda_{\text{em}} \sim 570\text{--}760$ nm; $\phi_{\text{F}} = 0.03$ (toluene), high triplet yield, long lived (ms) triplet with well characterised T-T absorption spectrum [129, 130].</p>
<p>Compound</p> <p>5.1 H₂TTPP (tetraphenylporphyrin)</p>			
<p>5.2 ZnTTPP</p>			

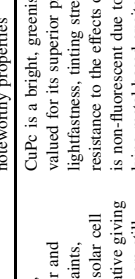
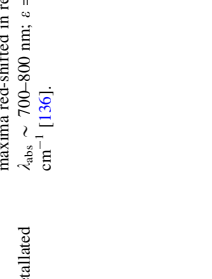
(continued)

Table 4.1 (continued)

Compound	Structure	Specific uses	Physical, photophysical and noteworthy properties
5.3 TMPyP (5,10,15,20-Tetrakis(1-methyl-4-pyridinio)porphyrin tetra(<i>p</i> -toluenesulfonate))		TMPyP is a water-soluble porphyrin that finds use as a chelating agent for the quantitative analysis for many metals. TMPyP intercalates to G-quadruplexes (nucleic acid sequences rich in guanine which form a four-stranded structure) and has been used to study such structures.	Water soluble; $pK_{a1} = 0.8$, $pK_{a2} = 2.06$. $\lambda_{max} = 422$ nm, $\epsilon = 2.3 \times 10^5$ mol ⁻¹ dm ³ cm ⁻¹ (H ₂ O); in 1 M HCl (protonated), $\lambda_{max} = 445$ nm, $\epsilon = 2.9 \times 10^5$ mol ⁻¹ dm ³ cm ⁻¹ .
5.4 PROEP (platinum octaethylporphyrin)		Red triplet emitter with high quantum yield for OLEDs which has shown exceptionally high efficiency (~7%) at low injection current [131]. Used as a dopant in host materials like 4,4'-bis(N-carbazolyl)-1,1'-biphenyl (CBP) and Alq ₃ (6.1). Has also been used as a phosphorescent dye in LEDs [132]. Widely studied as a phosphorescent oxygen sensor. The Pd analogue is also used in oxygen sensors studies; it has weaker emission, but a much longer triplet lifetime.	Red r.t. phosphorescence ~650 nm depending on solvent, host material and processing conditions, $\phi_p = 0.45$ (deoxygenated toluene/DMF, r.t.), $\tau_p = 83$ μ s [103, 128].
5.5 Pc (phthalocyanine)		Intensely blue/green coloured, widely used as a pigment. Properties can be varied by metallation and/or ring substitution. Phthalocyanines form coordination complexes with most elements of the periodic table. These complexes are also intensely coloured and many are also used as pigments.	Poor solubility, (chloro)phthalene is a good solvent for phthalocyanines). Structured abs in the λ_{abs} range ~530–740 nm; intensely coloured, $\epsilon = 1.62 \times 10^5$ mol ⁻¹ dm ³ cm ⁻¹ at 699 nm; $\lambda_{em} \sim 650$ –800 nm; strongly fluorescence, $\phi_f = 0.6$ (chloro)phthalene), moderate triplet yield [125, 133].

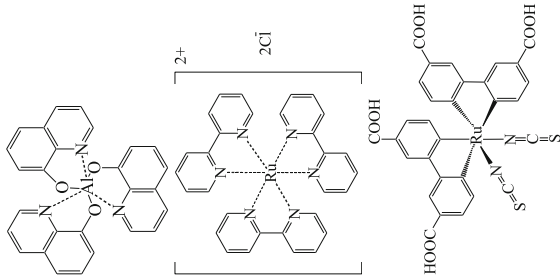
(continued)

Table 4.1 (continued)

Compound	Structure	Specific uses	Physical, photophysical and noteworthy properties
5.6 CuPc (copper phthalocyanine)		<p>First developed as a pigment, phthalocyanine, in the mid-1930s. Due to its brilliant colour and stability, it is a standard pigment used in paints, printing ink and packaging. The first OPV solar cell was made using CuPc and a perylene derivative giving 1% efficiency [134]. CuPc and derivatives are still leading materials used in OPV solar cell research. The analogous ZnPc is also a widely used absorber in OPV solar cells. Bulk hetero-junction solar cells using ZnPc as the donor and C60 as the acceptor have shown efficiencies greater than 2.5% [135]. Fluorine derivatives of ZnPc, such as hexadecafluorophthalocyanine, have shown promise for use in photodynamic therapy (PDT).</p>	<p>CuPc is a bright, greenish-blue pigment, highly valued for its superior pigment properties such as lightfastness, tinting strength, covering power and resistance to the effects of alkalis and acids. CuPc is non-fluorescent due to the presence of a low lying metal-based excited state. The corresponding ZnPc is intensely coloured, $\lambda_{\text{abs}} \sim 600\text{--}750\text{ nm}$; $\epsilon = 2.82 \times 10^5\text{ mol}^{-1}\text{ dm}^3\text{ cm}^{-1}$ at 674 nm, and is moderately fluorescent, $\phi_{\text{F}} = 0.3$; it also has a fairly high triplet yield [125, 133].</p>
5.7 Naphthalocyanine		<p>Potential use in OLEDs, OPV and OFETs. Used as a component in the development of IBM's single-molecule logic switch. Metallated derivatives also find use as gas sensors and in PDT.</p>	<p>Absorbs strongly in the NIR with the absorption maxima red-shifted in relation to 5.5 and 5.6. $\lambda_{\text{abs}} \sim 700\text{--}800\text{ nm}$; $\epsilon = 23,800\text{ mol}^{-1}\text{ dm}^3\text{ cm}^{-1}$ [136].</p>

(continued)

Table 4.1 (continued)

Molecule	Structure	Specific uses	Physical, photophysical and noteworthy properties
6. Aluminium(III), iridium(III) and ruthenium (II) complexes. Tris(8-hydroxyquinoline)aluminium(III) was the first material to be used in efficient OLEDs, and continues to be important for devices. Ir(III)-based triplet emitters have attracted substantial interest for OLED technology, with several highly efficient green devices reported along with blue, yellow and red. There are many Ru(II) bipyridine and terpyridine complexes. Many are phosphorescent with long-lived (μs) triplets which are efficient photooxidants and photoreductants. The long-lived phosphorescence is quenched by oxygen, which has led to their use as oxygen sensors. Ruthenium complexes which absorb light throughout the visible spectrum are currently the most widely used sensitizers for dye-sensitized solar cell (DSC) research.	 <p>The image shows three chemical structures. On the left is Alq3, a complex of aluminum coordinated to three 8-quinolinolyl groups. In the middle is [Ru(bpy)3]2+, a ruthenium complex with three bipyridine ligands and two chloride counterions. On the right is N3, a ruthenium complex with a bis(2,2'-bipyridyl)-4,4'-dicarboxylate ligand, a diisothiocyanato ligand, and two carboxylic acid groups.</p>	Green electroluminescent emitter for OLEDs [137].	Relatively high quantum yield of electroluminescence; broad fluorescence band peaking at ~ 478 nm (in methanol/ethanol at 77 K). Emission bands at 578 and 605 nm are assigned to phosphorescence; 478 nm band is assigned to delayed fluorescence [138].
6.2 Tris(bipyridine) ruthenium(II) dichloride		[Ru(bipy) ₃] ²⁺ has been examined as a photosensitizer for both the oxidation and reduction of water. A [Ru(bipy) ₃] ²⁺ , persulfate long lifetime τ_T : 890 ns in acetonitrile, 650 ns in combination can be used as a water-soluble free water, and shows a broad band emission, $\phi_T = 0.05$ at radical initiator.	$\lambda_{\text{abs max}} = 452$ nm; $\epsilon = 1.15 \times 10^4$ mol ⁻¹ dm ³ cm ⁻¹ . The triplet excited state has a comparatively long lifetime τ_T : 890 ns in acetonitrile, 650 ns in water, and shows a broad band emission, $\phi_T = 0.05$ at $\lambda_{\text{em}} \sim 620$ nm.
6.3 N3 (<i>cis</i> -bis(isothiocyanato)bis(2,2'-bipyridyl)-4,4'-dicarboxylato)ruthenium(II))		Sensitizer used by O'Reagan and Gratzel <i>et al.</i> in their 1991 breakthrough work in the field of DSCs. Highly stable dye for solar cell N3 starts to absorb light at around 800 nm when sorbed applications. Has showed light to electric energy conversion efficiency of 7.9 % [139].	Broad λ_{abs} range ~ 310 –775 nm; $\lambda_{\text{abs max}} = 534$ nm; in moderate $\epsilon = 1.42 \times 10^4$ mol ⁻¹ dm ³ cm ⁻¹ (EtOH).

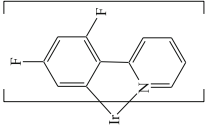
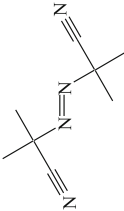
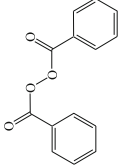
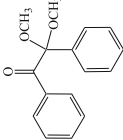
(continued)

Table 4.1 (continued)

Compound	Structure	Specific uses	Physical, photophysical and noteworthy properties
6.4 N719 (di-tetrabutylammonium <i>cis</i> -bis(isothiocyanato)bis(2,2'-bipyridyl)-4,4'-dicarboxylato)ruthenium(II)		Sensitiser for solar cells analogous to N3; however Broad has tetraethyl ammonium counter ions; this has a significant positive impact on the light to electric energy conversion efficiency. N719 is one of the most widely studied dyes for DSC applications. Has showed light to electric energy conversion efficiency of 11.1 % [140].	Broad λ_{abs} range \sim 310–775 nm; λ_{em} max = 535 nm; moderate $\epsilon = 1.36 \times 10^4 \text{ mol}^{-1} \text{ dm}^3 \text{ cm}^{-1}$ (EtOH). N719 has a moderate molar extinction coefficient (when compared to organic dyes) which limits solar cell efficiencies. Very stable dye for DSC research.
6.5 'Black' dye (tris(cyanato)-2,2',2''-terpyridyl-4,4',4''-tricarboxylate)Ru(II)		Panchromatic sensitiser for DSC. Has showed light to electric energy conversion efficiency of over 10 % [141].	Broad λ_{abs} range \sim 310–800 nm; λ_{em} max = 605 nm; moderate $\epsilon = 7.48 \times 10^3 \text{ mol}^{-1} \text{ dm}^3 \text{ cm}^{-1}$ (EtOH). Onset of absorption is 920 nm when sorbed to TiO ₂ . Very stable dye for DSC research; has been subjected to the equivalent of 10 years' exposure to the sun with no loss of performance [141].
6.6 Ir(ppy) ₃ tris[2-phenylpyridinato-C ² ,N]iridium(III)		Green emitter used in PLEDs, in a poly(9-vinylcarbazole) (PVK) matrix gives an efficiency of 7.5 % [103]. This was the first reported PLED device with an efficiency of greater than 5 %. Also used as an optical oxygen sensor.	Green emitter, λ_{em} max = 514 nm (solution) and 516 nm (film); $\phi_L = 0.40$ [103].
6.7 Ir(piq) ₃ (tris(1-phenylisoquinoline-C ² ,N)iridium(III))		Red-emissive complex used in PLEDs. Has achieved an external quantum efficiency of 10.3 % and a power efficiency of 8.0 % lm W ⁻¹ at 100 cd m ⁻² [103]. Originally, it was hoped that Ir(piq) ₃ could be directly applied as dopant into the polymer host for red emission. Unfortunately its use in LED technology is limited by its solubility which hinders cheap solution processing for device fabrication.	Red emitter; λ_{em} max = 624 nm; $\phi_L = 0.45$; $\tau = 1.25 \text{ ns}$ [142]. Use in OLED devices is limited by poor solubility and processability. Not soluble in many common solvents.

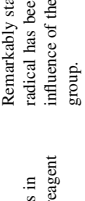
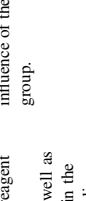

(continued)

Table 4.1 (continued)

Compound	Structure	Specific uses	Physical, photophysical and noteworthy properties
6.8 Ir(ppy) ₃ (tris[2-(2,4-difluorophenyl)pyridine]iridium(III))		This was one of the first blue OLED triplet emitters. However, its long term stability is limited which has led to a search for more stable phosphors for this spectral region.	$\lambda_{em} \sim 480$ nm (CHCl ₃).
7. Radical Initiators. These are substances that can produce radical species under mild conditions (i.e. have low bond dissociation energies and are thus inherently unstable) and promote radical reactions. Radical initiators are utilised in industrial processes such as polymer synthesis. Typical examples are halogen molecules, azo compounds, and organic peroxides. Here we concentrate on initiators that undergo cleavage upon UV/Vis irradiation, although they will also act as thermal radical initiators.			
Molecule	Structure	Specific uses	Physical, photophysical and noteworthy properties
7.1 AIBN (2,2'-azobis(2-methylpropanitrile))		Decomposes upon irradiation with UV, or upon heating, eliminating a molecule of nitrogen gas to form two 2-cyanoprop-2-yl radicals. These radicals can be used to initiate free radical polymerisations and other radical reactions. A classic example of a radical reaction that can be initiated by AIBN is the <i>anti</i> -Markovnikov hydrohalogenation of alkenes.	UV absorber; not water soluble; but soluble in methanol and ethanol. AIBN is highly toxic, but is a safer alternative to benzoyl peroxide (7.2) because the risk of explosion is far smaller. Decomposition temperature = 64 °C; slow decomposition at r.t.
7.2 Benzoyl peroxide		It is one of the most important organic peroxides in terms of applications and the scale of its production. Widely used initiator, curing agent, and cross-linking agent in polymerisation processes. Other major applications are based on its antiseptic and bleaching properties.	UV absorber; λ_{abs} max = 235 nm. Poor solubility in water; but soluble in ethanol and organic solvents. Decomposition temperature = 103 °C.
7.3 2,2-Dimethoxy-2-phenylacetophenone		Important photocuring agent used mainly for acrylic and unsaturated polyester resins. A great deal of work has been devoted to the unravelling of its photochemistry [143].	Primary reaction is a photochemical cleavage from a very short-lived triplet state ($\tau < 100$ ps) to radicals followed by fragmentation of the dimethoxybenzyl radical to methyl benzoate [143].

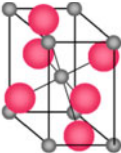
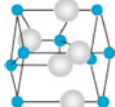
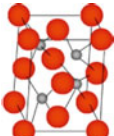
(continued)

Table 4.1 (continued)

Molecule	Structure	Specific uses	Physical, photophysical and noteworthy properties
8. Free radical traps (also known as free radical scavengers or spin traps). React with unstable short lived free radicals to form a relatively stable free radical (normally through the addition of the radical to the trap to form a nitroxide radical). Spin traps are normally used in conjunction with EPR spectroscopy for the detection and identification of short-lived free radicals. The identity of the radical can be inferred from the EPR spectrum of the spin adduct.			
8.1 TEMPO (2,2,6,6-tetramethyl-1-piperidinyloxy)		<p>TEMPO is widely used as a radical trap, as a structural probe for biological systems in conjunction with EPR spectroscopy, as a reagent in organic synthesis, and as a mediator in controlled free radical polymerisation. As well as alcohol oxidation, TEMPO also finds use in the oxidation of other functional groups, including amines, phosphines, phenols, anilines, sulfides and organometallic compounds [144].</p>	<p>Remarkably stable nitroxyl radical. The stability of the radical has been proposed to be due to the steric influence of the methyl groups which flank the nitroxyl group.</p>
8.2 CYPMPO		<p>CYPMPO is a free radical spin trap with excellent trapping capabilities toward hydroxyl and superoxide radicals in biological and chemical systems [145].</p>	<p>The high melting point (126 °C), low hygroscopic properties, and long shelf-life in aqueous solutions are significant practical advantages for use of CYPMPO.</p>
8.3 DEPMPO		<p>DEPMPO is frequently used as a spin trap for the measurement of superoxide by EPR spectrometry. Most efficient spin trap for the <i>in vitro</i> and <i>in vivo</i> detection of O₂⁻, S⁻ and C-centred free radicals.</p>	<p>DEPMPO is water-soluble, rapidly penetrates lipid bilayers, has low toxicity, and can be used <i>in vitro</i> and <i>in vivo</i>. Half-life is still fairly short at r.t. and thus measurements need to be made at low temperatures [146].</p>

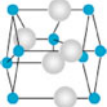
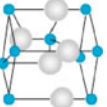
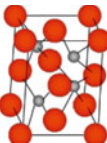
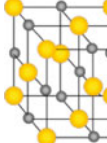
(continued)

Table 4.1 (continued)

Compound	Structure	Specific uses	Physical, photophysical and noteworthy properties
9.1 TiO ₂		<p>Common white pigment in paints, toothpaste, sunscreens and foodstuffs. Filters both UV-A and UV-B and used as nanoparticles in sunscreen formulations to increase transparency on the skin. It is the most widely studied semiconductor for DSC applications. Nano-particulate titania has a very high surface area which allows significant dye sorption to absorb visible light and to inject electrons into the conduction band (CB) of TiO₂ forming a PV device.</p>	<p>Relatively wide E_g semiconductor; direct band gap of $\sim 3.0\text{--}3.2$ eV (depending on crystal form). Stable, non-toxic oxide with a high refractive index ($n = 2.4\text{--}2.5$). The crystal form of TiO₂ is dependent on the method of production. <i>Anatase</i> and <i>rutile</i> forms are most common; rutile is the thermodynamically most stable form; anatase is the preferred form in DSCs, because it has a larger bandgap (3.2 vs. 3.0 eV) and higher CB edge energy which leads to a higher output voltage [147].</p>
9.2 ZnO		<p>Widely used as an additive in; plastics, ceramics, glass, cement, lubricants, paints, ointments, adhesives, sealants, pigments, foods, batteries, ferrites, fire retardants, and first aid tapes. Also used in emerging applications for transparent electrodes in LCDs; in energy-saving or heat-protecting windows, and in electronics as thin-film transistors and LEDs. Shows promise as a material for fast scintillators. Studied as a possible alternative to TiO₂ as a semiconductor for DSCs.</p>	<p>Relatively wide E_g semiconductor. The bandgap can be tuned across $\sim 3\text{--}4$ eV by doping. Most ZnO has <i>n</i>-type character (due to oxygen vacancies), even in the absence of intentional doping. Controllable <i>n</i>-type doping is easily achieved while reliable <i>p</i>-type doping remains difficult. Exhibits excitonic luminescence even at r.t. in the blue region with a relatively short lifetime (50 ps at 16 K) [148].</p>
9.3 ZnS		<p>In its dense synthetic form, ZnS can be transparent and is used as a window for visible and infrared optics. With addition of a suitable <i>activator</i>, ZnS finds use as a phosphor in several applications, from cathode ray tubes through X-ray screens to glow in the dark products. When silver is used as activator, the resulting colour is bright blue, manganese yields an orange/red colour and copper provides a long glow time and the familiar 'glow-in-the-dark' green colour. Cu-doped ZnS is used in electroluminescent panels.</p>	<p>Intrinsic, wide-bandgap semiconductor. The cubic form, (<i>zinc blende</i> structure) has a band gap of 3.54 eV at 300 K whereas the hexagonal form (<i>wurtzite</i>) has a band gap of 3.91 eV. Can be doped as both an <i>n</i>-type or <i>p</i>-type semiconductor. It may exhibit phosphorescence, due to impurities, on illumination with blue or UV light.</p>

(continued)

Table 4.1 (continued)

Molecule	Structure	Specific uses	Physical, photophysical and noteworthy properties
9.4 CdS		CdS is a pigment used in plastics. CdS and CdSe (9.5) are used in manufacturing of photoresistors, sensitive to visible and near NIR light. In thin-film form, CdS can be combined with a <i>p</i> -type semiconductor for PV applications; a CdS/Cu ₂ S solar cell was one of the first efficient cells to be reported (1954) [149]. Also used as a phosphor and in solid state lasers, and as nanoparticulate QDs.	Direct band gap semiconductor; $E_g = 2.42$ eV. Like ZnS (9.3), has two crystal forms: the more stable hexagonal, wurtzite, structure and the cubic, zinc blende, structure. The conductivity increases when irradiated with light (hence its use as a photoresistor). CdS pigments tend to have high thermal stability, good light and weather fastness as well as chemical resistance and high opacity.
9.5 CdSe		CdSe thin-film transistors were used in LCDs in 1973. Developed for use in optoelectronic devices, laser diodes, nano-sensing, biomedical imaging and film solar cells. CdSe QDs have potential use in optical devices, such as laser diodes that can cover a large part of the visible spectrum.	The wurtzite crystal structure is an important <i>n</i> -type semiconductor. Difficult to dope <i>p</i> -type, however <i>p</i> -type doping has been achieved using nitrogen. CdSe QDs have tunable absorption and emission across the visible spectrum.
9.6 CdTe		Used in thin film solar cells; has achieved a maximum efficiency, to date, of 16.5 %. This is lower than Si but at lower production costs. CdTe PV is the first thin-film PV technology to compete with crystalline silicon PV. Alloying with mercury gives a versatile infrared detector material (HgCdTe). Alloying with zinc gives an excellent solid-state X-ray and γ -ray detector.	Absorption range of bulk CdTe is dependent on sample thickness but generally λ_{abs} range ~ 475 – 850 nm. $E_g = 1.44$ eV at 300 K. Transparent in the IR out to wavelengths greater than 2000 nm Bulk CdTe is fluorescent at 790 nm; with QDs the fluorescence peak is tuneable through the visible range to the UV [150].
9.7 PbS		PbS is one of the oldest and most common materials for the detection of IR radiation. Can be used to measure radiation in either of two ways: by measuring the tiny photocurrent the photons cause, or by measuring the change in the material's electrical resistance; resistance change is the more commonly used method. PbS QDs have been studied for DSC applications.	At r.t., PbS is sensitive to radiation at wavelengths between approximately 1000 and 2500 nm. Cooling to 77 K shifts its sensitivity range to between approximately 2000 and 4000 nm. PbS has shown $\eta \sim 1.23$ % in DSCs [151].

(continued)

Table 4.1 (continued)

Compound	Specific use	Physical, photophysical and noteworthy properties
10.1 Europium(III) oxide	Widely used as a red phosphor in television sets and fluorescent lamps, and as an activator for yttrium-based phosphors. Europium photoluminescence is used in the anti-counterfeiting phosphors in Euro banknotes.	Red phosphorescent material.
10.2 Terbium (III) oxide	Terbium oxide is used in fluorescent lamps and TV tubes. Terbium green phosphors with Eu(II) blue phosphors and Eu(III) red phosphors provide a high-efficiency white light used for standard illumination in indoor lighting.	Green phosphorescent material.
10.3 Eu(II) based phosphors	Luminescence of Eu(II) depends on the host lattice, but tends to be on the blue side. Investigations of Eu(II) phosphors date back to the 1960s, first reported by Wanmaker <i>et al.</i> ABPO ₄ :Eu ²⁺ (A = Li, Na, K, B = Ca, Sr, Ba) have been extensively studied [152].	LiCaPO ₄ :Eu ²⁺ , phosphors have superior luminescence properties for UV-LED application among ABPO ₄ :Eu ²⁺ type phosphors because of their high quantum efficiency and thermal stability.
10.4 Lanthanide ions :Eu ³⁺ and Tb ³⁺	Lanthanide ions are visible to NIR ultra narrowband emitters with long luminescence lifetimes and thus have potential applications in lasing, up-conversion, and bioimaging. They have found use as potential emitters in OLEDs (see [38]).	Of the luminescent Ln ions, Eu ³⁺ and Tb ³⁺ are the two most extensively studied in practical applications. Luminescence is vibrationally quenched in common solvents. Lanthanide luminescence quenching can be suppressed by doping the lanthanide ions into the crystalline lattice of rare earth nanocrystals, e.g., LaF ₃ , NaYF ₄ , LaPO ₄ .
10.5 Nd:Y ₃ Al ₅ O ₁₂	Nd(III) is used to dope a host crystal structure of yttrium aluminium garnet (YAG) (the Nd ³⁺ and Y ³⁺ ions are of similar size) at ~1 % level to produce a solid-state lasing medium. The Nd ³⁺ provides the lasing activity in the crystal. Laser operation of Nd:YAG was first demonstrated by J. E. Geusic <i>et al.</i> at Bell Laboratories in 1964. More recently research has been carried out on ceramic Nd:YAG lasers [153].	The principle emission wavelength is 1064 nm (from a ⁴ F _{3/2} → ⁴ I _{11/2} transition), but for many applications, the IR is frequency-doubled or -tripled using non-linear optical materials Nd:YAG can be also made to lase at its non-principal wavelength. The line at 946 nm, doubled to 473 nm is typically employed in blue laser pointers, while a frequency doubled Nd:YVO ₄ diode pumped solid state (DPSS) laser can be used as a green laser pointer.


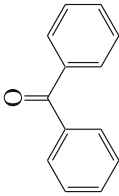
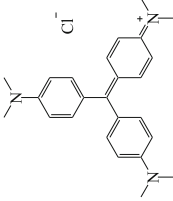
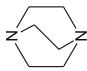
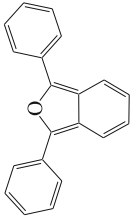
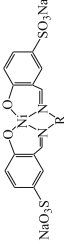
(continued)

Table 4.1 (continued)

Molecule	Structure	Specific uses	Physical, photophysical and noteworthy properties
10.6 Erbium(III) oxide		Erbium oxide is pink and is sometimes used as a colorant for glass, cubic zirconia and porcelain. It is particularly important as a near infrared emitted in optical data transmission. The Er(III) emission bands in the 1500–1600 nm region correspond to a region of high transmission in optical fibres. This is extensively used in high density communications, e.g. broadband internet or telecommunications.	Erbium oxides can up convert energy. Erbium oxide nanoparticles are visibly photoluminescent when excited at 379 nm (in water).
11. Miscellaneous compounds			
Compound	Structure	Specific uses	Physical, photophysical and noteworthy properties
11.1 Acridine orange (AO), N,N,N',N'-Tetramethylacridine-3,6-diamine		Fluorescent cationic dye, useful for fluorescence microscopy. Used in nucleic acid studies since it can be used to differentiate between DNA and RNA. AO intercalates with DNA (emitted radiation is green) and interacts electrostatically with RNA to form a complex where the emitted light is orange [126].	Similar spectrally to fluorescein when bound to DNA; λ_{ex} ~ 502 nm; λ_{em} max ~525 nm. When it associates with RNA λ_{obs} shifts to ~460 nm and λ_{em} max shifts to ~650 nm [126].
11.2 Avobenzene (Parsol)		Absorbs UV light over a wide range of wavelengths; widely used in 'broad spectrum' sunscreens.	UV absorber; λ_{obs} max = 357 nm. May photodegrade faster when used in combination with mineral UV absorbers like ZnO and TiO ₂ , though with the right coating, or doping, of the mineral particles this reaction can be reduced [154].
11.3 Anthraquinone		Building block of many dyes (e.g. 11.4). Very important precursor for the production of several drugs. Precursors of anthraquinone are also used in the production of hydrogen peroxide.	Colourless and very photochemically active with high ϕ_T and hydrogen abstraction from hydrogen donor solvents. Ring substitution, and introduction of routes for excited-state deactivation, notably proton transfer, gives the anthraquinone dyes e.g. 11.4.
11.4 Alizarin		Main ingredient for the manufacture of the madder lake pigments known to painters as rose madder and alizarin crimson. Used as a staining agent in biological research; stains free calcium and certain calcium compounds. Also used commercially as a red textile dye and, notably, is still the colour for French military cloth. Derivatives are commonly used as indicators of specific free ions and as pH indicators.	Reddish-orange solid and is very colour-fast.

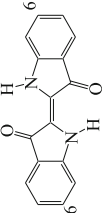
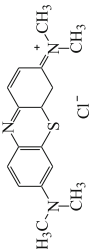
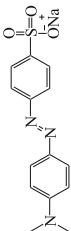
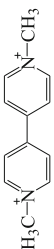
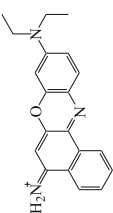
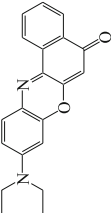
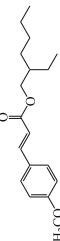
(continued)

Table 4.1 (continued)

Compound	Structure	Specific uses	Physical, photophysical and noteworthy properties
11.5 β -Carotene		β -carotene is a strongly-coloured red-orange pigment abundant in plants and fruits. Very low triplet energy acceptor. Energy transfer quencher of singlet oxygen.	λ_{abs} range ~ 350 – 520 nm; $\epsilon \sim 139,500$ mol $^{-1}$ dm 3 cm $^{-1}$; highly conjugated; deeply coloured; lipophilic, insoluble in water but soluble in diethyl ether and acetone. Very slightly soluble in methanol [155].
11.6 Benzophenone/hydroxybenzophenone		Benzophenone is a common photosensitiser. Free radical formation by hydrogen abstraction from solvent leads to use in UV-curing applications such as inks, imaging, and clear coatings in the printing industry. By way of contrast, hydroxy benzophenones with the OH group adjacent to the carbonyl are useful photostable UV absorbers because reversible proton transfer is an efficient deactivation route leading to very short lived excited-states.	Near UV absorbing with $\phi_T \sim 1$, and a triplet state which undergoes efficient solvent hydrogen abstraction with many solvents to generate ketyl and solvent radicals. Insoluble in water; soluble in benzene, THF, ethanol, propylene glycol.
11.7 Crystal violet (CV)		Used as a non-toxic stain for cells, DNA and bacteria. Important colouring dye for paper, printing inks and pen ink. CV is antibacterial and antifungal and thus finds medicinal use for treatment of skin conditions.	Intense visible absorption bands with λ_{abs} max = 590 nm; $\epsilon \sim 87,000$ mol $^{-1}$ dm 3 cm $^{-1}$. Absorption is pH dependent with the colour changing from purple through blue to yellow with decreasing pH. Shows very little fluorescence due to rapid non-radiative decay from the first excited singlet to the ground state in a few ps [156].
11.8 DABCO (1,4-diazabicyclo[2.2.2]octane)		Classic example of a hindered amine physical quencher of singlet oxygen; widely used as antioxidant to improve the lifetime of materials exposed to light, e.g. image dyes, laser dyes, probes and samples for fluorescence microscopy.	Effective physical quencher of singlet oxygen. Colourless and transparent throughout much of the UV, good solubility in many solvents.
11.9 DPBF (diphenylisobenzofuran)		Has been used as diagnostic tests for the presence of singlet oxygen in both chemical and biological processes.	λ_{max} in methanol = 410 nm; $\epsilon \sim 22,200$ mol $^{-1}$ dm 3 cm $^{-1}$. Strong blue fluorescence. DPBF reacts rapidly with singlet oxygen. The only reaction of DPBF with singlet oxygen is chemical. It does not react with ground state molecular oxygen or with the superoxide anion. The disappearance of DPBF in solution can be monitored by absorption and/or emission spectroscopy [124].
11.10 Disodium [NN'-ethylenebis(5-sulphosalicylideneiminato)]nickelate (II)		Typical Ni complex singlet oxygen quencher.	Water soluble, yellow/green complex.

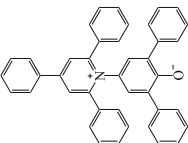
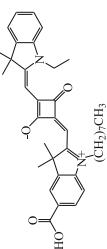
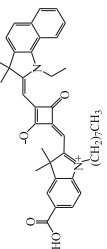
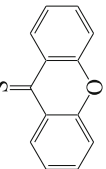
(continued)

Table 4.1 (continued)

Compound	Structure	Specific uses	Physical, photophysical and noteworthy properties
11.11 Indigo and tyrian purple		Indigo is mainly used as a fabric dye for the production of denim cloth for blue jeans. The closely related tyrian purple (mainly 6,6'-dibromoindigo), is a purple-red dye, obtained in minute amounts from sea snails and highly prized in antiquity.	λ_{abs} range \sim 520–680 nm; λ_{abs} max = 610 nm. Insoluble in water, alcohol, or ether; soluble in DMSO and chloroform. The dyeing process uses the reduced form of indigo, leuco-indigo, which is then oxidised to indigo on exposure to air.
11.12 Methylene blue (MB)		Widely used blue dye: a redox indicator in analytical chemistry (colourless when reduced or oxidised); efficient singlet oxygen sensitizer; standard compound for modelling TiO_2 photosensitised destruction of pollutants. The interaction of MB and DNA has been widely studied [157].	$E_T = 133.9 \text{ kJ mol}^{-1}$; λ_{abs} max \sim 670 nm; red fluorescence; high triplet and singlet oxygen yield [124]. Characteristic absorption spectrum which is dependent on a number of factors, including protonation, adsorption to other materials, the formation of dimers and higher-order aggregates depending on concentration, solvent and other interactions.
11.13 Methyl orange		Widely used azo dye: pH indicator and model compound for photodegradation studies. Also finds use as a biological stain.	Yellow in alkali, red in acid.
11.14 Methyl viologen (MV)		Charge transfer quencher, electron acceptor and transfer catalyst in redox reactions, use as an electron relay in photochemical systems designed for solar energy conversion.	Reduced MV is intensely blue with a characteristic absorption spectrum which makes monitoring its formation and decay relatively easy, and viologens can be used in electrochromic displays.
11.15 Nile blue		Stain used in biology; it may be used with live or fixed cells, and imparts a blue colour to cell nuclei. Derivatives of Nile blue are potential photosensitisers in photodynamic therapy of malignant tumours.	High fluorescence quantum yield in non-polar solvents. The absorption and emission maxima of Nile blue are strongly dependent on pH and solvent.
11.16 Nile red		Stain and polarity indicator. Nile red stains intracellular lipid red. Will not fluoresce in most polar solvents, however when in a lipid-rich environment can be intensely fluorescent, with colours varying from a deep red to strong yellow-gold emission [126].	Generally excitation/emission is 485/525 nm (552/636 nm in methanol), however, the fluorescence of the dye is heavily dependent on the solvent used, and in polar solvents it does not fluoresce at all.
11.17 Octyl methoxycinnamate (OMC)		Common UV-B filter used in various cosmetic formulations.	λ_{abs} max = 310 nm; $\epsilon \sim 24,000 \text{ mol}^{-1} \text{ dm}^3 \text{ cm}^{-1}$. On exposure to sunlight undergoes <i>trans</i> to <i>cis</i> isomerisation [158].

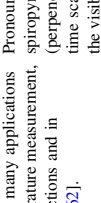
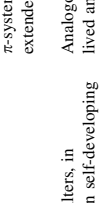
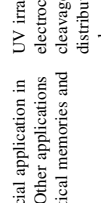
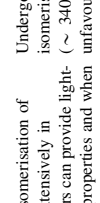
(continued)

Table 4.1 (continued)

Compound	Structure	Specific uses	Physical, photophysical and noteworthy properties
11.18 Reichardt's dye (2,6-Diphenyl-1,4-(2,4,6-triphenyl-1-pyridinio)phenolate)		Solvatochromic dye for use as a solvent polarity indicator [158].	Charge transfer transition with very high solvatochromism. The range of transition energies is extremely large, from 263.8 kJ mol ⁻¹ (453 nm) for water to 147.1 kJ mol ⁻¹ (882 nm) for tetrachloromethane [159].
11.19 SQ1		Blue organic sensitiser dye for DSCs. Device efficiencies of ca. 4.5 % have been achieved in a single dye system; has shown promise for use in co-sensitised DSC devices with $\eta \sim 8\%$ in combination with the Ru dye N719 [160].	High absorption coefficient ($\epsilon \sim 160,000 \text{ mol}^{-1} \text{ dm}^3 \text{ cm}^{-1}$) with a relatively narrow absorption band at λ_{abs} max $\sim 630 \text{ nm}$. Absorption shifts slightly bathochromically and broadens when anchored to TiO ₂ .
11.20 SQ2		Analogous to SQ1 but supposedly more stable in DSC devices. Commercialised for use in DSCs.	Slightly higher absorption coefficient than SQ1; λ_{abs} max $\sim 635 \text{ nm}$.
11.21 Xanthione		Xanthione, and aromatic thioketones in general, are exceptions to Kasha's rule, and as a consequence show unusual photophysics.	Red emitter. Direct fluorescence is from S ₂ ($\phi_F = 0.002\text{--}0.04$) rather than S ₁ due to a large S ₂ –S ₁ energy gap ($\Delta E \sim 7600 \text{ cm}^{-1}$). Strong spin-orbit coupling results in intense phosphorescence from the first triplet excited state T ₁ . Shows both E-type and P-type delayed fluorescence with thermally activated delayed fluorescence from S ₁ , and delayed fluorescence by triplet–triplet annihilation from S ₂ . The S ₂ ϕ_F and τ (450 ps) are very solvent dependent [161].

(continued)

Table 4.1 (continued)

12. Photochromics.	Structure	Specific uses	Physical, photophysical and noteworthy properties
<p>12. Photochromics. There are two main types of photochromic systems; (i) when the isomer obtained after irradiation is unstable, the back reaction occurs thermally and these are <i>T-type</i> (thermally reversible) and (ii) <i>P-type</i> (photochemically reversible), which contain structural units that can be converted to the original state photochemically, but not thermally. Most known photochromic compounds are <i>T-type</i> with two of the most extensively studied families being azobenzenes (12.1, 12.2, and 12.3) and spiropyrans (12.4) and spiropyrans (12.1, 12.2, and 12.3). Due to their thermal stability <i>P-type</i> switches are considered the most promising candidates for applications. Two common groups of <i>P-type</i> photochromics are diarylethenes (12.5) and furylfulgides (12.6). Photochromic compounds find applications in photonic devices such as erasable optical memory and photophysical switch components. Upon the discovery of the photochromic reactions of spiropyrans, (made by Fisher and Hirschberg in 1952), Hirschberg suggested using the phenomena for a "photochemical erasable memory", research into which continues today.</p>		<p>Extensively studied for use in many applications including: data storage, temperature measurement, as a trigger for biological reactions and in molecular optical switches [162].</p>	<p>Pronounced change in geometry on going from the spiropyran (SP) to the merocyanine (MC) form (perpendicular to planar), that occurs on the sub-ns time scale and shifts the absorbance from the UV into the visible spectral range. This is due to the planarity of the MC form, which allows the previously uncoupled π-systems of chromene and indoline to become extended across the entire structure [162, 163].</p>
12.2 Spirooxazine		<p>Proposed use in displays, as filters, in eye-protective laser goggles, in self-developing photography, photoswitching of protein activity, and in optical data storage.</p>	<p>Analogous to 12.1. Different relaxation times (a long-lived and short-lived component) at various temperatures indicate two distinctly different pathways back to the closed form (SP) [164].</p>
12.3 Naphthopyran		<p>Best known for their commercial application in the ophthalmic lens industry. Other applications include electronic devices, optical memories and photo-switches.</p>	<p>UV irradiation of the colourless closed form results in electrocyclic ring opening of the pyran moiety <i>via</i> cleavage of the C(sp²)-O bond. This produces a distribution of MC isomers which are intensely coloured. As is the case for 12.1 and 12.2, this is due to their extended conjugation and <i>quasi</i>-planar conformations [165].</p>
12.4 Azobenzene		<p>The photochromic <i>trans-cis</i> isomerisation of azobenzenes has been used extensively in molecular switches. Monolayers can provide light-controlled changes in surface properties and when incorporated into crown ethers gives switchable receptors.</p>	<p>Undergoes a reversible photochemical <i>trans-cis</i> isomerisation upon irradiation with UV light (~ 340 nm) [64]. The <i>cis</i> form is energetically unfavourable and as such returns back to the <i>trans</i> form by a thermal isomerisation pathway or <i>via</i> irradiation with longer wavelength visible light.</p>

(continued)

Table 4.1 (continued)

Compound	Structure	Specific uses	Physical, photophysical and noteworthy properties
12.5 Dithienylethene		<p>Can be used in both solid state and solution. Proposed use in optical data storage.</p>	<p>Undergoes open-closed ring isomerisation and not <i>cis-trans</i> isomerisation. Thus isomerisation requires very little change of shape which results in isomerisation in a solid matrix proceeding more quickly than with most other photochromic molecules. Closed ring form is thermally stable; ring opening is achieved with visible light.</p>
12.6 Fulgides and fulgimides	<p>X = O (fulgides) X = NR (fulgimides)</p>	<p>Used in recording media, particularly in erasable optical memory devices.</p>	<p>Possess high temperature stability and high fatigue resistance; usually lack fluorescence but fluorescent derivatives are possible. The closed coloured form can be reversed to the open bleached form by visible light (>500 nm).</p>

The aim of this chapter was to provide an overview of the most common and useful photochemical materials and their primary photophysical properties that allow for use, or potential use, in a given application. In this vein, we have presented a comprehensive table detailing the most common structures, physical and photophysical properties, and specific applications of each of the classes of photochemical materials discussed.

References

1. Griffiths J (1976) *Colour and constitution of organic molecules*. Academic Press, London
2. Christie RM (2001) *Colour chemistry*. Royal Society of Chemistry, Cambridge
3. Tilley R (2011) *Colour and the optical properties of materials*, 2nd edn. Wiley, Chichester
4. Reinen D, Lindner G–G (1999) The nature of the chalcogen colour centres in ultramarine-type solids. *Chem Soc Rev* 28:75–84
5. Ball P (2002) *Bright earth, the invention of colour*. Penguin, London
6. Głowacki ED, Voss G, Leonat L et al (2012) Indigo and tyrian purple—from ancient natural dyes to modern organic semiconductors. *Israel J Chem* 52:540–551
7. Nozik AJ, Beard MC, Luther JM et al (2010) Semiconductor quantum dots and quantum dot arrays and applications of multiple exciton generation to third-generation photovoltaic solar cells. *Chem Rev* 110:6873–6890
8. Cox J (2003) A quantum paintbox. *Chem Br* 39:21–25
9. Booth K, Hill S (1998) *The essence of optoelectronics*. Prentice Hall, London
10. Webb AR (2006) Considerations for lighting in the built environment: non-visual effects of light. *Energy Build* 38:721–727
11. Lister GG, Lawler JE, Lapatovich WP, Godyak VA (2004) The physics of discharge lamps. *Rev Mod Phys* 76:541–598
12. Leverenz HW (1949) Luminescent solids (phosphors). *Science* 109:183–195
13. Feldmann C, Jüstel T, Ronda C, Schmidt PJ (2003) Inorganic luminescent materials: 100 years of research and applications. *Adv Funct Mater* 13:511–516
14. Levine AK, Palilla FC (1964) New highly efficient red-emitting cathodoluminescent phosphor (YVO₄-Eu) for color television. *Appl Phys Lett* 5:118–120
15. Commission Internationale de L'Éclairage (CIE) (1986) *Colorimetry*. Publication Report No. 15.2, IEC/CIE, Vienna
97. Fairman HS, Brill MH, Hemmendinger H (1997) How the CIE color-matching functions were derived from Wright-Guild data. *Color Res Appl* 22:11–23
17. Jüstel T, Nikol H, Ronda C (1998) New developments in the field of luminescent materials for lighting and displays. *Angew Chem Int Ed* 37:3084–3103
18. Förster T (1959) Transfer mechanisms of electronic excitation. *Disc Faraday Soc* 27:7–17
19. Dexter DL (1953) A theory of sensitized luminescence in solids. *J Chem Phys* 21:836–850
20. Bürmen M, Pernuš F, Likar B (2008) LED light sources: a survey of quality-affecting factors and methods for their assessment. *Meas Sci Technol* 19:122002
21. Schadt M (2009) Milestone in the history of field-effect liquid crystal displays and materials. *Japan J Appl Phys* 48:03B001
22. Eden JG (2006) Information display early in the 21st century: overview of selected emissive display technologies. *Proc IEEE* 94:567–574
23. Hung LS, Chen CH (2002) Recent progress of organic electroluminescent materials and devices. *Mater Sci Eng R* 39:143–222
24. Bamfield P (2001) *Chromic phenomena*. Royal Society of Chemistry, Cambridge

25. Steranka FM, Bhat J, Collins D et al (2002) High power LEDs—technology status and market applications. *Phys Stat Sol (a)* 194:380–388
26. Dupuis TD, Krames MR (2008) History, development, and applications of high-brightness visible light-emitting diodes. *J Lightwave Technol* 26:1154–1171
27. Holonyak N, Bevacqua SF (1962) Coherent (visible) light emission from Ga(As_{1-x}P_x) junctions. *Appl Phys Lett* 1:82–83
28. Nakamura S, Mukai T, Senoh M (1994) Candela-class high brightness InGaN/AlGaIn double heterostructure blue light emitting diodes. *Appl Phys Lett* 64:1687–1689
29. Ye S, Xiao F, Pan YX et al (2010) Phosphors in phosphor-converted white light-emitting diodes: recent advances in materials, techniques and properties. *Mater Sci Eng R* 71:1–34
30. Grandjean N (2010) LED light sources (light for the future). *J Phys D Appl Phys* 43:350301 and following articles
31. Salbeck J (1996) Electroluminescence with organic compounds. *Ber Bunsenges Phys Chem* 100:1667–1677
32. Tang CW (1982) Organic electroluminescent cell. U.S. Patent Number 4,356,429 (Eastman Kodak Company)
33. Friend RH, Burroughes JH, Bradley DD (1993) Electroluminescent devices. U.S. Patent Number 5,247,190 (Cambridge Research and Innovation Limited)
34. Friend RH, Gymer RW, Holmes AB et al (1999) Electroluminescence in conjugated polymers. *Nature* 397:121–128
35. Grimsdale AC, Chan KL, Martin RE et al (2009) Synthesis of light-emitting conjugated polymers for applications in electroluminescent devices. *Chem Rev* 109:897–1091
36. Thompson ME, Burrows PE, Forrest SR (1999) Electrophosphorescence in organic light emitting diodes. *Curr Opin Solid State Mater Sci* 4:369–372
37. D'Andrade BW, Forrest SR (2004) White organic light-emitting devices for solid-state lighting. *Adv Mater* 16:1585–1595
38. Evans RC, Douglas P, Winscom CJ (2006) Coordination complexes exhibiting room temperature phosphorescence: evaluation of their suitability as triplet emitters in organic light emitting diodes. *Coord Chem Rev* 250:2093–2126
39. Kamtekar KT, Monkman AP, Bryce MR (2009) Recent advances in white organic light-emitting materials and devices (WOLEDs). *Adv Mater* 22:572–582
40. Liu B, Bazan GC (2004) Homogeneous fluorescence-based DNA detection with water-soluble conjugated polymers. *Chem Mater* 16:4467–4476
41. Davies ML, Douglas P, Burrows HD et al (2011) Effect of aggregation on the photophysical properties of three fluorene–phenylene-based cationic conjugated polyelectrolytes. *J Phys Chem B* 115:6885–6892
42. Thomas SW, Joly GD, Swager TM (2007) Chemical sensors based on amplifying fluorescent conjugated polymers. *Chem Rev* 107:1339–1386
43. Achyuthan KE, Bergstedt TS, Chen L et al (2005) Fluorescence superquenching of conjugated polyelectrolytes: applications for biosensing and drug discovery. *J Mater Chem* 15:2648–2656
44. Coakley KM, McGehee MD (2004) Conjugated polymer photovoltaic cells. *Chem Mater* 16:4533–4542
45. Montalti M, Credi A, Prodi L, Gandolfi MT (2006) *Handbook of photochemistry*, 3rd edn. CRC Press, New York
46. Balzani V, Bolletta F, Scandola F (1980) Vertical and nonvertical energy transfer processes. A general classical treatment. *J Am Chem Soc* 102:2152–2163
47. Lehn J-M (1990) Perspectives in supramolecular chemistry—from molecular recognition towards molecular information processing and self-organization. *Angew Chem Int Ed* 29:1304–1319
48. Wilkinson F, Helman WP, Ross AB (1995) Rate constants for the decay and reaction of the lowest electronically excited singlet state of molecular oxygen in solution. An expanded and revised compilation. *J Phys Chem Ref Data* 24:663–677

49. Wilkinson F, Brummer JG (1981) Rate constants for the decay and reaction of the lowest electronically excited singlet state of molecular oxygen in solution. *J Phys Chem Ref Data* 10:809–999
50. Henbest K, Douglas P, Garley MS, Mills A (1994) Persulphate quenching of the excited state of ruthenium(II) tris-bipyridyl dication: thermal reactions. *J Photochem Photobiol A Chem* 80:299–305
51. Bouas-Laurent H, Dürr H (2001) Organic photochromism (IUPAC technical report). *Pure Appl Chem* 73:639–665
52. Olive AGL, Del Guerzo A, Pozzo J-L, Desvergne J-P (2007) Photoimerization of soluble tetracene derivatives using visible light. *J Phys Org Chem* 20:838–844
53. Hirshberg Y (1950) Photochromie dans la serie de la bianthrone. *Compt Rend Acad Sci* 231:903–904
54. Brown GH (ed) (1971) *Photochromism*. Wiley-Interscience, New York
55. Smith GP (1967) Photochromic glasses: properties and applications. *J Mater Sci* 2:139–152
56. Armistead WH, Stookey SD (1964) Photochromic silicate glasses sensitized by silver halides. *Science* 144:150–154
57. Crano JC, Flood T, Knowles D et al (1996) Photochromic compounds: chemistry and application in ophthalmic lenses. *Pure Appl Chem* 68:1395–1398
58. Corns SN, Partington SM, Towns A (2009) Industrial organic photochromic dyes. *Color Technol* 125:249–261
59. Dürr H, Bouas-Laurent H (eds) (1990) *Photochromism: molecules and systems*. Elsevier, Amsterdam
60. Crano JC, Guglielmetti RJ (eds) (2001) *Organic photochromic and thermochromic compounds*, vols 1 and 2. Plenum, New York
61. Irie M (2000) Photochromism: memories and switches. *Chem Rev* 100:1683 and following articles
62. Favaro G, Irie M (eds) (2011) Special issue on photochromism. *J Photochem Photobiol C* 12:71–236
63. Wyman GM (1955) The *cis-trans* isomerization of conjugated compounds. *Chem Rev* 55:625–657
64. Zimmerman G, Chow LY, Paik UJ (1958) The photochemical isomerization of azobenzene. *J Am Chem Soc* 80:3528–3531
65. Ercole F, Davis TP, Evans RA (2010) Photo-responsive systems and biomaterials: photochromic polymers, light-triggered self-assembly, surface modification, fluorescence modulation and beyond. *Polym Chem* 1:37–54
66. Hampp N (2000) Bacteriorhodopsin as a photochromic retinal protein for optical memories. *Chem Rev* 100:1755–1776
67. Matsuda K, Irie M (2004) Diarylethene as a photoswitching unit. *J Photochem Photobiol C* 5:169–182
68. Yokoyama Y (2000) Fulgides for memories and switches. *Chem Rev* 100:1717–1739
69. Corval A, Kuldová K, Eichen Y et al (1996) Photochromism and thermochromism driven by intramolecular proton transfer in dinitrobenzylpyridine compounds. *J Phys Chem* 100:19315–19320
70. Naumov P (2006) Photochromism of *ortho*-nitrobenzylpyridines: a brief overview. *J Mol Struct* 783:1–8
71. Irie M, Miyatake O, Uchida K (1992) Blocked photochromism of diarylethenes. *J Am Chem Soc* 114:8715–8716
72. Pina F, Petrov V, Laia CAR (2012) Photochromism of flavylum systems. An overview of a versatile multistate system. *Dyes Pigments* 92:877–889
73. Uchida M, Irie M (1993) Two-photon photochromism of a naphthopyran derivative. *J Am Chem Soc* 115:6442–6443
74. Parthenopoulos DA, Rentzepis PM (1989) Three-dimensional optical storage memory. *Science* 245:843–845
75. Towns A (2012) Olympian colour chemistry. *Chem Ind* 76:32–35

76. Wang PY, Wu CJ (1997) Photochromic behavior of some phenoxyanthroquinone dyes in solution and on polyester substrate. *Dyes Pigments* 35:279–288
77. Cheng T, Lin T, Brady R, Wang X (2008) Photochromic fabrics with improved durability and photochromic performance. *Fibers Polym* 9:521–526
78. Moore GE (1965) Cramming more components onto integrated circuits. *Electronics* 38:4–7
79. Kawata S, Kawata Y (2000) Three-dimensional optical data storage using photochromic materials. *Chem Rev* 100:1777–1788
80. Tsujioka T, Irie M (1998) Fluorescence readout of near-field photochromic memory. *Appl Opt* 115:119458–119460
81. Balzani V, Credi A, Venturi M (2008) Molecular devices and machines. Concepts and perspectives. Wiley-VCH, Weinheim
82. Natali M, Giordani S (2012) Molecular switches as photocontrollable “smart” receptors. *Chem Soc Rev* 41:4010–4029
83. de Silva AP, McClenaghan ND (2004) Molecular-scale logic gates. *Chem Eur J* 10:574–586
84. <http://www.zyvex.com/nanotech/feynman.html>. Accessed 25 August 2012
85. Feringa BL (ed) (2001) Molecular switches. Wiley-VCH, Weinheim
86. Feringa BL (2001) In control of motion: from molecular switches to molecular motors. *Acc Chem Res* 34:504–513
87. Russew M–M, Hecht S (2010) Photoswitches: from molecules to materials. *Adv Mater* 22:3348–3360
88. Balzani V, Credi A, Venturi M (2009) Light powered molecular machines. *Chem Soc Rev* 38:1542–1550
89. Leo WR (ed) (1994) Techniques for nuclear and particle physics experiments, 2nd edn. Springer, Berlin
90. Hepp A, Heil H, Weise W et al (2003) Light-emitting field-effect transistor based on a tetracene thin film. *Phys Rev Lett* 91:406–410
91. Takahashi T, Takenobu T, Takeya J, Iwasa Y (2007) Ambipolar light-emitting transistors of a tetracene single crystal. *Adv Funct Mater* 17:1623–1628
92. Katraró R, Ron A, Speiser S (1979) Photophysical studies of coronene and 1,12-benzperylene. Self-quenching, photoquenching, temperature dependent fluorescence decay and temperature dependent electronic energy transfer to dye acceptors. *Chem Phys* 42:121–132V
93. Glushko V, Thaler MSR, Karp CD (1981) Pyrene fluorescence fine structure as a polarity probe of hydrophobic regions: behavior in model solvents. *Arch Biochem Biophys* 210:33–42
94. Lakowicz JR, Knutson JR (1980) Hindered depolarizing rotations of perylene in lipid bilayers. Detection by lifetime-resolved fluorescence anisotropy measurements. *Biochemistry* 19:905–911
95. Armstrong N, Wightman M, Gross E (2001) Light-emitting electrochemical processes. *Annu Rev Phys Chem* 52:391–422
96. Hoven CV, Garcia A, Bazan GC, Nguyen TQ (2008) Recent applications of conjugated polyelectrolytes in optoelectronic devices. *Adv Mater* 20:3793–3810
97. Vaschetto ME, Monkman AP, Springborg M (1999) First-principles studies of some conducting polymers: PPP, PPy, PPV, PPyV, and PANI. *J Mol Struct Theochem* 468:181–191
98. Rehahn M, Schlüter AD, Wegner G (1990) Soluble poly(para-phenylene)s 3. Variation of the length and the density of the solubilizing side chains. *Makromol Chem* 191:1991–2003
99. Yang Y, Pei Q, Heeger AJ (1996) Efficient blue polymer light-emitting diodes from a series of soluble poly(paraphenylene)s. *J Appl Phys* 79:934–939
100. Burroughes JH, Bradley DDC, Brown AR et al (1990) Light-emitting diodes based on conjugated polymers. *Nature* 347:539–541
101. Li J, Sun N, Guo ZX et al (2002) Photovoltaic devices with methanofullerenes as electron acceptors. *J Phys Chem B* 106:11509–11514

102. Grüner JF, Hamer P, Friend RH et al (1994) A high efficiency blue-light-emitting diode based on novel ladder poly(p-phenylene)s. *Adv Mater* 6:748–752
103. Li Z, Meng H (eds) (2007) *Organic light-emitting materials and devices*. CRC Press, New York
104. Takahashi K, Seto K, Yamaguchi T et al (2004) Performance enhancement by blending an electron acceptor in TiO₂/polyphenylenevinylene/Au solid-state solar cells. *Chem Lett* 33:1042–1043
105. Yang M, Zhang Q (2004) Organic light emitting diodes based on multi-wall carbon nanotubes (MWNTs) modified electrode. *J Mater Sci* 39:3777–3778
106. Shen F, He F, Lu D et al (2006) Bright and colour stable white polymer light-emitting diodes. *Semi Sci Tech* 22:L16–L19
107. Moses D (1993) High quantum efficiency luminescence from a conducting polymer in solution: a polymer laser dye. *Synth Met* 55:22–27
108. Chen L, McBranch DW, Wang HL et al (1999) Highly sensitive biological and chemical sensors based on reversible fluorescence quenching in a conjugated polymer. *Proc Nat Acad Sci USA* 96:12287–12292
109. Gerard M, Chaubey A, Malhotra BD (2002) Application of conducting polymers to biosensors. *Biosens Bioelectron* 17:345–359
110. Scherf U, Neher D (eds) (2008) *Polyfluorenes: Advances in Polymer Science*. Springer, Berlin
111. Davies ML, Burrows HD, Morán MC et al (2009) Cationic fluorene-based conjugated polyelectrolytes induce compaction and bridging in DNA. *Biomacromolecules* 10:2987–2997
112. Liu B, Bazan GC (2004) Homogeneous fluorescence-based DNA detection with water-soluble conjugated polymers. *Chem Mater* 16:4467–4476
113. Garnier F (1998) Field-effect transistors based on conjugated materials. In: Müllen K, Wegner G (eds) *Electronic materials: the oligomer approach*. Wiley-VCH, Weinheim
114. Tsiminis G, Ruseckas A, Samuel IDW, Turnbull GA (2009) A two-photon pumped polyfluorene laser. *Appl Phys Lett* 94:253304-1-253304-3
115. Price S, Stuart A, Yang L, Zhou H (2011) Fluorine substituted conjugated polymer of medium band gap yields 7% efficiency in polymer–fullerene solar cells. *J Am Chem Soc* 133:4625–4631
116. Scheinert S, Doll T, Scherer A et al (2004) Organic field-effect transistors with nonlithographically defined submicrometer channel length. *Appl Phys Lett* 84:4427–4429
117. Landi BJ, Raffaella RP, Castro SL, Bailey SG (2005) Single-wall carbon nanotube–polymer solar cells. *Prog Photovolt Res Appl* 13:165–172
118. Do H, Reinhard M, Vogeler H et al (2009) Polymeric anodes from poly(3,4-ethylenedioxythiophene):poly(styrenesulfonate) for 3.5% efficient organic solar cells. *Thin Solid Films* 517:5900–5902
119. Kubin RF, Fletcher AN (1982) Fluorescence quantum yields of some rhodamine dyes. *J Lumin* 27:455–462
120. Casey KG, Quitevis EL (1988) Effect of solvent polarity on nonradiative processes in xanthene dyes: Rhodamine B in normal alcohols. *J Phys Chem* 92:6590–6594
121. Schäfer FP (1990) *Dye lasers*, 3rd edn. Springer, Berlin
122. Duarte FJ, Hillman LW (1990) *Dye laser principles*. Academic, New York
123. De Bernardo S, Weigele M, Toome V et al (1974) Studies on the reaction of fluorescamine with primary amines. *Arch Biochem Biophys* 163:390
124. DeRosa MC, Crutchley RJ (2002) Photosensitized singlet oxygen and its application. *Coord Chem Rev* 233–234:351–371
125. Seybold PG, Gouterman M, Callis J (1969) Calometric, photometric and lifetime determinations of fluorescence yields of fluorescein dyes. *Photochem Photobiol* 9:229–242
126. Johnson I, Spence MTZ, *Molecular probes handbook—a guide to fluorescent probes and labelling technologies*, 11th edn. Life Technologies, Carlsbad

127. Noukakis D, Auweraer MV, Toppet S, De Schryver FC (1995) Photophysics of thiacyanocyanine dye in organic solvent. *J Phys Chem* 99:11860–11866
128. Jabbour GE, Wang JF, Peyghambarian N (2002) High-efficiency organic electrophosphorescent devices through balance of charge injection. *Appl Phys Lett* 80:2026–2028
129. Barnett GH, Hudson MF, Smith KM (1975) Concerning meso-tetraphenylporphyrin purification. *J Chem Soc Perkin Trans 1* 1401–1403
130. Strachan JP, Gentemann S, Seth J et al (1997) Effects of orbital ordering on electronic communication in multiporphyrin arrays. *J Am Chem Soc* 119:11191–11201
131. Baldo MA, O'Brien DF, You Y et al (1998) Highly efficient phosphorescent emission from organic electroluminescent devices. *Nature* 395:151–154
132. Cleave V, Yahsioglu G, Barny PL et al (1999) Harvesting singlet and triplet energy in polymer LEDs. *Adv Mater* 11:285–288
133. Whalley M (1961) Conjugated macrocycles. Part XXXII. Absorption spectra of tetrazaporphins and phthalocyanines. Formation of pyridine salts. *J Chem Soc* 866–869
134. Tang CW (1986) Two-layer organic photovoltaic cell. *Appl Phys Lett* 48:183–185
135. Pfuetzner S, Meiss J, Petrich A et al (2009) Thick C60:ZnPc bulk heterojunction solar cells with improved performance by film deposition on heated substrates. *Appl Phys Lett* 94:253303-1–253303-3
136. Kumar GA, Santhosh C (2003) Spectral studies and radiative characteristics of naphthalocyanine molecules in DMF. *Mater Lett* 57:2315–2319
137. Tang CW, Van Slyke SA (1987) Organic electroluminescent diodes. *Appl Phys Lett* 51:913–915
138. Hoshi T, Kumagai K, Inoue K et al (2008) Electronic absorption and emission spectra of Alq3 in solution with special attention to a delayed fluorescence. *J Lumin* 128:1353–1358
139. O'Regan B, Grätzel M (1991) A low-cost, high-efficiency solar cell based on dye-sensitized colloidal TiO₂ films. *Nature* 353:737–740
140. Nazeeruddin MK, De Angelis F, Fantacci S et al (2005) Combined experimental and DFT-TDDFT computational study of photoelectrochemical cell ruthenium sensitizers. *J Am Chem Soc* 127:16835–16847
141. Nazeeruddin MK, Péchy P, Renouard T et al (2001) Engineering of efficient panchromatic sensitizers for nanocrystalline TiO₂-based solar cells. *J Am Chem Soc* 123:1613–1624
142. Deaton JC, Young RH, Lenhard JR et al (2010) Photophysical properties of the series fac- and mer-(1-phenylisoquinolino[2,2′](x)(2-phenylpyridinato-NC2′)₃ – x iridium(III) (x = 1–3). *Inorg Chem* 49:9151–9161
143. Fischer H, Baer R, Hany R et al (1990) 2,2-Dimethoxy-2-phenylacetophenone: photochemistry and free radical photofragmentation. *J Chem Soc Perkin Trans 2* (5):787–798
144. Iwamoto S, Kai W, Isogai T et al (2010) Comparison study of TEMPO-analogous compounds on oxidation efficiency of wood cellulose for preparation of cellulose nanofibrils. *Polym Degrad Stabil* 95:1394–1398
145. Kamibayashi M, Oowada S, Kameda H et al (2006) Synthesis and characterization of a practically better DEPMPO-type spin trap, 5-(2,2-dimethyl-1,3-propoxy cyclophosphoryl)-5-methyl-1-pyrroline N-oxide (CYPMPO). *Free Radic Res* 40:1166–1172
146. Dambrova M, Baumanca L, Kalvinsha I, Wikberg JES (2000) Improved method for EPR detection of DEPMPO-superoxide radicals by liquid nitrogen freezing. *Biochem Biophys Res Commun* 275:895–898
147. Hagfeldt A, Boschloo G, Sun L et al (2010) Dye-sensitized solar cells. *Chem Rev* 110:6595–6663
148. Zhang XT, Liu YC, Zhi ZZ et al (2002) Temperature dependence of excitonic luminescence from nanocrystalline ZnO films. *J Lumin* 99:149–154
149. Reynolds D, Leies G, Antes L, Marburger R (1954) Photovoltaic effect in cadmium sulfide. *Phys Rev* 96:533–534

150. Bube RH (1955) Temperature dependence of the width of the band gap in several photoconductors. *Phys Rev* 98:431–433
151. Mali SS, Desai SK, Kalagi SS et al (2012) PbS quantum dot sensitized anatase TiO₂ nanocorals for quantum dot-sensitized solar cell applications. *Dalton Trans* 41:6130–6136
152. Zhang S, Nakai Y, Tsuboi T et al (2011) The thermal stabilities of luminescence and microstructures of Eu²⁺-doped KBaPO₄ and NaSrPO₄ with β -K₂SO₄ type structure. *Inorg Chem* 50:2897–2904
153. Lu J, Yagi H, Takaichi K et al (2004) 110 W ceramic Nd³⁺: Y₃Al₅O₁₂ laser. *Appl Phys B* 79:25–28
154. Vielhaber G, Grether-Beck S, Koch O et al (2006) Sunscreens with an absorption maximum of ≥ 360 nm provide optimal protection against UVA1-induced expression of matrix metalloproteinase-1, interleukin-1, and interleukin-6 in human dermal fibroblasts. *Photochem Photobiol Sci* 5:275–282
155. Zechmeister L, Polgar A (1943) Cis-trans isomerization and spectral characteristics of carotenoids and some related compounds. *J Am Chem Soc* 65:1522–1528
156. Naguiba YMA, Steel C, Young MA (2001) Decay kinetics of photosensitized triplet crystal violet in acetonitrile. *J Photochem Photobiol A-Chem* 141:33–38
157. Tuite EM, Kelly JM (1993) New trends in photobiology: photochemical interactions of methylene blue and analogues with DNA and other biological substrates. *J Photochem Photobiol B-Biol* 21:103–124
158. Pattanaargson S, Munhapol T, Hirunsupachot P, Luangthongaram P (2004) Photoisomerization of octyl methoxycinnamate. *J Photochem Photobiol A-Chem* 161:269–274
159. Reichardt C (1994) Solvatochromic dyes as solvent polarity indicators. *Chem Rev* 94:231–2358
160. Holliman PJ, Davies ML, Connell A et al (2010) Ultra-fast dye sensitisation and co-sensitisation for dye sensitized solar cells. *Chem Commun* 46:7256–7258
161. Ho CJ, Motyka AL, Topp MR (1989) Picosecond time-resolved S₂ → S₀ fluorescence of xanthione in different fluid solvents. *Chem Phys Lett* 158:51–59
162. Seefeldt B, Kasper R, Beining M et al (2010) Spiropyrans as molecular optical switches. *Photochem Photobiol Sci* 9:213–220
163. Landgraf JK, Braun M, Özçoban C et al (2012) Ultrafast dynamics of a spirocyan in water. *J Am Chem Soc* 134:14070–14077
164. Chibisov AK, Görner H (2001) Photochromism of spirobenzopyranindolines and spironaphthopyranindolines. *Phys Chem Chem Phys* 3:424–431
165. Ercole F, Malic N, Davis TP, Evans RA (2009) Optimizing the photochromic performance of naphthopyrans in a rigid host matrix using poly(dimethylsiloxane) conjugation. *J Mater Chem* 19:5612–5623
166. Gray GW, Kelly SM (1999) Liquid crystals for twisted nematic display devices. *J Mater Chem* 9:2037–2050
167. Lumileds Corporation (2004) Luxeon Reliability. Application Brief AB25 11

Chapter 5

Atmospheric Photochemistry

Rod S. Mason

Abstract The main photochemical processes occurring in the Earth's atmosphere and their effects on its chemistry and structure are described. The solar flux and its interaction with the components of air are discussed in Sect. 5.1. Of these, O₂ is the most photochemically active, UV absorption causing photodecomposition into ground state and excited state O atoms (Sect. 5.2). This causes differential heating of the atmosphere as the solar flux passes through. Without this, the air in thermal equilibrium cools with increasing altitude due to the effect of gravity. Combining the two effects creates the distinct layers (Sect. 5.3) known as the tropo-, strato-, meso- and thermo-spheres. Other designations e.g. the high altitude (D–F) regions containing high charge density are due to photo-ionisation. The detailed photochemistry of each region is discussed in Sects. 5.4–5.7, dominated at high altitude by oxygen atom and ozone reactions, which culminates in the stratospheric ozone layer. Ozone depletion due to the photochemistry involving chlorofluorocarbons is discussed. Comparatively little UV penetrates through to the troposphere, except enough to induce the formation of OH. It is the secondary reactions of OH which set off the oxidative chain reactions which dominate low altitude chemistry and initiates ground level ozone production. The combination of strong sunlight and automobile emissions causes photochemical smog. Aerosols play a vital role in dissolving the soluble reactants and oxidised hydrocarbons formed, thus removing them from the atmosphere by deposition as rain, and completing the cycle of pollutant emission and removal from the atmosphere.

R. S. Mason (✉)

Physical Science Solutions Ltd, 28 Fernhill Close, Blackpill, Swansea SA3 5BX, UK
e-mail: rodsamason@gmail.com

R. S. Mason

Physical Chemistry, Institute of Mass Spectrometry, College of Medicine, Swansea University, Singleton Park, Swansea SA2 8PP, UK

5.1 Introduction

Atmospheric chemistry is driven almost entirely by photochemical reactions, which result from the interaction of air with solar radiation. Table 5.1 lists the main components of air, in order of their abundance, and Fig. 5.1 shows the extraterrestrial solar spectrum in comparison with the spectrum at ground level, to demonstrate the significant level of attenuation depending on wavelength. There are clear strong absorption bands, for example between 750 and 3500 nm, due to the presence of CO₂, O₃, CH₄ and H₂O. Back-scattering also occurs, both off individual molecules (Rayleigh effect) and particulates (Mie effect); in the latter case, particularly off clouds. Chemical reaction, however, is initiated mostly by absorptions in the UV causing decomposition, and the most important process is the photodissociation of O₂ ($\lambda < 240$ nm). The next most important is dissociation of O₃ ($\lambda < 320$ nm), which itself is a secondary by-product of the O₂ reaction. Other important primary photochemical reactions involve NO₂, etc. (see Table 5.2). Whilst photochemically active, O₂ is still a relatively stable gas with an average residence time (see below for definition) in the atmosphere of ~ 2500 years, which compares with a few minutes, days or months (depending on its location) for ozone.

Table 5.1 Gases contained in air with abundance levels >0.01 ppm, bond dissociation energies (BDE), photodissociation thresholds (λ_{thresh}), and residence time (τ_{res}) in the atmosphere

Gas	Abundance (% or ppm by vol.)	^a BDE (298 K) (kJ mol ⁻¹)	^b Photodissociation threshold (λ_{thresh}) (nm)	^c Residence time
N ₂	78.1 %	945	<127	$\sim 2 \times 10^7$ yrs
O ₂	20.9 %	498	<240	~ 2500 yrs
Ar	0.93 %			
H ₂ O ^d	0.4 % (0–4 % at surface)	498	<240	~ 9 days
CO ₂ ^e	0.039 %	532	<225	~ 5 yrs
Ne	18 ppm			
He	5.2 ppm			
CH ₄	1.8 ppm	438	<273	~ 9 yrs
Kr	1.1 ppm			
H ₂	0.6 ppm	436	<274	~ 4 yrs
N ₂ O	0.3 ppm	167	<716	~ 94 yrs
CO	~ 0.1 ppm	1077	<111	~ 0.2 yrs
Xe	0.09 ppm			
O ₃ ^d	0–0.07 ppm	105	<1139	2–3 weeks
NO ₂ ^d	~ 0.02 ppm	305	<392	^f

^a Reference [1]

^b As given by the formula $\lambda_{\text{thresh}} = hc/\text{BDE}$, where h = Planck's constant, c is the velocity of light

^c As given in Ref. [2]

^d Variable depending on location, season, time of day etc.

^e As at July 2011, rising by ~ 1.5 ppm per annum [3]

^f Half-life in unpolluted air, in the absence of UV, is >50 days

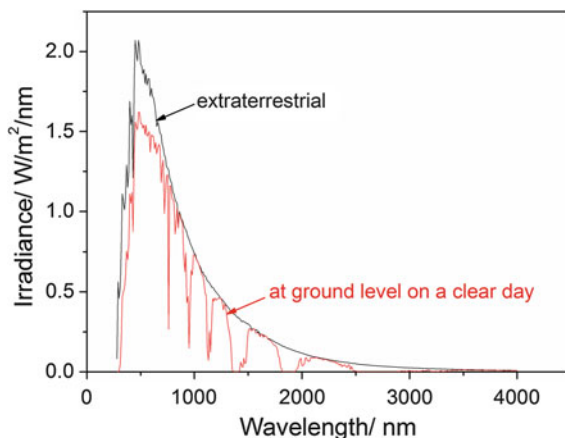


Fig. 5.1 Solar spectrum: comparison between extraterrestrial and ground level fluxes. The data used are taken from Ref. [4]

Incident radiation, I_λ , which survives after penetrating the atmosphere to a specific altitude, z , is called the *actinic flux*. Its value not only depends on z , but also the location with respect to the Earth's surface, the time of day and year (and hence the angle of the sun), and the weather conditions (e.g. cloud cover or pollution levels). The azimuthal angle of the sun, θ , matters because the solar flux passing through a unit area of a plane perpendicular to the incident line from the sun, is spread over a larger area when the receiving surface is set at an angle ($\theta > 0^\circ$) with respect to that plane. The incident flux per unit area of the surface is less by the factor $\cos\theta$; therefore, as is very well known, the flux at the poles tends to zero in the winter ($\theta \rightarrow 90^\circ$).

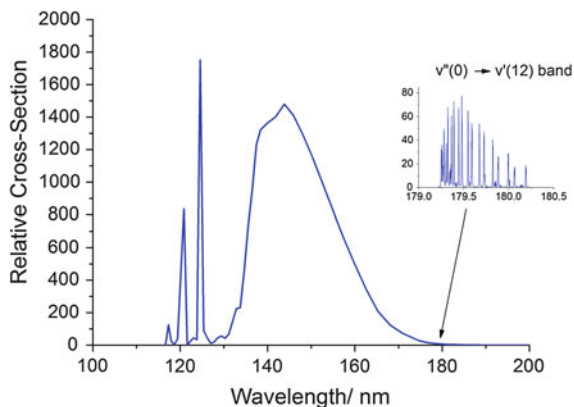
The thermodynamic threshold for molecular decomposition is the molecule's lowest bond dissociation energy (BDE), also shown in Table 5.1, and this determines the absolute maximum wavelength ($\lambda_{\max} = hc/\text{BDE}$ where h is Planck's constant and c is the speed of light), above which photodecomposition is energetically impossible. The most abundant gases require wavelengths < 240 nm, which are at relatively very low intensities, even in the extraterrestrial solar spectrum. Whether photons below λ_{\max} are actually absorbed, or not, depends of course on the absorption spectrum of the molecule concerned. Thus, Fig. 5.2 shows the O_2 UV absorption spectrum, which rises through a low intensity discrete banded system (*Schumann-Runge*) from ~ 195 nm up to ~ 175 nm, and then as a continuum up to a maximum at ~ 140 nm. The rate coefficient (*i.e.* the probability) for photodecomposition in the atmosphere, e.g. for the reaction:



is usually represented by the symbol J , which is given at a specific altitude by

Table 5.2 List of the most important photochemical reactions in the atmosphere, $X + h\nu \rightarrow$ products

X	Products	λ (nm)	Region
N ₂	N ₂ ⁺ + e ⁻	<80	Ionosphere
	N ⁺ + N + e ⁻	<51	
O ₂	O ₂ ⁺ + e ⁻	<102	Ionosphere
	O ⁺ + O + e ⁻	<66	
O ₂	O(³ P) + O(¹ D)	<240	Stratosphere and above
	O(³ P) + O(³ P)		
H ₂ O	H + OH	<240	Stratosphere and above
C _x F _y Cl _{2x+2-y} e.g. CF ₂ Cl ₂	Cl + C _x F _y Cl _{2x+1-y}	<220	Stratosphere and above
	e.g. Cl + CF ₂ Cl		
OCS	CO + S	<290	Stratosphere and above
O ₃	O(¹ D) + O ₂ (a ¹ Δ _g)	<310	Mainly stratosphere some troposphere
	O(³ P) + O ₂ (X ³ Σ _g ⁻)		
(ClO) ₂	Cl + ClO ₂	<400	Stratosphere
NO ₂	NO + O	<410	Throughout

**Fig. 5.2** UV absorption spectrum of O₂ (*inset*: part of the Schumann-Runge range, showing the X³Σ_g⁻(v = 0) to B³Σ_u⁻(v = 12) band in high resolution); data used were taken from Ref. [5]

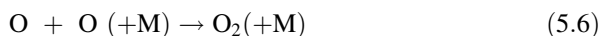
$$J(\text{s}^{-1}) = \int_{\lambda} I_{\lambda} \sigma_{\lambda} \phi_{\lambda} d\lambda \quad (5.2)$$

where I_{λ} is the actinic flux of photons of wavelength λ entering the reaction volume, σ_{λ} is the absorption cross-section, and ϕ_{λ} is the quantum yield for this reaction channel. The rate of reaction is then given by

$$R_z = J_z n_z \quad (5.3)$$

where n_z is the molecular density of the reacting gas, which obviously also changes with altitude.

There are three factors affecting the steady state density of gases of the atmosphere: total rate of emission into the atmosphere, residence time (τ_{res}) and altitude. τ_{res} is defined for a steady-state concentration of gas, measured, for example, as its total mass M kg in the containing volume, as the time taken to completely replace that gas. Thus if the total incoming flux of gas (from whatever source) into the containing volume is ΔM kg/yr (and since it is in steady state, that is also the total flux of the outgoing gas), then $\tau_{\text{res}} = M/\Delta M$ years. Gas residence times are therefore determined by their rates of formation (source) and removal (sink) from the atmosphere. For a given gas, there are usually many sources and sinks; the main source of O_2 for example is the photochemical biogenic reaction between carbon dioxide and water to form carbohydrates, whilst its main sink is the reverse process of organic oxidative decay. But there is (amongst other processes) a minor (<10 %) inorganic source caused by the photolysis of water vapour: reactions (5.4) to (5.6). This is self-limiting due to complete absorption of the necessary UV by the time it has penetrated towards the lower altitudes. There are also minor sinks, such as the surface oxidation of minerals. Whilst most of the sources and sinks for O_2 are known, in general, identification and quantification of all the sources and/or sinks of the atmospheric gases remains a significant stumbling block in the accurate predictive modelling of atmospheric chemistry.



Atmospheric residence times for significant gases in the atmosphere are given in Table 5.1. N_2 is very large because it is an unreactive gas and is relatively insoluble in water. You might expect CO_2 and O_2 to have similar values since these two gases are locked into the carbon cycle. However a major difference is that CO_2 dissolves and reacts readily in water to form carbonic acid. O_2 is relatively insoluble and therefore the main reservoir of O_2 is the atmosphere, whilst that for CO_2 is in the ocean. CO_2 therefore has a minor presence in the atmosphere, but the rates of formation and removal are similar to that of O_2 , hence the residence time of O_2 is about a thousand times longer.

Reactive gases have very short residence times; for example, the main source of O_3 is the photolysis of O_2 in the upper atmosphere, but since it is very reactive and decomposes readily, its residence time is only ~ 1 month in the stratosphere, but a few minutes or hours at ground level. It is dependent on its location in the atmosphere, the time of day etc. as is the case for all the other reactive trace components of the atmosphere.

The second factor affecting gas density is of course altitude. Gases with long residence times, such as O_2 , decrease exponentially in pressure with increasing altitude due to the decrease in the gravitational force. In general this is expressed in the barometric formula as

$$n_z = n_0 e^{z/H} \quad (5.7)$$

where H is called the *scale height* and for an ideal gas under idealised conditions is given by $H = RT/mg$, where R is the gas constant, T is the temperature (Kelvin), m is the relative molar mass and g is the acceleration due to gravity. For a gas mixture, m is the weighted molar mass of the mixture (thus $m_{air} = 28.8$) at 1 bar total pressure. The latter remains true only so long as the pressure is high enough for bulk transport properties to operate (*i.e.* the gas mixture behaves as if it were a single gas with the weighted average properties of the mixture). Above $z \approx 80$ km the gas density is reduced to $<4 \times 10^{14} \text{ cm}^{-3}$ (*cf.* $2.5 \times 10^{19} \text{ cm}^{-3}$ when $z = 0$), when the gas behaviour starts to depend on individual molecular properties, and gravitational separation therefore occurs with the lightest gases (H, H₂) becoming more prevalent towards the top of the atmosphere.

I_z is obviously greatest at the top of the atmosphere and decreases as it is absorbed or scattered, on its way down. As can be seen from Fig. 5.1, at ground level, radiation with $\lambda < 240$ nm has been completely absorbed; therefore the greatest degree of photochemical activity occurs in the upper atmosphere. In fact it comes to a maximum at about $z = 25$ km, in a region which is known as the stratosphere. Photodecomposition is a very minor reaction in the layer of air closest to the surface (the *troposphere*), affecting only trace gases with low bond energies, such as O₃ (see Table 5.1). This does not mean that photochemistry is not important in the troposphere; on the contrary, because of the chain reactions that ensue, it also is critical to the chemistry of the lower atmosphere. We start, however, with the most important processes.

5.2 Absorption of UV by O₂

Relevant potential energy (PE) curves for O₂ are shown in Fig. 5.3. The ground state ($X^3\Sigma_g^-$) and a number of bound excited states (not shown) and the repulsive state ($^5\Pi_u$) all correlate with the ground state atoms: O(³P) + O(³P). The excited bound state ($B^3\Sigma_u^-$) correlates with the first excited and ground state atoms O(¹D) + O(³P). The strong absorption spectrum in Fig. 5.2 is attributed mainly to the X → B transition, and is called the Schumann-Runge system. Transitions to intermediate states creating two ground state atoms do occur, but are relatively weak, because they are optically forbidden. The discrete banded part of the spectrum in Fig. 5.2 is due to rovibronic transitions into bound vibrational levels of the upper state. When absorptions occur into levels above the dissociation limit of the B state, they appear as a continuum, causing decomposition into the excited and ground state atoms. However a proportion of transitions ($\lambda > 175$ nm) into the B state leads to the formation of two ground state atoms *via* the predissociation route, due to the intersystem crossing from bound states of B to the repulsive Π state. The transition energy in excess of the minimum required to cause decomposition is dispersed in the form of the kinetic energy of the separating atoms. This creates ‘hot’ atoms, which are cooled by collisional transfer to surrounding molecules, which become heated. In the highest parts of the atmosphere, where the

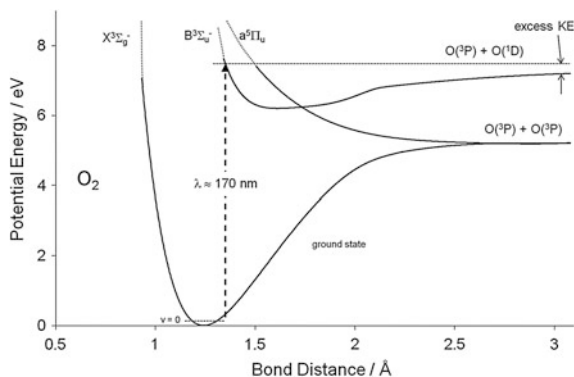


Fig. 5.3 Potential energy curves known to be important in the photochemistry of O_2 , showing vertical transition by absorption of a ~ 170 nm photon, to form kinetically ‘hot’ excited and ground state O atoms by photodissociation

pressure is very low, and collisions are therefore much less frequent, this region is characterised by the presence of ‘hot’ atoms, not only O, but also atoms of the other decomposed gases (e.g. N and H). Although, at this height, the internal energy of molecules remains cold, the existence of these kinetically hot atoms with a high mixing ratio give this very low pressure region of the atmosphere its description as the *thermosphere*.

In the lower parts of the atmosphere, the collisional dispersal of the excess kinetic energy leads to molecular heating, and proper equilibration of the energy distribution. The resulting increase in temperature of the air due to this effect reaches its maximum in the *stratosphere*.

5.3 Vertical Structure of the Atmosphere

The atmosphere is quite clearly and distinctly divided into a series of vertical layers of air (see Fig. 5.4), some of which have already been referred to. The layers are labelled (with increasing z): the *troposphere*, *stratosphere*, *mesosphere* and *thermosphere*, and they are caused by a combination of photochemistry, air temperature, and the effect of gravity on gas mixing due to convection. As discussed above, air pressure decays exponentially with increasing z , finally reaching the pressure of outer space at a distance $>10^5$ km; however 99.99 % of the air mass is located below $z = 100$ km. The depth of identified air layers is therefore a small fraction of the diameter of the Earth ($d = 12740$ km; the thickness of the troposphere is <0.12 % of this value). The stratosphere, which is photochemically the most active region, lies approximately in the range $10 < z < 50$ km (the actual boundaries vary with location, season and time of day).

The boundaries between the layers are delineated by reversals in the temperature gradient, which are as a direct result of the photochemistry. In the absence of

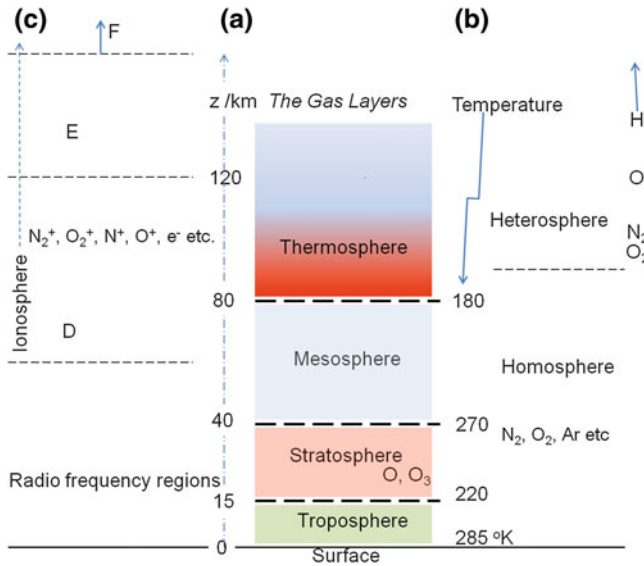


Fig. 5.4 Vertical structure of the atmosphere at a glance; **a** layers of air, and temperature, **b** chemical mixing, **c** radio wave reflection levels. Values given are very approximate, and depend on location and season

photochemistry the steady state average temperature at any point z , is determined by the fact that at each point the average kinetic energy (KE) of air molecules must be balanced by the potential energy (PE), *i.e.* the energy provided by the force due to gravity. If the KE was greater than this PE, the molecules would be able to escape, and be lost from the atmosphere; if it were less they would be pulled closer to the Earth's surface, until they were in balance. Therefore since gravity (and therefore PE) decreases, the air temperature also decreases with increasing z , an effect which is known as *adiabatic cooling*. It has a value of between 7 and 10 $K km^{-1}$, depending on the amount of water vapour present. Condensation is an exothermic process, therefore as the air cools, condensing water vapour makes an input into the energy balance, diminishing the degree of cooling.

As discussed above, absorption of radiation by air molecules and photodecomposition is also exothermic, and O_2 is the most abundant of the photochemically active gases present in the atmosphere. At high z , I_z is high, but n_z is low, and therefore R_z is low (see Sect. 5.3). At low z , n_z is high, but I_z is very low because of its absorption already in the upper atmosphere, and again R_z is low. Therefore R_z reaches a maximum at the intermediate altitudes, *i.e.* in the stratosphere where the *solar heating* effect more than offsets the *adiabatic cooling* effect. The result is that, whilst air temperature decreases with increasing z throughout the tropo- and meso-spheres, it increases throughout the stratosphere. The regions of temperature inversion at the boundaries are called the *tropo-, strato- and meso-pauses*.

Much of the heat generated is manifested in the kinetic energy of the photodecomposition products which are expelled from repulsive excited state potential energy surfaces (Fig. 5.3), following UV absorption. This excess kinetic energy is rapidly dispersed between all particles of the gas mixture and equilibrated across all energy modes (vibration and rotation) as a result of collision. However, above about 85 km, the air is so thin that the collision frequency is too low for the excess energy to equilibrate. The region therefore becomes dominated by the particles with high kinetic energy but very low molecular temperature, the disparity increasing with z . It is from this region, the *thermosphere*, that atoms and molecules (particularly H_2) escape the Earth's atmosphere. Since there is not thermal equilibrium, the notion of 'temperature' in this region is not strictly appropriate.

Despite direct absorption of solar radiation, and scattering, it is clear from Fig. 5.1 that the air is transparent to most of the incoming radiation, which therefore reaches and heats up the Earth's surface. The air is therefore heated mainly by contact with the surface which causes convection, thus leading to vertical mixing of the air. The mechanism is that a package of air heated above ambient at the surface expands and rises due to becoming less dense than surrounding air, setting up a convection current. The air packet would keep rising until it reaches surrounding air which is of the same density; as it rises, it expands due to the fall in pressure, so it cools, but it must lose energy to its surroundings faster than the rate of change of adiabatic cooling in order for the gas to equilibrate with the surrounding air and hence become stationary. It therefore tends to keep rising, unless it first hits a region of air which is already less dense than it ought to be if subject only to adiabatic cooling. The convection package therefore tends to rise until it hits the tropopause, where it meets air whose density is lower than demanded by the gravitational change, because of the solar heating effect. The tropopause therefore acts as a cap on the vertical movement of air from the troposphere to the stratosphere, making the two air masses quite distinct. Convection currents approaching the tropopause therefore change direction to the horizontal; this air cools, causing it to sink; the high pressure air sinking to the Earth's surface, turns and rushes into the low pressure region at the base of the rising convection column of air, thus setting up the gigantic vertical cyclic motions of air known as the Hadley cycles. When combined with the horizontal motions caused by the rotation of the Earth, this acts as a very efficient mixing mechanism (and of course the phenomenon we know as *weather*).

In contrast, convection currents are not possible in the stratosphere, because of the positive temperature gradient. Mixing there is caused by differential solar heating of the stratospheric gas across the latitudes and is known as *advection*. Air heated at the equator expands and moves towards the poles. Displaced air tends to rise at the poles and comes back down to replace the sinking heated air at the equator. An important point is that air on either side of the tropopause, moves horizontally and parallel, which makes mixing across the boundary difficult. The stratospheric air mass is therefore, partially isolated from that of the troposphere. Thus, whereas effective mixing within the troposphere may take only a few days or weeks, effective mixing across the boundary may take many months.

'Fast' reacting species (e.g. most pollutants) therefore never reach the stratosphere; only slow reacting species do so. An important example of the latter are of course the chlorofluorocarbons (CFCs) which are immune to both chemistry and photochemistry in the tropopause, and which therefore eventually congregate in the upper atmosphere, where they become subjected to much higher energy radiation, and photodecomposition, when their subsequent reaction can cause significant damage to the ozone layer.

The air at the top of the stratosphere is similarly capped by the temperature inversion of the stratopause, above which efficient vertical mixing again becomes possible. The mesosphere, where air pressure is still high enough for convection forces to operate, merges into the very low pressure region of the thermosphere, where gas molecules move more or less independently (movement is dominated by molecular transport in this region) and the kinetic 'temperature' resulting from photodecomposition is high.

There is therefore an effective temperature inversion at the mesopause (~ 80 km) which acts as a barrier to transport between the two layers of the meso- and thermo-spheres.

5.4 Photochemistry of the Thermosphere

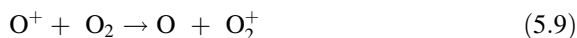
Very short wavelength solar radiation, EUV: $80 \leq \lambda \leq 103$ nm and X-rays: 1–10 nm, causes photo-ionisation (see Table 5.3), but is rapidly attenuated; restricting ionisation to $z > 60$ km: a region which is therefore also known as the *ionosphere* (but it encompasses both the thermosphere and part of the mesosphere, see Fig. 5.4).

The ions dominating during the daytime are therefore N^+ , O^+ , N_2^+ , O_2^+ and NO^+ . The charge density (cations and electrons) reaches values in the region of $>10^6$ cm^{-3} , which at this level has a mixing ratio of *ca.* 1 in 10^{11} . This compares with natural charge densities of $\sim 10^3$ cm^{-3} at ground level (caused mainly by ionising radiation emitted from radioactive materials), which is a mixing ratio of <1 in 10^{16} . For comparison, an electrical plasma, such as that produced in a low power electrical discharge lamp has charge densities in the region of 10^{11} cm^{-3} .

The chemistry that ensues is the reaction between ions and molecules, and ion-electron recombination, which is relatively fast for molecules, but slow for atomic ions.

Table 5.3 Photoionisation reactions in the ionosphere; IE is the ionisation energy, AE is the appearance energy for dissociative photoionisation, and the energies are also expressed in terms of the equivalent photon wavelength λ

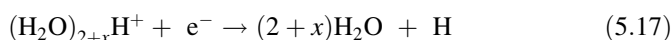
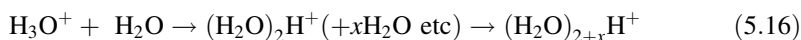
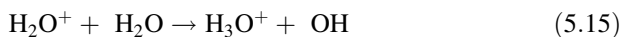
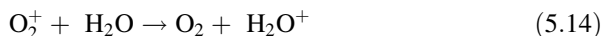
$h\nu + O_2$	$\rightarrow O_2^+ + e^-$	IE = 12.07 eV	$\lambda = 102$ nm
	$\rightarrow O^+ + O + e^-$	AE = 18.78	66
$h\nu + N_2$	$\rightarrow N_2^+ + e^-$	IE = 15.58	80
	$\rightarrow N^+ + N + e^-$	AE = 24.3	51
	etc.		



The *designation represents an excited state. There are, of course, many other reactions involving the less abundant species.

The free electrons which also congregate in this region are responsible for reflecting radio waves beamed from the Earth's surface. The optimum value of z for this occurrence depends on radio frequency, and a plot of reflection altitude versus frequency shows peaks. The higher frequencies penetrate to higher altitudes; e.g. there is a sharp peak at ~ 6.1 MHz, which penetrates up to about 750 km, and which early in the history of upper atmosphere research was used to designate the region where $z > 750$ km, as the F 'layer'. Likewise 'layers' E and D were also defined by lower frequency peaks. Although we now realise that they are not specific layers of air, partially isolated by their mixing properties, as we recognise today for the troposphere etc., the F, E and D regions are, however, still referred to in the literature as convenient markers for regions of the upper atmosphere. The E region stretches up from about 120 km, and the lower boundary of the D region is at the lower limit of the ionosphere at ~ 60 km. It therefore bridges the mesopause at 80 km (see Fig. 5.4).

In terms of ionic chemistry, O^+ dominates the F region, which is converted *via* reactions (5.8) and (5.9) to O_2^+ and NO^+ , and it is the latter molecular ions which dominate the E region. In the lower part of the D region, *i.e.* the mesosphere, which is the coldest part of the atmosphere, clustering results in the principal end product of ion–molecule reactions in air, *via* a complex series of reactions, which are clusters of water molecules bound to H^+ , *i.e.* $\text{H}^+(\text{H}_2\text{O})_n$ where n goes up to values >10 . These molecular ions are eventually removed by ion–electron recombination (5.17).

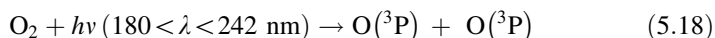


whereas chemical mixing in the tropo- and mesospheres is driven mainly by turbulent convection processes, and in the stratosphere is driven by advection, the

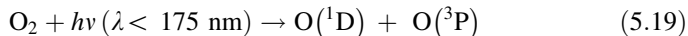
mixing at higher altitudes (>80 km), becomes dominated by molecular diffusion, the pressure becoming too low for the ‘bulk’ transport mechanisms of gases to operate. Gravitational separation therefore occurs and gases start to separate out according to their molecular mass, with the lightest components congregating towards the top of the atmosphere (see 5.7; H is proportional to $1/m$). Below that, turbulent mixing ensures that all the stable gases of the atmosphere, such as N_2 , O_2 , Ar and CO_2 , remain with the same fixed composition as at ground level. This is therefore sometimes referred to as the *homosphere*, and the heterogeneous region above that: the *heterosphere*.

5.5 Photochemistry of the Stratosphere

The most abundant solar radiation absorbent gas of the atmosphere, by far, is O_2 . Its absorption spectrum was shown in Fig. 5.3, and the most important reaction is photodissociation to create O atoms, reaction (5.18).



Shorter wavelength absorptions (in the Schumann-Runge range) give rise, reaction (5.19), to the first excited state $O(^1D)$, whose excess electronic energy is rapidly quenched by collision, (5.20).



It is higher energy transitions into the continuum of the B state, see Fig. 5.3, which lead directly to $O(^1D)$ formation. Requiring shorter wavelengths, this therefore tends to occur at higher altitudes than reaction (5.18), which dominates in the stratosphere.

O atom production leads directly to the formation of ozone, the simplified reaction sequence of which is now well established as:



The rate of O_2 photodissociation maximises high in the atmosphere above the equator, at ~ 40 km. Ozone, on the other hand, is a maximum at lower altitudes (~ 20 km) and towards the high latitudes, close to the polar regions. It is seasonal and the maximum levels occur in the spring time, *i.e.* March and April in the

Northern Hemisphere, but October in the Southern Hemisphere, when the equatorial photodissociation rate will have decreased. Whilst ozone will be produced over the whole of the stratosphere, the spring-time accumulation towards the poles is presumed to be due to a net transfer, over a period of months from the ‘hot’ low latitude, but high altitude region of the stratosphere, to the ‘cold’ high latitude, but low altitude regions at the poles.

The steady-state ozone concentration at any point is determined by the balance of O_2 photodissociation (5.1) and the removal mechanisms represented by reactions (5.22) and (5.23), and also the rates of transport in and out of the gas volume of interest, all of which vary depending on the conditions. The *chemical lifetime* (see Sect. 5.7.1 for a formal definition) of O_3 is very short at the top of the stratosphere, because of the high rate of its photodecomposition (5.22), and steady-state levels are relatively low, but it increases towards lower altitudes and higher latitudes, where it can be several months.

The vertical concentration profile increases significantly when passing down from the mesosphere into the stratosphere, reaching a maximum between 30 and 20 km (see Fig. 5.5), tending towards the higher z when close to the equator.

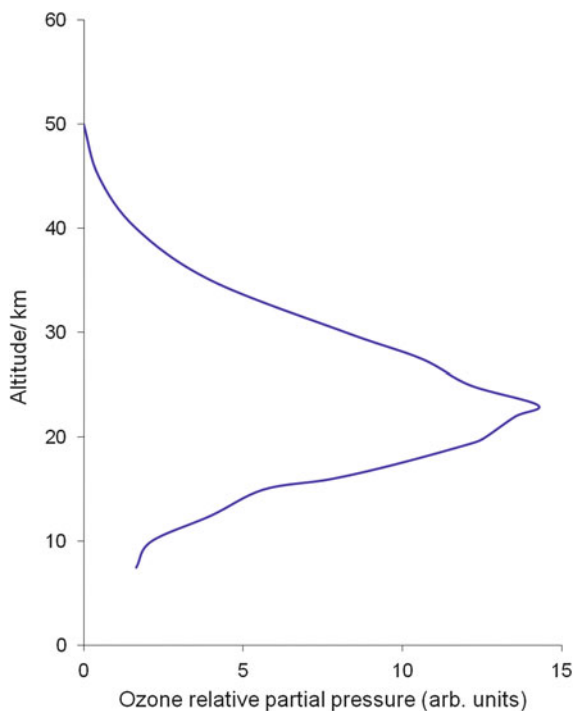


Fig. 5.5 Example of the vertical profile of ozone concentration; these data (averaged and smoothed) are extracted from Ref. [7] and represent balloon based measurements at 57° N and 107° W, during August in the years 1998–2004

It rapidly decreases across the tropopause, when the necessary UV levels have become effectively quenched. Spring-time levels in the stratosphere reach up to 10^{13} molecules cm^{-3} at a mixing ratio of ~ 5 ppm (e.g. if $z = 20$ km, where $p = 55.3$ mbar and $T = 220$ K). This compares with background ozone, at sea level in the mid-latitudes, which can be in the range of 20–45 ppb [6] ($\sim 5 \times 10^{11}$ cm^{-3} , $p_{\text{air}} = 1$ atm, $T = 293$ K). The source of most ozone at ground level, however, is different to that in the stratosphere.

The mechanism for net removal of ozone in the stratosphere is that of the catalytic chain reaction:

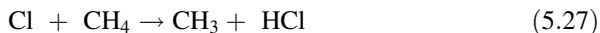


where X is thought to be mainly any one of the various trace gases present: H, OH, NO_x , Cl, and Br. Cl and Br are particularly effective, one atom possibly removing up to 10^4 O_3 molecules overall. The direct reaction (5.23) may contribute, but it is slow by comparison.

As has been discovered over the past 40 years, a principal contributor is $\text{X} = \text{Cl}$, and the principal source of Cl is chlorofluorocarbon pollutants. These entirely man-made materials, developed as highly efficient refrigerants, aerosol propellants and solvents, are inert in the troposphere. They are either gases or have a high vapour pressure and therefore all of them, unless deliberately destroyed, find their way into the atmosphere, and being highly stable, they ultimately end up in the stratosphere, where they do become vulnerable to photodecomposition, for example:



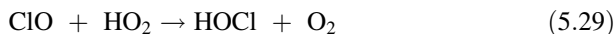
Levels of Cl from these anthropogenic sources now heavily outweigh natural sources (the most abundant of which is biogenic CH_3Cl , with a global mixing ratio at 550 ppt [8]). Their overall effect therefore is to remove ozone; the chemistry involved is, however, highly complex, since all these species react with many other species present, which may themselves react with ozone or even promote its formation. Of particular note is the formation of ‘reservoir’ species. For the $\text{X} = \text{Cl}$ reactions, an important example is HCl. It forms *via* the sequence:



and is eventually regenerated later as Cl by the reaction



Whilst in the HCl form it is inactive towards ozone, and therefore this sequence of reactions acts as a ‘holding’ mechanism, delaying the release of Cl, rather than necessarily actually permanently removing it from the mix. It is thought that as much as 70 % of stratospheric Cl is held in this form. Other ‘reservoir’ processes trap ClO, which temporarily forms HOCl and ClONO₂, in the reactions:



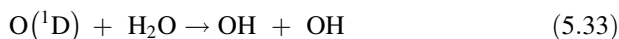
HO_2 is formed by the reaction:



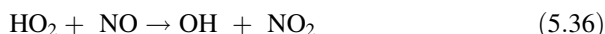
and H by the reaction:



OH is formed from $\text{O}(^1\text{D})$, mainly by its reactions with water and methane:



$\text{X} = \text{NO}_x$ is another important catalyst. The main source is the reaction sequence:



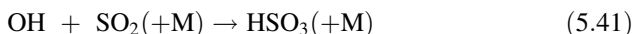
N_2O is an otherwise relatively unreactive trace gas, whose main source is biogenic emission. Each of the reagent species (OH, HO_2 , H, NO_2) themselves undergo many other reactions besides those shown, so that there is an intricate web involved in the final balance of O_3 in the stratosphere as a function of height, season, time of day and location. Model predictions of ozone depletion, not surprisingly, are very sensitive to the accuracy of laboratory kinetic data and the assumptions and approximations applied to these systems.

All the gases are held in a more or less 'steady' state, in which the net sink processes are thought to be removal via their longer lived reservoir species (HCl, HOCl, and ClONO_2 from above, but, for example, HNO_3 , HBr, BrONO_2 , and HO_2NO_2 may also be involved). These are all water soluble and it is thought that they eventually cross the tropopause where they dissolve in clouds and other aerosols and get 'rained' out of the atmosphere.

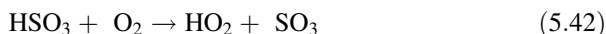
5.5.1 Heterogeneous Chemistry

Aerosols are also important in stratospheric photochemistry. They are thought to be formed as a result of the oxidation of dimethyl sulphide in the troposphere. This is formed from decaying organic matter (e.g. oceanic algae) and is emitted into the air where it breaks down to form carbonyl sulfide: COS. This is chemically stable

in the troposphere ($\tau = \sim 7$ years) and therefore is the most abundant atmospheric sulfur compound to be found. It therefore penetrates up into the stratosphere, where it becomes photolysed and oxidised to SO_2 , eventually forming H_2SO_4 .

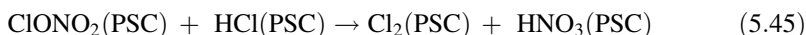


HSO_3 is converted to H_2SO_4 , possibly *via* reactions:



This highly hygroscopic molecule readily combines with water molecules to form an acid aerosol droplet. Other aerosols are formed by nucleation around mineral particles injected as a result of volcanic activity. Under very cold conditions, such as at the poles in winter, these aerosols freeze to form polar stratospheric ice clouds (PSCs), the surfaces of which provide a substrate for important heterogeneous catalytic processes. An example of this is the well-known ‘ozone hole’ effect. This arises because the steady state concentration of O_3 is sustained by the series of reactions (5.1) and (5.21)–(5.25). As already discussed, the sink mechanism (5.24) and (5.25) requires the presence of catalyst X, of which Cl atoms are nowadays the most important, and which are provided, such as reaction (5.26), mainly by the photolysis of CFCs present at trace levels in the upper atmosphere; and much of the Cl is temporarily locked up into the reservoir species such as HCl and ClO_x .

In the winter time, air from the equator, carrying the reacting ozone mixture, becomes trapped into a freezing cold mass (vortex) circling the pole, almost isolated from air in the lower latitudes, until spring time sunshine arrives. In the presence of PSCs HCl gets adsorbed onto the surface hence removing Cl from the gas phase and thus halting the O_3 removal process, which therefore remains at its steady-state level. It appears that a number of surface reactions involving adsorbed reservoir species occur, examples of which are:



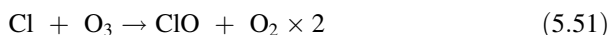
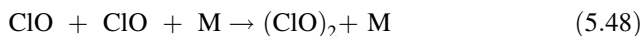
the products of which are retained until the onset of spring (*i.e.* October in the southern hemisphere, where the effect is most prominent). With the appearance of sunlight, evaporation occurs, releasing ‘large’ quantities of Cl_2 . This is very easily photolysed by visible light, the intensity of which is very much greater than the UV normally required for photodecomposition.



Cl atoms react with ozone to form ClO:



as part of the chain reactions (5.24) and (5.25); but the important reaction in the cold conditions of the Antarctic region is thought to be the formation of the $(\text{ClO})_2$ dimer. Aircraft based UV measurements show a direct correlation between O_3 depletion and ClO formation during ‘ozone hole’ formation. The low temperatures favour three body reactions such as (5.48) and (5.50), and $(\text{ClO})_2$ is easily photolysed to yield two Cl atoms leading to an increased removal rate for ozone.



The net reaction is equivalent to: $2\text{O}_3 + h\nu \rightarrow 3\text{O}_2$.

There are also lesser contributions from other catalytic species, such as BrO and NO_x , which are involved in similar reaction cycles.

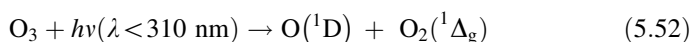
So, whereas for the winter and early spring the ozone cycle has lain dormant, the sink mechanism is triggered with the production of ‘large’ quantities of Cl atoms over a short period of time in the later spring, and O_3 concentrations rapidly decline by as much as one half over a few weeks (the so-called *ozone hole*). Of course the *status quo* is restored when the polar and lower latitude air masses start to mix effectively again. This effect did not appear to become significant (and was not observed until the early 1980s), until Cl catalysis became the dominant removal mechanism due to the build up of man-made CFCs in the atmosphere.

5.5.2 Ozone Levels and Life on Earth

There are two critical outcomes to the patterns of upper atmosphere ozone levels, which are vital to life on Earth. The first is the vertical layering of the atmosphere as already described. The second is the fact that, after O_2 , the O_3 filters out virtually all the remaining UV-B (280–315 nm) from the solar spectrum at the Earth’s surface. The DNA damage inflicted by extraterrestrial levels of UV would severely restrict the survival of life forms at the surface: it is O_2 combined with O_3 which provides the essential UV filter.

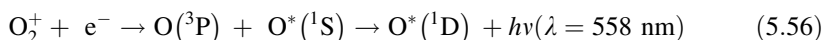
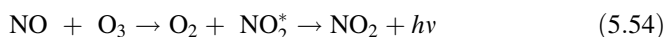
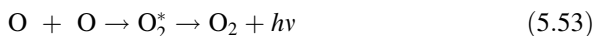
5.6 Photochemistry of the Mesosphere

Like the stratosphere, the mesosphere photochemistry is dominated by O₂, O₃, and O atom reactions. Being at a much lower pressure, the absolute concentrations are much lower, but the ratio of [O]/[O₃] is higher particularly because of the increased rate of reaction (5.22). A distinguishing feature of this reaction is the formation of the singlet D O atom and the singlet delta O₂ molecule, (5.52).



Both products are metastable, with long radiative lifetimes (110 s and 44 min respectively). The O(¹D) atom is however very rapidly converted, reaction (5.20), by collision with air molecules into the ground state O(³P), whereas O₂(¹Δ_g) (often called *singlet oxygen*) is collisionally much more stable. As a result, during the daytime, there is an accumulation of this excited molecule in the lower reaches of the mesosphere and the upper stratosphere, reaching values as high as 10¹⁰ molecules cm⁻³ (mixing ratio is at the ppm level). Despite its ‘forbidden’ nature, the O₂(¹Δ_g → ³Σ_g⁻) transition does occur, at 1270 nm, and forms the strongest emission in the daytime *airglow* (i.e. the *dayglow*), and is known as the Infrared Atmospheric Band. It is observable spectroscopically because of the very deep optical path lengths (tens of km) of the emission volumes which can be sampled during measurement. (Emission from the O₂(¹Δ_g → ³Σ_g⁻) transition can also be experimentally measured in the laboratory — see Chaps. 14 and 15).

At night there is a *nightglow*, but the emissions come from the top of the mesosphere, the thermosphere and ionosphere. The IR Atmospheric Band features, but so also do many chemiluminescent reactions due to, for example:



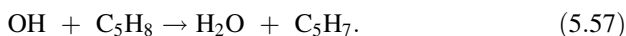
which emit in the visible part of the spectrum, and so can be observed by eye from space, as a glow on the edge of the night time atmosphere. Reactions (5.53)–(5.56) obviously also occur during the daytime in the meso- and stratospheres, but their emissions are impossible to detect by eye against the high intensity background solar radiation. The chemiluminescences can however be used spectroscopically to detect and monitor the gases involved.

These emissions of light occur over the whole upper atmosphere and should be distinguished from the *aurora* which are reactions induced by collisions with gas molecules at higher altitude, of charged cosmic particles captured in the Earth’s magnetic field, and frequently visible in the night sky of the northern and southern latitudes.

5.7 Photochemistry in the Troposphere

5.7.1 Non-Polluted Atmosphere

There are, of course, thousands of gaseous emissions into the atmosphere, other than N_2 , O_2 , H_2O , Ar and CO_2 . The latter are stable gases, whose fractional composition remains constant throughout the homosphere. But for most emissions the degree of mixing and their transport within the atmosphere depends on the *chemical lifetime* (τ_{chem}) of each species. This is best defined by example, such as the hydrogen abstraction reaction (5.57) which is one of the most important types of reaction in the unpolluted troposphere;



here the hydroxyl radical reacts with a hydrocarbon (in this case: isoprene emitted from the leaves of plants), to form water and another radical. This sets off a chain reaction, by which the hydrocarbon is eventually removed from the atmosphere. The rate of reaction is given by

$$\frac{\partial[\text{C}_5\text{H}_8]}{\partial t} = k[\text{OH}][\text{C}_5\text{H}_8] = k'[\text{C}_5\text{H}_8] \quad (5.58)$$

where t is the reaction time and k is the rate constant. If OH is assumed to be present at an approximately constant steady-state concentration, the rate equation is pseudo-first order, with pseudo-first order rate constant k' . The definition of the *lifetime* of a first order reaction is the time it takes for the reactant to decay by the fraction $1/e$ of its starting concentration, which is given by $1/k'$. According to the NIST Chemical Kinetics database, $k_{58} = 1 \times 10^{-11} \text{ molecules}^{-1} \text{ cm}^3 \text{ s}^{-1}$ at ambient temperatures. Since $[\text{OH}]_{\text{troposphere}} \approx 10^6 \text{ molecules cm}^{-3}$, then $k' = k[\text{OH}] \approx 10^{-4} \text{ s}^{-1}$, and τ_{chem} (isoprene) $\approx 10^4 \text{ s}$, *i.e.* $\sim 2.8 \text{ h}$. On a calm day (wind speed $< 1.6 \text{ km hr}^{-1}$) the molecules from such an emission source would therefore be carried no more than 5 km.

The main ingredients of air have a comparatively very long chemical lifetime and their residence time (τ) is therefore long. Thus it takes about 10^7 years to completely replace all the N_2 , 2500 years for O_2 and 120 years for CO_2 (not counting the continuous exchange with CO_2 dissolved in the oceans, the main reservoir for this gas; if counted the replacement time goes down to between 3 and 15 years [9]). The long-lived species therefore have plenty of time to cross the layer boundaries (e.g. the *tropopause*) and to mix effectively, so that the composition of the main ingredients remains the same up to the top of the homosphere.

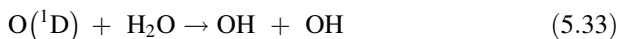
The great majority of gases emanate as volcanic, biogenic or radiogenic emissions from the surface. Whilst the original (prebiotic) atmosphere was dominated by volcanic emissions (e.g. N_2 , CO_2 and H_2O), it is now almost completely dominated by biogenic exchange, with radiogenic exceptions (such as Ar and He). Others, such as COS (see earlier), are the products of chemical or photochemical

reaction, in addition to the relatively minor volcanic input. Emissions with short lifetimes tend to remain confined to the troposphere. Some of these are inorganic, such as NH_3 , SO_2 or H_2S , but the vast majority are organic molecules. The longest-lived will obviously be more evenly distributed than the shortest. Methane, the main organic component of air, has a residence time measured in years, but there is a difference in its abundance between the northern (1750 ppm) and southern (1500 ppm) tropospheric hemispheres. This is due to the fact that two of its main sources are from farming: *i.e.* enteric fermentation in ruminants and rice growing, both of which are more concentrated in the northern hemisphere. It is exacerbated by the *intertropical convergence*. This is the boundary between air masses in the two hemispheres caused by the horizontal countermovement due to rotation of the Earth (west to east in the north, and the opposite in the south). At the convergence the air masses are therefore moving parallel to each other, so that transfer across the convergence is slower than within the hemispheres.

Others such as isoprene (C_5H_8), or the terpenes ($\text{C}_{10}\text{H}_{16}$) and related compounds (responsible for many plant smells), emitted by plants and trees have chemical lifetimes measured in hours, minutes or seconds and therefore never travel more than a few kilometres from their source, depending on the wind speed. In fact, the principal limitation on the lifetimes of shorter-lived organic species in the troposphere is their reaction with OH, which, although its background mixing ratio is in the 10^{-13} range, is therefore critical to tropospheric chemistry.

In the troposphere it is produced by a variety of reactions, but principally the photodecomposition of ozone. About 10 % of tropospheric O_3 results from its downward transport across the tropopause. Residual UV radiation at $\lambda < 310$ nm, penetrating the troposphere, causes photolysis, by reaction (5.52) to produce the singlet O atom.

Although $\text{O}(^1\text{D})$ is mostly quenched down to its ground state by collision (5.20) a small proportion reacts with water to form OH:

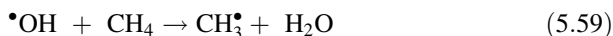


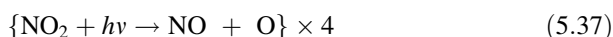
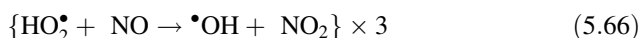
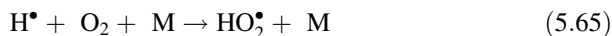
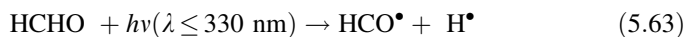
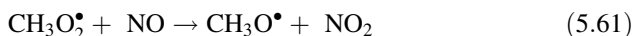
If NO_2 is present (for example in a polluted atmosphere), this too is broken down by UV (when $\lambda < 410$ nm):



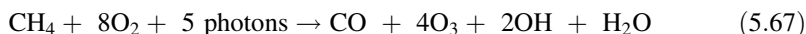
The $\text{O}(^3\text{P})$ atoms react with O_2 to reform O_3 by reaction (5.21) which again may lead back to OH formation, *via* photolysis reaction (5.52) which regenerates $\text{O}(^1\text{D})$. In an unpolluted atmosphere the main *sink* reaction for OH is reaction with CH_4 . It is this reaction which forms the backdrop to atmospheric chemistry in the troposphere. The sequence is complicated; Scheme 5.1 is the model suggested by Crutzen [10], and it illustrates the most likely oxidation route for most hydrocarbons emitted into the atmosphere.

Scheme 5.1: Oxidation of methane and formation of ozone





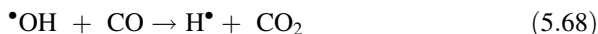
The overall reaction is therefore:



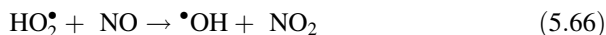
Once radicals are formed, either by photodecomposition or H abstraction, then they can react directly with O_2 to form a peroxide radical (5.60), which in the presence of NO and NO_2 can react to make an aldehyde (5.62), which breaks down in sunlight (5.63) to CO in this example. As shown, both NO_2 (5.61, 5.66 and 5.37) and HO_2 (5.62, 5.64 and 5.66) are thought to be involved in the chain; the former breaks down in sunlight ($\lambda \leq 410 \text{ nm}$) to $\text{NO} + \text{O}$ which gives rise to more O_3 formation, and catalyses the formation of more OH (5.66). Other hydrocarbons will lead to longer carbon chain products.

In this model, for every methane molecule which reacts, the sequence leads to 4 ozone and 2 hydroxyl radicals, extra. Formation of ozone in the lower troposphere is therefore catalysed by photochemical oxidation of organic molecules, but it does require comparatively high levels of NO (mixing ratio $> 5 - 10 \times 10^{-12}$) to be present. If it goes to completion, OH can react further with CO to make CO_2 thus completing the oxidation of methane (Scheme 5.2). At low NO levels, the net reaction is the destruction of ozone *via* the reaction with CO [Scheme 5.2b].

Scheme 5.2: Oxidation of CO and (a) formation *or* (b) removal of ozone

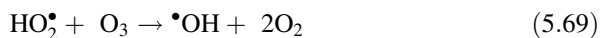


(a) in the presence of NO:





(b) without NO:



The main natural source of NO is reaction (5.35).



Ozone formation is enhanced when other more reactive organic molecules are present, such as on a hot day in the presence of vegetation; although the chemistry is more complex. Thus, for example, the heat haze above a pine forest is caused by emitted terpenes ($\text{C}_{10}\text{H}_{16}$) and other organic molecules which promote levels of both O_3 and NO_2 . The latter has a brown colour which can be seen. Thus, ozone levels and other associated gases, wax and wane with the presence of sunlight (along with other weather factors). The distribution of ozone at ground level therefore depends on local factors such as the vegetation. Figure 5.6 shows O_3 maps for average levels for three different years across mainland Britain. This shows ozone levels to be more concentrated in the rural areas such as the South West, Wales or northern Scotland. There are much more localised concentrations (although not so easy to see from these maps) in large city conurbations (London, Birmingham, Manchester etc.). The latter is not due to the vegetation, but is the well-known problem of air pollution. The difference between the years highlights the sensitivity to hours of sunshine experienced.

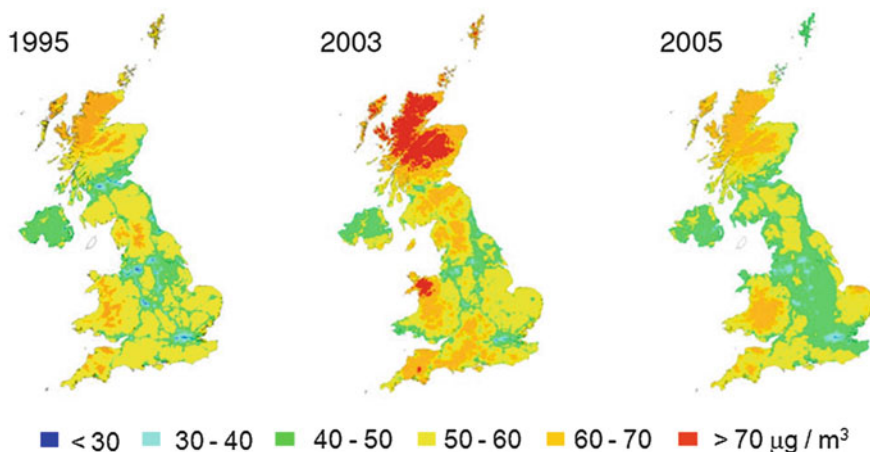
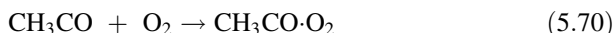


Fig. 5.6 Average annual mean distribution of ozone in the UK ($\mu\text{g m}^{-3}$), for various years. Reproduced and adapted with permission from Fig. 2.30 in Ref. [11] (Copyright 2008, DEFRA)

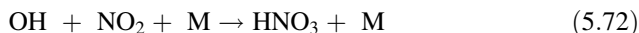
5.7.2 The Urban Polluted Atmosphere

Reactions in the polluted atmosphere are very similar to the natural background reactions, except for the intensity of reaction. The combustion engine, coal, oil and natural gas burning all pump large quantities of unburnt hydrocarbon fuel, and the products of combustion into the atmosphere. Automobile emissions are especially acute, pumping out petrol or oil fumes, partially burnt hydrocarbons, CO and NO (besides CO₂, a different sort of pollutant) into the local atmosphere. On a still sunny day this is a toxic combination which leads to high levels of photochemical reaction, especially promoted by the presence of excess NO, which helps catalyse the formation of high levels of O₃ and ultimately its removal. Whereas O₃ in the stratosphere is essential to life on earth, at ground level it is regarded as toxic at levels >200 ppb.

Among other products which build up during the day are NO₂, HNO₃, and partially oxidised hydrocarbons, such as formaldehyde. Another is peroxyacetyl nitrate (PAN). This is thought to result from the sequence of reactions:



PAN is also present at low pollution levels; and is thought to be reservoir species for NO₂ since it is broken down again, but relatively slowly, by sunlight; at high pollution levels (ppb) it is an intense eye irritant. NO₂ is ultimately removed mostly by its gas phase reaction (5.72) to make HNO₃, which is very soluble in water and therefore easily *rained out*.



On sunny still days, local low level boundary layers of air can form. This is exacerbated by certain geographical features, such as an onshore wind over a coastal plain bounded by hills or mountains. The boundary layer forms either as a result of a faster cooling of air with altitude close to the ground than the adiabatic cooling rate, in which case convection is inhibited (the early morning low level mist in river valleys), or the air above it becomes heated, making the localised solar heating rate greater than the adiabatic cooling rate, thus creating a layer of air which inhibits convection. This boundary layer, which is similar to the tropopause, but is temporary, acts as a cap just a few hundred metres from the surface, trapping the air mass below it and allowing pollutant emissions to build up (rather than being dispersed as normal). The Los Angeles basin is the usual example quoted, where high photochemical pollution is endemic, but many other cities around the world show similar levels of pollution. Figure 5.7 shows urban pollution levels recorded in Beijing, China during the winter months of 2001.

This very clearly demonstrates the correlation between emissions of NO_x and CO and the formation of O₃ (hydrocarbons are not shown). Hydrocarbons, NO and CO are emitted into the morning urban air by the morning rush-hour, peaking

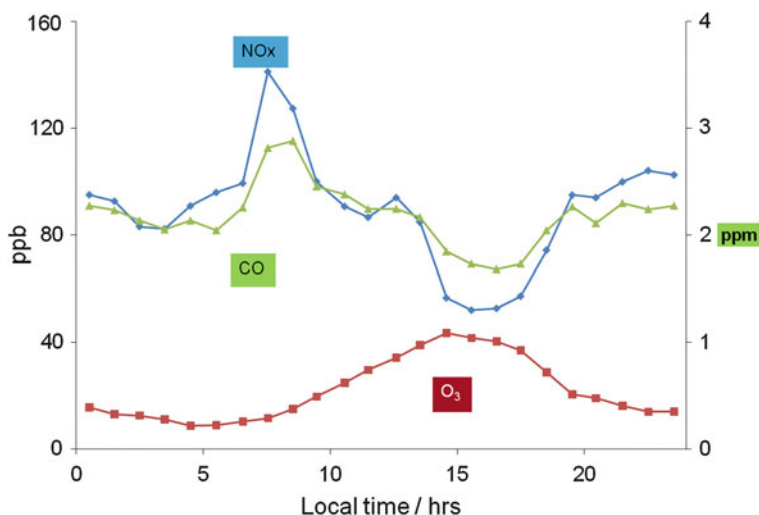
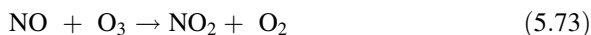


Fig. 5.7 Averaged diurnal variations of NO_x (ppb), CO (ppm) and O₃(ppb) in Beijing; Jan–Feb 2001; The data was extracted from Ref. [12]

at *ca.* 8.00 h. As the sunlight increases in intensity the chemistry illustrated by Schemes 5.1, 5.2 (but involving petroleum hydrocarbons, rather than CH₄) occurs, building up over the day, leading to higher levels of O₃ which peaks at *ca.* 15.00 h, when both NO_x and CO show a dip. A very fast reaction, not so far discussed, is (5.73), in which NO reacts with O₃ to form NO₂. Reactions (5.73) and (5.37) are so fast, compared to others, that the reactions in Scheme 5.3 may generate a photochemical steady state at the height of the day. Of (5.37) and (5.21), (5.37) is the rate determining step and so dictates the rate of formation of O₃. (5.73) dictates its rate of removal, and therefore under steady state conditions, their rates would equilibrate:

Scheme 5.3: A photochemical steady state?



$$J_{37}[\text{NO}_2] = k_{73}[\text{NO}][\text{O}_3] \quad (5.74)$$

and [O₃] is therefore given by:

$$[\text{O}_3] = (J_{37}/k_{73})[\text{NO}_2]/[\text{NO}] \quad (5.75)$$

where J_{37} is the actinic flux responsible for reaction (5.37). In bright sunlight therefore the removal reaction (5.73) has no significant effect on the ozone levels,

since ozone is rapidly regenerated from the product. However, in the evening when J_{37} is low, the reaction is a significant removal mechanism, hence in Fig. 5.7, O_3 dips and NO_x increases.

The higher levels of ozone recorded for unpolluted rural areas (Fig. 5.6) may at first seem counter-intuitive. It has been argued, however, that these higher rural levels of ozone are largely due to the relatively low levels of rural NO emission and hence the relative absence of reaction (5.73) as an efficient removal mechanism.

As discussed above, COS (present at 500 ppt) is thought to be the most abundant natural sulfur containing compound in the atmosphere and it has a long lifetime. Localised emissions of SO_2 are also common, both from automobiles and power station combustion of oil and coal. It is not an important contributor to the photochemistry of the atmosphere however, because of SO_2 's high *BDE* and its high reactivity. Its lifetime is therefore measured in days or weeks, becoming either oxidised to H_2SO_4 to form aerosols (as described earlier) or directly dissolving in existing aerosols (as does HNO_3), creating *acid rain*.

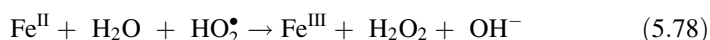
5.7.3 *Cleaning the Atmosphere*

Photochemical oxidation is an essential part of the natural cycle, keeping the atmosphere clean. This is achieved by converting insoluble trace components (e.g. CH_4) into partially oxidised soluble gases (e.g. aldehydes, acids). In general therefore, before they are ever completely oxidised the intermediate products dissolve in aerosol (or cloud) droplets. They may get further oxidised within those droplets, but the eventual outcome is that they precipitate to the surface, *i.e.* they are 'rained' out of the atmosphere. This is a very important process, since without it the atmosphere would become intensely polluted.

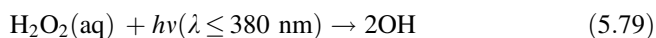
5.7.4 *Aerosol Photochemistry*

Aerosols are a suspension of either dust or water particles in air. They are formed by a variety of mechanisms. For example dry aerosols are created by wind erosion of rocks or soil, or emitted in volcanic emission. Wet aerosols are formed for example by the seeding action of dry particles in a humid atmosphere, when a hydrophilic dust particle (e.g. Fe_2O_3 or an aluminosilicate) collects a layer of water molecules onto itself (thickness of layer varies with changing humidity). A very important wet mechanism involves the sulphuric acid aerosol, formed as described for the stratosphere, but which occurs here at much higher densities. Oxidation reactions occur both at the surface and within the aerosol droplets, but its principal role is as a chemical sink. Gases such as OH, HO_2 , and H_2O_2 dissolve in aerosol droplets, thus tending to quench the gaseous photochemical cycle leading to ozone

production. SO_2 , HNO_3 and oxidised organics such as formaldehyde are also dissolved, which when it rains are thus carried back to the Earth's surface and out of the Earth's atmosphere. The atmosphere is thereby kept cleaned of organic and inorganic pollutants. The aqueous aerosol droplet typically has an inorganic (mineral) centre onto which water condenses, or from which it evaporates, depending on the time of day and humidity, leading to a surrounding aqueous layer which is up to 50 % of its weight. After gas absorption, the resulting solution is often highly acidic and contains mineral ions as hydroxy-complexes containing trace metals such as Fe(III) and Fe(II). These readily absorb photons in the range 290–400 nm, initiating a catalytic cycle which oxidises organic species present in the aerosol e.g. (5.76) to (5.78).



Hydrogen peroxide is itself photolysed by UV, within the droplet, to OH:



The aerosol therefore forms a potent oxidising environment being responsible for dissolution of SO_2 and formation of most tropospheric H_2SO_4 (by an aqueous mechanism), and the conversion of organics into organic acids. These, and dissolved HNO_3 , lead to the creation of acid rain in polluted environments.

5.8 Modelling

It is obvious that atmospheric chemistry is highly complex, with very many variables. These include solar radiation levels as a function of the sun's activity, season, time, altitude and location; absorption and scattering cross-sections as a function of wavelength; sources and sinks of both stable (e.g. O_2 , trace components) and reactant gas (e.g. O, N, NO_x , OH, $\text{O}(\text{D})$, etc.) densities, a knowledge of all possible reactions, and the thousands of associated rate coefficients as a function of pressure (P) and temperature (T); aerosol and cloud dispersions; air movements, gas transport properties and gas mixing mechanisms and efficiencies. It inevitably involves the need for laboratory data on the reaction kinetics, for detailed measurements on the identity and distribution of atmospheric species, and considerable approximation. *In-situ* identification and measurement particularly of trace reactive species is difficult. Attempts at integrating all these variables is done using numerical computer models. As usual for complex systems, the approach is intelligent guesswork as to what is thought to happen, to construct the model, and to fit the data to whatever experimental measurements are available. The simplest

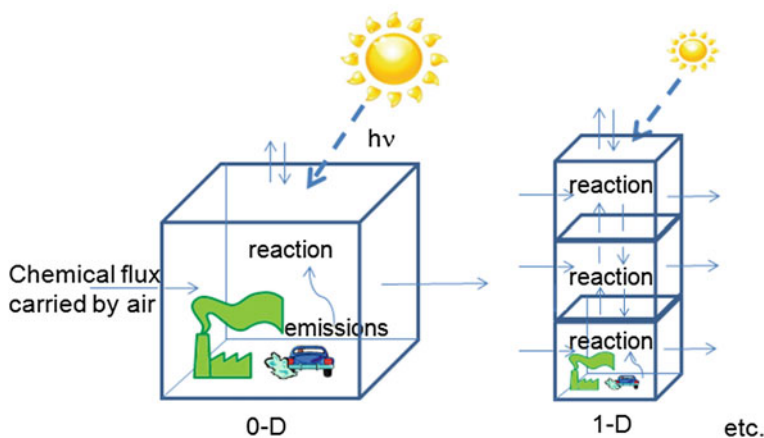


Fig. 5.8 Examples of 'Box' models

approach is the *Box model* (see Fig. 5.8). The box defines a fixed volume of space at a chosen site, which contains the set of reacting chemicals, as if it were a laboratory reactor in which all components are uniformly mixed, with a uniform temperature and pressure. Fluxes (chemicals carried by air movements and radiation) enter and leave at the surfaces of the box, and the differential equations describing the kinetics for each reaction are solved numerically to compute the concentrations of each chemical of interest, either as a steady state or as a function of time. This great simplification means that it is useful only as a first attempt at a problem, or where the information available, or the resources in time and computing, are severely limited.

For a single box at a set location, this is known as the 0D model. The next step up is a 1D model, exemplified by a vertical model in which the atmosphere is considered as a series of boxes one on top of the other as a function of altitude. The T and P in each box can then be different, determined by the physics, as well as radiation received, and the horizontal fluxes in and out. Exchanges of species between adjacent boxes make up the vertical fluxes, and thus such changes as the vertical distribution of ozone at a fixed point on the Earth's surface can be modelled, averaged and compared with vertical measurements made by balloon (see Fig. 5.5). The 2D model has both vertical and adjacent horizontal boxes, let us say along the lines of latitude. The computing power required goes up accordingly, as do the number of significant chemical variables. It has been found to be suitable for example in modelling ozone distribution across the stratosphere (such as measured by aircraft or satellite-based spectroscopic instruments), where perhaps up to 50 species involved in over 200 reactions might be considered. The 3D model has boxes extending vertically and horizontally, with both latitude and longitude. This is obviously the most realistic, especially if the box size is reduced to a sufficiently small volume that uniformity of distribution, and constant P and T within it, is also

realistic. This is what is really required to give global patterns of behaviour, but it is also highly complex and astronomically expensive.

The value of computer modelling is that it helps confirm our understanding of the processes. Where there is a poor fit between prediction and measurement it may indicate that there are important reactions occurring which have not yet been identified. The most famous example is the ozone hole problem which computer models at that time failed to predict and which led to the search for new mechanisms (heterogeneous reactions on polar stratospheric clouds). They are also often the only method of estimating levels of important intermediates, not otherwise possible to measure directly. The potential effects of adopting environmental strategies (e.g. the effect of phasing out CFCs) can also be tested. The degree of uncertainty is such, however, that even with the most sophisticated models, and despite the almost overwhelming political pressure for developing an orthodoxy (as in the climate change debate), a healthy scepticism is always necessary.

5.9 Concluding Remarks and Further Reading

What should be clear from this short account is the central role of O_2 , O atoms and O_3 in the photochemistry of the atmosphere. Ozone was first identified, as the smell produced by electrical discharge in air, as early as 1840 [13], and in 1880 Hartley [14] suggested that ozone in the upper atmosphere is responsible for the UV cut-off below 300 nm in the solar spectrum. It was proved to be so in the first part of the twentieth century and estimated that if all the ozone in the upper atmosphere was compressed down to 1 atm pressure it would be a layer only 3–5 mm thick (the ‘ozone blanket’). In the 1920s Dobson [15] invented the UV spectrometer for monitoring stratospheric ozone, a type which is still in use today. The Chapman model of the ozone cycle, reactions (5.1) and (5.21) to (5.23), was published in 1930 [16], and has proved to be essentially correct, but since modified (1960s [17]) to take account of the catalytic removal by H, OH, NO_x and particularly Cl, reactions (5.24) and (5.25). It was Molina and Rowland [18] who first realised the potential problems induced by fluorocarbons entering the atmosphere, in 1974. During the 1980s measurements using the humble Dobson spectrometer first identified the so-called ‘ozone hole’ problem [19], initially in the Antarctic, but later also in the northern hemisphere, and confirmed by satellite-based measurements. It was then that the world woke up to the global significance of problems induced by the pollution brought on solely due to human industrial activity.

At ground level, local pollution known as *smog* was known since the nineteenth century due to the industrial revolution and the burning of coal, causing the emission of SO_2 and other pollutants; but it was in the 1950s that ‘photochemical smog’ due to the combination of sunlight and car exhaust emissions was first described. In this too O_2 , O and O_3 play a central role, with the further addition of CO and NO_x and petrol fumes due to the ubiquitous combustion engine, and the oxidative chain reactions which ensue [20]. The route for the formation of OH in

the troposphere was first suggested in 1971 [21]. Whereas O_3 in the upper atmosphere is essential to the survival of life on Earth, at ground level, in the same mixing ratios it is a potential killer; nevertheless it is still an essential ingredient. Knowledge of all these processes is obviously essential to any control over the environment we might covet.

The main photochemical events in the atmosphere are by now all (probably) well-known, but there is still much to do to elucidate detailed mechanisms. Since the involvement of even very low abundance species can add up globally to make a significant contribution to the overall chemistry, advances mostly depend upon technological developments in analytical instrumentation, both for laboratory and global field measurements, enabling ever smaller concentrations of the short-lived species (important as intermediates) to be detected. Aided by space probe exploration, there is also increasing interest in extraterrestrial planetary atmospheres [22], particularly for the information that may be gleaned concerning the early development of our own.

There are many books devoted to atmospheric chemistry, which contain appropriate chapters on the photochemistry. Still one of the best, with an extensive bibliography, is Ref. [2]. Some other examples in press are:

- Holloway AM, Wayne RP (2010), Atmospheric chemistry. RSC Publishing, UK.
- Boule P, Bahnemann D, Robertson P (eds) (2010), Environmental photochemistry part 2, The handbook of environmental chemistry/reactions and processes. Springer-Verlag, Berlin Heidelberg.
- Seinfeld JH, Pandis SN (2006) Atmospheric chemistry and physics: from air pollution to climate change, 2nd edn. Wiley.
- Karol IL, Kiselev AA (2006) Photochemical models of the atmosphere and their application in ozonosphere and climate studies: A review. *Izvestiya Atmospheric and Oceanic Physics* 42: 1–31.
- Jacob D (1999) Introduction to atmospheric chemistry. Princeton University Press.
- Yung YL, DeMore WB (1998), Photochemistry of planetary atmospheres. Oxford University Press, USA.

References

1. Lide DR (ed) Handbook of chemistry and physics, 79th edn. CRC Press, Boca Raton
2. Wayne RP (2000) Chemistry of atmospheres, 3rd edn. Oxford University Press, Oxford
3. Trends in atmospheric carbon dioxide, US Department of Commerce, NOAA Research. <http://www.esrl.noaa.gov/gmd/ccgg/trends>. Accessed 21 June 2012
4. Yoshino K, Esmond JR et al (1992) High resolution absorption cross sections in the transmission window region of the Schumann-Runge bands and Herzberg continuum of O_2 . *Planet Space Sci* 40:185–192

5. CfA (Harvard-Smithsonian Center for Astrophysics) Molecular databases. <http://cfa-www.harvard.edu/amdata/ampdata/amdata.shtml>. Accessed 21 June 2012
6. Vingarazan R (2004) A review of surface ozone background levels and trends. *Atmos Environ* 38:3431–3442
7. Melo SML, Blatherwick R et al (2007) Summertime stratospheric processes at northern mid-latitudes: comparisons between MANTRA balloon measurements and the Canadian middle atmosphere model. *Atmos Chem Phys Discuss* 7:11621–11646
8. Aydin M, Saltzman WJ, De Bruyn W et al (2004) Atmospheric variability of methyl chloride during the last 300 years from an Antarctic ice core and firn air. *Geophys Res Lett* 31:L02109–L02109
9. This is a contentious figure because of its potential significance in climate change model predictions. In the literature a variety of values are quoted: Cawley GC (2011) On the atmospheric residence time of anthropogenically sourced carbon dioxide. *Energy Fuels* 25:5503–5513
10. Graedel TE, Crutzen PJ (1993) *Atmospheric change*. W H Freeman and Co, New York
11. The AQEG (2008) report: Ozone in the United Kingdom consultation document. www.defra.gov.uk. Accessed 21 June 2012
12. Li Z, Xiangde X et al (2005) Diurnal variations of air pollution and atmospheric boundary layer structure in Beijing during winter 2000/2001. *Adv Atmos Sci* 22:126–132
13. Schönbein CF (1840) On the odour accompanying electricity and on the probability of its dependence on the presence of a new substance. *Philos Mag* 17:293–294
14. Hartley WN (1880) On the probable absorption of the solar ray by atmospheric ozone. *Chem News* 26:268
15. Dobson GMB, Harrison DN et al (1926) Measurements of the amount of ozone in the Earth's atmosphere and its relation to the other geophysical conditions. *Proc R Soc Lond A* 110:660–693
16. Chapman S (1930) On ozone and atomic oxygen in the upper atmosphere. *Phil Mag* 10:369–383
17. Hunt BG (1966) The need for a modified photochemical theory of the ozonosphere. *J Atmos Sci* 23:88–95
18. Molina MJ, Rowland FS (1974) Stratospheric sink for chlorofluoromethanes: chlorine atom catalyzed destruction of ozone. *Nature* 249:810–814
19. Farman JC, Gardner BG et al (1985) Large losses of ozone in Antarctica reveal seasonal ClO_x/NO_x interaction. *Nature* 315:207–210
20. Haagen-Smit AJ (1972) Photochemical smog and ozone reactions. In: Gould RF (ed) *Advances in chemistry*, vol 113. American Chemical Society, Washington, DC
21. Levy H II (1971) Normal atmosphere: large radical and formaldehyde concentrations predicted. *Science* 173:141–143
22. Faraday Discussions (2010) *Chemistry of the planets*, vol 147. RSC publishing, Cambridge

Chapter 6

Photodegradation of Pesticides and Photocatalysis in the Treatment of Water and Waste

M. Emília Azenha, Andreia Romeiro and Mohamed Sarakha

Abstract A brief overview on the main photoprocesses applied to the treatment of water and wastewater is presented. The photodegradation methods that have been applied to the oxidation of organic pollutants are described. A review on advanced oxidation processes (AOP's) and photooxidation mechanisms in homogeneous and heterogeneous solution is presented and some practical applications discussed. Combinations of biological and chemical treatments are considered to be a good approach to improve the removal efficiencies and reduce costs.

6.1 Introduction

Water is critical and vital for life. As a consequence, environmental laws and regulations concerning its quality have become more stringent, in particular with reference to the presence of pesticides and other pollutants, such as chlorophenols, with admissible threshold values less than 0.5 micrograms per litre in water [1]. It is imperative to enforce the protection and correction of environmental problems

M. E. Azenha (✉) · A. Romeiro
Departamento de Química da Faculdade
de Ciências e Tecnologia da Universidade de Coimbra, 3004-535 Coimbra, Portugal
e-mail: meazenha@ci.uc.pt

A. Romeiro
e-mail: aromeiro@ci.uc.pt

M. Sarakha
Université Blaise Pascal U.F.R. Sciences et Technologies Laboratoire de Photochimie
Moléculaire, 24 avenue des Landais BP 80026 63171 Aubière Cedex, France
e-mail: mohamedsarakha@univ-bpclermont.fr

and thus adequate treatment of contaminated waters is of primary concern in order to preserve the natural ecosystem.

The increasing worldwide pollution of freshwater is mainly due to contamination of surface water and groundwater with chemical compounds arising from industrial discharges, excess use of pesticides or fertilizers applied in agriculture and leaching from landfilling of domestic wastes.

In order to cope with water scarcity and pollution of the hydrosphere, two main strategies of water treatment are applied: (1) chemical treatment of polluted drinking water, surface water, groundwater and (2) chemical treatment of wastewaters containing biocidal or non-biodegradable components.

Persistent organic chemicals present as pollutants in wastewater effluents can be found in ground water, as well as in surface waters. They have to be removed to protect water resources or to achieve drinking water quality. Unfortunately, the majority of organic pollutants, and in particular pesticides, are not biodegradable and are noted as biorecalcitrant organic compounds. Therefore, it is very important to develop eco-friendly methods capable of reducing a significant part of this pollution by destroying the toxic and hazardous organic pollutants.

Physicochemical methods, such as flocculation, membrane filtration or adsorption on activated carbon just transfer the pollutants from one phase to another without destroying them. Currently, the main progress in the decontamination of water is focussed on the use of advanced oxidation processes (AOP's) for the degradation of synthetic organic species resistant to conventional treatments, particularly those applying photochemical and photocatalytic reactions, which have the main advantage that they can be used for the treatment of relatively low levels of pollution in aqueous media [2, 3].

All AOP's are based largely on hydroxyl radical chemistry, generated *in situ* normally by using UV lamps or solar energy. The hydroxyl radical (HO^\bullet) has a high reduction potential (2.8 V) and is able to react rapidly and non-selectively with a wide range of organic compounds [4].

The most attractive feature of AOP's is that hydroxyl radical species are strongly oxidising and react with most organic substances, normally either by hydrogen abstraction or electrophilic addition to double bonds. Organic free radicals from the pollutant may react further with molecular oxygen to give a peroxy radical, initiating a sequence of oxidative degradation reactions, which may lead to complete mineralisation of the contaminant [5]. In addition, hydroxyl radicals may attack aromatic rings at positions occupied by a halogen, generating a phenol homologue. However, although hydroxyl radicals are among the most reactive species known, they only react slowly with chlorinated alkane compounds, which are frequent pollutants [6].

In this chapter, we describe the photodegradation methods applied to the oxidation of organic pollutants, namely pesticides. We have made the approach of the direct, sensitised and photocatalytic degradation of pollutants with a scheme of treating these in terms of the possible mechanisms. Further, we give an overview of AOP's in homogeneous and heterogeneous solutions and the corresponding mechanisms.

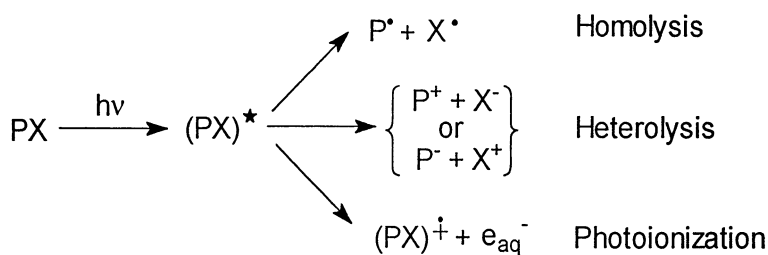
At the end, we will give examples of the treatment of some important pollutants in water.

6.2 Direct Photodegradation

Most pesticides show UV absorption bands at relatively short UV wavelengths (UV-A and UV-B). Since sunlight reaching the Earth's surface (mainly UV-A, with varying amounts of UV-B) contains only a very small amount of this short wavelength radiation [7], the direct photodegradation of pesticides by sunlight is expected to be, in general, of only limited importance.

Direct irradiation will lead to the promotion of the pesticides to their excited singlet states, which may then intersystem cross to produce triplet states. Such excited states can undergo, among other processes: (i) homolysis, (ii) heterolysis or (iii) photoionisation, as depicted in Scheme 6.1 [3].

The reader can find a variety of the literature for several chemical classes of pesticides in the review by Burrows *et al.* [3]. As a consequence of only limited direct photodegradation, in order to use solar energy to obtain significant degradation or mineralisation most research is directed towards photosensitised and photocatalytic reactions.



Scheme 6.1 Possible chemical events taking place upon direct photolysis [3]

6.3 Photosensitised Degradation

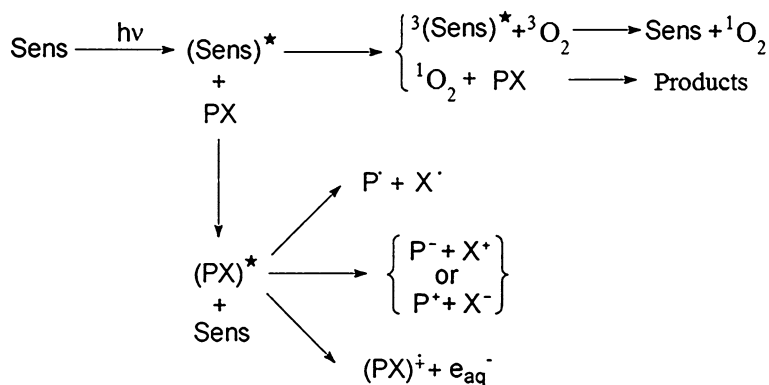
An important advantage of photosensitised photodegradation is the possibility of using light of wavelengths longer than those corresponding to the adsorption characteristics of the pollutant. Photosensitised degradation is based on the absorption of light by a strongly absorbing molecule that is not the pollutant (e.g. methylene blue, Rose Bengal, riboflavin, acetone, tris-2,2'-bipyridyl ruthenium (II), peroxy disulphate, porphyrins, phthalocyanines, etc.). Following light absorption, the photosensitiser (Sens) can transfer energy from its excited state to the pollutant, which can then undergo different intermolecular reactions or

intermolecular photophysical processes [3]. A second photophysical pathway which is of great importance in many systems, including photocatalysis, involves the intermolecular transfer of electronic energy from the excited sensitizer, as donor molecule (D^*) to an energy acceptor (A):



Probably, the most important cases of energy transfer for photocatalysis involve sensitisation by the triplet state of an appropriate donor and its interaction with the ground state (triplet) of molecular oxygen to form the highly reactive singlet oxygen (Scheme 6.2).

Photosensitisation may also involve redox processes such as those observed in the photo-Fenton process to produce hydroxyl free radicals (see Sect. 6.5).



Scheme 6.2 Chemical events taking place upon photosensitised photolysis involving energy transfer [3]

6.4 Photocatalytic Reactions/Heterogeneous Catalysis

Although different definitions have been suggested for photocatalysis, we will use photocatalytic reaction to mean cyclic photoprocesses in which the substrate photodegrades and spontaneous regeneration of the catalyst occurs to allow the sequence to continue indefinitely until all the substrate is destroyed [8, 9].

In conventional heterogeneous catalysis, the overall process consists of a sequence of events, which can be broken down into five elementary steps:

1. Diffusion of the reactants through the bulk to the surface.
2. Adsorption of at least one reactant.
3. Reaction in the adsorbed phase.
4. Desorption of the products.
5. Removal of products away from the interface.

In heterogeneous photocatalysis, the only difference with conventional catalysis lies in step 3, where the usual thermal activation is now replaced by photonic activation. The activation mode is not concerned with steps 1, 2, 4 and 5, although photoadsorption and photodesorption processes of some reactants, particularly oxygen, do exist. The photoinduced molecular transformations and reactions, involving electron transfer or energy transfer, will take place at the surface of the catalyst solely in step 3 as will be described later (Sect. 6.6). Therefore, a heterogeneous photocatalytic system for oxidative degradation of organic or inorganic compounds includes the following components: (1) a reactant; (2) a photon of the appropriate wavelength; (3) a catalyst surface (normally a semiconductor, such as TiO₂ or immobilised sensitisers, such as porphyrins or phthalocyanines, polyoxo-methalates etc.); (4) a strong oxidising agent [10, 11].

6.5 Advanced Oxidation Processes (AOP's)

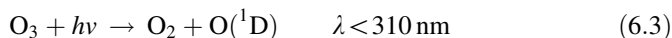
An improvement in oxidative degradation procedures for organic compounds is based on a group of catalytic and photochemical methods, which are referred to as *advanced oxidation processes* (AOP's), and which can be used in homogeneous or heterogeneous media. However, heterogeneous catalysts have the advantage that they can be recovered and reused.

Some of the most frequently used AOP's involve molecules that generate the hydroxyl radical (HO•) *in situ* in homogeneous or heterogeneous media. This can be achieved by various ways, such as:

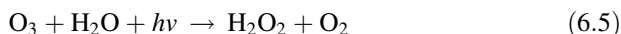
1. Addition of **hydrogen peroxide**, which undergoes homolysis upon photolysis:



2. Photolysis of **ozone**, either with the generation of atoms of singlet oxygen, which then react with water to generate HO•:

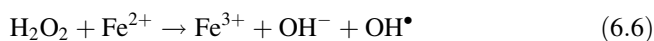


or through direct reaction with water to produce hydrogen peroxide:

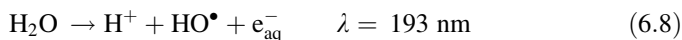


followed by its homolysis to generate hydroxyl radicals.

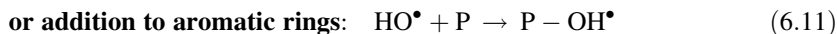
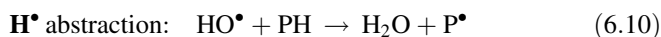
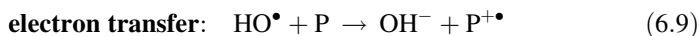
3. Aqueous photolysis of Fe³⁺, generated through oxidation of Fe²⁺ by H₂O₂—the **photo-Fenton** process:



4. Radiolysis (or vacuum UV photolysis) of water:



The HO^\bullet radical can then react by:

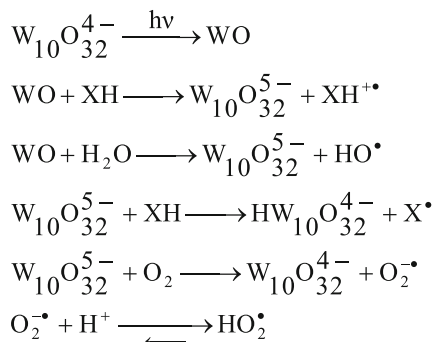


5. Polyoxometalates. Because of their excellent spectroscopic and electronic features, polyoxometalates (POMs) form an important family of compounds that can be used for several interesting applications such as redox and photoredox reactivity, conductivity and ionic charge effects [12]. In particular, these oxygen-bridged metal anion clusters are efficient photocatalysts and because of their wide range of redox potentials they may be used efficiently in various homogeneous oxidation and reduction reactions. These oxides, among them $\text{W}_{10}\text{O}_{32}^{4-}$, show good solubility, and have been intensively studied from the photochemistry point of view [13–15]. They have been shown to be promising candidates for treating contaminated and complex aqueous systems. The decatungstate polyoxometalate, which shows low toxicity, absorbs in the UV with a maximum at 320 nm. Its UV absorption spectrum clearly overlaps the solar emission spectrum indicating the possible use of this inexhaustible source of energy for the degradation of organic as well as inorganic substrates. Supported decatungstate can also be considered as a good candidate for the recovery of the photocatalyst for example on silica [16] and carbon fibres [17].

The application of tungstate-based photocatalysts was proposed by Satari and Hill [18]. These authors clearly showed that the light excitation of $\text{W}_{10}\text{O}_{32}^{4-}$ permits the oxidation of organic compounds with an effective cleavage of carbon-halogen bonds. This interesting application in the field of water decontamination has been seriously explored by Papaconstantinou and collaborators for the photochemical degradation and also efficient mineralisation of substrates such as chlorophenols and various chloroacetic acids [19, 20]. Within this work, a comparative study was carried out on the photocatalytic efficiency of TiO_2 and $\text{Na}_4\text{W}_{10}\text{O}_{32}$ at $\lambda > 300$ nm. The organic pollutants used were phenol, 4-chlorophenol, 2,4-dichlorophenol, bromoxynil, atrazine, imidachloprid and oxamyl in aqueous solution. TiO_2 was found to be the most effective photocatalyst in terms of the degradation rate and of the mineralisation of the compounds. However, the decatungstate anion appeared to be particularly efficient in the case of pesticides formulations, such as those prepared in the presence of surfactants [21]. Since mineralisation with decatungstate anions occurs over a longer time range, its use should be restricted only to pollutants that produce non-toxic intermediates.

Intensive studies have been devoted to obtain mechanistic information on photocatalysis by POMs that give a precise overview on the cascade of events, lifetime and quantum yield of formation of the primary intermediate species, which proceed after light absorption before leading to final reaction products [21–24]. These were performed using laser flash photolysis and pulse radiolysis, in combination with continuous photolysis studies. Within such studies, the light excitation of decatungstate leads to the formation of a very short lived charge transfer excited state (about 30 ps lifetime) which forms a longer lived species designated as WO with a formation quantum yield of 0.6. This latter species is most likely to be the reactive species in photocatalytic systems [23]. Furthermore, in aqueous solution, the photooxidation performance can be enhanced by the production of highly reactive hydroxyl radicals formed through the direct reaction of water with the excited decatungstates. In the presence of, for example, an organic substrate XH, WO reacts to form the one electron reduced species through either a hydrogen abstraction process or electron transfer. In aerated conditions, $W_{10}O_{32}^{5-}$ is then reoxidised by O_2 leading to the formation of the starting $W_{10}O_{32}^{4-}$, according to Scheme 6.3.

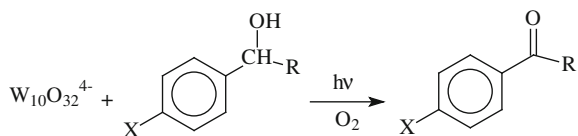
This type of photocatalytic cycle can efficiently be used for the degradation of organic substrates with the total recovery of the photocatalyst. They have also been used for the reduction of metal ions [25] and in simultaneous conversion of dye and hexavalent chromium using visible light illumination [26]. Some specific examples are described below.



Scheme 6.3 Photochemical primary processes upon excitation of $W_{10}O_{32}^{4-}$

i) Oxidation of Aryl Alkanols

A series of 1-aryl alkanols were investigated using polyoxometalates such as $W_{10}O_{32}^{4-}$ as a photocatalyst (Scheme 6.4). A clean oxidation reaction of the side chain of the aryl alkanol led to the formation of the aryl ketone. This process supports a hydrogen transfer mechanism as the rate determining step. The efficiency of the reaction was mainly determined in the presence of oxygen [27].

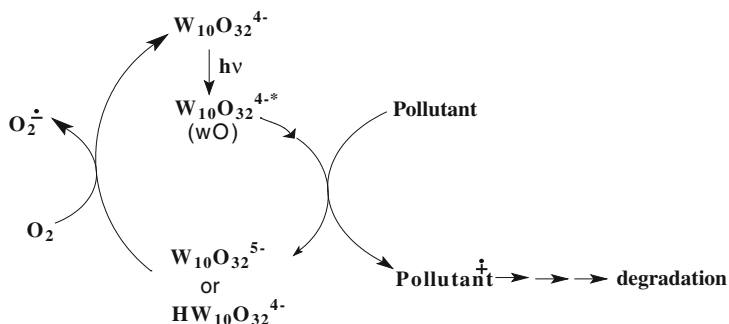


Scheme 6.4 Oxidation process induced by excitation of $W_{10}O_{32}^{4-}$

ii) Decolorisation of Dye Solutions and Pesticide Degradation

The photocatalytic degradation of textile and industry dyes (Brilliant Red X3B and Acid Orange 7) and pesticides was efficiently observed using POMs as inducers at $\lambda > 320$ nm. The photooxidative decomposition of Acid Orange (4[2-hydroxy-1-naphthyl]azo]benzene sulfonic acid) leads to the formation of several by-products that disappear in turn by excitation of POMs. Among them are 1-(4-hydroxyphenyl)azo-2-naphthol, 1-(phenylazo)-2-naphthol, 2-naphthol, 4-methyl-1-naphthol. Such reactivity demonstrates the involvement of an electron transfer process. In most cases, particularly in the presence of oxygen, the process leads to mineralisation of the solution showing the great reactivity of the POMs used towards the majority of the compounds (initial and intermediates) [28–30]. The following photocatalytic cycle has been proposed as shown in Scheme 6.5.

6. **Semiconductors** excited by appropriate energy photons. Two well-defined AOP's systems which have special interest, because natural solar light can be used, are heterogeneous photocatalysis with TiO_2 and homogeneous photocatalysis by the photo-Fenton process. These processes are covered in detail in the following sections.



Scheme 6.5 Photocatalytic cycle of $W_{10}O_{32}^{4-}$ in the presence of organic pollutant

6.6 Heterogeneous Photocatalysis by Semiconductors

Heterogeneous photocatalysis by semiconductor materials has gained increasing interest because, as a green technology, it can be widely applied both to environmental purification (non-selective process) and selective organic transformations of fine chemicals in both gas and liquid phases [31, 32].

Inorganic semiconductors (such as TiO_2 , ZnO , Fe_2O_3 , CdS and ZnS) can act as sensitizers for light-induced redox processes due their electronic structure, which is characterised by a filled valence band (VB) separated by a relatively small energy from an empty conduction band (CB) (see Chap. 4). The separation between the two bands is particular to each semiconductor, and is referred to as the *bandgap* (E_g). When the semiconductor is illuminated with light ($h\nu$) of energy greater than that of the bandgap, an electron is promoted from the VB to the CB, thus leaving a positive hole in the valence band; that is, absorption of light with sufficient energy (\geq the bandgap energy, E_g) leads to the formation of an electron/hole pair. In the absence of suitable scavengers, the stored energy is dissipated within a few nanoseconds by charge recombination. However, if a suitable scavenger or surface defect state is available to trap the electron or hole, recombination is prevented and subsequent redox reactions may occur. The valence band holes are powerful oxidants (+1.0 to +3.5 V vs. NHE (Normal Hydrogen Electrode)), depending on the semiconductor and pH, while the conduction band electrons are good reductants (+0.5 to -1.5 V vs. NHE). Most organic photodegradation reactions use the oxidising power of the holes either directly or indirectly. However, to prevent a build-up of charge one must also provide a reducible species to react with the electrons.

Within the large number of inorganic semiconductors that are known, TiO_2 and ZnO are the most commonly used in photocatalysis, due to both low cost and acceptable bandgap energy.

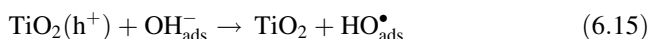
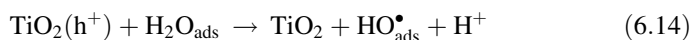
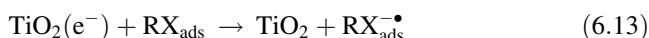
Titanium dioxide-based materials have proved to be the most suitable for the majority of environmental applications. TiO_2 is abundant, chemically inert, stable to photo- and chemical corrosion, inexpensive, relatively non-toxic, with good electronic and optical properties. However, it should be noted that the toxicity of TiO_2 in the form of nanoparticles is currently under study [33, 34]. TiO_2 is of special interest since it can use natural solar-UV radiation for excitation, which makes it a promising candidate in photocatalysis using solar light as energy source.

Considering the appropriate energetic separation between the valence and conduction bands in TiO_2 , which has to be overcome by the energy of a UV solar photon, the (VB) and (CB) energies are +3.1 and -0.1 V, respectively, such that the bandgap energy is 3.2 eV, which corresponds to absorption of near UV light ($\lambda < 387$ nm).

Under these conditions, valence band electrons are excited and move to the conduction band leaving behind holes; thus generating an electron/hole pair (e^- to h^+). The electron and holes must then migrate to the surface of the semiconductor to promote reduction and oxidation reactions of adsorbed species or of species that

are in close proximity to the surface of the semiconductor (Fig. 6.1). However, electron–hole recombination, at the surface or in the bulk of the catalyst competes with the above process and limits the overall quantum yield of photocatalytic reactions [35, 36]. Activation of this process proceeds through the excitation of the solid but not the reactants: there is no photochemical process in the adsorbed phase, but only a true heterogeneous photocatalytic reaction. The photocatalytic activity can be reduced by the electron–hole recombination, as described in Fig. 6.2, which corresponds to the degradation of the photoelectronic energy into heat.

The following chain reactions can be postulated:



The reaction mechanism described by Eqs. 6.14 and 6.15 appears to be of greater importance in oxidative degradation processes compared with the reductive route (Eq. 6.13), probably due to the high concentration of H_2O and HO^- molecules adsorbed at the particle surface with the generation of HO^{\bullet} a powerful oxidising species. Molecular oxygen, which must be present in all oxidative degradation processes, is the accepting species in the electron-transfer reaction from the conduction band of the photocatalyst (Eq. 6.16). The superoxide anion, and its

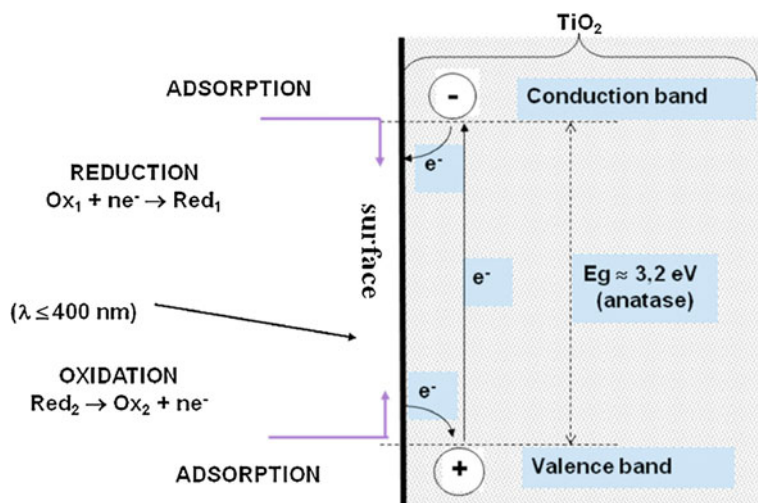


Fig. 6.1 Energy band diagram and activation of titanium dioxide (reproduced from Ref. [35] with personal permission of Jean-Marie Herrmann)

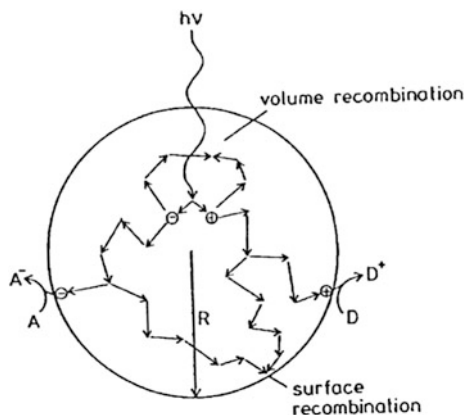
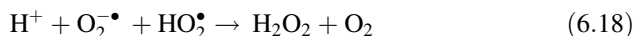
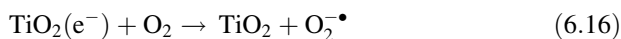


Fig. 6.2 Fate of electrons and holes within a spherical particle of TiO_2 in the presence of an acceptor (A) and (D) molecule (adapted with permission from Ref. [36], Copyright 1993, Elsevier)

protonated form, subsequently yield hydrogen peroxide (or peroxide anion) and molecular oxygen (Eq. 6.18).



Anatase and rutile are the most common forms of TiO_2 , and anatase is the most effective in photocatalytic wastewater treatment, mainly because it has a higher surface area and higher surface density of active sites for adsorption and catalysis. Brookite is not likely to be involved in photodegradation.

It has been pointed out that the photodegradation reaction rate is much more rapid with anatase than with rutile, and that the reaction rate is mainly affected by the crystalline state surface area and particle size of TiO_2 powder. However, these factors often vary in opposite ways, since a high degree of crystallinity is achieved through a high-temperature thermal treatment leading to a reduction in the surface area, while optimal conditions are required for photocatalysis. The photocatalytic activity of TiO_2 depends not only on the bandgap energy, but also, to a large extent, on its surface properties, which are affected both by the synthetic process [37] and the calcination atmosphere [38].

Although TiO_2 is cheap, the efficiency of the photocatalysis process with solar energy is low because only 10 % of the overall solar intensity is in the UV-A region where TiO_2 is excited. The effective goal now is to achieve TiO_2 -type photocatalysis with commercial viability using solar energy and high activity of photodegradation of pollutants. Within recent years, research has responded to this challenge. New TiO_2 photocatalysts have been synthesised by sol-gel or hydrothermal methods.

Doping the semiconductor with a variety of metal ions, such as Sn^{4+} , Au^{3+} , Bi^{3+} , Mg^{2+} , Ba^{2+} , etc. [39–42] has induced a bathochromic (red) shift, extending its absorption towards the visible light region. However, we should note that cationic doping may be detrimental for photocatalysis, since the doping cations may act as charge recombination centres [35]. Enhanced photocatalytic activity may be obtained by the introduction of non-metallic anions (N, C, S and F) [43–45], or by coupling two semiconductor systems TiO_2/CdS , $\text{TiO}_2/\text{SnO}_2$, TiO_2/ZnO , TiO_2/WO_3 [46, 47], in which there is coupling between a large gap semiconductor (3.2 eV TiO_2) and a smaller bandgap one. For example, in TiO_2/CdS the photogenerated electrons (2.4–2.6 eV in CdS) are transferred onto TiO_2 particles while the holes remain on the CdS particles, which makes long-term charge separation possible, by decreasing the recombination, and at the same time allowing the extension of the response of the photocatalyst into the visible region. Serpone et al. [46] provided the first report of the photocatalysed oxidation of phenols by coupled semiconductors in which the beneficial effect of charge transfer was demonstrated.

Immobilisation techniques on different supports have been also investigated. Among these materials, titanium dioxide with activated carbon, carbon nanotubes, activated carbon fibres, silica and alumina have all shown higher activity in photodegradations because of their surface properties, compared with TiO_2 alone [48, 49].

6.7 Photocatalysis in the Treatment of Water and Waste

Water purification treatment is currently a very hot subject within scientific research, and several books and reviews have been devoted to this problem [2, 3, 11, 36, 50–56]. One of the challenges facing water purification treatment is the elimination of low concentrations of toxic biorecalcitrants, particularly when present as components of complex mixtures, including chlorinated aromatics, pesticides, pharmaceuticals, hormones, surfactants, etc. [57, 58].

René *et al.* [63] indicate three scientific challenges in water quality problems caused by such micropollutants: (i) to develop and refine the tools to assess the impact of these pollutants on aquatic life and human health; (ii) the cost-effective and appropriate remediation and water treatment technologies must be explored and implemented, and (iii) usage and disposal strategies must be applied, coupled with intensive research and development of environmentally more benign products and processes.

TiO_2 has shown, so far, the best photocatalytic performance of all the inorganic semiconductors studied in the catalysed photodegradation of pesticides, and titania nanomaterials have been successfully used for the degradation of several classes of pollutants (pesticides, chlorinated aromatics, etc.), leading in some cases to complete mineralisation. However, these contrast, with the high cost of separation of the catalysts.

Photocatalysed degradation of s-triazine type herbicides with TiO_2 has been studied and it was observed that cyanuric acid is the final photoproduct [59–62].

This is photostable and complete mineralisation was not observed. In some countries restrictions on the use of s-triazines, such as atrazine, have been implemented, while in others, these have even been banned. Atrazine has, however, been detected above the recommended levels (0.1 ppb or $\mu\text{g dm}^{-3}$) throughout Europe and the United States and is considered as a priority toxic substance by the EC. Considerable efforts are being made to eliminate it from water.

Immobilised TiO_2 films have been tested in photocatalytic water treatment with atrazine but total mineralisation has not yet been achieved [63]. Microwave assisted degradation of atrazine with TiO_2 nanotubes, however, appears to be a good potential route way to mineralise atrazine [64].

Porphyrins and metalloporphyrins supported on TiO_2 also can degrade atrazine and 4-nitrophenol under visible light irradiation. However, lower efficiency is observed for atrazine than for the phenol. It is also possible to mineralise 4-nitrophenol with porphyrin/ TiO_2 based composites, and the addition of H_2O_2 improves this process when atrazine is used as substrate [65–67].

Indeed, porphyrins are good sensitisers for visible light sensitisation, with high extinction coefficients for their absorptions around 400 nm corresponding to the Soret band (see Chap. 4). They have been used as photosensitisers with polycrystalline TiO_2 in order to enhance the visible light-sensitivity of the TiO_2 matrix, and therefore increase its photocatalytic activity [67, 68]. For heterogeneous photocatalysis, immobilisation of porphyrins provides another route towards photodegradation of pesticides [69, 70].

Titanium dioxide in films has been proved to be a good photocatalyst towards degradation of chloroaromatics, such as chlorophenols [71], although overall mineralisation with chlorophenols has not been reported. Herrmann *et al.* [72] have studied the photocatalytic degradation with TiO_2 under solar irradiation of 2,4-dichlorophenoxyacetic acid leading to the complete mineralisation of the substrate.

Chlorophenols appear commonly in industrial effluents, but research into photocatalytic degradation of these compounds [73, 74] by TiO_2 indicates that mineralisation is not effective.

In order to have a practical application of these systems, both the use of visible light source and an enhanced degradation rate are essential. Doped TiO_2 semiconductors show photocatalytic activity for the photodegradation of phenol and chlorophenol using visible light [41, 43, 44, 75].

Coupled systems, such as TiO_2/WO_3 , have been tested with 4-chlorophenol, and have shown efficient degradation under visible light irradiation. A much higher hydroxyl radical concentration is found for the TiO_2/WO_3 system than using TiO_2 alone [47].

Immobilisation of TiO_2 on solid supports appears to be an attractive alternative avoiding the separation step in photocatalysis. Immobilisation of titanium dioxide has been adapted to a pilot scale solar photoreactor in a compound parabolic collector (CPC), and shown to be effective on the degradation and mineralisation of phenol and some emergent contaminants in a municipal effluent [57, 76].

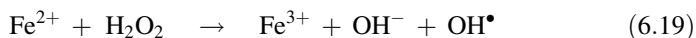
Sequential biological—advanced oxidative—biological processes are proving to be promising in photodegradation of chlorophenols as model substrates, and promote total degradation [77].

We have focused on triazines and chlorophenols, but the same methodology can be applied to other systems.

6.8 Photo-Fenton Reaction in the Treatment of Water and Waste Water

Among the various advanced oxidation processes, Fenton reactions and their combination with light, namely photo-Fenton reaction, have been efficiently used for the destruction of toxic and persistent organic pollutants [78–80]. Fenton treatment consists of the *in situ* formation of a highly reactive species, *i.e.* the hydroxyl radical. This is as an efficient oxidant ($E = 2.8 \text{ V vs. NHE}$) lower than fluorine (3.0 V) and higher than ozone (2.07 V) and hydrogen peroxide (1.78 V), which is able to react with almost all the organic compounds with rate constants close to those for diffusion controlled processes. Its reactions towards organic compounds can proceed *via* H-abstraction, electron transfer and/or addition to carbon–carbon unsaturated bonds.

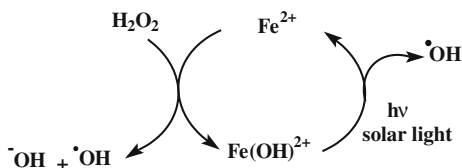
Even though the process is very complex, the production of the hydroxyl radical through the Fenton reaction is considered to be due to the interaction of hydrogen peroxide with ferrous ion, which occurs with a rate constant of $63 \text{ mol}^{-1} \text{ dm}^3 \text{ s}^{-1}$ [80–82].



The destruction rate of several organic pollutants was shown to increase when light illumination of the solution is used simultaneously with the above Fenton reaction. In this process, the iron salts (Fe^{2+} , Fe^{3+}) are used as photosensitisers and the hydrogen peroxide as an oxidising agent leading to a better production of hydroxyl radicals. The increase of the hydroxyl production rate is due to the involvement in the iron (III) photo reduction reaction of the iron aquacomplex, $[\text{Fe}(\text{H}_2\text{O})(\text{OH})]^{2+}$ (represented by $\text{Fe}(\text{OH})^{2+}$) through light excitation into the ligand to metal charge transfer transition (Eq. 6.20) [83–85].



Such a reaction regenerates ferrous ion showing that only low concentration of Fe^{2+} is needed in the system [86]. Moreover, the photo-Fenton process may proceed using photons of wavelength close to 500 nm in the case of mixtures of ferric ion and hydrogen peroxide. It can also be performed by solar irradiation making it a low cost process [79, 80, 87, 88]. The photocatalytic cycle may be presented as shown in Scheme 6.6.



Scheme 6.6 Photocatalytic cycle of iron in the photo-Fenton process

As shown in the photocatalytic cycle, the continuous production of hydroxyl radicals as well as the presence of hydrogen peroxide leads to the oxidation of the organic pollutants and also of the generated by-products. This phenomenon permits, in many cases, the total mineralisation of the solution [89].

6.9 Conclusions

In conclusion, current research on the degradation of organic pollutants has been focused on the combination of chemical (AOP's) processes and biological treatment and these have been tested on biorecalcitrant compounds such pesticides and chlorophenols [76, 90–92]. The results have shown that such AOP's have the ability to degrade the pollutants and produce by-products with high bio-degradation efficiency. Furthermore, by using the combination of biological and chemical treatments, in addition to improving the removal efficiencies, there is also a marked reduction of the overall costs, thus overcoming one of the main economic hindrance to practical exploitation.

Powdered TiO_2 is widely used in suspension (slurry) with excellent performance, but it requires filtration. Immobilisation of TiO_2 on solid supports such as glass, polymers and ceramics removes the need for filtration to separate the catalyst from treated water, making the process less expensive.

Solar photocatalytic degradation of water contaminants with titania and photo-Fenton catalysts has been carried out on a pilot-plant scale at the solar photo-chemical facilities of the *Plataforma Solar de Almeria* (PSA) in Spain, and show how solar photocatalysis is likely to become important within the next few decades in wastewater treatment and development of new AOP technologies [93, 94].

The testing and development of reactors to maximise the optical efficiencies are also being carried out at PSA. Unfortunately, at present there are no general rules for the photocatalysed degradation of several pollutants, and preliminary research is always required to optimise the best conditions.

References

1. Commission of the European Communities. Directive of the European Parliament and of the Council on environmental quality standards in the field of water policy and amending. Directive 2000/60/EC. COM (2006) 397 final, Brussels, July 2006
2. Legrini O, Oliveros E, Braun AM (1993) Photochemical processes for water treatment. *Chem Rev* 93:671–698
3. Burrows HD, Canle M, Santaballa JA, Steenken S (2002) Reaction pathway and mechanisms of photodegradation of pesticides. *J Photoch Photob B Biol* 67:71–108
4. Bielski BHJ, Cabelli DE, Arudi RL (1985) Reactivity of HO_2/O_2 -radicals in aqueous solution. *J Phys Chem Ref Data* 14:1041–1100
5. Buxton GV, Greenstock CL, Helman WP, Ross AB (1988) Critical review of rate constants for reactions of hydrated electrons, hydrogen atoms and hydroxyl radicals ($\text{HO}^\bullet/\text{HO}^-$) in aqueous solution. *J Phys Chem* 17:513–886
6. Haag WR, Yao CCD (1992) Rate constants for reaction of hydroxyl radicals with several drinking water contaminants. *Environ Sci Technol* 26:1005–1013
7. Murov SL, Carmichael I, Hug GL (eds) (1993) *Handbook of photochemistry*, 2nd edn. Marcel Dekker, New York
8. Braslavsky SE (2007) Glossary of terms used in photochemistry, 3rd edn. *Pure Appl Chem* 79:293–465
9. Kalyanasundaram K, Grätzel M (1993) Photosensitization and photocatalysis using inorganic and organometallic compounds. Kluwer Academic Publishers, Dordrecht
10. Faria J (2008) The heterogeneous photocatalytic process. In: Figueiredo JL, Pereira MM, Faria J (eds) *Catalysis from theory to application*. Coimbra University Press, Coimbra
11. Herrmann JM (2005) Heterogeneous photocatalysis: state of the art and present applications. *Top Catal* 34:49–65
12. Katsoulis DE (1998) A survey of applications of polyoxometalates. *Chem Rev* 98:359–388
13. Hill CL, Prosser-McCartha CM (1995) Homogeneous catalysis by transition metal oxygen anion clusters. *Coord Chem Rev* 143:407–455
14. Misono M (1987) Heterogeneous catalysis by heteropoly compounds of molybdenum and tungsten. *Catal Rev Sci Eng* 29:269–321
15. Papaconstantinou E (1989) Photochemistry of polyoxometalates of molybdenum and tungsten and/or vanadium. *Chem Soc Rev* 18:1–31
16. Kozhevnikov IV, Kloestra KR, Sinnema A, Zandbergen HW, Van Bekkum H (1996) Study of catalysts comprising heteropoly acid $\text{H}_3\text{PW}_{12}\text{O}_{40}$ supported on MCM-41 molecular sieve and amorphous silica. *J Mol Catal A Chem* 114:287–298
17. Gall RD, Hill CL, Walker JE (1996) Carbon powder and fiber-supported polyoxometalate catalytic materials. Preparation, characterization, and catalytic oxidation of dialkyl sulfides as mustard (HD) analogues. *Chem Mater* 8:2523–2527
18. Sattari D, Hill CL (1993) Catalytic carbon-halogen bond cleavage chemistry by redox-active polyoxometalates. *J Am Chem Soc* 115:4649–4657
19. Mylonas A, Papaconstantinou E (1994) Photocatalytic degradation of chlorophenols to CO_2 and HCl with polyoxotungstates in aqueous solution. *J Mol Catal* 92:261–267
20. Mylonas A, Hiskia A, Papaconstantinou E (1996) Contribution to water purification using polyoxometalates. Aromatic derivatives, chloroacetic acids. *J Mol Catal A Chem* 114:191–200
21. Texier I, Giannotti C, Malato S, Richter C, Delaire J (1999) Solar photodegradation of pesticides in water by sodium decatungstate. *Catal Today* 54:297–307
22. Texier I, Delouis J-F, Delaire J, Giannotti C, Plaza P, Martin M (1999) Dynamics of the first excited state of the decatungstate anion studied by subpicosecond laser spectroscopy. *Chem Phys Lett* 311:139–145
23. Tanielian C (1998) Decatungstate photocatalysis. *Coord Chem Rev* 178–180:1165–1181

24. Tanielian C, Duffy K, Jones A (1997) Kinetic and mechanistic aspects of photocatalysis by polyoxotungstates: a laser flash photolysis, pulse radiolysis, and continuous photolysis study. *J Phys Chem B* 101:4276–4282
25. Kim S, Yeo J, Choi W (2008) Simultaneous conversion of dye and hexavalent chromium in visible light-illuminated aqueous solution of polyoxometalate as an electron transfer catalyst. *Appl Catal B Environ* 84:148–155
26. Troupis A, Gkika E, Hiskia A, Papaconstantinou E (2006) Photocatalytic reduction of metals using polyoxometallates: recovery of metals or synthesis of metal nanoparticles. *C R Chimie* 9:851–857
27. Lykakis IO, Tanielian C, Orfanopoulos M (2003) Decatungstate photocatalyzed oxidation of aryl alkanols. Electron transfer or hydrogen abstraction mechanism? *Org Lett* 5:2875–2878
28. Troupis A, Triantis TM, Gkika et al (2009) Photocatalytic reductive–oxidative degradation of Acid Orange 7 by polyoxometalates. *Appl Catal B Environ* 86:98–107
29. Hu M, Xu Y (2004) Photocatalytic degradation of textile dye X3B by heteropolyoxometalate acids. *Chemosphere* 54:431–434
30. Rafqah S, Wong Wah Chung P, Forano C, Sarakha M (2008) Photocatalytic degradation of metsulfuron methyl in aqueous solution by decatungstate anions. *J Photochem Photobiol A Chem* 199:297–302
31. Anpo M (2000) Utilization of TiO₂ photocatalysts in green chemistry. *Pure Appl Chem* 72:1265–1270
32. Fox MA, Dulay MT (1993) Heterogeneous photocatalysis. *Chem Rev* 93:341–357
33. IARC (2006) Titanium dioxide Group 2B, Monographs on the evaluation of carcinogenic risks to humans. International Agency for Research on Cancer, World Health Organization, Lyon
34. Ramsden CS, Smith TJ, Shaw BJ, Handy RD (2009) Dietary exposure to titanium dioxide nanoparticles in rainbow trout, (*Oncorhynchus mykiss*): no effect on growth, but subtle biochemical disturbances in the brain. *Ecotoxicology* 18:939–951
35. Herrmann JM (2010) Photocatalysis fundamentals revisited to avoid several misconceptions. *Appl Catal* 99:461–468
36. Gerischer H (1993) Photocatalytic purification and treatment of water and air. In: Ollis DF, Al-Ekabi H (eds) Photocatalytic purification and treatment of water and air. Elsevier Science, Amsterdam
37. Nakamura M, Negishi N, Kutsuna S et al (2000) Role of oxygen vacancy in the plasma-treated TiO₂ photocatalyst with visible light activity for NO removal. *J Mol Catal A Chem* 161:205–212
38. Wu NL, Lee MS, Pon ZJ, Hsu JZ (2004) Effect of calcination atmosphere on TiO₂ photocatalysis in hydrogen production from methanol/water solution. *J Photochem Photobiol A* 163:277–280
39. Cao YA, Yang WS, Zhang WF et al (2004) Improved photocatalytic activity of Sn⁴⁺ doped TiO₂ nanoparticulate films prepared by plasma-enhanced chemical vapor deposition. *New J Chem* 28:218–222
40. Li FB, Li XZ (2002) Photocatalytic properties of gold/gold ion-modified titanium dioxide for wastewater treatment. *Appl Catal A Gen* 288:15–27
41. Venkatachalam N, Palanichamy M, Murugesan V (2007) Sol-gel preparation and characterization of alkaline earth metal doped nano TiO₂: efficient photocatalytic degradation of 4-chlorophenol. *J Mol Catal A Chem* 273:177–185
42. Yu J, Liu S, Xiu Z et al (2008) Combustion synthesis and photocatalytic activities of Bi³⁺ doped TiO₂ nanocrystals. *J Alloy Compd* 461:L17–L19
43. Liu S, Chen X (2008) A visible light response TiO₂ photocatalyst realized by cationic S-doping and its application for phenol degradation. *J Hazard Mater* 152:48–55
44. Anpo M, Takeuchi M (2003) The design and development of highly reactive titanium oxide photocatalysts operating under visible light irradiation. *J Catal* 216:505–516
45. Ohno T, Mitsui T, Matsumura M (2003) Photocatalytic activity of S-doped TiO₂ Photocatalyst under visible light. *Chem Lett* 32:364–36519

46. Serpone N, Maruthamuthu P, Pichat P et al (1995) Exploiting the interparticle electron transfer process in the photocatalysed oxidation of phenol, 2-chlorophenol and pentachlorophenol: chemical evidence for electron and hole transfer between coupled semiconductors. *J Photochem Photobiol* 85:247–255
47. Lin CF, Wu CH, Onn ZN (2008) Degradation of 4-chlorophenol in TiO₂, WO₃, SnO₂, TiO₂/WO₃ and TiO₂/SnO₂ systems. *J Hazard Mater* 154:1033–1039
48. Wang W, Serp P, Kalck P, Faria JL (2005) Photocatalytic degradation of phenol on MWNT and Titania composite catalysts prepared by a modified sol-gel method. *Appl Catal B Environ* 56:305–312
49. Wang W, Serp P, Kalck P et al (2008) Preparation and characterization of nanostructured MWCNT-TiO₂ composite materials for photocatalytic water treatment applications. *Mater Res Bull* 43:958–967
50. Khataee AR, Kasiri MB (2010) Photocatalytic degradation of organic dyes in the presence of nanostructured titanium dioxide: influence of the chemical structure of dyes. *J Mol Catal A Chem* 328:8–26
51. Schiavello M (ed) (1988) *Photocatalysis and environment: trends and applications*. Kluwer Academic Publishers, Dordrecht
52. Serpone N, Pelizzetti E (eds) (1989) *Photocatalysis, fundamentals and applications*. Wiley, New York
53. Herrmann JM, Guillard C, Pichat P (1993) Heterogeneous photocatalysis: an emerging technology for water treatment. *Catal Today* 17:7–20
54. Guillard C, Disdier J, Herrmann JM et al (1999) Comparison of various Titania samples of industrial origin in the solar photocatalytic detoxification of water containing 4-chlorophenol. *Catal Today* 54:217–228
55. Zepp RG, Helz GR, Crosby DG (eds) (1994) *Aquatic surface photochemistry*. Lewis Publishers, Boca Raton
56. Jansen F, Van Santen RA (1999) *Environmental catalysis*. Imperial College Press, London
57. Mazille F, Schoettl T, Klamerth N et al (2010) Field solar degradation of pesticides and emerging water contaminants mediated by polymer films containing titanium and iron oxide with synergistic heterogeneous photocatalytic activity at neutral pH. *Water Res* 44:3029–3038
58. Schwarzenbach RP, Escher BI, Fenner K et al (2006) The challenge of micropollutants in aquatic systems. *Science* 313:1072–1077
59. Pelizzetti E, Minero C, Carlin C et al (1992) Identification of photocatalytic degradation pathways of 2-Cl-S- triazine herbicides and detection of their decomposition intermediates. *Chemosphere* 24:891–910
60. Pelizzetti E, Carlin C, Minero C et al (1992) Degradation pathways of atrazine under solar light and in the presence of TiO₂ colloidal particles. *Sci Total Environ* 123–124:161–169
61. Minero C, Maurino V, Pelizzetti E (1997) Heterogeneous photocatalytic transformations of s-triazine derivatives. *Res Chem Inter* 23:291–310
62. Gianturco F, Chiodaroli CM, Bellobono IR et al (1997) Pilot-plant photomineralization of atrazine in aqueous solution, by photocatalytic membranes immobilising titanium dioxide and promoting photocatalysts. *Fresenius Environ Bull* 6:461–468
63. McMurray TA, Dunlop PSM, Byrne JA (2006) The photocatalytic degradation of atrazine on nanoparticulate TiO₂ films. *J Photochem Photobiol A Chem* 182:43–51
64. Zhanqi G, Shaogui Y, Na T, Cheng S (2007) Microwave assisted rapid and complete degradation of atrazine using TiO₂ nanotube photocatalyst suspension. *J Hazard Mater* 145:424–430
65. Granados-Oliveros G, Páez-Mozo EA, Ortega FM et al (2009) Degradation of atrazine using metalloporphyrins supported on TiO₂ under visible light irradiation. *Appl Catal B Environ* 89:448–454
66. Wang C, Li J, Mele G et al (2010) The photocatalytic activity of novel, substituted porphyrin/TiO₂-based composites. *Dyes Pigment* 84:183–189

67. Mele G, Del Sole R, Vasapollo G et al (2003) Photocatalytic degradation of 4-nitrophenol in aqueous suspension by using polycrystalline TiO₂ impregnated with functionalized Cu(II)-porphyrin or Cu(II)-phthalocyanine. *J Catal* 217:334–342
68. Wang C, Yang G-M, Li J et al (2009) Novel *meso*-substituted porphyrins: synthesis, characterization and photocatalytic activity of their TiO₂-based composites. *Dyes Pigm* 80:321–328
69. Silva M, Azenha ME, Pereira MM et al (2009) Immobilization of 5,10,15,20-tetrakis-(2-fluorophenyl)porphyrin into MCM-41 and NaY: routes toward photodegradation of pesticides. *Pure Appl Chem* 81:2025–2033
70. Silva M, Azenha ME, Pereira MM et al (2010) Immobilization of halogenated porphyrins and their copper complexes in MCM-41: environmentally friendly photocatalysts for the degradation of pesticides. *Appl Catal B Environ* 100:1–9
71. Mills A, Wang J (1998) Photomineralisation of 4-chlorophenol sensitised by TiO₂ thin films. *J Photochem Photobiol A Chem* 118:53–63
72. Herrmann JM, Disdier J, Pichat P et al (1998) TiO₂-based solar photocatalytic detoxification of water containing organic pollutants. Case studies of 2,4-dichlorophenoxyacetic acid (2,4-D) and of benzofuran. *Appl Catal B Environ* 17:15–23
73. Wuang KH, Hsieh YH, Chou MY, Chang CY (1998) Photocatalytic degradation of 2-chloro and 2-nitrophenol by titanium dioxide suspensions in aqueous solution. *Appl Catal B Environ* 21:1–8
74. Pera-Titus M, Garcia-Molina V, Banos MA et al (2004) Degradation of chlorophenols by means of advanced oxidation processes: a general review. *Appl Catal B Environ* 47:219–256
75. Huang DG, Liao SJ, Liu JM et al (2006) Preparation of visible-light responsive N-F-codoped TiO₂ photocatalyst by a sol-gel-solvothermal method. *J Photochem Photobiol A Chem* 184:282–288
76. Miranda-García N, Suárez S, Sánchez B et al (2011) Photocatalytic degradation of emerging contaminants in municipal wastewater treatment plant effluents using immobilized TiO₂ in a solar pilot plant. *Appl Catal B Environ* 103:294–301
77. González LF, Sarria V, Sánchez F (2010) Degradation of chlorophenols by sequential biological-advanced oxidative process using *Trametes pubescens* and TiO₂/UV. *Bioresource Technol* 101:3493–3499
78. Perez M, Torrades F, Doménech X, Peral J (2002) Removal of organic contaminants in paper pulp effluents by AOPs: an economic study. *J Chem Technol Biotechnol* 77:5425–5532
79. Sun Y, Pignatello JJ (1993) Photochemical reactions involved in the total mineralization of 2,4-D by iron(3+)/hydrogen peroxide/UV. *Environ Sci Technol* 27:304–310
80. Pignatello JJ, Liu D, Huston P (1999) Evidence for an additional oxidant in the photoassisted Fenton reaction. *Environ Sci Technol* 33:1832–1839
81. Kuo WG (1992) Decolorizing dye wastewater with Fenton's reagent. *Water Res* 26:881–886
82. Lipczynska-Kochany E (1991) Degradation of aqueous nitrophenols and nitrobenzene by means of the Fenton reaction. *Chemosphere* 22:529–536
83. Brand N, Mailhot G, Bolte M (1998) Degradation photoinduced by Fe(III): method of alkylphenol ethoxylates removal in water. *Environ Sci Technol* 32:2715–2720
84. Benkelberg HJ, Warneck P (1995) Photodecomposition of iron (III) hydroxo and sulfato complexes in aqueous solution: wavelength dependence of OH and SO₄⁻ quantum yields. *J Phys Chem* 99:5214–5221
85. Malato S, Blanco J, Richter C et al (1997) Low-concentrating CPC collectors for photocatalytic water detoxification: comparison with a medium concentrating solar collector. *Water Sci Technol* 35:157–164
86. Huang YH, Jen HY, Tsai HC, Chen HT (2010) Degradation of phenol using low concentration of ferric ions by the photo-Fenton process. *J Taiwan Inst Chem Eng* 41:699–704
87. Safarzadeh-Amiri A, Bolton JR, Cater SR (1996) The use of iron in advanced oxidation processes. *J Adv Oxid Technol* 1:1821

88. Perez M, Torrades F, Garcia Hortal JA, Doménech X, Peral J (2002) Removal of organic contaminants in paper pulp treatment effluents under Fenton and photo-Fenton conditions. *Appl Catal B Environ* 36:63–74
89. Preez-Moya M, Graells M, Castells G et al (2010) Characterization of the degradation performance of the sulfamethazine antibiotic by photoFenton process. *Water Res* 44:2533–2540
90. Al Momani FA, Shawaqfeha AT, Al-Zoubib H (2010) Comparison of different treatment alternatives for removal of pesticide from water solution. *J Chem Technol Biotechnol* 85:529–535
91. Ballesteros MM, Casas López JL, Oller I et al (2010) A comparative study of different tests for biodegradability enhancement determination during AOP treatment of recalcitrant toxic aqueous solutions. *Ecotox Environ Saf* 73:1189–1195
92. Essam T, Aly Amin M, El Tayeb O et al (2007) Sequential photochemical–biological degradation of chlorophenols. *Chemosphere* 66:2201–2209
93. Malato S, Blanco J, Vidal A, Richter C (2002) Photocatalysis with solar energy at a pilot-plant scale: an overview. *Appl Catal B* 37:1–15
94. Bauer R, Waldner G, Fallmann et al (1999) The photo-fenton reaction and the TiO₂/UV process for waste water treatment—novel developments. *Catal Today* 53:131–144

Chapter 7

Solar Energy Conversion

Luis G. Arnaut, Monica Barroso and Carlos Serpa

Abstract Photochemical conversion of solar photons is one of the most promising and sought after solutions to the current global energy problem. It combines the advantages of an abundant and widespread source of energy, the Sun, and Earth-abundant and environmentally benign materials, to produce other usable forms of energy such as electricity and fuels, without the negative impact of CO₂ or other greenhouse gas release into the atmosphere. Dye-sensitised solar cells (DSSC) and organic bulk heterojunction (BHJ) solar cells are two examples of such systems, allowing the conversion of visible sunlight into electricity by inorganic or organic semiconductor materials, which are inexpensive and easy to process on a large scale. Photocatalytic (PC) and photoelectrochemical (PEC) water splitting systems offer a solution to the problem of diffuse and intermittent sunlight irradiation, by storing the energy of solar photons in the form of clean energy vectors such as H₂. This chapter presents an overview of the technologies based on photochemical solar energy conversion and storage.

L. G. Arnaut (✉) · M. Barroso · C. Serpa
Department of Chemistry, University of Coimbra,
3004-535 Coimbra, Portugal
e-mail: lgarnaut@ci.uc.pt

M. Barroso
e-mail: m.barroso@imperial.ac.uk

C. Serpa
e-mail: serpaso@ci.uc.pt

M. Barroso
Department of Chemistry, Imperial College London, London, SW7 2AZUK

7.1 Introduction

Every day the Earth is supplied with an immense amount of energy by the Sun. Approximately 4.3×10^{20} J of photon energy hit the surface of our planet each hour, which is enough to cover our yearly energy needs [1–3]. This is our largest and most widely available renewable energy source and it is therefore surprising that solar-based energies contribute only a minute portion of the world's energy demand. On the other hand, fossil fuels, which supply $\sim 85\%$ of the current energy consumption [2], are finite and unevenly distributed beneath the Earth's surface. In addition, burning these leads to the release of harmful gases into the atmosphere. While the imminent depletion of fossil fuel and coal reserves is subject to some controversy, it is widely accepted that alternative energy sources, which avoid or compensate the release of anthropogenic CO_2 and other greenhouse gases, are urgently required.

Current solar energy technology and research are focused on the conversion of solar photons into electricity (photovoltaics), chemical energy (solar fuels) and heat (solar thermal). In this chapter we will explore the first two approaches.

Converting the energy from the Sun into electricity is a challenging but important task. However, large quantities of electrical energy cannot be stored easily and efficiently, and the intermittent nature of solar emission means that electric energy can only be obtained during daylight hours. This is not compatible with the rhythm of modern society. Solar fuel production is an attractive solution to this problem due to its potential to generate low-carbon energy carriers, which can store the energy contained in solar photons and effectively replace fossil fuels. The paradigm of the clean solar fuel technology is the light-driven splitting of water into hydrogen and oxygen gases, employing abundant and environmentally friendly semiconducting photoelectrode materials. Alternatively, solar water splitting can be combined with photochemical or electrochemical CO_2 reduction to generate carbon-based products that can be used either as fuels or feedstock for several reactions with industrial value.

The scientific and technical challenges posed by these strategies are manifold and range from the fundamental limitations related to inefficient light harvesting, charge separation and recombination, to applied aspects associated with device architecture and function. Although remarkable progress has been achieved in understanding the scientific basis of the processes involved in solar energy conversion, low overall efficiencies and high production costs remain major obstacles to the widespread use of solar energy technologies. Therefore, it is likely that the capturing, converting and storing solar energy will remain one of the most important topics of research in the coming years.

7.2 Dye-Sensitised Solar Cells

7.2.1 Fundamentals

Efficient dye-sensitised solar cells (DSSC) are based on the synergy between sensitiser dyes capable of absorbing sunlight, and convenient wide band gap nanocrystalline semiconductors. The existence of functional groups on the dye molecules capable of efficiently binding to the semiconductor surface (*the anchoring groups*) and the high surface area of nanocrystalline mesoporous materials, enable the binding of sufficient dye molecules to absorb most of the incident light, with the inherent potential of maximising the light harvested.

The basic photophysical properties of a dye molecule are maintained upon immobilisation on a semiconductor surface, but the interaction with the semiconductor may open new reactive routes and/or change the rate of particular photochemical processes. An example of the importance of these routes is the fact that some polypyridyl complexes, intrinsically photolabile in solution, become photostable when bound to the semiconductor titanium dioxide, and actually constitute the class of dyes that has enabled some of the most efficient cells constructed to date [4, 5].

In a dye-sensitised solar cell the fundamental new reactive route for the immobilised dye is an electron transfer reaction. The excited state generated by light absorption is a molecular excited state. Then, charge separation that follows light absorption requires an electron transfer from the molecular electron donor (the dye molecule) to the semiconductor (electron acceptor). Proper control of the kinetics of the this first electron transfer step is a primary condition for having an efficient dye-sensitised solar cell. The electron transfer leads to the formation of a *charged-separated state* constituted by the dye oxidised state (the dye cation or *hole*) and the electron on the semiconductor. One of the major origins of inefficiency in solar cells is the charge recombination of this pair. Dye-sensitised solar cells partly overcome the problem of charge recombination by completely separating the processes of light absorption, achieved by the sensitiser dye, and charge transport and collection. After the formation of the charge-separated state, electron transport occurs through the network of sintered semiconductor nanoparticles, whilst a suitable redox couple enables the regeneration of the sensitiser.

The schematic diagram in Fig. 7.1a, the energy level diagram of Fig. 7.1b and the chemical Eqs. 7.1–7.5 are parallel but complementary ways of describing a dye-sensitised solar cell. The equations are written for a generic sensitiser dye (S) but illustrate the most commonly used semiconductor (titanium dioxide, TiO_2) and the typical redox pair (I_3^-/I^-). The schematic diagrams can be followed through the description of the basic steps occurring in a typical DSSC: upon light absorption by the dye (Eq. 7.1) the excited dye (S^*) transfers an electron into the conduction band of the semiconductor (e_{cb}^-), resulting in an oxidised dye and a reduced semiconductor (this process is often termed electron *injection*, Eq. 7.2).

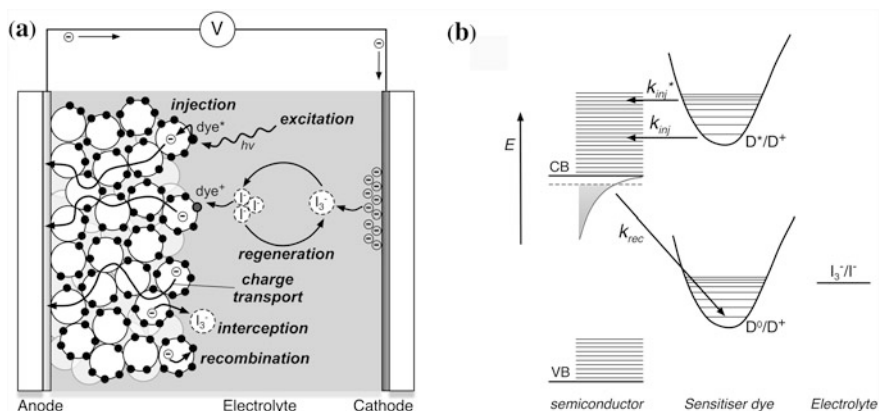


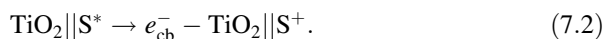
Fig. 7.1 **a** Schematic diagram illustrating the architecture and main electronic transition steps occurring in a typical DSSC. *White circles* represent semiconductor particles and the *black circles* the dye molecules; charge flow is represented by *arrows*. **b** Energy level diagram illustrating the relative energy position of DSSC main components: semiconductor, sensitizer dye and electrolyte. Electron injection from hot states (k_{inj}^*) and relaxed states (k_{inj}) of the excited dye, and charge recombination (k_{rec}) between the electron in the semiconductor conduction band and the dye cation, are represented by *arrows*

The injection process is in kinetic competition with the relaxation processes of the dye in its excited state (Eq. 7.3). Efficient electron transport within the semiconductor allows the collection of electrons on the back contact of the electrode, typically a thin layer of fluorine doped tin oxide (F:SnO₂, or FTO) or indium doped tin oxide (In:SnO₂, or ITO) deposited on a transparent substrate, like glass. This electrode is known as *photoanode* because it promotes the photo-oxidation of the sensitizer and moves electrons to the external circuit. The redox electrolyte in contact with the sensitised semiconductor reduces the oxidised dye, regenerating the sensitizer, and transports the resulting positive charge to the counter electrode (Eq. 7.4). This electrode (the *cathode*, as it collects positive charges) is usually a conducting glass covered with a transparent platinum or carbon thin coating. An external circuit connecting this sandwich-like structure allows the transport of the collected electrons from the anode to the cathode. These electrons will promote the reduction of the redox mediator (Eq. 7.6), closing the circuit. Well-known sources of efficiency loss in DSSC involve transfer of electrons across the semiconductor/electrolyte interface, either to oxidised dye molecules (charge recombination, Eq. 7.5) or to the oxidised component of the redox couple (charge interception, Eq. 7.7).

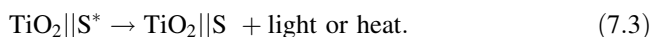
Excitation:



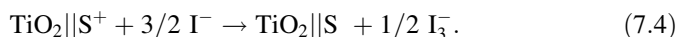
Injection:



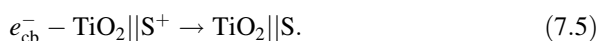
Relaxation:



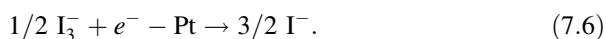
Dye regeneration:



Charge recombination:



Charge transport:



Charge interception:



Developments in DSSCs depend on our understanding and control of the fundamental kinetic and thermochemical nanoscale phenomena that govern the ‘conversion of photon energy into electron energy’, namely on the interfacial electron transfer and charge transport dynamics. Efficient dye-sensitised solar cells depend on the fine-tuning of the energies of the states implicated and of the rates of the processes involved.

In an electric insulating material the energy gap between the highest occupied energy state, the *valence band* and the *conduction band* (that in a molecular analogy would be an excited state) is of tens of eV. For semiconductors this gap can be as small as 1 eV, which enables, even at ambient temperature, some excited electrons to partially fill the conduction band, giving the material electrical conduction properties. The particular energetic position of the conduction band in some wide band gap semiconductors (for example rutile TiO_2 , $E_g = 3.2$ eV) allows molecular excited states of suitable sensitizer molecules to efficiently populate the semiconductor conduction band. For efficient electron injection to occur in a DSSC, the energy of the excited dye should be higher than the conduction band of the semiconductor. The importance of energy matching between the dye excited state and the semiconductor conduction band can be demonstrated by comparing the sensitisation of distinct semiconductors by $\text{Ru}(\text{dcbpy})_2(\text{NCS})_2$ (N3) (structure shown in Chap. 4: compound 4.3) [6–8]. The conduction band edge of TiO_2 is below the LUMO of N3, whereas the conduction band edges of niobium pentoxide (Nb_2O_5) and zirconium dioxide (ZrO_2) are above it (0.2–0.3 and 0.9–1.0 eV, respectively). As expected, spectroscopic probing reveals the absence of conduction band electron population for excited N3- ZrO_2 (550 nm excitation), as the conduction band is too negative to allow electron injection from N3. Excitation of N3 at 650 nm excites the dye to the lowest vibrational level of the sensitizer’s excited state. In these conditions the appearance of N3^+ , as a probe of electron injection, was only observed for N3- TiO_2 , consistent with the fact that the

energy of the lowest vibrational level of N3 excited state lies below the bottom of the other semiconductor conduction bands. But, for 450 nm excitation, high injection yields were observed for both TiO₂ and Nb₂O₅-sensitised semiconductors. This observation of excitation wavelength dependence of the electron injection yields, is consistent with the observation of extremely fast photoexcited electrons transfer even from vibrational ‘hot’ states of the sensitiser into the semiconductor conduction band. The observed electron injection has a dispersive kinetics regime with components on the femto- and pico-second timescale, competing with nuclear relaxation ($k_T \sim 10^{12} \text{ s}^{-1}$), and thus allowing non-thermalised electron transfer. It could be expected that the electron injection yield would not decrease when shifting the conduction band edge more negative (enhancing the cell potential), but the observation of dispersive kinetics for electron injection, including slow components, forecasts that this is not entirely the case [9].

The optimal working conditions of DSSCs are a result of quite favourable differential kinetics. It is energetically possible for the injected electron to recombine back into the dye, but the rate at which this occurs in an optimised device is quite slow compared to the rate that the dye recaptures an electron from the electrolyte. Why is such slow recombination observed after such a fast electron injection? Transport of photoinjected electrons through the semiconductor particle network occurs with a rate of micro- to milliseconds, so the reason is not the fast electron removal through the semiconductor. Are there also energy, geometrical or spatial constraints? The answer to these questions offers a good opportunity to briefly explore the next pair of equations:

$$k_{\text{ET}} = \frac{2\pi}{\hbar} H^2 FC(\alpha\Delta G). \quad (7.8)$$

$$H = H_0 \exp[-\beta(r - r_0)] \quad (7.9)$$

Following Fermi’s Golden Rule (Eq. 7.8), the interfacial electron transfer rates depend on the overlap of the sensitiser dye electronic orbital distribution function with the wide continuum of energy levels of the semiconductor, the electronic coupling factor H^2 , and on the overlap between the vibrational levels involved in the transition [10]. This nuclear vibration factor (Franck-Condon factor, FC) is explicitly dependent on the relative energetics of these states. We can assume that solvent dynamics are not important in interfacial electron transfer since solvent molecules immediately adjust their positions to the newly formed charges. Under these conditions, and if the electronic coupling is high enough, the rate becomes solely controlled by the nuclear vibration of the electron donor and acceptor and thus dependent on the Gibbs energy change resulting from the electron transfer, ΔG . However, if the electronic coupling is low enough, the rate will depend both on ΔG and the H value. As a consequence, when the electronic coupling is weak, geometry and distance will also affect the electron transfer rates, as shown in Eq. 7.9.

Considering electron injection, a sensitiser directly bound to the semiconductor allows a strong electronic coupling between the vibronic levels of the excited

sensitizer and the high density of acceptor states, thus a high value of H . Under these conditions the injection rate should follow the FC factor Gibbs energy dependence, and this indeed was observed [11]. It was also observed that the existence of (non-conjugated) spacers between the sensitizer and the TiO_2 nanoparticles lead to an exponential reduction of the electron injection rate (see Eq. 7.9) [11]. These observations are consistent with the understanding of the fast electron injection as described by Eqs. 7.8 and 7.9.

What about the much slower electron recombination? The nuclear FC factor shows an almost quadratic dependence on ΔG , leading to an inverted region, where the reaction rates become slower as the reactions become more exergonic. Such energy constraints may be the reason behind the slow recombination. Although such behaviour was observed for particular systems [12], it was found that this could not be the general explanation. In fact, ΔG for electron recombination for some of the more efficient polypyridyl sensitizers is not exergonic enough to be in the inverted region. So, only diminished electron coupling can explain the slow recombination observed for such dyes. How can a high electronic coupling for direct electron transfer (injection) become a low coupling for recombination? Equation 7.9 suggests that if the distance for electron recombination is higher than the distance for electron injection, the recombination rate would decrease exponentially. A quite interesting example is given by the molecular modelling of the N3 dye relevant orbitals for electron transfer. The appropriate orbital for electron injection (the LUMO) is located on the bipyridyl rings, closely bound to the semiconductor, whereas the relevant orbital for charge recombination (the HOMO) is located on the NCS groups, away from the semiconductor surface. In this particular case, distance constraints lead to optimum conditions for fast electron injection and slow recombination, as favourable molecular electronic distribution takes the 'hole' away from the semiconductor [13].

TiO_2 electron interception by species in the electrolyte is also in kinetic competition with electron transport through the semiconductor. Again, for optimised devices this reaction is rather slow. For this particular reaction the I_3^-/I^- redox pair has the advantage that the loss of photoinjected electrons to I_3^- is relatively slow, as a consequence of the fact that the reaction involves the transfer of two electrons and the breaking of the I-I bond [14]. The fact that the interception reaction is slow is probably the main reason why the majority of the high efficiency DSSCs reported to date use the I_3^-/I^- redox pair mediator.

Naturally the rate of electron transport through the semiconductor to the anode, in direct competition with recombination and interception, is pertinent in the overall performance of a DSSC. Photo-injected electrons are transported by diffusion in a free random walk [15] as a result of an electron concentration gradient. The diffusion time will depend on the distance to the anode (the semiconductor film thickness) and the diffusion coefficient of electrons. But electrons also seem to become trapped within the semiconductor particles for some time (picoseconds to nanoseconds). This trapping and thermal release (detraping) mechanism requires energy, and is important in retarding charge recombination in DSSCs. The process

is particularly dependent on the position of the Fermi level in the semiconductor and the outcome is a small apparent diffusion coefficient.

On the other side of the sandwich-like DSSC, electron transfer from the counter electrode to species in the electrolyte should be very fast. For the iodide redox pair, since platinum at the cathode acts as a catalyst, breaking the I-I bond, the regeneration of the chemisorbed iodide ions is fast.

If the above *kinetic* considerations are fundamental for the DSSC performance, we should emphasise that *energetic* considerations are also essential. For example, tuning the photophysical properties (absorption, HOMO and LUMO energies) and redox characteristics of the sensitizer dye with the semiconductor band gap and redox pair potential is crucial. Efficient regeneration by the electrolyte needs the energy level of redox potential to be equal to or higher than the ground state of dye (HOMO). There is a quest for dyes that improve the solar spectrum harvest coverage to lower energy photons, so that the LUMO energy level become closer to the HOMO level, as in the diagram in Fig. 7.2. This should not be made at the expense of the dye redox potential, because in that case both the HOMO and LUMO energy levels would shift up in that same diagram. An example is the comparison between N3 and $\text{Ru}(\text{dcb})_3^{2+}$ dyes. N3 shows better photon collection in the red part of the spectrum, but $E^\circ(\text{Ru}^{\text{III/II}})$ is lower [16]. This means a relative loss of driving force for the regeneration of the N3 cation (although in this particular case this loss is not sufficiently high to compromise regeneration).

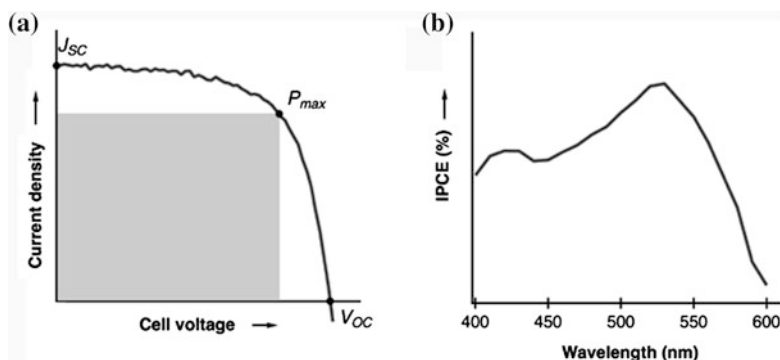


Fig. 7.2 Illustration of the spectroelectrochemical characterisation of a laboratory scale DSSC with a nanocrystalline TiO_2 film sensitised with the RuN3 dye, measured under simulated AM 1.5G solar irradiation (100 mW cm^{-2}); electrolyte composition: methoxypropionitrile with 0.6 M propylmethylimidazolium iodide, 0.1 M LiI, 0.1 M tert butylpyridine, and 0.1 M iodine or guanidium thiocyanate; 5 μm thick TiO_2 film (9 nm particles) and scattering layer. **a** J - V curve, **b** IPCE spectrum (Courtesy of Patricia Jesus, Coimbra Chemistry Centre). In an optimised RuN3 DSSC the J_{sc} reaches a value 20 mA cm^{-2} and the maximum incident photon to current efficiency reaches 85 % [25]

7.2.2 Device Construction and Characterisation

Although other semiconductors have been investigated, the use of the wide band gap metal oxide semiconductor titanium dioxide (TiO_2) nanocrystals was revealed to be crucial to present day state-of-the-art solar cell overall performance. The size and morphology of the particles used are of extreme importance. For 15 nm diameter particles in a 10 μm transparent thick film there is a 1,000-fold increase in surface area, compared with a single crystal of equal projected area. This fact enables the adsorption of large quantities of dye, resulting in efficient light harvesting. Typically, the TiO_2 particles are present only in the form of anatase or as a mixture of 80 % anatase and 20 % rutile. A key point on the performance of the anode semiconductor film is the quality and characteristics of the colloidal TiO_2 paste used. Preparation of this paste may be a complex procedure [17, 18]; high performance DSSCs are obtained with homemade or commercially available nanoparticles mixed with additives such as α -terpineol and ethyl cellulose in acidic water/alcohol media [17]. Alternatively, commercially available pastes can be used. The best-performing nanocrystalline TiO_2 films are typically fabricated by squeeze-printing (*doctor blading*) or screen-printing of the paste, followed by high temperature sintering (400–500 $^\circ\text{C}$) in order to enable electron conduction between the nanoparticles. The counter electrode can also be deposited by a printing method. Typical cells consist of a transparent layer of 10–20 μm thickness made from 10–20 nm semiconductor particles. Improvements in light harvesting can be achieved by the introduction of a layer of larger TiO_2 particles (100–400 nm). This scattering layer is particularly important when using dyes with low absorbance in the red and near infrared, as the light reflections inside the film enhance substantially the optical path length.

Iodide/iodine is the most commonly used redox couple, but the electrolyte is typically a chemically complex mixture that includes not only the redox couple but also supplementary additives. A common electrolyte composition consists of methoxypropionitrile with 0.6 M propylmethylimidazolium iodide, 0.1 M LiI, 0.1 M *tert* butylpyridine, and 0.1 M iodine or guanidium thiocyanate. It was empirically observed that the presence of additives enhances device performance. It is known that additives shift the conduction band edge, but probably it is the decrease in the electron interception rate (Eq. 7.7), due to the adsorption of additives at the TiO_2 surface, that is most active in the device performance enhancement. This is possibly due to the blocking of active reduction sites or inhibition of close approach of electron acceptors to the TiO_2 surface.

The sensitiser dye constitutes the heart of the DSSC, allowing the use of the solar spectrum to drive electrons from a lower to a higher energy level, and ultimately generating the cell electric potential difference. Several efforts have been focused on the development of organic and organometallic dye molecules. Among them, polypyridylruthenium complexes, yielding solar-to-electric conversion efficiencies of 11 % with simulated sunlight proved to be among the most efficient sensitisers [19, 20]. In general, sensitiser dye molecules can be regarded

as being constituted by a light antenna part, a spacer and an anchor group. The anchor group provides proper attachment of the dye to the semiconductor. The number [21], nature [8] and position [22] of this anchor groups may vary. Carboxylic acid groups are the most commonly used.

The introduction of the electrolyte and the sealing of the cell are critical steps to assemble a durable DSSC. Although highly efficient and durable dye-sensitised solar cells need pure materials, complex and controlled procedures [23], reasonable cells can be constructed using commercial available lower cost materials and following simplified processing steps [24].

The overall DSSC performance can be accessed by measuring the incident photon-to-current conversion efficiency (IPCE) profile over the solar spectrum and the current–voltage (J – V) curves under illumination. The IPCE can be defined as the ratio between the number of electrons collected (the current density measured in the external circuit) and the number of photons with a given energy that reaches the cell. It is a collective measure of the cell performance, depending on electron injection (η_{inj}) and collection (η_{coll}) efficiencies, as well as on the light harvesting efficiency (LHE), Eq. 7.10. The IPCE can be assessed at each wavelength by measuring the short circuit photocurrent density ($J_{SC}/\text{mA cm}^{-2}$) under monochromatic illumination (λ/nm) with a given intensity ($I_{inc}/\text{mW cm}^{-2}$), Eq. 7.11. (hc/e is 1,240 nm, the wavelength of a photon of 1 eV energy). Due to sensitivity issues this is typically done by scanning the wavelength range of interest with chopped light while illuminating the cell with a bias light, and distinguishing the alternating current output signal from the total output current using a lock-in technique [26].

$$\text{IPCE}(\lambda) = \text{LHE}(\lambda)\phi_{inj}\eta_{coll} \quad (7.10)$$

$$\text{IPCE}(\lambda) = \frac{hc}{e} \times \frac{J_{SC}(\lambda)}{\lambda I_{inc}(\lambda)} = \frac{1240J_{SC}(\lambda)}{\lambda I_{inc}(\lambda)}. \quad (7.11)$$

Figure 7.2a presents the IPCE as a function of the wavelength measured for a DSSC made with the N3 dye and Fig. 7.2b shows the J – V curve for the same cell. Important information about the microscopic cell performance can be obtained from the current density at short circuit (J_{SC}), the open circuit photovoltage (V_{OC}) and the cell's fill factor (FF) defined as,

$$\text{FF} = \frac{P_{\max}}{J_{SC}V_{OC}} \quad (7.12)$$

where P_{\max} is the product of the photocurrent and photovoltage at the voltage where the power output of the cell is maximised.

Charge flow in a DSSC involves the conduction of electrons in the semiconductor nanoparticles and of ions in the electrolyte. The current achieved at short circuit, J_{SC} , depends on the electron injection yield and on electron conduction losses by recombination or interception. The cell voltage is associated with the buildup of electron density in the TiO_2 . The maximum potential produced under

illumination (V_{OC}) corresponds to the difference between the chemical potential of the electrons at the semiconductor and the chemical potential of the holes at the hole conductor. So, the device photovoltage depends on the redox couple, as it sets the electrochemical potential at the counter electrode and the semiconductor's electrons potential, determined by its Fermi level.

Ultimately the conversion efficiency of a DSSC, η_{DSSC} , is determined by the photocurrent density measured at short-circuit, the open-circuit photovoltage and the cell's fill factor, corrected by the intensity of the incident light (I_{inc}).

$$\eta_{DSSC} = \frac{J_{SC} V_{OC} FF}{I_{inc}}. \quad (7.13)$$

The characterisation of a DSSC device or the study of partial processes that occurs at such cells uses a series of optical and electrochemical techniques, either stationary or time-resolved. The studies cover a wide range of timescales, accompanying the wide time span of phenomena occurring in a DSSC (from fs/ps for electron injection to ms for electron transport). Optical transient absorption techniques (see [Chaps. 8, 14, 15](#)) are used in combination with transient electrical measurements to follow the appearance and disappearance of chemical species and charges on a DSSC [27].

7.2.3 Novel Approaches

The gap between the full potential of solar energy and our energy needs can only be met by raising the efficiency of the conversion processes. In DSSCs these efficiencies are still well below the theoretical limit. Reaching this limit is both a scientific and an engineering endeavour. Thermodynamic analysis established the efficiency limit of 27–31 % for photovoltaic conversion efficiency [28], based on several premises that new developments may overcome. These assumptions are: a single layer cell, one electron–hole pair formation per absorbed photon, thermal relaxation of the electron–hole pair energy into semiconductor band gap energy, illumination with non-concentrated light.

A DSSC is a complex device with complex interactions between the device components. Innovation in a particular component is intrinsically related to changes in the performance of other components. For example: chromophores that can collect light more efficiently would make it possible to reduce the semiconductor thickness, with the implication of reducing electron interception by oxidised redox species and consequently increasing electron concentration, but also allowing further exploration of redox couples, including solid-state hole conductors. In the following paragraphs we will focus on recent and forecasted advances in (i) sensitiser dyes, (ii) electron conduction and (iii) hole conduction.

In a perfect world the absorption spectrum of a dye-sensitised solar cell would be optimum for the solar spectrum, which means high molar absorption coefficients

below 900 nm. Research on dyes that effectively harvest the red and near-IR part of sunlight had significant progress over the last decade [5].

Due to its chemical instability, the weakest part of the Ru dyes is the SCN^- ligand [29]. Probably the most promising thiocyanate-free Ru complexes are cyclometalated complexes, showing IPCE with a maximum of 80 % and an absorption window that extends beyond 800 nm [5]. The presence of fluoride substitution in these ligands adjusts the electron density of the dye and allows the sharing of the positive charge of the oxidised dye between the central metal and the ligand, contributing to a rapid charge transfer to the iodide ions in the electrolyte [5]. Other recent optimisation efforts include the development of heteroleptic ruthenium complexes, with thiophene moieties attached to the bpy-ligand enhancing both the absorption coefficient and shifting the spectral response to the red [30].

More recently, research efforts have been focused on the design of new aromatic molecules, which can cover the whole visible solar light spectrum. Among them, interest has been focused on perylenes [31], phthalocyanines [32] and especially tetrapyrrolic macrocycles, which play an important role in natural photosynthetic pigments, like porphyrins [33], chlorins [33] and bacteriochlorins [30]. The long list of sensitisers even includes dyes from fruit extracts [34]. Examples of many of these structural classes can be found in Chap. 4.

The adsorption of dyes with complementary absorption characteristics can be used as a strategy for improving light harvesting. This panchromatic approach can be based on the adsorption of a dye mixture or a more sophisticated multi-dye layer sequence [35]. The IPCE spectral shape for the panchromatic cell results in the superimposition of the IPCE spectrum for single dyed cells, and the $J-V$ curves yield a higher value for the J_{SC} than for the corresponding single dyed cells.

Antenna structures, which use distinct chromophores for light absorption and electron injection have also been tried. Efficient energy transfer from the antenna dye to the injection dye is required [36, 37]. Another appealing idea for the improvement of DSSC efficiency is the use of dyes with a high ground-state S_0-S_2 excited state transition probability or capable of multiphotonic absorption. In conjugation with the appropriate conduction band energy semiconductors, these dyes would allow the injection of very energetic electrons and a consequent increase in the cell potential.

Quantum dots, with high absorbing coefficients in the visible, have also been used as sensitisers in DSSCs. Despite the high theoretical maximum efficiency the energy conversions obtained are still low. Recently, an energy conversion efficiency as high as 4.22 % was achieved with CdS and CdSe as co-sensitiser of TiO_2 , taking advantage of the two materials in light harvesting and electron injection [38].

New architectures for DSSCs include new photoanodes [9]. The expectation is that the transport of photogenerated electrons along new nanostructured materials, such as nanowires or nanotubes, will be faster than in a network of sintered titanium oxide particles. The random walk of electrons through the nanoparticle particles limits the collection of charges to the millisecond timescale. Reducing the

number of grain boundaries, which are obstacles to fast electron transport, would reduce the loss of charge carriers by recombination and interception and therefore increase electron collection. It has been demonstrated that the morphology of semiconductor films has an effect on the electron transport losses [39]. Changing the usual granular TiO₂ morphology into a columnar morphology leads to an increase in the short-circuit current, assigned to differences in electron transport with an increase in the electron lifetime in the TiO₂ columnar film. Those nanowire, nanorod or nanotube (and even some more unusual *nanoplant-like* [40]) semiconductor morphologies should have high surface area, otherwise this would require the design of new dyes with higher absorption coefficients in order to obtain efficient light harvesting.

Although the most commonly used redox couple to act as a hole transport medium is the I₃⁻/I⁻ this does not mean the couple is necessarily unique. Actually the space for improvement for DSSCs that use this redox mediator is mostly limited to improvements in better light harvesting dyes [41]. Corrosion, light absorption and diffusion limitations had been identified for the I₃⁻/I⁻ pair and it has been replaced successfully by cobalt-based redox systems [14], as well as by organic hole conductors [42]. Difficulties in sealing to prevent evaporation and water diffusion into the cell led to research into the substitution of liquid redox pair electrolyte, replacing the liquid for solid or quasi-solid hole-conduction media, such as polymeric, gel [43], or solid electrolytes [44].

Solid-state redox mediators or hole conductor materials would make it possible to construct completely solid-state DSSCs that will probably have considerable added commercial value. One of the main difficulties in substituting liquid electrolytes is the need for an 'interpenetration' of the sensitised metal oxide by the electrolyte, in order to have efficient contact between the sensitiser cation (the hole) and the mediator. Additionally, prospective solid hole collectors should have the following properties: the valence band of the hole collector material must be located above the bottom of the sensitiser dye ground state; it must be transparent throughout the visible spectrum, where the dye absorbs light; and the deposition of the solid material should be done without degrading the monolayer of sensitiser dye adsorbed on TiO₂.

In terms of stability, inorganic oxide semiconductors of Ni and Cu are among the very few oxides which have been shown to possess a suitable band gap and band-position, although the efficiency of the cells constructed with those compounds is still low [45, 46]. Both low intrinsic hole mobility and hindered penetration of the hole collector into the dyed mesoporous TiO₂ film (due to the bigger particle sizes compared to that of TiO₂ pores), seem to be the reason for the poor performance. A promising material is CuBO₂, which is transparent over a wide spectral range with suitable band gap and exhibiting high conductivity and hole mobility [47].

Polymer materials as a hole-transporting layer, in an all solid-state polymer-based DSSC, have also been devised. Cells with polymers such as poly(*N*-vinylcarbazole) forming a solid junction comprising nanocrystalline TiO₂/dye monolayer and hole transporter at which photo-induced charge separation proceeds, obtained a relatively

high conversion efficiency with a simple composition and a cheap polymer material [48]. In order to avoid the difficulty of polymer penetration into the porous TiO₂ *in situ* polymerisation of pre-penetrated monomers has been developed. Polymers prepared as carboxylated diacetylenes, were found to be efficient hole conductors [49]. Conjugation of dye and interfacial engineering with *in situ* polymerisation of poly(3,4 ethylenedioxythiophene (PEDOT, see Chap. 4: compound 4.10) yielded an average efficiency of 6.1 %, which represents a remarkable improvement for polymer-based DSSC [50].

We can expect that the joint efforts of molecular science and nanotechnology will tackle the problems that still persist so that efficient, low cost and environmental friendly DSSCs can be widely available in the near future.

7.3 Organic Solar Cells

7.3.1 Exciton Diffusion and Charge-Carrier Mobilities

Another very appealing concept for the conversion of light into electric power is the fabrication of organic photovoltaic cells with materials simply processed from solution. Such solar cells would combine low cost, large area, lightweight, flexibility and versatility.

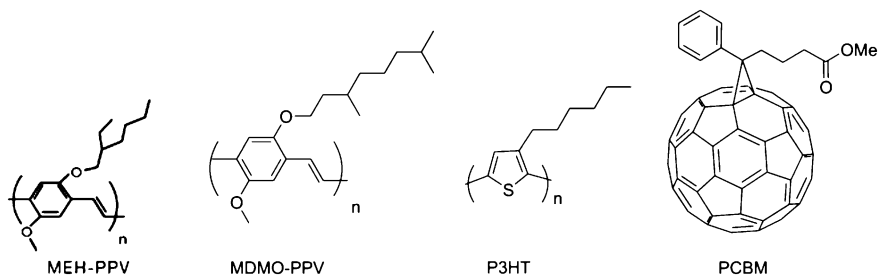
A first step in making efficient organic solar cells was reported by Tang in 1986, who reported a cell with a power conversion efficiency of 1 % under AM2 illumination [51]. These cells were made of one 30 nm thick layer of copper phthalocyanine deposited on ITO glass and, on the top of it, a 50 nm layer of a perylene tetracarboxylic derivative was deposited, followed by an opaque Ag layer. Charge separation was driven by the differences of electron affinities (and/or of ionisation potentials) between the two organic layers. Donor/acceptor bilayer devices have an intrinsic limitation. Organic molecules rarely exceed molar absorption coefficients of $10^5 \text{ mol}^{-1} \text{ dm}^3 \text{ cm}^{-1}$ in the most intense regions of the solar spectrum. Harvesting 90 % of the photons with such absorptivities requires a layer thickness of 100 nm. When one photon is absorbed by a layer of solid material made of such molecules, it originates a Coulombically bound electron–hole pair, or exciton, that must migrate to the donor/acceptor interface with the other layer before the exciton dissociates in a charge-separated state. This is an essentially diffusive process of an uncharged species, which must compete with its decay to the ground state. The exciton diffusion length, $L = (D\tau)^{1/2}$, determined by the exciton diffusion coefficient D and lifetime, must be of the same magnitude as the layer thickness to promote the efficient formation of charge-separated states. Singlet exciton migration can be understood in terms of long-range electrostatic coupling between the transition dipoles of initial and final states (Förster mechanism), whereas triplet excitons migrate *via* short-range exchange due to orbital overlap (Dexter mechanism see Chap. 1). The diffusion of singlet excitons is faster but this may be offset

by their shorter lifetimes, typically between 100 ps and 1 ns. An example of a material that exhibits a large exciton diffusion coefficient is a layer of pentacene molecules, for which $L = 70$ nm [52]. Further progress on bilayer organic solar cells depends on the availability of materials combining high visible and near-infrared absorbances with longer diffusion lengths.

The intrinsic limitation of the bilayer cells mentioned above was overcome in cells with a blend of bicontinuous and interpenetrating donor and acceptor materials. Bulk heterojunctions (BHJ) of interpenetrating materials increase the interfacial area between donor and acceptor and substantially reduce the distance that the exciton must travel before reaching an interface. If, additionally, the network is bicontinuous, the collection efficiency can, in principle, be also efficient.

The first report on BHJ solar cells showed that the carrier collection efficiency increased by two orders of magnitude from a cell with a pristine polymer, Ca/MEH-PPV/ITO, to a cell with a blend of the same polymer with a C₆₀ derivative, Ca/MEH-PPV:PCBM(1:4)/ITO, where Ca (or alternatively Al) is the cathode and ITO is the anode [53]. Scheme 7.1 shows the molecular structures of these and other materials currently employed in organic solar cells. This increase in efficiency was assigned to efficient charge separation in the BHJ between the polymer and C₆₀, followed by high collection efficiency through the bicontinuous network of internal donor–acceptor heterojunctions. In principle, the high work function of the anode metal (positive electrode) should extract holes from a close lying donor HOMO, and the lower work function of the cathode (negative electrode) should match the energy of the acceptor LUMO and collect the electrons. The open circuit voltage, V_{OC} , of the cell would be the difference between the LUMO and HOMO energies, which should have ohmic contacts with the negative and positive electrodes, respectively. In such ohmic contacts, charge transfer of electrons or holes between the metal and the semiconductor occurs in order to align the Fermi level of the negative electrode with the energy of the LUMO of the acceptor, and to align the Fermi level of the positive electrode with the energy of the HOMO of the donor. BHJ cells have both the donor and acceptor moieties in simultaneous electrical contact with both the anode and the cathode, and the electrons transported by the PCBM network have a non-negligible probability of diffusing/hopping to the ‘wrong’ yet proximate hole-extracting ITO electrode. In practice, the internal field across the 100–200 nm thickness film of a BHJ cell drives the holes from MEH-PPV to the ITO electrode (high-work function contact of ≈ 4.7 eV) and the electrons from C₆₀ to the Ca (or Al) electrode (low-work function contacts of 2.9 or 4.2 eV, respectively). The small change in V_{OC} when going from Al to Ca is assigned to the pinning of the Ca work function to the LUMO of PCBM (3.7 eV). Additionally, it was found that the photocurrent depends on the effective applied voltage, which supports the idea that photocurrents in these BHJ devices are field-driven, and that diffusion only plays a minor role [54].

The conjugated polymers employed in BHJ solar cells have exciton diffusion lengths ranging from 5 to 20 nm [54], but the proximity between donor and



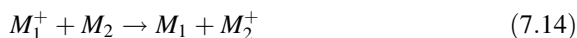
Scheme 7.1 Molecular structures of poly[2-methoxy-5-(2'-ethyl-hexyloxy)-1,4-phenylene vinylene] (MEH-PPV), poly[2-methoxy-5-(3',7'-dimethyloctyloxy)-1,4-phenylene vinylene] (MDMO-PPV), poly(3-hexylthiophene) (P3HT), [6]-phenyl- C_{61} -butyric acid methyl ester (PCBM) (see also [Chap. 4](#): compounds 4.2, 3, 4 for more information about these polymers)

acceptor materials solves the problem of increasing the exciton diffusion length above the optical absorption depth. On the other hand, BHJs raise the issues of hole and electron mobilities in the bicontinuous network. A low mobility favours electron–hole bimolecular recombination that reduces charge collection, and also increases the resistivity of the layer that decreases the device fill factor. The relatively high hole mobilities, the optical band gaps at the low energy of the visible, the high molar absorption coefficients and the ease of preparation of thin films and blends with other materials, have made conjugated polymers the most common solar radiation absorbers and hole transporters in organic solar cells. Scheme 7.1 presents some examples of conjugated polymers currently employed in such cells. However, it must be realised that the charge carrier mobilities of crystalline inorganic semiconductors are in the order of $10^3 \text{ cm}^2 \text{ V}^{-1} \text{ s}^{-1}$, whereas the hole mobility of P3HT is $5 \times 10^{-3} \text{ cm}^2 \text{ V}^{-1} \text{ s}^{-1}$ and the electron mobility of PCBM is $2 \times 10^{-3} \text{ cm}^2 \text{ V}^{-1} \text{ s}^{-1}$, and both are considered high for organic materials [55]. Fullerene derivatives such as PCBM are frequently employed as electron acceptors in BHJ cells both because they have a LUMO level allowing efficient photoinduced electron transfer from the donor and because their spherical geometry leads to isotropic 3D electron transport that is particularly appropriate for disordered media.

The modest charge-carrier mobilities of organic semiconductors are intrinsic to their charge transport mechanisms. The total mobility in π -conjugated materials has contributions from two intrinsic mechanisms: charge-transport resulting from the electronic coupling between adjacent molecules and from electron-vibration coupling [56]. The electronic coupling mechanism is characterised by the exponential decrease of the effective electron transfer frequency with the donor–acceptor distance and can be understood in terms of electron tunnelling. Intermolecular electronic coupling in glasses of organic molecules typically shows an exponential decrease of the electron transfer frequency with donor–acceptor distance with a decay $\beta = 1.65 \text{ \AA}^{-1}$ (*i.e.*, the transfer frequency decreases by a factor of 4×10^{-3} for each 3.3 \AA intermolecular jump, see Eq. 7.9) [57]. Another measure of the electronic coupling between adjacent molecules can be found in

exciplexes, which have electron transfer frequencies reduced by a factor *ca.* 7×10^{-3} for such intermolecular jumps [58].

Electron-vibration couplings can also contribute to the charge mobility in organic semiconductors because the geometry relaxation from neutral to charged organic species can be rather large and lead to trap sites. Electron-vibration coupling in individual organic molecules is apparent in the vibrational structure of their electronic spectra, or, when the generation of charges is involved, in their photo-ionisation spectra. In crystals or polymers, this coupling is more appropriately referred as electron-phonon coupling because it involves the collective oscillations of the atoms in a crystal or polymer. The localisation of an electron (or a hole) on a given site of the material is due to the deformations in molecular and lattice geometries that locally minimises its energy. In some cases the contribution of the molecular modes to the electron-phonon coupling can be identified, as in PPV-like systems in which the phenyl ring is replaced by a biphenyl moiety revealing a coupling of the excited state to a torsional mode of the chain [59]. These changes in nuclear geometry are closely related to the reorganisation energies employed in electron-transfer theories. However, it is consensual that the main contribution to the relaxation energy in organic crystals comes from intramolecular modes, with the lattice giving only a minor contribution [56], whereas in solution the relative roles of intramolecular and solvent modes remain controversial [60, 61]. Electron-phonon coupling contributes to charge-carrier mobility because of the hopping motion, which can be described as a transition from a charge being localised entirely on one molecule or segment (M_1) to its being localised entirely on another one (M_2). Charge transport occurs by a sequence of steps such as:



In the presence of physical (disorder) and chemical (dopants) defects, additional trap sites, of unequal energies, are introduced in the organic semiconductor. Their presence also contributes to charge mobility with more pathways for the hopping motion. The rate of transfer between non-equivalent sites can be formulated according to the golden rule of quantum mechanics as the product of an electronic and a Franck-Condon factor, Eq. 7.8 [62]. This latter factor is a function of the relative free-energy of such sites and of an intrinsic free-energy barrier (usually named reorganisation energy). It should be noted that the escape from a trap with large energy stabilisation with respect to the thermal energy available, will be difficult and will impair charge mobility. In summary, the charge carrier mobilities in organic semiconductors are due to tunnelling, which dominates at low temperatures, and to hopping motion, which shows the thermal activation of the Franck-Condon factor.

New materials with higher charge carrier mobilities have been investigated. The conductance of organic molecules is related to their HOMO-LUMO gap. For example, *n*-alkanes have very high HOMO-LUMO gaps that lead to $\beta \approx 0.9 \text{ \AA}^{-1}$, whereas conjugated molecules with alternating double and single

bonds have smaller HOMO–LUMO gaps and transport electrons more efficiently. The lowest value of β was measured for oligothiophenes, $\beta = 0.1 \text{ \AA}^{-1}$ [63]. Carbon nanotubes and graphene sheets attain the limit of zero energy gap but these species behave as molecular wires rather than semiconductors, and are useless for solar cells because V_{OC} is limited by the energy difference between the HOMO and the LUMO. A good compromise between semiconductor behaviour and ballistic electron transfer seems to be reached by short single-walled carbon nanotubes [64]. The spread of the electrons over a large volume in such conjugated systems also reduces the electron–phonon coupling to negligible values.

7.3.2 Charge Separation Efficiencies

When BHJs are present, the exciton can reach the donor/acceptor interface within its lifetime. The energy offset between the molecular orbitals of the donor and acceptor at the BHJ favours charge transfer and the formation of a charge-transfer exciton. However, only exciton dissociation into free charge carriers at this interface can generate photocurrent, and this is in competition with geminate recombination in the CT exciton. Once formed, the charges migrate to the electrodes unless bimolecular recombination of the dissociated charge carriers occurs. These processes are illustrated in Fig. 7.3.

The charge-transfer exciton formed at the BHJ has the hole predominantly located in the donor HOMO and the electron in the acceptor LUMO. Their Coulomb attraction, for electron–hole separations of 0.5–1 nm, gives a CT exciton binding energy of a few tenths of eV, which is much greater than $k_B T$ (0.025 eV). Entropy drives charge carrier separation and diffusion away from the interface but this alone is insufficient to give high charge separation efficiencies. In some cases these CT excitons exhibit weak charge-transfer optical absorptions similar to those observed for CT species in solution, and/or red-shifted and broadened emission similar to that of exciplexes. The degree of charge separation in CT excitons is intermediate between that of excitons and that of fully dissociated charges. In solution, the dissociation of exciplexes into solvent-separated ion pairs or free radical ions was found to occur for solvents with dielectric constants $\epsilon \geq 7$ at room temperature and at higher solvent polarities for higher temperatures [57], in agreement with the Lippert–Mataga relationship. Conventional solar cells, such as those based on silicon *p-n* junctions, have $\epsilon = 12$ and the separation of charges is spontaneous. The same occurs in DSSCs because TiO_2 has $\epsilon \approx 80$. However, organic semiconductors typically have $\epsilon \approx 2\text{--}4$, and achieving efficient charge photogeneration is a key challenge [65].

In view of the binding energies of thermalised CT excitons, their predominant mode of decay is expected to be charge recombination (rate constant k_{rec} in Fig. 7.3). The observed photocurrent is unlikely to originate from such excitons. It has been proposed that CT excitons can avoid geminate recombination by separating into free charge carriers immediately after the electron transfer at the BHJ

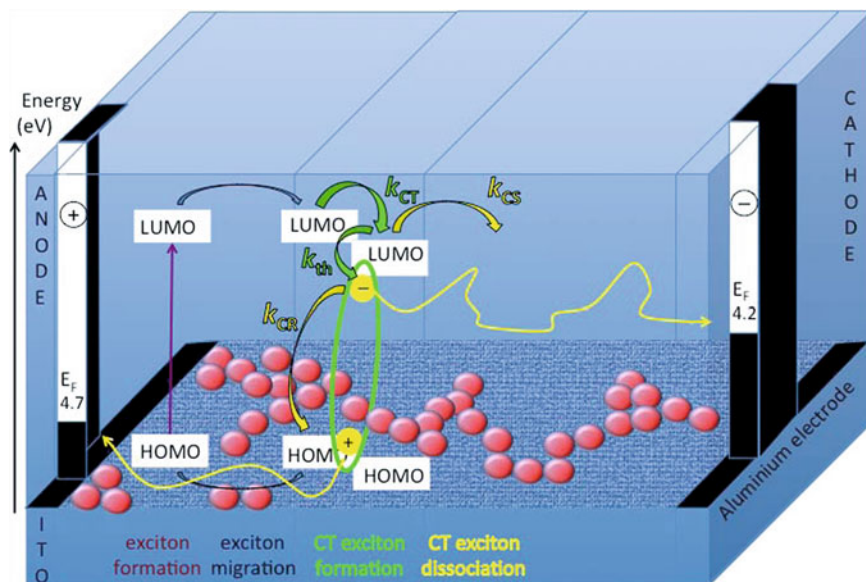


Fig. 7.3 Electronic state diagram and (in *horizontal* perspective) schematic charge photogeneration and transport in a polymer:fullerene photovoltaic cell. The migration of the exciton to the BHJ generates a CT exciton that may dissociate into free charge carriers, recombine to the ground state or intersystem cross to the triplet exciton (not shown in this figure). Charge separation is believed to occur from a hot exciton, in competition with its thermalisation. The built-in electric field created by the electrode work function differential drives the electrons to the cathode and the holes to the anode

and before the hot CT exciton dissipates its excess photon energy. This excess energy is viewed as kinetic energy that assists the electron and/or the hole in escaping from the Coulomb potential, yielding charge-separated states where the electron and hole are hardly Coulombically bound [66]. Thus, the excess energy of the hot carriers governs the initial separation distance between electron and hole, and, consequently, the dissociation efficiency. According to this view, the rate constant for charge separation of the hot exciton (k_{CS}) is in competition with the thermalisation rate (k_{th}), Fig. 7.3 [67], and the internal conversion of the hot exciton will reduce the charge-separation efficiency. Moreover, the requirement of excess thermal energy to drive charge separation is also detrimental for the photovoltaic device efficiency because the excess energy needed to create hot excitons will be lost. A correlation between excess energy and the yields of free charge carriers was recently reported [68].

The current view of the exciton dissociation into free charge carriers assumes that it only occurs at the interface between donor and acceptor materials. Model calculations on pentacene/ C_{60} heterojunctions gave a decrease in the electron transfer rate of 2×10^{-7} for a 3.3 Å intermolecular separation that, if correct, would make long-distance electron transfer irrelevant for such materials. However, this distance

dependence corresponds to $\tau = 4.6 \text{ \AA}^{-1}$ [63], which is clearly excessive in view of the experimental data obtained with matrixes where it is known that electron transfer from an electronically excited donor to an acceptor arrested in rigid media takes place over a range of distances [57]. A more reasonable value would be $\tau = 1 \text{ \AA}^{-1}$ [57], which for activationless electron transfer allows for an exciton to dissociate within 50 fs and generate an electron–hole pair 4 Å apart. A distribution of electron–hole distances is not unlikely for activationless exciton dissociations in BHJ solar cells, and would generate charge carriers with small Coulombic attractions.

The dissociation of an exciton in a polymer/fullerene BHJ does occur within tens of fs. This may allow both the presence of hot excitons and for electron transfer to a distribution of electron–hole distances. The subsequent transport of the free holes delocalised on polymer chains is also very fast and has two contributions. The initial hole mobility is comparable to the polymer intrinsic mobility and is assigned to hot holes. These cool down at a fast rate of $(1/180) \text{ fs}^{-1}$ and are trapped at an initial rate of $(1/860) \text{ fs}^{-1}$ [69]. At longer times, the conductivity decreases and represents the equilibrium population of mobile and trapped charge carriers.

The description given above ignored the presence of triplet states. Triplet excitons are formed directly by intersystem crossing in the polymer singlet excitons (rate constant k_{isc}), or may result from geminate recombination in the charge-transfer state. The formation of such triplet excitons is detrimental for device efficiency because their energy is insufficient to produce free charge carriers. The direct formation of triplet excitons can be minimised by increasing the amount of acceptor present in the blend film because this reduces the singlet exciton lifetime. For example, 5 wt % of PCBM quenches >70 % of the singlet exciton luminescence of polythiophene films [68]. When the energy of the singlet exciton is higher than that of the electron acceptor, energy transfer will become competitive with electron transfer and the singlet state of the acceptor will be formed. This opens a new channel to form triplets when fullerenes are employed as acceptors because fullerenes have fast intersystem crossing rates and smaller singlet–triplet splitting than polythiophene films. The singlet and triplet state energies of solid C_{60} are $E_S = 1.70 \text{ eV}$ and $E_T = 1.55 \text{ eV}$ [63], whereas those of polythiophene films are $E_S = 2.1 \text{ eV}$ and $E_T = 1.2 \text{ eV}$ [70]. Thus, when $E_S(\text{polymer}) > E_S(\text{fullerene})$ singlet energy transfer from polythiophene to C_{60} will dominate over electron transfer, will be followed by fast intersystem crossing in the fullerene, and then by triplet energy transfer from C_{60} to polythiophene, yielding more polymer triplet excitons. On the other hand, when $E_S(\text{polymer}) < E_S(\text{fullerene})$, the yield of free charge carriers depends upon the kinetics of charge dissociation (k_{CS}) relative to geminate recombination to the ground state (k_{rec}) and intersystem crossing to the triplet exciton (k_{isc}).

It was mentioned before that the internal field across the BHJ cell drives electrons to the cathode and reduces the probability of diffusion to the hole-extracting ITO electrode. Nevertheless, it is energetically favourable for an electron in the LUMO of PCBM to transfer to the ITO electrode, where it recombines with a hole and erodes device efficiency. This leakage can be countered by an

interfacial 10 nm layer deposited on the ITO electrode composed of a material with a relatively high-lying LUMO, well-aligned for blocking electrons. Additionally, a transparent layer of intermediate hydrophobicity can improve the adhesion and electrical contact between the hydrophilic ITO surface and the typically hydrophobic organic semiconductors. Finally, with appropriate HOMO-level alignment with the active layer, such an interfacial layer would also improve hole transport. An interfacial layer capable of reducing the dark current and increasing V_{OC} was recently reported [71].

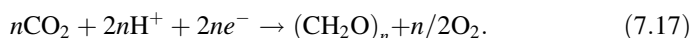
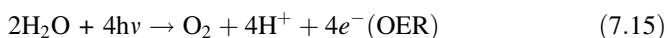
7.3.3 Challenges and New Developments

Most efforts to improve the performance of organic solar cells concentrate today on bulk heterojunction photovoltaic devices, most often using conjugated polymers as donors and fullerene derivatives as acceptors. At present, the most efficient BHJ solar cells employ P3HT as donor and PCBM as acceptor and reach power conversion efficiencies of 5 %. However, with a rather narrow long-wavelength absorption band and a 1.90 eV band gap, P3HT can only absorb *ca.* 30 % of the solar photons. Further improvement of the efficiency of such cells will require new polymer donors with an extended absorption edge to match solar terrestrial radiation, higher carrier mobility and better energy alignment with acceptors to reach a high open circuit voltage. Many research efforts have been dedicated to the development of organic semiconductors with such properties [63], but there is a caveat against polymers with low band gaps: in BHJ cells this is accompanied by a decrease in V_{OC} cancelling the benefit of an absorption increase. Moreover, the preparation and purification of such polymers is far from trivial, and their long-term stability is questionable. Alternatively, we may witness a renaissance of molecular donors, originally developed for bilayer organic solar cells, with properties designed for BHJ solar cells. The original applications favoured planar molecules with a strong propensity to adopt a horizontal orientation on substrate. It is believed that BHJs require isotropic charge transport and molecular donors with 3D geometries may offer new opportunities for organic solar cells [72].

The fabrication of BHJ solar cells with large V_{OC} and efficient charge separations remains a challenge. According to the model where the excess thermal energy of the exciton is necessary to overcome its Coulombic binding energy, efficient charge separation will require donor/acceptor blends with a large LUMO level offset, which is detrimental to the V_{OC} and overall efficiency of the cell, and/or polymers with lower electron–phonon couplings, which will reduce k_{th} and k_{isc} . Alternatively, the model based on a distance distribution of electrons and holes as a result of weakly distance-dependent electron transfer rates, suggests that increasing the lifetime of the exciton will lead to a wider distribution of distance and more charge carriers escaping from the electron–hole Coulombic potential. Ultimately, with energy levels, band gaps, charge separations and mobilities simultaneously optimised, single-layer polymer/fullerene solar cells may reach an efficiency of 11 % [54].

7.4 Solar Fuels

The diffuse and diurnal nature of solar irradiation represents a significant obstacle to the widespread use of solar energy as a viable alternative to fossil fuels or coal. One way to circumvent this problem is to store the energy coming from the Sun in other usable forms of energy, such as fuels. Natural photosynthesis accomplished by plants and bacteria shows that it is indeed possible to directly convert and store the energy contained in solar photons in the form of energy dense chemical bonds. With this inspiration from nature, extensive research in the last four decades has been focused on the development of artificial systems that can efficiently promote the photosynthesis of chemical fuels from water and, ideally, from carbon dioxide. In both these fuel synthesis processes, the *oxygen evolution reaction*, OER, supplies the electrons and protons (Eq. 7.15) required for the *hydrogen evolution reaction*, HER (Eq. 7.16) or hydrocarbon synthesis from CO₂ reduction (Eq. 7.17). The energy required to break the original chemical bonds and form new ones can be obtained from sunlight, provided that suitable photosystems are employed which are capable of capturing the photon energy and drive the redox reactions.



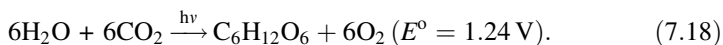
Hydrogen is one the most attractive next generation energy carriers; it is potentially more efficient than conventional fuels and environmentally benign. Its low density means that per gram, a much higher energy can be harvested from hydrogen than from gasoline, for example. Additionally, hydrogen can be obtained from the splitting of water and, when combined with oxygen in a fuel cell to produce electricity, it generates water as the only reaction product. Therefore, solar assisted splitting of water employing Earth-abundant and non-toxic photocatalytic systems provides a clean pathway for the generation of fuel and is often viewed as the holy grail of renewable energy [1]. The electrolysis of water can be driven by sunlight through the combination of a photovoltaic unit, which converts the photons from the Sun into electric current and generates a certain voltage, and an electrolyser that uses the voltage produced to drive the electrolysis reaction. Alternatively, the splitting of water can also be achieved using high temperatures to drive the decomposition process. This thermal water splitting (or thermolysis) typically occurs at very high temperatures, a requirement that considerably restricts the range of materials that can be employed in the process and limits the commercial viability of this technology. Direct photocatalytic (PC) or photo-electrochemical (PEC) water splitting employ inexpensive and non-toxic semiconductor materials and are, therefore, more attractive answers to the problem of conversion and storage of solar energy [73].

The first report of a semiconductor-based photoelectrochemical water splitting cell by Fujishima and Honda in 1972 offered a new approach to utilise sunlight as an energy source, in a time when renewable alternatives to fossil fuels were actively sought [74]. This discovery was quickly followed by the search for new semiconductor materials, particularly metal oxides, which could be employed as photoelectrodes to simultaneously harvest sunlight and catalyse the photolysis of water [75]. Biomimetic or bioinspired photochemical systems, combining photosensitiser units and molecular catalysts, have also been actively pursued in the last decades [76, 77]. Technological improvements in the synthesis and characterisation of nanomaterials, progresses in the fundamental understanding and theoretical modelling of semiconductors, and advances in the field of natural photosynthesis have led to the development of a multitude of new and improved water splitting systems, as will be discussed in the following sections.

7.4.1 Natural Photosynthesis

Over billions of years, plants, algae and bacteria have developed the capacity to harvest and store solar energy into chemical bonds by converting water and CO_2 into energy dense compounds, like glucose. Mimicking this function using artificial systems has become one of the most active areas of chemical research in the last decades, due to the prospect of generating renewable energy carriers and simultaneously mitigating the impact of CO_2 in the atmosphere.

Natural oxygenic photosynthesis in higher plants requires an intricate structure that is responsible for the tasks of light harvesting and concentration, charge generation and separation, and catalysis of water splitting into oxygen and protons (light process) and CO_2 reduction (dark process). This complex machinery resides in the chloroplasts, in the leaves of green plants, where chlorophyll molecules in the reaction centres—Photosystems II (PSII) and I (PSI)—are photoexcited by red solar photons. Additional energy is obtained from antennae complexes composed of chlorophylls and carotenoids, which absorb light of a wide range of wavelengths and funnel this energy to the reaction centres. Upon excitation of the P680 chlorophyll dimers in PSII, charge generation is followed by a sequence of electron transfer steps that result in the spatial and temporal separation of charges, minimising recombination processes, but at the expense of a significant loss of energy. For this reason, two reaction centres, Photosystems I (PSI) and II (PSII), are needed to supply the energy necessary for the photosynthesis reaction:



The electrons required to regenerate the chlorophyll molecules in PSII are then obtained from the oxidation of water by the $\text{Mn}_4\text{O}_5\text{Ca}$ cluster in the oxygen-evolving complex (OEC). This catalyst is responsible for the activation of water

and for the translation of one-electron photochemical steps into the multi-proton/multi-electron oxidation reaction (Eq. 7.15). The vital importance of good kinetic and thermodynamic control is well-evidenced in photosynthesis, where it avoids the loss of charges by recombination, and accounts for the mismatch between the rate of solar illumination and the slow reaction kinetics, particularly in the case of water oxidation. The efficiency of energy conversion in natural systems can reach up to 7 %, although in most cases less than 1 % of the solar energy is effectively converted into chemical energy [78], the overall conversion efficiency being determined by the relative rates of the processes described above. The application of the working principles derived from natural photosynthesis is therefore particularly valuable for the design and development of photochemical solar fuel production systems.

7.4.2 Semiconductor-Based Water Splitting

The splitting of water into molecular oxygen and hydrogen (Eq. 7.19) is a kinetically and thermodynamically demanding reaction.

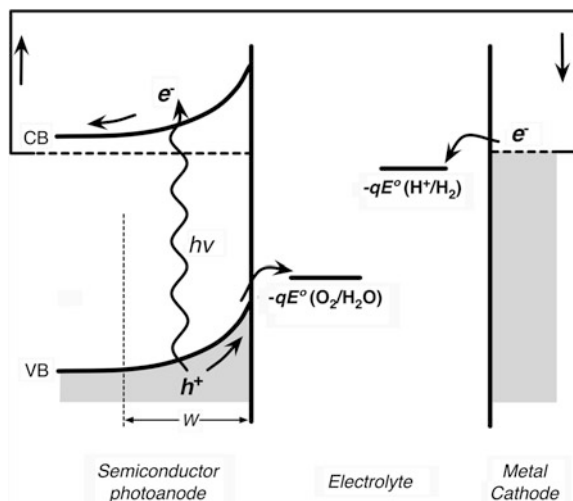


The conversion of one molecule of H_2O into H_2 and $\frac{1}{2}\text{O}_2$ is an uphill reaction (the Gibbs free energy, ΔG° , increases) and therefore thermodynamically unfavourable under standard conditions. Using the Nernst equation and considering that this process involves the transfer of two electrons per hydrogen molecule formed, the energy required per electron transferred can be calculated as $\Delta E^\circ = 1.23 \text{ V} \approx 1,000 \text{ nm}$, which establishes the ideal energy requirement for water splitting to occur and the threshold excitation wavelength in the case of a light-driven reaction. This thermodynamic analysis, however, is only valid for the multi-electron reactions (Eqs. 7.15 and 7.16), whereby the transfer of multiple electrons and protons is concerted. If the photolysis of water proceeds *via* different mechanisms, the energetic cost is higher (Table 7.1), despite the kinetic benefit. This interplay between thermodynamic and kinetic limitations requires the development of suitable catalyst materials, as is the case of the $\text{Mn}_4\text{O}_5\text{Ca}$ cluster in natural photosynthesis.

The photoelectrochemical water splitting cell reported in the seminal work of Fujishima and Honda employed a TiO_2 single crystal photoanode combined with a Pt metal counter electrode, placed in separate containers with water-based electrolytes [74]. Irradiation of the photoanode with UV light led to the formation of oxygen gas at the semiconductor/electrolyte interface while hydrogen gas was evolved at the cathode. A typical single band gap photoelectrochemical water splitting cell, like the one just described is illustrated in Fig. 7.4. In this example, the photoactive electrode is constructed from an *n*-type semiconductor (where the majority carriers are electrons, e^-), although the same principles apply to *p*-type electrodes (with holes, h^+ , as majority carriers).

Table 7.1 Standard electrode potentials for the single- and multi-electron water oxidation and proton reduction reactions (at pH 7)

	Half-cell reaction	E° versus NHE (V)
O1	$\text{H}_2\text{O} \rightarrow \text{HO}^\cdot + \text{H}^+ + e^-$	2.33
O2	$2\text{H}_2\text{O} \rightarrow \text{H}_2\text{O}_2 + 2\text{H}^+ + 2e^-$	1.35
O3	$2\text{H}_2\text{O} \rightarrow \text{O}_2 + 4\text{H}^+ + 4e^-$	0.82
R1	$\text{H}^+ + e^- \rightarrow \text{H}^\cdot$	-2.20
R2	$2\text{H}^+ + 2e^- \rightarrow \text{H}_2$	-0.41

**Fig. 7.4** Schematic energy band diagram for an ideal photoelectrochemical cell with a single-absorber semiconductor photoanode and a metal cathode for light assisted water splitting. The electrochemical potentials for the oxygen evolution reaction (OER) and hydrogen evolution reaction (HER) are represented by $-qE^\circ$, where E° represents the reduction potential for the corresponding redox couples

A detailed description of the working principles and different designs of photoelectrochemical cells is outside the scope of this work and only the main aspects will be discussed here. For further information on this topic the reader is referred to a number of comprehensive review articles [79, 80] and book chapters [81, 82].

When the semiconductor is put into contact with a liquid electrolyte containing a redox couple, thermodynamic equilibrium dictates that electrons will flow between the semiconductor and the electrolyte solution until the electrochemical potential (or Fermi level) on both sides of the interface is the same. This movement of charges results in the development of an electric field across the interface, which compensates the difference between the Fermi level position in the semiconductor before equilibrium and the electrochemical potential of the redox pair. If the semiconductor is *n*-type, the presence of ionised donor species leads to an excess of positive charges, which are spread out over a depletion region with

width W ; the solution will accommodate the excess of negative charges in the narrower region near the interface, known as the Helmholtz layer. Therefore, n -type electrodes are typically employed as photoanodes (where the oxidation of the electrolyte occurs) because the electric field in the solid causes an upward band bending that directs the minority carriers (h^+) to the semiconductor/electrolyte interface. Upon excitation of the photoanode with photons of energy higher than the band gap, electrons are excited to the conduction band of the semiconductor, while holes are left in the valence band. The band bending will cause electrons to move across the electrode to the back electric contact, while holes diffuse to the semiconductor/electrolyte interface, where they will promote the oxidation of water [$E^\circ(\text{O}_2/\text{H}_2\text{O}) = 1.23 - 0.059 \times \text{pH}$, V vs NHE]. Simultaneously, photo-generated electrons are transported through the external circuit to the counter electrode, where hydrogen will be evolved [$E^\circ(\text{H}^+/\text{H}_2) = 0 - 0.059 \times \text{pH}$, V vs NHE]. It then becomes clear that the feasibility of water splitting in the above photoelectrochemical cell requires certain criteria to be met by the semiconductor photoelectrode. First, the position of the conduction and valence band edges must straddle the water oxidation and proton reduction potentials, while the band gap energy should be 1.6–2.4 eV per electron–hole pair generated to drive both half-reactions and account for energy losses, e.g. kinetic losses. Another important requirement is that the mobility of photoinduced charge carriers is sufficiently high to allow their transport to the corresponding junctions (semiconductor/electric contact and semiconductor/liquid junctions for electron and hole, respectively) before recombination occurs. Additionally, fast surface reaction is desirable to avoid kinetic competition with surface electron–hole recombination. Finally, it is important that the semiconductor materials employed in water splitting systems are chemically stable under the reaction conditions. To date, no such material that meets all these criteria has been found [83].

Due to the intrinsic kinetic and thermodynamic constraints, the water oxidation reaction (Eq. 7.15) is usually considered the bottleneck of the whole water splitting process, and for that reason it has been extensively investigated. The requirement of chemical stability under oxidising conditions makes metal oxides and oxometalates particularly suitable for photoanode applications. Typically, in these materials the valence band consists of O $2p$ orbitals and the conduction band is formed by the valence orbitals in the metals and, as a consequence, the valence band is relatively fixed around 3.0 ± 0.5 eV versus NHE while the conduction band (and band gap) is tuned by the metal ions. Several transition metal oxides have been extensively investigated, both in the early days of photoelectrochemical water splitting research [84–86], and in recent years [83, 87]. The energy diagram for a number of photoanode materials is presented in Fig. 7.5, where the potentials for the oxidation and reduction of water are also shown, for guidance. Among those materials, TiO_2 [88], Fe_2O_3 [89], and WO_3 [90], have received particular attention. Given the position of the conduction band edges, more positive than the hydrogen evolution potential, water photolysis with Fe_2O_3 and WO_3 photoanodes will require additional energy, in the form of an external bias, to occur. Conversely, in the case of TiO_2 , unassisted water photolysis would be expected under

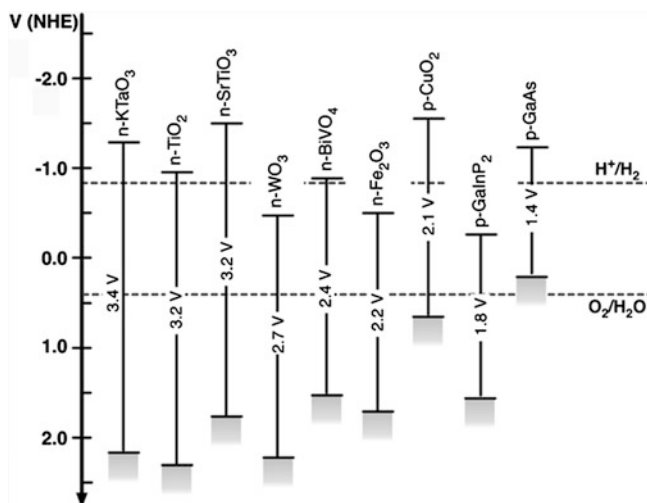


Fig. 7.5 Energy band diagram with the positions of the conduction and valence band edges *versus* NHE for selected semiconductors typically used in photoelectrochemical water splitting. For guidance, the reduction potentials for the water oxidation and reduction are also represented (*dashed lines*)

UV light illumination. In practice, however, this reaction requires an excess energy due to the existence of various activation barriers. This overpotential can be overcome by the application of an external electrical bias or chemically, by creating a pH gradient between the anode and cathode half-cells as shown in Fujishima and Honda's experiment [74]. Charge carrier dynamics studies of TiO₂, WO₃ and Fe₂O₃ by transient absorption spectroscopy under water splitting conditions have revealed that losses due to slow surface kinetics and fast electron-hole recombination are responsible for large oxygen evolution overpotentials and low photocurrents, resulting in poor water splitting efficiencies [91–95]. Several strategies have been used to overcome these limitations, namely through material nanostructuring [96, 97] and the use of surface co-catalysts [98–100], aimed at reducing electron-hole recombination and accelerating the rate of interfacial charge transfer, respectively.

The development of photocathode materials for either single- or dual-absorber cells has also received considerable attention [80, 101, 102]. Thermodynamic equilibrium dictates that *p*-type semiconductors will exhibit upward band bending when in contact with a liquid electrolyte. This behaviour is the opposite to that of *n*-type semiconductors described previously, and will result in the movement of photogenerated electrons towards the semiconductor–electrolyte interface while the holes are driven into the bulk of the electrode, towards the electrical back contact. At the surface, provided that the energy carried by the electrons is sufficient, H₂ is evolved. As discussed previously, one of the electronic properties of metal oxides that makes them suitable for water photo-oxidation purposes is the O 2*p* character of the valence electrons, which places the VB edge at potentials

~ 1.5 V positive of $E^\circ(\text{O}_2/\text{H}_2\text{O})$. The implication is that, for metal oxides with visible light absorption ($E_g > 3$ eV), the potential of the CB band edge will be very close or positive of $E^\circ(\text{H}^+/\text{H}_2)$, and photoelectrochemical proton reduction becomes thermodynamically unviable in these systems. Two examples of exception to this rule are SrTiO_3 and KTaO_3 , with VB and CB band edges suitable for both oxidation and reduction of water. However, despite the favourable driving force, in the few reports of unassisted proton reduction by these materials, hydrogen quantum yields observed were very low, possibly due to additional kinetic limitations. Cu_2O , an intrinsic *p*-type semiconductor with a direct band gap of 2.0 eV, is another exception, although in this case VB ≈ 0.9 V implies that water photo-oxidation is unfeasible. This Cu(I) oxide has been investigated by several research groups as an example of a catalytically active, easily processable material, based on widely available elements [103–108]. The main drawback of cuprous oxide is its instability in aqueous solutions, however, Grätzel and co-workers have shown that protecting this material with a combination of thin metal oxide layers (TiO_2 , Al:ZnO) can avoid photocorrosion, while activation with Pt nanoparticles allows the evolution of hydrogen with photocurrents as high as -7.6 mA cm^{-2} at 0 V versus NHE [109]. There are also several non-oxide materials employed as photocathodes for water splitting. One such example is *p*-type InP, with a band gap of 1.35 eV and the conduction band edge ~ 0.4 V negative of the redox potential for water reduction. This material has been extensively investigated [110] and several modifications have been proposed, particularly by surface attachment of proton reduction catalysts, such as Ru, Re and Rh, resulting in solar to hydrogen conversion efficiencies of 11–13 % [111]. However, scarcity of indium and the transition metal catalysts utilised renders this approach commercially unviable. Another example, *p*-type GaP, is stable in aqueous solution, has an indirect band gap of 2.3 eV and a conduction band edge more negative than the redox potential for proton reduction (-1.0 V vs NHE). However, as discussed previously for a few *n*-type materials, the small diffusion length of minority carriers compared to the absorption depth of visible light hampers the performance of this material by leading to very high recombination losses. Metal catalysts have also been used to increase the catalytic activity of *p*-Si electrodes ($E_g = 1.12$ eV) and conversion efficiencies up to 6 % have been measured upon visible light irradiation of the photocathode [112].

Photocatalytic water splitting using semiconductor nanoparticles suspended in the aqueous electrolyte is an alternative to the photoelectrochemical approach (where bulk semiconductor electrodes are employed) [113]. Although the same basic principles of photoelectrochemical water splitting apply to these systems, these are sometimes preferred because they are easier to process and their optical and electronic properties are more easily tuned than in bulk materials. Such advantages, however, are counterweighed by the fact that in photocatalytic systems the separation of water splitting products is not easily achieved, resulting in recombination and the formation of a potentially explosive mixture of O_2 and H_2 , both of which are highly undesirable.

Water oxidation and proton reduction half reactions are generally investigated separately, as discussed above, to allow the fine-tuning and optimisation of light harvesting, charge separation and catalytic properties of each of the units. Assembling the two components, photoanode and photocathode, in one complete cell that accomplishes unassisted visible light-driven water splitting is an extremely challenging task and few reports of such devices are known to date. A particularly successful photocatalytic system, capable of achieving water splitting with an apparent quantum yield of 6.3 % upon monochromatic light excitation, was reported by Domen *et al.* [114]. This two-step, microheterogeneous, non-sacrificial system is composed of Pt-loaded WO_3 (oxidation) and Pt-loaded ZrO_2/TaON (reduction) nanoparticles, and an I^-/IO_3^- redox mediator. The good performance observed for this assembly has been ascribed, in part, to the suppression of electron-hole recombination in ZrO_2/TaON particles. Additionally, efficient forward reactions between the redox couple and the photocatalysts (oxidation of I^- at the cathodic moiety and reduction of IO_3^- at the anodic moiety) prevented further losses associated to back electron transfer. The importance of a careful control of charge-carrier dynamics is well exemplified in this case, where surface modification of the particulate photocatalysts and introduction of a shuttle redox mediator play essential roles. Unassisted PEC water splitting has also been shown by Turner *et al.* in 1998 [115], with a system where the photosensitive electrode was a monolithic PEC/PV tandem device formed by the combination of a p/n GaAs cell (at the bottom) and a p/n GaInP₂ cell (on the top), interconnected with a tunnel diode. This arrangement ensured the complementary absorption of visible and near-infrared spectral regions by the top ($E_g = 1.83$ eV) and bottom ($E_g = 1.42$ eV) cells, respectively. Simultaneously, the relative band edge positions and diode interconnection facilitated the movement of electrons towards the electrode surface, while holes were directed to the electrical back contact. In the cell arrangement described, hydrogen was evolved at the photoelectrode and oxygen at the Pt counter electrode, resulting in an overall conversion efficiency of 12.4 %. Unfortunately, in addition to the high cost of the component materials this device was shown to be unstable, rapidly degrading under operation conditions. Nocera *et al.* have also reported an example of a fully synthetic and inorganic system capable of achieving photoelectrochemical water splitting without an external bias, or even any external electric circuit [116]. This new architecture consists of a commercial triple junction amorphous silicon solar cell interfaced with oxygen and hydrogen evolving catalysts. For the oxidation reaction, a Co-OEC is chosen, while for the H₂ evolution reaction a NiMoZn alloy is employed. Relatively high conversion efficiencies were calculated for this “artificial leaf”—4.7 % for the wired configuration and 2.5 % for the wireless—although the entire system was only stable for 10 h.

Other multi-component assemblies have been proposed that incorporate molecular components—sensitisers, electrocatalysts, or both—although unassisted photoelectrolysis failed to be observed with reasonable efficiency on any of such devices. A dye-sensitised PEC cell was first reported by Mallouk *et al.* [117]. In this artificial photosynthetic system, the photoanode is composed of a nanostructured

TiO₂ film deposited on FTO glass and sensitised with a Ru(bpy)₃²⁺ dye. This sensitiser is simultaneously attached to the TiO₂ nanoparticles through phosphonated ligands, and to IrO₂ water oxidation catalyst nanoparticles through malonate functional groups. Spectroscopic studies have shown that selective excitation of the dye with visible light (532 nm) lead to fast and efficient electron injection into the conduction band of TiO₂, as in a typical dye-sensitised solar cell. The corresponding quantum yield for water splitting, however, is very low because the multi-electron water oxidation reaction is slower than charge recombination in these systems.

7.4.3 Biomimetic Water Splitting

Homogeneous water splitting assemblies inspired by natural photosystems are usually composed of a photosensitiser, electron donor and acceptors, and catalytic units capable of accumulating multiple charges and promoting the oxidation or reduction of water [76, 118]. The unique photophysical and electrochemical properties of [Ru(bpy)₃]²⁺ make it the sensitiser of choice for most of these systems and modifications in the structures of ligands can be used to further modulate these properties. These remarkable qualities of ruthenium polypyridyl complexes are responsible for their utilisation not only as sensitisers but also as water splitting catalysts, particularly in photochemical water oxidation applications. In fact, a large number of the molecular oxygen evolution catalysts known to date are based on Ru(II) as the catalytic metal centre [119], mostly due to the robustness of the metal–ligand bonds formed, which increase the stability of the complexes in higher oxidation states. The ‘ruthenium dimer’, reported by Meyer in 1982 [120], *cis,cis*[(bpy)₂(H₂O)Ru^{III}ORu^{III}(H₂O)(bpy)₂]⁴⁺, is the first and probably most well-known ruthenium-based molecular water oxidation catalyst, capable of evolving O₂ in the presence of Ce^{IV} as an oxidising agent. Since the first report of the catalytic properties of the ruthenium dimer, several other catalysts have been developed, which differ in the number and nature of the metal centres [121].

Manganese, the metal of choice in Nature [122], has served as inspiration for the development of numerous Mn-based molecular catalysts, particularly those including Mn atoms linked by μ -oxo bridges, as seen in the OEC [123]. Several molecular iridium complexes have also been reported in the literature in the past few years and among them, [Ir^{III}(L)₂(H₂O)₂]⁺, with L = 2-(2-pyridyl)phenylate anion [124] and analogue ligands, have been reported to catalyse water in the presence of Ce^{IV} with considerably high turnover numbers (>2,500). Molecular catalysts for the evolution of hydrogen have also been extensively explored and are typically inspired by natural hydrogenase enzymes, with iron or nickel–iron binuclear centres as catalytic sites. A significant research effort is currently devoted to the assembly of water splitting catalysts, such as those described above, with visible light absorbing photosensitisers, for efficient photocatalytic activity [125].

Table 7.2 Standard electrode potentials for the single- and multi-electron reduction of carbon dioxide (in an aqueous solution at pH 7) [126]

	Half-cell reaction	E° (V)
R3	$\text{CO}_2 + e^- \rightarrow \text{CO}_2^-$	-1.90
R4	$\text{CO}_2 + 2\text{H}^+ + 2e^- \rightarrow \text{CO} + \text{H}_2\text{O}$	-0.52
R5	$\text{CO}_2 + 2\text{H}^+ + 2e^- \rightarrow \text{HCO}_2\text{H}$	-0.61
R6	$\text{CO}_2 + 4\text{H}^+ + 4e^- \rightarrow \text{HCHO} + \text{H}_2\text{O}$	-0.48
R7	$\text{CO}_2 + 6\text{H}^+ + 6e^- \rightarrow \text{CH}_3\text{OH} + \text{H}_2\text{O}$	-0.38
R8	$\text{CO}_2 + 4\text{H}^+ + 8e^- \rightarrow \text{CH}_4 + \text{H}_2\text{O}$	-0.24

7.4.4 Fuel Synthesis from CO₂ Photoreduction

Fuel synthesis from photochemical CO₂ reduction, mimicking closely the natural process of carbohydrate synthesis, is particularly attractive from the sustainability point of view, as it combines the storage of solar energy with the mitigation of the negative environmental impact of carbon dioxide present in the atmosphere. Also importantly, the chemical fuels produced in this way (particularly methanol) are easy to transport and benefit from a network of infrastructures already in place, which makes these energy carriers potentially more attractive than hydrogen. As a consequence, research focused on the photochemical or photoelectrochemical reduction of CO₂ has grown considerably in recent years.

The single electron reduction of CO₂ requires high energy and generates a highly unstable product, *i.e.* CO₂⁻ (Table 7.2, R3). Introduction of multi-electron processes significantly decreases the energetic requirement and increases the stability of CO₂ reduction products (Table 7.2, R4–R8), but requires suitable catalysts to manage the multiple proton couple electron transfer steps, as in the case of water oxidation discussed in Sect. 7.4.1. So far, several successful systems for the reduction of CO₂ to formate (CO) have been reported. Conversely, more useful reduction products, like methane or methanol, which require multiple electron and proton transfers, have proved difficult to obtain by direct photochemical reduction.

As seen for the case of hydrogen evolution, *p*-type semiconductors have been extensively investigated for the heterogeneous photoelectrochemical reduction of CO₂. Also in this case, thermodynamic criteria require semiconductors with a conduction band energy more negative than the reduction potential of carbon dioxide to drive the reaction. From Table 7.2 it becomes clear that this condition will significantly limit the number of suitable visible light absorbing semiconductor materials capable of reducing carbon dioxide directly to methanol or methane. Homogeneous photochemical CO₂ reduction has also been actively sought. For this type of approach, the photochemical system is typically composed of a photosensitiser, a catalyst, and a sacrificial agent or electron relay (for charge management). Typical light absorbers include transition metal complexes, particularly Ru(bpy)₃²⁺, and organic dyes such as *p*-terphenyl and phenazine, while the most efficient molecular catalysts typically consist of Re or Ru polypyridine

complexes, and Ni and Co macrocycle complexes. For a detailed analysis and a more complete list of these systems the reader is referred to a number of comprehensive reviews on this topic [127–130]. Despite the extensive research, however, no photo/electrocatalyst system has yet been found that is capable of efficiently reducing CO₂ with low overpotentials and high selectivity.

7.5 Conclusions

The Sun has great potential to supply our energy needs. The main obstacles to its widespread utilisation as the main source of sustainable energy are the high costs of conversion and storage when compared to fossil fuels and coal. Enormous scientific and technological progress has been made in the last decades and we are now much closer to efficient solutions that can enable us to benefit from such a copious energy resource. A detailed understanding of the factors that govern the function of photovoltaic and photoelectrochemical cells, and effective strategies to produce materials with enhanced light harvesting and charge separation properties to increase overall solar-to-chemical conversion efficiencies, remain important scientific endeavours.

Extensive fundamental characterisation of ‘traditional’ dye-sensitised solar cells has been accomplished, and the processes of charge generation and transfer are fairly well described. The biggest challenge in this field appears to reside in the technological development of devices. Nonetheless, important scientific advances, like the replacement of organic electrolytes for water-based ones [131] and the development of new fully organic dyes, show that there is space for improvement and that target efficiencies can potentially be achieved. Organic photovoltaics, a younger research field, has experienced a fast growth as it benefited from the fundamental knowledge base already available for DSSCs and which is transversal to both fields. Recent years have seen a significant increase in record efficiencies for organic photovoltaic devices at the laboratory scale, while new polymer materials, donor–acceptor blends and device architectures are reported nearly on a daily basis.

Solar fuel production is the area with most modest performances at present but the wealth of new semiconductor and molecular catalysts reported in recent years, combined with the important advances achieved in the understanding of the mechanisms of the oxidation and reduction of water, suggest that significant progress can be rapidly attained and higher solar-to-chemical conversion efficiencies can be envisaged. Finally, the development of artificial photosystems aimed at the photochemical/photoelectrochemical conversion of CO₂ into energy dense hydrocarbons shows great promise despite the limited number of systems capable of promoting the multi-electron reduction reactions, such as those leading to the formation of methanol and methane.

References

1. Lewis NS, Nocera DG (2006) Powering the planet: chemical challenges in solar energy utilization. *Proc Natl Acad Sci U S A* 103:15729–15735
2. Barber J (2009) Photosynthetic energy conversion: natural and artificial. *Chem Soc Rev* 38:185–196
3. Cook TR, Dogutan DK, Reece SY et al (2010) Solar energy supply and storage for the legacy and nonlegacy worlds. *Chem Rev* 110:6474–6502
4. O'Regan B, Grätzel M (1991) A low-cost, high efficiency solar cell based on dye sensitized colloidal TiO₂ films. *Nature* 335:737–740
5. Bessho T, Yoneda E, Yum J-H et al (2009) New paradigm in molecular engineering of sensitizers for solar cell applications. *J Am Chem Soc* 131:5930–5934
6. Moser J-E, Grätzel M (1998) Excitation-wavelength dependence of photoinduced charge injection at the semiconductor-dye interface: evidence for electron transfer from vibrationally hot excited states. *Chimia* 52:160–162
7. Ellingson RJ, Asbury JB, Ferrere S et al (1998) Dynamics of electron injection in nanocrystalline titanium dioxide films sensitized with [Ru(4,4'-dicarboxy-2,2'-bipyridine)₂(NCS)₂] by infrared transient absorption. *J Phys Chem B* 102:6455–6458
8. Benkő G, Kallioinen J, Korppi-Tommola JEI et al (2002) Photoinduced ultrafast dye-to-semiconductor electron injection from nonthermalized and thermalized donor states. *J Am Chem Soc* 124:489–493
9. Martinson ABF, Hamann TW, Pellin MJ et al (2008) New architectures for dye-sensitized solar cells. *Chem Eur J* 14:4458–4467
10. Arnaut LG, Formosinho SJ, Burrows HD (2007) Chemical kinetics. From molecular structure to chemical reactivity. Elsevier, Amsterdam
11. Tachibana Y, Haque SA, Mercer IP et al (2001) Modulation of the rate of electron injection in dye-sensitized nanocrystalline TiO₂ films by externally applied bias. *J Phys Chem B* 105:7424–7431
12. Kuciauskas D, Freund MS, Gray HB et al (2001) Electron transfer dynamics in nanocrystalline titanium dioxide solar cells sensitized with ruthenium or osmium polypyridyl complexes. *J Phys Chem B* 105:392–403
13. Durrant JR, Haque SA, Palomares E (2006) Photochemical energy conversion: from molecular dyads to solar cells. *Chem Commun* 31:3279–3289
14. Wang H, Nicholson PG, Peter L et al (2010) Transport and interfacial transfer of electrons in dye-sensitized solar cells utilizing a Co(dbbp)₂ redox shuttle. *J Phys Chem C* 114:14300–14306
15. Peter L (2009) “Sticky Electrons” transport and interfacial transfer of electrons in the dye-sensitized solar cell. *Acc Chem Res* 42:1839–1847
16. Ardo S, Meyer GJ (2009) Photodriven heterogeneous charge transfer with transition-metal compounds anchored to TiO₂ semiconductor surfaces. *Chem Soc Rev* 38:115–164
17. Ito S, Chen P, Comte P et al (2007) Fabrication of screen-printing pastes from TiO₂ powders for dye-sensitized solar cells. *Prog Photovolt Res Appl* 15:603–612
18. Zhang D, Ito S, Wada Y et al (2001) Nanocrystalline TiO₂ electrodes prepared by water-medium screen printing technique. *Chem Lett* 30:1042–1043
19. Grätzel M (2005) Solar energy conversion by dye-sensitized photovoltaic cells. *Inorg Chem* 44:6841–6851
20. Nazeeruddin MK, Angelis FD, Fantacci S et al (2005) Combined experimental and DFT–TDDFT computational study of photoelectrochemical cell ruthenium sensitizers. *J Am Chem Soc* 127:16835–16847
21. Kilså K, Mayo EI, Brunshwig BS et al (2004) Anchoring group and auxiliary ligand effects on the binding of ruthenium complexes to nanocrystalline TiO₂ photoelectrodes. *J Phys Chem B* 108:15640–15651

22. Odobel F, Blart E, Lagr e M et al (2003) Porphyrin dyes for TiO₂ sensitization. *J Mater Chem* 13:502–510
23. Ito S, Murakami TN, Comte P et al (2008) Fabrication of thin film dye sensitized solar cells with solar to electric power conversion efficiency over 10%. *Thin Solid Films* 516:4613–4619
24. Smestad GP, Gr tzel M (1998) Demonstrating electron transfer and nanotechnology: a natural dye-sensitized nanocrystalline energy converter. *J Chem Educ* 75:752–756
25. Nazeeruddin MK, Humphry-Baker R, Liska P et al (2003) Investigation of sensitizer adsorption and the influence of protons on current and voltage of a dye-sensitized nanocrystalline TiO₂ solar cell. *J Phys Chem B* 107:8981–8987
26. Guo X-Z, Luo Y-H, Zhang Y-D et al (2010) Study on the effect of measuring methods on incident photon-to-electron conversion efficiency of dye-sensitized solar cells by home-made setup. *Rev Sci Instr* 81:103106–103114
27. Anderson AY, Barnes PRF, Durrant JR et al (2010) Simultaneous transient absorption and transient electrical measurements on operating dye-sensitized solar cells: elucidating the intermediates in iodide oxidation. *J Phys Chem C* 114:1953–1958
28. Gr tzel M, Moser J-E (2001) Solar energy conversion. In: Balzani V (ed) *Electron transfer in chemistry*, vol V. Wiley-VCH, Weinheim, pp 588–644
29. Moser J-E, N oukakis D, Bach U et al (1998) Comment on “Measurement of ultrafast photoinduced electron transfer from chemically anchored Ru-dye molecules into empty electronic states in a colloidal anatase TiO₂ film”. *J Phys Chem B* 102:3649–3650
30. Cao Y, Bai Y, Yu Q et al (2009) Dye-sensitized solar cells with a high absorptivity ruthenium sensitizer featuring a 2-(hexylthio)thiophene conjugated bipyridine. *J Phys Chem C* 113:6290–6297
31. Balraju P, Kumar M, Deol YS et al (2010) Photovoltaic performance of quasi-solid state dye sensitized solar cells based on perylene dye and modified TiO₂ photo-electrode. *Synth Met* 160:127–133
32. Cid J-J, Garc a-Iglesias M, Yum J-H et al (2009) Structure–function relationships in unsymmetrical zinc phthalocyanines for dye-sensitized solar cells. *Chem Eur J* 15:5130–5137
33. Campbell WM, Jolley KW, Wagner P et al (2007) Highly efficient porphyrin sensitizers for dye-sensitized solar cells. *J Phys Chem C* 111:11760–11762
34. Garcia CG, Polo AS, Iha NYM (2003) Fruit extracts and ruthenium polypyridinic dyes for sensitization of TiO₂ in photoelectrochemical solar cells. *J Photochem Photobiol A* 160:87–91
35. Park N-G (2010) Light management in dye-sensitized solar cell. *Korean J Chem Eng* 27:375–384
36. Amadelli R, Argazzi R, Bignozzi CA et al (1990) Design of antenna-sensitizer polynuclear complexes. Sensitization of titanium dioxide with [Ru(bpy)₂(CN)₂]₂Ru(bpy(COO)₂)₂²⁻. *J Am Chem Soc* 112:7099–7133
37. Gajardo F, Leiva AM, Loeb B et al (2008) Interfacial electron transfer on TiO₂ sensitized with an axially anchored trans tetradentate Ru(II) compound. *Inorg Chim Acta* 361:613–619
38. Chiu W-H, Lee C-H, Cheng H-M et al (2009) Efficient electron transport in tetrapod-like ZnO metal-free dye-sensitized solar cells. *Energy Environ Sci* 2:694–698
39. Thimsen E, Rastgar N, Biswas P (2008) Nanostructured TiO₂ films with controlled morphology synthesized in a single step process: performance of dye-sensitized solar cells and photo water splitting. *J Phys Chem C* 112:4134–4140
40. Tiwari A, Snure M (2008) Synthesis and characterization of ZnO nano-plant-like electrodes. *J Nanosci Nanotech* 8:3981–3987
41. Boschloo G, Hagfeldt A (2009) Characteristics of the iodide/triiodide redox mediator in dye-sensitized solar cells. *Acc Chem Res* 42:1819–1826
42. Zhang Z, Chen P, Murakami TN et al (2008) The 2,2,6,6-tetramethyl-1-piperidinyloxy radical: an efficient, iodine-free redox mediator for dye-sensitized solar cells. *Adv Funct Mater* 18:341–346

43. Wang P, Zakeeruddin M, Moser J-E et al (2003) A stable quasi-solid-state dye-sensitized solar cell with an amphiphilic ruthenium sensitizer and polymer gel electrolyte. *Nature Mater* 2:402–407
44. Durrant JR, Haque SA (2003) Solar Cells Solid Compromise. *Nature Mater* 2:362–363
45. Li B, Wang LD, Kang BN et al (2006) Review of recent progress in solid-state dye-sensitized solar cells. *Sol Energy Mater Sol Cells* 90:549–573
46. O'Reagan BC, Lenzmann F, Muis R et al (2002) A solid-state dye-sensitized solar cell fabricated with pressure-treated P25-TiO₂ and CuSCN: analysis of pore filling and IV characteristics. *Chem Mater* 14:5023–5029
47. Snure M, Tiwari A (2007) CuBO₂-A p-type transparent oxide. *Appl Phys Lett* 91:092123
48. Nobuyuki I, Miysaka T (2005) A solid-state dye-sensitized photovoltaic cell with a poly(*N*-vinyl-carbazole) hole transporter mediated by an alkali iodide. *Chem Commun*, 1886–1888
49. Wang Y, Yang K, Kim S-C et al (2006) In situ polymerized carboxylated diacetylene as a hole conductor in solid-state dye-sensitized solar cells. *Chem Mater* 18:4215–4217
50. Liu X, Zhang W, Uchida S et al (2010) An efficient organic-dye-sensitized solar cell with in situ polymerized poly(3,4-ethylenedioxythiophene) as a hole-transporting material. *Adv Mater* 22:E150–E155
51. Tang CW (1986) Two-layer organic photovoltaic cell. *Appl Phys Lett* 48:183–185
52. Yoo S, Domercq B, Kippelen B (2004) Efficient thin-film organic solar cells based on pentacene/C60 heterojunctions. *Appl Phys Lett* 85:5427–5429
53. Yu G, Gao J, Hummelen JC et al (1995) Polymer photovoltaic cells: enhanced efficiencies via a network of internal donor-acceptor heterojunctions. *Science* 270:1789–1791
54. Blom PWM, Mihailetschi VD, Koster LJA et al (2007) Device physics of polymer:fullerene bulk heterojunction solar cells. *Adv Mater* 19:1551–1566
55. Jarzab D, Cordella F, Lenas M et al (2009) Charge transfer dynamics in polymer-fullerene blends for efficient solar cells. *J Phys Chem B* 113:16513–16517
56. Coropceanu V, Cornil J, da Silva Filho DA et al (2007) Charge transport in organic semiconductors. *Chem Rev* 107:926–952
57. Gomes PJS, Nunes RMD, Serpa C et al (2010) Exothermic rate restrictions in long-range photoinduced charge separations in rigid media. *J Phys Chem A* 114:2778–2787. *Correc J Phys Chem A* 2114:10759–11760
58. Serpa C, Gomes PJS, Arnaut LG et al (2006) Electron transfer in supercritical carbon dioxide: Ultraexothermic charge recombination at the end of the “Inverted Region”. *Chem Eur J* 12:5014–5023
59. Bässler H, Schweitzer B (1999) Site-selective fluorescence spectroscopy of conjugated polymers and oligomers. *Acc Chem Res* 32:173–182
60. Marcus RA, Sutin N (1985) Electron transfers in chemistry and biology. *Biochim Biophys Acta* 811:265–322
61. Arnaut LG, Formosinho SJ (1998) Modelling intramolecular electron transfer reactions in cytochromes and in photosynthetic bacteria reaction centres. *J Photochem Photobiol A Chem* 118:173–181
62. Kestner NR, Logan J, Jortner J (1974) Thermal electron transfer reactions in polar solvents. *J Phys Chem* 78:2148–2166
63. Baxter J, Bian Z, Chen G et al (2009) Nanoscale design to enable the revolution in renewable energy. *Energy Environ Sci* 2:559–588
64. Javey A, Guo J, Wang Q et al (2003) Ballistic carbon nanotube field-effect transistors. *Nature* 424:654–657
65. Clarke TM, Durrant JR (2010) Charge photogeneration in organic solar cells. *Chem Rev* 110:6736–6767
66. Zhu X-Y (2009) Charge-transfer excitons at organic semiconductor surfaces and interfaces. *Acc Chem Res* 42:1779–1787
67. Brédas J-L, Norton JE, Cornil J et al (2009) Molecular understanding of organic solar cells: the challenges. *Acc Chem Res* 42:1691–1699

68. Ohkita H, Cook S, Astuti Y et al (2008) Charge carrier formation in polythiophene/fullerene blend films studied by transient absorption spectroscopy. *J Am Chem Soc* 130:3030–3042
69. Nemeč H, Nienhuys H-K, Perzon E et al (2009) Ultrafast conductivity in a low-band-gap polyphenylene and fullerene blend studied by terahertz spectroscopy. *Phys Rev B* 79:245326–245333
70. Seixas de Melo J, Silva LM, Arnaut LG et al (1999) Singlet and triplet energies of a-oligothiophenes: a spectroscopic, theoretical, and photoacoustic study. *J Chem Phys* 111:5427–5433
71. Hains AW, Liu J, Martinson ABF et al (2010) Anode interfacial tuning via electron-blocking/hole-transport layers and indium tin oxide surface treatment in bulk-heterojunction organic photovoltaic cells. *Adv Funct Mater* 20:595–606
72. Roncali J (2009) Molecular bulk heterojunctions : an emerging approach to organic solar cells. *Acc Chem Res* 42:1719–1730
73. Turner J, Sverdrup G, Mann MK et al (2008) Renewable hydrogen production. *Int J Energy Res* 32:379–407
74. Fujishima A, Honda K (1972) Electrochemical photolysis of water at a semiconductor electrode. *Nature* 238:37–38
75. Chen X, Shen S, Guo L et al (2010) Semiconductor-based photocatalytic hydrogen generation. *Chem Rev* 110:6503–6570
76. Yagi M, Kaneko M (2000) Molecular catalysts for water oxidation. *Chem Rev* 101:21–36
77. Sala X, Romero I, Rodríguez M et al (2009) Molecular catalysts that oxidize water to dioxygen. *Ang Chem Int Ed Engl* 48:2842–2852
78. Blankenship RE, Tiede DM, Barber J et al (2011) Comparing photosynthetic and photovoltaic efficiencies and recognizing the potential for improvement. *Science* 332:805–809
79. Nozik AJ, Memming R (1996) Physical chemistry of semiconductor–liquid interfaces. *J Phys Chem* 100:13061–13078
80. Walter MG, Warren EL, McKone JR et al (2010) Solar water splitting cells. *Chem Rev* 110:6446–6473
81. van de Krol R (2012) Principles of photoelectrochemical cells. In: van de Krol R, Grätzel M (eds) Photoelectrochemical hydrogen production. *Electronic Materials: Science & Technology*, vol 102. Springer US, pp 13–67
82. Miller EL (2010) Solar hydrogen production by photoelectrochemical water splitting: The promise and challenge. In: *On solar hydrogen & nanotechnology*. Wiley, pp 1–35
83. Osterloh FE (2008) Inorganic materials as catalysts for photochemical splitting of water. *Chem Mater* 20:35
84. Memming R (1980) Solar-energy conversion by photoelectrochemical processes. *Electrochim Acta* 25:77–88
85. Hardee KL, Bard AJ (1976) Semiconductor electrodes. *J Electrochem Soc* 123:1024–1026
86. Harris LA, Wilson RH (1978) Semiconductors for photoelectrolysis. *Ann Rev Mater Sci* 8:99–134
87. Kudo A, Miseki Y (2009) Heterogeneous photocatalyst materials for water splitting. *Chem Soc Rev* 38:253–278
88. Anpo M, Takeuchi M (2003) The design and development of highly reactive titanium oxide photocatalysts operating under visible light irradiation. *J Catal* 216:505–516
89. Sivula K, Zboril R, Le Formal F et al (2010) Photoelectrochemical water splitting with mesoporous hematite prepared by a solution-based colloidal approach. *J Am Chem Soc* 132:7436–7444
90. Liu X, Wang F, Wang Q (2012) Nanostructure-based WO₃ photoanodes for photoelectrochemical water splitting. *Phys Chem Chem Phys* 14:7894–7911
91. Pendlebury SR, Cowan AJ, Barroso M et al (2012) Correlating long-lived photogenerated hole populations with photocurrent densities in hematite water oxidation photoanodes. *Energy Environ Sci* 5:6304–6312

92. Pendlebury SR, Barroso M, Cowan AJ et al (2011) Dynamics of photogenerated holes in nanocrystalline α -Fe₂O₃ electrodes for water oxidation probed by transient absorption spectroscopy. *Chem Commun* 47:716–718
93. Cowan AJ, Tang JW, Leng WH et al (2010) Water splitting by nanocrystalline TiO₂ in a complete photoelectrochemical cell exhibits efficiencies limited by charge recombination. *J Phys Chem C* 114:4208–4214
94. Tang JW, Durrant JR, Klug DR (2008) Mechanism of photocatalytic water splitting in TiO₂, reaction of water with photoholes, importance of charge carrier dynamics, and evidence for four-hole chemistry. *J Am Chem Soc* 130:13885–13891
95. Cowan AJ, Barnett CJ, Pendlebury SR et al (2011) Activation energies for the rate-limiting step in water photooxidation by nanostructured α -Fe₂O₃ and TiO₂. *J Am Chem Soc* 133:10134–10140
96. Cesar I, Sivula K, Kay A et al (2009) Influence of feature size, film thickness, and silicon doping on the performance of nanostructured hematite photoanodes for solar water splitting. *J Phys Chem C* 113:772–782
97. Brilllet J, Grätzel M, Sivula K (2010) Decoupling feature size and functionality in solution-processed, porous hematite electrodes for solar water splitting. *Nano Lett* 10:4155–4160
98. Zhong DK, Cornuz M, Sivula K et al (2011) Photo-assisted electrodeposition of cobalt-phosphate (Co-Pi) catalyst on hematite photoanodes for solar water oxidation. *Energy Environ Sci* 4:1759–1764
99. Barroso M, Mesa CA, Pendlebury SR et al (2012) Dynamics of photogenerated holes in surface modified α -Fe₂O₃ photoanodes for solar water splitting. *Proc Natl Acad Sci U S A*. doi:10.1073/pnas.1118326109
100. Barroso M, Cowan AJ, Pendlebury SR et al (2011) The role of cobalt phosphate in enhancing the photocatalytic activity of α -Fe₂O₃ toward water oxidation. *J Am Chem Soc* 133:14868–14871
101. Heller A (1984) Hydrogen-evolving solar cells. *Science* 223:1141–1148
102. Heller A, Aharonshalom E, Bonner WA et al (1982) Hydrogen-evolving semiconductor photocathodes: nature of the junction and function of the platinum group metal catalyst. *J Am Chem Soc* 104:6942–6948
103. Barreca D (2009) The potential of supported Cu₂O and CuO nanosystems in photocatalytic H₂ production. *Chemosuschem* 2:230–233
104. de Jongh PE, Vanmaekelbergh D, Kelly JJ (2000) Photoelectrochemistry of electrodeposited Cu₂O. *J Electrochem Soc* 147:486–489
105. Engel CJ, Polson TA, Spado JR et al (2008) Photoelectrochemistry of porous p-Cu₂O films. *J Electrochem Soc* 155:F37–F42
106. Hara M (1998) Cu₂O as a photocatalyst for overall water splitting under visible light irradiation. *Chem Commun* 3:357–358
107. Hu CC, Nian JN, Teng H (2008) Electrodeposited p-type Cu₂O as photocatalyst for H₂ evolution from water reduction in the presence of WO₃. *Sol Energy Mater Sol Cells* 92:1071–1076
108. Siripala W, Ivanovskaya A, Jaramillo TF et al (2003) A Cu₂O/TiO₂ heterojunction thin film cathode for photoelectrocatalysis. *Sol Energy Mater Sol Cells* 77:229–237
109. Paracchino A, Laporte V, Sivula K et al (2011) Highly active oxide photocathode for photoelectrochemical water reduction. *Nat Mater* 10:456–461
110. Szklarczyk M, Bockris JOM (1984) Photoelectrocatalysis and electrocatalysis on p-silicon. *J Phys Chem* 88:1808–1815
111. Aharon-Shalom E, Heller A (1982) Efficient p-InP(Rh-H alloy) and p-InP(Re-H alloy) hydrogen evolving photocathodes. *J Electrochem Soc* 129:2865–2866
112. Dominey RN, Lewis NS, Bruce JA et al (1982) Improvement of photoelectrochemical hydrogen generation by surface modification of p-type silicon semiconductor photocathodes. *J Am Chem Soc* 104:467–482
113. Maeda K, Domen K (2010) Photocatalytic water splitting: recent progress and future challenges. *J Phys Chem Lett* 1:2655–2661

114. Maeda K, Higashi M, Lu D et al (2010) Efficient nonsacrificial water splitting through two-step photoexcitation by visible light using a modified oxynitride as a hydrogen evolution photocatalyst. *J Am Chem Soc* 132:5858–5868
115. Khaselev O, Turner JA (1998) A monolithic photovoltaic-photoelectrochemical device for hydrogen production via water splitting. *Science* 208:425–427
116. Reece SY, Hamel JA, Sung K et al (2011) Wireless solar water splitting using silicon-based semiconductors and earth-abundant catalysts. *Science* 334:645–648
117. Youngblood WJ, Lee S-HA, Maeda K et al (2009) Visible light water splitting using dye-sensitized oxide semiconductors. *Acc Chem Res* 42:1966–1973
118. Andreiadis ES, Chavarot-Kerlidou M, Fontecave M et al (2011) Artificial photosynthesis: from molecular catalysts for light-driven water splitting to photoelectrochemical cells. *Photochem Photobiol* 87:946–964
119. Concepcion JJ, Jurss JW, Brennaman MK et al (2009) Making oxygen with ruthenium complexes. *Acc Chem Res* 42:1954–1965
120. Gersten SW, Samuels GJ, Meyer TJ (1982) Catalytic oxidation of water by an oxo-bridged ruthenium dimer. *J Am Chem Soc* 104:4029–4030
121. Duan L, Xu YH, Gorlov M et al (2010) Chemical and photochemical water oxidation catalyzed by mononuclear ruthenium complexes with a negatively charged tridentate ligand. *Chem Eur J* 16:4659–4668
122. Armstrong FA (2008) Why did nature choose manganese to make oxygen? *Phil Trans R Soc B Biol Sci* 363:1263–1270
123. Kurz P (2009) Oxygen evolving reactions catalysed by manganese-oxo-complexes adsorbed on clays. *Dalton Trans* 31:6103–6108
124. McDaniel ND, Coughlin FJ, Tinker LL et al (2007) Cyclometalated iridium(III) aquo complexes: efficient and tunable catalysts for the homogeneous oxidation of water. *J Am Chem Soc* 130:210–217
125. Herrero C, Lassalle-Kaiser B, Leibl W et al (2008) Artificial systems related to light driven electron transfer processes in PSII. *Coord Chem Rev* 252:456–468
126. Fujita E (1999) Photochemical carbon dioxide reduction with metal complexes. *Coord Chem Rev* 185–186:373–384
127. Doherty MD, Grills DC, Muckerman JT et al (2010) Toward more efficient photochemical CO₂ reduction: use of scCO₂ or photogenerated hydrides. *Coord Chem Rev* 254:2472–2482
128. Morris AJ, Meyer GJ, Fujita E (2009) Molecular approaches to the photocatalytic reduction of carbon dioxide for solar fuels. *Acc Chem Res* 42:1983–1994
129. Takeda H, Ishitani O (2010) Development of efficient photocatalytic systems for CO₂ reduction using mononuclear and multinuclear metal complexes based on mechanistic studies. *Coord Chem Rev* 254:346–354
130. Kumar B, Llorente M, Froehlich J et al (2012) Photochemical and photoelectrochemical reduction of CO₂. *Ann Rev Phys Chem* 63:541–569
131. Law C, Pathirana SC, Li X et al (2010) Water-based electrolytes for dye-sensitized solar cells. *Adv Mater* 22:4505–4509

Chapter 8

Radiolytic and Photolytic Production of Free Radicals and Reactive Oxygen Species: Interactions with Antioxidants and Biomolecules

Ruth Edge

Abstract This chapter discusses a variety of free radicals and other reactive oxygen species that are biologically and medically relevant. Radiolytic and/or photochemical methods of production for each reactive oxygen species are shown and for each type of reactive oxygen species some antioxidant and/or biomolecule interactions are discussed. Additionally, the techniques of laser flash photolysis and pulse radiolysis are described in detail and a comparison of the two techniques is made

8.1 Introduction

Other than the obvious exceptions, such as pigmented skin cells, the rods and cones in the eye and photosynthetic cells in plants and bacteria, most cells are not very sensitive to light. However, the presence of a photosensitiser, which can be exogenous or a cellular component, may induce damage possibly leading to cell death.

Photosensitisation in the presence of molecular oxygen can be classified into two pathways (shown in Fig. 8.1). A type I mechanism occurs *via* electron or hydrogen atom transfer from a substrate (RH) to the triplet state of a sensitiser ($^3\text{sens}^*$); this produces a carbon-centred radical (R^\bullet). This carbon-centred radical can then go on to react with oxygen producing a peroxy radical (RO_2^\bullet). A chain reaction follows, with RO_2^\bullet attacking other substrates, thus, generating more carbon-centred radicals, propagating the oxidation. A type II mechanism generates singlet oxygen *via* energy transfer from $^3\text{sens}^*$ to ground state molecular oxygen.

R. Edge (✉)

Dalton Cumbrian Facility, The University of Manchester, Westlakes Science and Technology Park, Moor Row, Cumbria, CA24 3HAUK
e-mail: ruth.edge@manchester.ac.uk

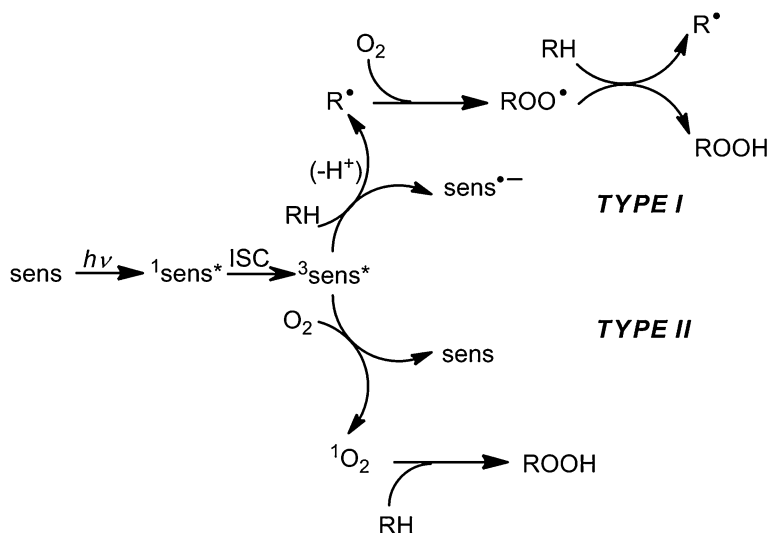


Fig. 8.1 Reaction scheme for photosensitised oxidation, showing type I and type II initiation

Additionally, many free radicals are produced in the body during normal metabolic processes (see, for example, [1, 2]) and they are usually very reactive species, having one unpaired electron and a spin multiplicity of two. Radicals can be neutral, positively or negatively charged, and are, essentially, either oxidising or reducing species, depending on their reduction potentials and those of the substrates they react with.

Lipids, proteins and DNA are all susceptible to attack by both singlet oxygen and free radicals [3, 4]. Cellular damage is both dependent on the location of the sensitizer and permeation of the sensitizer to the target site. It has been suggested that many diseases, including atherosclerosis [5], cancer [4], age-related macular degeneration [6] and neurological disorders [4], such as Alzheimer's disease, as well as the ageing process in general [7], are all associated with singlet oxygen and/or free radical production.

A range of defense systems have evolved to scavenge these species and to repair slight cellular damage. Substances which afford these defense mechanisms are known as antioxidants and can be classified into two categories, preventative antioxidants and scavenging antioxidants.

The preventative antioxidants include superoxide dismutase (SOD), catalase and glutathione peroxidase, as well as metal chelators. There are three types of SOD enzyme, containing different metals, which all catalyse the dismutation of superoxide [8]. Due to SOD enzymes generating H_2O_2 , catalase and glutathione peroxidase work together with SOD to remove H_2O_2 by converting it to harmless compounds. Catalase converts H_2O_2 to oxygen and water, while glutathione peroxidase oxidises reduced glutathione and also generates water [9]. Metal chelators, such as protoporphyrin IX and albumin, are used to prevent iron or copper from catalysing the Haber–Weiss reaction [10], which produces the hydroxyl radical.

The radical scavenging antioxidants are non-enzymatic and are found in plasma, lipoproteins and membranes. It is these types of antioxidant reactions that this Chapter will concentrate on, since many of these antioxidants can be increased by dietary supplementation and, therefore, could be used medicinally to prevent oxidation by radicals and other reactive oxygen species.

This category of antioxidants can be subdivided into water soluble and lipid soluble antioxidants. Nevertheless, they all act in a similar manner when scavenging reactive oxygen species. Radicals usually react with these antioxidants as a redox system, hence, the difference in reduction potentials of the species involved is a factor in determining how efficiently the reaction proceeds. An antioxidant can either react by donating an electron or a hydrogen atom to the radical, thus producing a stable compound and an antioxidant-derived radical (non-redox reactions can also occur, such as addition).

In the electron transfer case, the antioxidant radical cation can subsequently deprotonate producing the neutral radical, and there is much evidence to suggest that the interaction of antioxidants with peroxy radicals proceeds *via* this mechanism [11]. However, for the antioxidant to be effective its radical must either be stable and thus, not initiate other chain reactions by attacking other substrates, or it must be recycled by an enzyme or another antioxidant compound whose radical has a lower reduction potential. Scavenging antioxidants also react with singlet oxygen in two ways, either physical or chemical quenching [12]. Physical quenching occurs *via* electron exchange energy transfer producing the triplet state of the antioxidant and molecular oxygen. This reaction must predominate over chemical quenching, which will destroy the antioxidant, to give prolonged protection.

The major water-soluble antioxidant present in plasma, is ascorbic acid (vitamin C) [13]. At physiological pH it is present as ascorbate (AscH^-) and, due to its strong reducing potential, it is capable of scavenging many reactive oxygen species. Other water soluble antioxidants capable of radical scavenging include uric acid, albumin-bound bilirubin and glutathione [13, 14]. The lipid-soluble antioxidants include ubiquinol, carotenoids, flavonoids and other polyphenols, as well as the tocopherols (vitamin E) [14, 15]. Indeed, α -tocopherol is generally considered to be the most important lipophilic antioxidant [16].

This chapter will describe both pulse radiolytic and flash photolytic methods for the generation of a variety of biologically relevant free radicals and reactive oxygen species in solution, giving examples of antioxidant/biomolecule interactions with each species.

8.2 Experimental Techniques: Laser Flash Photolysis and Pulse Radiolysis

Flash photolysis is a useful technique for studying transient species, such as excited states and radicals, which are too short lived to be detected by conventional absorption spectroscopy [17].

An intense short pulse of UV or visible radiation is used to electronically excite the sample, and the subsequent absorption changes are probed spectrophotometrically. The technique was first introduced by Norrish and Porter in 1949 [18] and at this time gas-filled discharge lamps were used, limiting the time resolution, which is principally governed by the duration of the excitation pulse, to microseconds. This is now usually termed conventional flash photolysis. However, with the development of laser pulsed techniques in place of flash excitation, the time resolution has been progressively reduced to subpicosecond, particularly with the use of mode-locked solid state lasers. Much current work utilises nanosecond time resolution with pulsed lasers such as ruby, neodymium and excimer lasers.

One advantage of laser excitation is that monochromatic light allows excitation selectivity. Hence, laser flash photolysis has become an extremely useful method which is widely used in the investigation of many transient species, including biradicals, photoisomers, and photo tautomers, as well as excited states and radicals. Laser flash photolysis is also discussed in more detail in [Chaps. 14 and 15](#).

Pulse radiolysis is another technique for generating free radicals and excited states *in vitro* [17, 19, 20]. This technique is complementary to laser flash photolysis and has the ability to generate radicals in high yields, which is often impossible by laser flash photolysis. Thus, pulse radiolysis is often the preferred method for generation of radicals while flash photolysis is preferred for generating electronic excited states.

Pulse radiolysis emerged about ten years after laser flash photolysis and uses similar principles to study the effects of high energy radiation upon molecules. The laser excitation source used in flash photolysis is often replaced by a beam of electrons in pulse radiolysis, although X-rays, γ -rays, and other energetic particles, such as protons, neutrons, and α - or β -particles may also be used. The beam and sample are housed in a shielded room due to the potentially lethal effects of the ionising radiation and the detection equipment is outside this shielding. The energy of the pulsed beam can be varied as can the pulse length. Hence, the dose of radiation which the sample receives can be altered *via* variation of these parameters.

The transient species produced by either technique are usually monitored *via* the transient absorption changes induced, though other methods of detection can also be used, such as Raman spectroscopy and electron paramagnetic resonance spectroscopy (EPR). Briefly, a monitoring light, e.g. a xenon arc lamp (possibly pulsed) is focused through the sample cell, which, for pulse radiolysis, is normally a flow cell which can be operated from outside the shielding, since the sample is destroyed by the radiation and, therefore, a fresh sample is needed after each pulse, unlike with laser flash photolysis (unless the sample photodegrades rapidly). The monitoring light passes through the sample cell perpendicular to the laser or ion beam and, after passing through the sample, it is collimated into a monochromator and a photodetector, for pulse radiolysis it is first reflected by planar front mirrors out of the shielded radiation area. Changes in the photodetector current are recorded as changes in voltage on an oscilloscope, which can be PC interfaced for analysis and storage of the data.

Even though the experimental apparatus for pulse radiolysis and laser flash photolysis are very similar their initial effects on the samples are very different. In pulse radiolysis, unlike laser flash photolysis where it is the solute which is excited, the energy from the ionising radiation is absorbed by the most abundant species, which in dilute solutions is the solvent. Upon absorption of the radiation the solvent-derived intermediates can interact with the solute thus forming solute transient intermediates. Hence, in pulse radiolysis the choice of solvent is extremely important in determining the type of species formed.

However, despite the initial differences in the two techniques they can both ultimately produce the same species, although the efficiency of their generation is expressed differently. In laser flash photolysis the efficiency is expressed by the quantum yield (ϕ) which is equivalent to the number of excited intermediates formed per absorbed photon. In contrast, in pulse radiolysis the effects of the ionising radiation are measured in G values, which are the number of excited intermediates produced per 100 eV of absorbed energy.

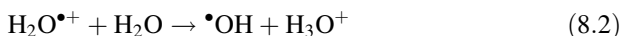
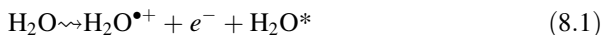
Solute excited states and radicals produced using pulse radiolysis can be formed *via* recombination, direct excitation, or energy transfer from excited solvent and sub-excitation electrons. Mechanisms for some common solvents are discussed below, since they are solvent specific. Thus, by appropriately choosing the experimental conditions, specific radicals or excited states can be generated.

Non-polar solvents, such as hexane and benzene, produce high yields of excited states *via* ion recombination, and relatively low yields of radical ions. In contrast, polar solvents like methanol, acetonitrile and water support high yields of radical ions with low excited state yields, due to solvation and stabilisation of the initial ions, particularly the electrons, leading to a slow rate of ion recombination. In intermediate polarity solvents, such as acetone, approximately equal amounts of radicals and excited states are generated. Hence, generally it is better to study solute excited states with pulse radiolysis in non-polar solvents and solute radicals or radical ions in polar solvents. This is often not possible due to insolubility in the preferred solvent, but if the transients are being monitored *via* transient absorption spectroscopy and they have high molar absorption coefficients then low yields need not be problematic.

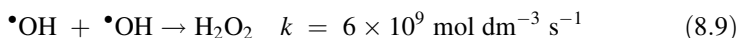
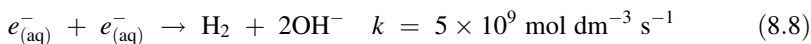
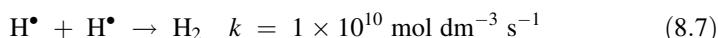
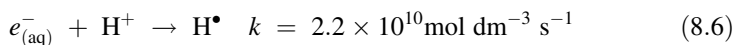
8.2.1 Radiolytic generation of radicals and excited states in various solvents

8.2.1.1 Water

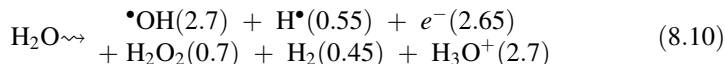
The radiolysis of water occurs in two stages, firstly excited states (H_2O^*), cations and electrons are produced (reaction 8.1), then a variety of reactions occur, also generating hydrogen atoms and hydroxyl radicals (reactions 8.2–8.4) and the electron loses energy *via* excitation and ionisation of other molecules and becomes solvated (reaction 8.5).



Reaction 8.2 occurs in 1.6×10^{-14} s [17] which is faster than the recombination of $\text{H}_2\text{O}^{\bullet+}$ and $e_{(\text{aq})}^-$ (reaction 8.3). These species can then rapidly react with each other so that further hydrogen atoms are generated *via* reaction 8.6 and reactions 8.7–8.9 produce hydrogen and hydrogen peroxide.

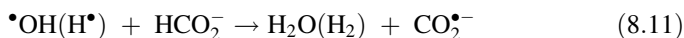


Many of the radicals formed will recombine to form water and the protons and hydroxide ions eventually neutralise one another. Thus, the ultimate products of water radiolysis (within a ns) in an argon or nitrogen saturated solution are given in reaction 8.10 with the G values shown in parentheses [17, 21].



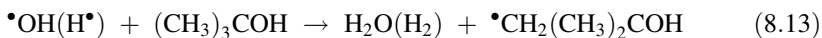
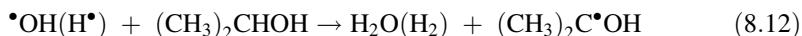
Of these products it is the three radical species which are the most reactive. The solvated electron and hydrogen atom have reduction potentials (E_0) of -2.87 and -2.30 V versus the standard hydrogen electrode (SHE), respectively [22], and hence they are extremely reactive reductants. The hydroxyl radical is a highly oxidising species with a reduction potential (E_0) of 2.65 V *vs* SHE [22].

Since a restricted radical source is needed for many studies, specific scavengers can be utilised to produce exclusively reducing or oxidising conditions. In order to selectively produce reduced products of the solute, sodium formate can be added to the solution in a high concentration. The formate anion reacts with the oxidising hydroxyl radical and with the hydrogen atom (reaction 8.11) forming $\text{CO}_2^{\bullet-}$ which is reducing and has a reduction potential of -1.9 V *vs* SHE [23], so it is not as reactive as the solvated electron.

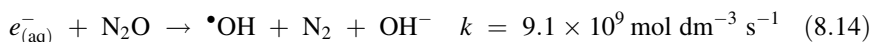


Alternatively, alcohols such as isopropanol or *tert*-butanol can be used to remove hydroxyl radicals (reactions 8.12 and 8.13). Isopropanol also effectively

scavenges hydrogen atoms ($k = 5 - 7 \times 10^7 \text{ mol dm}^{-3} \text{ s}^{-1}$ [24, 25]) whereas *tert*-butanol does not ($k = 2 \times 10^5 \text{ mol dm}^{-3} \text{ s}^{-1}$ [25]).

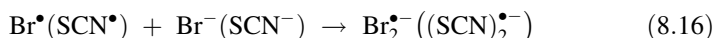


Predominantly oxidising conditions can be produced by saturating the solution with nitrous oxide gas (N_2O), which reacts with the solvated electron to generate further oxidising hydroxyl radicals (reaction 8.14). The reducing hydrogen atoms also react with nitrous oxide, producing more $\text{OH}\bullet$ and nitrogen, though with a much slower rate constant ($k = 2.1 \times 10^6 \text{ mol dm}^{-3} \text{ s}^{-1}$ [26, 27]).



Nitrous oxide saturation can also be used with other solvents to remove the electron although the $\text{O}\bullet^-$ produced may not generate $\text{OH}\bullet$ as it does in water but little is known about the reactions of N_2O in other solvents. However, in N_2O saturated cyclohexane, nitrogen and hydrogen are produced together with the oxygenated product, cyclohexanol [28].

In some cases when oxidising conditions are required, milder oxidants may be needed, because the hydroxyl radical can react with the solute forming adducts as well as *via* electron transfer. Hydroxyl radicals can be converted into milder (one-electron) oxidants by the addition of halides, thiocyanate or azide ions (reactions 8.15–8.17). In fact, halide radical reactions occur in atmospheric chemistry, particularly in urban cloud droplets, as well as in marine water radical reactions [29].



8.2.1.2 Methanol

Methanol is a useful polar solvent for solutes which are insoluble in water. The radiolysis of methanol yields a number of intermediates including $\text{CH}_3\text{O}\bullet$, $\text{H}\bullet$, $\bullet\text{OH}$, and $\text{CH}_3\bullet$ as well as $e_{(\text{MeOH})}^-$ and $\bullet\text{CH}_2\text{OH}$. The first four radicals above all react with methanol itself, yielding more $\bullet\text{CH}_2\text{OH}$. Hence, the initial reaction reduces to reaction 8.18.



Both of the species, $e^-_{(\text{MeOH})}$ and $\bullet\text{CH}_2\text{OH}$ are reducing and will react with the solute to generate its radical anion.

Also useful for samples insoluble in water are detergents, since it is possible to study oxidation and reduction reactions *via* electron transfer through the water-detergent interface.

8.2.1.3 Hexane

This non-polar aliphatic hydrocarbon solvent has relatively short-lived excited states ($\tau_{s1} < 1$ ns), and as such, upon absorption of radiation the major process is solvent ionisation (reaction 8.19) producing the hexane radical cation ($\text{C}_6\text{H}_{14}^{\bullet+}$) and the electron (e^-). As the electron is not readily solvated in hexane, it will either recombine with the hexane radical cation or react with the solute (S) (reactions 8.20 and 8.21). The parent radical cation can also react with the solute, as in reaction 8.22.



Fast recombination of solute radical anions and cations (reaction 8.23) or of solute radical anions with hexane radical cations (reaction 8.24) yields first excited singlet and triplet states of the solute (S^*). Further solute triplet states may be produced *via* intersystem crossing.

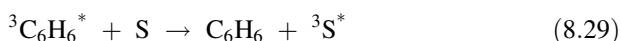
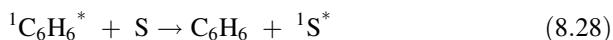
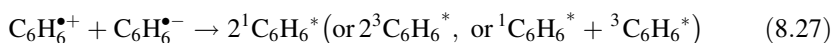
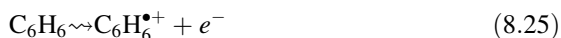


Two types of ion are involved in ion recombination. Geminate ions, which constitute 90 % of the total, recombine within a few nanoseconds since the positive and negative ions which are formed do not escape each others influence. The other 10 % of the ions do escape each others influence and are termed 'free' or non-geminate. They recombine over microsecond time scales. The high percentage of geminate ions in hexane explains why non-polar solvents support high yields of excited states and low yields of radical ions.

8.2.1.4 Benzene

The aromatic hydrocarbon benzene differs from hexane since it has relatively long-lived excited singlet and triplet states. ($\tau = 20$ ns and 3 μs , respectively). Thus, solute excited states may be generated *via* energy transfer from the benzene

excited states. Again, intersystem crossing may occur, yielding more triplet states. The following reactions (8.25–8.29) illustrate the radiation chemistry of benzene with a solute (S). (Reactions 8.20–8.24 can also occur, with benzene replacing hexane).



8.3 Production of Radicals and Reactive Oxygen Species and their Reactions

8.3.1 Hydroxyl radical

As discussed above (in Sect. 8.2.1.1) the hydroxyl radical is one of the primary products in the radiolysis of water and can almost be exclusively produced by saturating the solution with N_2O . Other methods of $\bullet\text{OH}$ production include, the photolysis of dilute solutions of hydrogen peroxide [30] and the metal-ion catalyzed Haber–Weiss reaction which can also occur *in vivo* [10].

The hydroxyl radical is a highly oxidising species, having a reduction potential of 2.31 V vs SHE at pH 7 [31], higher in acidic solutions [22]. Thus, it is capable of oxidising many organic compounds, such as the flavour compound methional [32] and the anti-inflammatory drug metiazinic acid [33]. It can also abstract hydrogen atoms from C to H groups e.g. in aliphatic amino acids [34] and add across C=C double bonds e.g. in the purine bases [35] and in the spin traps often used to detect it, such as DMPO [36]. It has a pK_a of 11.9 and so forms $\text{O}^{\bullet-}$ in highly basic solutions, which can sometimes react *via* a different mechanism. For example, a study by Neta *et al.* has shown that for aromatic compounds with aliphatic chains $\bullet\text{OH}$ will preferentially add to the aromatic ring whilst $\text{O}^{\bullet-}$ will abstract a hydrogen atom from the aliphatic chain [37].

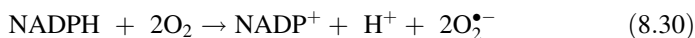
A wide range of flavonoid antioxidants have been studied for their ability to scavenge $\bullet\text{OH}$ radicals produced by photolysis of hydrogen peroxide and analysed using spin-trapping and HPLC [36]. It was found that those flavonoids containing the most hydroxyl groups in the aromatic B-ring were the best scavengers. They found that the C-3 hydroxyl group was the most important, as did a more recent study using a salicylate probe for detection in a modified CUPRAC (cupric ion

reducing antioxidant capacity) assay [38]. Additionally, the presence of a carbonyl group in the C-4 position increased the reactivity significantly, with catechin shown to quench only 2/3 the amount of $\bullet\text{OH}$ as quercetin. In the spin-trapping study [36] the flavones were shown to exhibit similar quenching capacities to the flavanone, naringenin, suggesting that the presence of a double bond between the C-2 and C-3 groups has no effect on the scavenging capacity. However, the newer study showed that the presence of this double bond increased scavenging [38].

The reactions of $\bullet\text{OH}$ radicals with the polyphenolic antioxidant bergenin have been monitored using pulse radiolysis [39]. Multiple reaction pathways have been shown to occur, with radical addition being the major process and one electron oxidation only a minor process. Both radical addition and hydrogen abstraction were shown to produce reducing radicals that react readily with oxygen to yield peroxy radicals, suggesting that bergenin may act as a prooxidant.

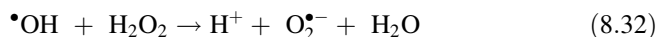
8.3.2 Superoxide Radical Anion and its Protonated Form

Superoxide can be produced in a number of ways, radiolytically, photochemically, electrochemically [40], enzymatically (*via* xanthine oxidase) [41] or prepared from potassium superoxide [42]. Biologically it is generated mainly in phagocytic cells helping them to inactivate foreign bodies, such as viruses and bacteria [43]. When these cell types are activated for phagocytosis an increase in oxygen consumption (of at least 10 fold) is triggered and there is rapid reduction of the oxygen to superoxide. This reaction is catalysed by plasma membrane-bound NADPH (reduced form of nicotinamide adenine dinucleotide phosphate) oxidase, reaction 8.30.



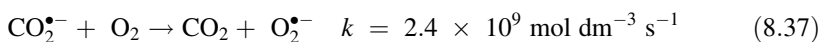
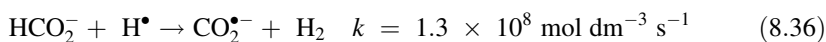
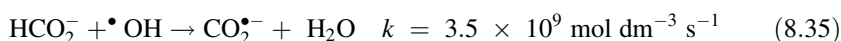
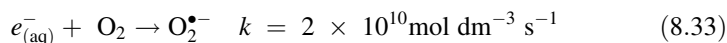
Several subcellular organelles, including mitochondria, microsomes and chloroplasts, generate superoxide during electron transport, usually via the autooxidation of various biomolecules, such as reduced cytochrome C and reduced flavins, as well as haemoglobin and myoglobin (see, for example, [1]).

Photochemical production of $\text{O}_2^{\bullet-}$ can be achieved in two ways. Firstly, by the photolysis of concentrated hydrogen peroxide solutions, where the initially produced hydroxyl radicals go on to react with the hydrogen peroxide to produce superoxide [44]:



The other method is to generate it *via* reduction of a donor triplet, such as a flavin, to its radical anion, which will reoxidise simultaneously reducing molecular oxygen [45].

Radiolytic production of $\text{O}_2^{\bullet-}$ is achieved in oxygen saturated aqueous solutions containing formate. Of the primary radicals produced upon water radiolysis, both the hydrated electron and the hydrogen atom react rapidly with oxygen to produce $\text{O}_2^{\bullet-}$. The hydroxyl radicals (and the hydrogen atom) react with the formate to produce the carbon dioxide radical anion and this radical anion reacts with oxygen generating further $\text{O}_2^{\bullet-}$ [46].



In aqueous, and other protic media, superoxide is not very reactive, due to its negative charge, high activation energy and high energy of solvation (usually it acts as a mild reductant, although it can also act as an oxidant). However, it is the dissociated form of the hydroperoxyl radical (HO_2^\bullet), a weak acid, and this is more reactive. For example, HO_2^\bullet is capable of initiating peroxidation of polyunsaturated fatty acids (PUFA), whereas $\text{O}_2^{\bullet-}$ cannot. The hydroperoxyl radical has a $\text{p}K_a$ of 4.8 [47], thus at physiological pH only a small amount of superoxide will be present in the protonated form. However, in aqueous solutions both of these species (HO_2^\bullet and $\text{O}_2^{\bullet-}$) can react with themselves or each other producing hydrogen peroxide which can then, in turn, react with superoxide generating the hydroxyl radical.

Many antioxidants have been shown to react with superoxide, such as ubiquinone [48], curcumin [49] and ascorbic acid/ascorbate [50]. A variety of flavonoids and other plant antioxidants have been tested for their superoxide scavenging ability [51], with those compounds containing ortho-trihydroxy groups showing the highest rate constants for scavenging. While those containing the ortho-dihydroxy (catechol) group have rate constants for superoxide scavenging of about one order of magnitude lower and the rate constants for those with only a monohydroxy group were shown to be 2–3 orders of magnitude lower. More recently, Silva *et al.* [52] have synthesised and studied some flavonoid derivatives, 3-alkylpolyhydroxyflavones, in which the C-3 hydroxyl group on the chromone ring has been replaced by an alkyl chain. *Via* pulse radiolysis studies of the reaction of superoxide with these compounds they have shown that different alkyl chain lengths allow the compounds to penetrate into the micelles to different depths, therefore, suggesting that cellular distribution can be selectively modified to improve the inhibitory effect on damage due to reactive oxygen species.

8.3.3 Singlet Oxygen

Ground state molecular oxygen has a spin multiplicity of 3 (*i.e.* it is in a triplet state, $^3\Sigma_g^-$) with the two unpaired electrons being in the degenerate pair of π^* orbitals. The two lowest electronic excited states of oxygen in the gas phase are singlet states ($^1\Delta_g$ and $^1\Sigma_g^+$) with the $^1\Delta_g$ state being the lower lying and as such being commonly referred to as singlet oxygen (1O_2) [53].

1O_2 can be produced in a number of ways, e.g. peroxide decomposition, high frequency discharge and energy transfer [53]. The most common mechanism for its production is *via* energy transfer from the excited state of a photosensitiser to ground state molecular oxygen. The low energy level of 1O_2 ($E = 0.98$ eV or 94.5 kJ mol $^{-1}$) means that many sensitisers have a high enough energy in their singlet and triplet states to convert molecular oxygen to its excited state. This means that the quantum yield of 1O_2 production can reach two. For both singlets and triplets to be quenched by molecular oxygen in this way, the singlet state lifetime must be long and the energy difference between the singlet and triplet state ($\Delta E(S_1 - T_1)$) and the triplet state energy must both be higher than $E(^1O_2)$. Hence, 1O_2 production most often occurs from triplet states only, since usually $\Delta E(S_1 - T_1)$ is too low and the lifetime of the singlet state is too short. Typical triplet sensitisers are dyes like methylene blue, rose bengal and eosin, although many other compounds are capable of sensitising singlet oxygen due to the relatively small energy difference between the ground state ($^3\Sigma_g^-$) and excited state ($^1\Delta_g$). Usually, the triplet state of the sensitiser is generated *via* laser flash photolysis (see Chap. 15) but pulse radiolysis can also be used [54, 55] and, in fact, can produce more accurate triplet-induced 1O_2 yields. This is because photolysis initially generates only excited singlet states, whereas radiolysis generates both triplet and singlet excited states (usually in about a 3:1 ratio), thus less singlet state quenching by oxygen can occur and therefore less additional sensitiser triplet states are produced (*via* oxygen-enhanced intersystem crossing or by energy transfer).

In biological systems, sensitisers such as porphyrins, chlorophylls and riboflavin can sensitise 1O_2 production and this can lead to deleterious effects including DNA damage and lipid peroxidation [56, 57]. Once produced 1O_2 can react with and oxidise many cellular substrates but it has a limited lifetime and, if no reaction occurs, it decays to the ground state either radiatively or by solvent-induced non-radiative deactivation. The non-radiative process dominates in solution, and is governed by the vibrational frequencies of the solvent molecule. Thus, the lifetime of singlet oxygen is greatly influenced by the solvent, varying from a few milliseconds to a few microseconds compared with a half-life of 45 min in the gas phase [58]. The radiative component of the deactivation of 1O_2 has a maximum around 1270 nm for the (0', 0) transition (varying only a few nm with the solvent) and this decay can be used for monitoring 1O_2 (see Chap. 15).

1O_2 may be quenched either chemically or physically by antioxidants, with chemical quenching ultimately destroying the quencher. Physical quenching can occur either *via* collisional energy transfer, which is the reverse of the reaction by

which $^1\text{O}_2$ is formed and is the process by which carotenoids quench $^1\text{O}_2$ or via charge transfer with electron donors, such as amines [53]. Various antioxidants have been shown to quench singlet oxygen, for example the tocopherols [59]. One class of antioxidants which quench $^1\text{O}_2$ very efficiently is the carotenoids and many studies have been carried out on their quenching and on their protection against $^1\text{O}_2$ mediated photo-oxidation reactions. Foote and Denny [60] were the first to show that β -carotene inhibits photosensitised oxidation and was, therefore, able to efficiently quench $^1\text{O}_2$. Farmilo and Wilkinson [61] showed that electron exchange energy transfer quenching is the principal mechanism of carotenoid photoprotection against $^1\text{O}_2$, leading to the carotenoid triplet state (reaction 8.38), although, chemical quenching also occurs in a minor process destroying the carotenoid [62].



Once produced ${}^3\text{CAR}^*$ returns to the ground state dissipating the energy as heat or it can be quenched physically *via* enhanced intersystem crossing by oxygen.

Many carotenoids have been studied to investigate the influence of different structural characteristics on the ability to quench $^1\text{O}_2$ and it has been observed that the quenching ability increases with increasing number of conjugated double bonds, n , and the increasing wavelength of the $\pi\pi^*$ absorption maximum, reflecting increased exothermicity in the energy transfer as the energy of ${}^3\text{CAR}^*$ decreases, see Fig. 8.2 [63, 64].

Studies have also been undertaken in more biologically relevant environments, such as micelles and dipalmitoylphosphatidylcholine (DPPC) liposomes [64, 65] where the quenching rate constants are still found to be high and in the liposome study [65] little difference was observed in the quenching when the $^1\text{O}_2$ was generated by either water or lipid soluble photosensitisers. Cellular studies have also shown carotenoids to be efficient quenchers of singlet oxygen, for example in isolated photosystem II reaction centres [66] and in protecting *ex vivo* lymphocytes from $^1\text{O}_2$ damage [67].

8.3.4 Peroxyl Radicals

Peroxyl radicals are formed in the oxidation of many organic and biological molecules and they can propagate chain reactions. They are usually formed *via* the reaction of oxygen with carbon-centered radicals. Lipid peroxyl radicals are produced during lipid peroxidation, which is a complex process but can be divided into stages [3]:

1. Initiation; production, and subsequent attack of a polyunsaturated fatty acid (PUFA) side chain by R^\bullet , RO_2^\bullet or $^1\text{O}_2$, producing a lipid radical (capable of reacting with oxygen).

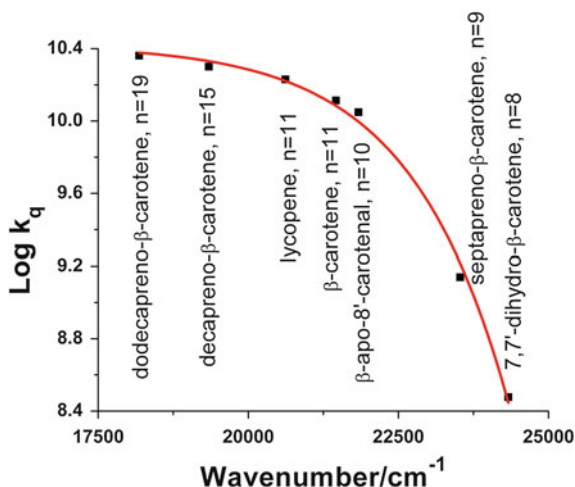


Fig. 8.2 Graph showing the relationship between the rate constant for $^1\text{O}_2$ quenching (k_q) and the wavenumber of the lowest energy ground state absorption maximum for a range of carotenoids in benzene, adapted from [64]

2. Propagation; the fatty acid peroxy radical (PUFAO_2^\bullet) abstracts a hydrogen atom from another PUFA molecule.



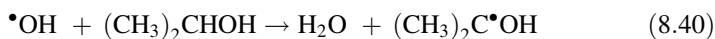
The resulting PUFA^\bullet can react with oxygen and a chain reaction is initiated so that lipid hydroperoxides accumulate until:-

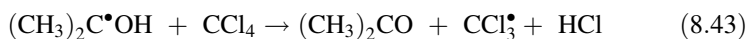
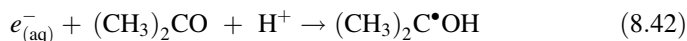
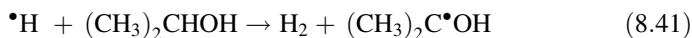
3. Termination; leads to non-radical products.

The accumulated lipid hydroperoxides can, however, react with metal complexes, generating even more alkoxy and peroxy radicals.

A wide range of peroxy radicals can be produced both photochemically and radiolitically, *via* reaction of oxygen with the corresponding alkyl radical, and their methods of production and reaction rates with a variety of compounds have been detailed by Neta *et al.* [68].

The peroxy radical that has been most extensively studied for its interactions with antioxidants is the trichloromethyl peroxy radical ($\text{CCl}_3\text{O}_2^\bullet$), which is produced during the metabolism of CCl_4 *via* reaction of the trichloromethyl radical (CCl_3^\bullet) with oxygen [69] and is known to cause hepatotoxicity and other types of tissue injury. Pulse radiolysis is normally used to generate this radical and in primarily aqueous solutions it is prepared in air saturated solutions by adding carbon tetrachloride, 2-propanol and acetone and is produced *via* the following reactions [70].



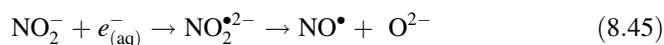


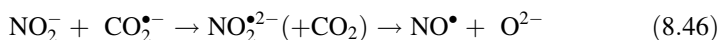
$\text{CCl}_3\text{O}_2\bullet$ reacts with ascorbic and uric acid [71], as well as bilirubin [72] and glutathione [73] *via* electron transfer. However, with tryptophan and carotenoids another reaction also occurs, suggested to be radical addition [74, 75]. For the carotenoids the proposed adduct decays to yield more radical cation and for the carotenoid, astaxanthin, the radical cation is not formed initially but is formed solely through the proposed addition radical [75]. The one electron reduction potential of astaxanthin radical cation has been shown to be higher than several other carotenoids [76], so it may be that it is very close to that of $\text{CCl}_3\text{O}_2\bullet$ so that electron transfer is very slow.

8.3.5 NO_x

Nitrogen monoxide, or nitric oxide ($\text{NO}\bullet$) as it is more usually called, is involved in many biological functions. It is formed in activated macrophages and neutrophils where it is produced from the amino acid L-arginine [77] and is involved in killing bacteria. It is also generated by a range of cells as an intercellular messenger and acts as a vasodilator [78]. When $\text{NO}\bullet$ is present in excess it is thought to be cytotoxic [79] and humans are exposed daily to this substance from cigarette smoke as well as exhaust fumes (the cytotoxicity may well be mediated by other species derived from $\text{NO}\bullet$). $\text{NO}\bullet$ reacts readily with oxygen forming nitrogen dioxide ($\text{NO}_2\bullet$), which is also a major air pollutant and has been shown to trigger lipid peroxidation [80]. $\text{NO}\bullet$ can also rapidly react with superoxide producing peroxyntirite (OONO^-) [81] and, since both radicals are generated in many cell types, there is a high likelihood of them being able to react. Peroxyntirite is stable at basic pH values, but is the salt of peroxyntirous acid, a weak acid with a $\text{p}K_a$ of 6.8 [81], hence if produced *in vivo* nearly half will protonate to peroxyntirous acid. Rapid rearrangement of the peroxyntirous acid to H^+ and nitrate (NO_3^-) then occurs, with competing decomposition generating $\text{NO}_2\bullet$ and $\bullet\text{OH}$ [82]. The nitrate radical ($\text{NO}_3\bullet$) can also be formed, *via* reaction of ozone with $\text{NO}_2\bullet$ and, as with all NO_x , it is an air pollutant (see Chap. 5) and is found in cigarette smoke [83].

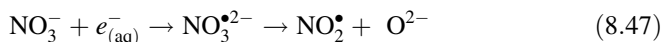
$\text{NO}\bullet$ is stable as a gas in oxygen free environments and it can be selectively generated using pulse radiolysis in argon-saturated aqueous solutions *via* reaction of nitrite with $e_{(\text{aq})}^-$, using formate to scavenge $\text{OH}\bullet$ forming $\text{CO}_2^{\bullet-}$ *via* reaction 9.11 and the following reactions [84]:





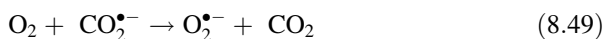
It can also be produced photolytically, for example from S-nitroso complexes [85] or nitrite [86].

NO_2^\bullet is also a stable gas and can be produced radiolytically using a mixture of nitrate and nitrite in argon saturated water in a $\sim 10:1$ ratio [87]. The nitrite reacts with the hydroxyl radical and the nitrate reacts preferentially with the aqueous electron:



Photochemically, NO_2^\bullet has been produced directly from nitrite or *via* the nitrite reaction with the triplet state of nitronaphthalene [86, 88].

$\text{ONOO}^-/\text{ONOOH}$ can be generated radiolytically either from reactions 8.47 and 8.48, above (using less nitrate so that the remaining $\bullet\text{OH}$ can react with NO_2^\bullet [87]) or in air saturated aqueous nitrite solutions containing formate. In this case reaction 8.45 will proceed as above but oxygen can compete for $\text{CO}_2^{\bullet-}$ and superoxide will be produced (reaction 8.49). This can then react with NO^\bullet generating peroxyxynitrite (reaction 8.50) [89].



$\text{ONOO}^-/\text{ONOOH}$ can also be generated by photolysis of nitrite/formate solutions. NO_2^- is converted to NO^\bullet and $\bullet\text{OH}$, then $\bullet\text{OH}$ reacts with formate (reaction 8.11) and reactions 8.49 and 8.50 proceed as above [90].

NO_3^\bullet can be produced by pulse radiolysis of concentrated nitrate or nitrous acid solutions [91], so that NO_3^\bullet is formed directly from the electron pulse, or *via* flash photolysis of ceric nitrate solutions [92]. Both of these methods present problems, as NO_2^\bullet will also be produced when using the pulse radiolysis method (*via* reaction 8.47) and the ceric ion from the laser method has a high reduction potential (1.28 V vs SHE [93]) and so is also a powerful oxidising agent itself.

NO^\bullet is not a highly reactive species and is relatively unreactive towards the antioxidants glutathione and ascorbate [85, 94]. Flavonoids were found to quench NO^\bullet but the rate constants determined were also quite low (up to $4 \times 10^2 \text{ mol dm}^{-3} \text{ s}^{-1}$) [95]. In fact, NO^\bullet has been shown to act as an antioxidant itself and can terminate the propagation process of lipid peroxidation [96]. Flavonoids have also been shown not to react efficiently with $\text{ONOO}^-/\text{ONOOH}$ [97], though ascorbate is oxidised (by one electron) by it [98]. It does react with carotenoids and tocopherols [99, 100], though not *via* one electron transfer, and β -carotene has been shown to protect lymphocytes from $\text{ONOO}^-/\text{ONOOH}$ induced damage [90].

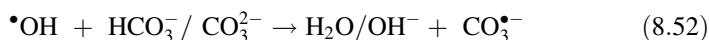
NO_2^\bullet and NO_3^\bullet are both more powerful oxidising species, each reacting with a range of antioxidants. NO_2^\bullet usually reacts by one-electron oxidation, as observed for β -carotene [101], though addition across double bonds is possible [102] and it has been shown that β -carotene in hexane is completely destroyed by 2 equimolar amounts of NO_2^\bullet , with the absorption spectra gradually decreasing and blue-shifting, possibly indicating a gradual decrease in conjugation [103]. Carotenoids are also able to protect lymphocytes from NO_2^\bullet induced damage [67, 88, 90]. NO_3^\bullet reactions are more complex and can occur *via* electron transfer, addition and hydrogen abstraction [91, 104, 105].

8.3.6 Carbonate Radical

The carbonate radical ($\text{CO}_3^{\bullet-}$) can be produced through the reaction of peroxynitrite with CO_2 (reaction 8.51) and this could occur *in vivo* [106]:



$\text{CO}_3^{\bullet-}$ is a highly oxidising radical with a reduction potential of 1.59 V *vs* SHE [107] and it can be produced radiolytically very easily, *via* the quenching of $^\bullet\text{OH}$ by carbonate in nitrous oxide saturated solutions [107]:



It can also be produced by the photoionisation of carbonate or of carbonate metal complexes [108]. It has an optical absorption maximum at 600 nm with an absorption coefficient of $1830 \text{ mol}^{-1} \text{ dm}^3 \text{ cm}^{-1}$ [108]. For a long time, it was assumed that this radical exists at neutral pH as the protonated form (HCO_3^\bullet), but it is now firmly established that above pH 0 the radical exists in the deprotonated state [109].

$\text{CO}_3^{\bullet-}$ reactions with antioxidants and biomolecules occur mainly *via* one electron transfer (for example the interaction with tea polyphenols [110]), and it has recently been shown to directly oxidise guanine bases [111] however, hydrogen abstraction and addition can also occur [112]. The rate constants for $\text{CO}_3^{\bullet-}$ reaction with amino acids were found to be lower for the aliphatic amino acids than for those containing sulfur, and aromatic amino acids and derivatives showed a range of reactivities, with the indole derivatives, such as tryptophan, reacting most efficiently [113]. Enzyme interactions with $\text{CO}_3^{\bullet-}$ were also monitored in this study and their reactivity reflected the reactivity of their constituent aromatic amino acids, with enzymes, such as lysozyme and trypsin (which contain tryptophan) having rate constants comparable to that of tryptophan itself and in ribnuclease A (which contains no tryptophan) the quenching was similar to that of tyrosine.

8.3.7 Sulfur-Containing Radicals

A wide range of sulfur radicals have been reported. Sulfur dioxide ($\text{SO}_2^{\bullet-}$), sulfite radical ($\text{SO}_3^{\bullet-}$), sulfate radical ($\text{SO}_4^{\bullet-}$) and peroxomonosulfate radical ($\text{SO}_5^{\bullet-}$) can all be formed from sulfur dioxide, which is an environmental air pollutant, as well as from sulfites and bisulfites used as preservatives [114–118] and methods of their production and their reactivity has been previously reviewed [119]. Briefly, $\text{SO}_2^{\bullet-}$ acts as a one electron reductant whereas the others are all oxidising species with $\text{SO}_4^{\bullet-}$ being the strongest one electron oxidant [117–119].

Many sulfur radical cations have also been reported and it has been suggested that they might be intermediates in biological redox processes. Their production and reaction has been the subject of an extensive review by Glass [120]. The most important biologically are sulfide ($\text{RS}^{\bullet+}$) and disulfide radical cations ($\text{RSSR}^{\bullet+}$) which are produced upon $\bullet\text{OH}$ radical reaction with biological sulfides, such as the amino acid methionine, and so can be easily generated *via* laser flash photolysis and pulse radiolysis [121, 122]. These radicals have been shown to be oxidising but the reaction mechanisms can be complex. For example, a disulfide radical cation can be converted to the corresponding radical anion ($\text{RSSR}^{\bullet-}$) by reaction with thiolate as has been observed for cysteamine oxidation by lipoate radical cations [123]. This is because the reaction proceeds with $\text{RSSR}^{\bullet+}$ oxidising thiolate by one electron transfer forming a neutral thiy radical (RS^{\bullet}) and this then equilibrates with excess thiolate to yield $\text{RSSR}^{\bullet-}$ (reactions 8.53 and 8.54), thus turning an oxidising species into a reducing one. $\text{RSSR}^{\bullet-}$ can also be generated *via* one electron reduction of disulfides [124].



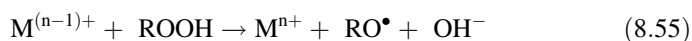
Neutral organosulfur (or thiy) radicals (RS^{\bullet}) can also be produced *in vivo* by hydrogen abstraction from, or oxidation of, biological thiols (either *via* antioxidant repair mechanisms or *via* peroxidase catalysed oxidation), such as glutathione, the drug penicillamine and proteins containing the amino acid cysteine. They can also be easily generated by radiolysis and photochemically, for example from $\bullet\text{OH}$ reaction with thiol, and the production, both *in vitro* and *in vivo*, and reactions of these radicals have been discussed in several reviews [124–126]. These neutral radicals react with oxygen to give thiol peroxy radicals (RSOO^{\bullet}), these can then react with another thiol to give a sulfinyl radical (RSO^{\bullet}) or photoisomerise to sulfonyl radicals (with both oxygens bonded to sulfur, RSO_2^{\bullet}), which can also add oxygen to give sulfonyl peroxy radicals ($\text{RSO}_2\text{OO}^{\bullet}$) [127].

Ascorbate and α -tocopherol can repair $\text{RSSR}^{\bullet+}$ and RS^{\bullet} by electron transfer, and RS^{\bullet} have been shown to abstract hydrogen from polyunsaturated fatty acids. [124, 126] RSO^{\bullet} have been found to be relatively stable while RSO_2^{\bullet} abstract hydrogen atoms, though at very slow rates, and $\text{RSO}_2\text{OO}^{\bullet}$ have been suggested to be much more reactive [127, 128], with sulfonyl peroxy radicals from cysteine

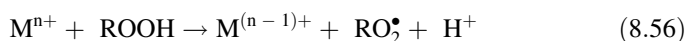
reacting rapidly with DNA and free bases by both hydrogen abstraction and addition. [129] Destruction of β -carotene has been observed by xanthine-oxidase initiated RS^\bullet , with both ascorbic acid and the water soluble tocopherol analogue, Trolox, preventing its destruction [125]. The β -carotene reaction probably occurs *via* addition as seen by Everett *et al.* for the reaction of glutathione thyl radicals. They also observed quenching of RSO_2^\bullet by β -carotene with both an electron transfer and an addition reaction occurring [101].

8.3.8 Alkoxy and Phenoxy Radicals

Alkoxy and phenoxy (RO^\bullet) radicals are generated *in vivo* from complexed transition metals (M) and organic hydroperoxides (e.g. lipid hydroperoxides) *via* catalysed electron transfer reactions:



The oxidised metal complex, M^{n+} , is then capable of breaking down peroxides, producing peroxy radicals (RO_2^\bullet):



Aliphatic alkoxy radicals have reduction potentials of about 1600 mV *vs* SHE at pH 7 making them better oxidising agents than alkyl peroxy radicals ($E^7 \sim 1000$ mV *vs* SHE) [130]. Phenoxy radicals usually have even lower reduction potentials, e.g. phenoxy radical ($C_6H_5O^\bullet$) with $E^7 \sim 900$ mV *vs* SHE and tocopheroxy radical with $E^7 \sim 500$ mV *vs* SHE [130], and these can also be produced *in vivo via* the oxidation of phenols, such as the amino acid tyrosine, flavenoids and other phenolic antioxidants (e.g. tocopherols), or *via* the reduction of quinones.

Radiolytically, RO^\bullet can be produced *via* the electron reaction with hydroperoxides or quinones [131, 132] or *via* the one electron oxidation of phenolic compounds [133]. RO^\bullet radicals can also be generated photolytically *via* photochemical reduction of quinones, photodecomposition of peroxides or *via* direct photolysis of phenols [134–136].

Alkoxy radicals react with a variety of antioxidants and biological compounds, such as *t*-butoxy radical reaction with a range of fatty acids, generating *t*-butanol and a fatty acid radical *via* hydrogen abstraction [135]. Introducing unsaturated bonds into the fatty acids was seen to increase the abstraction rate constant. These radicals have also been seen to react with the antioxidants quercetin, crocin and crocetin, ascorbate and Trolox, as well as with the DNA bases, thymidine and adenosine [131]. In the case of quercetin its phenoxy radical was observed, and this would be expected to occur for Trolox as well, though the authors used competition kinetics to monitor this reaction rather than direct monitoring of the product.

Phenoxy radicals of tyrosine in the enzyme lysozyme have been observed to react with α -tocopherol, ascorbate and urate, repairing the tyrosine amino acid

[137]. Again, this reaction with tocopherol produces another phenoxyl radical, the α -tocopheroxyl radical. However, antioxidant reactions with the α -tocopheroxyl radical have also been studied and it has been observed to be quenched by ubiquinol-10 [138], as well as by glutathione and ascorbate [139, 140] regenerating α -tocopherol. α -Tocopherol is an important antioxidant due to its position in the membrane, with the phytyl tail being anchored in the hydrophobic section and the chromane ring positioned near the membrane interface, thus, allowing reactions with free radicals in both the aqueous and lipid phases [14]. These repair reactions may be especially important *in vivo* as they can prevent α -tocopherol depletion. The repair by ascorbate is thought to occur *via* concerted electron and proton transfer and not by simple hydrogen atom transfer ($k = 3 \times 10^5 \text{ mol dm}^{-3} \text{ s}^{-1}$ in lipid bilayers) [140]. The resulting ascorbate radicals are fairly unreactive and can be reconverted to ascorbate (AscH^-) and dehydroascorbate (Asc) [50]. The dehydroascorbate can then regenerate ascorbate *via* a glutathione peroxidase catalysed reaction with glutathione (GSH) yielding non-reactive, non-radical products [14]:



8.4 Conclusions

A large range of free radicals and other reactive oxygen species (ROS) can be produced biologically and *in vivo* and a variety of antioxidant species quench these ROS. Pulse radiolysis and laser flash photolysis are useful techniques for producing these radicals and ROS and for studying their reaction mechanisms.

The quenching reactions often generate another radical species, usually an antioxidant radical or radical ion, (though addition radicals are also possible) and these can then go on to react with other biomolecules or radicals. For example, carotenoid radical cations have been shown to oxidise the amino acids tyrosine and cysteine, so have pro-oxidant ability [141].

Each step in the reaction cascade that occurs upon the quenching of a free radical should generate a more stable and less reactive species. However, the presence of certain gases and metals can affect this and produce products which are more reactive, such as oxygen addition to carbon-centered radicals or to RS^\bullet producing the more reactive peroxy radicals (or sulfonyl radicals) [68, 127]; nitric oxides reaction with superoxide to give peroxynitrite [81], and the reaction of peroxynitrite with carbon dioxide to yield nitrogen dioxide and carbonate radicals [106]. Thus, an antioxidant can become pro-oxidant under certain conditions unless another antioxidant is present in sufficient amounts to quench the initial species produced in a competing reaction before any pro-oxidant reaction can occur. Therefore, knowing the reaction rates and mechanisms of antioxidant/biomolecule interactions with radicals and reactive oxygen species can help to predict biological anti/pro-oxidant capacity.

References

1. Nohl H (1990) Is redox-cycling ubiquinone involved in mitochondrial oxygen activation? *Free Rad Res Comms* 8:307–315
2. Benzie IFF (1996) Lipid peroxidation: a review of causes, consequences, measurement and dietary influences. *Int J Food Sci Nutr* 47:233–261
3. Pryor WA (1994) Free radicals and lipid peroxidation: what they are and how they got that way. In: Frei B (ed) *Natural antioxidants in human health and disease*. Academic Press Inc, New York
4. Kehler JP, Smith CV (1994) Free radicals in biology: sources, reactivities, and roles in the etiology of human diseases. In: Frei B (ed) *Natural antioxidants in human health and disease*. Academic Press Inc, New York
5. Leake D (1995) The french paradox. *The Biochemist* 17:12–15
6. Marak GE, de Kozak Y, Faure JP (1990) Free radicals and antioxidants in the pathogenesis of eye diseases. In: Emerit I, Packer L, Auclair C (eds) *Antioxidants in therapy and preventative medicine*. Plenum Press, New York
7. Greenstock CL (1986) The role of free radicals in radiation chemical aging. *Proc React Kinet* 14:249–265
8. Fridovich I (1983) Superoxide radical: an endogeneous toxicant. *Ann Rev Pharmacol Toxicol* 23:239–257
9. Bhabak KP, Mugesh G (2010) Functional mimics of glutathione peroxidase: bioinspired synthetic antioxidants. *Acc Chem Res* 43:1408–1419
10. Kehler JP (2000) The Haber–Weiss reaction and mechanisms of toxicity. *Toxicol* 149:43–50
11. Jovanovic SV (1991) Antioxidant mechanisms: electron v's H-atom transfer. In: Davies KJA (ed) *Oxidative damage and repair*. Pergamon Press, Oxford
12. Simic MG (1991) Antioxidant compounds: an overview. In: Davies KJA (ed) *Oxidative damage and repair*. Pergamon Press, Oxford
13. Niki E (1991) Antioxidant compounds. In: Davies KJA (ed) *Oxidative damage and repair*. Pergamon Press, Oxford
14. Briviba K, Sies H (1994) Nonenzymatic antioxidant defense systems. In: Frei B (ed) *Natural antioxidants in human health and disease*. Academic Press Inc, New York
15. Krinsky NI (1988) Membrane antioxidants. *Ann New York Acad Sci* 551:17–33
16. Ingold KU, Webb AC, Witter D et al (1987) Vitamin E remains the major lipid-soluble chain-breaking antioxidant in human plasma even in individuals suffering severe vitamin E deficiency. *Arch Biochem Biophys* 259:224–225
17. Bensasson RV, Land EJ, Truscott TG (1983) Flash photolysis and pulse radiolysis. Contributions to the chemistry of biology and medicine. Pergamon Press, Oxford
18. Norrish RGW, Porter G (1949) Chemical reactions produced by very high light intensities. *Nature* 164:658
19. Dorfman LM (1963) Pulse radiolysis: fast reaction studies in radiation chemistry. *Science* 141:493–498
20. Keene JP (1964) Pulse radiolysis apparatus. *J Sci Instrum* 41:493–496
21. Von Sonntag C (1987) Chemical basis of radiation biology. Taylor & Francis Ltd, London
22. Schwartz HA (1981) Free radicals generated by radiolysis of aqueous solutions. *J Chem Educ* 58:101–105
23. Simic MG (1990) Pulse radiolysis in study of oxygen radicals. *Methods Enzymol* 186:89–107
24. Neta P, Schuler RH (1971) Rate constants for reaction of hydrogen atoms with compounds of biochemical interest. *Radiat Res* 47:612–627
25. Alam MS, Rao BSM, Janata E (2001) A pulse radiolysis study of H atom reactions with aliphatic alcohols : evaluation of kinetics by direct optical absorption measurement. *Phys Chem Chem Phys* 3:2622–2624

26. Czapski G, Peled E (1968) On the pH-dependence of G_{reducing} in the radiation chemistry of aqueous solutions. *Isr J Chem* 6:421–436
27. Janata E, Schuler RH (1982) Rate constant for scavenging of e_{aq}^- in N_2O saturated solutions. *J Phys Chem* 86:2078–2084
28. Holroyd RA (1968) The reaction of nitrous oxide with excited molecules in the radiolysis and photolysis of liquid alkanes. In: Gould RF (ed) *Radiation chemistry II. Advances in Chemistry Series*. American Chemical Society, Washington
29. Herrmann H, Majdik Z, Ervens B et al (2003) Halogen production from aqueous tropospheric particles. *Chemosphere* 52:485–502
30. Harbour JR, Chow V, Bolton JR (1974) An electron spin resonance study of the spin adducts of OH and HO_2 radicals with nitrones in the ultraviolet photolysis of aqueous hydrogen peroxide solutions. *Can J Chem* 52:3549–3553
31. Koppenol WH (1989) Generation and thermodynamic properties of oxyradicals. In: *CRC critical reviews in membrane lipid oxidation*, vol 1. CRC Press, Boca Raton
32. Bors W, Lengfelder E, Saran M (1976) Reactions of oxygen radical species with methional: a pulse radiolysis study. *Biochem Biophys Res Commun* 70:81–87
33. Bahnemann D, Asmus K-D, Willson RL (1981) Free radical reactions of the phenothiazine, metiazinic acid. *J Chem Soc Perkin Trans II*:890–895
34. Shinohara H, Imamura A, Masuda T et al (1979) Molecular-orbital study on the partial reactivity of hydrogen of various amino-acids in the abstraction reaction by hydroxyl radical. *Bull Chem Soc Japan* 52:1–7
35. Steenken S (1989) Purine bases, nucleosides and nucleotides: aqueous solution redox chemistry and transformation reactions of their radical cations and e^- and OH adducts. *Chem Rev* 89:503–520
36. Husain SR, Cillard P (1987) Hydroxyl radical scavenging activity of flavinoids. *Phytochemistry* 26:2489–2491
37. Neta P, Hoffman MZ, Simic M (1972) Electron spin resonance and pulse radiolysis studies of the reactions of OH and O^- radicals with aromatic and olefinic compounds. *J Phys Chem* 76:847–853
38. Özyürek M, Bektaşoğlu B, Güçlü K et al (2008) Hydroxyl radical scavenging assay of phenolics and flavonoids with a modified cupric reducing antioxidant capacity (CUPRAC) method using catalase for hydrogen peroxide degradation. *Anal Chim Acta* 616:196–206
39. Singh U, Barik A, Priyadarsini KI (2009) Reactions of hydroxyl radical with bergenin, a natural poly phenol studied by pulse radiolysis. *Bioorg Med Chem* 17:6008–6014
40. Sawyer DT, Nanni EJ, Roberts JL (1982) The reaction chemistry of superoxide ion in aprotic media. *Adv Chem Ser* 201:585–600
41. McCord JM, Fridovich I (1968) The reduction of cytochrome c by milk xanthine oxidase. *J Biol Chem* 243:5753–5760
42. Valentine JS, Curtis AB (1975) A convenient preparation of solutions of superoxide anion and the reaction of superoxide anion with a copper (II) complex. *J Am Chem Soc* 97:224–226
43. Markert M, Andrews PC, Babior BM (1984) Measurement of O_2^- production by human neutrophils. The preparation and assay of NADPH oxidase-containing particles from human neutrophils. *Methods Enzymol* 105:358–365
44. Nadezhdin A, Dunford HB (1979) Oxidation of nicotinamide adenine dinucleotide by hydroperoxyl radical, a flash photolysis study. *J Phys Chem* 83:1957–1961
45. Vaish SP, Tollin G (1971) Flash photolysis of flavins. V. Oxidation and disproportionation of flavin radicals. *J Bioenerg* 2:61–72
46. Bielski BHJ, Cabelli DE, Arudi RL et al (1985) Reactivity of HO_2/O_2^- radicals in aqueous solution. *J Phys Chem Ref Data* 14:1041–1100
47. Bielski BHJ, Allen AO (1977) Mechanism of the disproportionation of superoxide radicals. *J Phys Chem* 81:1048–1050

48. Maroz A, Anderson RF, Smith RAJ et al (2009) Reactivity of ubiquinone and ubiquinol with superoxide and the hydroperoxyl radical: Implications for in vivo antioxidant activity. *Free Radical Biol Med* 46:105–109
49. Mishra B, Priyadarsinia K, Bbhide MK et al (2004) Reactions of superoxide radicals with curcumin: probable mechanisms by optical spectroscopy and EPR. *Free Radical Res* 38:355–362
50. Cabelli DE, Bielski BHJ (1983) Kinetics and mechanism for the oxidation of ascorbic acid/ascorbate by HO₂/O₂⁻ radicals. A pulse radiolysis and stopped-flow photolysis study. *J Phys Chem* 87:1809–1812
51. Taubert D, Breitenbach T, Lazar A et al (2003) Reaction rate constants of superoxide scavenging by plant antioxidants. *Free Radical Biol Med* 35:1599–1607
52. Silva AMS, Filipe P, Seixas RSGR et al (2008) One-electron reduction of superoxide radical-anions by 3-alkylpolyhydroxyflavones in micelles. Effect of antioxidant alkyl chain length on micellar structure and reactivity. *J Phys Chem B* 112:11456–11461
53. Gorman AA, Rodgers MAJ (1981) Singlet molecular oxygen. *Chem Soc Rev* 10:205–231
54. Gorman AA, Hamblett I, Land EJ (1989) A pulse radiolysis based singlet oxygen luminescence facility. *J Am Chem Soc* 111:1876–1877
55. Land EJ (1991) Time-resolved luminescence-pulse radiolysis determination of the fractions of porphyrin photosensitizer triplets giving rise to singlet excited oxygen on quenching by ground state triplet oxygen. *J Photochem Photobiol A Chem* 61:165–170
56. Piette J (1991) Biological consequences associated with DNA oxidation mediated by singlet oxygen. *J Photochem Photobiol* 11:241–260
57. Girotti AW (1990) Photodynamic lipid peroxidation in biological systems. *Photochem Photobiol* 51:497–509
58. Badger RM, Wright AC, Whitlock RF (1965) Absolute intensities of the discrete and continuous absorption bands of oxygen gas at 1.26 and 1.065 μ and the radiative lifetime of the ¹ Δ_g state of oxygen. *J Chem Phys* 43:4345–4350
59. Neely WC, Martin JM, Barker SA (1988) Products and relative reaction rates of the oxidation of tocopherols with singlet molecular oxygen. *Photochem Photobiol* 48:423–428
60. Foote CS, Denny RW (1968) Chemistry of singlet oxygen. VII. Quenching by β -carotene. *J Am Chem Soc* 90:6233–6235
61. Farmilo A, Wilkinson F (1973) On the mechanism of quenching of singlet oxygen in solution. *Photochem Photobiol* 18:447–450
62. Liebler DC (1993) Antioxidant reactions of carotenoids. *Ann New York Acad Sci* 691:20–31
63. Oliveros E, Braun AM, Aminian-Saghafi T et al (1994) Quenching of singlet oxygen (¹ Δ_g) by carotenoid derivatives: Kinetic analysis by near infra-red luminescence. *New J Chem* 18:535–539
64. Edge R, McGarvey DJ, Truscott TG (1997) The carotenoids as antioxidants—a review. *J Photochem Photobiol B: Biol* 41:189–200
65. Cantrell A, McGarvey DJ, Truscott TG (2003) Singlet oxygen quenching by dietary carotenoids in a model membrane environment. *Arch Biochem Biophys* 412:47–54
66. Telfer A, Dhami S, Bishop SM et al (1994) β -Carotene quenches singlet oxygen formed in isolated photosystem II reaction centers. *Biochemistry* 33:14469–14474
67. Boehm F, Edge R, Burke M et al (2001) Dietary uptake of lycopene protects human cells from singlet oxygen and nitrogen dioxide—ROS components from cigarette smoke. *J Photochem Photobiol B: Biol* 64:176–178
68. Neta P, Huie RE, Ross AB (1990) Rate constants for reactions of peroxy radicals in fluid solutions. *J Phys Chem Ref Data* 19:413–513
69. Connor HD, Thurman RG, Galizi MD et al (1985) The formation of a novel free radical metabolite from CCl₄ in the perfused rat liver and in vivo. *J Biol Chem* 261:4542–4548
70. Packer JE, Willson RL, Bahnmann D et al (1980) Electron transfer reactions of halogenated aliphatic peroxy radicals: measurement of absolute rate constants by pulse radiolysis. *J Chem Soc Perkin Trans II*:296–299

71. Neta P, Huie RE, Maruthamuthu P et al (1989) Solvent effects in the reactions of peroxy radicals with organic reductants. Evidence for proton-transfer-mediated electron transfer. *J Phys Chem* 93:7654–7659
72. Mohan H, Gopinathan C (1990) Oxidation reactions of bilirubin by peroxy radicals in aqueous-solutions. *Radiat Phys Chem* 36:801–804
73. Cudina I, Jovanovic SV (1988) Free radical inactivation of trypsin. *Radiat Phys Chem* 32:497–501
74. Packer JE, Mahood JS, Willson RL et al (1981) Reactions of the trichloromethylperoxy free radical ($\text{Cl}_3\text{COO}^\bullet$) with tryptophan, tryptophanyl-tyrosine and lysozyme. *Int J Radiat Biol* 39:135–141
75. Hill TJ, Land EJ, McGarvey DJ et al (1995) Interactions between carotenoids and the CCl_3O_2 radical. *J Am Chem Soc* 117:8322–8326
76. Edge R, Land EJ, McGarvey DJ et al (1998) Relative one-electron reduction potentials of carotenoid radical cations and the interaction of carotenoids with the vitamin E radical cation. *J Am Chem Soc* 120:4087–4090
77. Monacada S, Palmer RMJ, Higgs EA (1989) Biosynthesis of nitric oxide from L-arginine. A pathway for the regulation of cell function and communication. *Biochem Pharmacol* 38:1709–1715
78. Palmer RMJ, Ferrige AG, Moncada S (1987) Nitric oxide release accounts for the biological activity of endothelium-derived relaxing factor. *Nature* 327:524–526
79. Arroyo PL, Hatch-Pigott V, Mower HF et al (1992) Mutagenicity of nitric oxide and its inhibition by antioxidants. *Mutat Res* 281:193–202
80. Pryor WA, Lightsey JW (1981) Mechanisms of nitrogen dioxide reactions: initiation of lipid peroxidation and the production of nitrous acid. *Science* 214:435–437
81. Koppenol WH, Moreno JJ, Pryor WA et al (1992) Peroxynitrite, a cloaked oxidant formed by nitric oxide and superoxide. *Chem Res Toxicol* 5:834–842
82. Richeson CE, Mulder P, Bowry VW et al (1998) The complex chemistry of peroxynitrite decomposition: new insights. *J Am Chem Soc* 120:7211–7219
83. Ingrosso G (2002) Free radical chemistry and its concern with indoor air quality: an open problem. *Mirochem J* 73:221–236
84. Buxton GV, Greenstock CL, Helman WP et al (1988) Critical review of rate constants of hydrated electrons, hydrogen atoms and hydroxyl radicals ($^\bullet\text{OH}/^\bullet\text{O}^-$) in aqueous solution. *J Phys Chem Ref Data* 17:513–886
85. Wood PD, Mutus B, Redmond RW (1996) The mechanism of photochemical release of nitric oxide from S-nitrosoglutathione. *Photochem Photobiol* 64:518–524
86. Treinin A, Hayon E (1970) Absorption spectra and reaction kinetics of NO_2 , N_2O_3 , and N_2O_4 in aqueous solution. *J Am Chem Soc* 92:5821–5828
87. Løgager T, Sehested K (1993) Formation and decay of peroxynitrous acid: a pulse radiolysis study. *J Phys Chem* 97:6664–6669
88. Boehm F, Tinkler JH, Truscott TG (1995) Carotenoids protect against cell membrane damage by the nitrogen dioxide radical. *Nature Med* 1:98–99
89. Goldstein S, Czapski G (1995) The reaction of NO^\bullet with O_2^- and HO_2^\bullet a pulse radiolysis study. *Free Rad Biol Med* 19:505–510
90. Boehm F, Edge R, McGarvey DJ et al (1998) β -Carotene with vitamins E and C offer synergistic cell protection against NOx. *FEBS Lett* 436:387–389
91. Neta P, Huie RE (1986) Rate constants for reactions of NO_3 radicals in aqueous solutions. *J Phys Chem* 90:4644–4648
92. Dogliotti L, Hayon E (1967) Transient species produced in the photochemical decomposition of ceric salts in aqueous solution. Reactivity of NO_3 and HSO_4 free radicals. *J Phys Chem* 71:3802–3808
93. Connelly NG, Geiger WE (1996) Chemical redox agents for organometallic chemistry. *Chem Rev* 96:877–910
94. Jackson TS, Xu A, Vita JA et al (1998) Ascorbate prevents the interaction of superoxide and nitric oxide only at very high physiological concentrations. *Circ Res* 83:916–922

95. van Acker SABE, Tromp MNJL, Heanen GRMM et al (1995) Flavonoids as scavengers of nitric oxide radical. *Biochem Biophys Res Commun* 214:755–759
96. Rubbo H, Radi R, Anselmi D (2000) Nitric oxide reaction with lipid peroxyl radicals spares α -tocopherol during lipid peroxidation. *J Biol Chem* 275:10812–10818
97. Tibi S, Koppenol WH (2000) Reactions of peroxynitrite with phenolic and carbonyl compounds: flavonoids are not scavengers of peroxynitrite. *Helv Chim Acta* 83:2412–2424
98. Bartlett D, Church DF, Bounds PL et al (1995) The kinetics of the oxidation of L-ascorbic acid by peroxynitrite. *Free Rad Biol Med* 18:85–92
99. Pannala AS, Rice-Evans C, Sampson J et al (1998) Interaction of peroxynitrite with carotenoids and tocopherols within low density lipoprotein. *FEBS Lett* 423:297–301
100. Hogg N, Joseph J, Kalyanaraman B (1994) The oxidation of α -tocopherol and trolox by peroxynitrite. *Arch Biochem Biophys* 314:153–158
101. Everett SA, Dennis MF, Patel KB et al (1996) Scavenging of nitrogen dioxide, thiol, and sulphonyl free radicals by the nutritional antioxidant β -carotene. *J Biol Chem* 271:3988–3994
102. Pryor WA, Lightsey JW (1981) Mechanisms of nitrogen dioxide reactions: initiation of lipid peroxidation and the production of nitrous acid. *Science* 214:435–437
103. Kikugawa K, Hiramoto K, Tomiyama S et al (1997) β -Carotene effectively scavenges toxic nitrogen oxides: nitrogen dioxide and peroxynitrous acid. *FEBS Lett* 404:175–178
104. Barzaghi P, Herrmann H (2004) Kinetics and mechanisms of reactions of the nitrate radical (NO_3^\bullet) with substituted phenols in aqueous solution. *Phys Chem Chem Phys* 6:5379–5388
105. Venkatachalapathy B, Ramamurthy P (1996) Reactions of nitrate radical with amino acids in acidic aqueous medium: a flash photolysis investigation. *J Photochem Photobiol A: Chem* 93:1–5
106. Meli R, Nauser T, Latal P (2002) Reaction of peroxynitrite with carbon dioxide: intermediates and determination of the yield of $\text{CO}_3^{\bullet-}$ and NO_2^\bullet . *J Biol Inorg Chem* 7:31–36
107. Huie RE, Clifton CL, Neta P (1991) Electron transfer reaction rates of the carbonate and sulfate radical anions. *Radiat Phys Chem* 38:477–481
108. Chen S, Cope VW, Hoffman MZ (1973) Behavior of $\text{CO}_3^{\bullet-}$ radicals generated in the flash photolysis of carbonatoamine complexes of cobalt (III) in aqueous solution. *J Phys Chem* 77:1111–1116
109. Bisby RH, Johnson SA, Parker AW et al (1998) Time-resolved resonance Raman spectroscopy of the carbonate radical. *J Chem Soc Faraday Trans* 94:2069–2072
110. Miao J-L, Wang W-F, Pan J-X (2001) The scavenging reactions of nitrogen dioxide radical and carbonate radical by tea polyphenol derivatives: a pulse radiolysis study. *Radiat Phys Chem* 60:163–168
111. Lee YA, Yun BH, Kim SK et al (2007) Mechanisms of oxidation of guanine in DNA by carbonate radical anion, a decomposition product of nitrosoperoxycarbonate. *Chem Eur J* 13:4571–4581
112. Clifton CL, Huie RE (1993) Rate constants for some hydrogen abstraction reactions of the carbonate radical. *Int J Chem Kinet* 25:199–203
113. Chen S-N, Hoffman MZ (1973) Rate constants for the reaction of the carbonate radical with compounds of biochemical interest in neutral aqueous solution. *Radiat Res* 56:40–47
114. Brandt C, van Eldik R (1995) Transition metal-catalyzed oxidation of sulfur (IV) oxides. Atmospheric-relevant processes and mechanisms. *Chem Rev* 95:119–190
115. Mottley C, Harman LS, Mason RP (1985) Microsomal reduction of bisulfite (aqueous sulfur dioxide)—sulfur dioxide anion free radical formation by cytochrome P-450. *Biochem Pharmacol* 34:3005–3008
116. Mottley C, Mason RP, Chignell CF (1982) The formation of sulfur trioxide radical anion during the prostaglandin hydroperoxidase-catalyzed oxidation of bisulfite (hydrated sulfur dioxide). *J Biol Chem* 257:5050–5055
117. Das TN, Huie RE, Neta P (1999) Reduction potentials of $\text{SO}_3^{\bullet-}$, $\text{SO}_5^{\bullet-}$, and $\text{S}_4\text{O}_6^{\bullet 3-}$ radicals in aqueous solution. *J Phys Chem A* 103:3581–3588

118. Neta P, Huie RE, Harriman A (1987) One-electron-transfer reactions of the couple $\text{SO}_2/\text{SO}_2^-$ in aqueous solutions. Pulse radiolytic and cyclic voltammetric studies. *J Phys Chem* 91:1606–1611
119. Neta P, Huie RE, Ross AB (1988) Rate constants for reactions of inorganic radicals in aqueous solution. *J Phys Chem Ref Data* 17:1027–1284
120. Glass RS (1999) Sulfur radical cations. *Top Curr Chem* 205:1–87
121. Bonifačić M, Hug GL, Schöneich C (2000) Kinetics of the reactions between sulfide radical cation complexes, $[\text{S} \cdot \cdot \cdot \text{S}]^+$ and $[\text{S} \cdot \cdot \cdot \text{N}]^+$, and superoxide or carbon dioxide radical anions. *J Phys Chem A* 104:1240–1245
122. Bobrowski K, Hug GL, Pogochi D et al (2007) Sulfur radical cation-peptide bond complex in the one-electron oxidation of S-methylglutathione. *J Am Chem Soc* 129:9236–9245
123. Bonifačić M, Asmus K-D (1984) Radical reactions in aqueous disulphide-thiol systems. *Int J Radiat Biol* 46:35–45
124. Asmus K-D (1990) Sulfur-centered free radicals. *Methods Enzymol* 186:167–180
125. Kundu SC, Willson RL (1995) Thiyl (sulfhydryl/thiol) free radical reactions, vitamins, β -carotene and superoxide dismutase in oxidative stress: design and interpretation of enzymatic studies. *Methods Enzymol* 251:69–81
126. Wardman P, von Sonntag C (1995) Kinetic factors that control the rate of thiyl radicals in cells. *Methods Enzymol* 251:31–45
127. Sevilla MD, Becker D, Yan M (1990) The formation and structure of the sulfoxyl radicals RSO^\bullet , RSOO^\bullet , RSO_2^\bullet , and $\text{RSO}_2\text{OO}^\bullet$ from the reaction of cysteine, glutathione and penicillamine thiyl radicals with molecular oxygen. *Int J Radiat Biol* 57:65–81
128. Horowitz A, Rajbenbach LA (1975) The free radical mechanism of the decomposition of alkylsulfonyl chlorides in liquid cyclohexane. *J Am Chem Soc* 97:10–13
129. Razskazovskii Y, Sevilla MD (1996) Reactions of sulphonyl peroxy radicals with DNA and its components: hydrogen abstraction from the sugar backbone versus addition to pyrimidine double bonds. *Int J Radiat Biol* 69:75–87
130. Buettner GR (1993) The pecking order of free radicals and antioxidants: lipid peroxidation, α -tocopherol, and ascorbate. *Arch Biochem Biophys* 300:535–543
131. Erben-Russ B, Michel C, Bors W et al (1987) Absolute rate constants of alkoxy radical reactions in aqueous solution. *J Phys Chem* 91:2362–2365
132. Land EJ, Mukherjee T, Swallow AJ et al (1983) Reduction of the naphthazarin molecule as studied by pulse radiolysis. *J Chem Soc Faraday Trans 1*(79):391–404
133. Bansal KM, Fessenden RW (1976) Pulse radiolysis studies of the oxidation of phenols by $\text{SO}_4^{\bullet -}$ and $\text{Br}_2^{\bullet -}$ in aqueous solutions. *Radiat Res* 67:1–8
134. El'tsov AV, Studzinskii OP, Grebenkina VM (1977) Photoinitiation of the reactions of quinones. *Russ Chem Rev* 46:93–114
135. Small RD Jr, Scaiano JC, Patterson LK (1979) Radical processes in lipids. A laser photolysis study of t-butoxy radical reactivity toward fatty acids. *Photochem Photobiol* 29:49–51
136. Allen NS, Parkinson A, Loffelman FF et al (1983) Flash Photolysis and antioxidant activity. *Polym Degrad Stab* 5:403–413
137. Hoey BM, Butler J (1984) The repair of oxidized amino acids by antioxidants. *Biochim Biophys Acta* 791:212–218
138. Mukai K, Kikuchi S, Urano S (1990) Stopped-flow kinetic study of the regeneration reaction of tocopheroxyl radical by reduced ubiquinone-10 in solution. *Biochim Biophys Acta* 1035:77–82
139. Bisby RH, Parker AW (1991) Reactions of the α -tocopheroxyl radical in micellar solutions studied by nanosecond laser flash photolysis. *FEBS Lett* 290:205–208
140. Bisby RH, Parker AW (1995) Reaction of ascorbate with the α -tocopheroxyl radical in micellar and bilayer membrane systems. *Arch Biochem Biophys* 317:170–178
141. Burke M, Edge R, Land EJ et al (2001) One-electron reduction potentials of dietary carotenoid radical cations in aqueous micellar environments. *FEBS Lett* 500:132–136

Chapter 9

Photomedicine

Marina K. Kuimova and David Phillips

Abstract This chapter discusses the various modalities of photomedicine, an interdisciplinary branch of medicine that involves the study and application of light with respect to health and disease. The following main concepts are covered: Photodynamic Therapy (PDT) for the treatment of cancer, PDT for bacterial infections, vascular PDT, photochemical internalisation, photochemical tissue bonding and the use of lasers in medicine.

9.1 Photomedicine: An Introduction

The notion that light can cure diseases goes back to ancient civilisations, when people worshipped the Sun and believed in the health-giving and protective properties of sunlight. It was not, however, until the late part of the nineteenth century, that the scientific discipline of ‘photomedicine’ was born. The official birth of photomedicine began with the discovery by the Danish physician Niels Finsen that artificial UV light from a carbon arc lamp could efficiently cure facial lesions (*lupus vulgaris*), which commonly develop on tuberculosis sufferers. Finsen consequently received the Nobel Prize in Physiology or Medicine in 1903 *‘in recognition of his contribution to the treatment of diseases, especially lupus vulgaris, with concentrated light radiation, whereby he has opened a new avenue*

M. K. Kuimova (✉) · D. Phillips
Chemistry Department, Imperial College London, Exhibition Road,
London SW7 2AZ, UK
e-mail: m.kuimova@imperial.ac.uk

D. Phillips
e-mail: d.phillips@imperial.ac.uk

for medical science' [1]. Attention to the beneficial properties of light continued after a chance discovery in 1900 by Oscar Raab, a medical student in Munich, Germany, that the combination of the drug *acridine red* and light killed microorganisms. Raab was able to establish [2] that the acridine drug alone or light alone were not able to cause any damage to *Infusoria* and thus a prototype for contemporary Photodynamic Therapy (PDT) treatment (*vide infra*) was first documented. Indeed, based on Raab's findings about photodynamic effects, his advisor Professor Tappeiner in collaboration with Jesionek performed the first PDT treatment of a patient with skin cancer, using eosin as the photosensitiser [2].

Today, photomedicine is an interdisciplinary branch of medicine that involves the study and application of light with respect to health and disease. Photomedicine is closely connected with medical practice in various fields including oncology, dermatology, ophthalmology, surgery, dentistry, optical diagnostics, cardiology and many others.

The following topics are of interest to practical photomedicine:

- (1) the effect of light upon skin;
- (2) the diagnostic uses of light, by luminescence;
- (3) the therapeutic uses of light.

Ultraviolet (UV) radiation is the part of the electromagnetic spectrum emitted by the sun which is of major importance to human health. The higher energy UV-C radiation (100–280 nm) is absorbed efficiently by atmospheric constituents (ozone, water vapour, oxygen and carbon dioxide), however most radiation in the UV-A range (315–400 nm) and about 10 % of UV-B rays (280–315 nm) reach the surface of the Earth. Small amounts of UV radiation are essential for human health, e.g. for the production of vitamin D (see below), yet overexposure may result in acute and chronic health effects, in particular on the human skin. The most harmful consequence of the overexposure to sunlight is skin cancer, both carcinomas and malignant melanoma. We will not dwell on this aspect of photomedicine here, as the various harmful effects of light upon skin along with currently available prevention strategies are discussed in [Chap. 4](#). Likewise, photodiagnosis is discussed in detail in [Chap. 10](#).

In the present Chapter we will mainly focus on the beneficial effects light can make on human health and on its many therapeutic applications. In order to follow a historical timeline, we will start by discussing the only beneficial effect of UV radiation from sunlight on human health: vitamin D synthesis.

9.2 Vitamin D Synthesis

Vitamin D is essential in the body's calcium metabolism and is formed in the skin from previtamin D, which is in turn synthesised from 7-dehydrocholesterol under exposure to UV light. The deficiency of vitamin D causes rickets, which manifests itself as deformities of the skeleton, enlargements of the head, bending of the spine

and legs, which become unable to sustain body weight. This collection of symptoms was very common in developed countries in the late nineteenth century, and up to 90 % children in cities suffered from this condition. Fortunately, in the early twentieth century the importance of UV light in avoiding rickets was recognised and by 1920 artificial UV light was used to cure rickets and it is now rare [3]. (The use of light in the industrial synthesis of vitamin D is discussed in [Chap. 2.](#))

9.3 Phototherapy of Hyperbilirubinemia

Another impressive example of the beneficial properties of UV/blue visible light is the phototherapy of jaundice. About 50 % of new born babies suffer from hyperbilirubinemia, which is caused by the inability of an infant to excrete the substance bilirubin as fast as it is being produced by the body. In an adult, bilirubin is bound by albumin in the blood stream, and is transported into the liver, where it is conjugated to glucuronic acid with the help of the enzyme uridine diphosphate glucuronyl transferase. The conjugate is then excreted into the bile. In a new born baby this process can be inefficient due to the delayed maturation of the enzyme. This leaves bilirubin to circulate in the blood stream and above a certain concentration it appears as a yellow pigmentation in the skin due to the deposition of a lipid soluble form. This pigmentation is known as *jaundice*. As bilirubin is toxic, in particular to the cells of the central nervous system, hyperbilirubinemia has to be treated promptly, to avoid irreversible brain damage in infants.

It turns out that the treatment of this condition is simple. Exposure of newly born infants to the UV light reduces jaundice and bilirubin levels in the blood. This was first reported by Cremer in *Lancet* in 1958 [4], and since this time the treatment has been used successfully to treat hyperbilirubinemia world wide.

The chemistry behind this UV light treatment of jaundice, long debated, was finally unravelled in 1979 by McDonagh *et al.* [5]. The team demonstrated that irradiation with UV light causes *cis-trans* isomerisation in bilirubin and thus renders the products of photoisomerisation water-soluble. This is all that is required to make bilirubin excretable.

9.4 PDT of Cancer

Perhaps the most widely applied technique in photomedicine, and the one responsible for most research effort, both fundamental and applied, is PDT. We will now discuss the principles, mechanism and application of PDT, as well as the techniques of photochemical tissue bonding, photochemical internalisation and PUVA therapy, which share photochemical principles with PDT. The reader can refer to the following recent reviews [6, 7] and monographs [8, 9] for more detailed information on the PDT mechanism and its applications.

PDT can be broadly defined as administration to a patient of a non-toxic drug called a photosensitiser, followed by the illumination of the lesion/diseased tissue with visible light. These actions lead to the generation of cytotoxic species resulting in cell death and destruction of the lesion. PDT is a minimally invasive procedure and has been successfully applied to the treatment of a range of cancerous diseases and, more recently, in ophthalmology to treat the wet form of AMD. In many cases the PDT treatment is a viable alternative to surgery and is characterised by an excellent cosmetic outcome with minimal scarring.

Photodynamic action relies on the fact that the photosensitising drug is non-toxic to cells and tissues in the dark, but upon activation with visible light of the appropriate wavelength in the presence of molecular oxygen, the photosensitiser generates reactive oxygen species (ROS). A schematic Jablonski diagram visualising all the processes leading to ROS production is shown in Fig. 9.1. Primarily, ROS comprise of the reactive singlet state of molecular oxygen, $O_2(^1\Delta_g)$, obtained through energy transfer from the triplet state of the photosensitiser to the ground state triplet oxygen, $O_2(^3\Sigma_g^-)$. This process is known as the Type II mechanism of PDT and is considered to be the major route of phototoxicity. Other photochemical products can originate from the triplet state of the photosensitiser through an electron transfer pathway (Type I mechanism of PDT). The Type I mechanism produces reactive species containing an unpaired electron, e.g. superoxide anion O_2^- and hydroxyl radical OH^\bullet . The generation and photochemical reactions of ROS are discussed in more detail in Chap. 8.

Both singlet oxygen, $O_2(^1\Delta_g)$, and radical intermediates are characterised by short lifetimes, are unstable and can react efficiently with cellular components such as proteins, lipids and DNA, thus causing irreversible damage to the affected cells. This damage leads to cell death through apoptosis or necrosis and results in eradication of unwanted tissues, e.g. cancerous lesions or unwanted vasculature (in tumour treatments or in AMD).

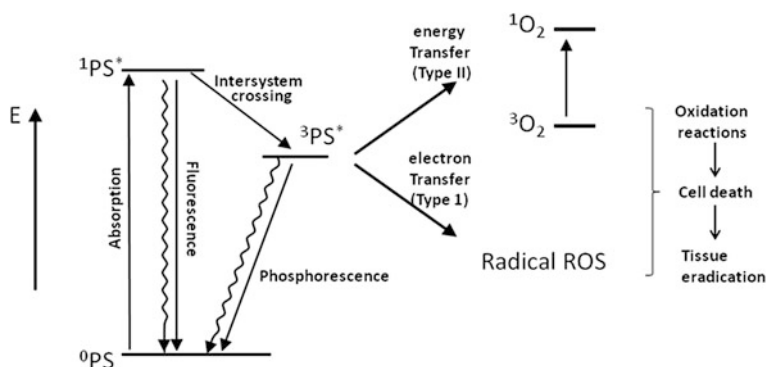


Fig. 9.1 Simplified Jablonski diagram visualising the processes leading to production of reactive oxygen species (ROS) following photosensitisation

The key components of PDT are the photosensitiser, light and molecular oxygen. Oxygen is the most likely acceptor of either energy or electrons, generating either singlet oxygen $O_2(^1\Delta_g)$ or oxygen-containing radicals. Therefore a high concentration and constant supply of oxygen in tissues under treatment is essential for efficient PDT. The immediate consequence of this requirement is that large hypoxic tumours are not suitable for PDT treatment. Another immediate implication is that the light dosimetry, as well as the fluency of light in PDT protocols need to be considered carefully to allow proper tissue re-oxygenation to achieve maximum clinical outcome.

The PDT photosensitiser has to possess a number of key properties, which include absorption in the red region of the spectrum (600–800 nm), allowing photoactivation within deeper tissues, the ability to generate efficiently singlet oxygen, selective uptake by malignant cells and minimal dark toxicity. We will consider each of these properties in turn.

Deep light penetration into tissue is extremely important, in order to achieve treatment of thicker segments of tissue as well as deeper lying lesions. The depth of light penetration is dependent upon the optical properties of the tissue and the wavelength of the light used. Water in biological tissues starts to absorb at wavelengths longer than 900 nm, whereas at wavelengths less than 650 nm absorption by endogenous chromophores such as haemoglobin and scattering by macromolecules becomes dominant. Thus, an ideal PDT photosensitiser should be activated at wavelengths where the absorbance of biological tissues is minimal, that is in the range from 700–950 nm, the so-called ‘tissue therapeutic window’ (Fig. 9.2).

The first clinical photosensitiser, called Photofrin[®] (Fig. 9.3), was approved in 1990. While it is still used in a number of PDT applications, it has a number of

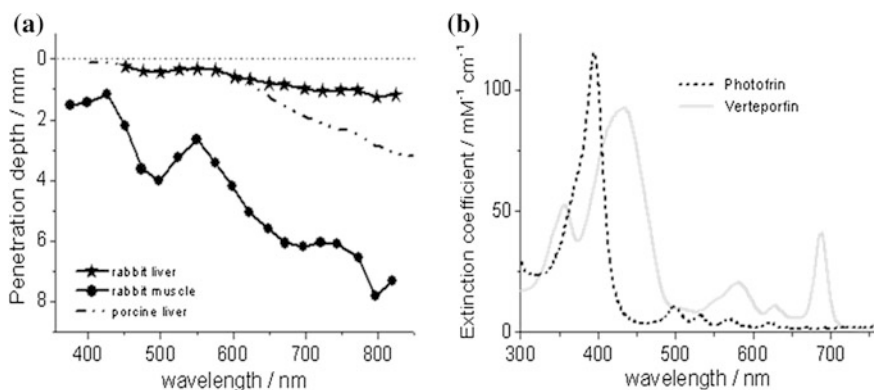


Fig. 9.2 **a** The depth of light penetration into tissue as a function of irradiation wavelength, data taken from [10, 11]. The range from 700–950 nm is called ‘tissue therapeutic window’ due to the minimal absorbance of biological tissues in this range. **b** The absorption spectra of the first generation photosensitiser Photofrin[®] as compared to the second generation photosensitiser Verteporfin

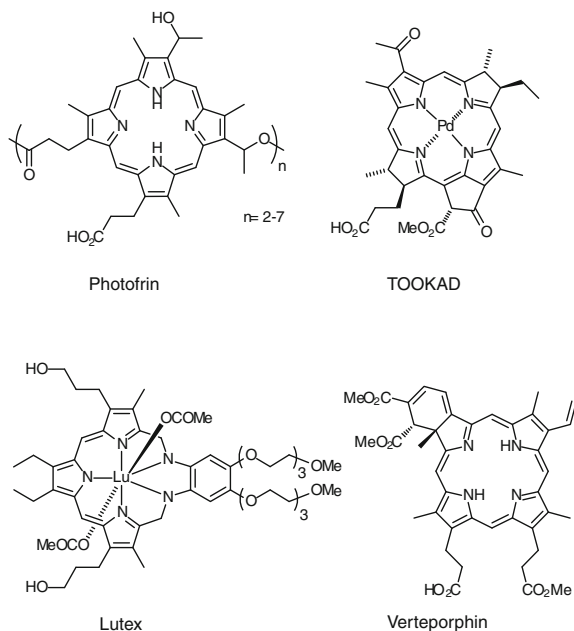


Fig. 9.3 The structures of clinical PDT photosensitizers Photofrin[®], TOOKAD[®], Lutex[®] and Visudyne[®]

limitations including poor absorption in the red (the lowest energy absorption maximum is at 630 nm, Fig. 9.2b, and this transition has a very low molar absorption coefficient). In recent years efforts have concentrated on so-called second generation photosensitizers with substantially improved properties over Photofrin[®]. The majority of these second generation photosensitizers are based on modified tetrapyrrolic macrocycles (porphyrinoids) with excellent absorption profiles at longer wavelengths. These include both naturally derived and synthetic chlorins/bacteriochlorins, benzoporphyrin derivatives and (na)phthalocyanines. Figure 9.2b shows the absorption spectrum of Photofrin[®] compared to that of the second generation photosensitizer Visudyne[®]. The benefit of using the latter drug to achieve both efficient tissue penetration and the efficient absorption of light by the drug are obvious, especially considering the low molar absorption coefficient of Photofrin[®] ($\epsilon = 3200 \text{ mol}^{-1} \text{ dm}^3 \text{ cm}^{-1}$ at 630 nm *vs* $\epsilon = 4 \times 10^4 \text{ mol}^{-1} \text{ dm}^3 \text{ cm}^{-1}$ for Visudyne[®] at 690 nm).

Several promising photosensitizers with activation wavelengths in the far-red or near infrared regions are currently in clinical trials. The structures of several clinical PDT photosensitizers are shown in Fig. 9.3. TOOKAD[®], a palladium bacteriochlorophyll derivative with excitation at 763 nm is currently in phase II clinical trials for the treatment of prostate cancer (*via* vascular targeted PDT, *vide infra*). Lutetium texaphyrin (motexafin lutetium, Lutex[®]) which combines the advantages of water solubility, selective localisation, and the ability to be activated

by deeply penetrating far-red light ($\lambda_{\text{ex}} = 732 \text{ nm}$) is currently in phase I/II clinical trials, while the chlorin derivative verteporfin (Visudyne[®]) is clinically approved for the treatment of AMD.

Singlet oxygen is considered to be the main cytotoxic intermediate in PDT, although contributions from the Type I electron transfer mechanism, generating oxygen radicals cannot be excluded. The ultimate proof for the involvement of either species in PDT *in vivo* would be the direct detection of these intermediates in the treated area, however due to their short lifetimes and high reactivity, such detection is a daunting task. It is a common practice to assess the potency of PDT photosensitisers by measuring their quantum yield of singlet oxygen production, ϕ_{Δ} . It has to be noted, however, that the photosensitisers' efficiency *in vitro* and *in vivo* does not always correlate with the simple trend derived from the photo-physical properties, and *in vivo* properties depend crucially on the intracellular localisation of the drug.

The singlet oxygen quantum yields of clinical photosensitisers in solution vary from 0.1 to 1.0 and are strongly solvent dependent [12]. The latter phenomenon is often due to aggregation or self-association of hydrophobic photosensitisers, in particular in aqueous environment, and can cause complications in designing PDT photosensitisers. Association is governed by the hydrophobic/hydrophilic balance and is promoted for amphiphilic molecules with asymmetrically located polar or charged groups. In general, the fluorescence and most frequently the singlet oxygen quantum yields of aggregated species are much lower than those of monomers, thus reducing their PDT efficiency. Most crucially, the formation of such aggregates might also have an effect on subcellular localisation and pharmacokinetics of the photosensitiser. Since aggregation can be affected by binding to serum proteins or lipids, the photosensitiser behaviour is even more convoluted and sometimes poorly understood *in vitro* and *in vivo*.

An important advantage of PDT as a treatment modality is its dual selectivity towards lesions *vs* normal tissues, which is achieved through (i) preferential uptake of the photosensitiser by diseased cells and (ii) the selective application of light. We will now discuss both of these localisation strategies in turn.

Preferential uptake of the photosensitiser by diseased tissue is desirable in PDT and, if achieved, can overcome the main problem of this treatment modality, *i.e.* the enhanced skin photosensitivity in patients long after the treatment is complete. Photosensitivity occurs as a result of the low concentration of the photosensitising drug present in the skin of a patient, which causes painful effects upon exposure to sunlight. As a result, many patients have to remain in the dark until the photosensitiser has completely cleared from their body, which can take up to 1 month in the case of Photofrin[®]. Preferential or exclusive uptake of the PDT drug to diseased tissue will leave the patient free to be exposed to sunlight after the treatment, as no photosensitiser will be found in the skin. In principle, specific uptake can be achieved in several ways. Most commonly, tumourous tissues have poorer lymphatic drainage than healthy tissues and this leads to a somewhat higher concentration of the drug at the target lesion site (typically 4:1 tumour *vs* the healthy tissue). To improve on this rather low (passive) selectivity, more potent targeting

strategies are being currently developed, including attachment of photosensitisers to ligands showing high specificity for the tissues of interest [13, 14]. The possible ligands include monoclonal antibodies and antibody fragments, as well as cell penetrating peptides, which specifically recognise cancer markers. By displaying remarkably high specificity to a certain receptor, which is either over expressed in the tumour or is only present in specific tumour types, these photosensitiser/ligand constructs ensure targeted delivery of the light sensitive drug. These photosensitisers, which have favourable photophysical properties, but are also suitable for conjugation to biomolecules are known as third generation PDT photosensitisers.

On the subject of skin photosensitivity it is fitting to mention porphyria, which belongs to a group of inherited or acquired disorders of certain enzymes in the heme biosynthetic pathway. The main problem with porphyria is the accumulation of porphyrins, which are the heme precursors in the body. While porphyrins are non-toxic at biologically relevant concentrations, they become toxic to tissue at high concentration. Deficiency in the enzymes of the porphyrin biosynthetic pathway leads to insufficient production of heme, which plays a central role in cellular metabolism, and accumulation of porphyrins. The high concentration of porphyrins manifests itself by either neurological complications or by skin problems. The presence of porphyrins in the skin in porphyria patients is therefore akin to skin photosensitivity in PDT.

There is one case, however, where accumulation of a porphyrin from precursors can be used for therapeutic purposes, namely aminolevulinic acid (ALA) PDT [15, 16]. ALA is an endogenous precursor of protoporphyrin IX, which is converted into heme by the cellular machinery. When exogenous ALA is provided to the cell through topical application, protoporphyrin IX accumulates in high amounts and can be used successfully as a photosensitiser in PDT treatment. ALA PDT is particularly successful in treating of skin tumours and actinic keratoses.

The second mechanism for achieving selectivity in PDT lies in the fact that the photosensitiser is harmless to cells in the absence of light and thus cell death can be localised exclusively at the irradiated site, where the ROS are produced. Since ROS have a very short lifetime their diffusion, and therefore the spatial domain of activity, is restricted. For example, the lifetime of the most important ROS, singlet oxygen, in an aqueous environment is 3.5 μs [17], which is expected to shorten further in a cellular environment due to its reactions with intracellular targets. Other potent ROS of radical nature display even shorter lifetimes. This means that the diffusion distance of ROS is on the order of 100 nm or less (compared with the typical cell size of 10–100 μm) and thus the primary damage through photodynamic action only occurs at the intracellular level. An important consequence of such short diffusion distances of ROS is that the subcellular localisation (i.e. targeting vulnerable organelles within cells) as well as the selective accumulation of photosensitisers in diseased cells are important factors in determining PDT efficacy. Photosensitiser/ligand constructs, discussed above, can play an important role in targeting PDT action to a vulnerable intracellular domain, as well as to the tissue/organ of interest.

The other important development, based on the fact that the ROS diffusion distance is limited to hundreds of nanometres, utilises the fact that the irradiated volume in PDT can be as small as $1 \mu\text{m}^3$, when femtosecond pulsed lasers are used as an excitation source. Precise localisation of excitation light should, in principle, allow the treatment of tissues without any damage to surrounding structures, which is crucial in the treatment of sensitive tissues such as those found in the eye and the brain of the patient. See Sect. 9.11 for more details of this emerging treatment modality: two-photon excited PDT (TPE PDT).

9.5 Vascular Targeted PDT and PDT of AMD

The vasculature of the tumour is an important target for PDT [18]. As tumours grow, they typically develop an extended vascular network, which enables efficient nutrient delivery to the tumour and the trafficking of metabolic waste away from the tumour. Disruptions of this network can serve as a very efficient way to ‘starve’ the tumour and stop its proliferation, *i.e.* instead of directly killing the malignant cells, PDT might be used efficiently to indirectly induce tumour death by damage to tumour stroma. An additional benefit stems from the PDT-induced inflammation activated by the damage to the vasculature, which is capable of activating the body’s immune system, important in maintaining long-term tumour control.

This vascular targeting strategy has so far shown very promising results. The vascular targeting of the photosensitiser can be achieved by active or passive means, the former using the ligands and vectors over-expressed by the tumour, as discussed above. The ligands to endothelial cell markers (VEGF receptors, tumour endothelial markers) are commonly used for active vascular targeting. Passive delivery uses the fact that following an intravenous injection, the concentration of the photosensitiser in the blood plasma remains high for some time, typically < 60 min. Selective irradiation of affected tissue shortly after the drug injection will thus result in destruction of blood vessels carrying the drug and the desired tumour vascular shutdown. Several drugs are currently in stage I or II clinical trials for vascular PDT, primarily **TOOKAD[®]**, shown in Fig. 9.3.

Perhaps the most important application of vascular PDT is the treatment of the wet form of Age-related Macular Degeneration (wet AMD) [19, 20], the disease characterised by overproliferation of the blood vessels in the macula, behind the retina. This abnormal growth of blood vessels causes bleeding and scarring, and leads to loss of central vision in patients. Wet AMD is currently the most common source of blindness in the Caucasian population over 60. The photosensitiser verteporfin (trade name **Visudyne[®]**), Fig. 9.3, is clinically approved for the treatment of wet AMD, and several other sensitizers (e.g. lutetium texaphyrin known as **Lutex[®]**) are currently in clinical trials.

It has been recognised that in many cases central and peripheral blood vessels of the tumour respond differently to vascular PDT, with peripheral vessels being

less susceptible to the treatment. This trait might have dangerous consequences and cause tumour recurrence. As often is the case with the treatment of tumours, a promising solution might be combination therapy, e.g. combining vascular PDT with antiangiogenic therapy (e.g. medication-driven approach limiting the growth of the new blood vessels), to target survival and repair pathways for endothelial cells in the vasculature. Such strategies employing PDT in combination with VEGF antibodies or with COX inhibitors have shown very promising therapeutic results.

9.6 Bacterial PDT

A variety of infective diseases can be treated using PDT [21, 22]. The use of PDT effectively overcomes a major problem associated with antibiotics, *i.e.* the development of resistance of microorganisms to many classes of antibiotics.

Photodynamic inactivation of microbial cells can be achieved upon irradiation of a suitable photosensitiser with visible light and effectively circumvents the mechanisms for resistance. The photosensitiser is typically administered topically, e.g. by spray formulation, and is expected to interact closely with the bacterial wall, to enable the most potent killing action through destruction of the bacterial membrane. As such, most photosensitisers designed for bacterial PDT are positively charged (targeting gram-positive bacteria) or contain targeting moieties such as poly-charged peptides.

Light irradiation of the photosensitiser produces either radical intermediates (through the Type I process) or singlet molecular oxygen (through the Type II process). In the case of the Type I process, the most common species formed is the superoxide radical $O_2^{\bullet-}$, which can be further converted to OH^{\bullet} through the Fenton reaction (Chap. 6). Similarly to the case of PDT of cancer, it is generally accepted that singlet oxygen sensitisation is the most important mechanism of bacterial inactivation; however there is some evidence to the contrary. For example, it has been demonstrated that the Type I mechanism is predominant in bacterial PDT using sulphonated aluminium phthalocyanines as photosensitisers [23].

Since no resistance can be developed by bacteria to either singlet oxygen, or reactive radicals, photodynamic inactivation of microbial cells may provide an alternative where antibiotics are no longer working. This may be vital for patients undergoing cancer therapy, or HIV patients who demonstrate resistance to antibiotics. A very successful case for bacterial PDT has been made in dentistry for treatment of oral infections, in particular in the elderly, showing persistent oral infections. PDT treatments are being developed for a variety of infections, including tuberculosis and leishmaniasis.

9.7 Photochemical Internalisation

The utilisation of macromolecules in the therapy of cancer and other diseases is becoming increasingly important. In many cases the targets of such macromolecular therapeutics are intracellular, however many of these drugs can only enter the cell through the endocytotic pathway. In this case, degradation of macromolecules in endocytotic vesicles after uptake by endocytosis is a major problem for therapeutic application. Photochemical internalisation is an emerging technique for efficient light-directed delivery of endocytosed macromolecules and/or drugs into the cytosol, based on light-assisted rupture of the vesicles containing the drug, once inside the cell [24, 25].

Photochemical internalisation uses the fact that following the activation by light of photosensitisers, located in endocytotic vesicles, ROS assist in breaking of the vesicular membranes and thus the therapeutic macromolecules can be released from the endocytic vesicles. They are then free to reach their target of action before being degraded in lysosomes. Photochemical internalisation has been shown to stimulate intracellular delivery of a large variety of macromolecules and other drugs that do not readily penetrate the plasma membrane. Examples include DNA delivered as gene-encoding plasmids or by means of viruses, peptide nucleic acids and chemotherapeutic agents such as bleomycin and doxorubicin. The efficacy and specificity of photochemical internalisation can be further improved by combining the macromolecules with targeting moieties, such as the epidermal growth factor.

9.8 Photochemical Wound Healing

Photochemical tissue bonding (PTB) is a light-activated method for tissue repair, where photodynamic action of the drug applied to tissue surfaces, particularly on the surfaces of the wounds, induces covalent crosslinking of proteins across the surfaces [26, 27]. The thus formed *nanosutures*, a result of a photochemical process, probably mediated by singlet oxygen, create an immediate water-tight seal. PTB has distinct advantages over conventional sutures, staples and glues and is suitable for wide variety of surgical applications, including sealing corneal and skin incisions and reconnecting peripheral nerves, blood vessels and tendons. A pilot clinical study at the Wellman Center for Photomedicine (Massachusetts General Hospital) has compared the novel photochemical wound healing technique and traditional sutures for closure of skin wounds and has shown the process to be safe and to cause less scarring than sutured closure. The representative image, Fig. 9.4, shows closure of a skin wound that was made to remove a skin cancer, either using common interrupted sutures on one half of the wound (on the right) or photochemical tissue bonding (on the left). The redness on the right half is

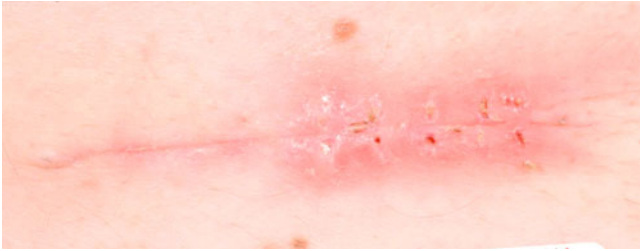


Fig. 9.4 The closure of a skin wound (an elliptical excision) that was made to remove a skin cancer. The closure of this type of wound includes two steps. First the sides of the wound were brought together with deep sutures. Then superficial sealing was done by using interrupted sutures on one half (*right*) and photochemical tissue bonding using Rose Bengal as a photosensitiser (532 nm irradiation) on the other half (*left*). The image shows the appearance of the wound 2 weeks after surgery just after the sutures were removed. The image courtesy of Prof. Irene E. Kochevar, the Wellman Center for Photomedicine (Massachusetts General Hospital)

caused by reaction to the sutures. The left half shows only a thin line where the wound sides were sealed with photochemical tissue bonding.

9.9 PUVA Therapy

PUVA is a treatment for eczema, psoriasis and vitiligo, which uses psoralen (furocoumarin molecule) as a photosensitiser, excited with UVA irradiation. The mechanism of PUVA action is similar to that of PDT, with photodynamic action utilising either a Type I or Type II mechanism. Psoralens are typically found in plants. They were known as early as ancient Egypt, but were only synthesised in a pure form in the 1970s. For PUVA therapy, psoralen can be taken orally or can be applied directly to the skin. PUVA therapy is highly effective at clearing skin problems such as psoriasis.

9.10 Use of Lasers in Surgery

The discussion of photomedicine would not be complete without several words on light sources. In PDT the selection of a light source is of utmost importance and is normally satisfied by using a laser. The ideal light source will deliver the correct wavelength showing good overlap with the absorption spectrum of the photosensitiser and sufficient power of visible light, resulting in reasonable treatment times. However there are several noteworthy applications of lasers in photomedicine which do not require the use of a photosensitiser. This section lists some of these applications.

Kidney stone removal using laser lithotripsy was invented in the 1980s and has revolutionised the treatment. Laser pulses delivered through a fibre optic were used to pulverise the stones and thus effectively remove them from the urinary tract. Laser lithotripsy allows kidney stone removal avoiding surgery.

Selective photothermolysis is the modality of skin treatment with lasers through lesion destruction by photo-thermal mechanisms. The unwanted structure or tissue is targeted using a specific laser wavelength of light, with the intention of absorbing light into the target area alone. The energy directed into the target area produces sufficient heat to damage the target while allowing the surrounding area to remain relatively untouched.

Safe removal of vascular and pigmented birthmarks can be achieved by selective photothermolysis. Selective absorption of high-power laser pulses causes selective removal of the abnormal vessels or pigment cells, without damaging other structures and without scarring. These treatments are now widely used in dermatology. Likewise, permanent laser hair removal and tattoo removal also uses the principles of selective photothermolysis.

Selective laser trabeculoplasty, a non-destructive laser treatment, has been developed on the basis of laser thermolysis, to treat glaucoma. Glaucoma is a common eye disease causing progressive, irreversible loss of vision, which is often associated with increased pressure of the fluid in the eye. Selective laser trabeculoplasty uses a 50 μm laser spot, aimed at the trabecular meshwork in the eye, to stimulate the opening of the mesh to allow more outflow of aqueous fluid. While a cure for glaucoma is not available, selective laser trabeculoplasty offers a good maintenance treatment and can be repeated as required several times without the damage to the eye.

9.11 New and Developing Treatment Modalities: Two Photon Activation

We have discussed earlier in this chapter how the efficiency of PDT can be improved by targeting photosensitisers to a specific cellular target. Precise localisation of the drug has the potential to improve on the treatment efficacy by delivering more molecules to the place where they will be most effective and to reduce the damage to healthy tissues. In this section we will discuss the emerging strategies for targeting in PDT and laser ablation based on a different irradiation regime.

9.11.1 Two-Photon PDT

The increasing availability of short-pulsed lasers is stimulating much research activity into novel ways of utilising the non-linear optical properties of materials.

Of particular interest for us here is the utilisation of multiphoton processes requiring high energy pulses. Such multiphoton processes have caused much excitement in the last decade and offered novel solutions for biological and medical applications, in particular, multiphoton imaging and two-photon excited PDT (TPE PDT) [28, 29].

As discussed in earlier chapters, the absorption of a single photon of appropriate wavelength excites the molecule from the ground state (S_0) to the first excited singlet state (S_1), from which it can undergo a series of photochemical processes. In PDT these photochemical reactions ultimately result in production of ROS and in ensuing cell death. In simultaneous two photon excitation (TPE), near-infrared light of twice the wavelength required for the S_0 – S_1 transition can be used to produce the excited state of the photosensitiser. The sensitiser is then deactivated in the normal way by either luminescence (which may be utilised in imaging applications) or by photophysical or photochemical processes to produce cytotoxic species, which eradicate cells and tissue (as utilised in PDT).

A clear benefit of TPE PDT over conventional one photon PDT is that it provides the means to excite chromophores in the near-infrared spectral region (700–900 nm), enabling deeper penetration of useful light, due to minimised tissue absorption and scattering in the *tissue optical window* (Fig. 9.2a). However the major advantage of TPE PDT stems from the fact that biphotonic absorption depends on the square of the light intensity, so it is confined to the focal volume of the laser where the intensity is the highest. The latter factor yields considerably better spatial resolution for TPE imaging, compared to monophotonic confocal imaging, due to reduced out-of-focus blur. Likewise, TPE PDT has potential advantages in the treatment of sensitive tissues such as found in the wet form of age related macular degeneration (wet AMD) in the eye by reducing out-of-focus damage to adjacent healthy tissue.

Naturally, for TPE PDT and imaging applications to be successful, photosensitisers must be created which combine both desirable biological and photophysical properties with high two-photon absorption cross-sections to enable the efficient use of biphotonic excitation. In recent years several classes of efficient TPE PDT sensitisers have been reported [30–33]. For example, it has been demonstrated that TPE PDT using a conjugated porphyrin dimer and 900 nm pulsed excitation from a Ti–Sapphire laser (150 fs) can efficiently occlude a single blood vessel in an animal model, avoiding any damage to surrounding blood vessels in a 3D sample [33].

9.11.2 Nanosurgery

Similarly to TPE PDT, intense laser light can be used in two-photon laser ablation of tissues, termed *nanosurgery*. The major benefit of using femtosecond laser pulses for nanosurgery is high peak intensities that reduce the energy threshold for tissue removal (ablation) and enable laser ablation to proceed with a low-energy

source. With this method, single axons inside the nematode *Caenorhabditis elegans* (*C. elegans*) were cut successfully by using near-infrared laser pulses with relatively low pulse energies of 10–40 nJ at the specimen (200 fs pulses) [34].

In nanosurgery no specific photosensitiser is added to achieve the nanoscale tissue removal. The minimal energy used is consistent with measured optical breakdown thresholds in transparent materials. At these low energies, mechanical effects due to plasma expansion and shock waves are also significantly reduced with respect to other laser ablation techniques using nanosecond pulsed lasers, that require much higher energies. Thus nanosurgery using femtosecond pulsed lasers utilises multiphoton processes to evaporate very small volumes ($1 \mu\text{m}^3$) of a tissue with no heat accumulation and thermal damage to the environment. This for example enables the surgeon to cut axons at the nano-scale resolution with minimal damage to the micro-environment and no damage to neighbouring axons [35].

9.12 Conclusions

In this Chapter we aimed to demonstrate that photomedicine is a vibrant and actively developing branch of medicine that involves the study and practical applications of light-initiated processes, with respect to health and disease. While the early medical treatments involving light have been in use since the late nineteenth century, the new concepts and modalities continue to emerge today. With a significant amount of research conducted in theoretical and practical aspects of light-induced medicine and adjoining fields today, from basic chemistry of photosensitisation and biochemistry of cell death to optimisation of PDT procedures in clinical trials, we believe that the future of photomedicine is bright.

Acknowledgments The current work of MKK in the areas of biological imaging and photomedicine is supported by the UK's Engineering and Physical Sciences Research Council (EPSRC) in the form of the Career Acceleration Fellowship (EP/E038980/1) and this support is gratefully acknowledged.

References

1. The Nobel Prize in Physiology or Medicine 1903. http://nobelprize.org/nobel_prizes/medicine/laureates/1903/index.html
2. Raab C (1900) Ber die wirkung fluoreszierender stoffe auf infu-soria. *Z Biol* 39:524–546
3. Tappeiner H, Jesionek H (1903) Therapeutische versuche mit fluo-reszierenden stoffen. *Munch Med Wschr* 50:2042–2044
4. Rajakumar K (2003) Vitamin D, cod-liver oil, sunlight, and rickets: a historical perspective. *Pediatrics* 112:e132–e135
5. Cremer RJ, Perryman PW, Richards DH (1958) Influence of light on the hyperbilirubinaemia of infants. *Lancet* 1:1094

6. McDonagh AF, Lightner DA, Woolridge A (1979) Geometric isomerization of bilirubin-IX and its dimethyl ester. *J Chem Soc Chem Commun* 3:110
7. Dolmans DEJGJ, Fukumura D, Jain RK (2003) Photodynamic therapy for cancer. *Nat Rev Cancer* 3:380–387
8. Wilson BC, Patterson MS (2008) The physics, biophysics, and technology of photodynamic therapy. *Phys Med Biol* 53:R61–R109
9. *Advances in photodynamic therapy: basic, translational and clinical* (2008) Hamblin MR, Mróz P (eds), Artech House, London
10. Photodynamic therapy methods and protocols; series: methods in molecular biology (2010) In: Gomer CJ (ed), vol. 635. A product of Humana press, p 294
11. Wilson BC, Jeeves WP, Lowe DM, Adam G (1984) Light propagation in animal tissues in the wavelength range 375–825 nanometers. *Progr Clin Biol Res* 170:115–132
12. Ritz J-P, Roggan A, Isbert C, Müller G, Buhr HJ, Germer CT (2001) Optical properties of native and coagulated porcine liver tissue between 400 and 2400 nm. *Lasers Surg Med* 29:205–212
13. Wilkinson F, Helman WP, Ross AB (1995) Quantum yields for the photosensitized formation of the lowest electronically excited singlet state of molecular oxygen in solution. *J Phys Chem Ref Data* 24:663
14. Hudson H, Boyle RW (2004) Strategies for selective delivery of photodynamic sensitizers to biological targets. *J Porphyrins Phthalocyanines* 8:954–975
15. Sharmon WM, van Lier JE, Allen CM (2004) Targeted photodynamic therapy via receptor mediated delivery systems. *Adv Drug Deliv Rev* 56:53–76
16. Hongcharu W, Taylor CR, Chang Y et al (2000) Topical ALA-photodynamic therapy for the treatment of acne vulgaris. *J Investigative Dermatol* 115:183–192
17. Peng Q, Warloe T, Berg K et al (1997) 5-Aminolevulinic acid-based photodynamic therapy—clinical research and future challenges. *Cancer* 79:2282–2308
18. Egorov SY, Kamalov VF, Koroteev NI et al (1989) The lifetime of singlet oxygen. *Chem Phys Lett* 163:421–424
19. Chen B, Pogue BW, Hoopes PJ, Hasan T (2006) Vascular and cellular targeting for photodynamic therapy. *Critical Rev Eukariotic Gene Express* 16:279–305
20. Arnold J, Kilmartin D, Olson J et al (2001) Verteporfin therapy of subfoveal choroidal neovascularization in age-related macular degeneration: Two-year results of a randomized clinical trial including lesions with occult with no classic choroidal neovascularization—verteporfin in photodynamic therapy report 2. *Am J Ophthalmol* 131:541–560
21. Arnold J, Kilmartin D, Olson J et al (2001) Photodynamic therapy of subfoveal choroidal neovascularization in pathologic myopia with verteporfin—1-year results of a randomized clinical trial—VIP report no. 1. *Ophthalmology* 108:841–852
22. Hamblin MR, Hasan T (2004) Photodynamic therapy: a new antimicrobial approach to infectious disease? *Photochem Photobiol Sci* 3:436–450
23. Jori G, Fabris C, Soncin M et al (2006) Photodynamic therapy in the treatment of microbial infections: Basic principles and perspective applications. *Lasers Surg Med* 38:468–481
24. Phillips D (1997) Chemical mechanisms in photodynamic therapy with phthalocyanines. *Prog React Kinetics* 22:175–300
25. Berg K, Selbo PK, Prasmickaite L et al (1999) Photochemical internalization: A novel technology for delivery of macromolecules into cytosol. *Cancer Res* 59:1180–1183
26. Hogset A, Prasmickaite L, Selbo PK et al (2004) Photochemical internalisation in drug and gene delivery. *Adv Drug Delivery Rev* 56:95–115
27. Kamegaya Y, Farinelli WA, Echague AVV et al (2005) Evaluation of photochemical tissue bonding for closure of skin incisions and excisions. *Lasers Surg Med* 37:264–270
28. Tsao S, Yao M, Henry FP et al (2010) A phase I/II trial of photoactivated tissue bonding (“nanosuturing”) for excisional wound closure. *J Investig Dermatol* 130:S42–S42
29. Bhawalkar JD, Kumar ND, Zhao CF, Prasad PN (1997) Two-photon photodynamic therapy. *J Clin Laser Med Surg* 15:201

30. Fisher WG, Partridge WP, Dees C, Wachter EA (1997) Simultaneous two-photon activation of type-I photodynamic therapy agents. *Photochem Photobiol* 66:141–155
31. Dy JT, Ogawa K, Satake A, Ishizumi A, Kobuke Y (2007) Water-soluble self-assembled butadiyne-bridged bisporphyrin: a potential two-photon-absorbing photosensitizer for photodynamic therapy. *Chem Eur J* 13:3491–3500
32. Balaz M, Collins HA, Dahlstedt E, Anderson HL (2009) Synthesis of hydrophilic conjugated porphyrin dimers for one-photon and two-photon photodynamic therapy at NIR wavelengths. *Org Biomol Chem* 7:874–888
33. Arnbjerg J, Jimenez-Banzo A, Paterson MJ et al (2007) Two-photon absorption in tetraphenylporphycenes: are porphycenes better candidates than porphyrins for providing optimal optical properties for two-photon photodynamic therapy? *J Am Chem Soc* 129:5188–5199
34. Collins HA, Khurana M, Moriyama EH et al (2008) Blood-vessel closure using photosensitizers engineered for two-photon excitation. *Nat Photonics* 7:420–424
35. Yanik MF, Cinar H, Cinar HN et al (2004) Functional regeneration after laser axotomy. *Nature* 432:882

Chapter 10

Photochemistry in Medical Diagnostics

Huw D. Summers

Abstract Photochemicals play a leading role in the diagnosis of disease, being widely used in assays of whole cells, of protein levels and in genetic analysis. This chapter looks at a number of selected examples of photochemical diagnostics, aiming to give an overview of the principles of their use through case studies of the techniques most commonly employed within the clinical setting. These cover blood based diagnostics, fluorescence assays using immunochemistry and the photochemical analysis of DNA. The chapter concludes with a look to the future and consideration of the role of novel nanocrystal photochemicals in the burgeoning field of Nanomedicine.

10.1 Introduction

The application of photochemicals to diagnose disease dates back to the nineteenth century and the pioneering work of Sir George Stokes on the fluorescent properties of quinine [1]; interestingly the first practical spectrofluorometer was developed in the 1950s to monitor quinine in its role as an anti-malarial drug [2]. As the science of fluorescence spectroscopy was developed in the early twentieth century by people such as Alexander Jabłoński, Theodor Förster and Gregorio Weber its medical application correspondingly increased. Today fluorescence assays are widely used throughout medicine to diagnose disease, to track the response to treatment programs and to monitor the general health of patients. This

H. D. Summers (✉)
Centre for Nanohealth, Swansea University, Singleton Park,
Swansea SA2 8PP, UK
e-mail: h.d.summers@swansea.ac.uk

pervasiveness of photochemistry in the clinical arena is due to the unrivalled sensitivity, accuracy and portability of optical sensors; characteristics that have stemmed from the constant technological advances in the chemical compounds and the light sources and detectors used in the detection of their fluorescence. In many cases the performance of photo-techniques has meant that they have replaced prior, well-established approaches e.g. in the switch from radiochemical to photochemical assays.

The requirements for photochemical sensors in medicine is the same as in other biological applications; in addition to the general requirement for high optical efficiency and wide dynamic range the photo-active compound must be stable in the biological environment, or behave in a predictable manner, and most importantly be capable of targeting to the tissue or cell of interest. An exhaustive review of medical photochemistry is beyond the scope of this chapter which rather concentrates on a selection of case studies to provide an introduction by way of examples. These reflect widely used techniques to be found in daily use in many hospitals and give a glimpse of photochemistry being used to diagnose disease in blood, tissue, cells and in chromosomes.

10.2 Blood Diagnostics

The analysis of patient blood is one of the most widely used diagnostics of health through direct sample measurement. The monitoring of pH and the gas pressure of O_2 and CO_2 is routinely used to assess patients during the course of a treatment regime or following surgery [3, 4]. Blood pH indicates whether the patient is acidotic or alkalemic, O_2 and CO_2 levels provide a measure of respiratory capacity, whilst CO_2 also reports on general metabolic processes. Standard procedure involves taking a sample of arterial blood from the patient and then sending this to a central laboratory for analysis. This is inevitably time-consuming and does not match the clinical time frame in which the levels of these blood markers changes over minutes; there is therefore a pressing need for rapid and robust quantitative measures that can be performed at the bedside or operating theatre [5]. The wide range of assays possible using photo-chemicals and the high sensitivity of optical measurements make photonic approaches highly appropriate to these demands.

10.2.1 *pH and CO_2 Measurements*

One of the most widely used photo-chemicals for pH measurement is fluorescein [6], which displays complex optical properties dependent upon its ionic form (See Chap. 4, compound 4.3). In particular only the two anionic forms present at high pH are fluorescent. Fluorescein can be used a wavelength ratiometric probe

through its pH dependent absorption in the blue-green part of the spectrum (absorption measurements at 450 and 495 nm are frequently used). One limitation here is the relatively weak absorption and emission using 450 nm excitation and so alternatives such as hydroxypyrene trisulfonate (HPTS) (see Fig. 12.1), which displays strong pH dependent absorption and emission due to ionisation of hydroxyl groups, have been developed [7].

CO₂ is indirectly measured by sensing of the pH of a bicarbonate buffer solution in equilibrium with the blood CO₂, where the Henderson–Hasselbalch relationship (see Eq. 12.9) allows calculation of CO₂ from the pH value [8]. Optical sensing methods for pH and CO₂ are discussed in more detail in Chap. 12.

10.2.2 O₂ Sensing

Collisional quenching of fluorescent probes by oxygen molecules is commonly employed to measure oxygen concentration. This leads to decreases in fluorescence intensity and lifetime (see Chap. 12). To gain high sensitivity and hence detection of low O₂ concentrations (and low cost sensors) long lifetime probes are required; metal ligand complexes (MLCs) such as ruthenium(II) tris(1,10-phenanthroline) with microsecond lifetimes are therefore commonly used [9, 10]. Many MLCs exhibit absorption maxima between 400–500 nm wavelengths and so can be excited with inexpensive blue LEDs; the microsecond dynamics of their fluorescence decay also makes it relatively straight forward and inexpensive to measure decay lifetime using silicon photodetectors, either directly in the time-domain or *via* phase-based measurement using frequency dependent excitation (see Chap. 14).

10.3 Immunoassays

Immunoassays are based on the body's evolved system of antibodies for molecular recognition. The mammalian immune system can evolve a virtually unlimited number of antibodies to different antigen molecules; for photochemistry this provides a readymade targeting technology, through which fluorescent probes can be selectively attached to diseased cells or specific sub-cellular compartments within cells. Immunofluorescence assays are therefore widely used in medical diagnostics.

10.3.1 *Antibodies and Antigens*

Antibodies are molecules, produced by the immune system, of very specific form. They are produced by B cells in response to antigens (antigen \equiv **antibody generator**). Each antibody has a unique recognition element (antigen binding site) that structurally matches its partner antigen, *i.e.* there is a three-dimensional shape match between antibody and antigen akin to that between a lock and key [11, 12]. It is this highly selective identification and binding mechanism that makes antibodies ideal for diagnostic assays [13]. Extremely dilute molecules that are known biomarkers of disease can be located and selected from the myriad background of similar molecules through the use of their bespoke antibody. The antibodies are generated by one of two methods:

1. Introduction of the target antigen into an animal system and subsequent harvesting from the blood serum, in this case *polyclonal antibodies* are generated—a number of different antibodies will be produced that recognise different binding sites of the antigen.
2. Production of *monoclonal antibodies* from a single B-cell using cell culture techniques—a single antibody type is produced with a single antigen binding format [14]. This avoids the multi-specificity that arises from the use of polyclonal antibodies.

Identification of recognition events is done through detection of emissions from radiochemicals or photochemicals tagged to the antibody–antigen pair.

10.3.2 *Development of Immunofluorescence*

The first steps in the development of fluorescent antibody staining were made by Coon *et al.* at the Harvard medical school in the early 1940s [15]. They initially used anthracence isothiocyanate as a labelling fluorophore, however the pronounced spectral overlap of the anthracence emission ($\lambda_{\max} \sim 400$ nm) with tissue autofluorescence led them to an alternative—fluorescein-isocyanate (FTIC), which has an emission maximum at 520 nm. Coon was able to demonstrate that when attached to *Pneumococcus* antibodies the fluorescein did not prevent antibody binding, that bright fluorescence could be seen in organ tissue sections from mice infected with the bacterium and that the antibody labeling could differentiate between different strains of the *Pneumococcus*. Immunofluorescent staining or imaging of this sort is now routinely used in the detection and identification of infectious diseases.

The use of immunolabelling as a quantitative assaying protocol dates back to the late 1950s and the work of Yalow and Berson on the detection of blood hormones [16]. Using radiochemical markers they developed a simple and effective assay based on the competitive binding of antibodies. Radioactive insulin was

attached to insulin antibodies; these were then mixed with blood samples containing native insulin. As the blood borne insulin binds to antibodies it replaces the radioactive species and this is monitored as a time dependent decay in total radioactivity from the sample. This *Yalow–Berson method* is one of a range of *radioimmunoassay* techniques that are extremely sensitive and can detect antigen concentrations in the picomolar range. The idea that small molecules such as insulin could stimulate antibody production was extremely controversial at the time, Yalow and Berson's original paper was rejected from the journal *Science* and only accepted into the *Journal of Clinical Investigation* after the authors agreed to substitute the words '*insulin antibody*' for '*insulin-binding antibody*' in the title [17]. It is interesting to note that in 1977 Yalow was awarded the Nobel prize in Medicine '*for the development of radioimmunoassays of peptide hormones*'.

Today the approach first outlined by Yalow and Berson has developed to incorporate enzyme-activation of photochemicals allowing easier detection *via* optical fluorescence [18–23]. Enzyme-linked immunosorbent assays (ELISA) or enzyme immunoassays (EIA) use antibody binding to antigens and enzymes on a substrate to create a surface on which target recognition followed by washing produces bound enzymes. Addition of a suitable enzyme substrate produces a fluorescent signal that is proportional to the amount of antibody–antigen binding. Thus the antibodies recognise the molecule of interest and the enzymes amplify the read-out signal through multiple binding of enzymes onto each antibody–antigen pair. One of the most commonly employed enzyme-substrate pairs used in ELISA is horseradish peroxidase and diaminobenzidine; oxidation of this benzidine derivative in the presence of hydrogen peroxide converts it to a fluorescent form [24].

10.3.3 Immunofluorescence Assay Types

Immunofluorescent assays can be implemented in a number of different ways and are categorised by their structure of the protocol used. The main classifications are depicted in Fig. 10.1.

In *direct* or *primary* assays the fluorescently labelled antigen binds directly to the target antibody, providing one photochemical reporter per antibody. In the *competitive* or *substitution* form of this assay both labelled and unlabelled antigens compete to bind to the antibodies; this is the basis of the Yalow–Berson method, where antigen concentration is measured by its displacement of fluorescent reporter antigens. In *indirect* or *secondary* immunoassays two antibodies are used; the primary antibody binds to the antigen to be detected, and a secondary, fluorescently labelled antibody is then used to bind to a different molecular motif of the antigen. This indirect technique brings two main advantages: (i) multiple fluorophores can be attached to the secondary antibody to provide signal amplification and (ii) many different primary antibodies can be developed whilst maintaining the same fluorescently labelled secondary antibody. This minimises the requirement for development of potentially expensive fluorescently labelled antibodies.

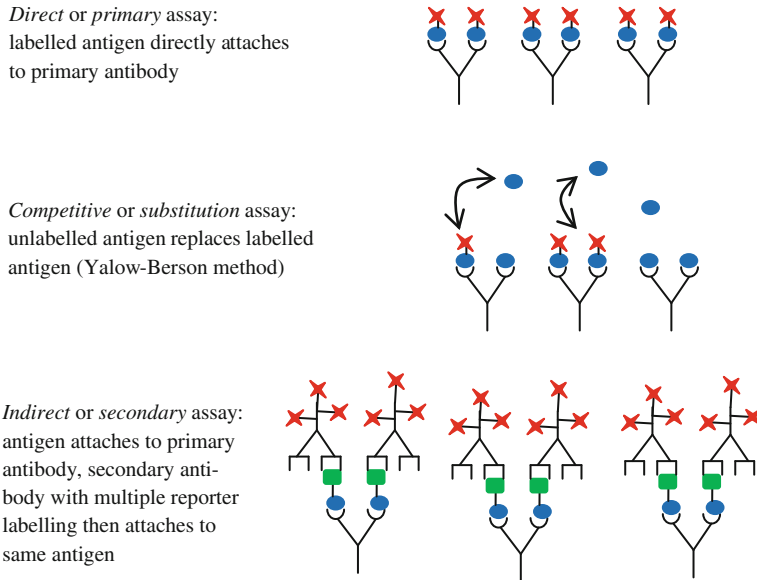


Fig. 10.1 Immunofluorescent assay types

10.4 Gene Level Diagnostics

The use of stains to enhance image contrast in biological tissues and cells has been common since the earliest days of microscopy when Antoni van Leeuwenhoek (1632–1723) used saffron to dye muscle fibres. The first applications sought to identify structures which are otherwise invisible as the bulk of cellular material is transparent in the optical regime. The use of stains in medical diagnosis began in the nineteenth century with Carl Weigert's work on the identification of blood disorders through dye absorption, Paul Ehrlich's discovery of trypan red which kills the protozoa responsible for sleeping sickness and the work of Hans Gram whose bacterial staining techniques led to the classification of gram positive and gram negative cells. Technological development has been a constant theme ever since the first synthetic dye—mauveine, an aminobenzene with an intense purple colour, was discovered by William Perkin in 1856. One strand of this development has been the unravelling of the cell's structure through the use of photochemical compounds with first whole cells, then sub-cellular organelles, and finally chromosomes and individual genes being identified. In modern medicine diagnosis is now commonly implemented at the genetic level through the staining of DNA sequences within whole cells using fluorophores. This method attaches fluorophores to specific target sequences of DNA within chromosomes allowing identification of numerical and structural abnormalities, monitoring of the effects of therapy, recognition of tumour cells and a host of pre-birth diagnoses from foetal DNA, e.g. Down's syndrome.

10.4.1 Karyotyping

The complete set of human chromosomes in their condensed form, just prior to cell division, is called the human karyotype. This can be visualised using staining procedures developed over the past 30 years that use selective binding of fluorescent dyes to DNA that is rich in either adenine–thymine (A–T) or cytosine–guanine (C–G) nucleotide pairs [25, 26]. The presence of the dye produces distinctive banding of the chromosomes which can be visualised under a microscope. A–T areas are known as G-bands as they stain with Giemsa stain and G–C bonding areas are correspondingly known as R-bands because they form the reverse of the G-band pattern (see Fig. 10.2). Examination of these chromosome banding patterns provides a ready measure of chromosome number and fidelity and can be used in diagnosis of diseases such as cancer, where polyploidy cells are common (cells containing multiple chromosome copies), or genetic disorders where, the banding patterns are altered due to DNA miscoding.

10.4.2 Fluorescence *In Situ* Hybridisation (FISH)

Whilst karyotyping provides a means to genetic disease diagnosis it is non-specific and subjective, relying on expert assessment by someone ‘trained in the art’. To obtain greater precision and reliability *in situ* DNA hybridisation techniques have been developed that bind specific, fluorescently-labelled RNA sequences (ribo-probes) to matching base sequences on chromosomes within cells [27–30]. A wide variety of probes, matching specific sequences of DNA, are available, having been developed as part of the Human Genome Project. Individual DNA sequences have

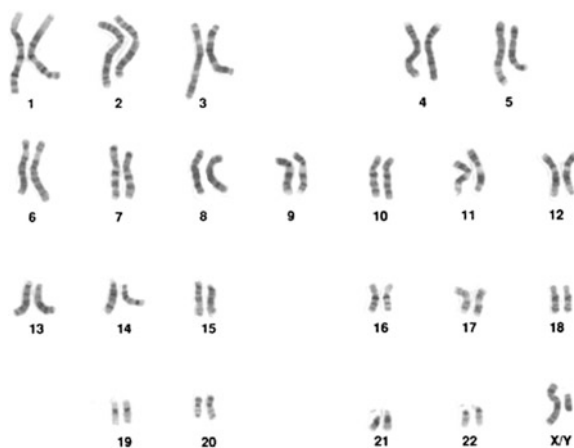


Fig. 10.2 Karyotype of a human male (reproduced with permission from the National Human Genome Research Institute: <http://www.genome.gov/>)

been added into the genetic material of continually replicating bacteria populations. Each population maintains a single bacterial artificial chromosome (BAC) that can be grown, extracted, and fluorescently labelled. These fragments are on the order of 100 thousand base-pairs and are the basis for most FISH probes. Thus disease specific DNA sequences can be identified or whole chromosome counting done [31–40]. The procedure is shown schematically in Fig. 10.3; cellular DNA is denatured by heating and then hybridised with the fluorescent, probe RNA sequences. Imaging *via* fluorescent microscopy then allows identification of disease positive samples.

10.4.3 Development of Fluorescent Probes for DNA

The earliest detection probes were labelled with radioisotopes making them expensive, difficult to work with and of limited lifetime. Fluorescent nucleotide labels were developed in the 1970s [29] and have since expanded in sensitivity and range to the point where multi-colour FISH can reveal all 24 human chromosomes simultaneously [41–45] and even track the dynamics of DNA expression within living cells [46–48]. A variety of fluorophores have been used for DNA labelling typically with an individual fluorophore, selectively attached to each base, A, G, C and T. The first generation used consisted of fluorescein, nitrobenzoxadiazole (NBD), tetramethylrhodamine and Texas Red [49], all of which can be excited with a single laser line at 488 nm. They are attached to DNA using an aliphatic amino group. Whilst this group can be excited by a single source and have differing emission maxima, in practice dual excitation at 488 nm and 514 nm is necessary to ensure relatively equal emission intensities as absorption at 488 nm is weak for Texas Red and tetramethylrhodamine. Considerable overlap in the emission spectra also brings difficulties in unambiguous identification. Improved

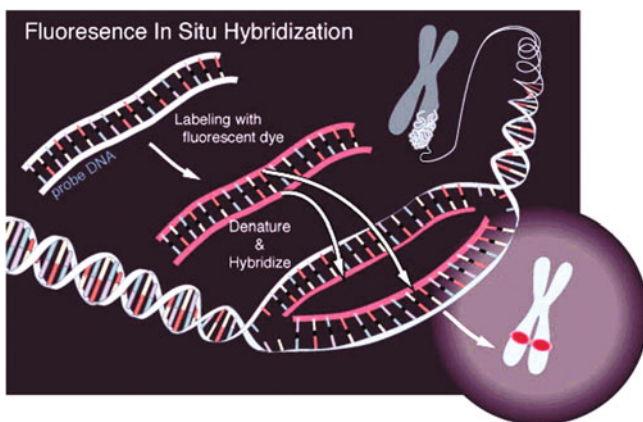


Fig. 10.3 Schematic of FISH procedure (reproduced with permission from the National Human Genome Research Institute: <http://www.genome.gov/>)

dye sets have used directly fluorescent dideoxynucleotides [50] that can be used as terminators for FISH riboprobes. With common excitation at 488 nm these probes have fluorescence intensities that differ by less than a factor of two. It is noteworthy that these fluorescence reporters can be incorporated into DNA without disruption of the base pairing and remain photo-active. Non-covalent fluorescent probes for DNA are also discussed in Chap. 12.

The increasing number of accessible target DNA sequences has led to growing popularity of FISH in the last two decades. Alongside this there has been a corresponding increase in the number of simultaneously detected probes, firstly by the incorporation of ever more spectrally distinct fluorophores and then by the use of digital encoding schemes. Specific DNA sequences can be identified by unique colour code and intensity combinations (optical bar-coding), such that dozens of targets can be detected [51]. Current advances in nanoparticle fluorophores promise to extend this to simultaneously recognise thousands of target sequences [52].

10.5 Future Applications: Nanomedicine

The maturation of nanotechnology in the twenty-first century has the potential to revolutionise many areas of science and engineering and one of the most important of these is health and medicine. Nanomedicine is defined in its widest aspect as *'the application of nanotechnology to further human health'* and is an area of tremendous potential because of the fundamental properties of material at the nanoscale and the natural affinity of nanoparticles and biological molecules. The control and analysis of matter at the nanoscale provides novel materials with unique properties determined by quantum physical laws and with massive surface area to volume ratios relative to the bulk state. Together these attributes provide ultra-sensitive sensing capability in which the ideal combination of high responsiveness and large sensing area can be realised [53]. The nanoscale is that of molecules and so the application of nanotechnology to human health finally allows medicine to be performed directly on the molecular initiators of disease [54–56] bringing increased sensitivity, intelligent targeting of drugs and the potential for personalised therapeutic programs, customised for each patient. Photochemistry is playing a leading role within this nanomedicine revolution as photonic nanoparticles can be readily substituted for traditional fluorescent agents. This brings highly novel technology to bear within established diagnostic platforms and so accelerates the technology take-up within the clinical environment (see Fig. 10.4).

10.5.1 Quantum Dots: Fluorescent Nanocrystals

Fluorescent nanoparticles are commonly referred to as *quantum dots*, reflecting the quantum nature of the optoelectronic processes that lead to their light emission [57].

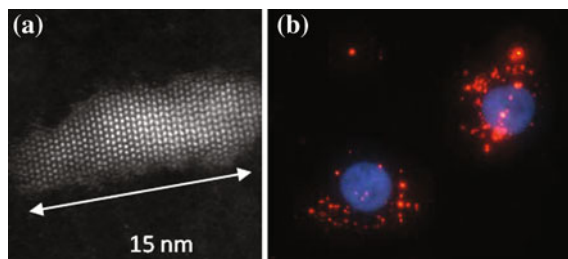


Fig. 10.4 **a** Electron micrograph of a CdTe nanocrystal. **b** Fluorescence image of CdTe nanocrystals in MCF-7, breast cancer cells, the endosome encapsulated nanoparticles are visible as discrete sources of *red* fluorescence (*blue* emission is from a nuclear dye)

They consist of nano-sized crystals of semiconductor compounds, usually formed from group II and VI elements e.g. CdSe, CdTe, ZnS. Reduction of the crystal size leads to quantum confinement of the electronic states in the conduction and valence bands of the semiconductor and this leads to a fluorescence emission wavelength that is controlled by size. As the crystal shrinks to diameters <100 nm, the quantum confinement energies increase dramatically and the emission wavelength is blue-shifted (see Fig. 10.5). This tuning of optical properties revolutionises photochemistry as now a multitude of different fluorescence wavelengths can be realised using the same chemical compound. The CdSe quantum dot system that is most commonly available can produce emission spanning the whole of the visible spectrum from the same CdSe nanocrystal. In addition to this customisability, quantum dots provide additional benefits for photochemical assays, including (i) their optical absorption is through a band of high energy states and hence their absorption spectrum is broad, making multiple emitting dots excitable with a single wavelength source; (ii) these inorganic crystals are also more robust in comparison to traditional fluorophores, being virtually immune to photo-degradation; (iii) finally, the typical size of quantum dots ($\sim 2\text{--}20$ nm) means that they are

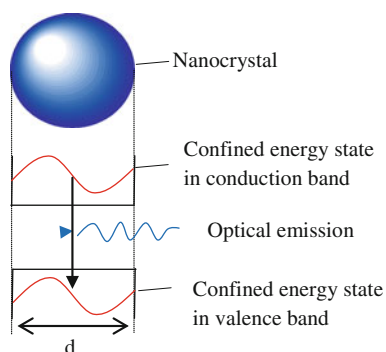


Fig. 10.5 Quantum dot tuning. As the crystal diameter, d , is decreased the confined energy states move apart leading to higher photon energy emission

internalised into cells through the natural process of endocytosis [58] and have a relatively large surface area for decoration with targeting ligands such as antibodies or with drug molecules. The photophysical properties of quantum dots are discussed in detail in [Chap. 4](#).

10.5.2 Medical Applications of Nanophotonics

Most of the early applications of quantum dots have used them as direct replacements of traditional photochemicals in the common diagnostic assays detailed in this Chapter. However the potential applications of photonic nanocrystals extend far beyond these current protocols, in particular nanomedicine will bring diagnostics and therapeutics advances through multi-functional nanoparticles. The ultimate vision is of specifically targeted nanocomposites, with an attached cargo of drug molecules, identifying and entering diseased cells and then releasing the therapeutic agent to induce cell death [59, 60]. Specific examples of multi-functional activity include the fluorescent identification of diseased cells and their subsequent removal through photoactivation of the nanoparticle (a nanomolecular version of photodynamic therapy (PDT)—see [Chap. 9](#)); and thermal treatment of tumour cells through selective tuning of optical absorption in gold–silica nanoparticle composites allied with magnetic resonance guided temperature measurement [61]. The revolution promised by nanomedicine is a suiting end point to this review of photochemistry in the medical domain as it is the ultimate example of how photochemistry, in its role as an enabling technology, is all important in driving advances in our ability to diagnose and treat disease.

References

1. Stokes GG (1852) On the change of refrangibility of light. *Phil Trans R Soc* 142:463–562
2. Udenfriend S (1995) Development of the spectrophotofluorometer and its commercialization. *Protein Sci* 4:542–551
3. Severinghaus JW, Astrup PB (1987) History of blood gas analysis. *Int Anesthesiol Clin* 25:1–224
4. Royston BD (1993) Continuous monitoring of arterial blood gases. *Int Anesthesiol Clin* 31:1–22
5. Mahutte CK (1994) Continuous intra-arterial blood gas monitoring. *Intensive Care Med* 21:487–494
6. Ohkuma S, Poole B (1978) Fluorescence probe measurement of the intralysosomal pH in living cells and the perturbation of pH by various agents. *Proc Nat Acad Sci USA* 5:3327–3331
7. Clement NR, Gould JM (1981) Pyranine (8-hydroxy-1,3,6-pyrenetrisulfonate) as a probe of internal aqueous hydrogen ion concentration in phospholipid vesicles. *Biochemistry* 20:1534–1538

8. Vurek GG, Feustel PJ, Severinghaus JW (1983) A fiber optic pCO₂ sensor. *Ann Biomed Eng* 11:499–510
9. Bacon JR, Demas JN (1987) Determination of oxygen concentrations by luminescence quenching of a polymer immobilized transition metal complex. *Anal Chem* 59:2780–2785
10. Draxler S, Lippitsch ME, Klimant I et al (1995) Effects of polymer matrices on the time-resolved luminescence of a ruthenium complex quenched by oxygen. *J Phys Chem* 99:3162–3167
11. Alberts B, Johnson A, Lewis J et al (1994) *Molecular biology of the cell*, 3rd edn. Garland, New York
12. Pier GB, Lyczak JB, Wetzler LM (2004) *Immunology, infection, and immunity*. ASM Press, Washington
13. Vo-Dinh T, Sepaniak MJ, Griffin GD, Alarie JP (1993) *Immunosensors: principles and application*. *Immunomethods* 3:85–92
14. Kohler G (1986) Derivation and diversification of monoclonal antibodies. *Science* 233:1281–1286
15. Coons A, Creech HJ, Jones RN (1941) Immunological properties of an antibody containing a fluorescent group. *Proc Soc Exp Biol Med* 47:200–202
16. Berson S, Yalow R (1959) Quantitative aspects of the reaction between insulin and insulin-binding antibody. *J Clin Invest* 38:1996–2016
17. Yalow RS (1977) Radioimmunoassay: a probe for fine structure of biologic systems. In: *Nobel lecture in medicine*
18. Oellerich M (1984) Enzyme-immunoassay: a review. *J Clin Chem Clin Biochem* 22:895–904
19. Dodeigne C, Thunus L, Lejeune R (2000) Chemiluminescence as diagnostic tool. A review. *Talanta* 51:415–439
20. Blake C, Gould BJ (1984) Use of enzymes in immunoassay techniques. A review. *Analyst* 109:533–547
21. O'Sullivan MJ, Bridges JW, Marks V (1979) Enzyme immunoassay: a review. *Ann Clin Biochem* 5:221–240
22. Weissmann G, Bloomgarden D, Kaplan R et al (1975) A general method for the introduction of enzymes, by means of immunoglobulin-coated liposomes, into lysosomes of deficient cells. *Proc Nat Acad Sci USA* 72:88–92
23. Van weemen BK, Schuur AHWM (1971) Immunoassay using antigen-enzyme conjugates. *FEBS Lett* 15:232–236
24. Horobin RW, Kiernan JA (2002) *Conn's biological stains. A handbook of dyes, stains and fluorochromes for use in biology and medicine*, 10th edn. Cromwell Press, Oxford
25. Gustashaw KM (1991) Chromosome stains. In: Barch MJ (ed) *ACT cytogenetics laboratory manual*, 2nd edn. The association of cytogenetic technologists. Raven Press, New York
26. Langer PR, Waldrop AA, Ward DC (1981) Enzymatic synthesis of biotin-labeled polynucleotides: novel nucleic acid affinity probes (nucleotide analog/DNA and RNA polymerase/avidin-sepharose/antibiotin antibody/immunoprecipitation). *Proc Nat Acad Sci USA* 78:6633–6637
27. Femino AM, Fay FS, Fogarty K, Singer RH (1998) Visualization of single RNA transcripts in situ. *Science* 280:585–590
28. Gall JG, Pardue ML (1969) Formation and detection of RNA–DNA hybrid molecules in cytological preparations. *Proc Nat Acad Sci USA* 63:378–383
29. Rudkin GT, Stollar BD (1977) High resolution detection of DNA–RNA hybrids in situ by indirect immunofluorescence. *Nature* 265:472–473
30. Bauman JG, Wiegant J, Borst P, van Duijn P (1980) A new method for fluorescence microscopical localization of specific DNA sequences by in situ hybridization of fluorochrome labelled RNA. *Exp Cell Res* 128:485–490
31. Nederlof PM, van der Flier S, Raap AK et al (1989) Detection of chromosome aberrations in interphase tumor nuclei by non-radioactive in situ hybridization. *Cancer Genet Cytogenet* 42:87–98

32. Levsky JM, Singer RH (2003) Fluorescence in situ hybridization: past, present and future. *J Cell Sci* 116:2833–2838
33. Van der Ploeg M (2000) Cytochemical nucleic acid research during the twentieth century. *Eur J Histochem* 44:7–42
34. Raap AK (1998) Advances in fluorescence in situ hybridization. *Mutat Res* 400:287–298
35. Levsky JM, Shenoy SM, Pezo RC, Singer RH (2002) Single cell gene expression profiling. *Science* 297:836–840
36. Cremer T, Lichter P, Borden J et al (1988) Detection of chromosome aberrations in metaphase and interphase tumor cells by in situ hybridization using chromosome-specific library probes. *Hum Genet* 80:235–246
37. Devilee P, Thierry RF, Kievits T et al (1988) Detection of chromosome aneuploidy in interphase nuclei from human primary breast tumors using chromosome specific repetitive DNA probes. *Cancer Res* 48:5825–5830
38. Hopinan AHN, Kamaekers FCS, Raap AK et al (1988) In situ hybridization as a tool to study numerical chromosome aberrations in solid bladder tumors. *Histochemistry* 89:307–316
39. Brown J, Horsley SW, Jung C et al (2000) Identification of a subtle t(16;19)(p13.3;p13.3) in an infant with multiple congenital abnormalities using a 12-colour multiplex FISH telomere assay, M-TEL. *Eur J Hum Genet* 8:903–910
40. Stebbins GL (1950) Variation and evolution in plants. Chapter XII: The karyotype. Columbia University Press, New York
41. Kottler M (1974) From 48 to 46: cytological technique, preconception and the counting of the human chromosomes. *Bull Hist Med* 48:465–502
42. Nederlof PM, van der Flier S, Wiegant J et al (1990) Multiple fluorescence in situ hybridization. *Cytometry* 11:126–131
43. Schröck E, du Manoir S, Veldman T et al (1996) Multicolor spectral karyotyping of human chromosomes. *Science* 273:494–497
44. Chudoba I, Plesch A, Lörch T et al (1999) High resolution multicolor-banding: a new technique for refined FISH analysis of human chromosomes. *Cytogenet Cell Genet* 84:156–160
45. Tyagi S, Kramer FR (1996) Molecular beacons: probes that fluoresce upon hybridization. *Nat Biotechnol* 14:303–308
46. Boulon S, Basyuk E, Blanchard JM et al (2002) Intra-nuclear RNA trafficking: insights from live cell imaging. *Biochimie* 84:805–813
47. Contag CH, Bachmann MH (2002) Advances in in vivo bioluminescence imaging of gene expression. *Annu Rev Biomed Eng* 4:235–260
48. Politz JC, Singer RH (1999) In situ reverse transcription for detection of hybridization between oligonucleotides and their intracellular targets. *Methods: a companion to methods in enzymology* 18:281–285
49. Smith LM, Sanders JZ, Kaiser RJ et al (1986) Fluorescence detection in automated DNA sequence analysis. *Nature* 321:674–679
50. Prober JM, Trainor GL, Dam RJ et al (1987) A system for rapid DNA sequencing with fluorescent chain-terminating dideoxynucleotides. *Science* 238:336–341
51. Fauth C, Speicher MR (2001) Classifying by colors: FISH-based genome analysis. *Cytogenet Cell Genet* 93:1–10
52. Han M, Gao X, Su JZ, Nie S (2001) Quantum-dot-tagged microbeads for multiplexed optical coding of biomolecules. *Nat Biotechnol* 19:631–635
53. Roduner E (2009) Size matters: why nanomaterials are different. *Chem Soc Rev* 35:583–592
54. Scheinberg DA, Villa CH, Escorcia FE, McDevitt MR (2010) Conscripts of the infinite armada: systematic cancer therapy using nanomaterials. *Nat Rev Clin Oncol* 7:266–276
55. Davis ME, Chen Z, Shin DM (2008) Nanoparticle therapeutics: an emerging treatment modality for cancer. *Nat Rev Drug Disc* 7:771–782
56. Ferrari M (2005) Cancer nanotechnology: opportunities and challenges. *Nat Rev Cancer* 5:161–171

57. Norris DJ, Bawendi MG, Brus LE (1997) Optical properties of semiconductor nanocrystals (quantum dots). In: Jortner J, Ratner M (eds) *Molecular electronics*. Blackwell Science, Oxford
58. Zhang S, Li J, Lykotrafitis G et al (2008) Size-dependent endocytosis of nanoparticles. *Adv Mat* 20:1–6
59. Koo OM, Rubinstein I, Onyuksel H (2005) Role of nanotechnology in targeted drug delivery and imaging: a concise review. *Nanomedicine* 1:193–212
60. Janib SM, Moses AS, MacKay JA (2010) Imaging and drug delivery using theranostic nanoparticles. *Adv Drug Deliv Rev* 62:1052–1063
61. Hirsch LR, Stafford RJ, Bankson JA et al (2003) Nanoshell-mediated near-infrared thermal therapy of tumors under magnetic resonance guidance. *Proc Nat Acad Sci* 100:13549–13554

Chapter 11

Photochemical Imaging

Gareth B. Evans, Michael B. Ledger and Henry H. Adam

Abstract Photochemical imaging is dominated by silver halide technology. The early history of photography is described while introducing the essential ingredients of modern photography. The technology is described by reference to modern materials and current understanding of the photochemical processes involved. At the core is the photolysis of silver halide crystals leading to the formation of latent images. Their manufacture and chemical and spectral sensitisation are briefly described. The development of the silver images is explained. Variations on the technology of development lead to the variety of types of familiar and less familiar photographic products. Non-silver photographic systems have also provided significant commercial imaging systems, for example, Blueprints, Diazotypes and dichromated colloid/polymer systems. The last was important in the early development of photography and is still exploited today. The principles of electrophotographic systems are also briefly described.

11.1 Introduction

The topic of ‘photochemical imaging’ immediately suggests photography, ‘drawing with light’ and in particular the familiar silver halide photography. When people are asked what they would save first if fleeing from a fire in their homes

G. B. Evans (✉) · M. B. Ledger · H. H. Adam
Kodak Ltd Research Laboratory (retired), Middlesex, UK
e-mail: gbe@evansgb.plus.com

M. B. Ledger
e-mail: mbledger@yahoo.co.uk

H. H. Adam
e-mail: harry.adam@btinternet.com

they usually opt for their photo albums. Photographs are important, not only to the individual but to so many industrial processes and as historical records. The history of photographic science, dating as far back as the early eighteenth century, includes some of the first observations of the chemical effects of light. In other words, photochemical effects were recorded even before the emergence of the science of chemistry as we would recognise it today.

There are several other technologies which use light to make images which are not called photography. Photopolymerisation (not involving silver salts) and its application to materials used in the printing industry are covered in [Chap. 13](#). Also, photochromism is mentioned in [Chap. 4](#). These will not, therefore, be included here. A number of photochemical imaging technologies of minor commercial importance also exist and these will be mentioned but not described in detail. We will, in very brief form, include electrophotography for completion because of its importance despite the lack of chemical change in the process.

Also included are some of the chemical and physical steps which immediately follow the initial interaction of silver halide materials with light. The story of these imaging processes would not be complete without them and they serve to illustrate the diverse applications of the common photochemical process of silver halide photolysis.

11.1.1 Requirements of Imaging Systems

In this chapter and elsewhere in this book, various technologies applied to imaging systems are described. As well as printed images we are familiar with projected images in the cinema and television images at home. Before looking at the various exploitations of photochemical imaging systems including those based on silver, we should therefore first consider more generally what is required of all imaging systems, particularly colour systems. We can then see how the available processes can be tailored to suit particular applications.

We will first look briefly at black-and-white (B and W) imaging where all aspects of imaging except colour are, of course, still important. Images are composed of component areas of different apparent brightness or *luminance*. In printed images these variations are quantified as (optical) densities ranging from the darkest ‘shadow’ areas to the brightest ‘highlight’ areas. The term *tone* refers to the position of an area on a scale of luminance. The *tone-reproduction* is then the relationship between the densities of the various parts of the original and the corresponding parts of the reproduced image. This relationship is not necessarily 1:1 or even linear for a variety of physical and perceptual reasons. Elements of an imaging system must translate an input signal into a resulting output which contributes to a satisfactory final image. A display screen must convert an electronic signal into, for example, a luminous image. A photographic reflection print must convert a light exposure of an image capture device into an image density in the viewed print.

Most original scenes contain a much wider range of luminance than can be reproduced in an imaging system. Our eyes and the brain's processing of the image information have remarkable capabilities for coping with the challenge of tone reproduction and colour perception. A good example is the now obsolescent cathode ray tube (CRT) display technology. Black areas in TV images are never actually darker than the darkness of the screen when switched off, yet we take some convincing of this fact when we see the displayed image with a full range of tone reproduction including what seem to be very black shadow areas. They seem black only in relation to the bright areas in the image. For printed materials such as photographs, the perceived depth of blacks is limited, as with TV screens, by the amount of light reflected from the darkest possible areas. In the case of B and W silver halide prints these areas are where the maximum amount of silver is developed. Silver scatters light as well as absorbing it, so some of the light used to view the image is inevitably reflected from the darkest areas into the observer's eye. In practice, the maximum density of a silver reflection image is about 1.7, that is a maximum luminance range on a linear scale of only 50:1. This is well short of the range of a typical scene. A well-lit scene can often have density range of over 4.0 or 10,000:1 in luminance terms. Shadows are less interesting than bright parts of an image so we do tolerate a limited density range for most imaging purposes.

Images produced with black inks do better because inks tend to scatter light less than silver, but surface (Fresnel) reflections impose practical limits here as well. Transparent images are capable of much greater ranges, but are usually limited to a density range of around 3.5, because to provide more density would come with a cost to other factors, for example of reduced speed, sharpness and ease of chemical processing without much perceived quality benefit.

After tone-reproduction, image sharpness, *i.e.* the ability to reproduce detailed shapes, is probably the most important requirement. The issues here are largely apparent and need not be discussed in detail. The number of picture elements in a structured image such as a half-tone printed image or screen resolution in a TV monitor are obvious influences. In silver halide photography, sharpness is linked in practice to other aspects of performance such as sensitivity (speed), tolerance of films to a wide range of exposure levels and the graininess of images. Compromises are needed in the design of the materials to optimise the mix of these performance factors. For all but the highest speed films adequate sharpness is now achieved relatively easily. One limiting factor (apart from the most frequent cause of sharpness loss, namely poor focusing) is the optics of the print material. While the imaging layer of a print can be capable of being very sharp, it is exposed and viewed above a light-reflecting support. Ideally, light would bounce back from low-density areas of an image without penetrating into the support, but often in practice, cost considerations usually dictate that less light-scattering material than ideal is contained in the support. Consequently, light penetration is significant and this inevitably includes lateral penetration and loss of sharpness. An important consideration here is, however, the ability of the eye to perceive differences in sharpness beyond a limit (about 7 lines per mm), which many imaging systems can achieve without too much difficulty today.

For colour materials, the colour reproduction requirements are driven again by the nature and performance of our own imaging system of human vision. We need to take a look at how our colour vision works and then how to fool it into thinking a reproduced image using light sources or coloured dyes and pigments is a good reproduction of the experience of viewing an original image.

Figure 11.1 shows the spectral response of the three sets of cone cells [1] responsible for colour vision. The curves are normalised to show equal maximum responses, but in fact the blue-sensitive cones are much less sensitive than the 'green' and 'red'. Blue colours are therefore seen as relatively dark but the blue response is vital in determining how we see a variety of colours.

Monochromatic light will produce a response in the three sets of cones dependent on its wavelength. The total response determines the perceived brightness and the relative responses produce the experience of colour. The colour which we experience depends on this primary response, though it can be modified significantly by later processing by the brain. Surprisingly perhaps, the red and green responses overlap considerably, but this is an essential requirement if we are to experience a wide range of colours. If the responses were completely separate, then within each envelope, the colour sensation would be independent of wavelength and we would experience only three spectral colours. In practice, we are able to distinguish subtle differences in hue, particularly in the green/yellow region, an ability which was invaluable in the leafy, grassy environment our ancient ancestors evolved in.

Usually of course we do not see monochromatic light, but a continuous spectrum of wavelengths. The responses we experience are the integrals of the effects of the component monochromatic contributions to the spectral distributions of the light we sense. The results still add up to a set of three responses from the three sets of cones. The challenge for a colour imaging system is to generate, for each part of the image, at least approximately, the same three responses and therefore the same colour and lightness sensations as would have been experienced on viewing the reproduced original.

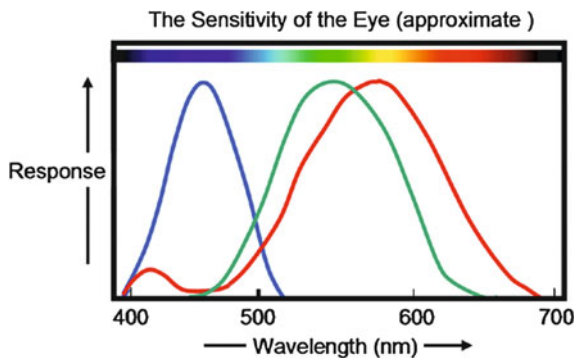


Fig. 11.1 The spectral sensitivity of the three sets of cone receptor cells

There are two broad classes of image display systems. The *additive* system uses light sources to create a pattern of light to form the image. We need a suitable set of emitters. Conveniently, if we limit the wavelength ranges of an emitter to between approximately 400 and 500 nm we see this as ‘blue’. Using the range 500–600 nm gives us a green sensation and the band from 600 to 700 nm gives us red. These correspond only approximately to the spectral responses of the three sets of cones, but systems based on red, green and blue (RGB) emitters do in practice prove an effective means of reproduction. This set of three emitted colours, are then our additive *primary colours*. The television screen is perhaps the most familiar example. Figure 11.2a shows the array of emitters of a CRT TV screen. The spectral emission of each emitter set usually spreads beyond the boundary wavelengths mentioned above with some sacrifice in colour reproduction including the gamut of colours available for the sake of improved brightness and dynamic range (contrast). Figure 11.2b showing overlapping RGB circles, demonstrates the making of three different colours from each combination of two of the RGB emitters and ‘white’ from all three. The colours are a little dull because of the black gaps between the individual emitters. By adjustment of the relative brightness of each set of emitters satisfactory reproduction of a variety of colours can be achieved. This is in part due to the contribution of the eye/brain’s ability to interpret the physical sensing of light and make adjustments for errors in colour balance. Additive colour systems are not confined to emissive systems. Film systems such as Dufay Colour and Polachrome used RGB colorants as colour filters for projected images (see Sect. 11.2.3.2).

The other class of display system is the *subtractive* system. Here, images include both reflection prints, such as conventional colour photographs or printed pages and transmission prints, such as slides and projected movie cinema images. These images provide the light sensed by the eye from a combination of a light source and colorants which modify the light source in an image-wise manner. For reflection prints the light source is the ambient light under which the print is viewed, while for transmission prints a back-light such as a light-box or a projector

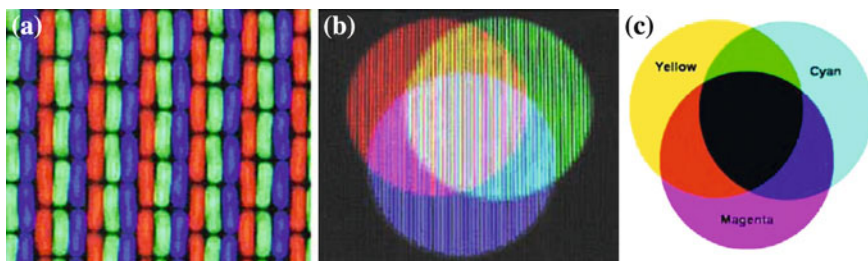


Fig. 11.2 **a** *R*, *G* and *B* emitting pixels of a CRT screen. **b** Overlapping additive colours produce the three subtractive primaries and ‘white’. **c** Two overlapping subtractive primaries remove two additive primaries leaving an additive primary. When all three overlap *black* is produced

bulb provides the light. The colorants' role is to modify the amounts of red, green and blue light seen by our eyes by absorbing ideally only one of them.

To do this, cyan, magenta and yellow colorants are used (see Fig. 11.2c). These absorb red, green and blue light respectively. This set of colorants (CMY) are therefore known as the *subtractive primaries* [2]. Where two primaries overlap, two of the RGB colours are subtracted leaving the third. The colorants are provided in the form of dyes and pigments (insoluble colorants) in media such as printing inks, ink-jet inks, electrophotographic toners and photographically produced dyes. They are often supplemented by a black colorant (K) to adjust tone-scale, improve sharpness and deepen black areas in CMYK systems [3].

In colour photography the three dyes are usually generated as part of the process of development of the silver halide emulsion. This process is described more fully later. Figure 11.3 illustrates how the negative/positive colour system reproduces an original colour pattern using the subtractive primaries. Light of various colours is provided by the original scene or object, usually by reflected or otherwise modified light. The object to be reproduced in this diagram provides red, green and blue areas as well as white (all three together), and black (none). These areas are imaged onto the first material, the negative camera-film. The film is made up of three layers [4] with other layers in between to prevent cross-talk between the colour responses. In each layer the silver halide crystals are *sensitised* to one of the RGB spectral regions. The photochemistry of the responses of the dyed crystals

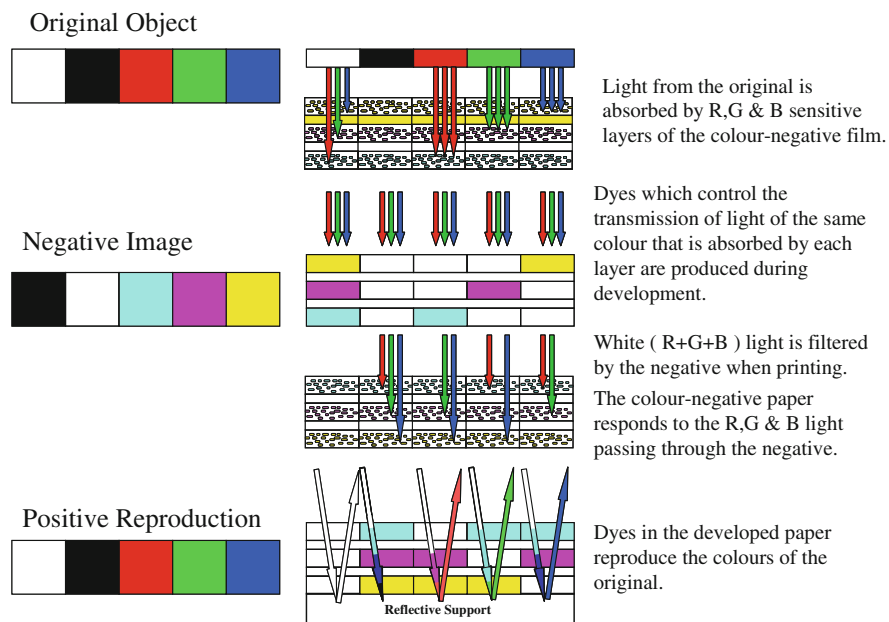


Fig. 11.3 Schematic diagram of the negative/positive colour photographic system

is described in more detail later. The blue-sensitive, yellow-forming layer is above the other imaging layers and immediately above a yellow-coloured filter layer made from silver nanoparticles [5]. This is mainly because the silver halide crystals used in films absorb and respond to blue light which needs to be filtered before the light passes to the green and red sensitive layers. The crystals in the green layer are sensitised with a green-absorbing dye which provides a degree of filtration of green light passing to the red-sensitive layer.

The exposed film is then processed and dyes are produced which absorb in the same spectral region that was used to expose the layers in which they are formed to provide the negative image. To produce the positive image, the negative is then illuminated by polychromatic light and used to expose the print material. Photographic paper has a different layer order from that of film. This is not for any good imaging reason but to overcome a problem of non-uniform response in the bottom layer caused by unevenness of the paper support. Rather than solve this problem by using smoother paper, it is mitigated by using the yellow-forming layer on the bottom. As we have observed before the eye is not very sensitive to blue light and therefore sees yellow (white minus blue) as a bright colour. Variations in its brightness are therefore of less importance. The blue-sensitive layer, though, is now no longer able to have the first bite at the blue light. To provide a response to blue light sufficiently different from the other two layers, it needs to use much faster silver halide crystals.

The colour negative-positive silver halide system has evolved over a long time during which sophisticated chemical devices have been introduced to overcome deficiencies. Section 11.2.3 describes the basic colour-forming chemicals which couple with developing agents. In modern materials some of these are themselves coloured so that when they form the required dye, the disappearance of their own colour corrects for the spectral defects of the dyes formed. Other couplers release agents which inhibit the development of the silver halide crystals. These *development-inhibitor releasing* (DIR) couplers are remarkably effective in providing mitigation of a number of deficiencies. The details of their effects are beyond the scope of this book but can be found in a number of books describing photographic technology for example “The Theory of the Photographic Process” [6]. They reduce graininess by limiting the amount of dye formed from each silver halide crystal thus allowing more crystals to participate in forming the image. The migration of inhibitor to adjacent layers provides some colour reproduction benefits and their lateral migration enhances image edges and therefore apparent sharpness.

All these sophisticated chemical functions are readily performed arithmetically in digital imaging systems but until recently the combination of image quality, robustness and permanence of silver halide prints has been difficult to match. For that reason we will look first at the earliest and most important photochemical imaging system, silver halide photography.

11.2 Silver Halide Photography

Before we look in detail at the core photochemical process of silver halide photolysis and the amplification of the photochemical response resulting from chemical development we will first explore the early history of imaging technology. By doing so will introduce the essential elements of modern photographic systems.

11.2.1 Early History

11.2.1.1 The Building Blocks

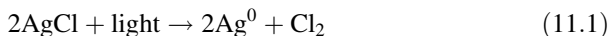
As is often the case, there are times in science and technology when a few people were doing similar things at the same time and it is sometimes uncertain as to who knew what and when. The historical accounts are often distorted by personal rivalries, races to be 'first', and the promotion of ideas, personalities and products. We can however recognise the major building blocks of the photographic system as we would recognise it today and the inventive combinations which enabled useful systems to be realised.

Firstly, we require a means of creating a pattern of light on a light-sensitive material. We need a camera. By the time useful light-sensitive materials were discovered cameras had been around a long time. The earliest reference to what we would now call a *camera obscura* dates from the fifth century BC by the Chinese philosopher Mo-Ti, who described an inverted image created by light passing through a hole in a wall of a darkened room [7] and falling on the opposite wall. A number of people described the principle and practice of imaging with this arrangement in increasing detail including the Islamic physicist Alhazen, Da Vinci and later, Johannes Kepler, who first coined the term *camera obscura*, the Latin for a dark room. Smaller, portable devices improved their versatility and their use in art enabled a breakthrough in the accuracy of perspective in paintings by, for example, Jan Vermeer. These devices, then, allowed the capture of ephemeral images and were in the wings awaiting the discovery of suitable materials before permanent images could be recorded.

The discovery of light-recording materials came along a lot later than the earliest cameras, but some considerable time before what many would recognise as the 'birth' of photography often attributed to the Frenchman Joseph Nicéphore Niépce in 1826. A hundred years earlier than Niépce's first photographs, Johann Heinrich Schultze, a German professor of anatomy, probably made the first images using light [8, 9]. In 1725 Schultze was experimenting with silver compounds and had impregnated powdered minerals such as chalk and gypsum with silver nitrate. Initially he had been using nitric acid for another purpose but this contained some silver and Schultze identified silver as the active ingredient. A jar of the material exposed to sunlight darkened on the side facing the sun and Schultze established

that light rather than heat caused the darkening. He went a crucial step further as far as photography is concerned, and partly covered the exposed surface of powder by gluing on pieces of paper not just randomly but with shapes cut out, for example, of letters. We now call these images *photograms* to distinguish them from images produced by projection. As far as the photochemistry is concerned it was probably halide impurities in the chalky substrate which enabled the formation of silver halides which we now know to be particularly effective light recorders.

Half a century later, Carl Wilhelm Scheele, more famous for his discovery of oxygen, described the reduction of silver chloride to silver metal by light in 1779:



He also noted that violet light was more effective than light of longer wavelength. This was at the time when Lavoisier was overthrowing the Phlogiston Theory and establishing chemistry as a respectable science, so photochemistry can claim to be as old as chemistry itself. Scheele also provided a potential method of fixing silver images. Knowing that silver chloride was soluble in ammonia [10], he showed that ammonia dissolved un-reacted silver chloride from the exposed, darkened powder leaving the black photolytic silver.

At the beginning of the nineteenth century, Thomas Wedgwood the scientist son of the potter Josiah Wedgwood experimented with silver nitrate. Sir Humphrey Davy presented a paper [11] based on Wedgwood's work to the Royal Institution in 1802. Again, Wedgwood's first light-sensitive materials were produced by applying silver nitrate to substrates such as paper and leather and, fortuitously present halide ions, may explain the photosensitivity. He was aware of Scheele's work on silver chloride, probably through Joseph Priestley, a fellow member of the Lunar Society, and recognised the increased sensitivity to light of paper soaked with silver nitrate by a subsequent treatment with hydrochloric acid. Despite his best efforts he failed to make the images permanent, by preventing unexposed areas eventually darkening and destroying the image. This seems somewhat surprising in view of Scheele's observation of the effect of ammonia on exposed silver chloride. Facing apparent defeat in his attempts to make his images permanent, he, as did Schultze before him, turned to other interests.

11.2.1.2 The First Permanent Images

The light sensitivity of silver-treated materials was therefore well known to those later in the nineteenth century seeking to make permanent images. These included the Frenchman, Nicéphore Niepce. He succeeded in producing images using, at first, silver nitrate-treated paper in 1816 [12] but like Wedgwood he did not discover a way to "fix" the images and make them permanent so he looked elsewhere. He was interested in lithography and familiar with the materials involved so he experimented with bitumen of Judea. In 1822 he attempted to produce photograms using bitumen on lithographic stones and copper plates. The bitumen was hardened by the

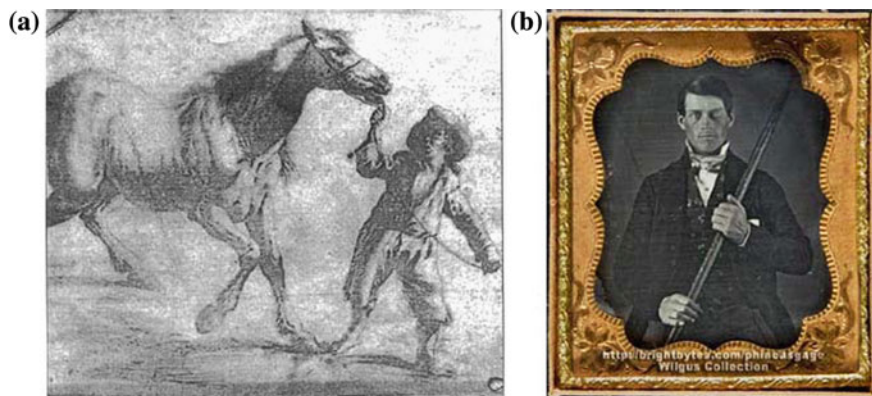


Fig. 11.4 **a** The first known permanent photographic image (reproduced with kind permission from Ref. [13], Copyright 2002, the Bibliotheque National de France). **b** A daguerreotype of Phineas Gage (reproduced with kind permission of Jack and Beverley Wilgus—Ref. [15]) (laterally reversed to show features correctly)

action of prolonged exposure to light though it is possible that it was heat, either directly or from light absorption which was responsible for the hardening due to the consequent evaporation of the lighter fractions in the bitumen. Nevertheless, he was able to produce a difference in solubility of the bitumen layer which could be revealed by treatment with primrose oil and kerosene mixtures. Etching with nitric acid provided a surface which could be inked to provide a positive image which could then be transferred to paper. The earliest surviving print, shown here in Fig. 11.4a, ‘*Cheval et son Conducteur*’ sold in Paris in March 2002 and is thought to date from 1825. It is essentially a ‘photocopy’ of a seventeenth century Dutch print made by contact printing rather than with a camera [13]. The light levels available in a camera obscura are of course much lower than can be used for photograms but Niepce persevered and eventually in 1826 produced the first permanent photographic image using a camera, a picture of the roof-tops of his home. He called the images ‘Heliograms’. He is therefore widely considered to be the inventor of photography despite the earlier technology because of the combination of a camera and a light-sensitive material.

It was a major achievement but it has to be said that the quality was not very good. The sun moves a long way in 8 hours and the etching process produced either black or white with few greys in between. In terms of photography as we understand it today it was a technological blind alley, though the use of photo-resists to produce printing plates was a direct precursor of the very important modern photolithography and photofabrication methods (see Chap. 13).

Niepce went to England to promote his invention through the Royal Society but he did not receive the publicity he sought because he was reluctant to divulge some of his techniques and on those grounds was refused endorsement. This probably persuaded him to team up with Louis Daguerre and this formal partnership seems

to have been crucial to the development of the first commercially successful photographic material, the *Daguerreotype*.

Daguerre was an imaginative and successful stage-set designer and saw his work dismantled frequently. Aware of the *camera obscura* he too sought a way to use this device to record images of his work and of course much else. Niepce and Daguerre worked on refinements to Niepce's earlier ideas but they lead nowhere. Niepce died soon after in 1833 and Daguerre using the knowledge of silver-based materials he had gained from his partner, went on to develop a process which was the first successful photographic system. Niepce had produced images in bitumen layers coated on silver plated copper and treated them with iodine vapour. This darkened unexposed areas of the metal surface thus providing an alternative method to etching for providing a positive image.

Daguerre's vital contribution was to discover that surfaces coated with silver iodide were light-sensitive and when exposed, the resulting photolytic silver could form an image. More importantly, the poor image could be revealed or "developed" by mercury vapour which was deposited in an image-wise manner forming a reflective mercury/silver amalgam. It is said, but not recorded [14], that the discovery was made when Daguerre, left an exposed iodised silver plate with no visible image on it in a drawer. A few days later when the drawer was opened the plate showed a visible image. This was subsequently proved to be due to the presence of mercury vapour in the drawer and the Daguerreotype was born (see Fig. 11.4b). The mercury treatment produced a much more visible and positive image, the lighter areas consisting of an array of reflective dots of mercury/silver amalgam.

The other vital building block used by Daguerre in 1837 (probably learned from Niepce and used 3 years previously by Fox Talbot) was a method of 'fixing' the images using 'cooking' salt solution to dissolve unexposed silver iodide thus rendering them permanent. This also improved image contrast.

Many such images from the decades following the commercial release of Daguerre's system are still in existence today due to the roaring success of this technology [15]. Again though, we must accept that the Daguerreotype's flaws, particularly the fact that only a single image could be obtained, were fatal and the system was overtaken.

11.2.1.3 The Birth of Modern Photography

William Henry "Fox" Talbot was in his teens when Niepce experimented with silver based light-sensitive materials but he must have been a fast learner. He had been a classics and mathematics scholar at Cambridge, a Fellow of the Astronomical Society at 22, a Fellow of the Royal Society at the age of 32. His interests included botany, deciphering cuneiform inscriptions and the Bible. He was also a member of the British parliament. It is for his contribution to photography, of course, that he is best remembered. Though the novelty of his work is sometimes exaggerated, he connected several known technical ingredients in a new way and developed a system which can be seen as the origin of the negative/positive

photographic systems still in use today. In 1833 he mused in his writings that it would be “charming” if the views he was experiencing could be captured as permanent images using a camera obscura. This is of course the year that Niepce, who had already successfully achieved a similar ambition, died. It was also before the introduction of the Daguerreotype in 1839 and Fox Talbot was convinced that he had made the first silver-based photographs. His earliest surviving photograph is the famous negative picture of a window taken in 1835 in his home Lacock Abbey, produced by exposing silver-sensitised paper.

To sensitise the paper it was treated successively with solutions of silver nitrate and sodium chloride which precipitated silver chloride crystals. After drying, the paper was given a final treatment with a solution of silver nitrate, gallic acid, and acetic acid. This increased the speed of the paper. We can now recognise this treatment as a form of chemical sensitisation of the silver chloride which we call ‘r-type’ or ‘reduction sensitising’, *i.e.* the production of groups of aggregated silver atoms on the surface of the silver chloride. We will deal with the details of the photochemistry of the image forming process later.

While experimenting with the sensitisation of paper, Talbot observed that high chloride levels reduced sensitivity. Daguerre had also used salt solutions to fix images. Talbot’s and Daguerre’s systems were obviously quite different and Daguerre’s considerably more advanced in 1839. Daguerreotypes were sharp while Talbot’s were not, even before they had been used to produce positives using contact exposure of a second piece of paper through the paper negative, a process which further degraded the image. Talbot’s method though had a significant advantage. It was possible to make multiple copies of a negative. When other pieces of the jigsaw fell into place this was a crucial advantage and the negative/positive system went on to dominate photography until the twenty-first century. One such piece was an improved fixing material provided by Sir John Herschel, who suggested the use of sodium thiosulfate in 1839, though this suggestion seems to have been borrowed from the reverend Reade [16, 17], who reported its use 2 or 3 years before. Herschel also coined the term “photography” in 1839 as well as advising Talbot to wax the negative image to improve its optical properties.

At this stage exposure times were extremely long. Daguerreotype portraiture involved clamping people’s heads for tens of minutes. This was despite some degree of visual amplification of the silver image by mercury. Talbot’s system involved exposure times of an hour or so despite his use of a small “mouse-trap” versions of a camera obscura having recognised that focussing the light onto a smaller area increased exposure intensity.

The formation of photolytic silver was still a very inefficient process but more significantly, all the silver in the image comes from photolytic silver and even if one silver atom resulted from one absorbed photon, exposure times would still be very long. We need another piece of the jigsaw.

Another vital breakthrough which Talbot made occurred as a result of another chance observation in 1840. His process involved a final treatment of the paper with a gallic acid solution, which the Reverend Reade [18] had combined with silver nitrate to produce light-sensitive materials. It seems that Talbot had exposed

some sensitised paper which did not work well, so he applied the gallic acid solution again. This treatment revealed the image resulting from the earlier exposure. In other words he had discovered that it was not necessary to expose the paper until the image was visible. It could be exposed briefly and the hidden or “latent” image could be revealed by the chemical treatment that developed the image. The development process amplifies the effects of light by a huge amount. We will also look at this process in more detail later.

Having reduced exposure times to minutes rather than hours Talbot had a viable system and described the ‘Calotype process’ in 1841 (from *Kalos*, meaning beautiful in Greek) by which time he had explored other halides and settled on silver iodide. Talbot’s grip on his process was maintained by patents and this unfortunately slowed technological progress, since not only potential suppliers, but even practitioners of photography had to pay royalties to make photographs. The quality of images using the Calotype process was impressive, even though it was limited by exposure and copying steps using paper. When the wet ‘*collodion*’ process was introduced by Frederick Scott Archer in 1851, it provided a way round this optical limitation. *Collodion* is cellulose nitrate made from gun cotton and as a soluble polymer could be coated onto glass plates, where it provided a host layer for the production of silver halide crystals. The exposure was made immediately after sensitisation and development was carried out with gallic acid. If dried, these layers were less responsive to light, so unlike the Calotype process, the photographic material could not be made and stored for later use.

In other words, the photographer was the photographic manufacturer and the processor and had to carry both his factory and laboratory, as well as his studio. However, the improvement in tone-scale and definition provided by collodion’s fibre-free layer compensated for this inconvenience. Furthermore, it was left unpatented and became the dominant method of negative production. For producing the positive print albumen-coated paper was normally employed. It is estimated that in 1866, at the height of its popularity, 6 million eggs were used in the UK for this purpose. Although there was no fundamental reason why albumen-based papers could not have been developed chemically, they were in practice developed by light.

Continued non-image wise exposure to light reveals a difference between exposed and unexposed crystals created during image capture. The exposed crystals or ‘grains’ darken more quickly as the production of photolytic silver accelerates, a process known as *latensification*. These so-called ‘Print-Out Papers’ or ‘POPs’ were preferred presumably because the process required less skill and no chemical processing. Exposure times were of less importance than during image capture. Prints could also be made easily by the growing army of amateur photographers. Most of the prints surviving from the nineteenth century used this photochemical method of production.

A further step forward was the separation of the production of the silver halide crystals from the coating of the substrate, such as glass or paper, with the sensitising materials. This allowed greater control over the formation and any subsequent treatment of the crystals and it also enabled crystal dispersions, which the

photographic industry now calls *emulsions* [19], to be made and coated on an industrial scale.

We now have the ingredients of modern silver halide photography, the small cameras, silver halide sensitised materials, a chemical development process allowing the copying of good quality photographs, and a method of fixing the developed image. We have not yet discovered how to extend the sensitivity of the materials to green and red light, how to get colour images or how to produce crystals which give direct positive images. It is time now to look at the chemistry of imaging in more detail with reference to modern materials. In doing so, we will fill in these gaps. A summary of the history of the development of component imaging technologies is provided in Fig 11.5.

Today, silver halide photographic materials have reached the last stages of their improvement. Digital image capture is now replacing film for a number of reasons. At the time of writing, film is still preferred for making movie films because of the infrastructure of the cinema industry and the need for large, bright projected images. Silver-based print materials for still images are steadily being displaced by temporary display and other non-photographic print technologies, particularly ink-jet, though electrophotographic printing may still eventually emerge as the dominant technology for hard copy. Many people still get their digital holiday snaps printed on silver halide paper at the supermarket. Leaving this uncertain peering into the future of imaging we should take time to celebrate the achievement of the refinement of silver-based materials resulting in the stunning images we have become used to enjoying. The level of performance of modern materials is nothing short of a miracle. Not only have several chance observations been involved in the story so far, but the sheer arithmetic of the chemistry of photography is remarkable as we shall see. Let us first look at some more details of image capture.

11.2.2 Silver Halide Photolysis

The silver halide, AgCl, AgBr, AgI and mixtures thereof, are all crystalline solids, being substantially insoluble in water, with pK_{sp} of *ca.* 10, 13 and 16 respectively. Photographic materials consist of a suitable support (polyester film, paper, glass) on which is coated one or more layers containing small crystals of silver halide (sizes varying from *ca.* 100 nm to 5 μm , depending on the application) prepared by carefully controlled precipitation methods. By controlling such factors as temperature, rate of addition and halide concentration, dispersions (or ‘emulsions’ as the photographic industry traditionally calls them) of silver halide crystals with specific composition, size, size distribution and morphology are reproducibly prepared on large scale (up to *ca.* 1000 mol or more of silver halide per batch). Precipitations are always carried out in the presence of a colloid stabilising agent, traditionally gelatin, which binds to the surfaces of the crystals, preventing agglomeration and, to some extent, affecting the final crystal habit. Gelatin is also

Early History of Photographic Technology

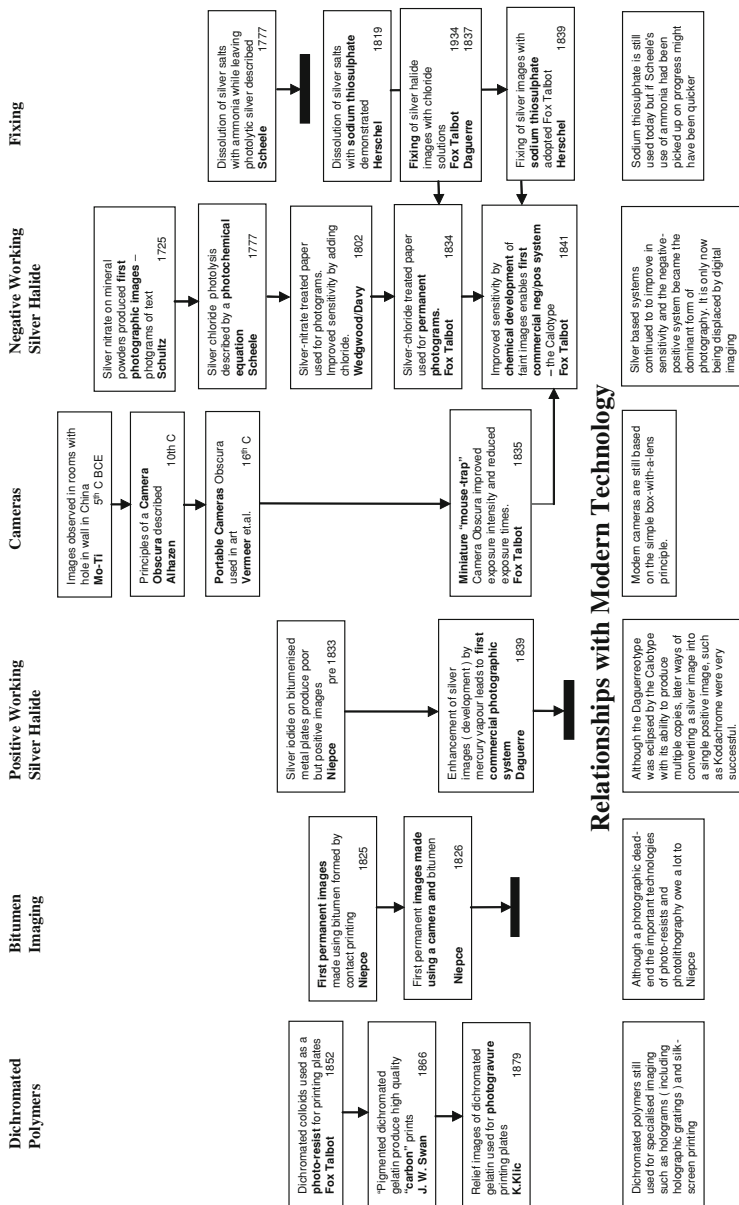


Fig. 11.5 A summary of the development of component technologies leading to modern photochemical imaging systems

the carrier medium for the coating stage, so that the various layers in a photographic material are actually layers of dried gelatin containing the various chemical components, including the emulsions, coated over the support material.

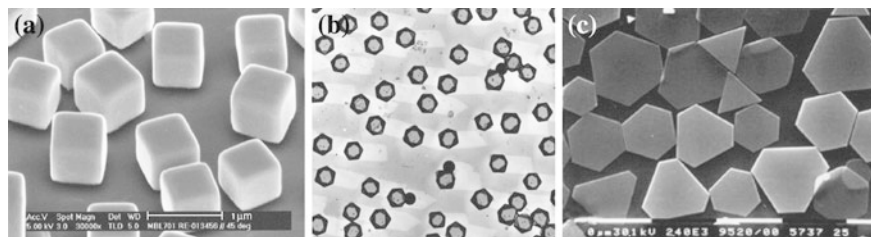


Fig. 11.6 Examples of silver halide emulsions. [Note: **a** and **c** are scanning electron micrographs of AgX crystals; **b** is a transmission electron micrograph of gold-shadowed carbon replicas of octahedral AgX crystals with the substrate fixed out]. Micrographs reproduced with courtesy of Eastman Kodak Company

AgCl and AgBr have face-centred cubic lattices (rock salt structure), while pure AgI adopts a variety of forms, including cubic sphalerite and hexagonal wurtzite, though a thermally unstable body-centred cubic form is also known to exist. In practice, most photographic products use AgCl, AgBr, or mixed phase Ag (Cl, Br) or Ag (Br, I) emulsions.

Figure 11.6 shows electron micrographs of some typical photographic emulsions, illustrating the variety of crystal shapes used. Emulsion choice depends on performance criteria dictated by the specific product application—considerations such as photographic speed (*i.e.* sensitivity to light), image contrast, processing factors (*i.e.* ease of development), image quality (graininess, contrast, tone scale, etc.) and cost all impacting on the final design.

All the emulsion types shown in Fig. 11.6 contain crystals with face-centred cubic lattice structure. The variety of shapes reflects differences in the rates of growth of [100] versus [111] faces and, in the case of the tabular grains in Fig. 11.6c the presence of crystallographic twin planes. The doubly-twinned crystals in (c) are particularly advantageous for the achievement of high sensitivity (camera speed) with minimal image graininess. These crystals, with their large surface area to volume ratio, combine a large capture cross-sectional area for light absorption with a relatively low mass per crystal. Thus, for a given coated mass of silver, there are more imaging centres per unit area, making for improved image graininess (or ‘granularity’).

In the absence of deliberately added growth modifiers, AgCl emulsions are invariably composed of cubic crystals. The natural morphology for AgBr is also cubic, but it is found that the presence of excess bromide ion during the precipitation inhibits the growth of [111] faces. Thus, a moderate bromide ion excess results in the formation of cubo-octahedral crystals with distinct [111] faces exposed at the corners. Increase the bromide ion concentration further, and regular octahedra can be produced (Fig. 11.6b). Still higher bromide levels encourage the formation of twin planes, with a progression from singly- to doubly- to multiply-twinned crystals as the Br^- concentration increases (Fig. 11.6c). The pattern for mixed halide crystals is broadly similar, with the presence of iodide in the lattice tending to push morphology somewhat further towards octahedral/twinned. Apart

from bromide ion, other substances are also known to be effective ‘growth modifiers’, influencing the final morphology of an emulsion by preferentially binding to one of other type of crystallographic face.

11.2.2.1 The Emulsion Precipitation Process

In the modern photographic industry, the precipitation process itself most often entails the continuous flow delivery of aqueous solutions of silver nitrate and alkali metal halide into a reactor containing an aqueous gelatin solution. Solution addition rate, temperature, halide excess and pH are all important variables and are generally tightly controlled to predetermined levels specific for a given emulsion formulation. It is also vital to ensure efficient high shear mixing of the incoming reactant streams as well as good bulk turnover of the reactant mixture. The silver and salt solutions are typically very concentrated (perhaps 3–4 mol dm⁻³). The precipitations follow a classic nucleation followed by growth mechanism. The mixing reagent streams constitute a zone of very high supersaturation, leading to the spontaneous formation of silver halide (AgX) nuclei. The initially formed nuclei are inherently unstable, being prone to dissolution *via* the Gibbs–Thomson effect. In a dynamic process called *Oswald Ripening*, the smaller particles redissolve and their material is deposited on other nuclei. Within fractions of a second from the start of the precipitation, the number of particles in the reactor increases, passes through a maximum and then falls to a stable number (provided reagent addition rate is properly controlled); from that point on in the precipitation, the final particle size (*i.e.* volume) is primarily a function of the number of moles of silver added to the reactor. Some emulsion preparations might involve several stages if, for example, a zoned halide distribution within crystals was desired or if the emulsion was to be of the ‘core–shell’ variety used for the direct positive (‘Reversal F’) process in which case two separate precipitation stages would be required.

All other things being equal, the final mean size of crystals in an emulsion depends on three main factors:

1. Reagent addition rate, especially in the early ‘nucleation’ stages of the reaction.
2. Net AgX solubility: influenced by temperature, halide excess (through the equilibria: $\text{AgX} + \text{X}^- \rightleftharpoons \text{AgX}_2^- + \text{X}^- \rightleftharpoons \text{AgX}_3^-$, etc.) or the presence/absence of another silver halide solvent (e.g. ammonia, thioethers etc).
3. The net number of moles precipitated (for a given nucleation regime).

By appropriate control of the precipitation variables, ‘monodisperse’ emulsions composed of crystals with near identical size (and shape) can be prepared. Such emulsions might be desirable for an application where very high contrast photographic response is required. Other product applications might call for a broader size distribution.

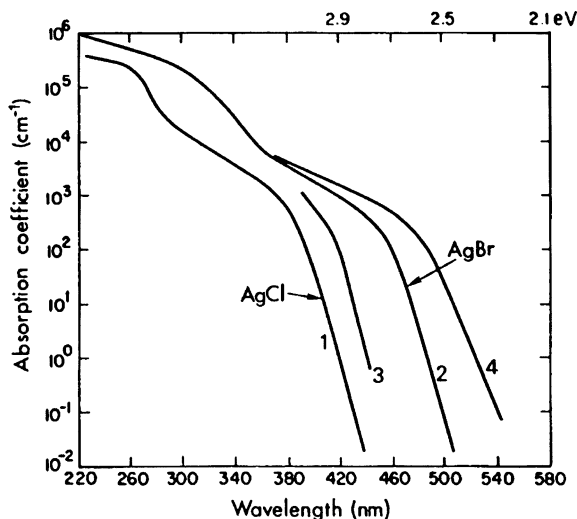


Fig. 11.7 Silver halides absorption spectra: (1) AgCl, (2) AgBr, (3) AgCl_{0.9}Br_{0.1} and (4) AgBr_{0.97}I_{0.03}. [Adapted with permission from Ref [22]. Copyright 1988, Taylor and Francis Ltd (tandfonline.com)]

11.2.2.2 Physical Properties of the Silver Halides

The silver halides are semiconductors, that is, their electronic structure is best described by the solid state model in which atomic orbitals overlap extensively to form occupied valence bands together with conduction bands that are unoccupied in the absence of external perturbation (*i.e.* in the dark at normal temperatures). All the halides absorb light in the UV region of the electromagnetic spectrum, with AgBr, AgI and mixed salts also absorbing into the visible out to *ca.* 500 nm (Fig. 11.7).

There are two main regions of absorption, corresponding to so-called ‘direct’ and ‘indirect’ transitions. The weaker absorption at longer wavelengths represents the indirect, forbidden transitions, which gain intensity *via* lattice vibrations (*phonons*). Absorption of a photon promotes an electron from the valence band to the conduction band, shown by the blue arrow in Fig. 11.8.

The silver halides exhibit photoconductive properties, since, electrons in the conduction band are mobile and free to migrate throughout the crystal structure. The positively charged hole left behind in the valence band is also mobile but with much lower mobility. The precise chemical nature of the hole species, h^+ , differs for each halide type. In the case of AgCl, the hole has been shown to be largely ‘self-trapped’, existing as a distinct Jahn–Teller distorted AgCl₆⁴⁻ species [20, 21]. In the case of AgBr, it is thought that the hole occupies a silver ion vacancy site from where it can migrate *via* an exchange mechanism to a neighbouring lattice site. The presence of silver ion vacancies is a consequence of the Frenkel defect whereby, at a given temperature, a certain number of silver ions are thermally

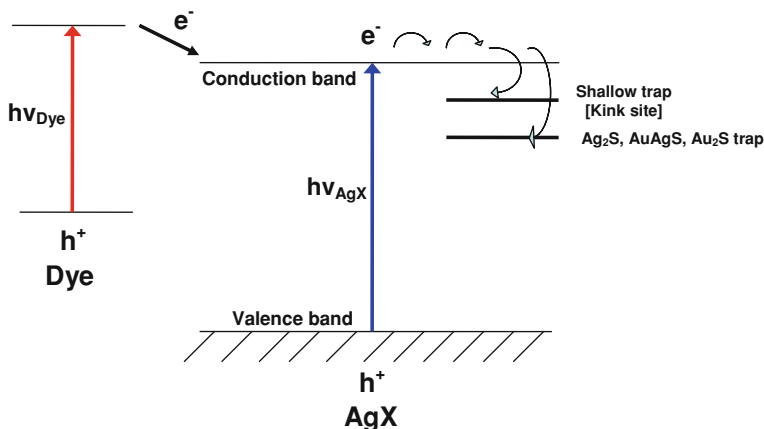


Fig. 11.8 Band model for silver halides

promoted from their normal lattice positions to occupy so-called *interstitial* sites. The defect may be considered to arise because of the significant difference in size (ionic radius) between the silver and halide ions, with Ag^+ being much the smaller. The equilibrium number of interstitial silver ions in AgBr is greater than that in AgCl , owing to the larger size of the Br^- ion versus Cl^- . The Ag^+ *vacancies* left behind experience a net negative charge, rendering them favourable for hole localisation. Interstitial silver ions are the carriers responsible for the dark electrical conductivity exhibited by the silver halides and, as we shall see, they play an important role in the photographic process.

11.2.2.3 Formation of the Latent Image

The photographic process relies on the fact that photogenerated conduction band electrons react with interstitial silver ions to produce clusters of Ag^0 atoms on the surface of an exposed crystal. With sufficient exposure to light, AgX materials will, in fact, darken, due to the formation of metallic silver. This process, called *print-out*, was actually exploited in some non-processable, low cost, recording papers to produce fairly low density black-on-white traces. The same print-out effect is used today in some silver chloride based photochromic glasses. The dark reversibility of the photochromism in this case is due to the total bleaching of the photolytic silver by the slowly diffusing positive holes such that there is no net conversion to Ag^0 . The substantially non-reversible darkening witnessed in gelatin-based coatings of AgX results from the scavenging of positive holes at the AgX surface by naturally occurring reducing moieties in the gelatin matrix.

Print-out materials are, of course, exceedingly 'slow' in a photographic sense, requiring a relatively large exposure to light in order to generate a visible effect. The miracle of modern silver-based photography is that images can be recorded

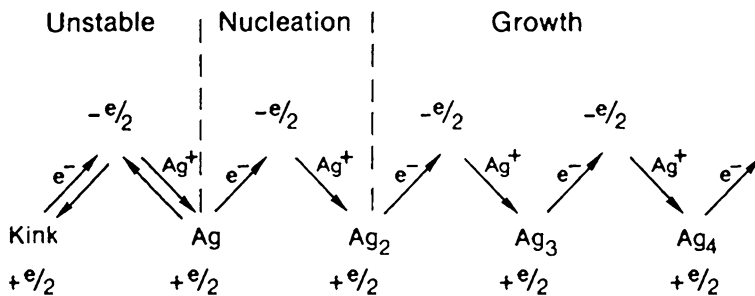


Fig. 11.9 The mechanism of latent image formation. [Adapted from Ref. [22] with kind permission from Taylor and Francis Ltd (tandfonline.com)]

with minimal exposure (and therefore very short exposure times for camera films). Such exposures generate no visible change in the recording medium until it is *developed*. It is found that clusters containing four or more Ag^0 atoms are effective catalysts for the chemical reduction of AgX particles to metallic silver by a solution of suitable reducing agent (the *developer*). The presence of one or more such developable clusters on the surface of an AgX particle constitutes a so-called *latent image*. The mechanism [22] by which latent image is believed to be formed is illustrated in Fig. 11.9.

The mobile conduction band electrons diffuse rapidly through the crystal until they find their way into shallow traps on the grain surface (Fig. 11.8). These traps are thought to be associated with crystalline imperfections that inevitably exist at the crystal surface as a result of incomplete ionic layers and partial co-ordination of lattice Ag^+ and X^- ions. These defects will carry a net electrostatic charge. Some of the kink sites on cubic [200] faces, for example, possess a net $+e/2$ charge, making them attractive trap sites for electrons. Once an electron is trapped there, the net electrostatic charge switches from $+e/2$ to $-e/2$ rendering the site attractive to mobile interstitial silver ions (Ag_i^+) and resulting in the formation of a silver atom: $\text{Ag}_i^+ + e^- \rightarrow \text{Ag}^0$ thereby resetting the trap charge to $+e/2$. A second electron may then be trapped at the same site, followed by reaction with another Ag_i^+ to give Ag_2^0 and so on.

Points to note about this mechanism are:

- Single silver atoms, Ag^0 , are unstable and require little thermal energy to re-ionise with the injection of the electron back into the conduction band.
- An Ag^0 atom at a kink site represents a slightly more favourable (*i.e.* deeper) trap for electrons than the original ‘empty’ trap.
- Ag_n^0 centres with $n \geq 2$ are relatively stable.
- Ag_2^0 and Ag_3^0 centres are *not* catalysts for development.

This mechanism, first proposed by Gurney and Mott in 1938 [23], helps to explain how an AgX crystal may be rendered developable by the absorption of a

very small number of photons. An important feature of the mechanism is the reversible nature of the steps leading to the formation of an initial Ag^0 atom (labelled ‘unstable’ in Fig. 11.9). In principle, a single Ag_4^0 cluster is capable of catalysing the development of the whole crystal on which it sits. Since typical emulsion crystals contain from 10^6 to 10^9 Ag^+ ions, this represents an enormous amplification factor. In practice, loss processes reduce the net quantum efficiency so that even in the most sensitive modern materials, crystals require the absorption of perhaps 10–15 photons to create at least one Ag_4^0 cluster.

11.2.2.4 Chemical Sensitisation

So far, however, we have only considered the performance of untreated AgX emulsions. Emulsions, as precipitated, are in fact not very sensitive to light—at least not by the standards of modern day photography. Untreated, or *primitive*, emulsions suffer from two major drawbacks: (a) inefficiencies in latent image formation and (b) lack of any sensitivity throughout much of the visible light region of the spectrum (see Fig. 11.7). This is why in the early days of photography those wishing to have their portraits taken would need to sit still for quite a long time! Following the explosion of interest in synthetic dyes initiated by William Perkin in the mid nineteenth century, it was soon realised that the sensitivity of photographic plates could be increased by adding certain dyes to the emulsions. This process of spectral sensitisation continued to be developed and investigated throughout the long history of silver halide photography (see Sect. 11.2.2.5).

Some of the early photographic plates probably also gained a little extra sensitivity from interaction with impurities in the raw materials (silver, halide salt, gelatin). One of those impurities was most likely sulfur since by the 1920s it was realised that by deliberately treating AgX grains with labile sulfur compounds (sodium thiosulfate being commonly used), their sensitivity to light could increase several-fold. This treatment, called *chemical sensitisation* or *chemical ripening*, is known to decorate the surfaces of AgX grains with clusters of Ag_2S . Sulfur sensitisation serves to enhance the electron-trapping capability of sites on the AgX surface, in part at least by slightly deepening the intrinsic traps provided by crystalline imperfections though the reversibility of the steps in Fig. 11.9 still applies. Some time later, in the 1940s, it was found that the inclusion of gold in the sensitisation could increase sensitivity even further.

The beneficial effects of sulfur + gold sensitisation can be best understood in the context of the loss processes which exist in unsensitised material. The two most important loss processes are (a) recombination and (b) image dispersity. The recombination of the primary photoproducts, electrons and positive holes, which competes with the formation of latent image Ag_n^0 clusters, is most likely to occur at either very high or very low light intensities. At high intensities, the high concentration of holes and electrons within a crystal enhances the probability of second order encounters. At low intensities, the electrons will spend more of their time in

the conduction band, owing to the reversible nature of the initial steps in the latent image formation process (see Fig. 11.9), thereby increasing the probability that they will encounter a trapped hole before a stable Ag_2^0 centre can be produced. Another adverse effect of high intensity exposures is the excessive number of different sub-developable Ag_2^0 and Ag_3^0 centres that form as a result of dispersity, i.e. too many different stable centres competing for photoelectrons. The loss processes occurring at low and high intensity exposures are examples of so-called *reciprocity failure*, whereby the quantum efficiency of latent image formation is reduced. Sulfur sensitisation mitigates against both these loss processes to some extent by ensuring more rapid electron trapping and increased stability of electrons in shallow trap sites. Gold is believed to make little difference to trap depths, its main role being to enhance the catalytic ability of the latent image centres at the development stage, thereby significantly reducing high-intensity reciprocity failure by rendering smaller Ag_n^0 centres developable. Certain transition metal dopants, generally introduced during the precipitation stage, can also help to offset reciprocity failure effects. For example, Ir(III) dopants act as temporary shallow electron traps. Such traps will release their electrons relatively slowly back into the conduction band, making a high intensity exposure resemble a lower intensity exposure with regards to the rate at which Ag_n^0 centres are nucleated, thereby reducing dispersity losses.

11.2.2.5 Spectral Sensitisation

The net effect of successful chemical sensitisation is to increase the sensitivity of AgX materials by >10X. This statement applies to the situation in which light is absorbed directly by AgX. Whilst sulfur sensitisation imparts a very low level of light absorption at longer wavelengths, which may have benefited the early pioneers of photography, the use of dyes is essential for achieving good spectral sensitivity throughout the visible (and into the infrared) region. Furthermore, it is necessary to be able to *selectively* sensitise emulsions to the blue, green and red regions in order to faithfully reproduce the colour information in a subject. The class of dyes found to be most effective for this purpose are the cyanines (see Chap. 4 for some examples). During the century and more that commercial photography has been in existence, literally thousands of cyanine dyes have been synthesised and screened for their possible application. Of these, only a relatively small number ever appeared in products. The great number of variables in the molecular architecture of dyes allows fine-tuning of their spectral properties. A typical vinylogous series of dyes is illustrated in Fig. 11.10a.

Many dyes have a tendency to aggregate. One class of aggregate, called *J-aggregates*, have characteristically sharp absorption spectra, making them particularly useful for sensitising in a narrow spectral region (see Fig. 11.10b). In addition to their spectral characteristics, other important dye properties include the degree of adsorption to silver halide surfaces (which depends on halide type and crystal habit) and solubility, whether organic solvent- or aqueous-based.

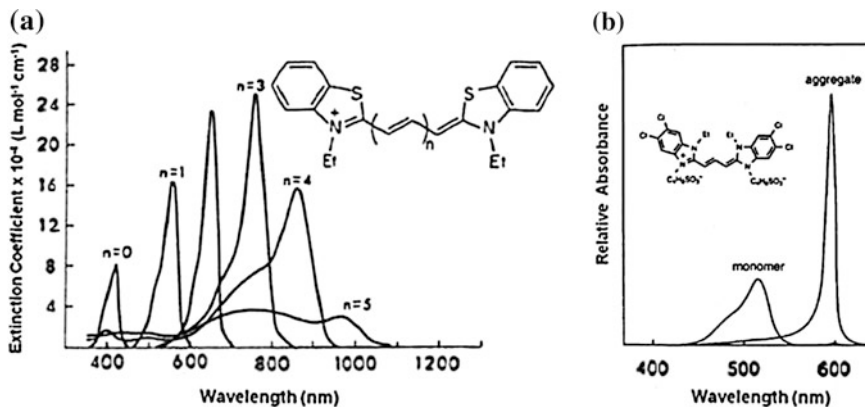


Fig. 11.10 Absorption spectra of cyanine dyes. **a** Absorption spectra of a vinylogous series of cyanine dyes in methanol solution [Adapted with permission from Ref. [62], p 197]. **b** Absorption spectra of monomeric and aggregated forms of a cyanine dye in solution. [Adapted with permission from Ref. [62], p 219]. Copyright 1977, Macmillan NY; Copyright 1989, jointly Macmillan NY and Eastman Kodak Company

The mechanism of spectral sensitisation has been shown to involve the direct transfer of an electron from the excited state of the dye into the AgX conduction band (see Fig. 11.8). In confirmation of this mechanism, excellent correlation has been demonstrated between the sensitisation capability of dyes and their electrochemical reduction potential. For the most efficient dyes, the quantum yield of the electron transfer step is close to 1.0. Using picosecond laser pulse excitation to measure the fluorescence decay rates of dyes adsorbed to AgX crystals, it has been shown that the electron transfer is very fast, with rate constants in the region of 10^{11} s^{-1} having been reported [24]. Once an electron has been transferred into the AgX conduction band, the latent image formation process ensues more or less as it does following direct absorption by AgX itself. The difference in the case of the dye-sensitised process is that the positive holes are trapped at the dye molecules.

Although chemical and spectral sensitisation markedly improve the yield of latent image silver centres for a given amount of absorbed photons, the photographic industry pays little attention to directly managing the fate of the positive holes produced on exposure. Apart from the few that are lost in recombination events, the holes either diffuse slowly to the crystal surface (following direct absorption by AgX) or are trapped temporarily at a dye molecule. Thereafter, they may be released as halogen or are consumed in chemical reaction with gelatin moieties. Hole attack on latent image centres, though possible, generally occurs with low probability in efficiently sensitised materials. At high surface coverages of certain *J*-aggregated dyes, migration of the dye-trapped hole through the dye layer is known to exacerbate latent image bleaching.

11.2.3 Photographic Development

11.2.3.1 Development of the Latent Image

The early silver halide systems for capturing images were very slow, requiring long exposure times to produce a sensible image. To make commercially successful consumer photography systems, camera shutter times needed to come down from the hours and minutes of early systems to fractions of a second. Sensitisation of the halide crystals was part of the story, but an equally important factor was the ability to take the tiny physical images formed in camera and make them useful at a later stage. This is the development process, where the latent image consisting often of clusters of only a few atoms could be converted into thousands of millions of atoms, and rendered visible to the eye. Typically the amplification factor in this process was of the order of 10^8 – 10^9 . In modern emulsions it takes only approximately four atoms of silver to make a latent image developable.

The key to this process is the catalytic effect of small clusters of metallic atoms on the surface of a silver halide crystal, which enhance the rate of reduction of the silver halide to metallic silver by a reducing agent (developer). This catalytic effect allows whole grains or crystals to be fully reduced to metal while neighbouring grains, without this catalyst, remained unreduced. This discrimination-between grains with latent image as opposed to those without-is only possible due to the differential rate of reduction caused by the catalytic effect. By tailoring the developer composition in combination with a fixed development time, temperature and pH, better and better discrimination was enabled along with shorter process times.

It should be said that development of the latent image can occur by virtue of the reduction of the original light sensitive silver halide either by virtue of the catalytically enhanced reduction rate described above (known as *chemical development* in the 'trade') or by the use of the catalytic action on a soluble silver salt introduced simultaneously with the reducing agent or by virtue of solubilising the primary halide and effecting reduction from it in its solubilised state. This is known as *physical development*. Physical development can be carried out either before fixation (see later) or post fixation; the latter is clearly not an option for chemical development. Despite the name, it is, of course, still a chemical development process.

The physical chemistries behind these processes are complex: the rate of development is dependent on many factors which include the nature [25] of the catalytic speck itself, its size, the reduction potential (See electrochemical explanations, for example [26, 27]) of the developer composition and the agitation of the process [28] to prevent undue concentration depletion. It also depends on the stage of the development process: typical negative emulsion systems are characterised by a slow initial rate (often referred to as an induction period) followed by a rapid acceleration and a final slowing as reagents are depleted. Many different compounds have been explored as developers alone and as combinations. Some combinations provided advantages in rates of development [29] compared to

expectations based on rate measurements of the components of these mixtures alone. (This is referred to as *superadditivity*). Development kinetics follow several stages depending on the process; typical chemical development of negative emulsions lead to a form of silver metal known as *filaments*. These hair-like strands of silver metal are the result of a growth pattern which typically starts as spherical, as the silver atoms are formed at a rate which is slow enough to allow them to diffuse uniformly over the surface of the expanding metal speck, but which suddenly explodes in rate and changes in configuration when the surface area becomes able to generate new silver faster than it can diffuse over it to maintain sphericity. At the very inception of development, with tiny latent images, Gibbs free energy (excess energy due to small size-Gibbs-Thomson [30] equation) plays a role in altering the effective reducing strength of the developer, allowing a relatively rapid expansion despite the small area of the developing speck. When the size is large enough to make this effect disappear, but is still small enough to continue spherical development, the development rate, although accelerating, is now at its slowest and it is thought that this phase is the cause of the observed 'induction period'.

Successful developing agents are characterised by having oxidation potentials within a specific range. Too strongly reducing in potential would cause non-exposed grains to be reduced while too weakly reducing would cause development rates to diminish below practical use. Experiments with redox buffers of constant and defined oxidation potential showed what the useful range was—already discovered empirically [31]. An example of a common black and white developer, cheap and available in large quantity, is hydroquinone, and this combined with a relatively recent discovery as a developer [32], phenidone, is a good example of the synergistic combination of two developers to produce a development rate greater than the sum of the rates for each developer used alone (superadditivity). For more on development kinetics and a discussion of the influence of the swelling of the matrix (gelatin), diffusion, temperature, superadditivity and pre-treatments of the latent image (such as latensification) see Ref. [6].

Consumer photographers have typically used the word "development" to mean the whole process of turning exposed film into useful images—usually prints. However to the technician, the development stage is the initial part of the process to amplify the latent image. The amplified image is not useful until stabilised and this requires the process of *fixation*, mentioned earlier in discussion of physical development. Residual unreduced silver halide must be removed to prevent its gradual darkening on exposure to light (printout) and if a colour image is to be generated, the developed silver must also be removed. Residual chemicals must be washed from the gelatin layers and the film must be dried without leaving optically interfering marks. These processes have their own complexities—but these are perhaps a step too far for the purposes of this chapter.

11.2.3.2 Extensions of the Development Process

The development of silver halide can be exploited in an impressively large number of ingenious ways. For example the now obsolete Dufay Colour and Polachrome film materials used R, G and B filter arrays in combination with a panchromatic (having sensitivity covering the entire visible spectrum) silver halide layers which were developed to give positive silver images which viewed through the same filter arrays gave full colour images [33].

The majority of systems, though, make use of the oxidised developing agent resulting from silver image formation to provide a number of useful imaging effects. A complete survey of such effects and products is not possible here and since these extensions of the development process involve no photochemistry they will not be discussed in detail. Nevertheless, these chemical chains of events, are enabled by the initial photolysis of the silver halide crystal leading to useful consequences and to a variety of important photographic systems and applications, so a few of the more important examples will be described briefly below.

Chromogenic development. The most obvious extension of the development process is probably the production of dyes, and the consequent ability to form colour images. Most colour photographs have been produced in this way. The first system based on chromogenic development was Eastman Kodak's Kodachrome system introduced in 1935. After an initial black-and-white development of the negative image the remaining undeveloped silver halide provided the oxidative driving force in subsequent colour forming stages. Because the dyes were formed where silver halide remained after the initial non-chromogenic development of the negative image, the resulting colour image was positive. These stages used a processing solution containing both a developer and a compound, which on coupling with the oxidised developer formed a dye. Both coupler and developer were soluble, but the dye formed from them was insoluble and remained near the silver halide crystal, which provided oxidised developer.

Selective exposure or *fogging* of each of the three layers sensitive to blue, green and red light allowed each layer to be developed separately. The blue-sensitive layer generated the complimentary yellow (blue-absorbing) dye, the green-sensitive layer formed the magenta dye, and the red layer formed the cyan dye. Bleaching of the silver back to silver halide and its removal by a solubilising fixing agent left a high quality colour image.

The first, hugely complicated, Kodachrome process was replaced by simpler forms, which still remained very complicated and difficult to control. Despite the difficult process, Kodachrome remained available until 2009. Soon after its introduction more easily processed colour films were introduced, for example, the Kodacolor system in 1942. In this system the coupler molecules included a *ballast*, a bulky oleophilic group which allowed them to be dissolved in a substantially hydrophobic solvent. The resulting solution could be dispersed in a gelatin solution by an emulsifying process and incorporated into the layers of the photographic material. These *incorporated coupler* films soon dominated the market. Modern systems use *N-N*-disubstituted *p*-phenylenediamine developers. Cyan dyes are

formed using phenols or naphthols. Magenta dyes are derived from pyrazolones or pyrazolotriazoles and yellows are formed using couplers containing an active methylene group, which is not part of a ring such as benzoylacetanilides.

All three colour-forming layers are developed simultaneously. When the colour image is formed during the development of the latent image these systems are negative working and require a partner colour negative print material to produce a positive colour image. Alternatively, a *reversal* process using a first black and white development step, followed by fogging and chromogenic reduction of the initially undeveloped silver halide to produce a positive colour image.

Tanning development. A number of silver-based imaging systems use oxidised developer to cross-link the gelatin matrix to produce and exploit a difference in physical behaviour between exposed and unexposed regions. This can be for example, hydrophilicity. The so-called *tanning developers*, such as hydroquinone and similar di- and tri-hydroxy benzenes, are oxidised to quinones which are capable of reacting with the amino groups of gelatin resulting in cross-linking. Areas where silver development occurs become harder and more hydrophobic, and therefore more receptive to oil-based inks, while undeveloped areas repel ink. Low-cost printing plates can be produced in this way.

In 'wash-off' systems the hardened areas of gelatin layers can be made to adhere to the support while unhardened areas when washed with warm water are removed completely. The resulting images are suitable for line images since the image is either of maximum or minimum density.

Perhaps the most familiar use of differential hardening is the Technicolor process. There have been various forms of Technicolor systems over the many decades of its use in cinematography. Originally, special cameras, which split the image into three different spectral regions, were employed despite their complexity and cost. The last generation used the same colour negative film stock to generate three (red, green and blue) images on a set of black and white films. These were exposed through their supporting film bases. The films included non-photographically active dyes to control the penetration of light so that only the highest exposures reached the top-most silver halide crystals. Development in a tanning developer resulted in gelatin hardening only next to the base with low exposure building up to complete hardening as exposure levels increased. After fixing, the films were washed in hot water which removed the gelatin which was insufficiently hardened to prevent dissolution.

The films were then soaked in dye solution, cyan dye for the film with red image information, magenta for the green and yellow for the blue. The dye-soaked layers were then contacted with a receiving layer in accurate register to form the final positive image. Technicolor was, for a long time, the preferred method for generating multiple copies of films because the intermediates were relatively cheap but in recent times its complexity and the lowering costs of silver halide print films have led to its displacement.

The related large-format products exploit an important aspect of the dye-transfer technique. The dye-transfer system allows a far wider selection of dyes than chromogenic dyes which are generated *in situ* during the development process. In particular, very stable dyes of excellent hue can be used to produce

high quality archival images. The control which the complexity of the process allows is valuable to some practitioners who consider the images achieved to be of the highest possible quality.

Other Colour Systems

Silver dye bleach. Chemical processing of silver halide materials can also be used to destroy dye. The azo-dye-bleach process [34] used in Ilfachrome (formerly Cibachrome) uses the developed silver to reduce azo dyes to colourless amine compounds. Positive images of high quality and excellent stability can be produced. These materials have long been popular with photographic artists for this reason.

‘Instant’ Colour Films. The Polaroid Corporation’s instant films provided a remarkable breakthrough in photography. We have seen that early photographers carried their materials and processing equipment with them as well as their cameras. Edwin Land challenged himself with integrating a processing laboratory into a small portable camera, about the same size as Talbot’s ‘mousetrap’ camera. The developers were incorporated into the film’s layers. Each developer was chemically attached to a dye of a colour appropriate to the silver layer it developed. As with Technicolor, this enabled the use of dyes which could be selected with less restrictive criteria. Very stable metallised dyes were used in later versions.

After exposure, processing was achieved by passing the film pack through rollers. This burst a pod containing a viscous alkaline solution, which was spread uniformly between the light-sensitive layers and a dye-receiving layer. The success of the system relied on control of the diffusivity of the dye-developer. On development, the oxidised dye-developer became relatively insoluble. The diffusion rates of the dye developers through the multilayer coatings to the image receiving layers was sufficiently slow that by the time they had travelled through adjacent layers sensitive to other wavelengths than those appropriate to their hue, these layers were developed and the three separate colour images did not significantly interfere with each other. This independence of the three colour channels was helped by using auxiliary developing agents which shuttled electrons between the dye developer and the developing silver crystals and speeded up development in each layer. Since silver development prevented the diffusion of dye-developer to the image-receiving layer the system was positive-working.

Polaroid’s film product technology was initially developed and manufactured by Kodak until Kodak decided it needed a comparable product and this required the invention of a different type of development chemistry. In Kodak’s PR10 ‘Instant Colour’ films a B and W developer was used and its oxidised form, created by silver development, oxidised an immobile molecule called a *redox dye releaser*, which then released a mobile dye [35]. Where development occurred dye was released to a receiving layer and this required new positive working emulsions, described in Sect. 11.2.4. The arrival of digital photography provided an alternative to the gratification of instant photography without the limitations and expense of instant films so they have all but disappeared.

11.2.4 Direct Positive Emulsions

Another of the many chance observations made during the history of photography led to silver halide emulsions which worked in a *positive* sense, *i.e.* when imaging light exposed the crystals they do not develop whereas unexposed crystals do. E. B. Knott working at Kodak in Harrow had exposed some film and was processing it when he accidentally switched the dark-room lights on. A positive image resulted. This was later explained by a colleague, G. Stevens. The emulsion Knott was using had high internal sensitivity due mainly to a rather chaotic crystal structure, providing effective trapping sites for electrons released by exposure. At moderate exposure levels only internal latent image was formed. The crystals did not develop in developer solutions which did not dissolve or disrupt the crystals and therefore detected only the surface latent image.

In the wet conditions of the developer solution however the trap sites on the surface became more effective. This meant that when exposed during development, the unexposed crystals, instead of producing internal silver, produced surface silver at sites previously uncompetitive with the internal sites. On the other hand, crystals which already had internal silver produced from the image exposure, continued to trap photoelectrons internally because the accumulation of silver at the trap sites made them more effective traps than those on the surface despite the change in exposure conditions. They therefore did not develop. A direct-positive system was thus discovered [36].

This understanding of the observation later led to the design of relatively defect free crystals with carefully controlled internal and surface sensitivity through chemical sensitisation. Crystals of silver bromide were precipitated and treated with sensitisers. Further deposits of silver bromide then buried the sensitivity centres. Figure 11.6b shows the resulting monodispersed crystals. These direct positive emulsions designed by F. Evans [37–39] were probably the first commercially exploited examples of crystals which were so perfectly formed and uniform. Previous emulsions contained a mixture of shapes and sizes due to relatively uncontrolled precipitation processes.

The role of the non-imagewise exposure in *Reversal F* emulsions is to produce conduction band electrons. Developers are very mild reducing agents and unless silver halide solvents such as thiosulfate are present or the crystal structure is disrupted by, for example, iodide, they only reduce silver halide at a significant rate when surface silver is present. Stronger reducing agents will provide electrons less discriminately, for example, hydrazides [40]. In this context these are usually referred to as nucleating agents and they provide the same effect as a non-imagewise exposure. This is done conveniently by including them in developer solutions or even more so by incorporating them in the photographic layers. These positive emulsions found application in Kodak's PR10 Film [41] and the related Ektaflex print materials. (See 'Other Colour Systems', above.)

11.2.5 X-Ray Imaging

One might expect that materials which are sensitive to electromagnetic radiation in the UV/Vis region are also responsive to more energetic radiation and this is indeed usually the case. Ionising radiation such as X- and gamma rays produce latent image silver in silver halide crystals. The initial interaction of such rays with exposed material, results in the generation of free, energetic ‘primary’ electrons. If the photon energy of the radiation is low it is possible that the photon is absorbed but has sufficient energy to eject an energetic *photoelectron*. Higher energy photons are more likely to give up a portion of their energy and be deflected while also producing an energetic electron, a process known as the *Compton effect*. The likelihood of ionisation depends on the density of electrons in the exposed material so silver bromo-iodides are preferred to the lighter halide combinations. Subsequent ionisation events are then caused by the interaction of the primary electrons with their source crystals or other crystals within their reach. On each occasion the electrons lose energy and eventually become incapable of further damage. The main differences from light exposure is that the initial photon and the released electrons are very much more energetic than light by up to about four orders of magnitude and that the energy is deposited effectively instantaneously.

Directly exposed X-ray films are used for what are known as ‘industrial’ applications such as searching for cracks in metal objects, for example oil pipelines. The films can be made handleable in light by packaging with light-opaque materials. An improvement in efficiency can be achieved by placing the film, in particular the coated side, next to a ‘screen’ made from a heavy metal such as lead. The screen absorbs X-rays more effectively than the film providing primary electrons some of which can expose the film. This indirect exposure supplements that achieved by direct exposure.

A much greater improvement to sensitivity is obtained using a fluorescent screen to convert the X-ray energy to light, which is then used to expose silver halide film. About 5 % of X rays are typically absorbed in directly exposed films. Intensifying screens can absorb up to 60 % of the incident X-rays, two screens are often used, one on each side of the film.

The screen materials are made from a variety of heavy metals compounds such as oxides, sulfides, aluminates or silicates of metals such as zinc, cadmium and tungsten. More efficient phosphors use lanthanides. The materials are usually ‘activated’ by dopants such as silver, copper and europium. These allow fine-tuning of the emitted wavelengths and optimisation of the efficiency of the materials. Typical materials are: M_2O_2S where M is Gd or La, doped, for example, with Tb, Eu, or Pr, or $Y_3(Al,Ga)_5O_{12}$ doped with Ce or Tb (see [Chap. 4](#) for more information on solid-state lanthanide phosphors).

The screen materials respond initially to X-rays in a similar way to that of directly exposed silver halide layers except that the excited screen compounds produce emitted light rather than the chemical change resulting in latent image. Interaction with the energetic electrons produced by the X-rays promotes valence-

band electrons to the conduction band or to levels below the conduction band provided by the dopants. The return of the electrons to the ground state provides the opportunity for emission of light.

The emitted light is efficiently harvested by spectrally sensitised film. In medical applications this increased sensitivity is an important contribution to reducing the doses of radiation suffered by the patient and/or to improving image resolution.

11.3 Non-Silver Imaging Systems

Over the last few decades there has been a fascinating technical and commercial battle between technologies competing to be dominant in the digital colour print market. It is still raging. During this period the lead in terms of commercial importance and predicted eventual pre-eminence has changed many times as technological progress has been made. Silver halide paper remains a major player despite predictions of its demise over 30 years ago.

Two other major technologies, ink-jet and thermal dye transfer (sometimes erroneously referred to as *dye sublimation*) systems are widely used but no photochemistry is involved so these will not be discussed further. Also omitted for the same reason is the thermal Autochrome system developed by Fuji for small-scale digital imaging.

Photochromism is discussed in [Chap. 4](#) and photopolymerisation as applied to photo-fabrication and printing is dealt with in [Chap. 13](#). Electrophotography does involve imaging with light even though no actual photochemistry occurs so it will be discussed briefly due to its commercial importance in imaging. Before doing so, we should also look at photochemical systems which have been largely supplanted by electrophotography and digital imaging technology but which once had an important place in commercial imaging.

11.3.1 Cyanotype Printing

Whenever we talk about a technical drawing describing a plan from which an object could be made, we use the term *blue-print*. Originally called the *Cyanotype process*, this imaging method was invented by the prodigious Sir John Herschel [\[42\]](#) in 1842. It is therefore almost as old as silver halide photography. At that time, and for a long time since, it had some advantages over silver based systems. For example, it was inexpensive to produce and relatively easily processed. Herschel used Cyanotypes to make copies of his own notes. It was, in fact, the system used in the first photographically illustrated book [\[43\]](#).

The Cyanotype process is the most successful of a family of imaging methods based on the photochemistry of iron compounds. The basic system involves the photochemical formation of the pigment Prussian Blue or iron(III) hexacyanoferrate,

which explains the name of the process (see Chap. 4). Ware [44, 45] has described a number of sensitising formulations using various ferric complexes of carboxylic acids including the commonly used citrates. He illustrates the photochemical imaging step with reference to ferric oxalate. On absorption of UV or blue light an electron is transferred from the oxalate ligand to the Fe(III) and the oxidised oxalate decarboxylates. The released Fe(II) reacts with potassium ferricyanide to give the permanent blue imaging pigment.

The exact nature of the imaging pigment produced, that is, the chemical make-up, the degree of hydration and the physical form, particularly particle size, depends on the starting materials, the preparation and the post-exposure treatment of the coated materials [46]. The formation of the intermediate Fe(II) can be also used to reduce metallic compounds including those of platinum to produce metallic images. Using gold chloride, Herschel produced purple images of metallic gold in the process he called the *Chrysotype process* [47]. Cyanotypes and the variations on them are still produced today but mainly for artistic purposes.

11.3.2 *Diazotype Prints*

Cyanotype blue-prints were, for about a hundred years, the dominant method of copying engineering drawings but they were displaced by *diazotype prints*. These were sometimes referred to as *white-prints*. Originally described in a patent in 1890 the first commercially successful system did not emerge until the 1920s, when the German company Kalle began to coat and sell products, expanding to England in 1926 using the trade name Ozalid. By the late 1940s diazo copying had largely replaced blue-prints.

Diazotypes rely on the destruction of a component in a reaction to form a dye, namely a diazonium salt. This was coated on paper or film alongside a phenolic compound under acid conditions. After contact exposure to intense UV irradiation the diazonium salt remaining, by virtue of being shielded from the light by the dark areas of the original, is allowed to couple with the phenol to produce dye by raising the pH. This was originally done by exposing the diazo material to ammonia vapour. The system had a number of significant disadvantages. The dye images were not stable. The ammonia or alternative amines needed to be vented from the working environment and two-sided originals could not be copied. These problems caused the system's eventual replacement by the more convenient electrophotographic methods emerging during the 1960s. Also, before these systems completed the take-over of office copying technology, silver halide systems such as Kodak's Verifax system, based on silver halide and tanning development avoided the problems with diazotypes albeit at higher materials costs.

During irradiation of the diazonium salt, nitrogen is generated. If the salt is coated in an appropriate transparent matrix, small bubbles of nitrogen are produced and these have been used to produce opaque areas which when viewed with specular light, provide dark image areas by scattering light away from the line of sight. The process was simple, materials are cheap and quite good resolution was possible.

11.3.3 The Mead “Cycolor” System

This ingenious system may have been the first application of visible light photo-initiation of polymerisation [48, 49]. The system has the considerable merit of ease of processing, at least as simple in practice as Polaroid’s and Kodak’s instant films. These are much more complicated, chemically and physically, as described in Sect. 11.2.3. Cycolor by comparison is simplicity itself, though lacking the exceptional sensitivity of silver halide materials it is only suitable for making prints.

As with any three-colour photographic system three dyes need to be deployed in an image-wise manner. Cycolor used a single coating containing micro-capsules which were called *cyliths*. Each cylith included a chromogenic compound, in this case a leuco dye, a photopolymerisable compound, namely, a functionalised acrylic monomer and a polymerisation initiator. On absorption of light, a single electron transfer to the singlet excited state of the dye from a partner borate ion occurs. The consequent boranyl radical initiates polymerisation. The initiators, dye-borate ion salts [50], typically cyanines are selectable and/or tuneable to provide the desired spectral response by means of the number of conjugated alkene units linking the fused heterocyclic end units. Blue-, green- and red-sensitive initiators can be then selected to provide three types of cylith. Each type included an image dye in *leuco* form which could be converted to a dye of a hue corresponding to the hue of the initiating dye. On exposure to a three-colour image each cylith hardened to a degree dependent on the amount of the light absorbed.

The processing step involved simply the compression of the exposed layer to rupture the cyliths and developer capsules and squeeze out the contents. The amount of *leuco* dye released depended on the degree to which the cyliths were hardened. Image dye was then produced from the *leuco* forms by the action of developers [51]. In the most compact formats of the system, the developer were encapsulated and coated in the same layer as the cyliths. The system did not reach the necessary quality/permanence/cost criteria to make it commercially viable in the longer term and so it remains a clever curiosity and unfortunately another imaging blind alley.

11.3.4 Dichromated Gelatin/Polymer Systems

The late 1830s was the time when silver-based imaging systems were emerging from the laboratories of such as those of Fox Talbot, Herschel and Daguerre. It must have been a time of intense activity as attempts to find other better systems were made. Herschel’s Cyanotype, based on iron salts is an example. Another metal, chromium, formed the basis of a number of useful printing methods some of which are still in use today.

The early dichromate materials used gelatin or albumen. Gelatin is still used today as well as polymers such as poly(vinyl chloride) (PVC) and poly(vinyl alcohol) (PVA). The first systems stemmed from the observations by a number of

people, including the Scottish experimenter Mongo Ponton [52], of the light sensitivity of materials treated with potassium dichromate. It was the ubiquitous Fox Talbot who first combined dichromates with colloids such as gum arabic and gelatin in 1852. The exposure-dependent hardening effect was used to control the diffusion of etching solutions through gelatin layers coated on metal printing plates. The more deeply an area was etched the more printing ink it retained and transferred to the paper print.

On exposure to light, dichromated gelatin becomes hardened or *tanned*. The photochemistry of this process does not seem to have been studied extensively until relatively recently including studies by Bolte *et al.* The initial reaction involves the photo-reduction of Cr(VI) to Cr(V) by amino groups in the gelatin. Further reduction to Cr(III) follows, and then the metal ion hosts the ligands provided by gelatin resulting in cross-linking and consequent hardening [53]. A similar mechanism is proposed in systems using polymers such as PVA, which do not contain amino groups [54, 55]. In PVA Cr(V) seems to be stable enough to participate in the cross-linking effect, at least temporarily.

In 1855 Lois Poitevin added a pigment, carbon, to the gelatin or mixtures of other natural gums. It took almost a decade and several experimenters to devise a commercially practical system. In 1866, J. W. Swan supplied 'carbon tissue' which was a thin paper coated by the user with sensitised pigmented gelatin. This was exposed when dry to a negative then contacted with a second paper sheet coated with clear gelatin. The first paper tissue was then stripped off and the exposed pigmented gelatin layer developed with warm water, revealing an image directly. These were known as *carbon prints* and the materials were improved to a stage when the image quality was remarkably high. This is due to a number of factors. The imaging layer is substantially non-scattering and can retain fine image detail. The photochemically active element is molecular, rather than a dispersion of crystals as with silver halide and the hardening effect proceeds in a linear fashion over a wide range of exposures resulting in accurate tone reproduction.

A number of printing techniques were enabled by dichromated gelatin. Most, such as *intaglio*, *aquatint* and *photogravure* methods involve the use of the material to produce relief images which could be inked to provide printing plates. More recently, dichromated gelatin has been used in silk-screen printing. It is applied to the screen material and exposed and washed with water. In exposed areas the holes between the fabric's fibres are blocked while unexposed areas allow ink through to the surfaces to be printed, ranging from paper and fabrics to metals.

Today, the main interest in dichromated polymer systems lies with holographic applications including the generation of diffraction gratings. The photochemical process is molecular, not amplified by a subsequent chemical step as in silver halide processing. Only the fact that macromolecules such as gelatin or PVA are involved provides some response beyond the simple molecular scale. This characteristic becomes a strength when exposure levels are unimportant. Then, the high optical resolution of a molecular process becomes an asset. For this reason dichromated polymer systems remain in use today having started life earlier than any photochemical system other than silver halide photography.

11.4 Electrophotography

The electrophotographic process is a major imaging system which dominates office copying, and, as image quality improves, is making inroads into the mainstream photomechanical printing industry. Although no chemical changes as such are involved, in view of its current importance and its commercial potential in imaging it is briefly described here. A thorough account of the technology and photophysics is provided by Weiss *et al.* [56].

The original invention was made by Chester Carlton and a patent applied for in 1939 [57]. Carlton coined the name *Xerography* (*dry printing*). Following the involvement of the Battelle Institute supported later by the Haloid corporation of Rochester, New York, the first commercial copier appeared in 1949. Twenty years later the company changed its name to the Xerox Corporation.

Modern printers have been made simpler, less expensive and more capable in terms of both versatility and speed as well providing good quality colour images but the basic principles of the system remain the same. The core of the system is a photoreceptor belt or drum. This is coated with a metallic conductive layer at earth potential. In the case of the commonly used organic photosensitive materials, a second layer, the charge-generating layer contains photoionisable molecules such as, phthalocyanines, perylenes or squarines (see Chap. 4). Above this a charge-transport layer is coated using for example poly(N-vinylcarbazole) which provides a conductive path at very high electric fields (Fig. 11.11).

Charge is applied to the belt by contact with a charged metal roller or exposure to a corona-generating charging unit. The latter includes a series of isolated wires at high voltage, typically ~ 6 kV, which generate a flow of ionised air molecules which then charge the surface of the belt to typically 600 V. During image

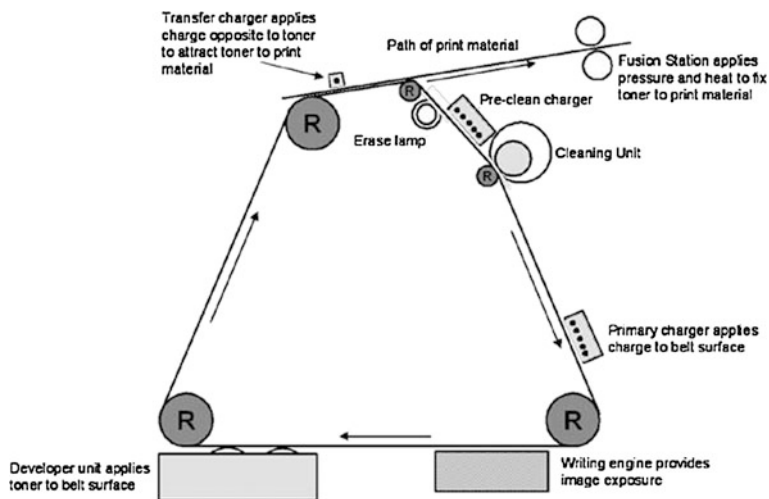


Fig. 11.11 A simplified diagram of an imaging mechanism in a typical photocopier

exposure light generates photoelectrons which are removed by the conducting sub-layer on the belt. The holes generated are transported through the upper layer and neutralise the surface charge. Today, the exposure is normally provided by digitally-controlled writing engines using lasers or LEDs.

Once the imagewise surface charge is produced it can be decorated by pigmented ‘toner’ particles. This is done by charging the particles using a *tribocharging* process. Often the toner particles are transported to the belt surface by using larger magnetic ‘carrier’ particles. These are mixed with the toner particles and the mixing process produces a transfer of charge from the toner particles to the carriers. The toner particles achieve a voltage opposite to the charge of the areas of the belt they are to be attracted to while the carrier particles have the same charge but at a lower voltage. The magnetic carriers form the bulk of the mixture which is picked up by a magnetic roller forming a ‘magnetic brush’ which can be used to apply the toner particles to the belt.

This process of converting an image in surface charge to a pattern of pigment particles is a development process which has an element of amplification by virtue of the mass of light-absorbing pigment compared with the amount of light used to discharge the belt to produce the image.

The pigmented image is then transferred with electrostatic assistance to the printed substrate. In the case of colour images an intermediate surface is usually used for indirect transfer of the four pigments which due to their light-scattering properties, as with photomechanical printing, include a final black pigment. Various other components of a printer are required to prevent image defects but are not included in this brief summary.

11.5 Conclusions and Further Reading

We have seen that the earliest descriptions of chemical processes include an equation involving light as a vital component. This reaction also involved silver halide, the predominantly important photochemical imaging material.

It is interesting to note that the two earliest imaging materials involved in the initial photolytic step of their imaging systems, namely silver halides and dichromated polymers are the only ones remaining in commercial use in any real sense. All the others have come and gone including the once important, iron-based blueprints. It is therefore curious that neither silver, chromium or iron had a high profile in the academic discipline of photochemistry. ‘Calvert and Pitts’ [58], one of the most widely used textbooks on photochemistry in the late twentieth century, barely mentions them at all.

The various forms of photochemical imaging including artistic, scientific and personal photography, X-ray imaging, photographic methods in the printing industry and photofabrication touch almost every aspect of our lives. Most of the decoration we see, the recorded memories we have, the manufactured goods we

use have at some point used photographic materials. The importance of photochemical imaging is difficult to exaggerate.

No single previous publication seems to cover the full scope of this chapter but there are several which provide wide scope and extensive detail. Although some are included in the references cited, the following books are recommended for further exploration:

The Origins of Photography (1982) by Helmut Gernsheim (Thames and Hudson, London) is an up-date of *The History of Photography* (1955) (Oxford University Press) by Helmut and his wife, who are major photographic collectors.

Out of the Shadows, Herschel, Talbot and the Invention of Photography (1992, Yale University Press, New Haven and London) recognises John Herschel's largely undervalued contributions including his support for Talbot.

The Keepers of Light (1979) by William Crawford (Morgan and Morgan, New York) covers important and obscure silver and non silver systems. Historical accounts are thorough and unusually accompanied by practical recipes for the reader to follow to reproduce the techniques described.

The Theory of the Photographic Process, (Ed. James T H [6]) in its various editions is the pre-eminent reference work for silver halide technology and science. It is however somewhat biased towards Kodak products since its authors are drawn from Kodak employees.

The following topics may be pursued using the references provided:

- Computer modelling of latent image formation [59, 60],
- Theory and practice of precipitation [61],
- Spectral sensitisation [62–65].

Another valuable source is *Photographic Sensitivity* (1995) by T. Tani (Oxford University Press, USA [66]) as is *The Handbook of Photographic Science and Engineering* [67]. A particularly useful source of mechanistic information for a range of systems is *Electron Transfer in Chemistry* (Ed. Balzani V, Volume 5, Wiley–VCH Germany), which includes sections on: photographic development, bleaching, spectral sensitisation; electrophotography; and photoinduced electron-transfer polymerisation initiating systems relevant to the Cyclic system and other photopolymer technologies.

References and notes

1. The rods in the retina respond to much lower light levels. They are saturated at normal light levels but at low levels they produce an achromatic response to the wavelength range below about 600 nm. Moonlit scenes are therefore lacking in colour. To become active the rods need to recover from the saturation caused by high light levels and this process of dark adaptation takes up to 30 min or so. Their activity can be preserved by using red illumination. For example, in a submarine if the red lights used were to fail suddenly the rods would still be responsive whereas white light failure would leave the crew essentially blind for several minutes

2. Artists may disagree. Artists' primaries are blue, red and yellow. Many do recognise that the best blue for mixing with yellow to get the best greens is 'Phthalo' blue, a phthalocyanine pigment which is in fact the best cyan available in the paint box. Also, Permanent Rose which is a decent magenta is often recommended for a mixing red. Since it is possible to get a blue from a cyan and magenta and a red from a magenta and yellow, while it is impossible to achieve a magenta or a cyan from a mixture of blue red and yellow, the traditional artists' case is weak if not simply wrong.
3. The letter K is used to avoid confusion with Blue.
4. In practice, two or even three layers make up each blue-, green- and red-sensitive sets of layers to improve the sensitivity/image structure (grain and sharpness) response.
5. Dispersion of very small silver particles can be highly coloured and of various hues depending on particle size. Carey-Lee silver is a suspension of very small silver particles of narrow size distribution. It provides a strong yellow colour and is removed conveniently during processing when the developed image silver is removed by bleaching and fixing.
6. James TH (ed) (1977) Theory of the photographic process, 4th edn. Macmillan Publishing Co Inc, USA
7. Wilgus J, Wilgus B (2004) What is a camera obscura? <http://brightbytes.com/cosite/what.html>. Accessed 14 July 2012
8. Rudnick L (2004) <http://www.photograms.org/chapter01.html>. Accessed 14 July 2012, refers to Adolfo Martinez in Phovision 221981 Arte y Proyectos Editoriales, S.L. p 4–5
9. Crawford W (1979) The keepers of light. Morgan and Morgan, New York, p 19
10. Gernsheim H, Gernsheim A (1955) The history of photography. Oxford University Press, Oxford, p 21
11. Wedgwood T, Davy H (1802) An account of method of copying paintings upon glass and making profiles by the agency of nitrate of silver. J Royal Inst 1:1
12. Crawford W (1979) The keepers of light. Morgan and Morgan, New York p235
13. Reproduced by kind permission from Bibliotheque National de France, the image appeared in "The Independent" Newspaper in the UK, Jan. 17, 2002 prior to its auction in Paris.
14. Crawford W (1979) The keepers of light. Morgan and Morgan, New York p24
15. The example of a Daguerreotype shown here, is reproduced with kind permission from the collection of Jack and Beverley Wilgus. It is of Phineas Gage who became famous after an accidental explosion drove the metal spike he is holding through his cheek and out through his forehead. The fact that he made a good physical recovery but suffered major personality changes made him one of the most famous medical cases of all time.
16. Gernsheim H, Gernsheim A (1955) The history of photography. Oxford University Press 66:69–73
17. Wood RD (1971) J.B.Reade, FRS and the early history of photography. Part 1. Annals of Science 27:47–83
18. Gernsheim H (1982) The origins of photography. Thames and Hudson, London, p 60ff
19. Photographers use this term to refer to the coated photographic layers while the term *dispersion*, as used in photographic technology, is applied to oil-in-water emulsions.
20. Hamilton JF (1988) The silver halide photographic process. Adv Phys 37:359–441 (and references therein)
21. Bennebroek MT, van Duijn-Arnold A, Schmidt J et al (2002) Self-trapped hole in silver chloride crystals. A pulsed EPR/ENDOR study at 95 GHz. Phys Rev B 66:054305
22. Hamilton JF (1988) The silver halide photographic process. Adv Phys 37:359–441
23. Gurney RW, Mott NF (1938) The theory of the photolysis of silver bromide and the photographic latent image. Proc Roy Soc (A) 164:151–167
24. Eachus R, Marchetti AP, Muentner AA (1999) The photophysics of silver halide imaging materials. Ann Rev Phys Chem 50:117–144
25. See, for example the effect of the inclusion of gold in a latent image on the resultant increase in development rate for small latent images resulting in an effective speed increase, due to the greater energy for deposition of silver on gold than on silver (underpotential). Hillson PJ, Adam HH (1975) On latent images of gold and silver. J Photogr Sci 23:104

26. Fleischauer PD, Shepherd JR (1974) Kinetics of the reaction between iron(II) and silver(I) catalyzed by silver nuclei on titanium dioxide surfaces. *J Phys Chem* 78:2580–2585
27. Faerman GP (1935) IXe Congrès Intern. De Photographie Scientifique et Appliquée, Paris. Editions Rev d'Optique, Paris 1936, p 198—and numerous other later studies
28. James TH (1977) The rate of development part 1—General kinetics of negative image development. In: James TH (ed) *The theory of the photographic process*, 4th edn. Macmillan Publishing Co Inc, New York; Collier Macmillan Publishers, London
29. Lee WE (1977) The rate of development part 2—Superadditivity. In: James TH (ed) *The Theory of the photographic process*, 4th edn. Macmillan Publishing Co Inc, New York; Collier Macmillan Publishers, London
30. Cramp JHW, Hillson PJ (1976) The dependence of the activation energy for development on the size of the latent image. *J Photogr Sci* 24:25
31. Hillson PJ (1958) The redox potential of the latent image. *J Photogr Sci* 6:97
32. Kendall JD (1940) Brit Pat 542,502, (1953) Brit J Photogr 100:56
33. Attridge GG (2000) Principles of colour photography p216. In: Jacobson RE, Ray SF, Attridge GG, Axford NR (eds) *The manual of photography*, 9th edn. Focal Press, Oxford
34. Gunter E, Matějček R (1971) Basic electrochemical aspects of the azo dye bleach process. *J Photogr Sci* 19:106–107
35. Hanson WT (1976) A fundamentally new imaging technology for instant photography. *Photogr Sci Eng* 20:155–160
36. Davey EP, Knott EB (1950) Brit. Patent 635,841
37. Evans FJ, Gilman P (1975) Comparison of the spectral sensitization of surface and internally sensitized core/shell octahedral silver bromide emulsions. *Photogr Sci Eng* 19:344–351
38. US Patent 3,761,276, 25 Sept 1973
39. US Patent 3,850,367, 26 Nov 1974
40. Evans GB, Magee PM, US Patent 4,416,969
41. Hanson WT (1976) A fundamentally new imaging technology for instant photography. *Photogr Sci Eng* 20:155–160
42. Herschel JFW (1842) On the action of the rays of the solar spectrum on vegetable colours and on some new photographic processes. *Phil Trans Royal Soc* 202:181–214
43. Schaff LJ (1992) Out of the shadows, Herschel, Talbot and the invention of photography. Yale University Press, New Haven, pp 130–131
44. Ware M (1999) Cyanotype: the history, science and art of photographic printing in Prussian blue. Science Museum and National Museum of Photography Film and Television, London
45. Ware M http://www.mikeware.co.uk/mikeware/Iron-based_Processes.html. Accessed 14 July 2012
46. Ware M (1995) The new cyanotype process. *Ag Plus Photogr* 7:74–81
47. Crawford W (1979) *The keepers of Light*. Morgan and Morgan, New York, pp 67–68
48. Paczkowski J, Neckers DC (2001) Photoinduced electron transfer initiating systems for free-radical polymerisation. In: Balzani (ed) *Electron transfer in chemistry: molecular level electronics, imaging, energy and environment*, vol V. Wiley-VCH, Weinheim, pp 516–585
49. Valdes-Aguilera O, Pathak CP, Shi J et al (1992) Photopolymerisation studies using visible light photoinitiators. *Macromolecules* 25:541–547
50. Chatterjee S, Gottschalk P, Davis PD, Schuster GB (1988) Electron-transfer reactions in cyanine borate ion pairs: photopolymerization initiators sensitive to visible light. *J Am Chem Soc* 110:2326–2328
51. Gottschalk P, Schuster GB, US Patent 4,772, 541
52. Crawford W (1979) *The keepers of light*. Morgan and Morgan, New York, pp 69–73
53. Djouani F, Israëli Y, Frezet L et al (2006) New combined polymer/chromium approach for investigating the phototransformations involved in hologram formation in dichromated poly(vinyl alcohol). *J Polym Sci Polym Chem* 44:1317–1325
54. Manivannan G, Changkakoti R, Lessard RA et al (1993) Primary processes in real-time holographic record material: dichromated poly(vinyl alcohol). *Proc SPIE* 1774:24–34

55. Bolte M, Pizzocaro C, Lafond C (1998) Photochemical formation of chromium (V) in dichromated materials: a quantitative and comparative approach. *Proc SPIE* 3417:2–11
56. Weiss DS, Cowdrey JR, Young RH (2001) Electrophotography. In: Balzani (ed) *Electron transfer in chemistry: Molecular level electronics, imaging, energy and environment*, vol V Wiley-VCH, Weinheim, pp 379–471
57. Carlton C (1939) US Patent 2,297,691
58. Calvert JG, Pitts JN Jr (1967) *Photochemistry*. Wiley and Sons Inc, New York
59. Hailstone RK, French J, De Keyser R (2004) Latent image formation in AgBr tabular grain emulsions: experimental studies. *Imag Sci J* 52:151–163
60. Hailstone RK, De Keyser R (2004) Latent image formation in AgBr tabular grain emulsions: computer simulation studies. *Imag Sci J* 52:164–175
61. Leubner IH (2009) *Precision crystallisation: theory and practice of controlling crystal size*. CRC Press Taylor and Francis Group, Boca Raton
62. Sturmer DM, Heseltine DW (1977) In: James TH (ed) *Theory of the photographic process*, 4th edn. Macmillan Publishing Co Inc., USA, p 194
63. Herz AH (1977) In: James TH (ed) *Theory of the photographic process*, 4th edn. Macmillan Publishing Co Inc, USA, p 235
64. West W, Gilman PB (1977) In: James TH (ed) *Theory of the photographic process*, 4th edn. Macmillan Publishing Co Inc., USA, p 251
65. Sturmer DM (2004) *Kirk-Othmer encyclopedia of chemical technology*. Wiley and Sons Inc., New York
66. Tani T (1995) *Photographic sensitivity*. Oxford series in optical and imaging sciences, vol 8. Oxford University Press, Oxford
67. Proudfoot NC (ed) (1997) *The handbook of photographic science and engineering*, 2nd edn. The Society for Imaging Science and Technology, Springfield

Chapter 12

Optical Sensors and Probes

Rachel C. Evans and Peter Douglas

Abstract Optical sensors and probes have emerged as valuable analytical tools for the detection of a variety of biologically and chemically important analytes in the last three decades. Our aim for this chapter is not simply to provide a catalogue of results from the literature, but rather to discuss the fundamental principles behind optical sensing and to provide a suitable entry point for new researchers in the field. We take a bottom-up approach to the design of an optical sensor, starting with the different optical parameters available for use in sensing and the various response mechanisms shown by different classes of optical probes. We then consider the various approaches available for translation of a molecular probe into an optical sensor platform, including the current state-of-the-art and future trends in sensor design.

12.1 Sensor or Probe?

Optical sensors and probes have become indispensable analytical tools for the detection of a wide range of chemical and biological species in industry, biotechnology, medicine and the environment. The principle behind optical sensing is the change in one or more optical property (e.g. absorbance, luminescence, refractive index) of a ‘smart’ molecule in the presence of the analyte. This change

R. C. Evans (✉)

School of Chemistry, Trinity College Dublin, Dublin 2, Ireland
e-mail: raevans@tcd.ie

P. Douglas

Chemistry Group, College of Engineering, Swansea University, Swansea, UK
e-mail: P.Douglas@swansea.ac.uk

is registered as the sensor or probe response and may provide both qualitative information, indicating the presence or absence of the analyte, and quantitative data, enabling determination of the analyte concentration. An optical response offers many advantages for sensing applications. The use of highly sensitive spectroscopic instruments to detect the signal permits extremely low analyte concentrations to be detected. The optical response is usually rapid, often reversible, and provides a route to non-invasive measurements. It is also possible to incorporate optical probes into miniaturised devices for use under non-laboratory conditions.

The distinction between an optical sensor and an optical probe has become somewhat blurred in recent times, with the two terms being used interchangeably. An optical sensor may be defined as a device that reacts to an external input (*i.e.* the analyte) by generating an optically measurable and reversible signal. Reversibility is the key to optical sensing, making it suitable for continuous and online monitoring situations. The definition of an optical probe is less straightforward. Often the response is driven by a binding interaction between the target analyte and the probe; when this occurs as a high-affinity interaction the probe response is irreversible. Such optical probes or indicators are more suited to single-shot measurements. In the case of reversible probes, however, the distinction between a sensor and a probe becomes hazy. In keeping with the description above, a molecular probe only truly becomes an optical sensor when immobilised within an integrated sensor platform; in other situations the term probe is more appropriate. However, for anyone interested in designing an optical sensor, consideration of the molecular probe requirements and response profile will often be the first point of call.

An exhaustive review of the extensive literature in the area is beyond the scope of this chapter. Many excellent books, chapters and review articles have already been dedicated to both the general area of optical sensors and probes, and more specifically to particular probe classes [1–5]. Rather, we will concentrate on the main factors that should be considered when designing an optical probe or sensor for a specific application. We first consider the optical parameters available for exploitation in sensing schemes, the methods available for detecting the optical response, and the information that can be inferred from them. This will be followed by a discussion of the various response mechanisms demonstrated by different classes of optical probes. Illustrative examples will accompany each section to highlight sensing applications for specific analytes. We will then consider the different approaches available for translation of a molecular probe into an optical sensor platform, including the current state-of-the-art and future trends in sensor design.

12.2 Optical Properties and Their Exploitation in Sensing

Optical sensors fall into two categories: (1) direct sensors, where the analyte is detected directly *via* some intrinsic optical property; (2) indirect sensors, where the

change in the optical response is reagent-mediated [4]. Commonly used direct and reagent-mediated optical sensing approaches for the most important types of analyte are summarised in Table 12.1. Given that direct sensing generally falls within the scope of direct spectroscopic analysis, here we will focus our discussion on reagent-mediated sensors. Since these do not require the analyte to exhibit a measureable optical parameter, they are particularly useful for those analytes, or concentrations, where direct sensing will not work. Reagent-mediated sensing is therefore suitable for a much wider range of analytes than direct sensing.

The response of an optical sensor or probe is determined from the change in its optical properties in the presence/absence of the analyte. When light strikes a solution or a solid containing a molecular probe, a number of different interactions are possible. If absorbed in an electronic transition, then the resultant excited-state will then be available to react with other species or to relax radiatively or non-radiatively. If the probe is immobilised within a solid support matrix, then scattering, refraction and reflection of the incident light may also be important. Alternatively, the primary response signal may arise from these light interactions at a responsive surface, rather than from a combination of interactions at discrete probe sites. The underlying principle of optical sensing is that the presence of the analyte affects the rate and/or efficiency of one or more of these processes to some extent. Since light has a number of measureable properties, such as wavelength, intensity, phase and polarisation, which are easily monitored with spectroscopic techniques, it is possible to correlate the change in any of these optical parameters with the analyte concentration. Absorption and photoluminescence are most commonly used to monitor the optical response and we will now consider these in more detail.

12.2.1 Absorption

The presence of the analyte may cause a change (e.g. a spectral shift, intensity change, formation of new band) in the absorption spectrum of the probe. This may be monitored using a spectrometer to quantitatively determine the analyte concentration. The detection limit will be determined by the probe sensitivity and the instrument limitations but $\sim 10^{-5}$ – 10^{-7} mol dm⁻³ is typical. When the absorbance change is a wavelength shift in the visible region it may cause an observable colour change, enabling qualitative or even semi-quantitative analyte detection by sight alone—*i.e.* a colorimetric sensor. This offers a distinct advantage in situations where rapid assessment of the analyte presence is required. The most familiar colorimetric probe is perhaps the pH universal indicator strip, which is impregnated with halochromic dyes, whose absorption properties, and therefore colour, are modified by pH.

Table 12.1 Examples of direct and reagent-mediated optical sensing methods for important analyte types. Note that not all direct or reagent-mediated methods indicated are equally useful for each example of analyte type

Analyte type	Example(s)	Direct	Reagent-mediated	Intermediate stage	Sensing method	Application(s)
<i>Elemental gas</i>	O ₂		Absorption Luminescence	Complexation Quenching	Spectral shifts Intensity/lifetimes Imaging	Blood gas Food packaging Biotechnology
<i>Small molecule gas</i> (pK _a active and pK _a used in sensing)	CO ₂ , NH ₃ , SO ₂	IR/Raman Luminescence	Absorption Luminescence	pK _a equilibrium [H ⁺ measured]	Spectral shifts Intensity/lifetime	Blood gas Environmental
<i>Small molecule gas</i> (non-pK _a active, or pK _a not used in sensing)	NO ₂ , H ₂ S, HCN, NO, anaesthetic gases	IR/Raman	Absorption Luminescence	Complexation atom quenching	Spectral shifts Intensity/lifetime	Environmental Blood gas
<i>Metal cations</i>	Na ⁺ , Ca ²⁺ , Mg ²⁺	Atomic	Absorption	Complexation RET	Spectral shifts	Blood/cell
Alkali/alkaline earth	Fe ³⁺ , Cu ²⁺ , Zn ²⁺ , Pb ²⁺ , Hg ²⁺ , Cd ²⁺	Absorption/ emission	Luminescence	Complexation Heavy atom quenching	Spectral shifts Intensity/lifetimes Imaging	electrolytes, Environmental
Transition metal						
Heavy metal						
<i>Anions</i>						
	Cl ⁻ , Br ⁻ , I ⁻ , NO ₂ ⁻ , NO ₃ ⁻ , H ₂ PO ₄ ⁻	UV/Vis absorption	Absorption Luminescence	Complexation atom quenching RET	Spectral shifts Intensity/lifetime Imaging	Blood/cell electrolytes
<i>Organics</i>						
Hydrocarbon	Petroleum oils	IR/Raman	Absorption	Adsorption	Spectral shifts	Environmental
Heteroatom	Thiols, phenols	UV/Vis	Luminescence	Complexation	Intensity	
Polyaromatics	Benzopyrenes	absorption				
<i>Biomolecules</i>						
	Glucose, fructose	Raman	Absorption	Complexation ICT	Spectral shifts Intensity/lifetimes	Health monitoring
<i>Biomacromolecules</i>						
	DNA, proteins	Intrinsic fluorescence Raman	Absorption Luminescence	Complexation Conformational shifts	Spectral shifts Intensity/lifetimes Anisotropy	Health monitoring Diagnostics

PET photoinduced electron transfer, RET resonance energy transfer, ICT intramolecular charge transfer

12.2.2 Photoluminescence

Photoluminescence can be used to detect an analyte in three ways: (1) the analyte itself is intrinsically fluorescent (direct sensing); (2) the analyte can be tagged with a fluorophore label; or (3) the analyte interacts with a luminescent probe. Direct sensing and fluorophore-tags are widely used in biomedical applications to probe cell environments. Many proteins are intrinsic fluorophores due to the presence of the aromatic amino acids tryptophan, phenylalanine and tyrosine. Analytes such as pH, CO₂, NH₃, O₂ and various cations and anions can be measured indirectly using luminescence probes.

Photoluminescence measurements are inherently more sensitive than absorption, enabling detection limits of $\sim 10^{-9}$ mol dm⁻³ to be readily achieved. Luminescence intensity and lifetime are the most commonly monitored properties; however fluorescence anisotropy, spectral shifts, and changes in vibrational fine-structure may all be used as probing parameters.

Intensity probes may be either fluorescent or phosphorescent. Often, the analyte causes a decrease, or *quenching*, of the emission intensity, which, for simple systems may be related to the analyte concentration using the Stern–Volmer equation (see Chap. 1). However, deviation from linear Stern–Volmer kinetics is common and more complex models are often required to calibrate the probe response. Simple intensity measurements may require only an excitation source and detector. However, these measurements are susceptible to signal drift due to fluctuations in the source intensity and variations in the probe concentration due to photodegradation or leaching. This problem can be overcome using wavelength-ratiometric detection, where an analyte-insensitive excitation or emission band is used as a reference. Spectral changes, such as wavelength shifts and variation of vibrational structure may provide information on the nature of the probe-analyte interaction. For example, the emergence of vibronic structure in the emission spectrum may indicate the formation of a probe-analyte complex, whereby the probe adopts a more rigid or ordered conformation in the presence of the analyte. Similarly, shifts in the emission wavelength may be used to identify changes in the local environment, such as polarity, of the probe.

Lifetime measurements offer the advantage of being unaffected by fluctuations in the excitation source intensity or probe concentration. Since triplet excited states typically have much longer radiative lifetimes than singlet states, they are particularly susceptible to interactions with other molecules. Quenching interactions can also be investigated using lifetime measurements and modelled using the τ^0/τ form of the Stern–Volmer equation. The form of the Stern–Volmer plot may also indicate whether the probe-quencher interaction occurs predominantly *via* static or dynamic quenching (see Chap. 1).

Fluorescence anisotropy may also be used as a response parameter. Upon excitation with polarised light, many fluorophores give polarised emission, with the extent of polarisation being given by the anisotropy, *r*. Changes in anisotropy, as a consequence of changes in probe tumbling, e.g. by probe binding or

unbinding, or changes in emission lifetime when emission and tumbling rates are comparable, can be used as probe response. Since polarisation anisotropy requires emission measurements at both vertical and horizontal polarisations the method already has a ratiometric character, and the long-term stability of the excitation source is less important than for analysis using a single intensity measurement. A ratiometric approach involving two lumophores has also been proposed, primarily because of the wide dynamic range it offers. In this method the analyte-sensitive probe, P , and the analyte-insensitive reference, R , are both lumophores, but exhibit different anisotropy values when isolated. The combined fluorescence from both species is used to determine the analyte concentration [6]. The measured anisotropy of the steady-state emission of a mixture of lumophores is given by the intensity-weighted average of the individual anisotropies, r_P and r_R :

$$r = r_P f_P + r_R f_R \quad (12.1)$$

where f_P and f_R are the fractional intensities of the two fluorophores and $f_P + f_R = 1$. Since the fluorescence intensity and anisotropy of R are constant, any change in either f_P or r_P will result in a change in the measured anisotropy. To maximise the range of anisotropy values attainable, the reference fluorophore is chosen to have a complementary anisotropy of either ~ 0 or ~ 1 , depending on the relative anisotropy of the probe, such that in combination, a dynamic range of almost one full unit (*i.e.* 0–1) is possible.

12.3 Probe Response Mechanisms

The precise response mechanism will depend on the probe-analyte combination and is often difficult to assign unambiguously. However, the response of most probes arises from one (or more!) of the following:

- analyte-induced change to the probe molecular structure;
- introduction of a competing kinetic process;
- physical change in the local environment of the probe.

12.3.1 Analyte-Induced Change to the Probe Molecular Structure

The most obvious mechanism by which the analyte may modify the molecular structure of the probe is the formation of an analyte-probe complex. The analyte may bind to the probe by either physical or chemical bonding. For reversible sensing the binding interaction should be completely reversible, otherwise the probe will be suitable only for single-shot measurements. Knowledge of the binding equilibria is critical when designing sensors based on this type of probe.

12.3.1.1 Binding Equilibria Theory

The theoretical basis for analyte detection *via* binding is the same regardless of the actual binding mechanism. If we consider a sensing medium, where the relative concentrations of the analyte, A , and the probe, P , are such that the analyte is present in excess so that binding does not alter analyte concentration, then an equilibrium will exist between the bound (P_B) and free (P_F) states of the probe. If the binding stoichiometry is 1 to 1, the dissociation equilibrium is given by:



and the dissociation constant, K_d , is defined as,

$$K_d = \frac{[P_F]}{[P_B]} [A]. \quad (12.3)$$

The fraction of bound states of the probe is given by:

$$\frac{[P_B]}{[P]} = \frac{[A]}{K_d + [A]} \quad (12.4)$$

where $[P]$ is the total concentration of the probe (*i.e.* $[P] = [P_F + P_B]$). An important result arises from this relationship: if a probe is to give a useful response the binding constant of the probe must be comparable to the analyte concentration. The useful range of analyte concentrations is typically restricted to $0.1K_d < [A] < 10 K_d$ [1]. Analyte concentrations outside of this range will produce only a limited change to the measured signal.

Where the instrumental response is the sum of two terms, one each for P_F and P_B , and each of these terms is linearly dependent upon the respective concentration then, irrespective of the nature of the response, the analyte concentration may be obtained from:

$$[A] = K_d \left(\frac{S - S_{\min}}{S_{\max} - S} \right) \quad (12.5)$$

where S_{\min} is the instrument signal when all the probe is free (zero analyte), S_{\max} is the instrument signal when all the probe is complexed (suitably high analyte concentration), and S is the instrument signal at the analyte concentration of interest, *i.e.* when the probe is partially-bound. If response is not the sum of two terms, or if these terms are not linearly dependent upon the respective concentrations, then Eq. 12.5 does not apply and a more complex calibration equation is necessary.

Changes in absorption or emission intensity

Changes in absorbance can be used with Eq. 12.5, provided absorption by both bound and unbound probe obey the Beer-Lambert law across the wavelength band of measurement.

Changes in emission intensity can also be used, but this requires more careful consideration of the experimental procedure. All measurements must be performed using the same instrumental configuration (slit widths, excitation wavelength etc.), optical pathlength and probe configuration. To compensate for variations in excitation intensity, or geometry, an additional unquenched lumophore which emits in a different spectral region to the probe can be added to provide an intensity-ratiometric measurement. Many researchers perform solution phase measurements using a titration technique, where aliquots of an analyte solution are sequentially added to a solution of the probe. When using this approach, it is important to consider and compensate for a reduction in probe concentration, due to dilution effects.

Spectral shifts

For an optical probe that displays a wavelength shift in absorption or emission on binding, the analyte concentration may be determined from a ratio of intensities at two wavelengths. This is known as a wavelength-ratiometric approach and avoids some of the limitations mentioned above for intensity-based sensing, since, the measurements are independent of probe concentration. Absorption-, excitation- and emission-based ratiometric measurements are all possible.

Chemical and physical binding mechanisms

Binding probes are widely used for sensing in physiological media. Common analytes include anions, cations and biomolecules such as polysaccharides, DNA and proteins. The probe must contain a chemical moiety which acts as a receptor binding site for the analyte and the selectivity will depend on its binding constant at this site. Chemical binding results in the formation of a formal covalent or ionic bond between the analyte and the probe, yielding a new chemical species whose optical properties differ from that of the probe [7]. Physical binding arises due to a weaker intermolecular interaction between the analyte and the probe, in the form of van der Waals, electrostatic or hydrogen bonds.

12.3.1.2 Chemical Binding Probes

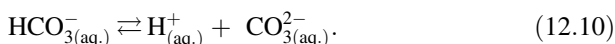
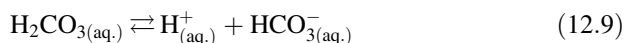
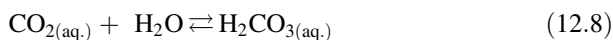
pH indicators: Colorimetric pH indicators are typically conjugated organic chromophores which contain a functional group that is pH sensitive due to its ability to participate in protonation-deprotonation equilibria. The ionised (Ind^-) and unionised (HInd) forms of the indicator are present in a concentration ratio determined by a logarithmic form of Eq. 12.5, *i.e.* the Henderson-Hasselbalch equation:

$$\text{pH} = \text{p}K_a + \log \frac{[\text{Ind}^-]}{[\text{HInd}]} \quad (12.6)$$

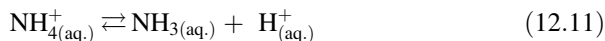
where $\text{p}K_a = -\log_{10}K_a$ and K_a is the acid dissociation constant. The two forms of the dye have different absorption spectra, so the relative concentration of either

form can be measured optically and related to changes in the pH. The dye pK_a indicates the centre of the measurable pH range at which the visible colour transition occurs. Although the pH response range for an individual indicator is quite narrow, a wide variety of indicators are available with responses spanning the entire pH scale [8] and mixed indicators can be used to give a solution or impregnated paper with a colorimetric response over a very wide pH range. Since the absorption bands arise due to $n-\pi^*$ and $\pi-\pi^*$ transitions, the observed colour change is determined by the degree of conjugation in the ionised and non-ionised dye forms. Luminescent pH indicators, where ionised and unionised forms of the indicator have different emission characteristics, are also available.

Carbon dioxide and ammonia probes: Optical sensors for CO_2 and NH_3 are based on pH-sensitive colorimetric or luminescent probes. When CO_2 dissolves in water it behaves as a weak acid, due to the following series of equilibria:



Thus, the pH of the aqueous solution in equilibrium with CO_2 gas is determined by the partial pressure, $p\text{CO}_2$, of carbon dioxide and an optical sensor for CO_2 may be designed by utilising a pH sensitive probe, P , which, on reaction with the protons generated in these equilibria, gives, HP^+ . The two forms of the probe must exhibit different spectral characteristics, such that, a detectable change in the absorption and/or emission profiles is observed upon protonation. Similar arguments may be applied to the development of optical sensors for ammonia based on the equilibrium:



Application

Two approaches have been adopted for $p\text{CO}_2$ sensing, namely (1) wet sensors and (2) plastic (solid-state) sensors. A wet sensor consists of a pH-sensitive probe dissolved in aqueous bicarbonate buffer solution, which is separated from the gaseous or liquid test medium by a gas-permeable membrane [9]. In plastic sensors, a polar pH-probe is immobilised in a thin polymer film. The probe is usually ion-paired with a lipophilic base such as a tetra-alkyl ammonium hydroxide. This ion-pair combination facilitates compatibility between the two components, whilst simultaneously eliminating the need for aqueous buffers due to the associated water of hydration. This makes it possible for these sensors to maintain their sensitivity to CO_2 , although they may show some humidity dependence. The requisites of a CO_2 probe are a suitable pK_a , a significant change in absorption or emission characteristics upon

protonation, and photostability. The luminescent probe 8-hydroxypyrene-1,3,6-trisulfonic acid (HPTS, Fig. 12.1) ($pK_a \sim 7.5$), which is highly fluorescent when unprotonated, satisfies these requirements. State-of-the-art sensors for CO_2 based on HPTS immobilised in a sol-gel matrix can achieve 80 ppm detection limits for sensing of CO_2 gas in the 0.03–30 % range [10].

Saccharide probes: Chemically-binding saccharide probes make use of the reversible formation of a cyclic ester between a boronic acid group attached to the probe (Fig. 12.1) and the diol moiety of saccharides. This interaction affects the Lewis acidity of the boron atom, which can influence the excited-state decay pathway of the probe. Often, this will result in the activation of a competing process, such as photoinduced electron transfer or resonance energy transfer (see Sect. 12.3.2). Spectral shifts in the UV/Vis absorbance spectrum may also be observed on binding.

Application

Continuous monitoring of blood glucose levels is particularly important for the management of diabetes. Since tear glucose levels are well-known to be elevated in hyperglycaemia sufferers, an optical glucose sensor comprised of a boronic acid containing fluorophore (BAF, Fig 12.1) based on a quarternised quinolinium nucleus, immobilised in a disposable contact lens has been developed [11]. The probe was incorporated into the sensor matrix simply by incubating the contact lens, made from a hydrophillic poly(vinylalcohol) polymer, in a concentrated aqueous probe solution. The hydrophilicity of the contact lens also enabled ready diffusion of the aqueous analytes in tears. The method was suitable for continuous non-invasive monitoring of tear glucose levels in the range 50–1000 mmol dm^{-3} , which is appropriate for physiological measurements.

Metal cation recognition probes: Some metals, notably the transition metals, readily form complexes with organic molecules, resulting in changes to optical properties, most commonly absorbance. This phenomenon is commonly exploited in standard methods for the spectrophotometric determination of metal cation concentrations [8] and standard test kits for a variety of metals are commercially available [12]. More complex probes based on a cation binding site linked to a fluorophore or chromophore reporter have also been developed [13]. The cation

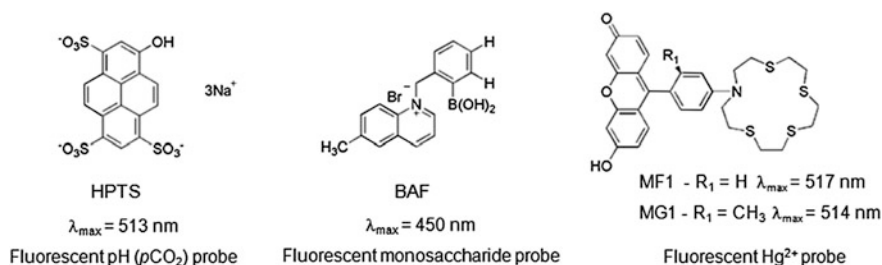


Fig. 12.1 Structures and characteristics of some typical chemical binding probes

receptor site is often a crown ether (monocyclic polyether) and selectivity to alkali, alkaline earth and transition metals can be achieved by varying the acceptor size, denticity or by substitution of the crown oxygen atoms with heteroatoms such as nitrogen and sulfur. The most stable complexes are usually formed when the crown diameter closely matches the cation ionic radius.

Application

The development of probes for the toxic heavy metals mercury, cadmium and lead in biological systems is of special interest. In this context, selectivity is particularly important since alkali and alkaline earth metals (e.g. Na^+ , K^+ , Ca^{2+} , Mg^{2+}) are usually present at much higher cellular concentrations. A series of probes based on a fluorescein-like xanthenone reporter and a ‘soft’ thioether receptor have been reported for the selective monitoring of Hg^{2+} (Fig. 12.1) [14]. A large fluorescence enhancement is observed on binding to Hg^{2+} in water, cells and tissue, due to the closing of an electron transfer deactivation pathway. Notably, one probe, MG1, which is structurally modified to restrict rotation between the receptor and emitter units, displays an emission quantum yield of 0.74 in its bound form, affording detection limits down to the 2 ppb range.

12.3.1.3 Physical Binding Probes

Anion recognition probes: The design of anion receptors poses more challenges than for their cation analogues. Anions have a lower charge to radius ratio than the isoelectronic cations meaning that electrostatic binding is often less effective. Anions also adopt a wide range of geometries including spherical (Cl^- , F^-), linear (CN^- , OH^-), trigonal planar (CO_3^{2-} , NO_3^-) and tetrahedral (PO_4^{3-}) [15]. While this phenomenon can be exploited to design shape-specific receptor sites, it is also more difficult to distinguish between anions with the same shape. Synthetic anion receptors may be positively charged or neutral. The positively charged acceptors are usually protonated nitrogen atoms or metal cations and anion binding occurs *via* electrostatic interactions. Neutral receptors bind anions *via* hydrogen bonding, ion–dipole interactions or coordinate anions at the Lewis acidic centre of a neutral organometallic ligand. The directionality of hydrogen bonds makes it possible to design receptors with specific shapes capable of differentiating between anions with different geometries. Commonly used hydrogen-bonding receptors include ureas, thioureas, pyrroles, indoles and triazoles. The addition of an optical reporter group to the receptor turns it into an optical probe for the anion. Various chromophores and lumophores have been used including anthracene, naphthalene, and 1,8-naphthalimide [15]. Dramatic changes in the ground-state absorption properties of the probe are often observed on anion binding, making them suitable for colorimetric detection [16, 17].

Indicator displacement assays (IDAs): These are a complementary approach to analyte recognition probes [17]. In the IDA method a colorimetric or fluorescent indicator is first allowed to bind reversibly to the receptor. A competitive analyte is

then introduced to the system causing the displacement of the indicator from the host, which in turn modulates the optical response of the indicator.

DNA probes and stains: Fluorescent probes and markers are often used to visualise and quantify nucleic acids such as DNA and RNA. Commonly used markers include DAPI (4'-6-diamidino-2-phenylindole), YOYO (homodimer of oxazole yellow YO), EtBr (ethidium bromide) and AO (acridine orange) (Fig. 12.2) [18]. These markers are weakly emissive in solution but exhibit a dramatic fluorescence enhancement on binding to DNA. The origin of this fluorescence enhancement is hotly debated and may differ for each dye. Two different binding modes are available, which enables site-specific probing of the DNA structure. YOYO, TOTO and EtBr are all examples of DNA intercalators – their planar fused aromatic ring structures enable them to slot in between the DNA base pairs, leading to significant π -electron overlap. DAPI, on the other hand, preferentially binds to AT-rich sequences in the DNA minor groove. Hydrophobic interactions and/or hydrogen-bonding stabilise this binding process. Acridine orange may be used to probe the secondary DNA structure. It intercalates with double-stranded (ds) DNA as a monomer, emitting green fluorescence (530 nm), but binds to single-stranded (ss) DNA as an aggregate which emits orange fluorescence (640 nm).

12.3.2 Introduction of a Competing Process by the Analyte

The second response mechanism is the situation where the presence of the analyte introduces a competing process which modifies the optical properties of the probe. Typically, the competing process activates or deactivates an alternative excited-state relaxation mechanism; consequently this response is limited to emission probes.

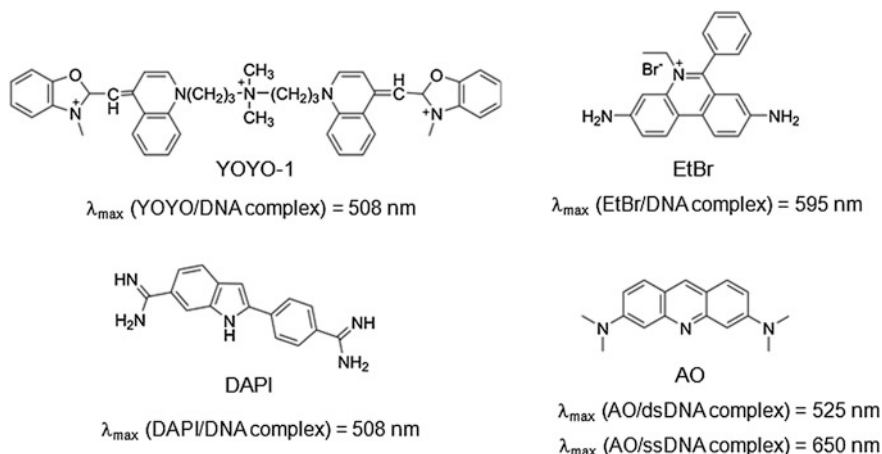


Fig. 12.2 Structures and optical characteristics of some common physical binding probes for DNA

Analyte control of competitive relaxation pathways can be induced by a dynamic collisional interaction between the analyte or analyte-generated quencher, and the probe emitter, or alternatively by analyte-binding, either directly to the emitter; at a site adjacent to the emitter; or to an adjacent molecule. It should be noted that these mechanisms are not mutually exclusive and assignment of the competing mode responsible for excited-state deactivation is often ambiguous. Discussion of these mechanisms based on the nature of the competitive process introduced is convenient.

12.3.2.1 Competition by Perturbation-Induced Intersystem Crossing

Perturbation quenching occurs when orbital overlap between the probe and quencher allows some property of the quencher to be shared with the probe excited-state. Neither probe nor quencher is chemically altered in the process. For example, the quencher may act as a heavy atom, causing non-radiative relaxation of the excited singlet state, S_1 , to the T_1 state *via* intersystem crossing and/or enhanced radiative relaxation from T_1 . Detection may then be based on quenching of S_1 , *i.e.* fluorescence quenching, or phosphorescence from the T_1 state.

Application

Perturbation quenching is particularly useful for detection of heavy atom halides and halocarbons [19]. The first optical sensor for halides was based on the fluorescence quenching of acridinium and quinolinium probes immobilised on a glass surface [19]. The detection limits followed the order Γ^- ($0.15 \text{ mmol dm}^{-3}$) < Br^- ($0.40 \text{ mmol dm}^{-3}$) < Cl^- ($10.0 \text{ mmol dm}^{-3}$). Two possible quenching mechanisms have been identified: electron transfer from the anion to the probe or heavy atom quenching. The enhanced sensitivity of the sensor to the iodide and bromide ions over chloride supports a heavy atom perturbation quenching mechanism, but the higher oxidation potentials of Γ^- and Br^- mean that they are also more likely to induce alternative competing processes such as photoinduced electron transfer (probably the quenching mechanism for *pseudo*-halides such as SCN^-). In a study using the probe *N*-methylquinolinium (Fig 12.3), analysis of the oxidation potentials for each quencher revealed a linear relationship between the quenching efficiency and the oxidation potential, suggesting that electron transfer was the predominant quenching mechanism [20]. Efficient quenching by Γ^- and Br^- and weaker quenching by Cl^- makes it particularly challenging to develop selective optical sensors for chloride, which is an important biological analyte due to its role in cellular pH, fluid adsorption and neuronal transmission processes.

12.3.2.2 Photoinduced Electron Transfer

PET involves the transfer of an electron from a donor, D, to an acceptor, A, following the absorption of light. The direction of electron transfer is determined

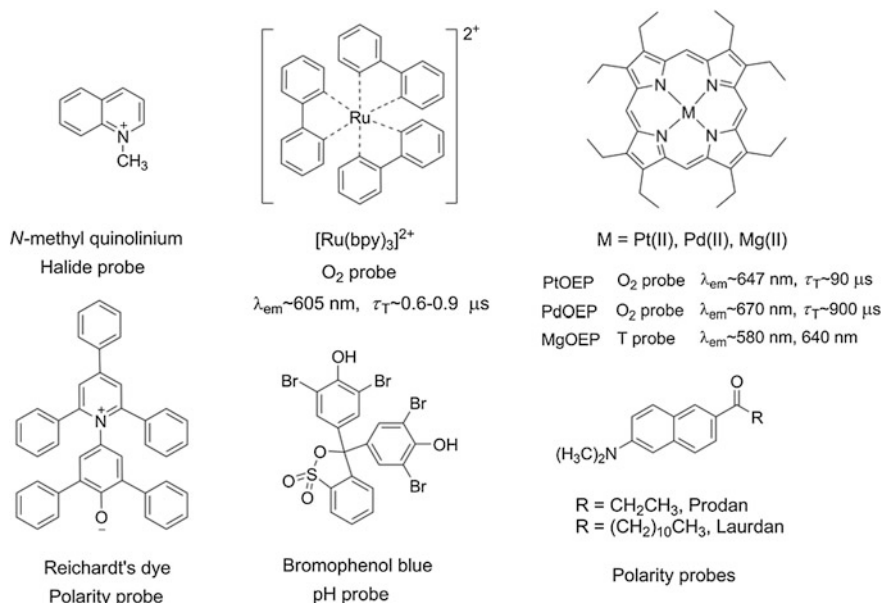


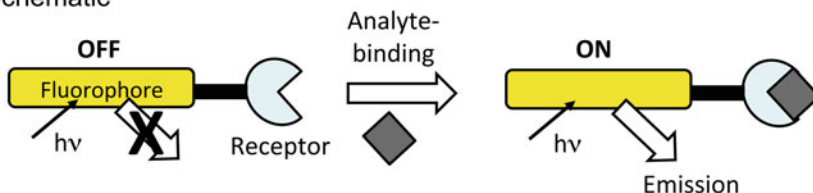
Fig. 12.3 Chemical structures of some non-binding optical probes and their applications

entirely by the oxidation and reduction potentials of the ground and excited states of the two species. Only a small thermodynamic driving force, ΔG_{PET} , is necessary for a high PET rate constant, k_{PET} . So for any D–A combination for which $\Delta G_{PET} \leq 0$, PET is expected to be very rapid compared to the radiative decay rate for typical fluorophores ($k_{rad} \sim 10^7$ to 10^9 s^{-1}). The resulting excited charge-transfer complex (D^+A^-)*, may either give charge transfer products or relax non-radiatively to the neutral A, D ground states, both of which result in emission quenching, or, alternatively, the complex may emit as an exciplex (Fig. 12.4).

PET has been exploited extensively for solar energy conversion (Chap. 7), however its application in the design of molecular probes is very much a field of on-going research. PET probes are typically molecular binding probes comprised of a lumophore reporter and an analyte receptor, linked by a non-conjugated spacer group. The lumophore absorbs light, resulting in the formation of an excited-state, which may luminesce, donate an electron, or, alternatively, accept an electron into the vacancy in the ground state. The receptor either accepts or donates an electron. Upon analyte-binding, the energy levels of the receptor are altered, such that the PET process is either switched on or off. Since PET competes with the radiative decay of the lumophore, luminescence measurements provide a method of quantifying the analyte concentration.

The choice of fluorophore determines both the direction of electron transfer and also the spectral response. While blue- and green-emitting PET probes are common, there is growing interest in the design of red emitters, which are more suitable for imaging/sensing in biological media (see Chaps. 9 and 10). The

(a) Schematic



(b) Molecular

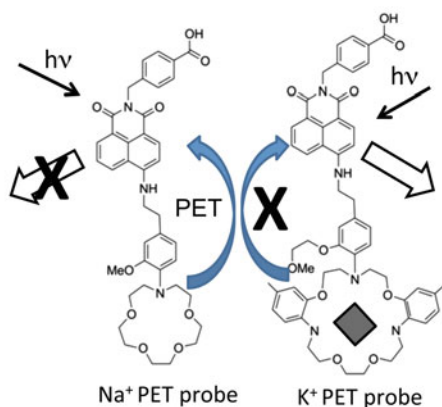


Fig. 12.4 (a) Schematic and (b) molecular representations of the PET mechanism in cation sensing (note the structure shown for an off-emission state is that for a Na^+ responsive probe, while the structure shown for an on-emission PET state is for a K^+ responsive probe)

distinct advantage of PET probes is that a dramatic change in the fluorescence intensity is observed on binding to the analyte, such that the terminology “OFF–ON” and “ON–OFF” is used to describe the response. Whether the probe is in its “ON” or “OFF” state will depend on how the redox potential of the receptor (and its subsequent influence on ΔG_{PET}) is affected by analyte binding.

Application

PET probes become very powerful sensors when the receptor is selective to a specific ion. For example, selective PET probes for Na^+ and K^+ have been designed using 4-amino-1,8-naphthalimide as the fluorophore and crown ethers of different sizes and composition as the receptors (Fig. 12.4) [21]. In the absence of the analyte, the probe is in the “OFF” state - the relative redox potentials (and energy levels) are configured in a way that it is thermodynamically favourable for electron transfer from the receptor to the fluorophore to occur, resulting in quenching of the luminescence. Upon excitation, PET from the receptor to the fluorophore is the main relaxation pathway. Exposure of the probe to the analyte results in the formation of the bound cation-receptor complex. This switches off the PET pathway—the probe is now in its “ON” state and fluorescence is observed. These ideas have been applied to design a variety of PET probes to detect alkali/alkaline earth, transition and main group metal ions, and anions [16, 21–23].

Moreover, the principles applied to design PET probes can be extended to molecular logic systems by adding additional receptors. For example, the fluorescence response from a receptor₁-spacer₁-fluorophore-spacer₂-receptor₂ type system may only emerge on binding of an analyte to each receptor site, thereby cancelling out the two possible PET pathways arising from the analyte-free receptor moieties.

12.3.2.3 Competition by Electron Exchange Energy Transfer

In electron exchange energy transfer, two electrons are simultaneously transferred between an excited state donor, D*, and ground state acceptor, A (see Chap. 1). Orbital overlap is required, and, since electron density falls off rapidly with distance, electron exchange is restricted to intermolecular distances of $< 8 \text{ \AA}$. The spin conservation rule is obeyed and this mechanism is possible for both singlet–singlet and triplet–triplet energy transfer.

Application

Electron exchange energy transfer *via* collisional quenching is the response mechanism shown by luminescence probes for oxygen. Oxygen quenching will be most efficient for long-lived probes immobilised in highly oxygen-permeable media. The trends and popularity of the probes used in oxygen sensing reflect this. While polyaromatic hydrocarbons ($\tau \sim 10$ to 100 ns) were the first lumophores to be extensively used in oxygen sensing, they have rapidly been superseded by organometallic compounds and metalloporphyrin derivatives of the heavy transition metals, which often exhibit room-temperature phosphorescence due to efficient singlet and triplet state mixing induced by the heavy atom effect. Group VIII transition metal complexes (primarily ruthenium(II) but also osmium(II) diimines) and platinum and palladium metalloporphyrins are among the most commonly used probes in oxygen sensing (Fig. 12.3) [24]. Their common traits include high emission quantum yields and long natural lifetimes ($\tau \sim 0.3$ to $5 \text{ }\mu\text{s}$ for transition metal complexes and $\tau \sim 90$ to $900 \text{ }\mu\text{s}$ for metalloporphyrins). It should be noted that oxygen quenching of triplets is so efficient that considerable care must be taken to work under anoxic conditions when using phosphorescence probes for analytes other than oxygen.

For optical sensing, the probe is immobilised in an oxygen-permeable host, such as a polymer film or sol–gel matrix. Consequently, the oxygen diffusion coefficient in the host matrix will also help to determine the quenching efficiency. For polymer matrices it has been shown that the relative sensitivity of the film to oxygen, given by $1/S_{50}$, the reciprocal of the partial pressure of oxygen, pO_2 , which results in 50 % quenching of the initial luminescence intensity, is dependent on the product of the probe lifetime and the oxygen permeability of the polymer. For example, a series of polymer films based on the probe platinum(II) octethylporphyrin (PtOEP) (Fig. 12.3) show $1/S_{50}$ values of 0.196, 0.081 and 0.0061 Torr^{-1} for ethyl cellulose (EC), cellulose acetate butyrate (CAB) and

poly(vinyl chloride) (PVC) hosts, respectively, where the oxygen permeabilities follow the order $EC > CAB > PVC$ [25]. Thus, with careful selection of the lumophore and polymer combination it is possible to tune the oxygen sensitivity of the film.

12.3.2.4 Competition by Resonance Energy Transfer (RET)

RET occurs *via* long-range dipole–dipole interactions and does not require direct molecular contact between the analyte and the probe. For RET to occur, a donor - acceptor system with spectral overlap is required, such that the emission spectrum of donor (D) overlaps with the absorption spectrum of acceptor (A). The acceptor may or may not be a lumophore. In RET sensors the presence of the analyte perturbs the electronic transitions of either the donor or acceptor in some way, so that the efficiency of the RET process is affected. Experimentally, RET shares many similarities with collisional quenching, typically resulting in a decrease the luminescence intensity and lifetime of the probe. Mechanistically, however, the processes are quite different and differ in both their concentration and distance dependencies.

RET offers many possibilities for sensing. The RET efficiency may be affected by changes in the analyte proximity, conformational changes induced by analyte binding, competitive analyte binding and/or displacement, or by analyte-induced changes in the absorption spectrum of the acceptor [26]. The RET process is monitored by measuring the luminescence intensity and/or lifetime of the donor. If the acceptor is also luminescent, this provides an additional response, which can be monitored and used in ratiometric measurements. The advantage of RET in sensing is that the requirements of suitable optical properties and sensitivity to the analyte are not demanded of a single molecule. The donor can be selected on the basis of its optical characteristics alone; it need not be sensitive to the analyte. The acceptor may itself be the analyte, or, it may be chosen on the basis of a change in its absorption spectrum in response to the analyte. Alternatively, the RET efficiency may change due to a fluctuation in the concentration of the acceptor in the proximity of the donor, as is the case for competitive protein-binding assays. In this situation, obtaining a donor and acceptor pair which meets the spectral overlap criterion for RET is easily attained by adding a fluorescent or chromophoric label to a protein-substrate pair.

Application

The absorbance response of pH indicators can be exploited in RET probes since changes in the spectral overlap integral will affect the RET efficiency. A sensor comprised of $[\text{Ru}(\text{dpp})_3]^{2+}$ (Fig. 12.3) as the donor, ion-paired with a pH indicator bromophenol blue as the acceptor, and immobilised in a plasticised PVC film, has been developed for the detection of ammonia. In the presence of the analyte, an increase in the deprotonated band of the pH indicator (which overlaps with the emission band of the donor) gives rise to RET, monitored by a decrease in the

luminescence intensity and lifetime of $[\text{Ru}(\text{dpp})_3]^{2+}$ [27]. A similar approach was used to design a sensor for $p\text{CO}_2$, where $[\text{Ru}(\text{dpp})_3]^{2+}$ was paired with the pH-sensitive acceptor Sudan III and immobilised in a silica sol-gel/ethyl cellulose hybrid matrix [28]. At low $p\text{CO}_2$ (high pH), Sudan III absorbs efficiently in the spectral region of the donor emission. As $p\text{CO}_2$ increases, the subsequent lowering of pH results in protonation of Sudan III, causing a shift in its absorption band to shorter wavelengths, thus inhibiting the RET pathway.

12.3.2.5 Amplified Fluorescence Quenching

Fluorescent conjugated polymers (CPs) merit special consideration as a sensing platform because they exhibit amplified or super quenching [29]. CPs are long-chain organic macromolecules which contain a strongly delocalised electronic structure along the polymer backbone. Upon photoexcitation, the excited states, which when considered as electron-hole pairs, are referred to as excitons (as in semiconductor photophysics), are free to migrate along the delocalised backbone. This process can be exploited for sensing as shown in Fig. 12.5. A local binding event or collision between the analyte at one local site on the polymer is accessible to any exciton on the chain, irrespective of where it was generated. Thus, for example, one analyte molecule can act as a potential quencher for hundreds of lumophores, and minor perturbations at a local site can affect the electronic properties of the entire polymer, thus enabling the detection of analytes at extremely low concentrations. The main modes of signal transduction are RET, PET and analyte-induced aggregation and/or conformational changes [29, 30]. Signal transduction is not restricted to luminescence quenching; changes to other optical properties such as absorbance, fluorescence enhancement and spectral shifts may also be amplified.

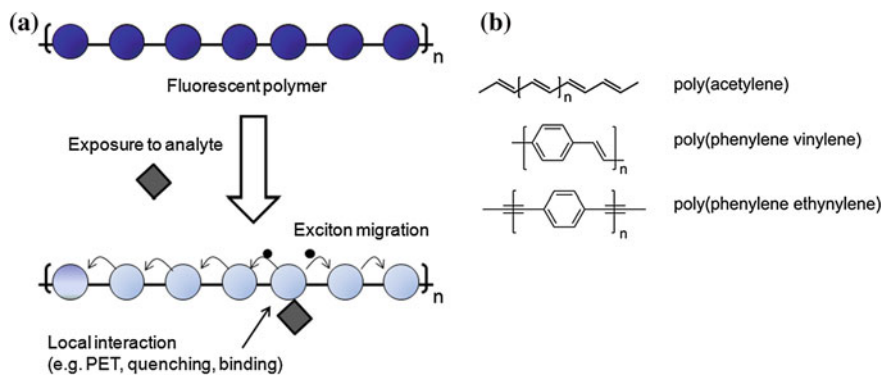


Fig. 12.5 (a) Schematic representation of amplified fluorescence quenching and (b) common conjugated polymer motifs used in optical sensing

Application

Conjugated polymers are good sensing platforms for the detection of vapours of nitroaromatic explosives such as trinitrotoluene (TNT) [31]. Fluorescence quenching occurs due to electron transfer from the conjugated polymer to the nitroaromatic species. Common classes of CPs used in nitroaromatics sensing are poly(acetylenes), poly(p-phenylenevinylenes), poly(p-phenyleneethynylenes) and polysilanes. CP sensor platforms have been successfully deployed outside the laboratory for the detection of hidden landmines, where impressive femtogram detection limits for TNT were obtained [32].

Conjugated polyelectrolytes (CPEs) contain ionic pendant chains anchored to the polymer backbone. In addition to water solubility, the charged nature of CPEs facilitates their interaction with charged analytes, such as metal ions, polyelectrolytes, proteins and oligo and polynucleic acids [30]. An ion-pair complex forms between the oppositely charged CPE and the analyte *via* both coulombic and hydrophobic interactions. For CPEs, amplified fluorescence quenching is therefore a combination of both efficient exciton migration and the formation of the ion-pair complex. Knowledge of the binding constant at the interaction site will therefore be important when evaluating the signal response.

12.3.3 Changes in the Probe Environment

Excited states and, to a lesser extent, the ground state may be sensitive to changes in environmental parameters such as temperature, pressure, viscosity and polarity. This manifests itself in a number of quantifiable parameters, such as: (i) spectral shifts; (ii) change in the emission quantum yield; (iii) change in the nature of the emissive state; (iv) change in non-radiative and radiative decay rates; (v) variations in the intensity and resolution of vibronic fine structure and (vi) the emergence of excimer or exciplex emission. These response mechanisms can be used to design sensor platforms to monitor both microscopic and macroscopic environmental parameters.

12.3.3.1 Polarity

All chromophores are affected by the polarity of the bulk environment to some extent. Some indicators exhibit more pronounced solvatochromatic behaviour, however, showing a pronounced shift in the position and sometimes intensity of an electronic absorption or emission band when the polarity of the medium is changed. The classic example is Reichardt's dye, which shows such an exceptionally large solvatochromatic shift (λ_{\max} shifts from 810 nm in diphenyl ether to 453 nm in water) that it was used to establish the commonly used $E_T(30)$ spectroscopic scale of solvent polarity [33].

Following excitation, changes in the electronic charge distribution can lead to a large shift in the dipole moment. The direction of the solvatochromic shift will therefore be determined by the relative magnitudes and directions of the ground (μ_g) and excited (μ_e) state dipole moments. If the dipole moment decreases along the direction of μ_g upon excitation, the ground state will be stabilised to a greater extent by solvation in media of increasing polarity, leading to negative solvatochromism (blue-shift). The reverse is true if the dipole moment increases along the direction of μ_g upon excitation. With increasing solvent polarity, the excited state is stabilised to a greater extent than the ground state, lowering its energy. The result is a red-shift in the absorption or emission band (positive solvatochromism).

In isotropic media, spectral shifts (excitation and emission) as a function of solvent polarity can be analysed using the well-established Lippert-Mataga theory [34, 35]. The application of polarity probes to biological systems is more complex due to the heterogeneity of the microenvironment. For example, the probe may be immobilised at a specific location on a protein or within a lipid membrane. Alternatively, it may be free to diffuse and will report the average polarity of a region of a few nm in radius. The ideal polarity probe will be sensitive to even small changes in the local environment polarity, signified by a dramatic change in its excited-state properties. This criterion is met by some polar fluorophores which undergo intramolecular charge transfer (ICT) upon excitation. Specific examples of ICT probes commonly used in polarity sensing are Prodan, Laurdan, and Nile Red. These probes exhibit a dramatic increase in dipole moment upon excitation due to ICT from the donor group (dialkyl amino) to the acceptor group (carbonyl). In addition to bulk polarity effects, the excited-state energy may also be affected by site-specific polarity effects, which provide more detailed information about the probe local environment and its nearest neighbours. Specific polarity effects arise due to localised interactions between functional groups on the probe and neighbouring molecules, for example hydrogen bonding. Experimental indicators for microenvironment polarity effects include loss (or gain) of vibrational structure to emission or absorption spectra and significant shifts in absorption/emission wavelength that cannot be explained by small changes in the solvent polarity alone. The latter effect may be identified, and quantified, by carrying out titration experiments, where the absorption and emission properties of the probe are studied by varying the percentage composition of the polar component in a solvent mixture.

Although molecular probes are extremely useful for monitoring microenvironment polarity, it is important to be careful in interpreting the results obtained. Each probe responds differently depending on the nature of the emissive state, the temperature and the molecular conformation. It is therefore important to perform detailed calibration experiments on the probe in isotropic media (e.g. in solution), before attempting to obtain meaningful and quantitative information from more complex anisotropic biological systems.

Application

Molecular probes are used extensively to investigate the microenvironment polarity of lipid membranes. Synthetic liposomes and vesicles that mimic the

geometry, topology and skeletal structure of cell membranes are often used as models for lipid bilayers. Prodan and Laurdan can inhabit both the hydrophobic interior of lipid bilayers and the polar water–lipid interface and have been used to monitor the membrane phase properties by probing the microenvironment in the bilayer [36, 37]. Specifically, variations in membrane water content induce red-shifts in the probe emission spectrum, which may be quantified using wavelength ratiometric measurements.

Laurdan has been used to probe the phase transitions in a 1,2-dipalmitoyl-sn-glycero-3-phosphocholine/cholesterol bilayer on exposure to chloroform [38]. In both cholesterol-poor and cholesterol-rich bilayers, the addition of chloroform resulted in an increase in the fluidity of the membrane. In the initial gel phase, diffusion is restricted and polarity induced red-shifts in the emission spectrum by local water molecules are not observed. On the addition of chloroform, the bilayer undergoes a phase transition to a more fluid-like state. The spectral response of the probe signals the change in its local environment polarity as a progressive red-shift in the emission band. The study showed that chloroform both loosens and rearranges phospholipid membranes, providing new evidence for the mode of action of general anaesthetics.

12.3.3.2 Viscosity

The microenvironment viscosity may also affect the excited state relaxation process. In fluid solution at ambient temperatures, solvent relaxation occurs much faster than radiative decay, and the probe emits from the solvent-relaxed excited state. However, in viscous solutions radiative decay may compete effectively with solvent relaxation, resulting in a broad emission band containing contributions from both the Franck–Condon and relaxed states. Temperature is also important, since a solution will become more viscous as the temperature is decreased. At very low temperatures, the fluorophore becomes immobilised in a viscous glass, and emission arises from a state very close in energy to the Frank–Condon state.

Application

Molecular rotors are fluorophores that exhibit strong variations in their fluorescence quantum yield depending on their intramolecular rotation—they can therefore be used as microenvironment viscosity probes. In viscous media, intermolecular rotations are slowed down, thus decreasing the efficiency of non-radiative relaxation and increasing both the fluorescence quantum yield and excited state lifetime. A conjugated zinc porphyrin dimer has been used as a molecular rotor to monitor intracellular viscosity increases following photoinduced cell death [39]. Following irradiation, efficient intersystem crossing to the triplet state occurs, which undergoes triplet-triplet annihilation with oxygen to produce cytotoxic singlet molecular oxygen, the species responsible for initiating cell death (see [Chaps. 8 and 9](#)). In low viscosity media the rotor adopts a planar conformation, which exhibits a broad emission band centred at 780 nm. In high viscosity

environments, intramolecular rotation becomes increasingly restricted and a twisted conformation is adopted, which emits at 710 nm. Fluorescence measurements based on these spectral shifts were used to quantify intracellular viscosity changes in single cells following irradiation. With increasing time after irradiation, a decrease in the emission peak at 780 nm, accompanied by an increase in the emission intensity at 710 nm, signified that the cell medium becomes more viscous upon death.

12.3.3.3 Spectroscopic Ruler

Due to its strong distance dependency, RET is also used as a 'spectroscopic ruler' to probe molecular distances in biological macromolecules, which can be used to identify molecular interactions and conformational changes (e.g. protein folding) in the local environment with high spatial (1–10 nm) and time (<1 ns) resolutions [40].

12.3.3.4 Temperature

A spectral shift due to interconversion between monomer and excimer/excplex emission can be exploited to develop temperature sensors for the macroscopic environment. For example, a thermochromic sensor film was developed by immobilising perylene in a polystyrene film with *N*-allyl-*N*-methylaniline (NA) [41]. In solution and in the absence of NA, perylene emits blue fluorescence ($\lambda_{\text{em}} = 475$ nm). In thin films and in the presence of NA, an additional broad red emission band is observed ($\lambda_{\text{em}} = 551$ nm), which is attributed to the perylene-NA exciplex. The fluorescence spectrum is temperature dependent: on heating between 25 and 85 °C the relative intensity of the blue monomer emission increases at the expense of the exciplex emission band, indicating that at higher temperatures the monomer-exciplex equilibrium is shifted in favour of the monomer. A wavelength ratiometric approach based on the relative intensities of the two emission peaks as a function of temperature was used to calibrate the sensor film [41].

12.3.3.5 Pressure

Changes to the fluorescence properties of a probe due to stacking effects can also be exploited in piezochromic macroscopic sensors. One such example is based on the liquid crystalline molecule cyano-substituted oligo(*p*-phenylene vinylene) (OPV), which forms columnar crystal stacks with pronounced π - π interactions, leading to excimer fluorescence [42]. In the solid state, the monomer emission is observed as a structured band in the green ($\lambda_{\text{em}} = 481$ nm). On exposure to external pressure, such as grinding with a pestle and mortar, the emission band is red-shifted ($\lambda_{\text{em}} = 548$ nm) and the vibrational structure is lost. The emission properties can be reversed upon heating the sample at ~ 130 °C. The choice of

temperature is significant as it determines the liquid crystalline phase that will be present. At 130 °C OPV is in a smectic phase, in which an ordered, layered architecture prevents excimer formation and monomer fluorescence predominates. Upon the application of force, or by heating to temperatures above 144 °C, OPV reverts to a nematic liquid crystal phase in which translational disorder facilitates the formation of dynamic excimers.

12.4 Advances in Sensor Design

An optical sensor platform consists of (1) an excitation source; (2) the sensor layer; and (3) a detector (Fig. 12.6). For luminescence-based sensors, the light source is usually tuned to the excitation wavelength that gives best probe selectivity. The sensor layer typically consists of a probe immobilised in an optically transparent, inert host matrix, which must be permeable to the analyte of interest.

Exposure of the sensor layer to the analyte induces a change in its optical properties, which is monitored by a detector such as a photodiode, spectrometer, or CCD camera. The optical signal is then converted into an electrical one for quantification. The sensor layer may be inserted into a bench-top spectrophotometer or, alternatively, the platform components may be partially or completely integrated within a stand-alone miniaturised device. For *in situ* work the sensor element may be spatially separated from both excitation source and detector, or added as a component to the sample under investigation as in fluorescence microscopy.

Current optical sensor research is motivated by the need for miniaturised, portable devices capable of selective and sensitive detection of multiple analytes in

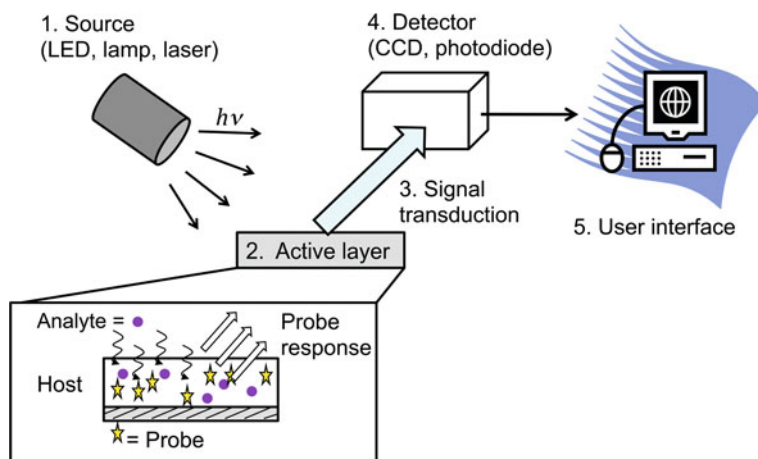


Fig. 12.6 Schematic representation of an optical sensor platform

real-life sensing environments. Less focus is being placed on the now well-established chemical and/or physical principles behind optical sensing and instead, efforts are directed at advances in device design, performance and field-viability, driven by the wide availability of low-cost electronic components, smart materials and improved detection techniques.

Fibre optic technology is widely used. Optical fibres are made from a cylindrical core surrounded by a cladding layer; both components are made from dielectric materials but with different refractive indices. If light enters the core within a critical angle, θ_c , it will undergo total internal reflection as it travels down the fibre. Energy is conserved at the core/cladding interface; however a portion of the electromagnetic field component, known as an evanescent field wave, penetrates a short distance (~ 20 nm) into the cladding. The interaction of this evanescent wave with an analyte may be used as a sensing platform. Removal or tapering of the fibre cladding exposes more of the evanescent field, such that it can be absorbed by, scattered by, or excite molecules located at the fibre surface. If the evanescent wave is generated in close proximity to a thin metallic layer, cooperative interaction with surface plasmons can lead to an enhanced effect known as *surface plasmon resonance* (SPR). Surface plasmons are collective oscillations of free electrons occurring at the interface between a metal and a dielectric. If a thin layer of a noble metal (e.g. Ag, Au) is inserted at the core/cladding interface, the p-polarised component of the evanescent field may excite surface plasmons in the metal layer. SPR sensors are extremely useful for studying adsorption events at surfaces, such as protein adsorption and biorecognition events [43].

12.4.1 *Integrated Sensor Devices*

Technological advances have made integration of the sensing element, excitation source, detector and electronics within a single miniaturised device possible. The most common semi-integrated devices are fibre optic sensors, or optodes, where the sensor layer is either coated on the tip of an optical fibre (for absorbance and luminescence sensing) or on an unsheathed section of the fibre (for evanescent wave sensing) [3]. Many fibre optic sensors are now commercially available (e.g. for oxygen [44]). The major advantage of fibre optics is that they enable light to be carried long distances, so that optodes can be used in remote or hazardous sensing environments, which may be inaccessible by other analytical techniques. Nonetheless, a separate light source and a detector to quantify the signal, are still required.

However, advances in miniaturised electronics mean that fully-integrated optical sensor devices are now a real possibility. Hand-held portable fluorescence spectrometers are now commercially available, enabling optical sensing to be taken out of the laboratory [44]. Low-cost inorganic *light-emitting diodes* (LEDs) emitting across the UV/Vis/NIR spectral region are already common excitation sources. These overcome the size, geometrical and electronic restrictions imposed

by traditional excitation sources such as lamps and lasers. The development of organic LED (OLED) technology has led to the development of truly integrated optical sensor platforms. Thin film *p-i-n* photodiode detectors can now be easily fabricated on glass or plastic substrates. Integrated sensor devices incorporating an OLED excitation source and a photodiode detector, and based on a luminescence quenching mechanism for the detection of a variety of analytes (e.g. O₂, glucose, ethanol) have been reported [45]. In these devices the sensor layer is deposited on one side of a transparent substrate, and the OLED excitation source is fabricated on the other side. The photodetector is placed behind the transparent OLED. Luminescence from the sensing layer transmits through the transparent layer and is measured by the photodetector. The availability of multi-pixel OLED arrays, suitable for use with a variety of lumophores, makes these compact devices ideal candidates for sensor microarrays for multi-analyte detection.

12.4.2 The Sensor Layer

Immobilisation of the optical probe in a permeable host matrix is a critical part of the sensor design process. The support matrix of choice varies between sensors, depending on the application requirements, and the final decision is usually based on the following considerations:

- probe-host compatibility;
- optical properties of the host e.g. refractive index, transparency;
- permeability of host to analyte;
- tendency for leaching (particularly for solution phase sensing).

The most commonly used host materials are polymers [46] and sol-gels [47]. Typical polymer hosts include organic glassy polymers (e.g. polystyrene), fluoropolymers, and cellulose derivatives. For polymers with a high glass transition temperature, a plasticiser is often added to make them more flexible and to improve analyte permeability. Sol-gel films are usually based on organically modified siloxanes (Ormosils), in which the surface Si-OH groups are replaced by Si-R groups (e.g. R = methyl, ethyl), rendering the surface hydrophobic. Ormosils are therefore suitable hosts for ambient and dissolved gas sensors.

Preparation of the sensor layer is relatively straight-forward: a known quantity of the probe is mixed with the polymer or sol-gel solution, which is then cast as a thin film *via* spin-coating, dip-coating or screen printing. The simplicity of this approach means that it is possible to add additional components to the layer, such as a reference dye for internal calibration or a scattering agent to improve sensitivity. The main disadvantage is that it is very difficult to ensure that the probe is homogeneously dispersed through the host layer. This can lead to a distribution of probe sites within the layer, which result in a variation in both the optical properties of the probe and its interaction with the analyte.

'PEBBLE' sensors (Probes Encapsulated By Biolegically Localised Embedding), consisting of one or more probes trapped in cross-linked polymer beads, have been developed as sensors for intracellular use in conjunction with fluorescence microscopy [48]. Intracellular cation and anion sensing is of great biological importance, but often, biomolecules will preferentially bind to the probe over the target analyte. The high-degree of cross-linking in the beads therefore serves to both trap the probe and to prevent biomolecules from entering the beads, whilst still allowing the permeation of small anions and cations.

12.4.3 Calibration and Amplification of the Sensor Response

In real analytical situations the sensor response for a specific analyte often suffers from interference from other environmental parameters. Moreover, fluctuations in excitation intensity, degradation and inhomogeneous distribution of the probe can all lead to drift in the sensor response, thus limiting the lifetime and reproducibility of devices. Self-compensating sensors contain an additional probe which independently monitors such changes, thus enabling correction of the sensor response to the analyte. For example, luminescence-based oxygen sensors are known to suffer from interference due to temperature fluctuations, whilst the response of optical glucose sensors oscillates due to a fluctuating supply of oxygen to glucose oxidase.

The optical response of many of the luminescence-based probes used in oxygen and pH sensors is temperature dependent. The incorporation of a temperature-sensitive reference probe (e.g. MgOEP, Eu(III) diketonate) enables internal calibration of the sensor response. Ideally the temperature probe should be insensitive to the analyte, but alternatively it can be immobilised in an analyte impermeable polymer bead. The design of multi-probe luminescence-based optical sensors is not trivial. Many probes exhibit very broad emission bands, meaning that the entire visible spectrum can be effectively covered by just two probes. Consequently, in the absence of both judicious selection of probes exhibiting the required analyte response and an independently-resolvable spectral response, multi-probe sensors are susceptible to considerable signal cross-talk and poor signal resolution. This effect is further exacerbated when indicator probes with overlapping absorption and emission bands are present at concentrations high enough to reach the critical distance (~ 5 to 7 nm) for RET to occur.

In some cases it may be advantageous to amplify the optical response, to improve the signal-to-noise ratio and therefore the sensor sensitivity. This may be achieved by the addition of inorganic colloidal nanoparticles, e.g. TiO_2 , to the sensor layer [10]. Since TiO_2 particles scatter all visible wavelengths more or less equally, their addition improves the interaction of light with the optical probe in the sensor layer, effectively increasing the surface area exposed to the analyte. Optimum scattering enhancement comes from colloidal particles whose diameter are ~ 0.5 times the probe emission wavelength. Alternatively, the signal may be

amplified using *metal-enhanced fluorescence* (MEF), where resonant coupling between surface plasmons from metal nanoparticles or a nanostructured metal film in close proximity to a lumophore probe can modify the radiative decay rate leading to enhancement of the fluorescence signal [49].

12.4.4 Evaluation of Sensor Response

Some applications require that the analyte distribution over relatively large areas is monitored in real time. This has been achieved by the development of *sensor paints*. Sensor paints consist of an optical probe dispersed in a viscous polymer solution, which can then be sprayed or painted onto the system of interest [50]. The sensor response is typically monitored using fluorescence imaging to obtain a quantitative image of the analyte distribution. Sensor paints have found considerable application for the measurement of the air pressure gradient across the surfaces of aeroplanes, spacecraft and racing cars in wind tunnels. As pressure sensitive paints (PSPs) contain an oxygen-sensitive luminescent probe, they more specifically measure the surface oxygen partial pressure gradient. Since many oxygen-sensitive lumophores exhibit cross-sensitivity to temperature, a second reference lumophore that corrects for excitation and temperature variations is often added. These ideas have been extended to monitor pH and oxygen gradients in marine environments and oxygen distribution across human skin [50].

Alternatively, it may be desirable to use a sensor which provides a quantitative response to the analyte that is easily detected by the eye alone. This is particularly useful for safety monitoring situations where a rapid indication of the analyte is required. While colorimetric sensors may appear well suited to this task, the detection limits of absorption-based devices are often inherently too low to be of practical use. To overcome this limitation, a series of luminescence-based sensors for the detection of oxygen using colour-change technology have been developed [51]. The sensor is prepared by incorporating two (or more) lumophores with different oxygen sensitivities and emission colours in a single device. In the presence of oxygen, the emission from each lumophore is quenched at different rates, resulting in a gradual “traffic-light” shift in the sensor emission colour across the red-yellow-green spectral region with increasing oxygen concentration (Fig. 12.7). This approach enables both rapid qualitative/semi-quantitative oxygen detection and quantitative measurements with high sensitivity, depending on the application requirements. However, since colour is a very subjective phenomenon, the objective description of colour changes can be challenging. The CIE (Commission Internationale de l'Éclairage) system of colorimetry provides a numerical description of colour, known as x,y colour coordinates, that is based on the sensitivity of the human eye to light across the visible spectral region (see Chap. 14). CIE x,y coordinates provide a particularly convenient system to describe the response of a luminescent colorimetric sensor when used in a qualitative or semi-quantitative way, enabling calibration and prediction of the sensor response.

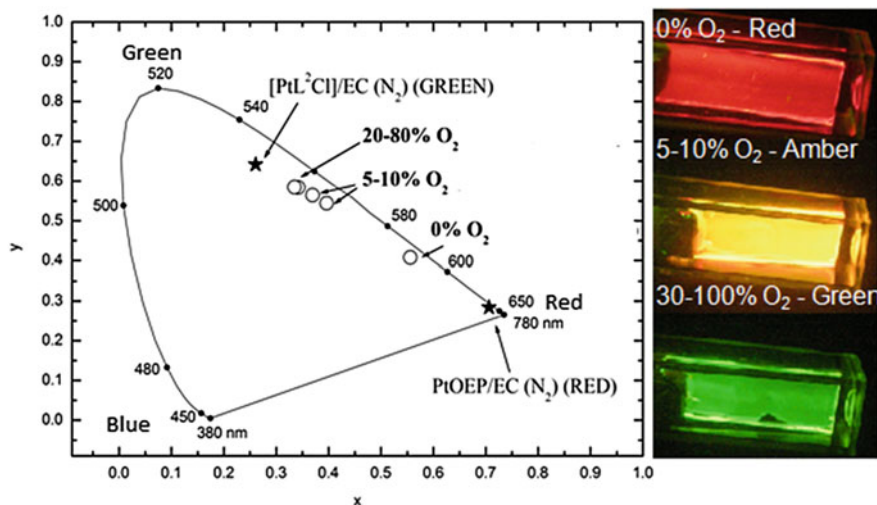


Fig. 12.7 CIE *xy* colour coordinates (*left*) and the observed sensor emission colour (*right*) of a dual-lumophore sensor at different % pO_2 . Revised from [51]

12.4.5 Multi-Analyte Sensing

The development of optical sensors that respond simultaneously and independently to different analytes is desirable for the analysis of complex samples. This requires a multiplexed approach, whereby the spectral and/or time-dependent optical response of the sensor must be resolved and unequivocally assigned to each individual parameter simultaneously. The most straight-forward approach to multiple analyte detection is to combine several analyte-specific sensors in a single miniaturised sensor array. For laboratory-based analysis, microwell plates are a cost-effective solution, with each well functionalised with a sensor specific to a given analyte. For field sensing, fibre optic bundles, composed of thousands of single core fibres bound together, but with each fibre maintaining its own independent light pathway, are promising. Each fibre in the bundle may be coated with a different optical probe, thus enabling simultaneous detection of multiple analytes. However, the disadvantage of both these approaches is that the inherent spatial distance between the sensors prevents the sample from being in contact with more than one sensor at the same time, thereby preventing truly simultaneous analyte detection.

In the truest sense, a multiplex sensor would use a single probe to detect each analyte. However, in practice, finding a single material capable of meeting this requirement is challenging. Multi-sensors (predominantly luminescence-based) which contain several analyte-specific probes in a single device are therefore more common [52]. However, determination of the correct probe combination is by no means trivial and requires similar considerations to those mentioned previously for

internal calibration probes. Two sensor configurations are possible: (1) a single-layer device in which multiple probes are homogeneously dispersed in a single host layer, or (2) a multiple-layer arrangement, where several probe-host blends for each analyte are immobilised as discrete layers. In single-layer sensors the individual probes are often immobilised in permeation-selective polymer beads to minimise signal cross-talk and to prevent analyte interference.

While dual-analyte luminescence-based sensors for a variety of parameters e.g. O_2/CO_2 , O_2 /temperature, O_2 /pH, O_2 /glucose are relatively common-place [52], a triple-sensor for pH, O_2 and temperature has only recently been realised [53]. The device was comprised of a single sensor layer in which polymer beads containing lumophores sensitive to either oxygen, temperature or pH were dispersed in a polyurethane hydrogel. Judicious selection of the polymer-lumophore combination enabled selective-permeation to the correct analyte. For example, the luminescence of the temperature-probe was considerably quenched by oxygen, but this effect was minimised by incorporating it into poly(vinyl chloride), which has a low oxygen permeability. Resolution of the response from each probe was achieved either by using an optical band-pass filter or, since emission decay times of each probe differed, gated (time-resolved) luminescence spectroscopy. It is interesting to note that most multi-sensors contain an oxygen-sensing component, since oxygen often acts as an interferent in sensors for other analytes. Moreover, oxygen is also consumed or produced during the chemical or enzymatic reactions used to detect CO_2 and glucose, and consequently monitoring fluctuations in the oxygen feedstock is essential for the reliable calibration of these sensors.

12.4.6 Optical Sensor Arrays

If several probes in an array respond to multiple analytes, but to a different extent, this may be utilised to quantify several analytes simultaneously. Low cost miniaturised detectors such as CCD cameras allow high-sensitivity imaging of the sensor array, enabling spectral changes (spectral shifts, intensity changes, shape variations and temporal response) in the presence of each analyte to be monitored. Image processing *via* pattern recognition then provides a qualitative and quantitative means of determining the analyte concentration. Frequently employed pattern recognition methods include principal component analysis (PCA), artificial neural networks (ANN), and linear discriminant analysis (LDA) [54, 55].

These cross-reactive sensor arrays are often called optoelectronic noses (for vapour or gas detection) or optoelectronic tongues (for detection in solution), since they aim to mimic the mammalian olfactory and gustatory systems, respectively, by producing a composite response that is unique to each analyte. Both luminescence-based and absorbance-based artificial noses and tongues have been developed for a wide range of analytes including organic vapours, ligating organic molecules and simple anions [54]. For example, an absorbance-based colorimetric array capable of differentiating between 19 different toxic industrial chemicals has

been developed [56]. In this array 36 different chemically-responsive dyes (e.g. acid indicators, base indicators, vapochromic, solvatochromic) were mixed with an ormosil host and printed as ~ 1 mm diameter dots onto a polymer membrane. The pattern of colour change across the array provided a unique molecular fingerprint for the analyte mixture with detection limits of ~ 2 to 500 ppm. A fluorescence-based cross-reactive array capable of identifying and quantifying metal cations in soft drinks has also been described [57]. Each probe in the array contained the same cation receptor (8-hydroxyquinoline) attached to a different conjugated chromophore. Metal complexation resulted in change in the resulting metallo-quinolinolate fluorescence (e.g. fluorescence enhancement, energy transfer, heavy metal quenching) yielding a fingerprint-like pattern of responses for each sensor-cation complex which could be discriminated by PCA and LDA.

12.5 Conclusions and Future Perspectives

In this chapter we aimed to demonstrate that while optical sensing is now well-developed, there is still considerable scope for new research in this vibrant and every-growing field. While the fundamental principles of optical sensing are well-established, there is still the need for new probes with superior optical properties, and also improved selectivity and sensitivity towards more unusual analytes. There have been significant recent advances in both the design of sensor platforms and strategies for improved device performance; however, there is still more to be done. Device miniaturisation, critical for the success of wireless sensor networks and remote sensing schemes, will continue to be a crucial area of growth and developments in the key areas of nanotechnology, microfluidics and plasmonics are likely to drive future trends. Optical sensing will continue to play an important role in real-time monitoring of environmental, health and security parameters, and with a significant amount of research being conducted in this field, long-range continuous monitoring across entire cities may soon become a reality.

References

1. Lakowicz JR (2006) Fluorescence sensing. In: Principles of fluorescence spectroscopy, 3rd edn. Springer, New York
2. Ramamurthy V, Schanze KS (2001) Optical sensors and switches. vol 7. Marcel Dekker, New York
3. Narayanaswamy R, Wolfbeis O (2004) Optical sensors. Industrial, environmental and diagnostic applications. Springer, Berlin
4. McDonagh C, Burke CS, MacCraith BD (2008) Optical chemical sensors. Chem Rev 108:400–422
5. Baldini F, Chester AN, Homola J (eds) (2006) Optical chemical sensors. NATO Science Series II: Mathematics, Physics and Chemistry. Springer, New York

6. Lakowicz JR, Gryczynski I, Gryczynski Z, Dattelbaum JD (1999) Anisotropy based sensing with reference fluorophores. *Anal Biochem* 267:397–405
7. Mohr GJ (2006) New chromogenic and fluorogenic reagents and sensors for neutral and ionic analytes based on covalent bond formation—a review of recent developments. *Anal Bioanal Chem* 386:1201–1214
8. Mendham J, Denney RC, Barnes JD, Thomas MJK (2000) Vogel's textbook of quantitative chemical analysis, 3rd edn. Pearson Education, Edinburgh
9. Mills A (2009) Optical sensors for carbon dioxide and their applications. In: Baraton MI (ed) *Sensors for environment, health and security*, NATO Science for peace and security series C: environmental security. Springer, New York
10. Dansby-Sparks RN, Jin J, Mechery SJ et al (2010) Fluorescent-dye-doped sol–gel sensor for highly sensitive carbon dioxide gas detection below atmospheric concentrations. *Anal Chem* 82:593–600
11. Badugu R, Lakowicz JR, Geddes CD (2003) A glucose sensing contact lens: A non-invasive technique for continuous physiological glucose monitoring. *J Fluoresc* 13:371–374
12. For example see: <http://www.mn-net.com/tabid/4650/Default.aspx>, <http://www.hach.com/nickel-cobalt-pocket-colorimeter-ii-test-kit/product?id=7640445220>. Accessed 27th July 2011
13. Valeur B, Leray I (2000) Design principles of fluorescent molecular sensors for cation recognition. *Coord Chem Rev* 205:3–40
14. Yoon S, Miller EW, He Q et al (2007) A bright and specific fluorescent sensor for mercury in water, cells and tissue. *Angew Chem Int Ed* 46:6658–6661
15. Beer PD, Gale PA (2001) Anion recognition and sensing: the state of the art and future perspectives. *Angew Chem Int Ed* 40:486–516
16. Gunnlaugsson T, Ali HDP, Glynn M et al (2005) Fluorescent photoinduced electron transfer (PET) sensors for anions; from design to potential application. *J Fluoresc* 15:287–299
17. Martínez-Máñez R, Sancenón F (2003) Fluorogenic and chromogenic chemosensors and reagents for anions. *Chem Rev* 103:4419–4476
18. Johnson I, Spence MTZ (eds) (2010) *Molecular probes handbook, a guide to fluorescent probes and labeling technologies*, 11th edn. Life Technologies, Inc., Eugene
19. Urbano E, Offenbacher H, Wolfbeis OS (1984) Optical sensor for the continuous determination of halides. *Anal Chem* 56:427–429
20. Jayaraman S, Verkman AS (2000) Quenching mechanism of quinolinium-type chloride-sensitive fluorescent indicators. *Biophys Chem* 85:45–57
21. Callan JF, de Silva AP, Magri DC (2005) Luminescent sensors and switches in the early 21st century. *Tetrahedron* 61:8551–8588
22. de Silva AP, Moody TS, Wright GD (2009) Fluorescent PET (photoinduced electron transfer) sensors as potent analytical tools. *Analyst* 134:2385–2393
23. de Silva AP, McCaughan, McKinney BOF, Querol M (2003) Newer optical-based molecular devices from older coordination chemistry. *Dalton Transactions*, 1902–1913
24. Amao Y (2003) Probes and polymers for optical sensing of oxygen. *Microchim Acta* 143:1–12
25. Douglas P, Eaton K (2001) Response characteristics of thin film oxygen sensors, Pt and Pt octaethylporphyrins in polymer films. *Sens Act B* 82:200–208
26. Birch DJS, Rolinski OJ (2001) Fluorescence resonance energy transfer sensors. *Res Chem Intermed* 27:425–446
27. Mohr GJ, Draxler S, Trznadelb K et al (1998) Synthesis and characterization of fluorophore-absorber pairs for sensing of ammonia based on fluorescence. *Anal Chim Acta* 360:119–138
28. von Bültzingslöwen C, McEvoy AK, McDonagh C et al (2003) Lifetime-based optical sensor for high-level $p\text{CO}_2$ detection employing fluorescence resonance energy transfer. *Anal Chim Acta* 480:275–283
29. Thomas SWT III, Joly GD, Swager TM (2007) Chemical sensors based on amplifying fluorescent conjugated polymers. *Chem Rev* 107:1339–1386
30. Liu Y, Ogawa K, Schanze KS (2009) Conjugated polyelectrolytes as fluorescent sensors. *J Photochem Photobiol, C* 10:173–190

31. Toal SJ, Troglor WC (2006) Polymer sensors for nitroaromatic explosives detection. *J Mater Chem* 16:2871–2883
32. Cumming CJ, Aker C, Fisher M et al (2001) Using novel fluorescent polymers as sensory materials for above ground sensing of chemical signature compounds emanating from buried landmines. *IEEE Trans Geosci Remote Sensing* 39:1119–1128
33. Reichardt C (1994) Solvatochromic dyes as solvent polarity indicators. *Chem Rev* 94:2319–2358
34. von Lippert E (1957) Spektroskopische bistimmung des dipolmomentes aromatischer verbindungen im ersten angeregten singulettzustand. *Z Electrochem* 61:962–975
35. Mataga N, Kaifu Y, Koizumi M (1956) Solvent effects upon fluorescence spectra and the dipole moments of excited molecules. *Bull Chem Soc Jpn* 29:465–470
36. Bagatolli LA, Gratton E (2000) Two-photon fluorescence microscopy of coexisting lipid domains in giant unilamellar vesicles of binary phospholipid mixtures. *Biophys J* 78:290–305
37. Gaus K, Gratton E, Kable EPW et al (2003) Visualizing lipid structure and raft domains in living cells with two-photon microscopy. *Proc Natl Acad Sci USA* 100:15554–15559
38. Turkyilmaz S, Chen WH, Mitomo H et al (2009) Loosening and reorganization of fluid phospholipid bilayers by chloroform. *J Am Chem Soc* 131:5068–5069
39. Kuimova MK, Botchway SW, Parker A et al (2009) Imaging intracellular viscosity of a single cell during photoinduced cell death. *Nat Chem* 1:69–73
40. Stryer L (1978) Fluorescence energy transfer as a spectroscopic ruler. *Ann Rev Biochem* 47:819–846
41. Chandrasekhara N, Kelly LA (2001) A dual fluorescence temperature sensor based on perylene/excimer interconversion. *J Am Chem Soc* 123:9898–9899
42. Kunzelman J, Kinami M, Grenshaw BR et al (2008) Oligo(p-phenylene vinylene)s as a “new” class of piezochromic fluorophores. *Adv Mater* 20:119–122
43. Homola J (2008) Surface plasmon resonance sensors for detection of chemical and biological species. *Chem Rev* 108:462–493
44. See: <http://www.oceanoptics.com>. Accessed 28th July 2012
45. Shinar J, Shinar R (2008) Organic light-emitting devices (OLEDs) and OLED-based chemical and biological sensors: an overview. *J Phys D Appl Phys* 41:133001
46. Mohr GJ (2006) Polymers for optical sensors. In: Baldini F, Chester AN, Homola J, Martellucci S (eds) *Optical chemical sensors*. Springer, New York
47. MacCraith BD, McDonagh C (2002) Enhanced fluorescence sensing using sol-gel materials. *J Fluoresc* 12:333–342
48. Buck SM, Koo YEL, Park E (2004) Optochemical nanosensor PEBBLEs: photonic explorers for bioanalysis with biologically localized embedding. *Curr Opin Chem Biol* 8:540–546
49. Aslan K, Lakowicz JR, Geddes CD (2005) Plasmon light scattering in biology and medicine: new sensing approaches, visions and perspectives. *Curr Opin Chem Biol* 9:538–544
50. Liu T, Sullivan JP (2004) *Pressure and temperature sensitive paints*. Springer, New York
51. Evans RC, Douglas P, Williams JAG et al (2006) A novel luminescence-based colorimetric oxygen sensor with a “traffic light” response. *J Fluoresc* 16:201–206
52. Stich MIJ, Fischer LH, Wolfbeis O (2010) Multiple fluorescent chemical sensing and imaging. *Chem Soc Rev* 39:3102–3114
53. Stich MIJ, Schaeferling M, Wolfbeis OS (2009) Multicolor fluorescent and permeation-selective microbeads enable simultaneous sensing of pH, oxygen, and temperature. *Adv Mater* 21:2216–2220
54. Anzenbacher P Jr, Lubal P, Buček P et al (2010) A practical approach to optical cross-reactive sensor arrays. *Chem Soc Rev* 39:3954–3979
55. Ciosek P, Wróblewski W (2007) Sensor arrays for liquid sensing—electronic tongue systems. *Analyst* 132:963–978
56. Lim SH, Feng L, Kemling JW (2009) An optoelectronic nose for the detection of toxic gases. *Nat Chem* 1:562–567
57. Palacios MA, Wang Z, Montes VA et al (2008) Rational design of a minimal size sensor array for metal ion detection. *J Am Chem Soc* 130:10307–10314

Chapter 13

Photochemistry in Electronics

Owen J. Guy, Gregory Burwell, Ambroise Castaing
and Kelly-Ann D. Walker

Abstract Photochemistry plays a critical role in modern semiconductor electronics, primarily through the use of photoactive polymers or photoresists in the lithographic processes used to fabricate semiconductor devices. Photoactive polymers have been extensively researched in order to develop resists that are chemically robust and that are able to produce sharp, well defined, high resolution features through photolithography. This chapter introduces photolithography and photoresists, and presents review of the photochemistry of some of the more important commercial photoresists. Miniaturisation of semiconductor devices for consumer electronics and sensors now places increasing demands on lithography processes. This has led to the development of sub-micrometer and now nanometer scale devices. A review of electron beam lithography and other high-resolution lithography techniques concludes this chapter.

O. J. Guy (✉) · G. Burwell · A. Castaing · K.-A. D. Walker
College of Engineering, Swansea University, Singleton Park,
Swansea SA3 8PP, UK
e-mail: o.j.guy@swansea.ac.uk

G. Burwell
e-mail: G.Burwell.436734@swansea.ac.uk

A. Castaing
e-mail: A.Castaing@swansea.ac.uk

K.-A. D. Walker
e-mail: K.D.Walker@swansea.ac.uk

13.1 Introduction

This chapter outlines some of the most important applications of photochemistry in electronics. Almost every step in the fabrication of electronic devices involves photoactive polymers called *photoresists*. Photoresists, applied as a thin layer on a semiconductor wafer, are used in the patterning of electronic devices and ‘micro-chips’ used in every modern electronic appliance. The process by which photoresists are patterned is called photolithography. *Photolithography*, which is explained in detail below, relies on a change in solubility of the photoresist polymer on exposure to light. Selective exposure of the resist and subsequent selective removal, allows the patterning of millions of micron-sized devices on a silicon wafer or other semiconductor substrate. Photolithography predominantly uses UV light to expose the photoresist.

Research on yet smaller (and therefore more dense and efficient) circuitry continues apace today. Photolithography is still the predominant technology used in the microelectronics industry, but polymers for extreme UV and electron beam lithography are becoming increasingly important as the evolution of electronic devices attempts to conform to Moore’s Law [1], by packing ever more devices onto the semiconductor wafer. There have been many developments in photolithography and the polymer chemistry of photoresists, all with the aim of enabling higher resolution device features to be fabricated. The limits of UV photolithography now appear to have been reached and research is currently focused on a host of techniques for patterning of features at the nanoscale. Nano-lithography techniques such as electron beam lithography and nanoimprint lithography are now used in mainstream industrial device processes. These methods utilise photochemistry to achieve nanoscale patterns. A summary of lithographic techniques for fabricating nanoscale structures is presented in this chapter.

13.2 Photolithography and Photoresists

Photolithography is in essence very similar to the process of photography, which is discussed in detail in [Chap. 11](#). As in photography, a light-sensitive material is selectively exposed to light in order to generate a picture, or a pattern. Photolithography uses a set of parameters: the tone, the sensitivity, the resolution and the contrast, to define the appropriate resist for specific exposure conditions in order to achieve a desired pattern. The tone determines which areas of the resist will be removed after exposure to light. Exposure of a positive tone resist enables the exposed resist to be removed using a chemical development process, whilst exposure of a negative tone resist makes the resist more difficult to remove with a developing solution. The sensitivity of the resist represents the amount of light, or dose, required to completely expose the resist film. The resolution is the minimum feature size attainable, and the contrast describes how abruptly, or sharply, features

can be defined using a particular resist layer thickness and light dose. A high contrast allows sharp edges and smaller features, while a low contrast resist, if combined with precise timing in the development process can allow the formation of 3D patterns.

Photoresists are photoactive polymers dissolved in a solvent to form a viscous liquid. The resists are used as protective or mask materials in electronic device fabrication processes. Photoresists undergo a photochemical reaction and subsequent change in their solubility on exposure to light. Photoresists can be categorised as positive or negative resists. Positive resists become more soluble when exposed to light whereas negative resists become less soluble.

Resists are applied to semiconductor wafers by dropping the polymer based liquid resist onto a substrate, which is then spun at 1000–6000 revolutions per minute (rpm) to form a thin coating. The spin-coated resist layer can be anything from tens of nanometres to several hundred micrometres in thickness—depending on the viscosity of the resist and the spin coating parameters (acceleration, spin speed and spin cycle duration).

The general principle of photolithography is to selectively expose the photoresist to light through a hard-mask (usually made from a patterned chrome layer on a glass or quartz substrate as shown for example in Fig. 13.1).

Light passes through the transparent areas of the hard mask and selectively exposes the photoresist layer. The solubility of a positive resist will increase on exposure to light, and can subsequently be selectively removed using a chemical developing solution. Negative resists behave in the opposite way, the light exposed areas becoming insoluble in the chemical developer whilst the soluble un-exposed areas can be removed. Negative photoresists often rely on a photo-initiated cross-linking reaction to generate an insoluble polymer. Figure 13.2 illustrates this process for both types of resist.

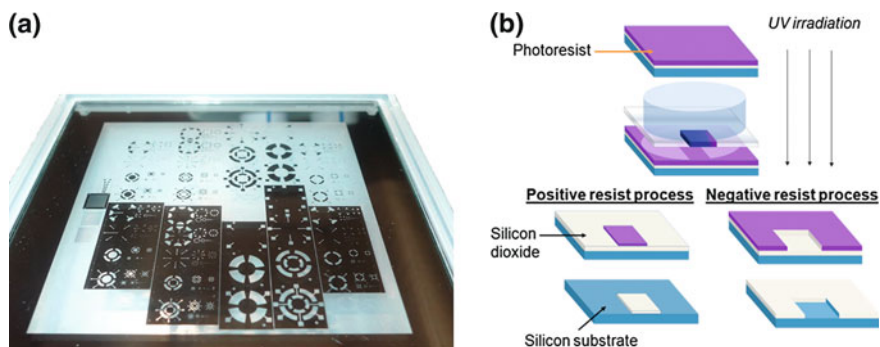


Fig. 13.1 **a** Chrome on quartz hard photomask. **b** Schematic illustration of photoresist (purple layer) exposure to UV light through a quartz-chrome hard mask. Exposure of positive resist (left) and negative resist (right) followed by resist removal and subsequent silicon dioxide (white layer) etching to selectively expose the silicon substrate (blue layer)

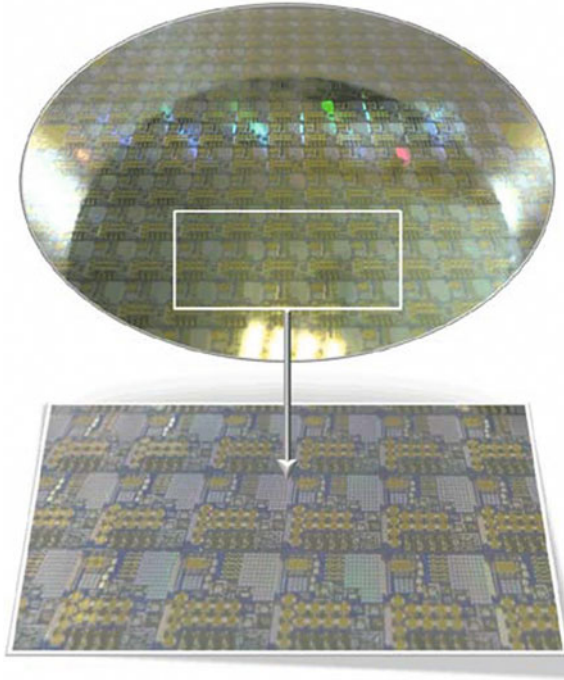


Fig. 13.2 Microelectronic devices fabricated on a silicon wafer. Devices are patterned using Novolak based photolithography

Following patterning of the photoresist layer, further process steps such as etching or metallisation can be carried out. The photoresist acts as a protective layer or mask, for example, protecting the substrate beneath from an etching process. In the example illustrated in Fig. 13.1b, the resist (purple) acts as a mask, initially protecting the silicon dioxide layer (white) from being etched by a hydrofluoric (HF) acid based etchant. Areas of silicon dioxide covered by the resist are protected from etching, whilst exposed silicon dioxide is etched away by the acid. Photoresists are used as protective masks in selective etching of silicon dioxide, silicon, silicon nitride and several metals. Resists, though partially inert to many etchants, will however degrade and be removed after time. Indeed, more aggressive etchants will remove resist layers quickly. The selectivity of the resist relative to the target etch material is thus critical. The selectivity is the ratio of the removal (etch) rate of the photoresist layer to the removal (etch) rate of the material to be etched (silicon dioxide in the above example). The higher this ratio, the longer the resist will remain intact and more of the target material can be etched away.

There are several methods that can be used to increase the endurance of the photoresist:

1. **Baking:** Baking the resist induces thermal cross-linking of the resist polymer. The resist thus becomes harder, less soluble and hence more difficult to remove. It also increases its resistance to chemical etchants.
2. **Resist thickness:** Thicker layers of resist can be applied to wafers by varying the spin coating conditions used to apply the resist to the semiconductor wafer. Decreasing the acceleration time and/or the spin speed (rpm) and/or the spin duration, would all result in a thicker resist layer. In addition more viscous resists can be used to yield much thicker protective layers. SU-8 is a commonly used epoxy-based negative photoresist. It is a highly viscous resist, which can form layers around 100 μm in thickness. Standard photoresists such as MicropositTM S1813TM (produced by Shipley a Rohm & Haas company) usually yield layers around 1 or 2 μm in thickness.

For some semiconductor processing steps such as ion-implantation or deep etching, the photoresist layer is insufficiently resilient to selectively protect the substrate material and a more durable mask material must be used. In these cases, silicon dioxide, silicon nitride or metal, 'hard masks', are often utilised. These materials are first patterned by photolithography using a photoresist to selectively protect the hard mask from etching. Once patterned, the hard mask provides greater selectivity to etching than a photoresist layer. Hard masks are also less penetrable than resist masks with respect to ion implantation. In Fig. 13.2, photolithography processes are used to pattern a hard silicon dioxide mask. This mask is then used to selectively protect the silicon substrate (blue layer) during further processing. In processes such as silicon reactive ion etching (RIE), the hard silicon dioxide mask is consumed during the etch process, but at a lower rate than the silicon is removed.

13.2.1 UV Light Exposure

The photochemistry of resists predominantly utilises molecules which absorb in the UV region of the electromagnetic spectrum. UV light is able to cleave bonds and create radicals which can crosslink polymers or modify functional moieties to create a change in solubility of chemical species after UV exposure, compared to pre-exposure. UV photochemistry was selected for lithographic processes for several reasons:

1. UV light is of shorter wavelength than visible light and thus a higher ultimate feature resolution can be obtained using UV photolithography.
2. UV light sources can be more effectively controlled (without interference from visible light sources).
3. Mercury lamp UV light sources give distinct linear light emission output at three UV wavelengths: 365.4 nm (I-line), 404.7 nm (H-line), 435.8 nm (G-line) [2]. (Emission spectra for mercury lamps are given in Chap. 14).

13.2.2 Chemistry of Photoresists

There are many photoresists available commercially. These can be categorised into positive and negative tone resists. Various formulations of resists have differing properties (viscosity, ultimate achievable resolution, substrate adhesion etc.). Several classes of resist have thus been developed for different electronic applications. For example, high-resolution photolithography for patterning of sub-micron transistors requires a different resist to that needed for deep silicon etching of micro-electro-mechanical-systems (MEMS) structures.

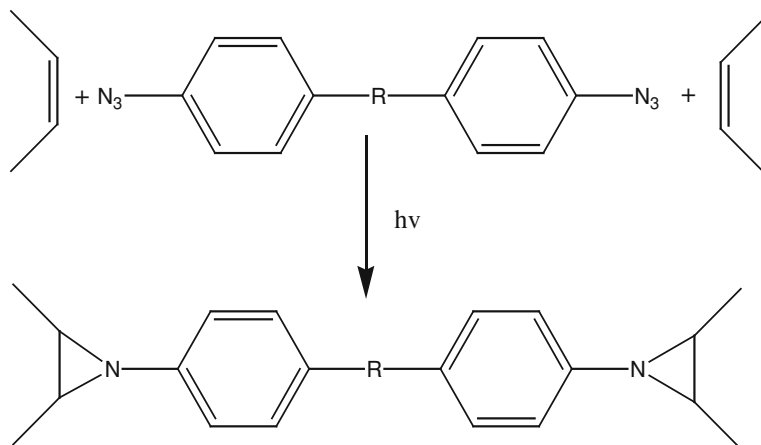
13.2.2.1 Negative Photoresists

Many negative photoresists rely on cross-linking reactions to create less soluble areas on exposure to light. Cross-linking refers to bonds formed between polymer chains creating a more rigid polymer matrix. Cross-links are formed by chemical reactions that are initiated by light, heat and/or pressure, or by the mixing of a non-polymerised or partially polymerised resin with various chemicals. Cross-linking is widely used in polymers or plastics to alter the properties of the polymer to become harder, more rigid and/or less soluble. It is much more difficult for solvent molecules to separate polymer chains in the cross-linked matrix, than in a non-cross-linked polymer. Cross-linked polymers tend only to swell in response to a solvent. There are many different cross-linking reactions that can be used in negative resists, some of which are highlighted below.

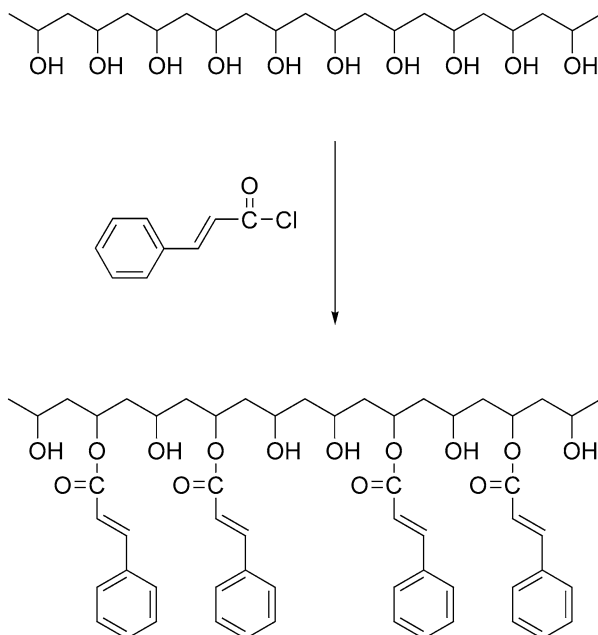
Early photoresists used polymers that could be cross-linked using a photo-initiated reaction. One example of a cross-linking resist is based on linking of poly-isoprene polymer chains *via* reaction with a bis-azide molecule [3]. The azide (N_3) group undergoes a photochemically initiated breakdown, releasing nitrogen (N_2) and also creating a very reactive nitrene group. Nitrene moieties are formed at both ends of the bis-azide molecule and the nitrene groups can react with two poly(*cis*-isoprene) chains to yield a cross-linked polymer. One of the most common reaction mechanisms is the formation of an aziridine ring (Scheme 13.1). Cross-linking of the polymer chains results in the polymer becoming less soluble, and the areas of polymer resist exposed to light are thus insoluble in the developing solution—constituting a negative tone resist.

Another example of a negative tone photoresist uses poly(vinyl cinnamate). The first step in the formation of an insoluble polymer is the esterification of poly(vinyl alcohol) (PVA) with cinnamate groups to yield poly(vinyl cinnamate) (Scheme 13.2).

The alkene groups of the cinnamate moieties subsequently undergo a [2 + 2] cycloaddition reaction under irradiation (Scheme 13.3). This cycloaddition results in a cross-linked polymer suitable as a negative tone photoresist [4].



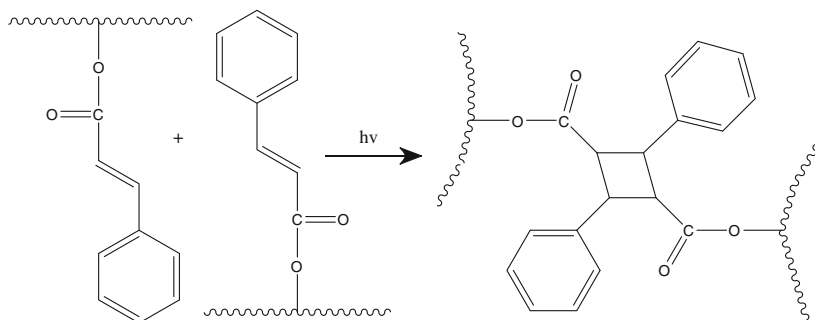
Scheme 13.1 Cross-linking of bis-azide with poly(*cis*-isoprene)



Scheme 13.2 Negative tone resist produced by partial esterification of poly(vinyl alcohol) to yield poly(vinyl cinnamate)

13.2.2.2 Positive Photoresists

Positive resists use an alternative approach to cross-linking. The objective is to use a photochemical reaction to create a more soluble material from an insoluble one.



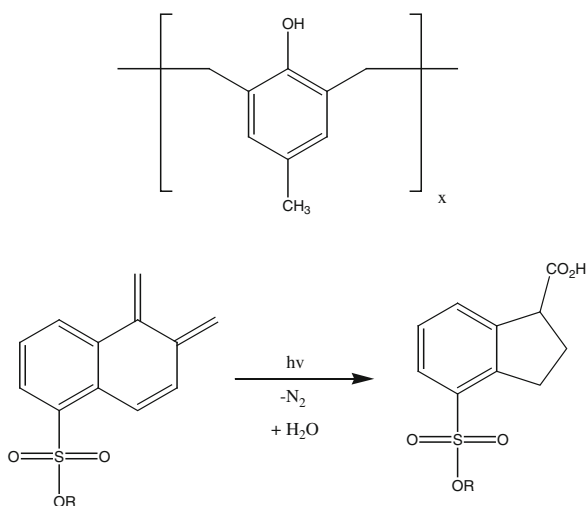
Scheme 13.3 Cycloaddition cross-linking of cinnamate groups

The approach is often to photochemically alter the functional groups of an insoluble molecule to convert the molecule into a soluble one. There are many different examples of this type of functional group conversion, but one of the most important is the class of polymers known as Novolaks [5].

Novolaks are phenol-formaldehyde type polymers. Novolaks are synthesised *via* a polycondensation reaction which is halted before the polymer becomes fully cross-linked. As Novolak polymers contain phenol units, they have reasonable solubility in aqueous base solutions. To act as a positive tone resist, the solubility of the Novolak polymer in basic solutions must be greatly enhanced. This can be achieved by using photochemically reactive additives. The additive used is a diazoanthraquinone, which undergoes a photochemically driven Wolff rearrangement reaction to produce a carboxylic acid (Scheme 13.4).

However, in the presence of suitable additives, the dissolution process can be greatly enhanced. The additives can be produced photochemically, leading to a useful photoresist system. In fact, Novolaks have been the ‘workhorse’ photoresists

Scheme 13.4 Wolff rearrangement of diazoanthraquinone to produce carboxylic acid



of the modern microelectronic revolution. The photoresist consists of Novolak polymer, with a small amount of diazonaphthaquinone dissolved in it. When irradiated, the diazonaphthaquinone undergoes a photochemical rearrangement.

The carboxylic acid produced is highly soluble in the base developing solution and the dissolution of this carboxylic acid enables the Novolak polymer to be dissolved much more readily in the base developer. In fact, the solubility of the Novolak polymer is increased by several orders of magnitude in comparison to the polymer in the absence of the carboxylic acid.

Novolak based resists that have not been exposed to UV light are therefore almost insoluble, but the exposed resist is highly soluble. Novolaks are therefore used as positive tone photoresists. Novolak chemistry has proved very effective for producing high resolution photolithographic patterns (Fig. 13.2) and is used extensively industry. An example of a Novolak-based commercial positive resist is S1813 from Rohm & Haas, which was developed for the microelectronics integrated circuits industry.

13.2.3 Photoresists for Micro-Electro-Mechanical Systems Processing

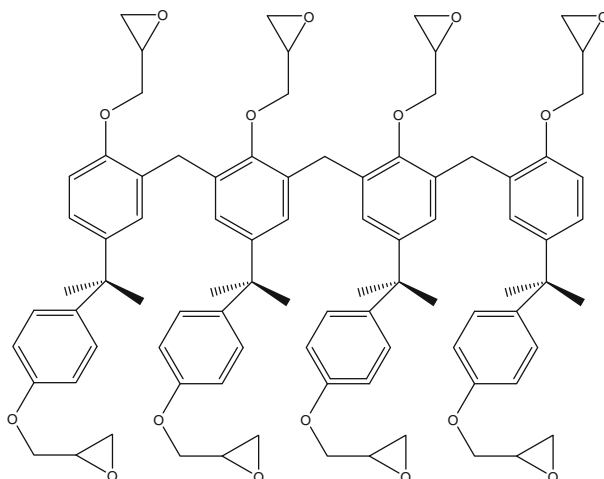
The microelectronics industry uses both positive and negative tone resists to pattern features from around 0.5 to several hundred micrometres in size. Smaller devices require high resolution processing with resists developed specifically for the microelectronics industry. Resist layers up to a few micrometres thick are usually sufficient for microelectronics device processing.

However, developments in the MEMS industry, which often relies on deep etching of silicon to fabricate micro-machine structures, require thicker resist layers and alternative polymer photoresists.

13.2.3.1 SU-8 Resist

A popular resist for MEMS processing is SU-8 [US Patent No. 4882245 (1989)]. This is a negative tone resist and is commonly applied as a layer, tens of micrometres in thickness. SU-8 was developed by Shell Chemicals and uses epoxy-based chemistry. Microchem [www.microchem.com] is one of the companies that now holds the licence for production and sale of SU-8 photoresists.

SU-8 (Scheme 13.5) is a very viscous polymer that can be spun or spread over a thickness ranging from 0.1 μm [6] up to 2 mm and can still be processed with standard contact lithography. It can be used to pattern high aspect ratio (>20:1) structures [7]. Its maximum absorption is for UV light with a wavelength of 365 nm. When exposed, SU-8's long molecular chains cross-link causing reduced solubility of the exposed resist.



Scheme 13.5 Molecular structure of SU-8 resist

SU-8 is highly transparent in the UV region, allowing fabrication of relatively thick (hundreds of micrometres) structures with nearly vertical side walls. After exposure and development, its highly cross-linked structure gives it high stability to chemicals and radiation damage. Cured cross-linked SU-8 shows very low levels of outgassing (the release of gasses from the polymer resist as a result of the resist being placed under vacuum conditions) in a vacuum [3]. However it is very difficult to remove, and tends to outgas in an unexposed state [4]. The main developer for SU-8 is 1-methoxy-2-propanol acetate.

SU-8 was originally developed as a photoresist for the microelectronics industry, to provide a high-resolution mask for fabrication of semiconductor devices. It is now mainly used in the fabrication of microfluidics (mainly *via* soft lithography) and micro-electromechanical systems (MEMS) (Fig. 13.3) and bio-MEMS applications [8]. This stems from its excellent biocompatibility—it is one of the most biocompatible materials known. SU-8 is now also used in conjunction with imprinting techniques such as nanoimprint lithography [2].

13.2.3.2 AZ-Series Resists

Several resists have been developed by AZ Electronic Materials for the MEMS industry. These resists are typically applied as thicker layers (around 8–50 μm in thickness). The thicker resist offers greater protection during the deep etch process encountered in MEMS device fabrication. These resists are positive tone and are based on diazonaphthaquinone/Novolak chemistry [13, 14].

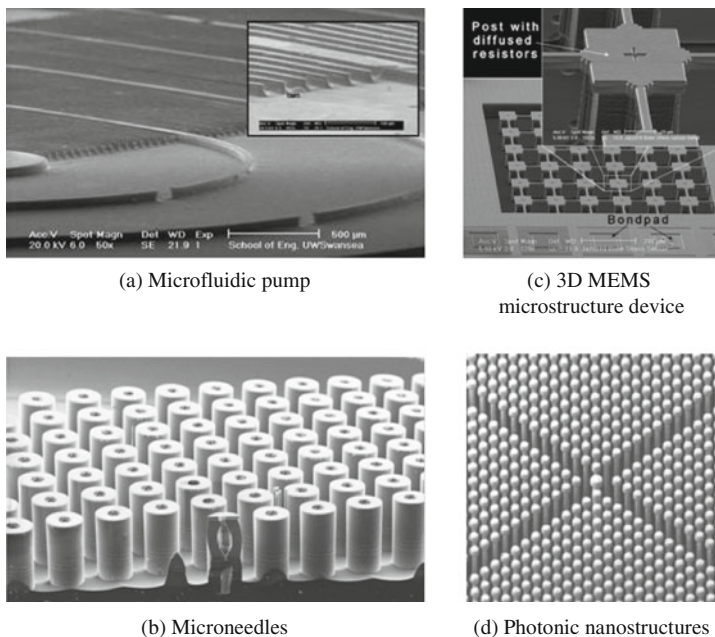


Fig. 13.3 MEMS 3D micro and nano structures produced by deep silicon etching. Deep etched silicon structures for microfluidic applications: **a** a microfluidic pump (image reproduced with kind permission from Springer Science and Business Media [9]); **b** hollow microneedles (images courtesy of Swansea University); **c** 3D MEMS device (images courtesy of F. Alfaro, G. K. Fedder, Carnegie Mellon University [10] and reproduced with permission from J. Micromech. Microeng. 19 (2009) 085016(13 pp) doi:10.1088/0960-1317/19/8/085016. Copyright (2009), IOP Publishing) [11]; and **d** nanophotonics structures (images courtesy of A.Q. Liu) [12]

13.2.4 Chemically Amplified Photoresists

Novolak, SU-8 and AZ photoresists provide excellent performance in microelectronics and MEMS applications. However, the increasing demands for higher resolution features and deep reactive ion etched MEMS structures place increasing demands on the photoresists used in these processes. Particularly important is the penetration of UV light into thick resist layers to effectively expose the resist layer all the way through. Insufficient or incomplete exposure can lead to non-discrete features and lower resolution patterns. High-resolution features in the microelectronics industry and sharp well-defined structures for MEMS devices are critical developments. Deep etched silicon structures, in MEMS devices, require particularly thick resist layers—often tens of microns or more. Efficient penetration of UV light into these layers is critical in producing well-defined structures with vertical sidewalls.

To counteract insufficient penetration of UV light into resist layers, higher powers and/or longer exposure times can be used to effect chemical change.

However, for device production, it is more desirable to utilise a low-power short duration process and perform the exposure process faster.

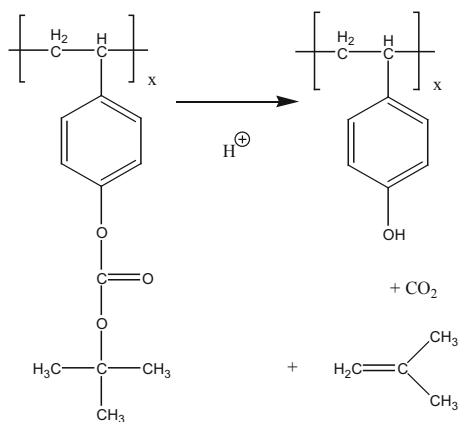
This issue has been addressed through clever polymer modification chemistry to maximise the effect of the light entering the resist layer. The process, developed by IBM, uses the concept of chemically amplified photoresists [15]. In this system, the original light exposure has a catalytic effect—initiating a series of secondary chemical reactions. It is these secondary chemical reactions that are responsible for the change in solubility needed for development. Chemically amplified photoresists therefore utilise one photon to initiate several secondary reactions, thus using the light much more effectively and enabling a more complete exposure of the resist. The chemical amplification process thus has a quantum yield which is much greater than one *i.e.* one photon causes several chemical reaction events.

A well-known example of the chemically amplified process uses a *t*-Boc-styrene polymer. Exposure of this polymer in the presence of an acid catalyst results in the protecting *t*-Boc groups decomposing to carbon dioxide and isobutylene, both gases that subsequently leave the coating (Scheme 13.6). The de-protection reveals phenolic moieties, which are soluble in aqueous base. This material can thus function as a negative tone photoresist [16].

Deprotection of the *t*-Boc groups is achieved by reaction with an acid, HX (Scheme 13.6). The acid is generated from photochemical decomposition of iodonium ($R_2I^+ X^-$) or sulfonium ($R_3S^+ X^-$) [17]. Deprotection of the *t*-Boc groups results in the formation of a styrene polymer with soluble phenolic side-chain groups. Thus the photoinduced creation of a soluble polymer from an insoluble one constitutes a positive chemically amplified photoresist.

Novolaks, can also be used in conjunction with photocatalysed acid generation. Chemically amplified resists can be used to fabricate very high resolution features with very little incident light required.

Scheme 13.6 Deprotection of Boc-styrene polymer to yield soluble phenol groups



13.3 Immersion Lithography

One method for extending the resolution of UV lithography beyond 193 nm—imposed by the diffraction limit of UV light—is immersion lithography. The ultimate resolution of a lithography system can be improved by passing light through a liquid medium [18]. In immersion lithography systems, projection optics with numerical apertures >1 can be constructed by filling the space between the lens and the photoresist with an immersion fluid with a refractive index, n , >1 [19]. The most practical and low-cost liquid for use as an immersion fluid is water, having a refractive index of 1.44 (at 193 nm). In addition, water does not generally interact with the resist, *i.e.* resists are primarily insoluble in water.

There are some obstacles to overcome before immersion lithography can be used in commercial systems [20], such as:

- contamination of the optical medium by the photoresist;
- formation of small bubbles that scatter light;
- damage to optical components from contaminated media;
- changes in the refractive index of the immersion liquid during exposure, resulting from fluid heating.

Some of these problems can be overcome using a top barrier coating to isolate the resist layer from the immersion medium [21]. Current state-of-the-art immersion photolithography systems utilise a wavelength of 193 nm [22]. Using optical techniques such as off-axis illumination and water immersion projection lenses, these systems can define feature sizes as fine as 38 nm.

13.4 Future Directions

The quest for smaller and smaller devices for more powerful and compact microchips for electronic applications requires device feature sizes beyond the diffraction limit of UV light. Industry is moving to ever-shorter irradiation wavelengths (193 nm) to obtain finer features. Aromatic-containing polymers are opaque at these short wavelengths, so new polymers and systems capable of absorbing short wavelength light are required.

Extensive research is being undertaken by the major corporations such as IBM, Bell Labs, Arch Corp, and many other high profile labs [23]. Chemical amplification is one of the techniques that are essential to achieving higher resolution features. Immersion lithography is also a promising technology with the capability of achieving 38 nm linewidths. Double-patterning techniques have the potential to reduce this resolution limit to 32 nm. Although impressive by today's standards, these figures are still far removed from the 10 nm resolution required for the next generation of electronics.

This has led to the development of a number of high-resolution lithographic techniques over the past two decades. Each of these techniques has its own advantages and disadvantages and some of the most important, including Extreme Ultraviolet (EUV), electron beam lithography and a variety of Nanoimprint Lithography (NIL) techniques are discussed below.

13.4.1 Extreme Ultraviolet Lithography

Extreme ultraviolet lithography (EUVL) is a promising technology for mass production at the scale of 10 nm [24]. The combination of small numerical aperture optics and small wavelengths enables superior ultimate resolution for these systems compared to their UV counterparts.

Utilising such small wavelength (high energy) photons in the system introduces new technical challenges for this type of lithography. This stems from the fact that EUV will interact with all forms of matter, including gases. Current EUV systems thus differ from their longer wavelength counterparts in two critical details: the system must be *in vacuo*, and employs reflective optics. Tin or xenon laser-produced plasmas are typically used as the source of EUV radiation [25].

Current highly reflective ($R > 65\%$) Bragg mirrors are optimised for wavelengths around 13 nm. These mirrors, comprised of layers of molybdenum and silicon, must be manufactured to an extremely high degree of accuracy. The Mo/Si multilayers act to reflect light by means of interlayer interference, or Bragg diffraction. Multilayers produced using magnetron sputtering can produce Mo/Si mirrors with reflectivities of 68 % [22, 26].

Since these mirrors are prone to degradation; good vacuums and oxidation protection are necessary to provide a practical lifetime for these optics systems [27]. A pressing issue in the development of EUV is the smoothness of the reflective mirrors. Mirrors are coated with up to 81 layers of reflective material and if EUV is to be used beyond the 32 nm manufacturing node, the mirrors will be required to be smooth and clean to within 1 atom.

The fact that EUV radiation interacts with all forms of matter has a number of implications for the development of suitable resists for EUVL. Finding a suitable material involves a trade-off between sensitivity, resolution, and line edge roughness (LER) [28]. Outgassing from the resist surface is also an issue when trying to maintain a good vacuum in the system [29]. Contamination from resist outgassing can reduce the lifetime of the system optics. A further trade-off therefore has to be made in the selection of EUV resists: resists that exhibit lower outgassing tend to be less sensitive, and *vice versa* [30, 31].

EUV photoresists exhibit properties of both optical photoresists and electron-beam resists (discussed below), since EUV photons generate secondary electrons. The resolution is limited by the effective point spread function, rather than the diffraction limit due to the wavelength.

Secondary electrons can travel as much as 50 nm [32] and there may also be long-distance backscattering effects in thin photoresist layers, due to secondary electrons from underlying layers. In particular, electrons with sufficient energy to dissociate a C–C bond (3.6 eV) exhibit a mean free path of around 20 nm.

Another issue that must be considered in relation to EUV is cost. The optics and masks for EUV are very expensive and the fact that the technique must be used in vacuum also significantly increases costs.

Line edge roughness becomes a significant concern at small line widths and when using thin photoresist films. The tradeoff between roughness and sensitivity means that it is difficult to produce sub-20 nm patterns using EUV lithography. However, this promising technology has been used to meet the specifications of the 32 and 22 nm nodes for the International Technology Roadmap for Semiconductors [33].

13.4.2 Electron Beam Lithography

Electron beam lithography (EBL) is similar to photolithography in many aspects, except that it uses a beam of electrons to expose the polymer resist and generate patterns on a surface, rather than a blanket UV light exposure. EBL is therefore a ‘direct-write’ technique and does not require a photomask. Very high-resolution nanoscale feature sizes can be written using EBL.

EBL has been considered a specialised technique because of the high equipment costs and the length of time required to ‘direct-write’ a large number of nanoscale features. It is used directly in industry for writing features, but the process is also used to generate exposure masks to be used with conventional photolithography. For commercial applications, electron beam lithography is usually produced using dedicated beam writing systems that are very expensive (>\$2 M USD).

However, EBL write times and tooling costs have decreased sufficiently so that EBL is now routinely used for creating the extremely fine patterns required by the modern electronics industry for integrated circuits. EBL is now often used in combination with photolithography to write-in very fine features such as the gate in a field effect transistor (FET) device.

Unlike optical lithography, where the resolution is limited by the wavelength of light used for exposure, the electrons in the beam have a wavelength so small that diffraction no longer defines the lithographic resolution (38.8 pm with an accelerating voltage of 1 kV, and 6.9 pm at 30 kV, as calculated considering the electron as a matter wave [34]).

The wavelength then, is not the limiting factor in electron beam optics. Rather, a combination of effects such as: the interaction between electrons (coulomb repulsion) within the beam, the interaction between the incident electrons and the returning secondary electrons, the cyclonic movement introduced by the magnetic lenses (in the plane perpendicular to the electron beam), along with the dimension

of the electron emitting source (filament or field emitting tip). The smaller the electron-emitting source is, the sharper the energy dispersion of the spot will be. State-of-the-art systems can reach a spot size of less than 1 nm.

Though a spot size as small as 1 nm is possible, in practice the ultimate resolution of electron beam lithography is limited to around 7 nm. In fact, it is quite difficult to achieve lithographic feature sizes of less than 10 nm due, mostly, to electron/matter interactions in the photoresist and in the substrate [35, 36]. These contributions can be attributed to two main types of scattering each of which can be treated separately and modelled by Gaussian distributions [37]. Inelastic scattering generates the secondary electrons that will expose the resist, or that can be used to image the surface. However, high energy electrons are only slightly deviated from the direction of the incident electron beam, thus increasing the electron energy reduces the lateral dispersion of secondary electrons.

Elastic collisions (backscattered electrons), though, consist of a large modification of the incident electron direction without any loss of energy and can be generated deep within the substrate. The back-scattered electrons can therefore be directed back to the surface in a location far from the incident beam, thus exposing the resist where it wasn't intended. Statistics predict that there is a high probability of exposure of the electron beam resist to backscattered electrons in the region around the incident electron beam. The radius of this exposure depends on parameters including the substrate type, the resist thickness and the incident electron energy. Successive exposures around the same area can therefore unintentionally fully expose the resist outside the defined writing area.

Electron beam lithography can comfortably be used to write features down to around 40 nm in size. However, when writing very small features in close proximity to one another using EBL, one must consider the proximity effect [38], whereby electrons from exposure of an adjacent feature spill over into the exposure of the originally written feature, effectively enlarging its image, and reducing its contrast, *i.e.*, difference between maximum and minimum intensity. Hence, the resolution of very small features in close proximity is difficult to control and for most resists, it is difficult to go below 25 nm lines and spaces. This effect, being statistical, cannot be completely eliminated, but can be partially predicted and compensated for, as illustrated in Fig. 13.4. Considerable effort from electron beam tool manufacturers has gone into counteracting the proximity effect and using an appropriate resist, it is now possible to write features of around 7 nm in size.

13.4.2.1 Electron Beam Resists

Electron beam resists are the recording and transfer media for EBL. The usual resists are polymers dissolved in a liquid solvent. Liquid resist is dropped onto the substrate, which is then spun at 1000–6000 rpm to form a coating—as in photolithography.

After baking out the casting solvent, exposure to the electron beam modifies the resist. As in optical lithography, there are two types of e-beam resists: positive tone

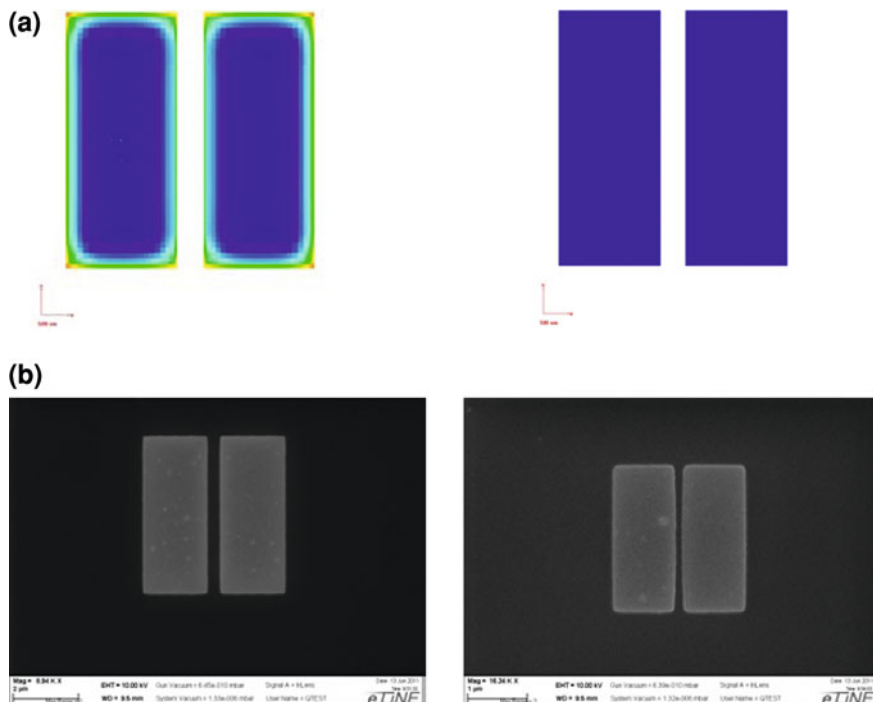
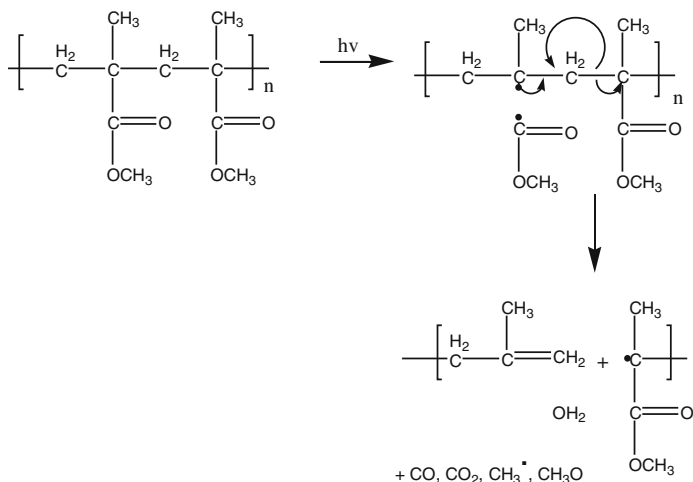


Fig. 13.4 **a** Illustration of the proximity effect created by backscattered electrons. **b** SEM image of features written using electron beam lithography with and without compensation for the proximity effect

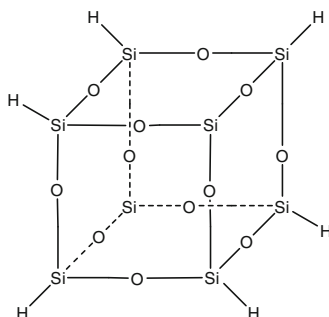
and negative tone, with the usual behaviour, *i.e.*, positive resists develop away at exposed regions, whereas in the case of negative resist the developed region remains after development.

Poly(methyl methacrylate) (PMMA) is the standard positive e-beam resist, usually purchased in two high molecular weight forms (495 or 950 kg mol^{-1}) in a casting solvent such as chlorobenzene or anisole. For example 950 kg mol^{-1} PMMA, 4 % in anisole is a commonly used solution. Electron beam exposure breaks the polymer into fragments (as shown in Scheme 13.7) that can be dissolved in a 1:1 MIBK:IPA developer (where MIBK is methyl isobutyl ketone and IPA is isopropyl alcohol).

PMMA based resists are suitable for fabricating device features with approximately 20 nm line widths. However, to achieve feature sizes below 20 nm it is necessary to use a resist developed for high-resolution line widths. One such resist is the negative tone electron beam resist hydrogen silsesquioxane (HSQ—Scheme 13.8) [39]. HSQ has a small grain size, which improves the ultimate resolution of the features obtainable. It can routinely be used to pattern sub-10 nm size features and indeed the smallest EBL structures reported have been obtained using HSQ [40–42]. HSQ has good etch resistance and good stability under



Scheme 13.7 Electron beam induced fragmentation of PMMA



Scheme 13.8 Molecular structure of hydrogen silsesquioxane (HSQ) before cross-linking

scanning electron microscope (SEM) inspection [43, 44]. After exposure to the electron beam, HSQ undergoes a cross-linking reaction and forms an amorphous silicon oxide structure. This amorphous material can be removed with tetramethyl ammonium hydroxide (TMAH), while the un-exposed HSQ material remains on the surface.

Electron beam lithography using HSQ often utilises a lift off process illustrated in Fig. 13.5. The lift-off process involves deposition of a material (often a metal) on top of a patterned resist layer. Where there is no resist present, the metal adheres to the semiconductor substrate. However, metal deposited on top of the resist can be removed when developing the resist.

An issue when using negative resists for lift-off processing however, is that negative resists usually produce an ‘over-cut’ profile. To resolve this problem, an intermediate layer of PMMA can be deposited beneath the HSQ layer and the

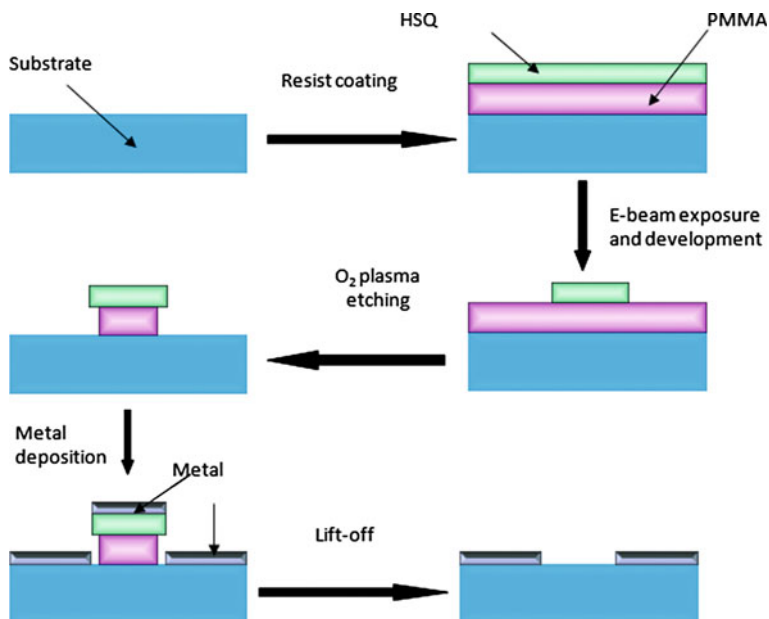


Fig. 13.5 Schematic diagram of the HSQ/PMMA bilayer resist for a negative tone lift-off process

substrate. The design from the HSQ is then transferred on to the PMMA layer using an oxygen plasma etch [45]. The resulting design then has an ‘undercut’ profile, allowing a lift-off process to be undertaken effectively, as shown in Fig. 13.5.

13.4.2.2 Electron Interference Lithography

Interference lithography uses the superposition principle to create an interference pattern to create fine, regular patterns. Interference lithography using electron beams is another possible path for patterning arrays with nanometre-scale periods [46]. This technique is therefore suitable for patterning regular, dense features over a large area.

At a given energy, the de Broglie wavelength of electrons is much shorter than that of a photon, allowing for finer features to be patterned. Though electron beam lithography is arguably more complicated in its execution, it is still the most practical method for concentrating the most energy into the smallest possible area on the resist. Compared to ‘direct write’ modes of electron beam lithography, interference techniques allow a pattern to be transferred into the resist with much higher throughput [47]. Electron interference lithography can utilise the same resists as ‘direct write’ EBL, such as PMMA [48].

13.4.3 Nanoimprint Lithography

Nanoimprint lithography is an alternative approach to patterning of nanoscale structures. In contrast to direct writing, using an electron beam or exposure using short wavelength radiation, NIL can be used for rapid replication of nanostructures, which can be fabricated over large areas. NIL has emerged as a potential lithography technique for the 32 nm device fabrication node and beyond because of its ability to faithfully reproduce sub-30 nm features with fidelity and high throughput [49].

The nanoimprint process utilises a patterned, 3D mould (template or stamp) to define patterns by embossing a soft polymer or liquid material. Once the material has completely filled the template cavities, it is hardened, using either a thermal or photochemical process, and the template is removed. The hardened imprinted polymer is an inverse 3D replication of the template mould. NIL uses a stamp or template to imprint or emboss a pattern into a polymer. The 3D polymer structures themselves may be used to create the desired nanostructures or alternatively, the polymer structures may be used as a protective mask to selectively protect a substrate during a subsequent process e.g. etching or deposition.

The main advantage of NIL techniques, over direct-write techniques such as electron beam lithography, is that NIL can be used for rapid replication of nanoscale features on a wafer substrate. There are several variations of NIL, developed by different manufacturers of NIL systems. The following sections give a brief overview of some of the most important concepts of NIL.

13.4.3.1 Master Stamp Creation

Common to all NIL techniques is the requirement for a ‘master’ stamp or template. The master is usually fabricated on silicon, glass or other rigid wafer substrate. For a nanoimprint process, the master must be patterned with nanoscale features using electron beam lithography.

13.4.3.2 Hot Embossing

Hot embossing is perhaps the most simple NIL technique, where the master stamp is imprinted into a soft polymer layer on a substrate (Fig. 13.6) [50]. The polymer and substrate are then heated, curing the polymer to form rigid polymer structures—the inverse of the structures on the master stamp. Once the polymer has been cured sufficiently, the master stamp is retracted, leaving the patterned polymer layer on the wafer substrate.

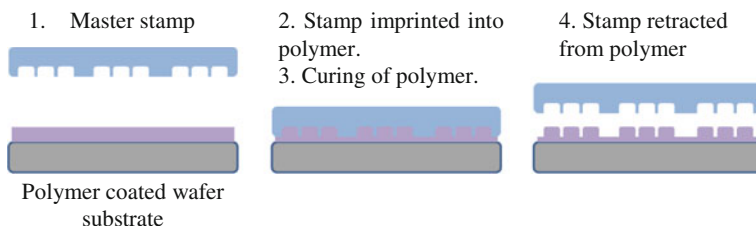


Fig. 13.6 Illustration of the hot embossing NIL process

13.4.3.3 Step and Flash NIL

Step and Flash NIL is similar to hot embossing except that a glass or quartz master must be used, rather than a silicon stamp. The reason for this is that the polymer curing step is achieved by exposing the template polymer to light—through the glass/quartz master (Fig. 13.7) [49]. The polymer-coated wafer is first imprinted with the nanostructured master stamp. UV light is then passed through the transparent quartz master to photochemically cure the polymer. The master is then retracted from the polymer, leaving behind the imprinted polymer.

Step and Flash Imprint Lithography (SFIL, a trademark of Molecular Imprints, Inc.) is a low-temperature, low-pressure UV-NIL process targeted for applications in complementary metal oxide semiconductor (CMOS) fabrication [51]. In this process, a low-viscosity liquid monomer fills the space between the template and a substrate and is then exposed to UV irradiation, which initiates a polymerisation that vitrifies the imprint fluid.

Although many variations on the imprint resist formulation exist, imprint resist formulations for UV-NIL applications generally consist of a solution containing a free radical generator and monofunctional, cross-linking, and etch-resistant monomers. The bifunctional crosslinking monomers are incorporated to provide the mechanical properties necessary for successful template separation from the cured imprint resist without deformation of high-resolution features or cohesive failure within the polymer. The etch-resistant monomers typically contain inorganic elements such as silicon to provide resistance to oxygen reactive ion etching. When the inorganic materials are exposed to oxidative environments, a nonvolatile inorganic oxide residue is generated that acts as an etch mask.

Acrylic or vinyl ether functional groups are incorporated due to their high polymerisation rate and high degree of conversion. Tough materials with tensile moduli over 100 MPa are required for faithful pattern replication at the nanometre scale. Further, the resist must contain at least 9 % silicon to provide sufficient oxygen etch resistance for pattern transfer [52, 53]. No current SFIL formulations produce easily strippable polymers due to the high degree of cross-linking (10–30 %) [53, 54].

SFIL formulations may be modified by replacing ethyleneglycol diacrylate, a nondegradable cross-linker, with a degradable (de-cross-linkable) cross-linker to

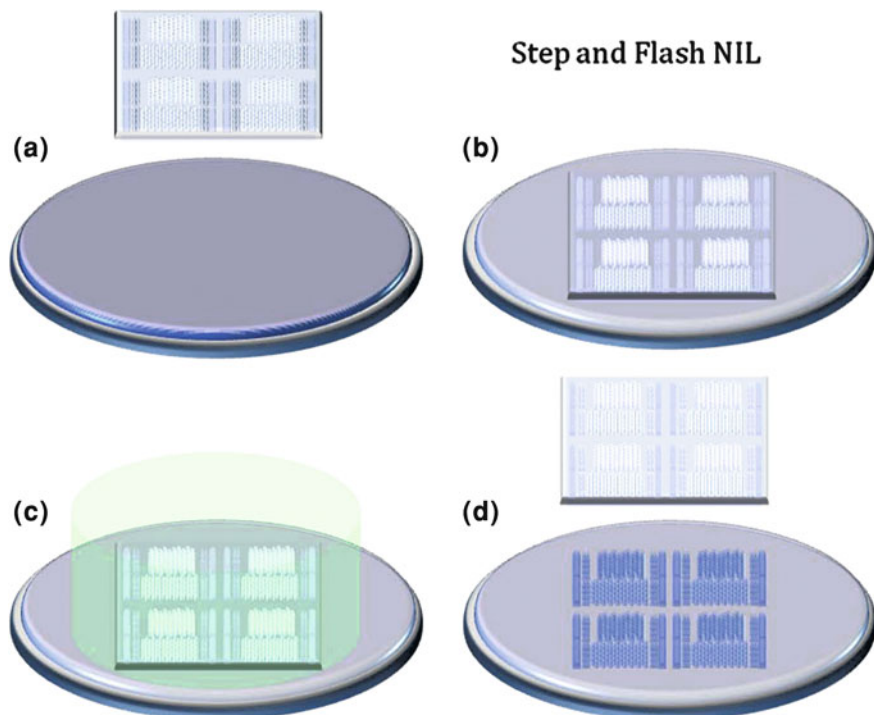


Fig. 13.7 Step and Flash Nano Imprint Lithography: **a** wafer coated in photoresist; **b** master stamp imprinted into resist; **c** UV curing 'flash' step to selectively harden resist; **d** stamp retracted from resist

enable stripping of the photopolymerised material with conventional solvents. Several de-cross-linking systems, such as Diels–Alder adducts, hydrogen-bonding monomers, degradable esters, and acetals, have been demonstrated elsewhere, but they have not been implemented in a UV-NIL process [55, 56]. Many potential degradable cross-linker designs create compatibility or solubility issues in standard imprint formulations, and the need for low viscosity and high molar concentration eliminates many of the candidates.

13.4.3.4 Soft Stamp Imprint Technology

NIL stamp sizes are often limited to areas of around 25 mm × 25 mm due to interactions between contaminant particles and the hard stamp. Hard silicon, glass or quartz stamps are inflexible when brought into contact with contaminant particles. If contaminant particles are present on the surface of the stamp or on the surface of the polymer coated wafer, these particles can cause significant damage to the stamp or to the wafer during the imprinting process. This damage is caused by the particle interacting with the stamp/wafer surface during the pressurised imprint

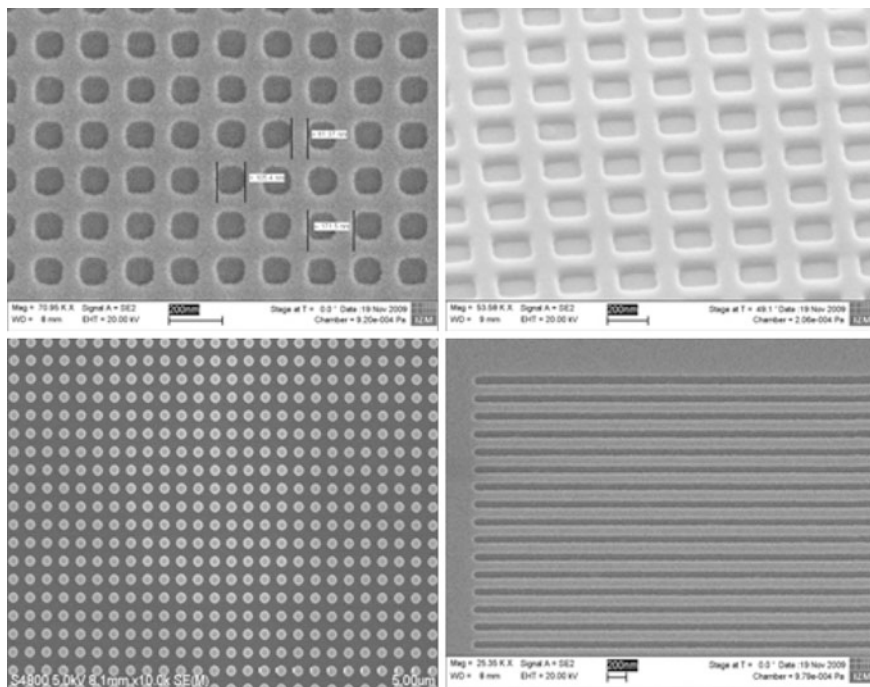


Fig. 13.8 SEM images of NIL (SCIL) photonic structures [images courtesy of Suss Microtec AG]

process. Thus, NIL should ideally be performed in a clean room with very low particle counts. To circumvent this issue, some manufacturers now use ‘soft stamp’ technology.

This process is essentially the same as the NIL method described above except for the use of a flexible soft stamp in place of the conventional hard silicon or quartz stamp. The soft stamp is fabricated using a polymer such as polydimethylsiloxane (PDMS). The polymer is coated onto a semi-flexible (thin glass) substrate and is imprinted with a silicon master (patterned using electron beam lithography or other nano-lithography technique). The imprinted PDMS is then photochemically cured and the master template is retracted, leaving behind the patterned PDMS on the flexible glass substrate. The glass/PDMS stamp then becomes the ‘soft stamp’. Because the PDMS is flexible, contaminant particulates tend to become embedded in the PDMS rather than damaging the substrate wafer. The more the NIL processes are repeated, the better the results tend to be, as particulates are absorbed into the PDMS layer.

As long as the particulates are not too large, transfer of the NIL patterns onto the polymer-coated wafer substrate is very effective, with very few voided areas. Large particles will of course still result in some voiding. Soft stamp technology

enables imprinting over much larger areas compared to standard hard stamp techniques and significantly improves yields. Hard stamp NIL is usually limited to 25 mm × 25 mm imprint areas whereas soft stamps have been used to print areas of up to 200 mm × 200 mm. Figure 13.8 shows some SEM images of structures fabricated using NIL.

13.4.3.5 Substrate Conformal Imprint Lithography

Substrate Conformal Imprint Lithography (SCIL) is a relatively new technique developed jointly by Phillips and Suss Microtec AG [57, 58]. It uses flexible soft stamp technology combined with an elegant vacuum controlled technique for the stamp imprint and retraction process.

The soft PDMS stamp allows large area imprinting and can lower the stamp fabrication cost, since thousands of copies can be reproduced from one master stamp. In addition, lateral stamp distortion and structure deformation caused by backside pressure during standard imprinting processes, which often restricts the resolution of UV-NIL using PDMS stamps to several hundreds of nanometres, can be minimised using the SCIL process [59].

The SCIL process uses a PDMS working stamp, replicated from the master, and glued onto a semi-flexible thin glass carrier. The use of the semi-flexible thin-glass substrate has two effects; firstly, the rigidity of the glass carrier avoids lateral stamp trapping caused by vacuum fixing on the stamp holder, and secondly the thin glass and PDMS are flexible enough to allow conformal imprinting over large areas.

Although the PDMS stamp can compensate for non-uniform flatness of the substrate, local stamp trapping caused by stamp replication can lead to non-conformal imprint or ‘bubbles’ when using a standard perpendicular stamp application imprint process. To achieve a substrate conformal contact between working stamp and substrate, the SCIL process relies on a sequential stamp approach in combination with the capillary forces of the liquid imprint resist. The approach of the flexible stamp starts from one side of the imprint stamp and spreads across the whole stamp sequentially by releasing the vacuum holding grooves step by step on the stamp holder.

This sequential contact mechanism prevents flexible stamp trapping and therefore ensures that the stamp follows exactly the undulating topography of the substrate. The application of capillary forces instead of backside pressure minimises structure deformation and lateral stamp distortion during the imprint process and can facilitate sub-10 nm resolution. After conformal contact over the entire substrate is carried out, the imprint resist layer is cured by UV-curing or diffusion of the solution into the PDMS stamp, in the case of using UV-curable NIL resist or imprint sol-gel, respectively. The automatic separation of the stamp from the substrate is performed by sequentially application of a vacuum to the grooves—in the reverse order to the original imprint process.



Fig. 13.9 Schematic of roll-to-roll nanoimprint lithography process

13.4.3.6 Roll-to-Roll NIL

NIL is one of the most promising techniques for high throughput replication of nanoscale structures. NIL can be used to process tens of wafers per hour, but for high-volume production of low-cost nanopatterned substrates for flat-panel displays, photonics, biotechnology and organic optoelectronics applications, a rapid throughput version of NIL is required.

A nanoimprint-based patterning technique that can be applied in a continuous roll-to-roll process to drastically increase the patterning speed is thus an attractive proposition. Continuous roll-to-roll nanoimprint processes are capable of replicating 300 nm line width optical grating patterns on both hard glass and flexible plastic substrates have been demonstrated [60, 61].

The R2RNIL nano-manufacturing process consists of two processing steps: (1) the coating process and (2) the imprinting-curing process. First, liquid phase UV-curable resist material is continuously coated on to the glass or flexible plastic (PET) substrate *via* a series of rollers. This provides a uniform coating of the UV-curable imprint polymer on the substrate. The imprint mould (stamp) is formed using a flexible ethylene tetrafluoroethylene (ETFE) polymer—replicated from a silicon master stamp using a standard NIL process.

Several ETFE soft stamps are then transferred on to a tensioned belt, which loops continuously over two rollers. The soft stamp imprints the nanoscale pattern onto the conveying coated substrate (Fig. 13.9). Continuous roll-to-roll imprinting has been demonstrated using a ~ 10 cm wide pattern. The polymer-coated substrate is imprinted and simultaneously UV cured, before the rolling stamp detaches from the imprinted polymer. The UV-curable polymer resist used is low viscosity liquid epoxysilicone [62].

13.4.4 Scanning Probe Nanolithography Techniques

In addition to the industry standard lithography techniques described above, there are a number of new nanolithography tools being developed by research groups. A number of these techniques are based on the use of scanning probes to ‘direct write’ nanoscale patterns onto a substrate. One of the more interesting techniques uses a scanning near-field optical microscope (SNOM) as a nanoscale lithography tool (SNOM is also discussed briefly in Chap. 14).

Near-field optical techniques are able to achieve resolutions beyond the diffraction limit ($\lambda/2$) by exploiting the properties of evanescent waves, which are not restricted by the effects of diffraction. Evanescent waves are non-propagating components of electric fields, which decay rapidly with increasing distance from their source.

SNOM is one such technique that utilises this phenomenon. Typically a sub-wavelength aperture is used to generate an evanescent electric field. Practically, light is passed down an optical fibre that has been drawn to a sharp tip with an aperture of nanoscale dimensions. The tip is often coated with a metal to help confine the light to the fibre optic core. If the probe aperture is sufficiently small, laser light that is passed through an optical fibre is confined to the probe and cannot propagate as illustrated in Fig. 13.10a. However, in the immediate vicinity of the aperture, non-propagating evanescent waves (or near-fields) are created that are not subject to diffraction effects and can be utilised to image nanoscale features. The resolution of SNOM is largely governed by the aperture of the SNOM fibre tip that can be as small as 20 nm in diameter [63].

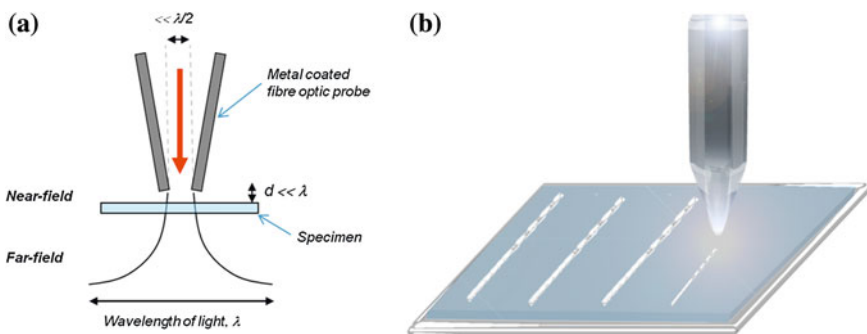


Fig. 13.10 **a** Schematic diagram depicting a metal-coated SNOM probe with sub-wavelength aperture. The aperture confines the light to the probe such that light cannot propagate. However, an evanescent near field exists within close proximity to the aperture which can be used to image a sample or write structures with resolutions beyond the diffraction limit. **b** Illustration of SNOM lithography using a metal-coated optical fibre tip

The SNOM technique has a reputation for being somewhat challenging. However, many of the difficulties encountered when using the instrumentation for imaging applications are not an issue when attempting photolithography. Moreover, optical fibre-based SNOM probes can be very effective tools for the selective exposure of resists to create nanoscale features (Fig. 13.10b). First reported by Betzig *et al.* [64], features of approximately 60 nm were written into Co/Pt multilayer films using visible light directed onto the films through an aluminium coated SNOM fibre probe. The authors noted that the feature size was dependent on the power used (up to a limit of 6 mW), beyond which the power was sufficient to cause damage to the aluminium coating on the probe resulting in increased feature widths.

Since this initial work, many developments of the technique have occurred. SNOM has subsequently been used to expose films of conventional photoresist to UV light emanating from the SNOM probe and to write patterns with line widths well beyond the limitations of diffraction [65]. Despite this success, the key to realising SNOM's full potential in photolithography applications is to minimise the thickness of the photoresist films. This point is critical since the evanescent electric field decays very rapidly with increasing distance from the probe's aperture. As such, the highest resolutions are achieved when self-assembled monolayers (SAMs) of photoactive medium are utilised—rather than standard polymer resists.

Sun *et al.* [65] demonstrated for the first time that SNOM could be utilised to write nanoscale features in SAMs. Well-ordered monolayers of alkylthiolates were adsorbed onto gold substrates and selected regions were subsequently exposed to UV light. In the presence of oxygen, the adsorbates oxidised to generate alkylsulfonates:



The oxidation products are only weakly bound at the gold surface and are readily displaced by immersion in a solution of a second thiol. The chemical pattern produced during this process was examined using atomic force microscopy (AFM) and structures as small as 25 nm were fabricated.

Sun and Leggett [66] further demonstrated the use of SNOM to fabricate features 20 nm in size in SAMs of alkanethiols on gold substrates. This additional study established that it is routinely possible to fabricate structures smaller than the SNOM probe aperture and that the dimensions of the written structures correlate with the substrate morphology. Sun and Leggett [66] conclude that non-radiative interactions, possibly plasmonic, between the metallic substrate and the fibre result in a focusing of the electric field beneath the aperture and that this is more pronounced when polycrystalline substrates with comparatively small grain sizes are used.

Further improvements have been realised and more recently Montague *et al.* [67] demonstrated SNOM's capability to generate photo-patterned structures in SAMs with dimensions as small as 9 nm, approximately 15 times smaller than the Rayleigh limit. SAMs consisting of alkylthiols functionalised with oligo(ethylene glycol) groups (OEG-functionalised SAMs) were used by Montague *et al.* [67].

The OEG-terminated monolayers were exposed to UV light and oxidised to yield sulfonates. These were subsequently used to fabricate protein nanopatterns.

There are, however, a number of remaining difficulties associated with SNOM that make near-field photolithography challenging. These issues should be addressed if the technique is to become a mainstay in device fabrication. The feature size depends heavily on the probe aperture size—if the aperture comes into contact with the sample or too much laser power is coupled into the probe, the aluminium coating may flake and result in the aperture size increasing—and as such increasing the size of the features written on the surface. Apertureless probe techniques are receiving attention in conventional SNOM applications due to localised field enhancement in close proximity to a metal probe. Apertureless techniques hold much promise in delivering superior resolutions in near-field lithography applications particularly when coupled with two-photon absorption processes

Another issue with respect to lithographic processing is the serial nature of scanning probe techniques. Mask-based lithography processes offer rapid fabrication of structures, whereas in scanning probe methods the probe must raster over the sample and can only write one feature at a time, making the process somewhat lengthy. Recently, ul Haq *et al.* [68] have developed instrumentation that performs high-throughput near-field photolithography on large scales. Their instrument, named the ‘Snomipede’, employs 16 parallel optical probes; the positioning of each is performed precisely and with an independent feedback mechanism. They propose that the principle of the Snomipede can be extended to include much larger arrays of probes. Moreover, they demonstrate that an array of probes can also be utilised effectively in fluid environments, which has advantages for applications outside of electronic device fabrication.

Although near-field lithography is still in its infancy, the technique holds much promise in nanofabrication. Careful selection of photoactive resist materials can produce structures that have comparative linewidths to those achievable using electron beam lithography. The potential offered by further advances in SNOM-based lithography techniques and the development of new SNOM resists must continue to be explored.

13.5 Conclusions

Though a number of lithographic techniques and corresponding resists have been outlined here, it should be stressed that there is no superlative technique that can render the others redundant. Rather than being competing techniques in a standard fabrication process, different lithographic techniques complement each other. For example, the versatility and high resolution of electron beam lithography is useful in conjunction with the high throughput and reliability of UV photolithography. It is therefore essential that these techniques and the supporting photochemistry be well understood for the outstanding progress in electronics to continue.

References

1. Moore GE (1995) Lithography and the future of Moore's law. *Adv Resist Technol Process* 2438:2
2. Burns K, Adams KB, Longwell J (1950) Interference measurements in the spectra of neon and natural mercury. *JOSA* 40:339–344
3. Miura K, Tomita Y (1978) Photo-sensitive bis-azide containing composition. US Patent 4,099,973
4. Haddleton DM, Creed D et al (1989) Photochemical crosslinking of main-chain liquid-crystalline polymers containing cinnamoyl groups. *Makromol Chemie Rapid Commun* 10:391–396
5. van Delft FC, Weterings JP, van Langen-Suurling AK et al (2000) Hydrogen silsesquioxane/novolac bilayer resist for high aspect ratio nanoscale electron-beam lithography. *J Vac Sci Technol B Microelectron Nanometer Struct* 18:3419
6. Franssila S (2004) Introduction to microfabrication. Wiley, New York
7. Lorenz H, Despont M, Fahrni N et al (1998) High-aspect-ratio, ultrathick, negative-tone near-UV photoresist and its applications for MEMS. *Sens Actuators A* 64:33–39
8. Voskerician G, Shive MS, Shawgo et al (2003) Biocompatibility and biofouling of MEMS drug delivery devices. *Biomaterials* 24:1959–1967
9. Eng P, Nithiarasu P, Guy O (2010) An experimental study on an electro-osmotic flow-based silicon heat spreader. *Microfluid Nanofluid* 9:787–795
10. Alfaro JF (2007) A multi axial bioimplantable MEMS array bone stress sensor. PhD thesis Carnegie Mellon University. http://www.ri.cmu.edu/publication_view.html?pub_id=5975
11. Alfaro JF, Weiss L, Campbell P et al (2009) Design of a multi-axis implantable MEMS sensor for intraosseous bone stress monitoring. *J Micromech Micromeng* 19:085016. <http://iopscience.iop.org/0960-1317/19/8/085016>
12. Teo SHG, Liu A, Singh J et al (2004) High resolution and aspect ratio two-dimensional photonic band-gap crystal. *J Vac Sci Technol B Microelectron Nanometer Struct* 22:2640
13. O'Brien J, Hughes P, Brunet M et al (2001) Advanced photoresist technologies for microsystems. *J Micromech Micromeng* 11:353
14. Dammel R (1993) Diazonaphthoquinone-based resists. SPIE, Washington
15. Ito H (1997) Chemical amplification resists: history and development within IBM. *IBM J Res Dev* 41:119–130
16. Postnikov SV, Stewart MD, Tran HV et al (1999) Study of resolution limits due to intrinsic bias in chemically amplified photoresists. *J Vac Sci Technol B Microelectron Nanometer Struct* 17:3335
17. Crivello JV, Shim SY (1994) Photoresist composition comprising a copolymer having a di-*t*-butyl fumarate. US Patent 5,346,803
18. Owa S, Nagasaka H (2003) Immersion lithography; its potential performance and issues. In: Yen A (ed) *Optical microlithography XVI*. Proceedings SPIE 5040, pp 724–733
19. Bratton D, Yang D, Dai J, Ober CK (2006) Recent progress in high resolution lithography. *Polym Adv Technol* 17:94–103
20. Hinsberg WD, Hoffnagle J, Wallraff G et al (2005) Evaluation of functional properties of imaging materials for water immersion lithography. *SPIE* 5753:508
21. Allen RD, Brock PJ, Sundberg L et al (2005) Design of protective topcoats for immersion lithography. *J Photopolym Sci Technol* 18:615–619
22. Wu B, Kumar A (2007) Extreme ultraviolet lithography: a review. *J Vac Sci Technol B Microelectron Nanometer Struct* 25:1743
23. Vladimirov N, Fréchet MJM, Yamada S et al (1999) Photoresists with reduced environmental impact: water-soluble resists based on photo-cross-linking of a sugar-containing polymethacrylate. *Macromolecules* 32:86–94
24. Wagner C, Harned N (2010) EUV lithography: lithography gets extreme. *Nat Photonics* 4:24–26

25. Jin F, Richardson M (1995) New laser plasma source for extreme-ultraviolet lithography. *Appl Opt* 34:5750–5760
26. Mirkarimi PB, Bajt S, Wall MA (2000) Mo/Si and Mo/Be multilayer thin films on Zerodur substrates for extreme-ultraviolet lithography. *Appl Opt* 39:1617–1625
27. Mertens B, Weiss M, Meiling H et al (2004) Progress in EUV optics lifetime expectations. *Micromech Micromeng* 73:16–22
28. Naulleau PP, Gallatin GM (2003) Line-edge roughness transfer function and its application to determining mask effects in EUV resist characterization. *Appl Opt* 42:3390–3397
29. Kobayashi S, Santillan JJ, Oizumi H et al (2009) EUV resist outgassing release characterization and analysis. *Micromech Micromeng* 86:479–482
30. Gonsalves K, Thiyagarajan M, Choi JH et al (2005) High performance resist for EUV lithography. *Micromech Micromeng* 77:27–35
31. Goethals A, Gronheld R, Leumissen L et al (2005) EUV resist screening: current performance and issues. *J Photopolym Sci Technol* 18:647–654
32. Lee KW, Yoon SM, Lee SC et al (2009) Secondary electron generation in electron-beam irradiated solids: resolution limits to nanolithography. *J Korean Phys Soc* 55:1720–1723
33. Wu B (2011) Next-generation lithography for 22 and 16 nm technology nodes and beyond. *Sci China Inf Sci* 54:959–979
34. De Broglie L (1924) Recherches sur la théorie des quanta. Thèse de doctorat, Faculté des Sciences de Paris, Paris
35. Fische P, Chou S (1993) 10 nm electron beam lithography and sub-50 nm overlay using a modified scanning electron microscope. *Appl Phys Lett* 62:2989–2991
36. Vieu C, Carcenac F, Pepin A et al (2000) Electron beam lithography: resolution limits and applications. *Appl Surf Sci* 164:111–117
37. Chang T (1975) Proximity effect in electron-beam lithography. *J Vac Sci Technol* 12:1271–1275
38. Parikh M (1979) Corrections to proximity effects in electron beam lithography. I Theory *J Appl Phys* 50:4371–4377
39. Peucker M, Lim M, Smith HI et al (2002) Hydrogen silsesquioxane, a high-resolution negative tone e-beam resist, investigated for its applicability in photon-based lithographies. *Microelectron Eng* 61:803–809
40. Mohammad M, Dew S, Evoy S et al (2011) Fabrication of sub-10 nm silicon carbon nitride resonators using a hydrogen silsesquioxane mask patterned by electron beam lithography. *Microelectron Eng* 88:2338–2341
41. Grigorescu A, van der Krogt M, Hagen CW et al (2007) 10 nm lines and spaces written in HSQ, using electron beam lithography. *Microelectron Eng* 84:822–824
42. Grigorescu A, Hagen C (2009) Resists for sub-20-nm electron beam lithography with a focus on HSQ: state of the art. *Nanotechnol* 20:292001
43. Lister K, Casey B, Dobson P et al (2004) Pattern transfer of a 23 nm-period grating and sub-15 nm dots into CVD diamond. *Microelectron Eng* 73:319–322
44. Henschel W, Georgiev Y, Kurz H (2003) Study of a high contrast process for hydrogen silsesquioxane as a negative tone electron beam resist. *J Vac Sci Technol, B Micro-electron Nanometer Struct* 21:2018
45. Yang H, Jin A, Luo Q et al (2008) Electron beam lithography of HSQ/PMMA bilayer resists for negative tone lift-off process. *Microelectron Eng* 85:814–817
46. Hasselbach F (1997) Selected topics in charge particle interferometry. *Scanning Microsc* 11:345–366
47. Ogai K, Kimura Y, Shimizu R et al (1995) Nanofabrication of grating and dot patterns by electron holographic lithography. *Appl Phys Lett* 66:1560–1562
48. Fujita S, Maruno S, Watanabe et al (1995) Periodical nanostructure fabrication using electron interference fringes produced by scanning interference electron microscope. *Appl Phys Lett* 66:2754
49. Palmieri F, Adams J, Long B et al (2007) Design of reversible cross-linkers for step and flash imprint lithography imprint resists. *ACS Nano* 1:307–312

50. Jaszewski R, Schiff H, Gobrecht J et al (1998) Hot embossing in polymers as a direct way to pattern resist. *Microelectron Eng* 41:575–578
51. Johnson SC, Bailey TC, Dickey MD et al (2003) Advances in step and flash imprint lithography. *Proc SPIE Int Soc Opt Eng* 5037:197–202
52. Le NV, Dauksher WJ, Gehoski KA et al (2005) Selective dry etch process for step and flash imprint lithography. *Microelectron Eng* 78:464–473
53. Mancini DP, Le N, Gehoski KA et al (2004) Sub-80-nm contact hole patterning using step and flash imprint lithography. *Proc SPIE-Int Soc Opt Eng* 5374:371–382
54. Kim E, Stacey N, Smith B et al (2004) Vinyl ethers in ultraviolet curable formulations for step and flash imprint lithography. *J Vac Sci Technol B Microelectron Nanometer Struct* 22:131
55. Ogino K, Chen J, Ober C (1998) Synthesis and characterization of thermally degradable polymer networks. *Chem Mater* 10:3833–3838
56. Chen X, Wudl F, Mal A et al (2003) New thermally remendable highly cross-linked polymeric materials. *Macromolecules* 36:1802–1807
57. Ji R, Hornung M, Verschuuren MA et al (2010) UV enhanced substrate conformal imprint lithography (UV-SCIL) technique for photonic crystals patterning in LED manufacturing. *Microelectron Eng* 87:963–967
58. Verschuuren MA (2010) Substrate conformal imprint lithography for nanophotonics. PhD thesis, Utrecht University
59. Ji R, Krueger A, Hornung M et al (2009) Full field nanoimprint on mask aligners using substrate conformal imprint lithography technique. *Acta Phys Pol* 116:S187–S189
60. Stuart C, Chen Y (2009) Roll in and roll out: a path to high-throughput nanoimprint lithography. *ACS Nano* 3:2062–2064
61. Ahn SH, Guo LJ (2009) Large-area roll-to-roll and roll-to-plate nanoimprint lithography: a step toward high-throughput application of continuous nanoimprinting. *ACS Nano* 3:2304–2310
62. Cheng X, Guo L, Fu P (2005) Room-temperature, low-pressure nanoimprinting based on cationic photopolymerization of novel epoxysilicone monomers. *Adv Mat* 17:1419
63. Hecht B, Sick B, Wild U et al (2000) Scanning near-field optical microscopy with aperture probes: fundamentals and applications. *J Chem Phys* 112:7761–7774
64. Betzig E, Trautman J, Wolfe R et al (1992) Near-field magneto-optics and high density data storage. *Appl Phys Lett* 61:142–144
65. Bozhevolnyi S, Vohnsen B (1997) Near-field optics with uncoated fiber tips: confinement and spatial resolution. *J Opt Soc Am B* 14:1656–1663
66. Sun S, Chong K, Leggett G (2002) Nanoscale molecular patterns fabricated by using scanning near-field optical lithography. *J Am Chem Soc* 124:2414–2415
67. Montague M, Ducker RE, Chong KSL et al (2007) Fabrication of biomolecular nanostructures by scanning near-field photolithography of oligo(ethylene glycol)-terminated self-assembled monolayers. *Langmuir* 23:7328–7337
68. ul Haq E, Liu Z, Zhang Y et al (2010) Parallel scanning near-field photolithography: the snomipede. *Nano Lett* 10:4375–4380

Chapter 14

The Photochemical Laboratory

Peter Douglas, Rachel C. Evans and Hugh D. Burrows

Abstract In this chapter we describe the basic photochemical instrumentation, instrument components and consumables, which make up a general photochemical laboratory. We consider factors such as sample preparation, optical properties of the sample, and contributions from background interferences, which can all affect the data obtained. We discuss the different accessories available, to optimise or perform more complex measurements such as fluorescence anisotropy and quantum yields. We do not consider in detail the more expensive systems required for specialised experiments, which are discussed in [Chap. 15](#), although we do describe the general principles of these methods. Finally, we describe a Photochemical Library, a reference to useful books, journals, organisations, websites, programs, and conferences for researchers in the field.

14.1 Introduction

The success of any photochemical or photophysical experiment will depend on knowledge of the reaction or process under investigation, an understanding of the instrumentation, and consideration of the experimental details. The theoretical

P. Douglas

Chemistry Group, College of Engineering, Swansea University, Swansea, UK
e-mail: P.Douglas@swansea.ac.uk

R. C. Evans (✉)

School of Chemistry, Trinity College Dublin, Dublin 2, Ireland
e-mail: raevans@tcd.ie

H. D. Burrows

Department of Chemistry, University of Coimbra, Coimbra, Portugal
e-mail: burrows@ci.uc.pt

aspects of photochemistry are covered in [Chap. 1](#) and also in several core textbooks (see [Sect. 14.12](#)); in this chapter we look at the experimental considerations and choice of instrumentation for photochemical experiments.

Although many of the requirements are the same, it is convenient to distinguish between what is necessary for synthetic applications of photochemistry and for spectral and photophysical studies. For the latter, sophisticated and fully-integrated steady-state and time-resolved instrumentation are now readily available and reasonably priced, making them accessible to many research laboratories. However, the simplicity of design and use means that these instruments are often treated as ‘black boxes’ and, consequently, inexperienced researchers can fail to take advantage of their full capacity. To get the best out of these instruments, it is important to understand the individual components and their limitations, to identify any potential artifacts or pitfalls that may distort the data, and to consider any sources of background interference. For photochemical synthesis the requirements are frequently less restrictive. However, it is vital to remember the First Law of Photochemistry (the *Grotthus–Draper law*)—the spectrum of the light source must have appropriate wavelengths that overlap with the absorption spectrum of the molecules of interest.

14.2 Controlling the Light

By definition, light plays a crucial role in any photochemical or photophysical experiment. The primary light source will be the excitation source (e.g., lamp, laser) used to irradiate the system under investigation to excite a molecule to an excited state, and a secondary monitoring beam might also be required. However, there will also be photons from the Sun or artificial lighting present and these must be eliminated or suitably minimised if controlled experiments are to be performed. In more complex optical arrangements, the light path will be controlled by a series of lenses, mirrors, slits and stops. Light management is therefore an important consideration at the start of any experiment.

14.2.1 Keeping the Light Out

Even on a dull day the intensity of both visible and near-UV light on the laboratory bench from windows and room lights is significant. A solution left out on the bench on a sunny day can easily receive more near-UV exposure than a sample under study in a fluorimeter or in an irradiation set-up. Aluminium foil is useful to wrap around flasks containing light sensitive solutions. For handling the most light-sensitive materials a darkroom with appropriate ‘safe-light’ is preferable.

14.2.2 *Putting the Light In*

The choice of excitation source will be determined by the sample and the nature of the experiment to be performed. Consideration must be given to the excitation wavelengths and source intensity required. These can be controlled by the use of monochromators and filters as necessary. Synthetic and steady-state experiments can be performed with continuous lamps or light-emitting diodes (LEDs). Time-resolved measurements, required for studying the kinetics of excited state reactions, need a pulsed light source such as a laser, pulsed LED, pulsed lamp or flash lamp, although for work in the ms–s range, a continuous lamp with a mechanical shutter can sometimes be used. The different light sources available are described below in Sect. 14.4.

14.2.3 *Following the Light Beam*

It is useful to see where the light beam travels in an optical arrangement. A piece of white paper will easily catch the path of the excitation beam of a fluorimeter in the sample compartment. In a darkened room, the monitoring beam of a spectrophotometer can similarly be followed if the instrument is set at 0 nm where the grating acts as a mirror, or even when set to pass green light, say 520 nm, to which the eye is most sensitive. A cell containing a fluorescent dye, or a plastic film or block of the same, is useful to follow a UV beam. A piece of white printing paper, which usually contains an optical brightener that will fluoresce blue under UV (See Chap. 4), will often suffice. Similarly, a solution, or plastic sheet, containing a fluorophore emitting in the window region of laser safety goggles can be used to safely see where a laser pulse is going while wearing the safety goggles. A piece of phosphorescent card, or paper painted with phosphorescent paint (available from many model shops), is a useful way to follow a pulse of light.

14.3 Sample Preparation

Photophysical and photochemical measurements can be performed on samples in a variety of forms, including: solutions, low-temperature glasses, powders, single crystals and thin films. The choice of sample form depends largely on the information one hopes to deduce from the experiment, or, for synthesis, the nature of the system. However, there are frequently specific considerations, such as the solubility or the amount of sample available. Measurements are perhaps most commonly made on solutions, and care must be taken not to introduce contaminants to the sample *via* the solvent. For solid samples, such as powders or films, light scattering from surfaces or crystallites can also introduce artefacts into the

spectrum. The main experimental considerations to take into account when preparing samples for photophysical characterisation are discussed below.

14.3.1 Solvents

Solvents come in various degrees of purity and cost. Fluorescence measurements are particularly sensitive to solvent impurities, so investing in a higher grade solvent may reduce time and frustration in the long run. The following general solvent grades (in increasing price) are commercially available (note that some manufacturers use different grade trade names).

1. **Reagent grade.** This is the lowest grade, suitable for general laboratory work.
2. **American Chemical Society (ACS) grade.** For general use requiring more stringent quality specifications.
3. **Analytical grade.** Prepared for analytical work with the level of specific important contaminants identified. However, higher chemical purity does not necessarily make the solvent more suitable for photochemical applications if there are still trace aromatic or other absorbing species. For example, 'water free' analytical grade ethanol is frequently obtained by azeotropic distillation with benzene, which absorbs light in the 254 nm region and is fluorescent.
4. **HPLC grade.** High purity, low residue on evaporation, and filtered, for use with HPLC systems incorporating absorbance detectors, with specified absorbances at specific wavelengths.
5. **Spectrophotometric.** Purified for spectrophotometric work. These are high-purity, low residue on evaporation, and with a clean UV spectrum with specified absorbances at specific wavelengths.
6. **Fluorimetric.** Some solvents are available specifically purified for fluorescence work.

Spectrophotometric and fluorimetric solvents can be very expensive; HPLC grades are often cheaper but with comparable optical specifications. Analytical grades can be cheaper still, and although not usually specified for absorbance, are of high general purity. Some solvents, e.g., chloroform, are supplied with stabiliser additives, so care should be taken to remove these [1] or to ensure they are unimportant for the work in hand. Some solvents are also available in anhydrous grades, but it is worth noting that these will pick up water very quickly if they are opened and handled under ambient conditions. Chemical suppliers' catalogues give detailed specifications of solvents; even so it is generally a prerequisite for any photochemical study to run a UV/Vis absorption spectrum of the solvent. For some photophysical studies, it may be advisable to purify solvents using standard procedures [1].

Judicious choice of solvent(s) is an important part of experimental design. The following are some important solvent parameters.

1. **Solvent cut-off wavelength.** Below this wavelength it is not possible to carry out any experiment that requires light to penetrate into or through the sample. The cut-off wavelengths for some common solvents are given in Table 14.1.
2. **Solvent polarity.** There are a variety of solvent polarity scales. Dielectric constant is probably the simplest bulk solvent physical parameter to consider, but measures of solvent polarity based on solvent–solute interactions at the microscopic molecular level, such as the interaction between solvent and solvatochromic dyes in the Reichart $E_T(30)$ scale [2], are also widely used. An increase in polarity will lower the energy of, and hence favour, all process involving charge separation, such as electron transfer, and charge transfer states, so a significant difference in behaviour in polar and non polar solvents indicates alternative charge transfer reaction routes or states (see Chap. 12).
3. **Solvent viscosity.** An increase in solvent viscosity will decrease the rate of molecular motion and reduce the rate of diffusion-controlled bimolecular interactions, such as those involved in dynamic quenching. For aqueous or alcoholic solutions, viscosity can easily be increased by use of poly-ols such as ethylene glycol or glycerol, either on their own or as part of a solvent mixture. These have the advantage that they are transparent through much of the UV/Vis. In addition, on freezing, they frequently form glasses, which are valuable for studying phosphorescence.
4. **Singlet oxygen lifetime.** This is highly solvent-dependent being particularly short in solvents containing $-OH$ groups, and much longer in deuterated and halogenated solvents. Particularly long singlet oxygen lifetimes are observed in carbon tetrachloride. The use of deuterated solvents can be a very useful tool in singlet oxygen studies.

Ensuring homogeneous dissolution of material in solvents is important. Ultrasonic baths or continued stirring under gentle heating may be used to dissolve more obstinate materials, though care should be taken to minimise the possibility of sample degradation by these methods. In some cases, samples become dispersed as micro-crystallites rather than dissolving to a homogeneous solution. While such

Table 14.1 Cut-off wavelengths of some commonly used solvents

Solvent	λ (nm)
Alkanes	195
Water	195
Acetonitrile	195
Methanol	210
Ethanol	210
Dichloromethane	220
Chloroform	240
Carbon tetrachloride	250
Benzene	280
Toluene	280
Tetrahydrofuran	280

solutions can look perfectly transparent, the presence of micro-crystallites can be detected from the observation of light scattering if a narrow light beam is passed through the solution, and sometimes by a high UV/Vis absorption 'baseline' which shows increasing 'absorbance' towards shorter wavelengths. For any material that has proved difficult to dissolve one or other of these simple checks for micro-crystallites is worth doing.

Even for solutions that are free of micro-crystallites, it is important to be aware of the possibility of solute aggregation, especially since the photochemical characteristics of aggregated species are often quite different from their molecular counterparts. Many organic compounds will aggregate at moderate concentration and this is particularly important for: large planar aromatic molecules which can associate through π - π interactions, non polar organics in polar solvents, polar organics in non-polar solvents, polymers generally, and charge bearing organics in water. Aggregation can be detected by changes in absorption, excitation or emission spectra, and also changes in emission quantum yields. Spectral changes due to aggregation are often quite small, as little as a minor deviation from a linear Beer-Lambert law, but in some cases, such as J-aggregate formation in cyanine dyes, they can be dramatic, and lead to a significant shift in the absorption band. Aggregation of organics in aqueous solution can often be reduced by addition of an organic co-solvent such as ethanol or acetonitrile, or a surfactant, which may isolate solute molecules in micelles, although the changes in solute environment these additions make should always be borne in mind.

Even when solutes are present as monomolecular species, concentration can influence photochemical measurements through inner filter effects (see later), and also photochemical reactions through, for example, self-quenching, triplet-triplet annihilation, and excimer formation.

14.3.2 General Laboratory Equipment for Solution Preparation

Glassware. The precision and accuracy required in any experiment is determined by the nature of the experiment itself. The tolerances of class A standard volumetric glassware: volumetric flasks, burettes, and pipettes are typically a few tenths of a percent of the glassware volume (tolerances for class B glassware are typically about twice that of class A glassware), but precision is usually better than this. Piston micropipettes which give a wide range of delivery volumes in the μ -ml range are available from a variety of suppliers e.g., Eppendorf, Gilson, Hamilton, Finnpiette, and pipettes of either fixed, or variable, volume are available. These have, depending on supplier and model, accuracy and precision typically in the range of a half to two percent of the maximum delivery volume, with highest imprecision/inaccuracy (which can be as much as 10-20 %) when using variable volume pipettes at the low volume end of their useable range. Regular calibration

is essential to ensure the accuracy and precision of these pipettes are retained over time. Glass syringes for use in μl – ml range are also available from a number of manufacturers, such as Hamilton, and these have accuracy and precision of about a percent of the maximum delivery volume. Typically then, routine solution make-up should be precise to a percent or so. This is usually better than that for most photochemical measurements such as yields and rate constants, so experimental precision should not generally be limited by solution preparation. For accurate work it is crucial to use volumetric glassware correctly and it is well worth consulting standard texts on the subject [3, 4]. The time spent reading the manufacturer's specifications and instructions for the correct use of pipettes, burettes, volumetric flasks, micropipettes, syringes, and other precision equipment, is time well spent. Solutions need to be well mixed to ensure homogeneous dissolution of the solute at the molecular level. In particular, adding solvent to make a volumetric flask 'up to the mark' can result in the neck of the flask being filled with solvent only, and a cursory inversion of the flask will not be adequate for thorough mixing.

Balance. An analytical balance capable of weighing ~ 100 – 200 g to 0.1 mg is suitable for most applications. For work where materials are limited, a six-figure balance may be useful, although the lower maximum weight, and increased care required for its use, mean that this is generally more an (expensive) addition to the lab rather than a replacement for a four figure balance. A four-figure balance is a precision instrument and requires treatment as such. For accurate work it is best placed on a vibration proof bench away from direct sun, drafts and thermal convection currents. When weighing to 0.1 mg, vessels should be handled with tongs rather than fingers because these can leave behind enough finger grease and moisture to add measurable weight to the vessel. Typically, repeat weighing on such an analytical balance can be made to ~ 0.2 mg and so working with ~ 20 mg of material gives $\sim 1\%$ precision; if significantly lower weights of material have to be used then it is important to be aware of the effect of this on the precision of subsequent experiments.

Optical determination of concentration. For a typical high absorber with a molar absorption coefficient, ϵ , of $\sim 10^4$ $\text{mol}^{-1} \text{dm}^3 \text{cm}^{-1}$ and molar mass ~ 200 g mol^{-1} , 20 mg will give enough for a 1 L solution with an absorbance of 1 . For most studies this is far too much solution, and may be a waste of a very valuable compound. However, if the molar absorption coefficient is known, determination of the concentration from absorbance using the Beer–Lambert law (Chap. 1) is easier and more reliable than trying to weigh out small amounts of material. For photochemical studies, the optical properties of the solution are often more important than using a specific concentration, and it is possible to avoid having to deal with large volumes of solution simply by the addition of small quantities of material to the required volume of solvent until the required absorption (and hence concentration) is obtained. A capillary tube, such as used for melting point determinations, or the tip of a glass Pasteur pipette, gently pressed into a sample is a convenient and disposable, contamination free, way to pick up a few mg of solid which can then be dissolved in solvent.

Sample concentrations should be tailored towards the measurement being performed, striking a careful balance between a good signal to noise ratio (see Sect. 14.8.2), minimisation of artefacts and preferably working within the linear response range of the instrument. Standard UV/Vis absorption spectrometers exhibit a linear response up to 2–3 absorbance units and for best results determination of molar absorption coefficients is usually performed on a series of solutions with an absorbance in the range 0.2–1.5. For standard emission measurements with 1 cm path length cells, however, the optical density at the absorption maximum should generally be kept below ~ 0.1 A to reduce gross inner filter effects (see Sect. 14.9). It is always advisable to run an absorption spectrum before and after any photophysical/photochemical experiment to see if sample degradation has occurred.

14.3.3 Optical Cells and Cuvettes

Gas and liquid samples are usually contained in optical cells or ‘cuvettes’. Solid powders can also be held in such cells but are more commonly made into a compact optically diffusing pellet, or pressed into a hollowed out receptacle with an open surface which can be exposed to the light source. Note that with all optical components, care must be taken to avoid scratching or touching optical surfaces; fingerprints can lead to extensive light scattering. Cell windows can be cleaned with ethanol and lens cleaning tissue.

Three types of materials are commonly used in the manufacture of optical cells: plastic, glass (optical glass, Pyrex, special optical glass) and quartz (UV silica, spectrosil). For standard measurements, cells of square cross section with a 1 cm pathlength are used. For absorption work, the cells have two polished faces, while emission cells have all four faces polished. Plastic cells, usually made from polystyrene, which are available as 1 cm path length absorption and emission cells, are very cheap, disposable, and, depending upon the plastic used, can be optically transparent down to ~ 280 nm. They are suitable for water and alcohol solutions but most other organic solvents dissolve the plastic. They are not made to the same tolerances as glass or quartz cells so should not be used for accurate absorption work, but they are excellent for non-demanding use in student laboratories. They are also good for preparing difficult samples, such as liquid crystals, which need a long time to stabilise. Glass and quartz differ in optical transmission properties; glass absorbs below about 320 nm, while UV grade silica has good transparency to ~ 160 –180 nm, depending upon thickness.

Quartz cells are significantly more expensive than those made of glass. Many different types of cell are available for specific applications: anaerobic, flow, micro, sipper, stirrer, stopcock, and others; examples of some of these cells are shown in Fig. 14.1. Cell manufacture catalogues are an excellent source of information about materials and what types of cell are commercially available [5]. Standard absorption cells typically have a 1 cm path length and square cross-

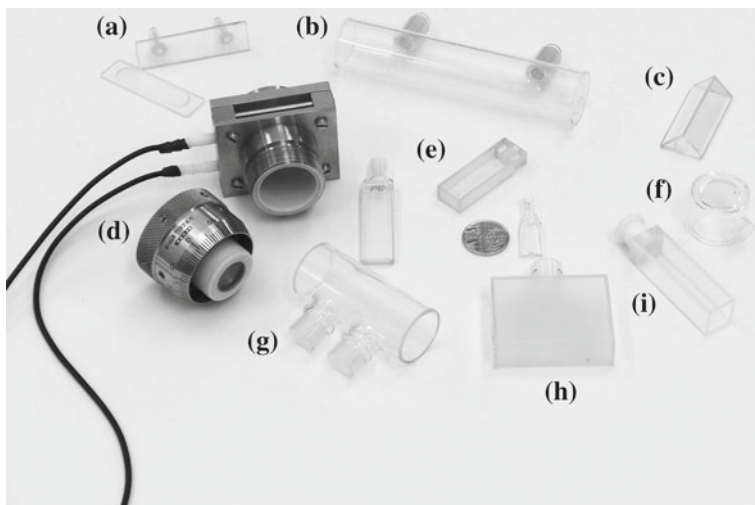


Fig. 14.1 Various absorption and emission cells. **a** Thin pathlength demountable flow cell; **b** 0 cm pathlength cylindrical absorption cell; **c** triangular emission cell for use with highly absorbing solutions; **d** variable path length absorption flow cell with stainless steel sleeve and screw; **e** standard 1 and 5 mm path length absorption cells, and micro cell; **f** 0.1 mm path length cylindrical cell (the 0.1 mm path length is behind the cell face placed down on the table); **g** 5 cm cylindrical absorption cell; **h** 4 cm absorption cell; **i** standard 1 cm emission cell. The 5p UK coin, included to give some idea of scale, has a diameter of 18 mm

section with a volume of about 3 ml, but a range of path lengths from 1 mm to 10 cm are readily available. A standard photochemical procedure is determination of the molar absorption coefficient from a Beer–Lambert plot of absorbance against concentration, and a collection of cells of different path lengths is very useful for this. Cells can be bought as ‘matched pairs’ with identical optical properties, for use as sample and reference in double beam spectrophotometers, but modern manufacturing methods and automatic background correction have reduced the need for such pairs somewhat.

Shorter path lengths down to 0.08 mm can be obtained using cells where the faces are demountable and a spacer of known thickness can be interposed between the cell faces, or where cell faces are brought together with one face on a screw thread and with path length read from a dial. Many spectrophotometers have the option of introducing a ‘beam mask’ to cut down the area of the light beam incident on the cell, so that small volume cells can be used, and many instrument manufacturers offer cell designs allowing measurement down to volumes of a few μl . The non-transmitting portion of cells may be made of black glass to prevent scatter and stray light.

Standard emission cells are also 1 cm square, and since the normal 90° optical arrangement is designed to pick up emission from the centre of the cell, both the excitation beam and the emission beams travel through *ca.* 0.5 cm of solution before being incident on the sample or collected by the detector. For anything

other than optically dilute solutions, absorption within these optical path lengths can distort excitation and emission spectra (so called *inner filter effects*). Emission cells of shorter pathlength for standard 1 cm cell holders must either be made with the solution held in the middle of the cell, e.g., 1 mm square wells in a 1 cm block, or held in an adapter which does this. Again many instrument manufacturers offer a variety of emission cells and cell holders, allowing measurement down to volumes of a few μL .

Low temperature phosphorescence measurements are most easily carried out at the boiling point of liquid nitrogen, 77 K, in a frozen organic glass. The sample is dissolved in an organic solution, which forms a transparent glass upon freezing, and the solution placed in a *ca.* 15 cm long tube of optical quartz (or glass if the near UV—visible spectral region is all that is required) of a few mm diameter. This is then immersed into liquid nitrogen held in a specially designed low temperature quartz Dewar which is equipped with a short protruding stem at the bottom into which the quartz tube fits (see Fig. 14.2). A reasonably snug fit is desirable for good repeatability of measurement, but if the fit is too tight there is risk of shattering the Dewar as the tube expands upon freezing. Excitation and emission measurements can then be made through the sides of the Dewar and tube. Two common problems with this arrangement are interference from nitrogen bubbles through the excitation or emission beams and a build-up of ice crystals in the liquid nitrogen. Bubbling can be reduced by a preliminary cooling and rinsing of the Dewar with liquid nitrogen followed by rapid filling immediately after the first rinse is discarded. Ice build-up can be minimised by keeping the liquid nitrogen sources covered. Care must be taken to ensure that the quartz tubes are warmed from the top down when being brought back up to room temperature. If warmed bottom first, expansion, as the solution in the bottom of the tube melts, may shatter the tube and/or eject solid material from the top of the tube. The glass tubes used for NMR are relatively cheap, easy to buy, and suitable for the visible spectral region. Quartz phosphorescence tubes are also available for the UV region.

Fig. 14.2 Silvered quartz Dewar and phosphorescence tube for low temperature work. The sample is placed in the narrow tube, which is then inserted into the vertically held liquid nitrogen filled Dewar. Excitation and emission is carried out through the unsilvered nipple on the Dewar. The 5p UK coin, included to give some idea of scale, has a diameter of 18 mm



Phosphorescence spectra and lifetimes are easy to measure using this arrangement but quantum yields are rather more difficult because of difficulty in repeatable positioning of the sample, the many curved surfaces in the light beams, and often a lack of knowledge of low temperature absorption spectra. The latter problem can be addressed, in part at least, if the sample fluoresces, since relative low temperature fluorescence and phosphorescence yields can be obtained from the individual and total emission spectra. Relative low temperature and room temperature fluorescence yields can then be obtained from emission spectra with the sample left in the same position, with allowance for temperature dependent changes in absorption spectra made by comparing excitation spectra at both temperatures. As a first approximation excitation spectra can be normalised assuming the area of the lowest energy absorption band is constant, *i.e.*, a temperature independent transition probability, and then allowance made for contraction of the solvent upon freezing to calculate the relative absorbances at the two temperatures. If it is possible to hold the Dewar in an absorption spectrometer then, provided the monitoring beam is narrow enough and aligned properly with the sample, reasonable low temperature spectra can be recorded. There are a number of solvents and solvent mixtures which form glasses at 77 K [6], but perhaps the easiest to work with for moderately polar systems is EPA (diethyl ether:isopentane:ethanol at 5:5:2 (v/v)), because it gives a relatively soft glass which does not shatter, while for non-polar compounds, 3-methylpentane, methylcyclohexane or isooctane all give good glasses. A more detailed discussion is given in [Chap. 15](#).

14.3.4 Removing Oxygen

At a concentration of $\sim 2 \times 10^{-4}$ mol dm⁻³ in air-equilibrated water and $\sim 2 \times 10^{-3}$ mol dm⁻³ in non-polar organic solvents, oxygen is a major reactive contaminant. In particular, it is a very effective triplet quencher. Oxygen can be removed from solution in one of two ways: (i) purging the solution with an inert gas, either oxygen-free nitrogen or argon; or (ii) *via* a series of freeze-pump-thaw cycles, with evacuation of the gas above the solid sample using a vacuum pump when the solution is frozen. In most cases inert gas purging is easiest, and it has replaced the freeze-pump-thaw method in most laboratories, although there is the suspicion that freeze-pump-thaw is most effective at removing the last traces of residual oxygen, and for studying long-lived triplet states it may still be the better method, particularly where information on lifetimes is needed.

Inert gas purging can be carried out with the sample *in situ*, with the gas delivered by a long syringe needle or thin Teflon tubing, using a fine needle valve on the cylinder to control gas flow, and with an adequate safety valve in the gas line, such as a balloon on a T piece, in case of blockage of gas flow. About 15–20 min purging is usually adequate, and it is a simple check to repeat the measurement in question before and after a further 5 min purge, to ensure

maximum oxygen removal. Results of the effect on fluorescence lifetimes from such purging are given in [Chap. 15](#). Once purging is complete the system can be sealed or gas flow continued but with the rate turned down to a lower level to ensure no return of oxygen into the sample. Care should be taken, particularly with volatile solvents, that purging does not transfer unacceptable levels of solvent vapour into the laboratory, and also that any change in concentration due to solvent loss is not critical to the experiment. Solvent loss can be minimised by pre-bubbling the gas through the solvent first to saturate it. Because of the risk of loss of solvent by purging, if comparison between aerated and oxygen free solution is required it is best to make measurements on the purged solution first and then shake the sample thoroughly in air before measuring under air equilibrated conditions.

14.4 Light Sources

Light sources are required to probe both the ground and excited state properties of a photoactive system, and also as a source of photons for photochemical reactions. The light source may be an integrated module of an instrument or a stand-alone component.

UV/Vis absorption measurements are used to probe and measure electronic transitions of ground and excited states and other short-lived species. Ground state absorption is usually obtained using continuous illumination lamps emitting in the UV and visible spectral regions. However, absorption measurements of excited states and other short-lived species may require a high intensity pulsed monitoring beam, (in addition to the excitation pulse required to generate the transient species in the first place), because continuous lamps cannot provide a high enough photon flux for adequate signal-to-noise ratio (S/N) for measurements over very short timescales.

Steady-state photoluminescence measurements use constant illumination and detection. The sample is irradiated with a continuous beam of light and the emission spectrum (or single-wavelength intensity) recorded. (In practice the excitation source may be ‘chopped’ at a few tens of Hz using a rotating disc chopper in the excitation beam with detection locked into the chopped signal in a method sometimes referred to as ‘AC mode’. This can be used to give a better background zero and more stable response since the portion of the beam ‘chopped out’ can be used with a reference detector to correct for wavelength, or time, dependent variations in excitation intensity. Providing the chopping frequency is much less than the excited-state lifetime, the steady-state excited-state concentration is the same as that for continuous irradiation.) The steady-state concentration of excited-states is reached on a timescale of a few excited-state lifetimes and since fluorescence typically occurs on nanosecond timescales, the fluorescent steady-state is reached essentially immediately upon excitation. However, because of their longer lifetimes, it may take a few seconds to reach the steady-state

concentration of phosphorescent excited-states. For time-resolved absorption and emission measurements a pulsed excitation light source must be used. This is discussed in more detail in [Chap. 15](#).

Steady-state and time-resolved measurements are related. The steady-state concentration of excited-states of a lumophore of lifetime τ is $R_{\text{abs}}\phi\tau$ where R_{abs} is the rate of absorption of photons, in $\text{E dm}^{-3} \text{ s}^{-1}$ (E is the Einstein, which corresponds to 1 mole of photons), and ϕ the quantum yield for excited-state formation. The total steady-state emission intensity is $R_{\text{abs}}\phi\tau/\tau_{\text{rad}}$ where τ_{rad} is the radiative lifetime. The instrument response depends on instrument optics and detector sensitivity, but for a given lumophore and constant R_{abs} , it is proportional to τ , and the introduction of any process, such as quenching, which reduces τ reduces instrument response proportionately, providing of course the instrument is operating in the linear range of the detector.

Working the other way, from decay curves to intensities, for a single lumophore decaying exponentially the integrated intensity across the decay (I_{ss}) is related to the excited state decay time by:

$$I_{\text{ss}} = \int_0^{\infty} I_0 e^{-t/\tau} dt = I_0 \tau \quad (14.1)$$

where I_0 is the emission intensity at time, $t = 0$, and τ is the corresponding emission decay time. So integrating the area under an emission decay curve gives a value proportional to the total number of emitted photons, *i.e.*, the total emission intensity. For a system of a number of lumophores or independent decay processes, the single term, $I_0\tau$, is replaced by a summation of such terms for each lumophore or process.

For photochemical reactions, as opposed to physical measurements, the key requirement of the lamp is high intensity, and, for maximum versatility, emission across a wide spectral range. In addition, for quantum yield measurements the light flux should be reasonably constant.

14.4.1 Continuous Light Sources

Spectral profiles and photographs of the most commonly encountered continuous light sources are shown in [Fig. 14.3](#). The Newport Corporation website (www.newport.com) is an excellent source of data on lamps and how to use them.

14.4.1.1 Tungsten Halogen Lamps

Tungsten iodide (also called tungsten halogen) lamps give a continuous spectrum with useful intensity from ~ 350 nm out into the near IR ([Fig. 14.3a](#)). The exact

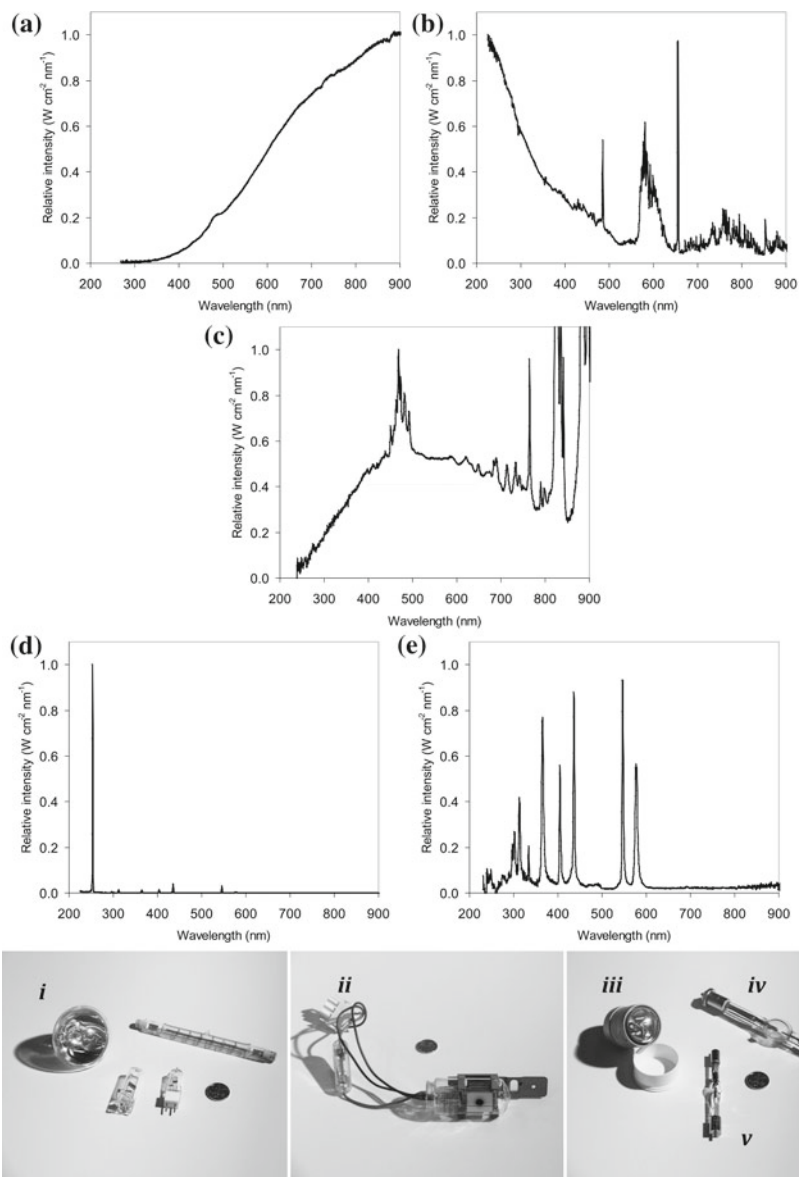


Fig. 14.3 Typical spectral profiles of **a** tungsten halogen, **b** deuterium, **c** compact continuous Xe arc, **d** low pressure and **e** medium pressure Hg lamps recorded with an Ocean Optics calibrated spectrometer. Note that the spectra are each individually normalised to a maximum of 1 and comparison of relative intensities between lamps cannot be made. Note also that when using a detector bandwidth wider than the emission line bandwidth, the measured relative intensities of lines compared to continuum varies with detector bandwidth, with the ratio of line-emission to continuum increasing with decreasing bandwidth. The lower panel shows photographs of commonly encountered lamps: **i** a variety of tungsten lamps, **ii** deuterium, **iii** compact xenon, **iv** a short arc xenon arc and **v** super pressure mercury lamp. The 5p UK coin, included to give some idea of scale, has a diameter of 18 mm

spectral distribution, which approximates to that of a black body, shifts to the blue as the temperature is increased, but the filament lifetime decreases rapidly with increasing operating temperature. Lamps ranging in electrical rating from mW to kW are readily available; those most commonly used in the laboratory are in the *ca.* 50–1000 W range. With a stabilised power supply the output from tungsten lamps can be very steady, and the combination of a spectral continuum and excellent output stability make these lamps ideal as visible light spectrophotometric monitoring sources. Since the total lamp output is varied by varying the size of the filament, then, for the same optical arrangement, increasing output does not directly correspond to increased intensity at the irradiation area, and for a small irradiation area, e.g., a spectrophotometer slit or small irradiation vessel, a 100 W lamp can be as effective as a 1000 W lamp.

Much of the input electrical energy ends up as heat, so the lamp housing can get very hot. For small power lamps, up to ~ 100 W, a well-ventilated housing may suffice, but for higher power lamps a fan is recommended. Due to the large amount of IR radiation it is useful to include either a filter of a few cm of water, or IR absorbing glass, or a ‘hot mirror’, between the source and sample (A ‘hot mirror’ is a dielectric filter that selectively reflects IR. Some hot mirrors must be placed at 45° to the source-sample axis while others require a 90° angle. Some may also reflect UV light, and if made of glass will also absorb UV. It is always worth measuring the absorption spectrum of any material placed in the light beam).

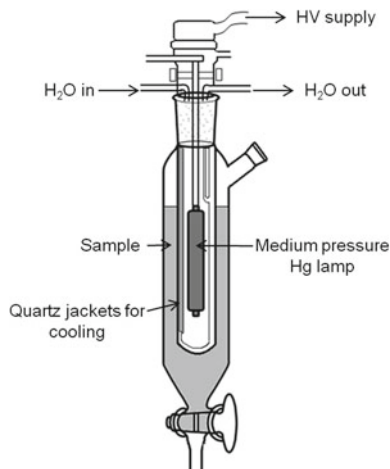
In dichroic tungsten lamps, a dichroic reflector which reflects visible light but absorbs IR helps increase the forward intensity of visible light while reducing the heating effect of IR radiation. Commercial irradiation sources for microscopy using dichroic lamps coupled to a fibre optic and a filter arrangement are useful reasonably high intensity, small area, visible light irradiation sources [7].

14.4.1.2 Arc Lamps

The highest intensity sources, other than lasers, are arc lamps, in which an electrical discharge is passed through a gas in a transparent, usually quartz, envelope. While lasers are brighter, the laser spot area is usually small and arc lamps are the brightest continuous large area illumination sources generally available, and as such are ideal irradiation lamps for synthesis and photodegradation studies. The gas and its pressure determine the emission spectrum. Mercury, xenon and deuterium are the most common gases employed. Xenon lamps are almost all high pressure (~ 30 atm) while mercury lamps may have a gas fill at low ($\sim 10^{-5}$ atm), medium (~ 2 – 5 atm) or high (> 100 atm) pressure, deuterium lamps are low pressure lamps.

Deuterium lamps are commonly used for UV spectroscopy. They give a moderately intense continuum of UV radiation from 360 nm down to 160 nm, with a weaker pseudo-continuum with strong line emission superimposed throughout the visible (Fig. 14.4b). Deuterium lamps with quartz envelopes generate ozone, a toxic chemical hazard formed *via* ionisation of O_2 molecules,

Fig. 14.4 Immersion well batch photochemical reactor



primarily from the radiation below 170 nm and ozone free deuterium lamps use a window material which absorbs below 180 nm. The combination of a deuterium and tungsten halogen lamp gives a continuum right through the UV/Vis/near-IR spectra region. Most UV/Vis spectrometers will use this arrangement, and there is usually an automatic lamp change as the instrument switches between lamps. Deuterium lamps can also be used as UV irradiation sources for the deep UV, in photolithography for example.

Continuous xenon (Xe) arc lamps are very high intensity visible light emitters with good yield of UV which decreases in intensity from about 400 nm downwards; emission also extends out into the near IR (Fig. 14.3c). Emission is a continuum with some high intensity emission lines from xenon, particularly around 420–480 nm and in the near IR, superimposed. Most fluorimeters use Xe-arc lamps as excitation source and these emission lines can be used for internal wavelength calibration e.g., the line at 467 nm can be used to calibrate the position of the excitation monochromator in a fluorimeter. Xe-arc lamps also make excellent high intensity irradiation sources for photochemical reactors. When fitted with a suitable 'Air Mass' filter they give a reasonable approximation to the solar spectrum and are widely used in solar simulators.

Continuous Xe-arc lamps are also used as high intensity monitoring beams for pulsed absorption work such as nanosecond flash photolysis, where, because of the short duration of measurement, a very high photon flux is required for adequate signal-to-noise ratios. Signal-to-noise ratio is proportional to the square root of the light intensity so the lamp is often pulsed to give a millisecond burst of even brighter illumination than that achievable in constant running.

A Xe-arc lamp requires an initial high voltage pulse of a few tens of kV to break down the gas between the electrodes to give electrical conduction. This pulse is intense enough to cause serious damage to sensitive electrical equipment close to the lamp or lamp power cables. It is therefore usual procedure to 'arc' the

Xe lamp before switching on any other electrical equipment in that section of the laboratory. Far UV emission through fused quartz will generate ozone and ozone-free Xe-arc lamps use fused quartz doped with titanium dioxide to block deep UV radiation (< 254 nm).

Mercury lamps are particularly rich in the UV, but also show line emission in the visible region. Low pressure lamps show narrow atomic lines, whereas emission from medium and high pressure lamps is subject to pressure broadening, although none give anything approaching a true continuum over a wide range of wavelengths. The intensity from high pressure lamps is significantly greater than for a low pressure lamp, and medium and high pressure mercury lamps are excellent intense UV sources. As shown in the spectra in Fig. 14.3d, e, they have a few very intense peaks (particularly the ones at 254, 312 and 365 nm). These can be isolated using appropriate filters to obtain nearly monochromatic light for quantum yield measurements.

A combined Xe–Hg lamp is also available. This gives a spectrum which is richer in the UV than a Xe lamp alone, but which also shows much greater line structure. The Xe–Hg lamp is used as a fluorimeter source when intense excitation in the mid/far UV is a particular requirement.

All of these lamps become very hot in operation and some cooling arrangement, such as water coils, a heat sink, a fan, or effective convective cooling is needed. Care is always required in operating high intensity lamps because of the intense UV and visible light, high voltages, and the very high temperature and pressure of the bulbs when running.

14.4.1.3 Spectral Lamps

Low pressure lamps with different gas fills, either rare gases, or reasonably volatile metals, e.g., Zn, Cd, Hg lamps, are available. They give emission spectra made up of a number of lines, characteristic of the element(s) used, and depending upon the element, lines can be found right across the UV/Vis/near IR range (see Fig. 14.3d for the spectrum of an Hg lamp). Spectral lamps are useful for wavelength calibration, and sodium lamps are used as a standard monochromatic source in a number of instruments, e.g., polarimeters and refractometers. Spectral lamps can also be used as excitation sources and irradiation sources for photochemical reactions. The company UVP provide them in a variety of sizes right down to a light length of 1.5 mm, and powers outputs, 2–30 W electrical energy and 0.04–20 mW cm⁻², under the trade name of PenRay[®] lamps [8].

14.4.1.4 Hand Held UV lamps

A UV lamp operating at 365 and 254 nm, as used for chromatographic visualisation, is a useful source for a quick check of luminescence from a sample. More powerful hand held ‘Black Light’ lamps, which emit at around 365 nm, are also

available, and these also make a useful lamp for a check on sample emission for samples which absorb at this wavelength.

14.4.1.5 Irradiation Reactors

Photochemical syntheses, as well as photodegradation studies, are usually performed in irradiation reactors; a variety of different designs are commercially available, depending on the specific application requirements. For synthetic photochemistry, immersion well reactors are commonly used (Fig. 14.4). The source, typically a low or medium pressure mercury lamp, is housed in a double-walled quartz jacket, which allows water-cooling and/or filtering of excitation radiation. The solution to be irradiated surrounds the lamp source, enabling homogenous irradiation.

14.4.1.6 LED Light Sources

LEDs (light-emitting diodes) are semiconductor devices that emit photons around a specific peak wavelength when an electrical current is passed through them. The colour of the emitted light depends on the composition of the semiconducting material, and a variety of emission wavelengths spanning the near UV, visible and NIR spectral regions, with typical emission bandwidths of a few tens of nm are available. Since LED light sources do not generate significant infrared radiation, an additional heat filter is not required. LED sources offer the additional advantages of low power consumption and long lifetime and are particularly useful as miniature light sources for instrument building. With the introduction of increasing legislation restricting the use of mercury vapour lamps, LEDs are likely to increase in importance as photochemical light sources in the future. They have the added advantage that they can often be tailored for specific applications, e.g., as flat-bed photoreactors, which are likely to be useful in areas such as water effluent treatment.

14.4.2 Pulsed Light Sources

14.4.2.1 Millisecond Pulses

A mechanical shutter or rotating disk with a continuous light source can be used to give pulses down to \sim ms timescales. Repetition rates of a few Hz can readily be obtained with a camera shutter, and up to about hundred Hz with a rotating disk. However, since a continuous source is used, the energy in a ms pulse will be quite weak. (Note that there is a risk that prolonged high intensity illumination will thermally distort fast shutter blades.) Photographic flash units are ms pulsed Xe

flash lamps. They will typically give ~ 10 μs – ms pulses of up to a few hundred joules (electrical energy) across the visible and near IR, and, if any plastic cover is removed, possibly into the UV depending upon the transmission characteristics of the bulb. Operated normally flash units give repetition rates of around 1–10 Hz or so, with higher repetition rates available from stroboscopic flash units.

14.4.2.2 Microsecond Pulses

High intensity μs Xe flash lamps are available. Emission is a continuum covering the UV/Vis and near IR, similar to a continuous Xe lamp, but the continuum is weaker with a much stronger line structure superimposed. Two types of lamps are commonly used: those used as excitation sources for lifetime measurements in the μs range, which give short duration pulses, typically 0.2–2 μs , but which are only a few tenths of a Joule electrical energy; and those used in μs flash photolysis, which give longer pulses, of around 10 μs duration, but with much higher energies, typically 10–1000 J.

14.4.2.3 Nanosecond Pulses

ns flash lamps. An electrical spark in a gas generates a ns pulse of light. The spectrum is typically a mixture of line and continuum across the UV/Vis/near IR, and is determined by the gas use. These ns flash lamps are most commonly used in time-correlated single photon counting (TCSPC) and are described in detail in [Chap. 15](#). They are not used as sources for many other instruments but they can be used to study emission in the ns– μs range using a fast photomultiplier with signal averaging over many pulses to compensate for the low pulse energy.

Pulsed diode lasers and pulsed LEDs. Diode lasers and LEDs can be pulsed or modulated and used as excitation sources for time-resolved measurements. LEDs can be operated with pulse rates up to ~ 50 MHz and pulse widths of ~ 1 –2 ns, enabling lifetimes of > 10 ns to be readily determined, and the good stability and pulse characteristics of these sources can allow the measurement of even shorter fluorescence lifetimes. A similarly wide range of emission wavelengths is available for pulsed LEDs as their continuous counterparts. Laser diodes differ from LEDs in that they emit monochromatic radiation (LEDs typically have a broader spectral profile). Pulsed laser diodes can achieve a repetition rate of up to several GHz, enabling rapid data acquisition. Pulse widths are shorter than for LEDs, typically ~ 50 ps, enabling facile determination of ns decay times. Currently available laser diode wavelengths include: 375, 390, 405, 420, 440, 473, 500, 510, 531, 596 nm and a number of wavelengths above 635 nm. Currently available LEDs wavelengths include: the full range from 250–380 in *ca.* 5–10 nm intervals, 450, 460, 475, 500, 600 nm. This is such a fast developing field that the introduction of many other pulsed laser diode and pulsed LED wavelengths can be expected in the near future.

14.4.2.4 Lasers

Lasers emit light through the process of stimulated emission. Both continuous wave (CW) and pulsed lasers are available, with pulsed lasers emitting radiation over timescales short enough to monitor even the fastest photochemical processes [9, 10]. The basic requirements for the generation of laser radiation are:

1. **Laser medium.** The laser medium contains a chemical system that exhibits a relatively long-lived excited state (*metastable* state), N_m , capable of undergoing stimulated emission. Stimulated emission requires the presence of a photon of energy $h\nu$ to induce radiative relaxation of the excited state to the ground state N_n :



The emitted photon travels in phase with and in the same direction as the initial photon. These two photons can similarly interact with additional excited states, stimulating the emission of further photons, resulting in light amplification (*laser* is an acronym for **light amplification by stimulated emission of radiation**). For stimulated emission to occur, the probability (or rate) of stimulated emission must exceed that of absorption. At thermal equilibrium, the relative population of the ground and excited state in a two-level system has $N_n > N_m$. As discussed in [Chap. 1](#), for stimulated emission to dominate absorption, a population inversion is required, such that $N_n < N_m$. To create this population inversion an energy source is needed and is provided in the form of an external *pumping* mechanism (see below). Solid-state, gaseous and liquid laser media are available.

2. **Optical resonance cavity.** To sustain laser action, the laser medium must be placed within an optical resonance cavity, which is confined by two highly reflecting mirrors. The mirrors are coated by alternate layers of high and low dielectric materials, such as TiO_2 and SiO_2 , to give almost total reflection at the laser wavelength. The photons emitted by the laser medium are reflected by these mirrors, confining them within the cavity and enabling the photon flux to sustain the conditions necessary for stimulated emission to occur. However, the mirrors, in fact, differ slightly in their reflectivity; the output mirror being specifically coated to allow around 1–10 % to leave the laser cavity forming the laser beam.
3. **Pumping mechanism.** In order to generate an excited-ground state population inversion, the laser medium must be pumped with energy—this may be provided by a light source, an electrical discharge or a chemical reaction.

Lasers offer four main advantages for time-resolved measurements over conventional light sources:

1. **Monochromatic emission.** Lasers emit light of a clearly defined single wavelength, or very narrow band of wavelengths, the energy of which is determined by the lasing medium. This enables selective excitation and observation of specific electronic transitions. Frequency doubling (or second harmonic generation), where the high laser intensity allows the conversion of two photons of frequency ν into a single photon of frequency 2ν when passed through a medium exhibiting nonlinear optical properties, such as a crystal of KH_2PO_4 , may be used to produce a wavelength that is one half of the fundamental wavelength of the laser. This can be subsequently combined, in a similar way, with the fundamental frequency to give a wavelength one third that of the fundamental, and frequency doubling the doubled beam gives a wavelength one quarter that of the fundamental.
2. **Very short pulses.** Pulses as short as 10 fs can be generated relatively easily, enabling ultrafast photochemical reactions and processes to be studied. Over the last decade, attosecond (10^{-18} s) laser pulses have been reported. However, their applications in photochemistry are limited to a few specific systems since Heisenberg's uncertainty principle dictates that these short pulses have relatively broad spectral bandwidths.
3. **High power.** The laser power is the amount of energy delivered by the laser per unit time in Watts ($W = \text{J/s}$). Pulsed lasers compress the emitted radiation into very short timescales, generating peak powers in the order of 10^4 – 10^9 W (10^9 W = 1 GW, the output of several power stations!). This enables excitation of even very weak transitions.
4. **Low divergence.** The laser beam is highly collimated, resulting in a low divergence angle (typically less than 1/100th of a degree). This allows laser radiation to travel long distances without spreading. Moreover, the laser beam can be focused onto a small, precisely located spot, enabling small sample volumes and high power densities.

Pulsed lasers are used to monitor the time-evolution of excited states, the formation of photochemical products and the kinetics of photoprocesses. The high intensity of the laser beam also enables very weak transitions to be excited, so that vibrational photochemistry and multiphoton transitions, which exhibit different selection rules, can be studied. [Chap. 15](#) provides further details about some of the experiments that may be performed using pulsed laser sources. [Table 14.2](#) gives details of the most commonly used lasers in photochemistry today. The key properties to consider for any particular application are: wavelength(s), pulse duration, and power. Simplicity of operation is another important factor.

Table 14.2 Properties of some pulsed lasers commonly used as excitation sources in time-resolved photoluminescence measurements. The reader is directed to Refs. [9, 10] for further information on lasers

Laser	Laser medium	Pumping mode	Wavelength(s)	Pulse duration	Power
Nd:YAG	Solid-state Nd ³⁺ ions embedded in yttrium aluminium garnet (Y ₃ Al ₅ O ₁₂)	Flash lamp, laser diode	Fundamental $\lambda = 1064$ nm Harmonic generation: 533 nm (2nd), 355 nm (3rd), 266 nm (4th)	~ 10 ns for Q-switched	2–50 W, continuous MW-GW, Q-switched
Dye	Liquid Organic dye in a non-absorbing solvent. Dye circulated from a reservoir to avoid problems from photodegradation and triplet state formation	Nitrogen laser Excimer laser Nd:YAG laser	Depends on dye: Stilbene (390–435 nm) Coumarin 102 (460–515 nm) Rhodamine G (570–640 nm)	Ring-dye laser—0.1 ps	1 MW
Ti:sapphire	Solid-state Ti ³⁺ doped aluminium oxide	Q-switched Nd:YAG CW argon	Broad absorption band of Ti ³⁺ enables tuning between 700–900 nm. Frequency doubling leads to wavelengths in 350–450 nm range	~ 10 ns Mode-locking generates ~ 10 –100 fs pulse	~ 3 W (for mode-locked oscillators) 50 GW for chirped-pulse

14.5 Selecting the Wavelength

For anything but a monochromatic source it is useful to have some wavelength selection, and this is achieved with filters or a monochromator.

14.5.1 Filters

Apart from filters for specific applications, it is useful to have a set of general use cut-off filters in the laboratory to remove damaging UV radiation in irradiation systems, and to block excitation light and low wavelength light to reduce scatter in detection systems. In many cases the judicious use of filters can significantly improve experiment design. Some instruments have integral absorption filters, which can be put into the excitation or emission beams to minimise stray light, second order effects (see below), or reduce light intensity. If internal filters are not available, filters can still be used, placed in the sample compartment, before and/or after the sample. There is a very wide range of filters of different characteristics available, which generally fall into three classes: (i) absorption filters, (ii) dielectric filters and (iii) neutral density filters. A selection of different filter types can be seen in Fig. 14.5.

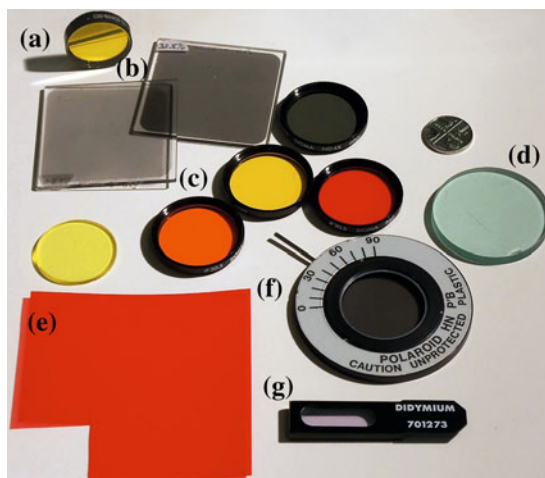


Fig. 14.5 A variety of typical filters. **a** An interference bandpass filter showing the typical mirrored surface of these types of filter; **b** two square silvered glass neutral density filters and a round neutral density filter of a colloidal dispersion in glass; **c** a series of round, coloured absorption ‘cut-off’ filters, and **d** a pale blue glass heat filter; **e** a ‘Wratten’ filter of dyed gelatin, which is flexible and easily cut to shape; **f** a polariser; **g** a didymium absorption wavelength standard. The 5p UK coin, included top left to give some idea of scale, has a diameter of 18 mm

Absorption filters are made using molecular or semiconductor materials dispersed in a support which is usually either glass, quartz, plastic or gelatin [11]. In these filters the incident energy not transmitted is absorbed within the filter, and care is required to ensure irradiation is not so intense as to cause the filter to shatter, or, in the case of plastic or gelatin filters, to melt. Care should also be taken when using such filters to ensure the filter itself is not luminescent, or, if it is, that any filter luminescence will not interfere with the experiment being performed. A luminescent filter on the detection side of an emission experiment can be a source of spurious results and consequent embarrassment!

Dielectric filters are made from a series of layers of thin dielectric coatings deposited onto a transparent, usually glass or quartz, support [12]. The structure of the dielectric coatings is such that interlayer reflections interfere constructively or destructively in the forward or backward directions, resulting in a filter which either reflects or transmits selected wavelengths of light. Since they operate on the principle of interference, the wavelengths transmitted/rejected depend on the angle of incidence the radiation makes upon the filter. If the instrument set-up means that light is incident upon the filter across a range of angles, then the filter performance can be significantly shifted from that with perpendicular irradiation. (This can be demonstrated easily by looking through a dielectric band-pass filter held up to a white light while shifting the angle of the filter with respect to the eye-to-source axis, a range of colours will be seen depending upon angle.) In these filters most of the rejected light is reflected, and they have a mirrored appearance. A range of dielectric filters are available: band-block, IR reflecting (hot) mirrors, visible reflecting (cold) mirrors, and band-pass filters. When selecting a band-pass filter it is important to consider the band-width required since a narrow bandwidth will result in lower transmission intensity. The best sources of information for these are manufacturers data books and catalogues [12].

Neutral density (ND) filters have a nominally constant absorption across the spectrum, and therefore reduce the light intensity for all wavelengths by the same fixed amount. They are either silvered glass or quartz, or colloidal carbon or metal in plastic or gelatin. They are very useful when determining the dependence of photochemical reaction yield on photon flux, which can be important in mechanistic studies. For example, the dependence of a steady-state yield, or transient absorption in flash photolysis, on the light intensity can show whether monophotonic, biphotonic or other processes are involved. ND filters are also useful to generally reduce light intensities in experimental arrangements to give matched transmission values or reduce intensities to keep within the linear range of detectors. Metal mesh filters are some times used as neutral density filters, but their effect depends upon where they are placed in the optical train. For example, when placed immediately before an irradiated sample, mesh filters reduce the area illuminated but do not reduce the intensity of the light on those areas which remain illuminated; therefore it can be expected that the apparent result of such an experiment will always be a linear dependence upon light intensity, even if the true dependence, as obtained using a true ND filter, is non-linear. If placed earlier in the optical train, e.g., immediately after the irradiation source, and before any beam

focussing, they may, depending upon the exact optical arrangement, act as reasonably uniform attenuators.

For some applications it is useful to have a filter solution rather than a solid filter. These are not commercially available but a list of useful solution filters is given in the literature [13]. These may be used in conjunction with absorbance filters. Often it is possible to use the solvent cut-off absorption wavelength (see Table 14.1) and/or one of the reaction components themselves to make up a filter to remove specific wavelengths relevant to the experiment. However care should be taken to check that such a filter solution remains effective throughout the experiment and is not subject to photochemical, thermal, or chemical, degradation. Special care should always be taken when interpreting spectra recorded using filters because light transmitted at the edge of the filter cut-off curve can result in a signal which looks like the edge of an absorption or emission band from the sample.

Solid-state reflectors and absorbers are often useful additions to an experimental set-up. MgO and BaSO₄ powders are widely used as white reflectance standards, (see Fig. 14.6), which reflect ~ 95 % of light between 400–700 nm and > 95 % of light 340–1400 nm, respectively [14]. A material that absorbs uniformly across the spectrum is also useful as a matt black paint coating to prevent scattering of light in optical instruments, and also as a uniform absorber for use in thermopiles and calorimeters which rely on the conversion of radiant energy to thermal energy. In thermopiles and surface calorimeters all of the incident energy is converted into heat in a very thin surface layer and care must be taken to limit the incident irradiation intensity to prevent damage to the absorbing surface. This is particularly important in calorimetric pulsed laser meters, where a single pulse may be sufficient to cause serious damage to a surface coated calorimetric detector. For

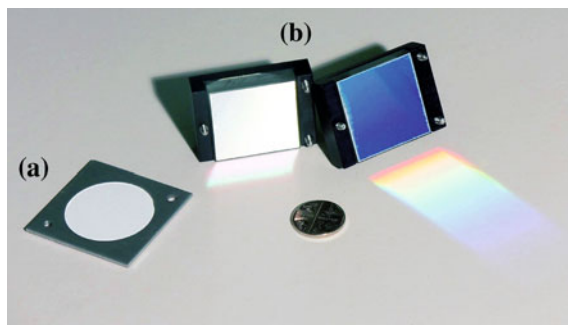


Fig. 14.6 **a** A diffuse reflectance plate used as a reference plate in an integrating sphere; **b** two diffraction gratings showing the effect of number of lines per mm on dispersion. The one in the *middle* of the photograph shows low dispersion because it has only 150 lines per mm (it is for use in the IR), while that on the *right*, showing better dispersion, is ruled with 600 lines per mm for use across the UV/Vis and near infrared (the *blue* colouring of the face of the grating is a consequence of the angle between camera, grating and light source). The 5p UK coin, included in the *middle* of the photograph to give some idea of scale, has a diameter of 18 mm

laser intensity measurements the absorber is often designed so that absorption occurs in the body of the detector element rather than just at the surface.

14.5.2 Monochromators and Spectrographs

The key elements of most monochromators are the diffraction grating, which disperses the radiation, and the entrance and exit slits. Some earlier systems used a prism for wavelength dispersion instead of diffraction gratings. A diffraction grating is a flat, or curved, surface which has a set of very closely spaced (100–1000's of lines per mm) parallel lines cut, etched, or deposited on it. When white light is incident upon the grating, interference between the light reflected from each line results in each wavelength of the incident beam being reflected at a different angle. Thus, the grating separates out the wavelengths in the original white light source and spreads then out into a fan of coloured light, a spectrum. The angular dispersion is proportional to the number of lines per mm on the grating, so a grating with a lot of lines per mm spreads the spectrum out across a wider beam than one with a few lines per mm (see Fig. 14.6). In the monochromator, part of this dispersed spectrum from the grating is made to fall upon the exit slit, which therefore only lets a certain band of wavelengths through. The wavelength of light passed through the monochromator is chosen by varying the angle the grating makes to the excitation and emission beams. This is usually achieved using a screw thread arrangement with wavelength measured directly from the number of turns of the screw. A diffraction grating does not diffract all wavelengths with equal efficiency, but rather shows a smooth curve of efficiency against wavelength. The blaze angle is the angle at which the grooves are cut into the grating, and by choice of this angle the wavelength at which the diffraction grating operates at maximum efficiency, the blaze wavelength, can be set. The transmission efficiency of a monochromator falls off either side of the blaze wavelength. Typically in a fluorimeter an excitation monochromator will be blazed at a lower wavelength than an emission monochromator. It is worth checking the blaze wavelength of any grating used.

Monochromators usually operate with equal input and exit slits. The light from a monochromator with input and exit slits of equal width illuminated by a spectrally uniform source is not strictly monochromatic, but is rather a range of wavelengths, which if plotted as intensity vs wavelength gives an isosceles triangle of light; the width at half height of this triangle of light is termed the *bandwidth* (or *bandpass*). The bandwidth of a spectrophotometer is determined by the instrument geometry, the number of lines per mm on the diffraction grating, and the slit widths on the monochromator. For monochromators with adjustable slits, the slit width is usually measured or given in mm, and the bandwidth, in nm, is then obtained by a conversion factor for the particular monochromator and diffraction grating used. A typical value for a 'fast' monochromator, *i.e.*, one which lets a lot of light through, would be about 4–5 nm per mm, but each instrument will have a

specific value. As slit width is narrowed spectral resolution is increased, but this is at the cost of reduced transmitted intensity.

The use of a monochromator often involves the compromise between best spectral resolution and best signal-to-noise-ratio (*S/N*). Because of the monochromator bandwidth, the measured absorption line is always broader than the true line. The degree of instrumental line broadening is determined by the ratio between the instrument bandwidth and the true bandwidth. An instrument bandwidth of $\sim 1/5$ th the true bandwidth will give a measured bandwidth only a few percent higher than the true bandwidth. Such a bandwidth ratio is acceptable for most applications and there is usually no advantage in using a bandwidth that is much narrower, since this results in lower *S/N* without any increase in spectral information (see Fig. 14.12). Monochromators have either a set of fixed slits or continuously variable slits—typically giving bandwidths in the range 0.1–10 nm. Narrow bandwidths are used in absorption studies in the gas phase; typical bandwidths for absorption studies in the gas phase are 0.1–2 nm; bandwidths for general solution phase emission spectroscopy are often wider, typically 1–20 nm; for time-resolved studies, *S/N* considerations usually mean relatively wide bandwidths, typically in the 2–30 nm range, are used. When using wide bandwidths care should be taken to make allowance for any deviation from the Beer–Lambert law arising from the wide bandwidth.

For a lamp-monochromator combination as an irradiation source for photochemical reactions the compromise is between maximum photon flux and spectral selectivity. Due to the need for a high photon flux, irradiations for photochemical reactions are usually carried out using wider bandwidths than those used in absorption or emission spectrometers. Bandwidth is a particularly important consideration when using sources that contain some line emission such as Hg or Xe lamps, since line emission within the bandwidth can dominate even though it is not the wavelength shown on the monochromator setting or readout.

A monochromator set at wavelength λ nm, will also transmit wavelengths of $\lambda/2$, $\lambda/3$, $\lambda/4$... nm, produced by second order, third order, fourth order, etc. dispersion. Thus, in the absence of any filtering, an excitation monochromator set at say 500 nm will also let through unwanted 250 nm radiation from the source. Similarly, scanning an emission monochromator to obtain the emission spectrum for a sample excited using say 225 nm radiation will show bands at 450 and 675 nm due to the second and third orders of the 225 nm excitation wavelength. If these artifacts become troublesome then judicious use of filters can usually remove them.

A monochromator is never perfect and there will always be some residual stray light transmitted for all wavelengths incident on the entrance slit. Stray light is particularly important when trying to measure intensities of wavelengths where the detector has poor sensitivity, e.g., using a photomultiplier tube (PMT) to measure near IR radiation. In such a case, stray light may be only a very low fraction of the total energy but if it falls in a region of high PMT sensitivity it may swamp the PMT response to the radiation of interest. Again, judicious use of filters can reduce the problem significantly. Some high-resolution instruments use two

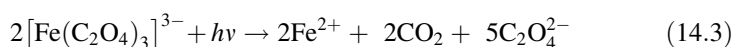
monochromators, one after the other, in a double monochromator arrangement, to reduce stray light.

A spectrograph has an entrance slit but no exit slit because the output is a long strip of light where the spectrum is spread out in a controlled manner and made incident on an array of discrete detector elements, or *pixels*, *i.e.*, a CCD or photodiode array. A spectrograph bandwidth refers to the entire wavelength range incident on the detector array. The optics of a spectrograph differ from those of a monochromator because of the need to bring all of the wavelengths to focus on the flat surface of the detector. The resolution of a spectrograph, *i.e.*, the ability to separate two spectral lines which are close together, is, for a given diffraction grating, determined by the entrance slit width, until this is reduced to the width of a single pixel when the spectrograph is at its limiting resolution with that particular grating and array. Thus increasing the amount of light incident on the detector by opening the entrance slit leads to a loss of resolution in a similar way that widening entrance and emission slits on a scanning monochromator gives a loss of resolution because of the increase in bandwidth.

14.6 Measurement of Light Intensity

Light intensity can be measured by a physical device, a *radiometer*, probably the simplest of which is a calorimetric detector which converts radiant energy into heat (see Fig. 14.7), or by a chemical change, an *actinometer*. A number of chemical actinometers, for both the solution and gas phase, are available, and the standard methodologies for their use are described in detail in the Handbook of Photochemistry (see Sect. 14.12.2). Potassium ferrioxalate is commonly used as a chemical actinometer in the UV-green spectral region ($\sim 250\text{--}500\text{ nm}$). A significant advantage of a chemical actinometer over a radiometer is that it can be placed in exactly the same optical position as a solution sample. In addition, relatively low intensities can be measured simply by integrating over a long time. The physical parameter measured differs for the two devices: actinometers give a response proportional to the photon flux, whereas many radiometers respond to the energy flux. If irradiation is over even a moderate spectral range, then, unless the spectral distribution is known, precise inter-conversion between photon and energy flux is not straightforward. If the spectral distribution is known, interconversion between energy and photon fluxes can be made using the average photon energy.

In a typical application using the potassium ferrioxalate actinometer, aqueous solutions of $\text{K}_3[\text{Fe}(\text{C}_2\text{O}_4)_3]$ are photolysed with monochromatic light, leading to reduction to iron(II) through the overall reaction:



The resulting Fe^{2+} is then determined spectrophotometrically as its 1,10-phenanthroline complex, and the total number of photons absorbed by the irradiated

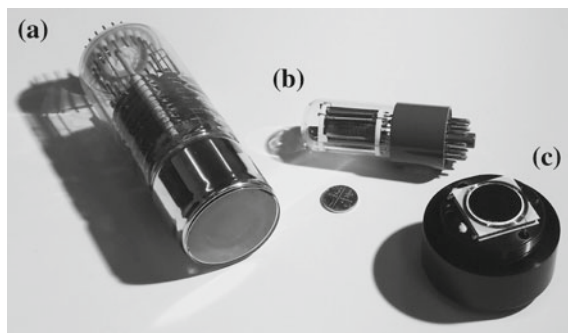


Fig. 14.7 **a** Front face PMT. The photosensitive surface, the photocathode, is at the front, at the back can be seen the pins used in the circuit to fix the dynode voltages. **b** A side window PMT. Here the photocathode is behind the grid towards the left centre of the device. **c** The thermoelectric detector element of a calorimetric laser power meter, the laser pulse is made incident on the thin black disc in the centre of the device, absorption converts the photon energy into thermal energy, which is subsequently measured using the thermoelectric effect in a thermopile immediately behind the disc. When in use the unit shown is held in a thermally isolated chamber which is screwed over the top of the detector element. The 5p UK coin, included in the *middle* of the photograph to give some idea of scale, has a diameter of 18 mm

solution per unit of time is then calculated from this, the irradiation volume, irradiation time and ferrioxalate decomposition quantum yield [6]. The ferrioxalate actinometer is simple to use and has excellent sensitivity over a wide wavelength range. Other systems, such as Reinecke's salt ($\text{NH}_4[\text{Cr}(\text{NH}_3)_2(\text{SCN})_4]$), are available for long wavelengths, while reusable photochromic systems have also been proposed as convenient chemical actinometers. These, and other systems for specific applications, are discussed in Ref. [6].

Chemical actinometers, such as these, are very convenient for determination of quantum yields of photochemical reactions. Typically, the amount of product formed in the reaction of interest on photolysis with monochromatic light is compared with the extent of reaction of the actinometer under the same conditions (irradiation time, etc.). The quantum yield is obtained using the product ratio and the quantum yield of the actinometer [13]. Corrections can be made for differences in absorbance, irradiation time or reaction media.

14.7 Detectors

The most important requirements of a detector are sensitivity and selectivity. The sensitivity determines the lowest signal that can be measured by the detector. Selectivity is achieved when the detector elicits a strong response to a specific input. All real measurements are affected to some extent by noise. The signal-to-noise ratio (S/N) is a measure of the desired signal against the background noise

(for example, one definition takes the S/N ratio as the difference of peak and background signal, divided by the square root of the background signal). Although various methods, such as the Savitzky–Golay algorithm [15] have been used to smooth data points, the overall sensitivity of the system is limited by the S/N ratio. Background noise includes electronic noise (random fluctuation of an electrical signal), but also external effects that may influence the measurement, such as vibrations, temperature or humidity fluctuations. Performing the experiment under controlled conditions may eliminate some of these external influences, but electronic noise will always be present. If the characteristics of the noise are known it may be possible to filter it or to reduce it by signal processing; for example, if the background noise fluctuates much more rapidly than the signal of interest, introducing an electronic filter with appropriate time constant, or post-collection averaging of data points over time will help reduce noise.

14.7.1 Photodiodes

Photodiodes are $p-n$ or $p-i-n$ junction semiconductors that generate a current or voltage upon irradiation with light that is proportional to the rate of photon absorption [16]. When light of energy greater than the band gap, E_g , strikes the photodiode, an electron is promoted from the valence band to the conduction band, leaving behind a hole. If this process occurs in the depletion (charge carrier free) zone of the junction, application of an external voltage sweeps the electrons and holes towards the cathode and anode respectively, generating a photocurrent. The current generated by the photodiode is proportional to the incident light power and the sensitivity is limited to one electron per photon absorbed (~ 0.5 A/W for ~ 2 eV photons, *i.e.*, ~ 620 nm). However, photodiodes are capable of measuring fairly high light intensities (~ 1 mW) with fast response times (~ 0.01 ns), making them suitable for measurement of laser powers, for example. Sensitivity can be improved using avalanche photodiodes, which operate under high reverse bias to enable multiplication of the charge carriers created by the initial electron–hole pairs created by photon absorption. This avalanche action enables the gain of the photodiode to be increased by several orders of magnitude. The wavelength sensitivity is determined by the semiconductor from which the photodiode is constructed: silicon photodiodes typically cover the ~ 400 – 1000 nm region and InGaAs photodiodes the region ~ 900 – 2500 nm.

14.7.2 Photomultiplier Tubes

Photomultiplier tubes (PMTs) (Fig. 14.7) have a light-sensitive cathode from which photoelectrons are ejected when illuminated. These primary photoelectrons are then accelerated by an electric field and made incident on a secondary emissive

layer which ejects many electrons for each, now high energy, incident photoelectron. These secondary electrons are, in turn, accelerated and made incident on another secondary emissive layer which ejects many more electrons. Repetition of this process at a number of secondary emissive layers (*dynodes*), leads to amplification of the current by as much as 10^8 electrons per photon. This current is collected at the photomultiplier anode as the output of the PMT, (although it is measured and recorded as a voltage across a resistor). Both the photomultiplier response and background noise depend on the photocathode and dynode voltages, and increasing the operating voltage significantly increases both sensitivity and noise. Photomultipliers need a very stable variable high voltage power supply that provides a few hundreds of volts, or a kV or so, to produce stable photocathode and dynode voltages. PMTs can be used in DC mode, in AC mode with a chopped light source which is most useful for low light levels, or in single photon counting mode. Photomultiplier tubes are the most sensitive and commonly used detectors for the 180–850 nm range. The wavelength sensitivity of some PMTs extends out to 1700 nm but for operation above *ca.* 850 nm photomultipliers must normally be cooled to *ca.* -80 °C to reduce thermal noise to an acceptable level. The time resolution of a conventional PMT is typically a few hundred ps but a change in design of the way electron amplification occurs has led to development of Multi-Channel Plate photomultiplier tubes, MCP-PMTs, which have time resolution in the tens of ps range. In ordinary PMTs amplification is brought about using a series of discrete dynodes whereas in MCP-PMTs amplification occurs within a honeycomb of capillaries each 6–20 μm diameter and coated with an electron emissive surface so that the whole capillary surface acts as an electron amplifier. The photocathode is placed a few mm from the multichannel plate so that the primary photoelectrons are caught in the capillaries of the plate and the electron current is amplified by secondary emission of electrons as the electron stream bounces back and forth from the walls of the capillary. MCP-PMT are the fastest photomultiplier tubes available but they are expensive and can be easily damaged by excessive light levels. Hamamatsu, a major manufacturer of photomultipliers, has an excellent photomultiplier handbook available online [17].

14.7.3 Charge-Coupled Devices

Charge-coupled devices (CCDs) are silicon-based imaging detectors containing a two-dimensional array of accumulating wells, or *pixels*. Each pixel is composed of a Si–SiO₂ metal–oxide–semiconductor (MOS) capacitor, which operates as a photodiode and a storage device, accumulating electric charge in proportion to the number of photons striking the depletion zone of each individual well. CCDs typically contain up to 500,000 pixels, and sensitivity can be several orders of magnitude better than a PMT at low light intensities. CCDs are commonly encountered in fluorescence microscopy—the charge at each pixel is read out after a specific time to construct a two-dimensional image. Peltier-cooled CCDs can

achieve dark noise counts of less than one electron per pixel per day, giving rise to high contrast low background noise images. CCDs can detect photons in the 400–1100 nm spectra range, with peak sensitivity normally in the range of 550–800 nm with quantum efficiencies of 40–60 % [16], and are currently proving attractive as detectors in reasonably priced miniature spectrometers and fluorimeters [18].

14.8 Data Collection, Analysis, and the CIE Representation of Colour

14.8.1 Digitisation

A detector operating in single photon counting mode provides a digitised response directly. Analog signals from detectors are usually digitised using an analog-to-digital (A-to-D) converter. For time resolved studies, in which a response is measured over a period of time, a digital oscilloscope is a very convenient A-to-D converter, but there are also plug-in A-to-D converters for PCs which, with appropriate software, can be used to convert a PC to a virtual oscilloscope. The two most important features of the oscilloscope, or signal recorder, are time resolution, and signal, *i.e.*, voltage, resolution. For ns flash photolysis a time resolution in the region of a few ns per data point is required, while for work with μ s pulsed lamps, pulsed Xe arc or flash lamps, resolution in the μ s range per point is required. A range of 1024–4096 data points per recorded event is typical.

Instruments usually digitise voltage signals into 8, 10, or 12, (or even 16) bit signals, *i.e.*, the voltage signal range is split into 256, 1024, or 4096 digital values. The sensitivity of the recorder is usually given by the size of the signal voltage that will give a full-scale deflection. Oscilloscope voltage ranges are usually specified as volt/div. with ten divisions (div.) full scale. Typical maximum sensitivities for oscilloscopes are 1–5 mV per div. *i.e.*, 10–50 mV full-scale, while low cost A-to-D converters are generally less sensitive. An increase in time resolution usually has an associated loss in finesse of digitisation, so most ns work is at 8 bit digitisation, while ms work, or wavelength or other scanning, can easily be 12 bit.

14.8.2 Signal to Noise Considerations

Signal-to-noise in photophysical measurements comes down to the ratio between the signal generated by photons incident on a detector, and the background noise of the detector and instrument electronics. Experimentally, S/N is usually increased by: increasing photon absorption by increasing sample concentration (although this is often fixed by the experiment); changing instrument settings to

increasing the number of photons incident on the detector per second; decreasing background noise by increasing the time constants of the electronics which results in effectively integrating the signal over a longer time; cooling the detector to reduce noise; or signal averaging. Increasing the number of photons incident per second usually has the associated penalty of reducing spectral resolution since the increase in photon flux is usually achieved by widening instrument monochromator slits. Increasing instrument time constants usually has the associated penalty of reducing the time resolution of the experiment, which may not be acceptable in fast time-resolved studies. Since the S/N ratio for an averaged signal improves as the square root of the number averaged, it is often time effective to average four signals, which doubles S/N. But it requires the average of 16 experiments to get a 4-fold improvement in S/N, so it is always best to optimise S/N instrumentally before having to rely on signal averaging to improve S/N. Furthermore, some experiments are not suitable for averaging, for example if there is a risk of photodegradation of the sample. Most experimental arrangements end up being a compromise between S/N, spectral resolution and time resolution. Knowing what is required from the experiment and how these three factors are related helps in making the optimum choice of experimental/instrumental variables.

14.8.3 Data Analysis

Most instruments have associated software for data analysis, but it is useful to be able to curve fit data independently of any particular software restrictions, so a method to export data as a number file, such as an ASCII file or similar, to general curve fitting programs (e.g., Table Curve, IGOR Pro, Origin) is useful. When decay curve fitting from lifetime studies, it is important to select the relevant section of the data for fitting. To give a common example; if the time over which data is collected is much longer than the decay itself then curve fitting can be dominated by the noise on the tail of the curve where the signal is essentially zero. The quality of a curve fit is always improved by addition of more parameters, but care has to be taken to ensure that the parameters are physically meaningful. A plot of the residuals, *i.e.*, the difference between experiment and theoretical data, is one of the most useful ways to evaluate the quality of the curve fit, a good curve fit should have residuals evenly distributed around zero for the whole curve. Examples are given in [Chap. 15](#). Most curve fitting programs also give the standard deviations for the various parameters used to create the curve, and these should be given along with the parameters themselves when reporting results.

14.8.4 Perception of Colour and Colour Representation

For many technological applications, the *colour* and *luminance* of the emitted light can be extremely important. Luminance is often used to characterise emission or reflection from a flat, diffuse surface and is an indicator of how much luminous power is perceived by the human eye looking at the surface from a particular angle of view, *i.e.*, how bright the surface will appear. Luminance is the luminous intensity per unit area projected in a given direction (in candela per square metre).

Colour perception in humans is initiated by the absorption of light by three different spectral classes of *cone cells* present in the retina, conveniently referred to as blue, green and red. Each class exhibits a different but overlapping spectral sensitivity, with maximum values at *ca.* 419, 531 and 558 nm respectively. The sum of the differing sensitivities is called the *photonic response* and displays a maximum value at 555 nm. However colour perception can be very subjective, and the description of colour differences can be quite challenging. Colorimetry and the trichromatic perception of colour are based on Grassmanns' laws [19, 20]:

1. Any colour may be matched by a linear combination of three other primary colours, provided that none of these may be matched by a combination of the other two.
2. A mixture of any two colours can be matched by linearly adding together the mixtures of any three other colours that individually match the two source colours.
3. Colour matching persists at all luminances.

In practice, experiments on the additive mixture of light prove that there are no three colours which when mixed additionally can duplicate all spectral colours. Whilst the mixture may exhibit the required spectral hue, it generally fails to duplicate the required saturation for that colour. The only approach to obtain a perfect match is the addition of a 'negative' colour, to desaturate the spectral hue. To overcome this problem in 1931 the CIE (Commission Internationale de l'Éclairage) defined a system based on colour coordinates to characterise the colour properties of light [19, 20]. The primary colours (X , Y and Z) in this system are theoretically defined super-saturated colours, which lie outside the bounds of the spectral locus, eliminating the need for 'negative' colours. In order to standardise this system, the CIE defined a secondary standard observer based on the differing sensitivity of the three classes of human cone cells. Consequently any colour, C , of wavelength, λ , may be expressed as:

$$C_{\lambda} = \bar{x}_{\lambda}X + \bar{y}_{\lambda}Y + \bar{z}_{\lambda}Z \quad (14.4)$$

where X , Y , Z are the system primaries (known as *tristimulus values*) and \bar{x}_{λ} , \bar{y}_{λ} and \bar{z}_{λ} are the colour-matching functions. The luminance and CIE colour response are obtained by determining the spectral energy distribution of a sample using a spectroradiometer and subsequently processing the data using appropriate software

containing the CIE colour matching curves. Alternatively, since values for the colour-matching functions as a function of wavelength are available in the literature [19, 20], the X , Y and Z tristimulus values may also be determined from properly corrected photoluminescence data in the visible region according to:

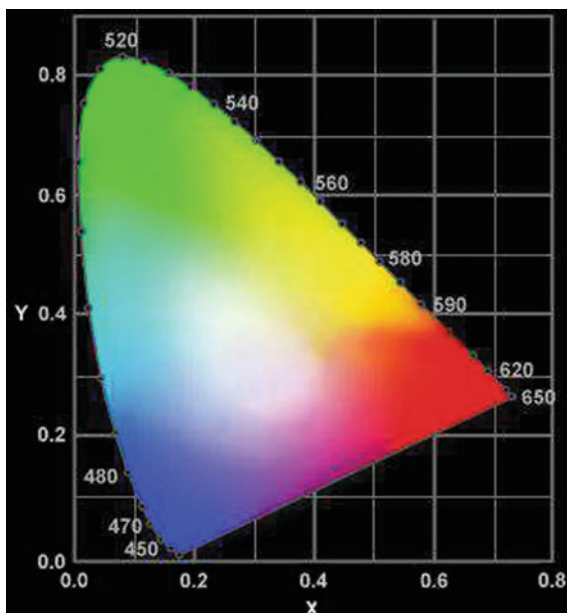
$$\left\{ \begin{array}{l} X = \sum_{\lambda=380}^{700} \bar{x}_{\lambda} E_{\lambda}(\Delta\lambda) \\ Y = \sum_{\lambda=380}^{700} \bar{y}_{\lambda} E_{\lambda}(\Delta\lambda) \\ Z = \sum_{\lambda=380}^{700} \bar{z}_{\lambda} E_{\lambda}(\Delta\lambda) \end{array} \right\} \quad (14.5)$$

where E is the emission intensity at wavelength, λ . To simplify the calculations, sampling wavelength bands ($\Delta\lambda$) at 5 or 10 nm apart is adequate. The *chromaticity* of a colour is specified by two parameters, x and y , known as *chromaticity* or *colour* coordinates, which are functions of the XYZ tristimulus values, given by:

$$x = \frac{X}{X + Y + Z} \quad y = \frac{Y}{X + Y + Z} \quad (14.6)$$

The x and y chromaticity coordinates are typically plotted in a two-dimensional grid known as the CIE (x,y)-chromaticity diagram (Fig. 14.8). The curve is made of the pure spectral colours from the blue to the red, covering the entire visible

Fig. 14.8 The CIE (x,y)-chromaticity diagram



spectrum (380–770 nm) and is known as the *spectral locus*. The two extremes of the spectral locus are connected by a straight line, the *purple boundary*, which represents colours which cannot be formed from any single part of the spectrum, but which must include a mixture of at least the two extremes of the visible spectrum. Consequently, the colours represented by the purple boundary are not pure spectral colours. The centre of the diagram is taken as the *white point*, whose coordinates are designated as (0.33, 0.33). The area restricted by the diagram, the spectral locus and the purple boundary encloses the domain of all colours.

14.9 General Instrumentation and Techniques

14.9.1 UV/Vis/NIR Spectrophotometer

A scanning UV/Vis spectrophotometer is essential; a schematic representation is shown in Fig. 14.9. Moderately priced instruments typically cover the wavelength range *ca.* 190–800 nm, but interest, and technological advances in detectors, have pushed the range available into the NIR, although at increased cost. Full wavelength instruments either scan each wavelength independently as a grating is rotated within a monochromator, or use a detector array with a spectrograph to give simultaneous measurement across the full spectral range. The latter are often referred to as ‘diode array’ spectrophotometers, and are particularly useful for kinetic studies where full spectra recorded at the same instant are preferred.

A typical scanning UV/Vis will use a tungsten lamp for ~ 320 –800 nm (and NIR if applicable), and a deuterium lamp for ~ 190 –320 nm, with an automatic lamp change, the position of which can usually be altered, within the ~ 300 –340 nm range. Internal wavelength calibration on start-up is often carried out using the 486.0 and 656.1 nm lines of the deuterium lamp. There are also a number of automatic filter changes as the spectrum is recorded, as filters are interposed in the light beam to reduce stray light and second order light. The detector is typically a photomultiplier tube for the UV and visible regions; and a cooled PbS detector for the NIR region. High-specification UV/Vis/NIR

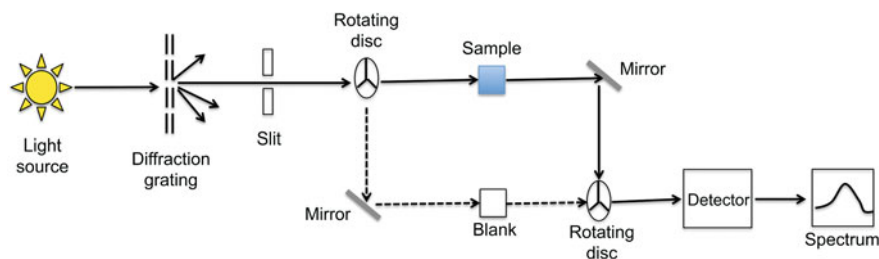


Fig. 14.9 Schematic of a dual-beam UV/Vis absorption spectrophotometer

spectrophotometers also incorporate an InGaAs detector to bridge the spectral gap between the PMT-PbS switching wavelength, thus ensuring high sensitivity across the entire measured range.

Most low to mid-range standard laboratory instruments have a fixed bandwidth of *ca.* 1–2 nm. More expensive instruments include variable slits, usually in fixed sizes but sometimes continuously variable, typically across the range 0.1–10 nm. Narrow slits are used for gas phase studies and narrow solution lines (such as in lanthanides, see Fig. 14.12), while wide slits are useful for matching absorption spectra to emission excitation spectra which are often recorded using a bandwidth wider than 2 nm. High specification instruments working with very narrow bandwidths may use a double monochromator arrangement to minimise stray light.

The design of the instrument sample compartment determines what can be studied. Typically, use of cells of up to 10 cm path length with a heating/cooling block for temperature control is easy, and some instruments allow the whole sample compartment to be removed so a custom built sample compartment can be inserted, or unusual samples studied. If the sample compartment lid needs to be removed for any samples of unusual shape, then a few layers of black cloth generally reduces stray light enough for measurement, although it is also a good precaution to dim the room light to the minimum convenient level, and to also check the effect of removing all room light completely.

Absorption of solids is usually measured using diffuse reflectance. Diffuse reflectance measurements typically use an integrating sphere, which replaces the normal spectrophotometer sample compartment. Diffuse reflectance relies upon the focused projection of the spectrometer beam onto the sample where it is reflected, scattered and/or absorbed. Both specular and diffuse reflectance will be generated by the sample. By placing either a diffusely reflective panel or a light absorbing cup at the angle of specular reflectance two different spectra can be recorded, *i.e.*, total reflectance or diffuse reflectance respectively. Reflectance, R , and concentration, c , are not linearly related, but, under certain circumstances the Kubelka–Munk function, $f(R)$ (Eq. 14.7), which assumes infinite sample dilution in a non-absorbing matrix, a constant scattering coefficient, s , and an infinitely thick sample, is linearly related to c :

$$f(R) = \frac{(1 - R)^2}{2R} = \frac{k}{s} = \frac{Ac}{s} \quad (14.7)$$

where R is the absolute reflectance of the sample, k is the extinction coefficient and A is the absorbance. It is often convenient, therefore, to present diffuse reflectance spectra in terms of the Kubelka–Munk function. k is the imaginary part of the complex index of refraction (the real part is given by the refractive index, n), which is related to the molar absorption coefficient by:

$$\varepsilon = \frac{4k}{\lambda} \quad (14.8)$$

Universal reflectance accessories to measure the absolute specular reflectance of polished surfaces and films are also available.

Absorption instruments can be single or double beam—the latter having a second light beam for a reference, or blank, which should contain everything except the compound of interest (e.g., solvent, buffer etc.). Due to absorption by cell materials and solvents, it is a useful check to run a preliminary spectrum of the blank against air, so that the cut-off wavelength of high blank absorbance, below which absorption measurements are meaningless, can be identified. Single beam variable wavelength, but non-scanning, UV/Vis spectrophotometers are relatively cheap instruments which are very useful for single wavelength kinetic studies or studies of absorbance changes arising from system response to external variables, such as sensor response studies. They are also excellent for optically matching solutions for relative quantum yield measurements.

Solution and gas phase spectra are usually presented in absorbance mode but can easily be transformed to transmittance using the Beer–Lambert law. Solid state spectra are presented as diffuse reflectance, the Kubelka–Munk function, or % reflectance, as described above. However, first, second, and even high, derivative spectra are also quite common. These higher derivative spectra are useful in picking out structure in spectra, showing vibrational shoulders etc., or components in mixtures [21].

Without doubt the most common error when first beginning to work with absorption spectroscopy is that of attempting to measure spectra of samples with absorbances which are too high for accurate measurement. A typical general laboratory instrument is usually reliable up to an absorbance of about 2–3, *i.e.*, with the sample transmitting at least 1–0.1 % of the incident light; although the range may have to be reduced in regions of the spectrum where lamp intensity or detector sensitivity is low, or if narrow slits are used. With such an instrument it is best, if possible, to work within the absorbance range of ~ 0.2 –1.7, but it is a relatively simple procedure to evaluate spectrophotometer performance using a solution which obeys the Beer–Lambert law at a range of concentrations, or the same solution in different path length cells, to cover a wide absorbance range. Stray light is much reduced by using a double monochromator arrangement and some double monochromator instruments claim a useful absorbance range of up to 8.

14.9.2 Steady-State Photoluminescence Spectroscopy

Figure 14.10 shows a schematic of modular components for emission spectroscopy. There is a wide range of fluorimeters available ranging from cheap non-scanning filter instruments to scanning instruments with very high specifications. A moderate price range scanning instrument will typically contain the following components: (i) a 150 W xenon lamp as excitation source; (ii) an excitation monochromator with variable slits with a diffraction grating blazed for maximum output in the UV; (iii) an emission monochromator with variable slits, and grating

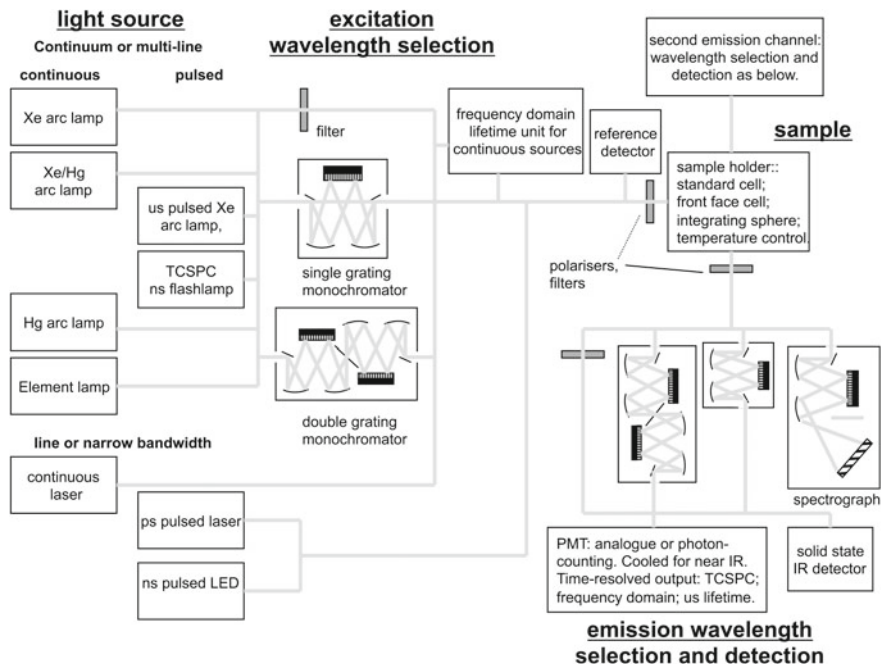


Fig. 14.10 Schematic of modular components for emission spectroscopy. The standard fluorimeter arrangement is: a Xe arc lamp as source; single grating monochromators for excitation and emission selection; and analogue or photon counting PMT as detector

blazed for the visible spectral region; and (iv) a red-sensitive photomultiplier, operating in either analogue, or perhaps photon counting, mode, as detector. Since xenon arc lamps are not very stable, a second reference detector is usually present to monitor and correct for variations in the excitation source intensity. More expensive instruments may use higher intensity lamps such as a 450 W xenon lamp, or have the facility to use an Hg or Hg/Xe lamp with their UV-rich line emission, and will use photon counting detection. Photon counting detection offers advantages over analogue measurements of both improved signal stability and improved signal to noise.

Polarisation studies are common in fluorescence spectroscopy. In the more expensive instruments internal polarisers may be automatically switched between horizontal and vertical alignments, otherwise polarisers placed in the sample compartment require manual switching. Plastic polarisers are relatively inexpensive but will absorb and be bleached by light below about 300 nm and so are unsuitable for UV work.

The instrument sample compartment once again determines what can be studied. Typically, right-angle geometry is used with standard 1 cm square cells for optically-dilute, transparent solutions. In other words, the sample emission is detected at 90° relative to the incident beam; this configuration minimises the

amount of incident light reaching the detector. A heating/cooling block for moderate temperature control is also quite standard. Smaller path length cells, across either the excitation beam, or emission beam, or both, are usually quite easily fitted into the 1 cm standard holder using an appropriate adaptor. Some instruments allow the whole sample compartment to be removed so a custom-built sample compartment can be inserted, or unusual samples can be studied. Again, a few layers of thick black cloth over any unusual samples in a dimly lit room generally reduces stray light enough for accurate measurement, unless the sample signals are particularly weak.

Sample cells with mirrors can enhance sensitivity by reflecting excitation light to give a double pass excitation, and by redirecting otherwise uncollected emission to the detector.

Opaque samples, films and solids are usually studied in the front-face configuration. In this arrangement, the incident beam is focused on the front surface of the sample and the emission is collected from the same region at an angle that minimises reflected and scattered light (typically 22.5° when the sample is orientated perpendicular to the excitation beam). For many instruments it is possible to buy solid-state sample holders which enable sample orientation angle to be altered; depending on the sample type and form, spectra may be improved by changing the sample orientation to an angle of 30° or 60° to the incident beam.

There are a number of common problems and artifacts in fluorescence spectroscopy (see also [Chap. 15](#)).

1. **Solvent Raman lines.** When operating even at moderate sensitivity, a fluorimeter will pick up the Raman lines from the solvent. Therefore the solvent blank will show both the scattered Rayleigh band, at the excitation frequency, and lower intensity Raman bands which are shifted from the excitation line by an energy corresponding to the solvent vibrational energy. Raman lines can be identified by: (a) their presence in the emission from the solvent blank alone; (b) the band shape, which is essentially the same as the excitation band, and therefore varies with excitation band width; (c) the position of a Raman band, which varies with excitation wavelength—shifting the excitation wavelength by 10 nm results in a *ca.* 10 nm shift in the position of the Raman band. Some solvents give stronger Raman bands than others, with high energy vibrations, such as OH and CH being particularly troublesome since these are shifted most from the excitation wavelength. If Raman bands are a significant problem then using CCl_4 as solvent which, because of the high atomic masses, has only low frequency Raman bands lying close to the excitation wavelength, may help. Raman bands, however, can be very useful for monochromator calibration and checking the S/N ratio of fluorimeters.
2. **Distorted excitation and/or emission spectra—inner filter and self absorption effects.** It is important to be aware of the optical geometry of the instrument and the absorption characteristics of the sample in the cell used. The excitation optics are usually arranged to focus the beam into the centre of the cell. In practice this gives a thin beam of excitation light, the width of which

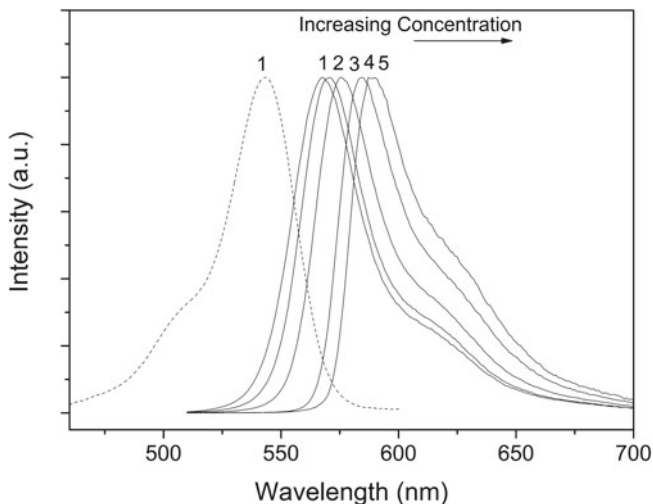


Fig. 14.11 The effect of concentration on the normalised emission spectrum of Rhodamine B in ethanol ($\lambda_{\text{ex}} = 500 \text{ nm}$). The concentrations are: **1** $1 \times 10^{-6} \text{ mol dm}^{-3}$; **2** $4 \times 10^{-6} \text{ mol dm}^{-3}$; **3** $8 \times 10^{-6} \text{ mol dm}^{-3}$; **4** $2 \times 10^{-5} \text{ mol dm}^{-3}$; **5** $4 \times 10^{-5} \text{ mol dm}^{-3}$. The UV/Vis absorption spectrum is also shown for **(1)** (*Dashed line*)

increases somewhat with slit width. Since the Beer–Lambert law indicates an exponential dependence of light transmittance upon optical pathlength, emission intensity is only proportional to absorption extinction coefficient at very low absorbances across the cell. If absorption is high then excitation light is absorbed even before it reaches the centre of the cell. At very low absorbance, the fraction of light absorbed is given by $2.303 \times A$; so even with an absorbance as low as 0.02 in a 1 cm cell, with emission measured from the centre of the cell, the incident light has been attenuated by 2.3 % by the time it reaches the middle of the cell, and a 2.3 % correction to intensity for the excitation spectrum is required. The optimum absorbance depends upon a number of factors, and sample concentration may be fixed by a variety of experimental requirements, but for typical preliminary fluorescence measurements using 1 cm cells, the optical density at the absorption maximum should be kept below 0.1 to reduce gross inner filter effects, and if precise excitation spectra are required it should, emission quantum yield allowing, be much less. In the most commonly used right-angle geometry the detector lens is arranged to collect light from the centre of the cell, and therefore any emission must pass through the sample solution between the centre and edge of the cell. With standard 1 cm cells this will be a 0.5 cm path length. If there is any significant absorption within this path length across the emission band then the emission band shape will be distorted by this ‘self-absorption’. This is most notable at the high energy side of a fluorescence band for fluorophores with a small Stokes’ shift. Figure 14.11 illustrates the problem of self-absorption in the emission spectrum

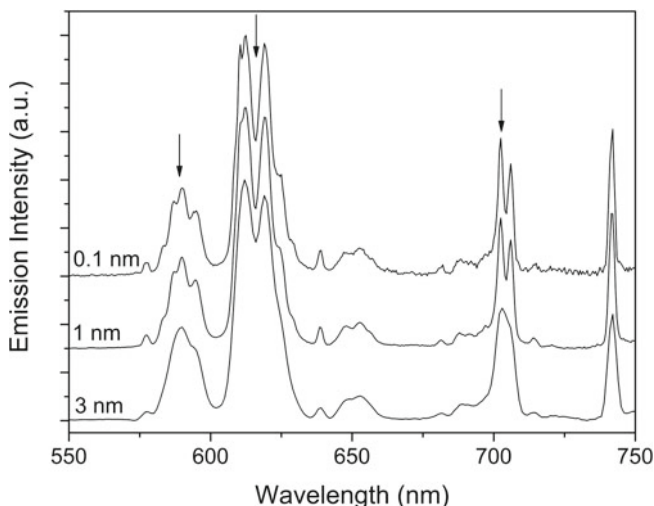


Fig. 14.12 The effect of varying the emission bandwidth on the photoluminescence spectrum of europium (III) (in $\text{Na}_{1.08}\text{K}_{0.5}\text{Eu}_{1.14}\text{Si}_3\text{O}_{8.5}\cdot 1.78\text{H}_2\text{O}$, $\lambda_{\text{ex}} = 393 \text{ nm}$). As the bandwidth increases from 0.1 to 3 nm, a gradual loss in the spectral resolution is observed, but S/N increases

of the laser dye Rhodamine B. As the concentration increases the emission spectrum shifts to longer wavelengths due to reabsorption of the higher energy emission, which results in a gradual shift in the fluorescence colour from green to orange to red. If emission ‘self-absorption’ is a problem, then either a lower concentration sample or a cell with a narrower path length along the emission path should be used.

- Second order transmission by monochromators.** As discussed earlier monochromators containing diffraction gratings will transmit light of wavelength $n\lambda$, where n is an integer. If these different order spectra become troublesome then a filter cutting off below the excitation wavelength on the excitation side, and a filter cutting off just above the excitation wavelength on the emission side will remove them.

14.9.2.1 Recording of Excitation and Emission Spectra

For an emission spectrum, the spectral resolution is provided by the emission monochromator, and so if spectral resolution is important the bandwidth of this monochromator should be set suitably narrow. The excitation bandwidth can be much wider, consistent with a suitably low level of scattered light and no overlap of emission and excitation bandwidths. Figure 14.12 illustrates the effect of varying the emission slit width on the resolution of the photoluminescence spectrum of a microporous europium(III) silicate ($\text{Na}_{1.08}\text{K}_{0.5}\text{Eu}_{1.14}\text{Si}_3\text{O}_{8.5}\cdot 1.78\text{H}_2\text{O}$). Lanthanide(III) ions typically exhibit sharp, line emission spectra, since their optical

transitions take place predominantly within the $4f$ manifold, where the electrons are largely shielded from crystal field effects by the filled $5s$ and $5p$ shells. If the emission slits are opened too widely, the fine-structure of the emission lines is poorly resolved. Reducing the slit width decreases the spectral bandwidth, thereby improving the resolution of closely spaced emission peaks, but with the penalty of decreasing S/N. Inevitably for weakly emitting samples, a compromise between spectral resolution and sufficient emission intensity must be made. In this instance, with standard detection electronics, longer integration times may be used to improve the S/N ratio.

For a full emission spectrum, the excitation wavelength is usually chosen to be on the high energy side of the longest wavelength absorption band. This is usually a better choice than the absorption maximum because it allows the full emission spectrum, which usually partly overlaps the absorption spectrum, to be recorded. Exactly how far away from the absorption maximum depends upon the Stokes shift, and the bandwidths required for suitable S/N.

The reverse arrangement of monochromator bandwidths applies for an excitation spectrum, and the emission wavelength is usually set to be on the low energy side of the highest energy emission band, for the same reasons as described above.

For both spectra the raw signal provided by the spectrometer is the wavelength dependence of the detector response to the light falling on it. For emission spectra this is not the same as the wavelength dependence of the emission from the sample; the two values differ because both the detector sensitivity and the efficiency of the optics between sample and detector vary with wavelength. For excitation spectra it is not the same as the relative efficiency of conversion of incident light into emitted light; here the two differ because the lamp output is not constant across the spectrum, and the efficiency of the optics between lamp and sample are wavelength dependent. Most spectrophotometers provide manufacturers correction factors, and spectra are usually automatically corrected using these correction factors. If these are not available then spectra can be corrected using the methods described below (Sect. 14.10.1).

14.9.2.2 Phosphorimetry

Fluorimeters which use a pulsed Xe lamp as the excitation source can be used for phosphorescence measurements down to lifetimes of about $10\ \mu\text{s}$ using electronic gating of the detection system, with both gate delay and gate width as variable operator set parameters. The sum of these must be less than the time between pulses unless mechanical shutters are used to isolate individual excitation pulses from the pulse train. In the absence of a single pulse facility, decay curves across *ca.* 10 ms are typically possible; if single pulses can be isolated then much longer decay curves can be obtained.

Fluorimeters which use a continuous light source can usually be adapted for phosphorescence work by addition of a phosphorimeter attachment, which is usually either a pair of mechanical shutters on the excitation and emission

monochromators which can be used in single shot or repetitive chopping mode, or, as in older phosphorimeters, a high speed “rotating can” with a slit in it, placed around the sample, so the slit alternately sweeps past the excitation and detection optics. The time resolution of these phosphorimeters is typically in the ms–s range.

14.9.2.3 Portable and Microvolume Spectrometers

There are a number of small portable spectrometers available, at reasonable cost, in which a fibre optic collector is attached to a small spectrograph-array spectrometer [18]. They are available with fibre optic of different diameters, which control light collection efficiency, and, in part, spectral resolution, and also different gratings and blazes for enhance sensitivity across particular spectral ranges. These are particularly useful for emission from unusual samples, or emitters fixed in particular experimental arrangements. When coupled to a white light source they can also be used for absorption measurements. Recently, spectrometers and fluorimeters have been developed which can be used with μl volumes of samples [22]. These are proving particularly valuable for fluorescence measurements on biological samples.

14.9.3 *Near Infrared Luminescence and Steady-State Singlet Oxygen Luminescence Studies*

The near IR ($\lambda > 700$ nm) spectral region is becoming increasingly important in the study of a wide range of inorganic and organic lumophores. Photomultipliers are available with sensitivity up to about 1700 nm, while solid state photodiodes can extend the spectral response of detectors to several μm . A particularly important application is in the detection and quantification of singlet oxygen. Many of the expensive fluorimeters can be fitted with an additional special monochromator and detector designed to measure the very weak emission from singlet oxygen centred at 1270 nm. An example is given Chap. 15. The monochromator is blazed for this wavelength range, and since the emission band is quite broad a wide bandwidth can be used. A cut-off filter is used to remove all lower emission wavelengths especially since visible light from sample emission in the second, or third, order spectra may interfere. Either a highly sensitive liquid nitrogen cooled photomultiplier or solid-state device is used as the detector. The presence of the characteristic emission band at 1270 nm is evidence of singlet oxygen production and the yield is determined in the same way as a fluorescence yield but this time using a known singlet oxygen generator as standard (see Chap. 15).

14.9.4 Time-Resolved Measurements

14.9.4.1 Time-Resolved Microsecond Emission Using Pulsed Xenon Lamp Excitation

Pulsed xenon lamps are available which give white light emission with pulse durations of a few 10 μs , and pulse frequencies of a few tens of Hz. The lamp intensity is high enough for emission work. Combination with an emission monochromator, excitation monochromator, and moderately fast detector gives a time resolved emission spectrometer operating over the UV/Vis range with a time resolution of a few μs , and at reasonable price. A number of commercial fluorimeters/phosphorimeters use pulsed xenon lamps with gated detection, rather than continuous lamps, as the excitation source. Fluorescence is detected with simultaneous gate and pulse; while longer lived emission can be isolated from fluorescence by delaying the detector gate. If gated detection is replaced by continuous monitoring then the full emission decay curve can be recorded. Averaging over a large number of pulses can be used to improve signal-to-noise for weak signals.

14.9.4.2 Microsecond Flash Photolysis

This is the classic photochemical time-resolved method developed by Porter and Norrish [23, 24]. Although now generally replaced in most laboratories by ns flash photolysis (see below) it is still the superior method for transient absorption studies at timescales longer than about 50 μs . The fundamental principles of the flash photolysis technique are discussed in [Chap. 8](#). Flash lamps with outputs typically of $\sim 10\text{--}100$ J and pulse durations of a few μs are used as the excitation source. It is worth noting that the pulse duration depends on its energy, and that lower energy, but shorter, pulses are preferred for many applications. The lamp emission spectrum is a white light continuum with atomic lines superimposed; the exact lamp wavelength output is determined by the choice of inert gas fill, with xenon being most commonly used. A tungsten lamp operated from a stabilised power supply makes a very stable monitoring beam for the visible and near UV. After travelling through the sample the monitoring beam is passed through a monochromator, and/or filters, for wavelength selection, before being incident on a moderately fast photomultiplier. A typical solution phase optical arrangement will have the sample held in 10 cm cylindrical path length cell, with two slightly longer flash lamps on either side, all in a reflective cylinder with aperture stops either side to help discriminate between monitoring beam and flash lamp pulse. The long path length means that relatively dilute solutions can be used which helps minimise second order processes for long-lived transients, such as triplet-triplet annihilation. A solution filter jacket around the sample, or gelatin sheet filters, can be used to give wavelength selection to the excitation light, and a thermostatted jacket can

be used for temperature dependent experiments such as the determination of reaction activation energies.

14.9.4.3 Nanosecond Absorption/Emission Using Laser Excitation (ns Flash Photolysis)

A schematic diagram of the typical experimental configuration for ns-flash photolysis experiments is shown in Fig. 14.13. A ns pulsed laser is used as the excitation source, with a fast kinetic spectrometer as the detection system. Most absorption systems use a 150 W xenon lamp as the monitoring source. Even this lamp, when operating in normal continuous mode, generates too few photons per nanosecond for good S/N across the ns– μ s range, and it is usual to provide an electrical pulse into the lamp which increases the output by a factor of ~ 50 , to give a relatively stable high intensity monitoring beam for $\sim 100 \mu$ s. The xenon arc pulse is synchronised with the laser system, so the laser pulse is timed to arrive during a flat portion of the monitoring beam (The temporal ‘shape’ of the monitoring pulse depends on the electrical pulse applied and can be altered somewhat using ferrite cores in the pulsing system). For times longer than a few hundred μ s the Xe lamp can be operated in non-pulsed mode, although, because of the poor stability of Xe lamps, for times longer than a hundred μ s, a stabilised tungsten lamp may well give a better signal. Aperture stops are set in the monitoring beam, before and after the sample, to ensure that the monitoring beam traverses that part of the sample exposed to the laser pulse, and also to reduce stray and scattered light. A shutter on the monitoring beam is also usually synchronised with the laser pulse to limit exposure of the sample to the intense xenon arc beam. Photodegradation of the sample can be a problem in ns flash photolysis, and regular checks on sample integrity are always worth carrying out. After passing through the sample the monitoring beam goes through a monochromator and then usually onto

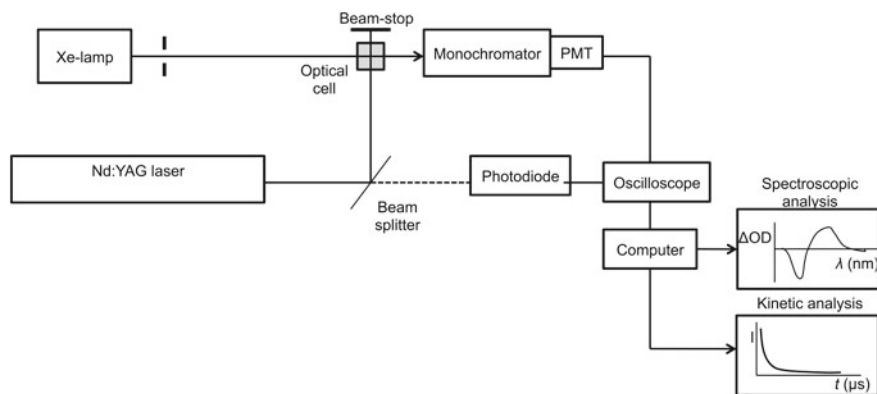


Fig. 14.13 Schematic of typical ns-flash photolysis instrumentation

a fast photomultiplier. Signal to noise considerations generally require a somewhat wider spectral bandwidth than is used in a conventional absorption spectrophotometer, but care must also be taken to prevent too much light being incident on the photomultiplier tube, since an excessive photomultiplier current is a major source of instrumental artifacts such as spurious signals, oscillating signals (“ringing”) and non-linear response. Most recording devices have an input impedance of $1\text{ M}\Omega$ and for ns timescales the photomultiplier output signal must be terminated with a $50\ \Omega$ load to limit current drain on the photomultiplier. However, as the time scales of interest increase a larger termination impedance can be used to increase the size of the signal voltage, and improve S/N.

The choice of laser determines which excitation lines are available. Any pulsed laser operating with high enough pulse energies, typically in the mJ range, can be used. The most commonly used is probably the Nd/YAG laser, which, with frequency doubling, tripling and quadrupling, gives lines at 1064, 532, 355, 266 nm, with pulse powers in the mJ range readily available (one Einstein of 355 nm radiation is 336 kJ, so a 10 mJ 355 nm pulse in 1 cm^{-3} is *ca.* $3 \times 10^{-5}\text{ E dm}^{-3}$ which is usually adequate for generation of measurable concentrations of transient species). Q-switched lasers generate pulses of a few ns lifetime, which generally limits the time resolution of the apparatus to a few tens of ns.

Computer-controlled equipment is available which will automatically record transient spectra across a specified spectral and temporal range. Often, a number of “shots” are made at each wavelength and the signals averaged. In addition, it is usually best to run the spectra at a series of random wavelengths (e.g. 490, 570, 420, 460, 530, 430 nm...) rather than at regular increasing or decreasing wavelengths (420, 430, 449, 450 nm...) to check for any problems associated with photodegradation of solutions. A preliminary examination would usually include such measurements but then a detailed examination of transient curves at specific wavelengths of interest should also be carried out to make sure that the timescales of transient spectra recorded are such to include all major spectral changes following absorption.

The usual optical arrangement has the sample in a 1 cm cell with the monitoring beam at 90° to the excitation pulse but narrower cells can be used, and it is also possible to arrange the laser beam and monitoring beam to be approximately collinear down the cell so both shorter and longer path length cells can be used.

ns-laser emission studies are generally easier than absorption. The same kinetic spectrometer can be used, but there is no need for the monitoring beam, the aperture stop on the emission side of the sample can be widened to allow more light through. Unless the emission is particularly strong, the monochromator bandwidth may need to be widened to collect enough light for an acceptable signal.

14.9.4.4 Time-Resolved Singlet Oxygen Studies

The lifetime of singlet oxygen is ideal for studies using laser generation on a ns timescale. Unfortunately the emission yield is very low, but there are fast detectors designed to measure the very weak emission from singlet oxygen centred at 1270 nm. A filter is used to select the wavelength range to avoid interference from second, or third, order emission spectra. Either a highly sensitive liquid nitrogen cooled photomultiplier, or solid state device is used as the detector. Yields can be obtained by comparison with the signal produced by a standard singlet oxygen generator in the same solvent and with the same absorbance at the excitation wavelength, preferably over a range of excitation pulse energies (see [Chap. 15](#)). Since the lifetime of singlet oxygen is highly solvent dependent, and the signal quality significantly improved by separating the timescale of the laser pulse from that of singlet oxygen decay, it is worth trying to work in solvents which give relatively long lifetimes; acetonitrile is a good polar solvent for singlet oxygen work, and hydrocarbons are suitable non polar solvents.

14.9.4.5 Time Correlated Single Photon Counting (TCSPC)

Instrumentation for TCSPC is described in [Chap. 15](#) and will not be discussed in detail here. A wide range of instruments is available, with cost generally increasing with: increasing time resolution arising from choice of excitation source *i.e.*, ns flash lamps, ns pulsed LEDs, or ps lasers; decreasing wavelength of excitation source; complexity of the detection equipment: filters, monochromator, polarisers; and time resolution and wavelength range of the photomultiplier used.

14.9.4.6 Phase Modulated (or Frequency Domain) Fluorimeter

This technique measures the phase shift, and change in degree of modulation, between a rapidly modulated excitation source and the subsequent modulated emission, which arises because of the time interval between excitation and emission in the sample (Fig. 14.14). The modulation in the emission intensity is measured for a number of excitation modulation frequencies. Best lifetime precision, and multi-component resolution, is achieved if measurements are made over a range of frequencies spread around $\sim 1/(2\pi\tau)$ Hz, where τ is the emission lifetime. Data from frequencies far removed from this value gives little information since: if the frequency of excitation modulation is much lower than this the emission modulation exactly matches that of excitation; while if it is much higher there is no measurable modulation in emission intensity. So the range of available modulation frequencies which can be generated, or measured, determines the range of lifetimes the instrument can be used for.

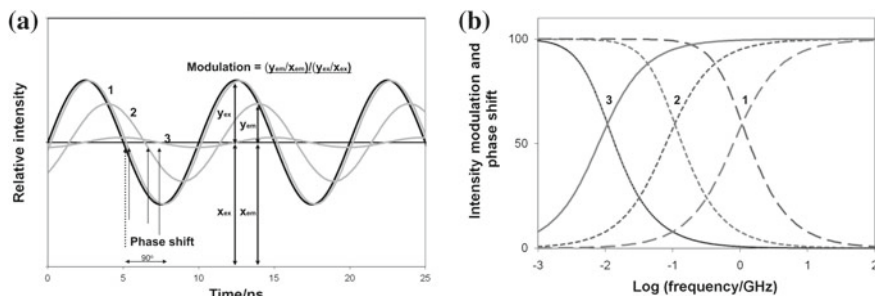


Fig. 14.14 **a** Modulation and phase shift of emission for lifetimes of: **1** 0.2 ns, **2** 2 ns, and **3** 20 ns (grey lines) in response to 0.1 GHz modulated excitation (black line). **b** Modulation and phase shift response as a function of frequency of intensity modulation. Modulation (decreasing with frequency) and phase shift (increasing with frequency) for lifetimes of: large dashed line, **1** 0.2 ns, short dashed line, **2** 2 ns, and solid line, **3** 20 ns. Note that as the excitation modulation frequency increases modulation decreases from a maximum of 1 to a minimum of 0, while at the same time phase shift increases from a minimum of 0 to a maximum of 90°, but these changes are most commonly shown as % of full range, as on the vertical axis in **b**

Either, or both, excitation source modulation frequency or detector response can limit instrument capabilities. Most standard commercial instruments have modulation frequencies up to a maximum of a few hundred MHz and are best suited for relatively long-lived fluorophores with high quantum yields. The excitation source is typically a modulated LED or laser diode, or for a wide wavelength range, light from a continuum steady-state source, such as a Xe arc lamp modulated with an electro-optical cell, such as a Pockels cell; detection is typically a fast photomultiplier, or multichannel plate photomultiplier. Polarizers are commonly used accessories. Such an instrument is ideally suited for lifetimes of a few ns, but will also measure, albeit with lower precision, lifetimes in range of 100's ps. GHz modulation frequencies are obtained with mode locked lasers with a fast multichannel plate photomultiplier and these allow lifetime measurements in the range of tens of ps.

A particular advantage of frequency domain lifetime measurements is that, by measuring a number of frequencies simultaneously, it is possible to make lifetime measurements very quickly, in as short a time as a few ms. Thus changes in excited-state lifetimes during chemical reactions can be studied in real time across the ms time domain. This matches that of the most commonly used chemical and biochemical fast reaction technique, stopped-flow, and stopped-flow accessories are available for commercial frequency domain fluorimeters. Because the measurements are quick, frequency domain measurements over a wide spectral range also provide an attractive method for obtaining time-resolved fluorescence spectra.

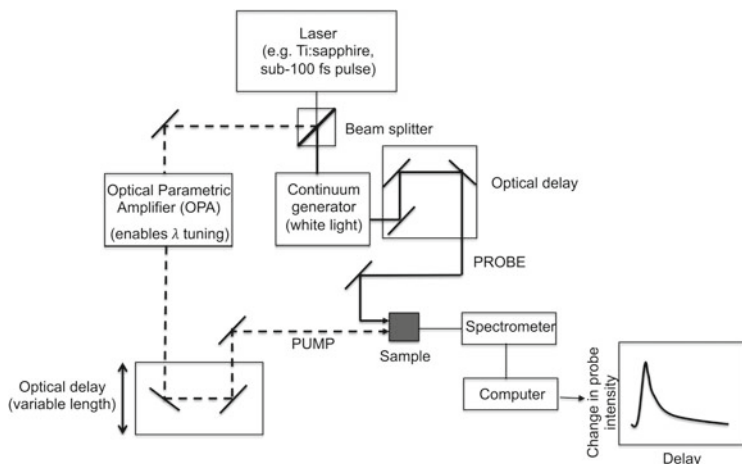


Fig. 14.15 Femtosecond pump-probe system

14.9.4.7 Ultrafast ps/fs Pump Probe Absorption Spectroscopy

Continuous monitoring at times much less than a nanosecond is limited by the response time of electronic components (particularly the photomultiplier) and poor S/N for continuous light sources on sub-ns timescales. However, many photochemical and photophysical processes occur on the sub-nanosecond timescale, including isomerism, internal conversion, energy transfer and electron transfer. The pump-probe method overcomes these limitations enabling reactions on the pico- and femtosecond timescale to be investigated. In pump-probe spectroscopy, two light pulses are generated from a single ultrafast (50–100 fs) laser source, which is typically a Ti:sapphire laser pumped by a diode or argon-ion laser (see Fig. 14.15). The first pulse is used to excite or *pump* the sample, the second to *probe* the changes induced in the system at a given time after excitation. The Ti:sapphire laser output is split into two pathways using a partially-reflecting mirror or beam splitter. Although the two laser pulses leave the beam splitter at the same time, they travel along different pathways so that they arrive at the sample at different times. The time resolution of the technique now no longer depends on the electronics but instead on the pathlength (using the speed of light, we can calculate that a 1 mm delay corresponds to 3.33 ps). The laser output is normally amplified and the wavelengths of both exciting and probe pulses can be tuned using an optical parametric amplifier (OPA). The monochromatic laser pulse may be transformed into a broad band continuum pulse covering the UV, visible and IR regions using various nonlinear optical effects. For example, this can be achieved simply by focusing the pulse into a cell containing a suitable liquid (e.g., water, D₂O, tetrachloromethane). The white light continuum pulse can then be used as analysing light to obtain the transient spectrum. The pump-probe method is

especially useful to monitor the dynamics of population of vibrationally excited states, however, the low absorption cross-section in the IR spectral region means that a high pump intensity ($\sim 10^{11} \text{ W cm}^{-2}$) is required. Similar methods involving splitting and introducing a time delay in laser pulses are also used to study ultrafast excited state emission processes in the technique of time-gated fluorescence upconversion [25]. The pump pulse is used to excite the fluorescence in the sample and then combined with the probe pulse in a nonlinear optical crystal (such as potassium dihydrogen phosphate, KDP) through sum-frequency generation to give the detected signal. This is then studied as a function of the optical delay to give time-resolved fluorescence with resolution of tens of fs.

14.9.5 Fluorescence Imaging

There is a wide range of commercially-available fluorescence microscopes available to meet all research budgets. Lower end models enable the observation of fluorescence from biological or materials samples at the micrometer level, with image capture if a camera is available. A larger budget will allow probing of sample depth, fluorescence lifetime measurements and high-end photography and video capture. Refurbished, second-hand and ex-demonstration microscopes are a good option for those with a limited budget. Optical microscopes tend to be extremely robust, so it is often possible to obtain a higher-specification instrument for a fraction of the price of a new microscope, and spare parts are relatively easy to find on the internet. It is also possible to convert a regular transmission microscope into a fluorescence microscope using LEDs as the excitation source—the Cheaposcope website gives an excellent description of how to achieve this [26].

Conventional wide-field fluorescence microscopes use vertical or *epi*-illumination, where the excitation source is typically a xenon arc or mercury lamp and the sample is irradiated from above. Excitation wavelength selection is achieved by first passing the light through a wavelength selection excitation filter. The transmitted light is then reflected from a dichroic mirror, through the microscope objective, where it is focused onto the sample. If the sample fluoresces, the emitted photons are collected by the same objective, passed back through the dichroic mirror, and are subsequently filtered by an emission filter, which removes unwanted excitation or background wavelengths. In a properly configured microscope, only the emission light should reach the eye or the detector. The limits of detection are therefore governed by the darkness of the background. Since the excitation light intensity is typically several orders of magnitude greater than the emitted fluorescence, an effective emission filter is crucial for good S/N.

The excitation filter, dichroic mirror and emission filter are typically housed in a single optical unit known as a *filter cube*. The filter cube provides a convenient means to change the excitation/emission wavelength range without direct handling of either the mirror or filters. The role of the dichroic mirror is to separate the excitation and emission light paths. Each dichroic mirror has a set wavelength

value at which it transmits 50 % of the incident light. The mirror reflects wavelengths below and transmits wavelengths above this value. To enable efficient separation of the excitation and emission light, the transition value should lie at a wavelength somewhere in between. Since the dichroic mirror is not 100 % effective, excitation and emission filters are used to minimise the effects of stray light. These filters are typically interference filters, which exhibit an extremely low transmission outside of their characteristic band pass. They are therefore very effective at selecting the excitation and emission wavelength range. Filter cubes containing various combinations of excitation and emission filters and dichroic mirrors suitable for use with most common fluorophores are available. Optical spectra for different filter cube types may be found in microscope manufacturer's catalogues.

The depth of field of an epifluorescence microscope is 2–3 μm and the maximum resolution is approximately equal to half the excitation wavelength (*i.e.* $\sim 0.2 \mu\text{m}$ for $\lambda_{\text{ex}} = 400 \text{ nm}$) [27]. If the sample is thicker than the depth of field, then out-of-focus fluorescence may result in blurred images. This problem may be overcome using *confocal fluorescence microscopy*. In contrast to conventional widefield microscopy, where the entire sample is irradiated, in a confocal microscope, a focused beam of light, typically from a laser, is scanned across the sample. The focused beam forms a series of diffraction-limited spots on the specimen, effectively dissecting it into optical sections. The fluorescence emitted by each optical section is separated from the incident beam by a dichroic mirror and focused by the objective lens through a pinhole aperture to a photomultiplier. The excitation intensity rapidly falls off above and below the plane of focus as the beam converges and diverges. This essentially confines the sample illumination to a specific area and depth, inhibiting excitation of the sample outside of the focal plane under examination. The optical path of the confocal microscope is additionally configured so that any fluorescence resulting from out-of-focus planes is blocked by the aperture, thus further attenuating any background interference. With certain fluorophores, two-photon fluorescence can also provide an excellent method for achieving depth profiling in imaging, particularly with biological samples. In this case, electronic excited states are produced by simultaneous absorption of two photons. For fluorophores emitting in the UV and visible this requires excitation in the near infrared, which provides the advantages for biological samples that this radiation is transmitted by tissues and that it is not normally damaging to biomolecules. Two-photon excitation needs a high photon flux, usually delivered by a pulsed laser. This has the advantage that the laser can be focused into a very small volume, providing high resolution. Chromophores for two-photon fluorescence possess certain requirements in terms of their structure and symmetry. However, a number of good two-photon fluorophores are now available. The area has been extensively reviewed [28, 29].

A number of more sophisticated fluorescence imaging techniques are available. **Fluorescence lifetime imaging microscopy (FLIM)** exploits the fact that the excited state lifetime is sensitive to its microenvironment to provide a contrast mechanism for imaging. By imaging the fluctuations of an excited-state lifetime

across a sample it is possible to obtain complementary information on local physical and chemical parameters such as viscosity, polarity and pH. **Fluorescence correlation spectroscopy (FCS)** measures the temporal fluctuation of fluorescence intensity due to translational motion, which may be correlated to physical parameters such as translational or rotational diffusion coefficients, molecular weights or aggregate size, or rate constants. An excellent discussion of the theory and applications of these and related fluorescence imaging methods may be found in the literature [30]. For FCS to work, it is important that solutions are very dilute and that the observation volume is very small. At the limit, it is possible to observe the fluorescence from a single molecule through the use of various advanced optical and detection methods. The behavior of one isolated molecule can be very different from that of an ensemble, and single-molecule spectroscopy and microscopy [31] are now important techniques for studying both chemical and biological systems.

The optical resolution (the distance between two points which can be distinguished) in microscopy is normally considered to be limited by the diffraction of light. Ernst Abbé showed in 1873 for optical devices that this diffraction limit is the wavelength of light divided by twice the numerical aperture of the imaging lens. This was thought for a long time to provide a limit on the resolution in optical microscopy, which with visible light corresponds to around a couple of hundred nm. However, over the last decade, a number of microscopic techniques, mainly based on photochemical processes, have been developed which allow sub-diffraction limited resolution. These are generally classified as super-resolution microscopy. The area is developing rapidly, and we will just mention three of these methods.

Near-field scanning optical microscopy (SNOM) overcomes the optical diffraction limit enabling very high spatial resolution at the sub-micron level and even single molecule detection. This uses a light source which is of nanometer dimensions obtained by the light passing through the tip of a nm dimension optical fibre [32]. In **stochastic optical reconstruction microscopy (STORM)**, photoswitchable fluorophores are used [33]. These are normally non-fluorescent but a certain percentage are transformed into emissive species upon photoswitching. These are then observed by single-molecule imaging and the centroid positions determined. The fluorophores are subsequently deactivated, a second group of photoswitchable fluorophores being converted into their emissive forms. These are imaged and the process repeated. In **stimulated emission depletion microscopy (STED)** [34], deactivation of excited states by stimulated emission at the edge of a fluorescent spot is used to inhibit the spontaneous emission of a probe. The overall effect is that it is possible to image samples on length scales smaller than the diffraction limit. Typically, two separate laser pulses are used, one to induce spontaneous emission and the other for stimulated emission depletion. However, it is possible to perform STED experiments using continuous wave lasers. With both STORM and STED, the use of dyes having appropriate photo-physical properties is of fundamental importance, and much research effort is being employed in the design and synthesis of appropriate systems.

14.9.6 Simple Test Rigs

With the wide availability of commercial instruments custom building of optical test rigs is less important than previously. However, a variety of simple optical rigs can be made with just a few components. A tungsten lamp with a stabilised power supply can act as either a very stable monitoring beam, or a moderate intensity irradiation source for the visible region. A xenon lamp is an excellent general purpose irradiation source for the UV/Vis region, and though less stable than a tungsten lamp, a beam splitter and photodiode detector can be inserted in the beam to monitor intensity variations when used as a monitoring beam for absorption or emission work. The light beams can be controlled using glass, or, for UV, quartz lenses, and iris apertures, or using fibre optics. A water filter, glass IR filter, or hot mirror will remove unwanted IR radiation, and either filters or a monochromator, will give wavelength selection as required for irradiation, excitation or absorption work. A photomultiplier running from a stabilised power supply is probably still the most convenient high sensitivity general purpose detector, but solid state detectors are also available. Cheap analogue-to-digital recording devices can be used to output signals from PM tubes and other recording devices directly in computers for data recording. There is a range of optical rails, stands, lenses and sample holders available from a number of commercial suppliers. A useful sample holder for irradiation of multiple samples is a “merry-go-round” in which samples are rotated in front of the beam, thus ensuring all samples are exposed under the same irradiation conditions irrespective of variations in lamp output.

14.9.7 Access to Infrastructure

The high costs associated with specialist ultrafast laser techniques can make their purchase prohibitive to many university research laboratories. However, centralised national and international research infrastructures hosting a variety of large scale sophisticated laser facilities are available to researchers. In Europe access to these facilities is currently obtained either *via* successful application to Laser Lab Europe (a European Union Research Initiative) [35] or directly to the research facility. Calls for proposals are launched at least annually and instrument time is allocated to the research on the basis of peer-reviewed evaluation of the proposal. Each facility hosts a variety of exotic techniques, enabling photoactive systems to be probed across a variety of timescales in different dimensions. For example, the STFC Central Laser Facility at the Rutherford Appleton Laboratory (UK) is home to optical tweezers, femtosecond pump-probe spectroscopy, time-resolved stimulated and resonance Raman spectroscopy, time-resolved linear and non-linear infrared transient spectroscopy, to name just a few techniques [36].

14.10 Reference Materials, Temperature Control, and Computer Programs

14.10.1 Reference materials: Absorption, Emission, Scattering

Although most modern spectrophotometers undergo automatic wavelength calibration upon start-up, using the emission lines from the deuterium lamp, and some fluorimeters may offer the same facility using the lines in the xenon lamp, reference materials are useful. For absorption spectrophotometry solid state filters, made of holmium and didymium oxide in a glass, with narrow reference absorption lines are available (See Fig. 14.5). For the UV, benzene vapour is an excellent standard for both wavelength and spectral resolution. The vapour pressure is sufficient that it is only necessary to put one drop of liquid benzene in a stoppered cuvette to get a good absorption spectrum.

To obtain corrected emission spectra, it is necessary to know the wavelength-dependent efficiency of the detector. The determination of correction factors can be a time-consuming process and several approaches are possible. For many commercial instruments, the manufacturer will supply correction files for emission and excitation spectra. While these are an invaluable assistance, it is advisable to exert caution when using them and make independent checks on their validity from time to time. One reliable method of doing this is to compare the experimental emission spectrum and known corrected emission spectrum of a standard emitter. Sets of standard emitters spanning the UV and visible regions are commercially available and their corrected emission spectra are available in the literature. If correction factors are not supplied by the instrument manufacturer, then they may be determined by measuring the wavelength-dependent photon output from a calibrated light source. Standard lamps for this purpose, and their spectral profiles, are available commercially. However, it is important to note that the spectral output of a lamp will vary with age. Alternatively, the spectral lamp output of the Xe lamp excitation source can be determined *in situ* using a *quantum counter* and a scatterer. A quantum counter emits with a quantum yield that is independent of the excitation energy over a defined spectral region. For example, concentrated rhodamine 6B solutions are often used for the spectral range between 300–600 nm. By scanning the excitation wavelength with the quantum counter in place, the relative photon output of the lamp can be obtained. A standard scatterer, such as barium sulfate or magnesium oxide, is then placed in the sample holder and a synchronous scan of the excitation and emission monochromators is performed. The resulting spectral output is then divided by wavelength dependent photon output of the lamp to yield the wavelength dependent sensitivity factors for the detection system (emission monochromator and detector). For further details on this method see the literature [37]. Fluorescence reference materials for

molecular spectroscopy in which the fluorophores are incorporated in poly(methyl methacrylate) blocks are available commercially, e.g., from Starna [5].

Magnesium oxide and barium sulfate are commonly used as scattering (diffuse reflectance) standards in the UV/Vis/NIR spectral regions as they scatter all wavelengths in this region efficiently and with reasonably uniform efficiency. However, there are some difficulties associated with using these materials including variation in reflectivity over time and on exposure to UV light. Moreover, the angular distribution of the scattered light can also show some wavelength dependence. To overcome the latter problem, integrating spheres have been developed, both for measurement of diffuse reflectance (absorption) spectra, and more recently, for the determination of emission quantum yields. An integrating sphere is typically a spherically shaped enclosure containing a hollow cavity that is coated with a highly reflective material (e.g., BaSO₄) which uniformly scatters light. Any photons which are incident with the highly reflective surface of the sphere wall are, by multiple scattering reflections, distributed equally to all other points in the sphere before eventually hitting the detector. This has the effect of eliminating the spatial and directional information of the scattered light. The use of an integrating sphere to determine emission quantum yields is described in [Chap. 15](#).

14.10.2 Temperature Control Units, and Cryostats

Most instrument manufacturers will make temperature control units for use at around a few tens of degrees from ambient, with either thermoelectric (Peltier) temperature control, or more simply a cell holder which allows water, or other liquid, circulation from an external temperature controlled bath. Cryostats are also available for precise very low temperature control, easily down to 77 K using liquid nitrogen cooling, less easily down to 4 K using liquid helium, and even to lower temperatures if required. A hot air blower, such as a hair dryer, is a convenient way to raise the temperature of a sample up to a few tens of degrees above ambient for the occasional experiment and a thermocouple or thermistor a convenient way to measure sample, or cell holder, temperature.

A quartz Dewar (Fig. 14.2) as described in [Sect. 14.3.3](#) is a relatively cheap alternative for low temperature work. 77 K is the most convenient temperature to work at, but thermostating at various other temperatures down to 113 K is possible using solid CO₂ or liquid nitrogen slush baths [1, 38]. If a thermocouple or thermistor can be placed in the Dewar the temperature can be monitored, and measurements made, as the whole assembly warms to ambient temperature.

14.10.3 Computer Programs

Molecular modelling. Molecular orbital modelling has reached the stage where it is possible to carry out useful electronic state modelling on a PC. It is mathematically convenient to use *Gaussian* equations rather than hydrogen like atomic orbitals for these calculations, and Gaussian programs are widely used in photochemical studies to give some theoretical insight into the nature of the transitions under investigation, and to calculate transition energies (wavelengths), and oscillator strengths, for comparison with those observed experimentally [39, 40]. Calculations for isolated molecules in the gas phase are most straightforward, but the effect of solvent can also be incorporated, most easily by considering the molecule of interest to be in the centre of a sphere of uniform dielectric constant but there are other models. Where a good match is obtained, the Gaussian molecular orbitals, and the atomic orbital coefficients used to generate them, can be used to help visualise the nature of the electronic transition. These programs can generate useful information such as the transition dipole, degree of charge transfer in the transition, and changes in atomic electron densities. Knowledge of those atoms of the molecular structure most involved in the orbitals of the transition, and also any atoms only slightly involved, is very useful in understanding substituent effects on transition energies [40].

Curve fitting programs. Most instruments have associated software for data analysis, but it is also useful to have some curve fitting programs available to explore custom designed models and models not included in the manufacturers software. We have found Table Curve from Jandel Scientific to be useful and fairly easy to use.

14.11 Safety

Aside from general laboratory precautions, the Photochemistry Laboratory has some more specific safety concerns that should be considered before undertaking any experiment.

High pressure lamps. Mercury and xenon arc lamps have high internal pressures even when not in operation. Follow the manufacturer's guidelines when changing and disposing these bulbs to avoid accidental breakages. In the event of breakage of a mercury lamp, the workplace safety protocol for a mercury spill should be followed. A mercury spill kit is a useful addition to any laboratory. Mercury lamps emit dangerous levels of UV radiation. It is important that if the lamp is not enclosed protective gloves and eyewear are used. If you are using a Hg lamp as the source in a fluorescence microscope, always ensure that appropriate filters are in place before looking down the eyepiece! Some Hg and Xe arc lamps produce ozone, which is toxic at relatively high concentration levels. Ozone-producing lamps should be used in lamp housings equipped with exhaust systems

in a well-ventilated room. Care should be taken with the high voltage start pulse of Xe lamps. Water cooling of any electrical equipment introduces another potential hazard.

Laser radiation. A laser produces an intense, highly directional beam of light. If directed, reflected, or focused upon an object, laser radiation will be partially absorbed, raising the temperature of the surface and even the interior layers of the object, potentially resulting in material deformation. The human body is vulnerable to laser radiation and exposure can result in serious tissue damage in the eye and skin. It is therefore essential that anyone working with a laser receives appropriate training and is familiar with the safe operating procedure. Most universities run a laser safety course which is a requirement for anyone intending to use lasers in their research.

Lasers are divided into a number of classes depending on the power of the beam and the wavelength of the emitted radiation. The weakest beams are designated Class 1, and are generally safe under all circumstances—these include laser pointers. Mode-locked Ti:sapphire, Q-switched Nd:YAG and dye lasers are all designated as Class 4 lasers, meaning they constitute a significant hazard if safety procedures are not strictly followed. Viewing of the beam and of specular reflections or exposure to diffuse reflections can cause eye and skin injuries.

Avoiding inadvertent exposure to the laser beam is an essential part of laser safety. Wherever possible, the laser optical path should be horizontal and well below eye level and ideally the beam path should be fully or at least partially enclosed. A beam dump should be inserted to terminate the beam path at some appropriate point and should be made from a material capable of absorbing the full intensity of the laser beam. All work with class 3B and four lasers should be carried out in a designated laser room, which should be clearly identified with a suitable warning notice and separate from the main laboratory. Lasers may also be required to have beam shutters or key-controlled interlocks to prevent operation if the laser casing or room door is open.

Laser protective eyewear fitted with appropriate filtering optics can protect the eyes from exposure to direct, reflected or scattered laser light and should always be worn if the experimental configuration involves an open beam or if there is a risk of accidental exposure. Laser goggles must be selected for the specific type of laser, to block or attenuate in the right wavelength range. Since laser goggles are subject to damage and deterioration, periodic inspection of these items should be part of the routine maintenance procedure.

High voltage electrical circuits. Many lasers are high voltage devices, typically 400 V upward for a small 5 mJ pulsed laser, and exceeding many kilovolts in higher powered lasers. This, coupled with high pressure water for cooling the laser and other associated electrical equipment, can create a greater hazard than the laser beam itself. Electrical equipment should generally be installed above ground level to reduce the electrical hazard in the case of flooding. Optical tables, lasers, and other equipment should be well grounded electrically.

Chemicals and laser dyes. The chemicals used in photochemical experiments, including laser dyes and solvents, may be harmful to health and should be handled appropriately in an adequately ventilated workspace.

14.12 The Photochemical Laboratory Library

While the following list of resources and useful information reflects our own research interests, with, for example, an emphasis on solution phase photochemistry, it should provide a good starting point for those interested in most aspects of photochemical research.

14.12.1 Books and Reviews

1. Reference handbooks

Montalti M, Credi A, Prodi L, Gandolfi MT (2006), Handbook of photochemistry, 3rd edn. CRC Press, Boca Raton. An essential reference book containing data tables for a wide range of compounds, and a variety of reference materials including: quantum yields, lifetimes, quenching rate constants, electrochemical potentials and solvent properties; as well as information on standard procedures used in chemical actinometry, determination of emission and excitation spectra correction factors, and quantum yield measurements; and also information on equipment such as lamps and filters.

Haynes WM (ed) (2011) CRC Handbook of chemistry and physics, 92nd edn. CRC Press Boca Raton, USA. Usually referred to as the Rubber Handbook in reference to the publisher of earlier editions, this is the first point of call when searching for physical or chemical constants, conversion factors, parameters, potentials, affinities, radii etc.

2. Photochemistry

Turro NJ (1991) Modern molecular photochemistry, University Science Books, California; Turro NJ, Ramamurthy V, Scaiano JC (2010) Principles of molecular photochemistry: an introduction, University Science Books, California; Turro NJ, Ramamurthy V, Scaiano JC (2010) Modern molecular photochemistry of organic molecules, University Science Books, California. The classic *Modern Molecular Photochemistry* recently underwent a comprehensive revision and is now available under the title *Modern Molecular Photochemistry of Organic Molecules*. It provides a detailed description of the

fundamental principles of molecular photochemistry, focusing in particular on organic photochemistry. The related primer *Principles of Molecular Photochemistry: An Introduction*, by the same authors, contains the introductory chapters of the main textbook.

Wardle B (2009) Principles and applications of photochemistry, Wiley. This book includes some excellent chapters on fluorescence sensors and probes, as well as a detailed description of more advanced fluorescence spectroscopy and imaging techniques.

3. Fluorescence and fluorescence spectroscopy

Lakowicz JR (2006) Principles of fluorescence spectroscopy, 3rd edn. Springer, Singapore. The big blue reference book for fluorescence spectroscopy and its applications. Detailed information provided on fundamental principles and theory, instrumental techniques and applications, and state-of-the-art applications.

Valeur B (2001) Molecular fluorescence: Principles and applications, Wiley. An excellent introductory textbook to the fields of photochemistry and photophysics and their applications.

4. Single photon counting

Becker W (2005) Advanced time-correlated single photon counting techniques, Springer. A detailed account of the principles and applications of time-correlated single photon counting.

5. Ultrafast processes

El-Sayed MA, Tanaka I, Molin Y (ed) (1995) Ultrafast processes in chemistry and photobiology, Blackwell. Some of the leading research workers in the field present brief accounts of ultrafast studies of reactions of interest in photochemistry and photobiology.

6. General spectroscopy

Banwell CN, McCash EM (1994) Fundamentals of molecular spectroscopy, 4th edn. McGraw-Hill, UK. An excellent easy to read undergraduate introductory text.

Hollas JM (2004) Modern spectroscopy, 4th edn. John Wiley and Sons Ltd, UK. This textbook contains an excellent chapter on lasers and laser spectroscopy.

7. Physical chemistry

Atkins P, de Paula J (2010) Physical chemistry, 9th edn. Oxford University Press, UK.

Winn JS (2001) Physical chemistry, Harper Collins, USA.

Two very good undergraduate texts, which differ in style.

8. Molecular quantum mechanics

Atkins P, de Paula J, Friedman R (2009) Quanta, matter and change: A molecular approach to physical chemistry, Oxford University Press, UK

Atkins PW, Friedman RS (2011) Molecular quantum mechanics, 5th edn. Oxford University Press, UK.

9. General chemistry, analytical chemistry, statistics

Mendham J, Denney RC, Barnes JD, Thomas MJK (2000) Vogel's quantitative chemical analysis, 6th edn. Pearson Education Ltd, UK. A comprehensive and detailed description of apparatus and methods used in quantitative chemistry and chemical analysis.

Skoog DA, West DM, Holler FJ, Crouch SR (2003) Fundamentals of analytical chemistry, 8th edn. Thomson Brooks/Cole, USA. An excellent standard undergraduate text, with more emphasis on instrumental methods than the above.

Armarego WLF, Chai, CLL (2003), Purification of laboratory chemicals, 5th edn. Elsevier. Procedures and processes for purifying organic, inorganic and organometallic chemicals.

Chatfield C. (1999) Statistics for technology, 3rd edn. (revised), CRC Press, Boca Raton, USA. Relatively easy to read and with plenty of illustrative examples.

10. Review articles

Glossary of terms in photochemistry (IUPAC Recommendations 2006), Prepared for publication by Braslavsky SE (2007) *Pure Appl Chem* 79:293–465. This gives detailed descriptions of the most important terms and concepts used in photochemistry.

Bonneau R, Wirz J, Zuberbuhler AD (1997) Methods for the analysis of transient absorbance data. *Pure & Appl Chem* 69:979–992. An excellent review of flash photolysis methods and common pitfalls in their use.

Wilkinson F, Helman WP, Ross AB (1995) Rate constants for the decay and reaction of the lowest electronically excited singlet state of molecular oxygen in solution. An expanded and revised compilation. *J Phys Chem Ref Data* 24:663–677. An excellent collection of data. The previous compilation: Wilkinson F, Brummer JG (1981) *J Phys Chem Ref Data* 10:809–999, also identified their preferred values, which helps when trying to decide which values to use from the many values given in the tables.

14.12.2 Websites

Some useful discussion of a wide variety of topics in photochemistry and photobiology can be found at dedicated websites such as that from the American Society of Photobiology (<http://www.photobiology.info/>) and the Outreach site from the Center for Photochemical Sciences, Bowling Green State University (<http://www.photochembgsu.com/main.html>).

14.12.3 Journals

Scientific journals specifically publishing fundamental research in photochemistry/ photophysics include:

- Photochemical and Photobiological Sciences (RSC)
- Journal of Photochemistry A: Chemistry, B: Biology, C: Reviews (Elsevier)
- Photochemistry and Photobiology (Wiley)
- Journal of Luminescence (Elsevier)
- Journal of Fluorescence (Springer)
- International Journal of Photoenergy (Hindawi)
- Sensors and Actuators B: Chemical (Elsevier)

However, as we have seen throughout this book, the applications of photochemistry and photophysics are hot topics in the scientific community and as such, research in this field is often published in many of the more general high-impact chemistry, physics and materials journals, including:

- Journal of the American Chemical Society
- Nature Photonics, and Nature Materials
- Angewandte Chemie
- Advanced Materials, and Advanced Functional Materials
- Chemical Communications, Chemical Science and RSC Advances
- Inorganic Chemistry
- Dalton Transactions
- Physical Chemistry Chemical Physics
- Journal of Physical Chemistry A, B and C

14.12.4 Instrument and Chemical Catalogues

Several instrument and chemical manufacturers produce extremely useful detailed reference catalogues, including:

The Molecular Probes® Handbook

Johnson I, Spence MTZ, *The molecular probes handbook-A guide to fluorescent probes and labeling technologies*, 11th edn. Life Technologies.

This provides a comprehensive guide of commercially-available fluorescence probes and labeling methods (including protocols), with particular emphasis on biological and biotechnological applications.

Hamamatsu Opto-semiconductor handbook

http://jp.hamamatsu.com/sp/ssd/tech_handbook_en.html (accessed May 2012)

Detailed information on semiconductor based light sources and detectors.

The Book of Photon Tools (2001, Oriel Instruments)

Unfortunately it is extremely difficult to obtain a copy of this excellent catalogue. If you don't own one already, it is possible to obtain some individual chapters *via* the Newport Corporation website (www.newport.com)—try using “Oriel Product Training” as your search term.

14.12.5 Professional Bodies and Conferences

The major continental professional bodies for photochemists are:

- European Photochemistry Association (EPA)
- Inter-American Photochemical Society (I-APS)
- Asian and Oceanian Photochemical Association (APA)
- The Japanese Photochemistry Association (JPA)

Similar groups exist for photobiology, including:

- American Society for Photobiology
- European Society for Photobiology

Partner members of each of these bodies may also have their own special interest groups e.g., Royal Society of Chemistry Photochemistry Group, German Group of Photochemistry (Fachgruppe Photochemie), Grupo Especializado de Fotoquímica (Real Sociedad Española de Química), Photobiology Association of Japan etc.

Some of the more specific photochemistry-related conferences series are listed below. Again, photochemistry/photophysics and their applications will also be key topics in more general conferences not listed below and new or one-time symposia

and summer schools in the field also frequently appear. Application-specific conferences are also not listed here.

- IUPAC Symposium in Photochemistry
- International Conference on Photochemistry
- Gordon Research Conference on Photochemistry
- Central European Conference on Photochemistry
- Asian Photochemistry Conference

References

1. Armarego WLF, Chai CLL (2003) Purification of laboratory chemicals, 5th edn. Elsevier, New York
2. Reichart C (1994) Solvatochromic dyes as solvent polarity indicators. *Chem Rev* 94:2319–2358
3. Mendham J, Denney RC, Barnes JD, Thomas MJK (2000) Vogel's quantitative chemical analysis, 6th edn. Pearson Education Ltd, UK
4. Skoog DA, West DM, Holler FJ, Crouch SR (2003) Fundamentals of analytical chemistry, 8th edn. Thomson Brooks/Cole, USA
5. www.starna.co.uk. Accessed 31 Aug 2012
6. Montalti M, Credi A, Prodi L, Gandolfi MT (2006) Handbook of photochemistry, 3rd edn. CRC Press, Boca Raton
7. Schott (www.schott.com) currently supply this type of illumination system for microscopy. Accessed 31 Aug 2012
8. www.uvp.com. Accessed 31 Aug 2012
9. Milonni PW, Eberly JH (2010) Laser physics. Wiley, New Jersey
10. Hollas JM (2004) Lasers and laser spectroscopy, Chapter 9, Modern spectroscopy, 4th edn. Wiley, UK
11. Suppliers include: Edmund optics. www.edmundoptics.eu. Accessed 19 June 2012; Acton optics and coatings. <http://www.princetoninstruments.com/optics/>. Accessed 19 June 2012
12. Semrock bandpass filters. <http://www.semrock.com/sets.aspx>. Accessed 19 June 2012; Newport optics. <http://www.newport.com/optical-filters/>. Accessed 19 June 2012
13. Calvert JG, Pitts JN (1966) Photochemistry. Wiley, New York Chapter 7
14. Jentof FC (2009) Ultraviolet-visible-near infrared spectroscopy in catalysis: theory, experiment, analysis and application under reaction conditions. In: Gates BC, Knözinger H (eds) Advances in catalysis, vol 52. Academic Press, Amsterdam
15. Savitzky A, Golay MJE (1964) Smoothing and differentiation of data by simplified least squares procedure. *Anal Chem* 36:1627–1639
16. Hamamatsu Opto-semiconductor handbook. http://jp.hamamatsu.com/sp/ssd/tech_handbook_en.html. Accessed 5 May 2012
17. Hamamatsu photomultiplier resource. <http://sales.hamamatsu.com/assets/applications>. - Accessed 5 May 2012
18. <http://www.oceanoptics.com/products/spectrometers>. Accessed 19 June 2012
19. Judd DB, Wyszecski G (1975) Color in business, science and industry. 3rd edn. Wiley, New York
20. Hunt RWG (1991) Measuring Colour. Ellis Horwood, Chichester
21. Talsky G (1994) Derivative spectrophotometry. VCH Publishers, New York
22. The thermo scientific NanoDrop fluorospectrometer. www.nanodrop.com. Accessed 31 Aug 2012

23. Thrush BA (2003) The genesis of flash photolysis. *Photochem Photobiol Sci* 2:453–454
24. Windsor MW (2003) *Photochem Photobiol Sci* 2:455–458 (Photochem Photobiol Sci 2003, volume 2, issue 5, is an issue in commemoration of George Porter)
25. Kahlow MA, Jarzęba W, DeBrull TP et al (1988) Ultrafast emission spectroscopy in the ultraviolet by time-gated upconversion. *Rev Sci Instrum* 59:1098–1109
26. The Cheaposcope. www.plantsci.cam.ac.uk/Haseloff/analysis/cheaposcope/index.html. Accessed 5 May 2012
27. Valeur B (2001) *Molecular fluorescence: principles and applications*. Wiley, Weinheim
28. Denk W, Strickler JH, Webb WT (1990) Two-photon laser scanning fluorescence microscopy. *Science* 248:73–76
29. Diaspro A, Robello M (2000) Two-photon excitation of fluorescence for three-dimensional optical imaging of biological structures. *J Photochem Photobiol B Biol* 55:1–8
30. Hausteib E, Schwille P (2007) Fluorescence correlation spectroscopy. Novel variations of an established technique. *Ann Rev Biophys Biomol Struct* 36:151–169
31. Moerner WE, Fromm DP (2003) Methods of single-molecule fluorescence spectroscopy and microscopy. *Rev Sci Instrum* 74:3597–3619
32. Rasmussen A, Deckert V (2005) New dimension in nano-imaging: breaking through the diffraction limit with scanning near-field optical microscopy. *Anal Bioanal Chem* 381:165–172
33. Bates M, Huang B, Dempsey GT et al (2007) Multicolor super-resolution imaging with photo-switchable fluorescent probes. *Science* 317:1749–1753
34. Hell SW (2009) Microscopy and its focal switch. *Nat Methods* 6:24–32
35. www.laserlab-europe.eu. Accessed 5 May 2012
36. www.clf.rl.ac.uk. Accessed 5 May 2012
37. Demas JN, Crosby GA (1971) Measurement of photoluminescence quantum yields. *J Phys Chem* 75:991–1024
38. Rondeau RE (1966) Slush baths. *J Chem Eng Data* 11:124
39. www.gaussian.com. Accessed 5 May 2012
40. Foresman JB, Frisch A (1996) *Exploring chemistry with electronic structure methods: A guide to using Gaussian*, 2nd edn. Gaussian, Pittsburg

Chapter 15

Experimental Techniques for Excited State Characterisation

J. Sérgio Seixas de Melo, João Pina, Fernando B. Dias
and António L. Maçanita

Abstract The characterisation of the excited state of a molecule implies the determinations of the different quantum yields and lifetimes. Additionally, complex kinetic systems are frequently observed and need to be solved. In this contribution, we give our particular way of studying systems of organic molecules where we describe how a quantum yield of fluorescence (in fluid or rigid solution, or in film), phosphorescence, singlet oxygen and intersystem crossing can be experimentally determined. This includes a brief description of the equipments routinely used for these determinations. The interpretation of bi- and tri-exponential decays (associated with proton transfer, excimer/exciple formation in the excited state) with the solution of kinetic schemes (with two and three excited species), and consequently the determination of the rate constants is also presented. Particular examples such as the excited state proton transfer in indigo (2-state system), the acid–base and tautomerisation equilibria in 7-hydroxy-4-methylcoumarin (3-state system), together with the classical examples of intramolecular excimer formation in 1,1'-dipyrenyldecane (2-state system) and 1,1'-dipyrenylpropane (3-state system) are given as illustrative examples.

J. S. S. de Melo (✉) · J. Pina
Department of Chemistry, University of Coimbra, 3004-535 Coimbra, Portugal
e-mail: sseixas@ci.uc.pt

J. Pina
e-mail: jpina@qui.uc.pt

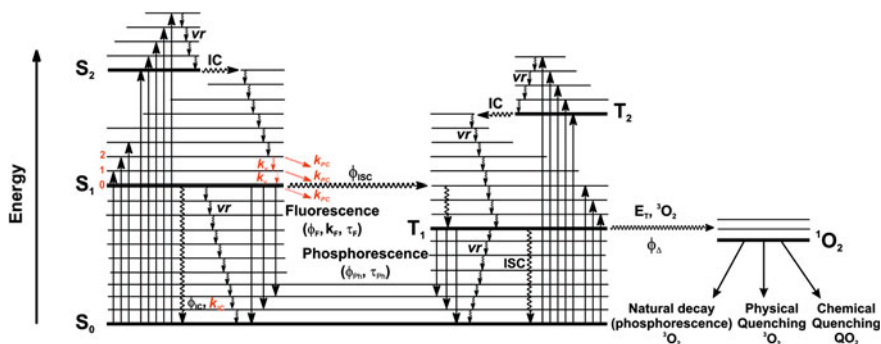
F. B. Dias
OEM Research Group, Department of Physics, Durham University, Durham DH1 3LE, UK
e-mail: f.m.b.dias@durham.ac.uk

A. L. Maçanita
Centro de Química Estrutural, Instituto Superior Técnico (IST), Lisbon, Portugal

15.1 General Jablonski Diagram: What parameters are needed to fully describe the excited state of a molecule?

The investigation of the excited state relaxation processes is one of the experimental key determinations to the interpretation of correlations between reactivity, stability and molecular structure. Prior to electronic excitation a molecule is usually in its ground electronic state. One of the few exceptions is molecular oxygen whose ground state is a triplet. Upon electronic excitation (1 fs) to any state above the first singlet excited state (S_1), deactivation occurs through internal conversion to the S_1 state, and here after vibrational relaxation to the lowest vibrational state of S_1 , the molecule further decays to its ground electronic state through several slower deactivation processes: radiative (fluorescence and phosphorescence) and radiationless (internal conversion and intersystem crossing), see Scheme 15.1. Photochemistry can compete with all the foregoing processes, including vibrational relaxation. This last process will be discussed in the context of the so-called vibronic effect, which will be described later in this chapter.

The general processes and deactivation mechanisms in Scheme 15.1 have been already described in Chap. 1. In this chapter, we will be mainly concerned with aspects associated with the experimental determinations of these parameters (energies, lifetimes, quantum yields and rate constants) and with particular emphasis on the determination of rate constants of reactions occurring in the excited states. These reactions include the formation of additional species (2, 3 and 4-state systems) or particular competition between deactivation processes—see the vibronic effect—and their dependence on the experiment conditions (solvent, temperature etc.).



Scheme 15.1 Jablonski-type diagram schematising the overall set of deactivation processes occurring upon excitation. vr vibrational relaxation; IC internal conversion; ISC intersystem crossing. In addition, the vibronic effect is illustrated in red, where k_v and k_{PC} are the vibrational relaxation constant and the photochemistry rate constant, respectively. This model for the fate of *quanta* absorbed into any vibrational level of any excited electronic singlet state excludes the occurrence of intersystem crossing

15.2 Characteristics of an Excited State

The lifetime of an excited state of a molecule is one of its fundamental characteristics; the others being its energy, quantum yields of decay processes and their respective rate constants. After generation of an excited population of molecules of concentration c_0 in the lowest vibronic state of S_1 , the concentration $c(t)$ at the time t after excitation decreases exponentially with time, according to the law $c(t) = c_0 e^{-t/\tau_0}$, where τ_0 is the reciprocal of the sum of the rate constants of all the decay processes available for this state. When the time t is equal to τ_0 , the concentration c has fallen to $1/e$ of its initial value. The value of τ_0 is defined as the lifetime of the excited state (Eq. 15.1). When the excited state is luminescent, the most common method to measure the lifetime consists in recording the luminescence decay. Since the luminescence intensity $I(t)$ is proportional to $c(t)$, it follows that $I(t) = I_0 e^{-t/\tau_0}$, with,

$$\tau_0 = \frac{1}{k_F + k_{IC} + k_{ISC}} \quad (15.1)$$

where k_F , k_{IC} and k_{ISC} are the rate constants for respectively the fluorescence, internal conversion and intersystem crossing. It is worth noting here that the foregoing exponential law does not hold when higher vibronic levels are excited and the decay includes the time region (fs-ps) where vibrational redistribution and relaxation occurs. In this time region, redistribution leads to oscillating functions and relaxation leads to additional negative exponential terms (rise times). These features become important in the particular case of competition between vibrational redistribution/relaxation and photochemistry. When fluorescence (or phosphorescence) is the only deactivation process, the value of τ is commonly designated as τ_F (or τ_P) with the meaning of radiative lifetime.

Additional excited state reactions add new pathways for energy dissipation, and consequently additional rate constants in (the denominator of) Eq. (15.1). Among these, we can find processes leading to the formation of new species (for example excimer formation, electron transfer or proton transfer) and/or quenching (e.g., energy transfer). Oxygen, present in all solvents in equilibrium with air, acts as a very efficient quencher, which is due to energy transfer to the triplet ground state of oxygen to generate singlet molecular oxygen (1270 nm, ≈ 1 eV), see Scheme 15.1. Obviously, the efficiency of diffusional oxygen quenching depends on the lifetime of the probe being quenched, and particularly on the nature and energy of the quenched state.

In the case of triplet states, due to their longer lifetimes, rigid matrices (frozen solutions or glasses for example) can be used to prevent diffusional collision between molecular oxygen and the probe, thus avoiding quenching. In the case of the singlet state, molecules with long lifetimes are highly sensitive to the presence of oxygen, whereas those with short lifetimes are only slightly affected. An important example of long-lived probes is pyrene, whose measured fluorescence lifetime (> 100 ns) critically depends on the oxygen content of the media; in

contrast, compounds with lifetimes shorter than 1 ns can generally be considered to be insensitive to the presence of oxygen. This can be easily explained with the Stern–Volmer equation (Eq. 15.2) [1].

$$\frac{\tau_0}{\tau} = 1 + k_q \tau_0 [\text{O}_2] \quad (15.2)$$

In liquid solutions at room temperature, the fluorescence of aromatic hydrocarbons or derivatives is known to be quenched by oxygen with a nearly diffusion-controlled rate constant. Values of k_q for more than 100 aromatic compounds in common solvents can be found in Ref. [2], as well as the concentration values of dissolved oxygen at 1 atm for *ca.* 70 common solvents. Let us take as an example 9,10-diphenylanthracene (DPA), whose lifetime is equal to 7.44 ns and $k_q = 1.7 \times 10^{10} \text{ mol}^{-1} \text{ dm}^3 \text{ s}^{-1}$, in cyclohexane at 20 °C, ($[\text{O}_2] = 2.4 \times 10^{-3} \text{ mol dm}^{-3}$). Substitution of these values in Eq. 15.2 yields $\tau_0/\tau = 1.30$. This means that, if oxygen is not removed from a solution of 9,10-diphenylanthracene, a significant difference will be observed in the lifetime of the probe, as shown in Fig. 15.1. However, suppose now that the lifetime is 1 ns. Now the ratio $\tau_0/\tau = 1.02$ and the effect of oxygen can be considered to be essentially negligible.

For fluorescent molecules with lifetimes ranging from 10 ns up to 500 ns, the influence of oxygen is even more relevant. For example, for pyrene (one of the most used, and probably most long-lived fluorescence probe), lifetimes values ranging between 382 and 650 ns can be found in the literature for the same solvent [2, 3].

One other way to observe this effect is by obtaining the rate constant for oxygen quenching from reorganisation of Eq. 15.2, leading to Eq. 15.3, and then compare the obtained values with those in the literature:

$$k_q = \left(\frac{1}{\tau_0(\text{with O}_2)} - \frac{1}{\tau_0(\text{without O}_2)} \right) \times \frac{1}{[\text{O}_2]} \quad (15.3)$$

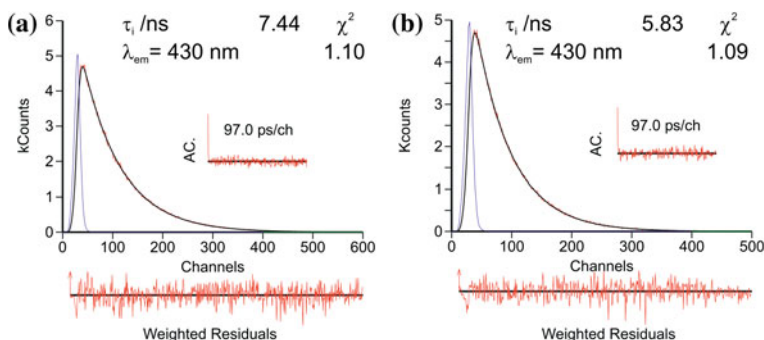


Fig. 15.1 Fluorescence emission decays for DPA (with $\lambda_{\text{ex}} = 373 \text{ nm}$) obtained in **a** previously degassed with nitrogen and sealed solution of cyclohexane and **b** in air-saturated solution of cyclohexane. The autocorrelation functions (AC), weighted residuals and χ^2 values, are also shown. The blue line is the pulse instrumental response

The values for pyrene and other aromatic hydrocarbons lifetimes are presented in Table 15.1. Note that the most dramatic change in the decay time values in the presence (for 0.21 atm pO_2) and absence of oxygen is displayed for pyrene. This is a clear consequence of its long lifetime, making it particularly sensitive to the presence of the oxygen quencher. Applying Eq. 15.2, and using the fluorescence lifetimes of common aromatic hydrocarbons provide rate constants for singlet state quenching by oxygen (k_q), which can be compared with those found in the literature [2] (see Table 15.1).

15.3 Quantum Yields and Energies

15.3.1 Quantum yields

From the Jablonski diagram, the different deactivation processes and the associated quantum yields and lifetimes are easily visualised. For all the deactivation processes the quantum yield is defined as the absolute ratio *quanta out/quanta in*. In the case of the fluorescence process:

$$\phi_F = \frac{\text{number of emitted fluorescence quanta}}{\text{number of absorbed quanta for a given singlet excited state}} \quad (15.4)$$

However, experimentally, room temperature fluorescence quantum yields (ϕ_F) can be determined by comparison with standards of known quantum yield (ϕ_F^{ref}). The emission quantum yields of these reference compounds should be independent of the excitation wavelength and the absorption and emission range of the sample (cp) and reference (ref) compound should match as much as possible. In practice, the quantum yield is determined by comparison of the integrated area under the emission spectra of optically matched solutions of the samples ($\int I(\lambda)^{\text{cp}} d\lambda$) and that of the suitable reference compound ($\int I(\lambda)^{\text{ref}} d\lambda$). The absorbance values should be kept as low as possible to avoid inner filter effects. In these conditions, using the same excitation wavelength, the unknown fluorescence quantum yield (ϕ_F^{cp}) is calculated using Eq. 15.5 [4],

$$\phi_F^{\text{cp}} = \frac{\int I(\lambda)^{\text{cp}} d\lambda}{\int I(\lambda)^{\text{ref}} d\lambda} \cdot \frac{\text{OD}_{\text{ref}}}{\text{OD}_{\text{cp}}} \cdot \frac{n_{\text{cp}}^2}{n_{\text{ref}}^2} \cdot \frac{f_{\text{des}}^{\text{cp}}}{f_{\text{des}}^{\text{ref}}} \cdot \phi_F^{\text{ref}} \quad (15.5)$$

where n_x is the refractive index of the solvents in which the compounds and the reference were respectively dissolved; OD_{ref} and OD_{cp} are the optical densities of the reference (ref) and compound (cp) at the excitation wavelength used. Since these experiments are done under usual laboratory conditions (room temperature and atmospheric pressure) and oxygen is present and dissolved in the solvent. In these conditions, oxygen must be removed ideally under several freeze-pump-freeze cycles. However, this is usually not practical. An alternative and more

Table 15.1 Fluorescence lifetimes (τ_F) for four different probes measured at 20 °C in the presence of oxygen and in argon-saturated solutions. Also presented are the literature values and the quenching rate constant by molecular oxygen (k_q). Data from Ref. [98] except where stated

Compound (solvent)	τ_F/ns ($p\text{O}_2 = 0.21$ atm)	τ_F/ns (in the absence of O_2 , Ar saturated solution)	τ_q/ns (literature)	$k_q/(\text{mol}^{-1} \text{dm}^3 \text{s}^{-1})$
Phenanthrene (cyclohexane)	15	55	57.5 (Ref. [2]) (n) 60.7 (Ref. [2]) (p) (Ref. [2])	2.0×10^{10} 2.3×10^{10} (Ref. [2])
Anthracene (cyclohexane)	4.65	5.25	5.24 (Ref. [5]) (Cx) 5.3 (Ref. [2]) (n) 5.8 (Ref. [2]) (p)	1.0×10^{10} 2.5×10^{10} (Ref. [2])
9,10-diphenylanthracene (cyclohexane)	7.44	5.83	7.5 (Ref. [6]) (Cx)	1.6×10^{10} (this work) 1.7×10^{10} (Ref. [2])
Naphthalene (cyclohexane)	16	102	100 (Ref. [7]) (Cx) 96 (Ref. [2]) (n) 105 (Ref. [2]) (p)	2.2×10^{10} 2.7×10^{10} (Ref. [2])
Pyrene (cyclohexane)	19	501	650 (Ref. [2]) (n) 190 (Ref. [2]) (p)	2.1×10^{10} 2.5×10^{10} (Ref. [2])

According to Ref. [2], (n) non-polar solvent, (p) polar solvent, (Cx) cyclohexane

straightforward approach consists in the introduction of a correction factor, f_{des}^x , that represents the degassing factor for the sample and reference compound, which is given by the ratio between the integrated area under the emission spectra in the absence and presence of oxygen. In general, the most used reference compound is quinine bisulfate [5], which ensures a good reliability in terms of the absolute value of the determined quantum yield (0.546 in 1 mol dm⁻³ aqueous H₂SO₄). However, because it is critical to guarantee the same absorption of sample and reference at the excitation wavelength, the required match of absorption spectra may not be possible with quinine bisulfate. A detailed list of other fluorescence standards can be found in Refs. [6, 7].

15.3.1.1 Fluorescence Quantum Yields at Low Temperature (77 K)

The fluorescence quantum yields at 77 K can be obtained by comparison with the spectrum at 293 K run under the same experimental conditions. Equation (15.6) is then applied [8],

$$\phi_{\text{F}}^{77\text{K}} = \frac{\int I(\lambda)^{77\text{K}} d\lambda}{\int I(\lambda)^{293\text{K}} d\lambda} \cdot \phi_{\text{F}}^{293\text{K}} \cdot f_c \quad (15.6)$$

where $\int I(\lambda)^x d\lambda$ is the integrated area under the emission of the sample at 77 and 293 K, $\phi_{\text{F}}^{293\text{K}}$ is the fluorescence quantum yield at 293 K and f_c is the factor that considers the “shrinkage” of the solvent volume (V) upon cooling, given by $V_{77\text{K}}/V_{293\text{K}}$.

15.3.1.2 Solid-State Fluorescence Quantum Yields

The solid-state fluorescence quantum yields in thin films can be obtained with the help of an integrating sphere, using the method outlined by de Mello et al. [9] and developed by Palsson and Monkman [10]. Equation (15.7) is used to determine the solid-state fluorescence quantum yields ($\phi_{\text{F}}^{\text{Solid}}$),

$$\phi_{\text{F}}^{\text{Solid}} = \frac{\int^{\text{cp}} I(\lambda) d\lambda}{\int^{\text{SA}} I(\lambda) d\lambda - \int^{\text{SS}} I(\lambda) d\lambda \cdot 10^{\Delta\text{OD}(\lambda_{\text{ex}})}} \quad (15.7)$$

where $\int^{\text{cp}} I(\lambda) d\lambda$ is the integrated area under the emission of the sample compound in the thin film (which excludes the integration of Rayleigh peak), $\int^{\text{SA}} I(\lambda) d\lambda$ is the integrated area under the Rayleigh peak of a sample containing only the quartz or sapphire disc support and $\int^{\text{SS}} I(\lambda) d\lambda$ is the integrated area under the Rayleigh peak in the emission spectra of the compounds under investigation in thin films. Since the emission from the samples is much weaker than the scattered excitation light (Rayleigh peak), the spectra are recorded with a filter that attenuates the

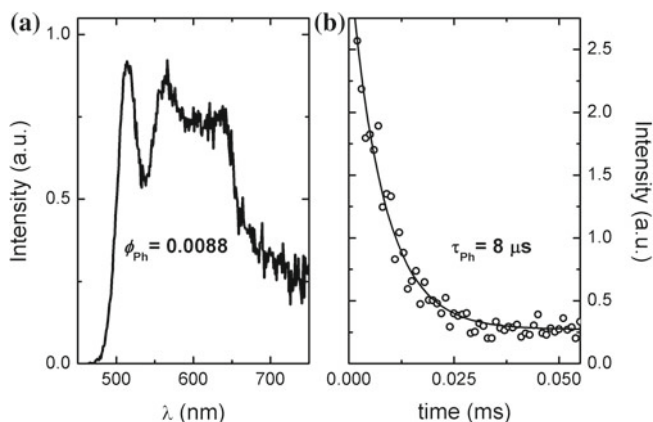


Fig. 15.2 Phosphorescence emission spectrum (a) and phosphorescence decay (b) for an oligothieryl-imidazole in ethanol glass at 77 K. (Reproduced with permission from Ref. [94], Copyright 2010, the American Chemical Society)

emission intensity at the excitation wavelength. This is considered in Eq. 15.7 by $10^{\Delta\text{OD}(\lambda_{\text{ex}})}$, the filter transmittance at the excitation wavelength.

15.3.1.3 Phosphorescence Quantum Yields

Phosphorescence measurements (spectra and decays, see Fig. 15.2) can be carried out in glasses at 77 K using a spectrometer equipped with a phosphorimeter unit (and an appropriate light source which can be a pulsed xenon lamp or a laser). The phosphorescence spectra should also be corrected for the wavelength response of the system.

Phosphorescence quantum yields (ϕ_{Ph}) are obtained by collecting the phosphorescence emission spectra from optically matched solutions (at the excitation wavelength) of the samples and the reference compound and by applying the following equation,

$$\phi_{\text{Ph}}^{\text{cp}} = \frac{\int I(\lambda)^{\text{cp}} d\lambda}{\int I(\lambda)^{\text{ref}} d\lambda} \cdot \frac{\text{OD}_{\text{ref}}}{\text{OD}_{\text{cp}}} \cdot \phi_{\text{Ph}}^{\text{ref}} \quad (15.8)$$

where $\int I(\lambda)^x d\lambda$ is the integrated area under the phosphorescence emission of the samples and the reference and $\phi_{\text{Ph}}^{\text{ref}}$ is the phosphorescence quantum yield of the reference compound. When possible, the phosphorescence quantum yields are determined using benzophenone ($\phi_{\text{Ph}} = 0.84$ in ethanol) as standard [2]. It is worth noting that, as with fluorescence (Eq. 15.5), in the determination of phosphorescence quantum yields, the same solvent should be used for the standard and sample. However, in the case that different solvents have to be used the correction introduced by the refractive index, n , in Eq. (15.5) is not necessary since the

phosphorescence quantum yields are obtained in rigid matrices and the properties of the solvent can be considered to be roughly identical.

15.3.1.4 Room-Temperature Singlet Oxygen Phosphorescence

Room-temperature singlet oxygen phosphorescence can be detected at 1,270 nm with the help of an appropriate detector (e.g., Hamamatsu R5509-42 photomultiplier cooled to 193 K in a liquid nitrogen chamber), and following laser excitation (at 266, 355 or 532 nm) of aerated solutions of the samples in a laser flash photolysis spectrometer [11]. In addition, the interposition of a 600-line diffraction grating, instead of the standard spectrometer grating (1,200-line), is needed to extend spectral response to the infrared.

In cases where the singlet oxygen phosphorescence emission intensity is sufficiently strong, measurements can be performed in a spectrofluorimeter using the Hamamatsu R5509-42 photomultiplier previously reported [12]. In both cases the use of a filter (Schott RG1000 for example), placed between the sample and the emission monochromator is essential to eliminate the first harmonic contribution of the sensitizer emission in the region below 850 nm. A characteristic singlet oxygen phosphorescence emission spectrum is shown in Fig. 15.3.

15.3.1.5 Singlet-Oxygen Formation Quantum Yields

When using the laser flash photolysis apparatus, the singlet oxygen formation quantum yields (ϕ_{Δ}) are obtained by direct measurement of the phosphorescence at 1,270 nm following irradiation of aerated solutions of the compounds. The ϕ_{Δ} values are determined by plotting the initial emission intensity for optically matched solutions as a function of the laser energy (Fig. 15.4) and comparing the slope with that obtained upon sensitisation with the reference compound (see Eq. 15.9). Biphenyl in cyclohexane ($\lambda_{\text{ex}} = 266$ nm, $\phi_{\Delta} = 0.73$ [13]), 1*H*-phenalen-1-one in toluene ($\lambda_{\text{ex}} = 355$ nm, $\phi_{\Delta} = 0.93$) or Rose Bengal in methanol ($\lambda_{\text{ex}} = 532$ nm, $\phi_{\Delta} = 0.76$) are generally used as standards [14].

$$\phi_{\Delta}^{\text{cp}} = \frac{\text{slope}^{\text{cp}}}{\text{slope}^{\text{ref}}} \cdot \phi_{\Delta}^{\text{ref}} \quad (15.9)$$

In a spectrofluorimeter, the sensitised phosphorescence emission spectra of singlet oxygen from optically matched solutions of the samples and that of the reference compound should be obtained in identical experimental conditions (see Fig. 15.3). The singlet oxygen formation quantum yield is then determined by comparing the integrated area under the emission spectra of the samples solutions ($\int I(\lambda)^{\text{cp}} d\lambda$) and that of the reference solution ($\int I(\lambda)^{\text{ref}} d\lambda$) and applying Eq. 15.10,

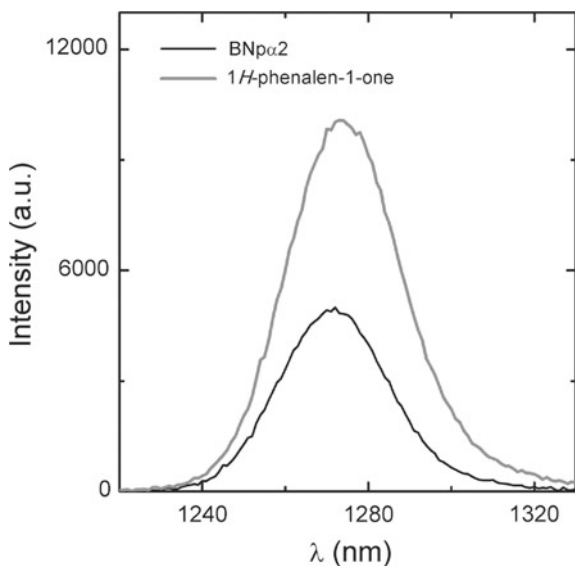


Fig. 15.3 Sensitised emission spectra of singlet oxygen in aerated toluene solutions of 1H-phenalen-1-one and a bis(naphthalene)-oligothiophene at 293 K. Reproduced with permission from Ref. [12], Copyright 2009, the Royal Society of Chemistry

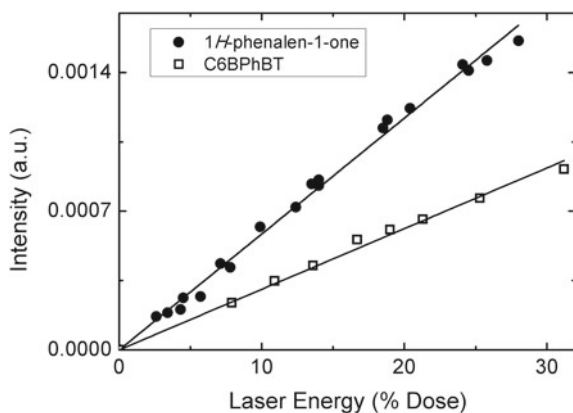


Fig. 15.4 Plots of the initial phosphorescence of singlet oxygen at 1,270 nm as a function of laser intensity for 1H-phenalen-1-one and an oligothiophene derivative in air-saturated toluene solutions at 293 K. Reproduced with permission from Ref. [95], Copyright 2006, the American Chemical Society

$$\phi_{\Delta}^{\text{cp}} = \frac{\int I(\lambda)^{\text{cp}} d\lambda}{\int I(\lambda)^{\text{ref}} d\lambda} \cdot \phi_{\Delta}^{\text{ref}} \quad (15.10)$$

with $\phi_{\Delta}^{\text{ref}}$ the singlet oxygen formation quantum yield of the reference compound.

15.3.1.6 Triplet–Triplet Transient Absorption Spectra

The transient triplet–triplet absorption spectra are collected by monitoring the optical density change at intervals of 5–10 nm over the range 250–850 nm and averaging at least 10 decays at each wavelength. First-order kinetics should be observed above the μs time range for the decays of the lowest triplet state. Special care should be taken in order to have low laser energy (≤ 2 mJ) to avoid multi-photon and triplet–triplet annihilation effects. All solutions should be degassed using the freeze-pump-thaw technique, or by bubbling with argon or nitrogen for ≈ 20 min, and sealed. The earlier is more accurate; however, for routine determinations, and for systems containing polymers, biomolecules, surfactants, etc., it is preferably to degas gently, which leads to the second method.

15.3.1.7 Triplet–Triplet Molar Absorption Coefficients Measurements

Singlet Depletion Method

This technique uses flash photolysis excitation and involves comparing the observed loss of ground state absorption with the gain in triplet absorption (see Fig. 15.5). The triplet molar absorption coefficients (ϵ_T) are determined according to the well-known relationship [4, 15],

$$\epsilon_T = \frac{\epsilon_S \cdot \Delta OD_T}{\Delta OD_S} \quad (15.11)$$

where ΔOD_S and ΔOD_T are the changes in optical density due to singlet depletion and to triplet absorption in the differential transient absorption spectra, respectively, and ϵ_S is the singlet molar extinction coefficient. Since assumptions

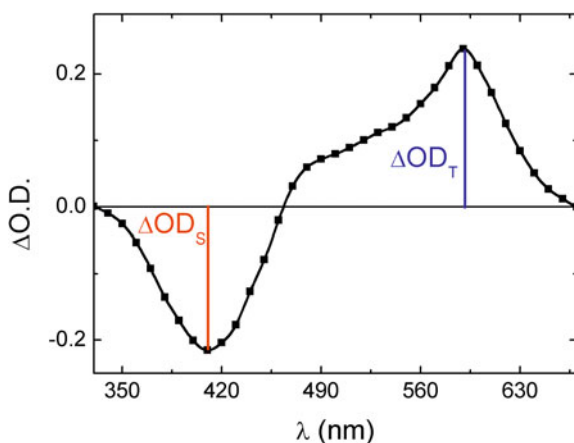
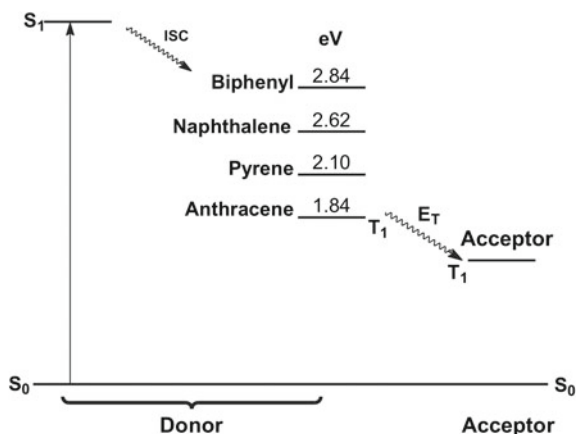


Fig. 15.5 Generic transient differential absorption spectrum



Scheme 15.2 Schematic representation of the energy transfer method used for determination of the triplet molar absorption coefficient in the laser flash photolysis apparatus

have to be made concerning the absence of absorption of the triplet state in the region of the ground state absorption, where the depletion is being monitored, this method is frequently associated with 50 or more percent error [16].

Energy Transfer Method

The energy transfer method is the most generally applicable method and involves sensitisation of the triplet state of the unknown compound (acceptor) by an appropriate energy donor in the triplet state (see Scheme 15.2). When using the flash photolysis technique, the unknown triplet–triplet molar absorption coefficient of the acceptor molecule can be obtained by comparison with that of the donor compound (with known molar absorption coefficient) by applying Eq. (15.12) [4].

$$\frac{\varepsilon_T^D}{\varepsilon_S^A} = \frac{\Delta OD^D}{\Delta OD^A} \quad (15.12)$$

where ΔOD^D is the maximum absorbance from the transient triplet–triplet absorption spectra of the donor in the absence of acceptor and ΔOD^A is the maximum absorbance of the acceptor triplet when both the donor and acceptor are present (see Fig. 15.6). For determination of ΔOD^A , additional corrections were taken into account, in particular, when the decay rate constant of the acceptor k_3 is not negligible. For this situation Eq. (15.13) should be applied [4];

$$\Delta OD_{\text{obs}}^A = \Delta OD^A \exp \left[-\frac{\ln k_2/k_3}{k_2/k_3 - 1} \right] \quad (15.13)$$

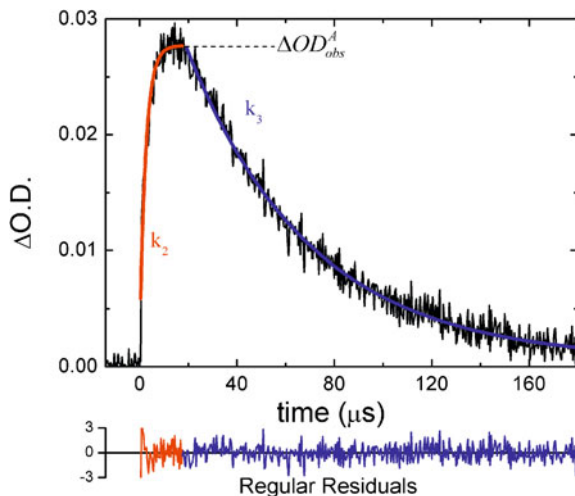


Fig. 15.6 Illustrative example of the shape of the triplet–triplet absorption decay obtained at the wavelength maxima of the transient absorption spectra of the acceptor in the presence of the donor

where k_2 is the donor decay rate constant in the presence of acceptor and ΔOD_{obs}^A is taken from the maximum observed in the triplet–triplet difference spectra of the acceptor in the presence of donor.

The decay in Fig. 15.6 clearly shows that the acceptor is being formed (by energy transfer from the donor) at the expense and during the decay of the donor (which occurs with a rate constant of $k_2 = 4 \times 10^5 \text{ s}^{-1}$) and then decays with a rate constant of $k_3 = 2 \times 10^4 \text{ s}^{-1}$.

Experimentally the samples under study are dissolved in solutions of relatively high concentrations of the donor compounds (10^{-2} – $10^{-4} \text{ mol dm}^{-3}$ solutions), while the concentration for the samples with unknown ϵ_T should be of $\sim 10^{-5} \text{ mol dm}^{-3}$.

15.3.1.8 Intersystem Crossing Quantum Yield Determinations

The singlet–triplet intersystem crossing quantum yields (ϕ_{ISC}) for the compounds with unknown values, ϕ_{ISC}^{cp} , but known triplet molar absorption coefficient, ϵ_T^{cp} , can be obtained by comparing the ΔOD_T^{cp} , in the triplet–triplet absorption maximum of the compounds, with the ΔOD_T^{ref} in the triplet wavelength absorption maximum of a reference compound with known intersystem crossing quantum yield, ϕ_{ISC}^{ref} , and triplet molar absorption coefficient, ϵ_T^{ref} , using Eq. (15.14) [17].

$$\phi_{\text{ISC}}^{\text{cp}} = \frac{\varepsilon_{\text{T}}^{\text{ref}}}{\varepsilon_{\text{T}}^{\text{cp}}} \cdot \frac{\Delta\text{OD}_{\text{T}}^{\text{cp}}}{\Delta\text{OD}_{\text{T}}^{\text{ref}}} \cdot \phi_{\text{ISC}}^{\text{ref}} \quad (15.14)$$

Care must be taken in order to have diluted solutions of the compounds and the reference optically matched at the laser excitation wavelength. Typically, we should have standards to obtain the $\phi_{\text{ISC}}^{\text{ref}}$ value for the three available wavelengths of a Nd:YAG laser: 266, 355 and 532 nm. Optical parametric amplifiers can be used to tune other wavelengths, but these are not always available and always reduce the laser intensity reaching the sample. Therefore, the ϕ_{T} values are generally determined using as standards naphthalene in ethanol ($\varepsilon_{\text{T}} = 24,500 \text{ mol}^{-1} \text{ dm}^3 \text{ cm}^{-1}$ at 415 nm, $\phi_{\text{T}} = 0.8$) when the laser excitation is with the fourth harmonic ($\lambda_{\text{ex}} = 266 \text{ nm}$) of a Nd:YAG, benzophenone in benzene ($\varepsilon_{\text{T}} = 7,220 \text{ mol}^{-1} \text{ dm}^3 \text{ cm}^{-1}$ at 530 nm, $\phi_{\text{T}} = 1$) with $\lambda_{\text{ex}} = 355 \text{ nm}$ and tetraphenyl-porphyrin in toluene ($\varepsilon_{\text{T}} = 6,000 \text{ mol}^{-1} \text{ dm}^3 \text{ cm}^{-1}$ at 790 nm, $\phi_{\text{T}} = 0.82$) for $\lambda_{\text{ex}} = 532 \text{ nm}$ [2, 15].

15.3.1.9 Photoacoustic Calorimetry

An alternative method to evaluate the intersystem crossing quantum yield is the photoacoustic calorimetry (PAC) technique, which requires previous knowledge of the triplet energy (see below). In a PAC experiment, the fraction of heat released following excitation with a laser pulse is measured by way of the resulting sound wave [18]. Using knowledge of the energies of the excited states involved (S_1 and T_1), and the quantum yield of fluorescence (ϕ_{F}), it is possible to determine the quantum yields for the non-radiative processes [18]. Moreover, it is also possible to split the relative contributions of the radiationless processes (heat released) into two components occurring in different time ranges: a fast and slow step (ϕ_1 and ϕ_2 respectively). The fast component results from the internal conversions, $S_n \sim S_1$ and $S_1 \sim S_0$, and the intersystem crossing to the triplet manifold, and lasts a few ns. The slower component is associated with radiationless processes originating from the lowest triplet state, thus occurring on a much longer time scale ($> 10 \mu\text{s}$). Longer lived processes are not detected using appropriate PAC transducers. Therefore, the process is considered ‘blocked’ at that energy level, and thus the deactivation of the system (as seen from PAC) stops in the triplet manifold. In this situation, it can be showed that the product of the singlet–triplet intersystem crossing yield (ϕ_{ISC}) and energy (E_{T}) is given by Eq. (15.15), [18, 19] where E_{vmax} is the energy of fluorescence (more correctly, the energy at the maximum fluorescence intensity taken as the Gaussian centre of the fluorescence band), and E_{hv} is the energy of the laser.

$$\phi_{\text{ISC}} \cdot E_{\text{T}} = (1 - \phi_1) \cdot E_{\text{hv}} - \phi_{\text{F}} \cdot E_{\text{vmax}} \quad (15.15)$$

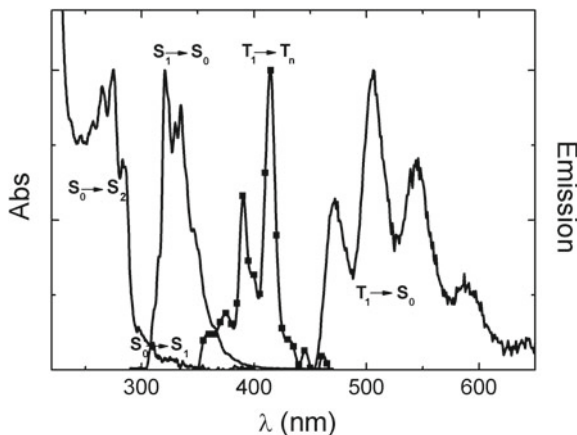


Fig. 15.7 Total electronic spectra including absorption ($S_0 \rightarrow S_{1,2}$), fluorescence ($S_1 \rightarrow S_0$), phosphorescence ($T_1 \rightarrow S_0$) and transient triplet–triplet absorption spectra for naphthalene in methylcyclohexane. The absorption, fluorescence and transient triplet–triplet spectra were acquired at 293 K, whereas the phosphorescence spectrum was recorded at 77 K

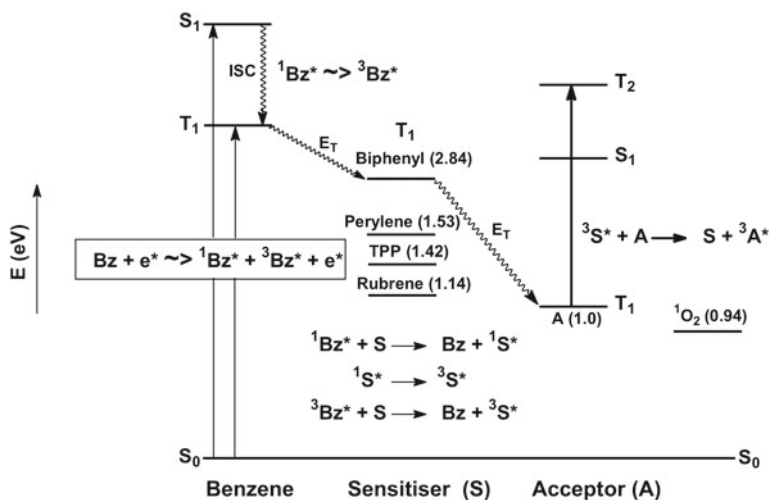
The photoacoustic calorimetry technique together with the triplet–triplet energy transfer method (see below) has been used to characterise the non-emissive triplet excited state of indigo, that is, to evaluate the intersystem crossing quantum yield and triplet energy values for this compound [20].

A value of $\phi_1 = 0.9952$ was obtained for indigo, and based on the triplet energy of indigo, $134.7 \text{ kcal mol}^{-1}$ (1.05 eV), and the values of $\phi_F = 0.0023$ [21], together with the energy of the singlet state $43.78 \text{ kcal mol}^{-1}$ (E_{vmax}), a value of $\phi_{\text{ISC}} = 0.0065$ was obtained [20]. In addition, this value was found in agreement with the value obtained for $\phi_{\Delta} = 0.0012$ [22], which validates the obtained ϕ_{ISC} value.

15.3.2 Triplet Energy Measurements

As mentioned before, the energy of the first triplet state T_1 can be taken from the 0–0 vibronic of the $T_1 \rightarrow S_0$ transition (or from the $S_0 \rightarrow T_1$ transition when induced by the external heavy atom effect [23]), or from the band onset. This is illustrated in Fig. 15.7 for naphthalene, which also includes the transient triplet–triplet absorption of this compound.

In the absence of phosphorescence, the triplet state energy can be obtained by the triplet–triplet energy transfer method as described in the next section [4, 24, 25].



Scheme 15.3 Schematic representation of the pulse radiolysis energy transfer technique applied to the characterisation of the triplet state (triplet energy determination)

15.3.2.1 Triplet–Triplet Energy Transfer

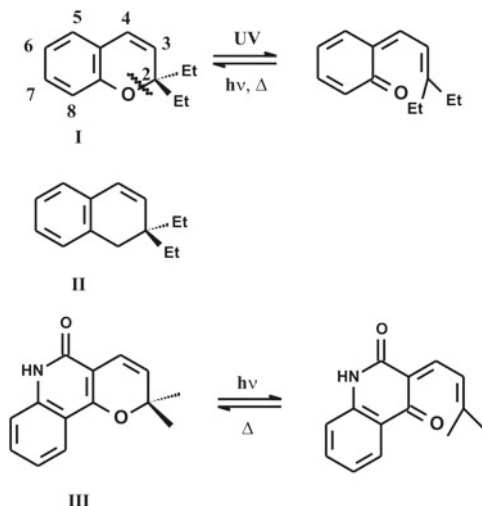
The absorption spectra of triplet states can also be obtained by the pulse radiolysis technique (see Chap. 8), which briefly consists of using 200 ns–2 μ s high-energy electron pulses from a 12 MeV linear accelerator, which is passed through solutions in a 2.5 cm optical path-length quartz cuvette attached to a flow system [26–28]. Optical spectra are normalised for the radiation dose and recorded using a spectrometer consisting of a xenon arc lamp, monochromator, photomultiplier and appropriate filters [27]. In the absence of appropriate sensitisers, pulse radiolysis of benzene solutions containing organic molecules can produce excited states and radical ions (see Sect. 8.2.1.4) [29–32]. However, upon pulse radiolysis of an argon-saturated solution of a donor D (in the sense that it can further transfer energy to an acceptor if present, for example 1×10^{-2} mol dm $^{-3}$ solutions of biphenyl) in benzene, the only significant species seen by transient absorption spectroscopy (within the time resolution used in this type of experiments; *i.e.* a few ns) is the triplet state of the donor (biphenyl). On this basis, triplet states of an acceptor (A), for example, a conjugated organic polymer or oligomer, can be selectively produced by energy transfer from appropriate donors which act as triplet sensitisers (S) following pulse radiolysis of benzene solutions as illustrated in Scheme 15.3 [33, 34].

The experiments are subject to the kinetically demanded concentration ratio $[Bz] \gg [S] \gg [A]$. This technique was applied to characterise the triplet state of conjugated oligomers and polymers where the concentrations of these were 10^{-5} mol dm $^{-3}$ (in terms of repeating units for the polymers), and they were dissolved in benzene solutions of biphenyl and degassed [11, 34–36].

Table 15.2 Triplet energy values (in eV) for several useful donor/acceptor compounds

Compound	Energy (eV)
Benzophenone	2.97
Biphenyl	2.84
9,10-Anthraquinone	2.71
Naphthalene	2.63
Terphenyl	2.52
1-Naphthaldehyde	2.44
Benzil	2.32
9-Fluorenone	2.19
Pyrene	2.10
Acridine	1.97
Anthracene	1.84
Azulene	1.68
Ferrocene	1.65
Perylene	1.54
Tetraphenyl-porphyrin (TPP)	1.43
Tetracene	1.27
Phthalocyanine	1.24
Rubrene	1.14
O ₂ (¹ Δ _g)	0.94
β-Carotene	0.91
Pentacene	0.78

This technique also allows the determination of the triplet energy of the compounds and is known as the triplet–triplet energy transfer method which was developed by Bensasson and Land [4, 24, 25]. Briefly, the procedure is as follows: the compound, with an unknown triplet level, is excited in the presence of a given compound whose triplet energy is known (see Table 15.2). If the unknown triplet is quenched, then its triplet energy level should lie above that of the standard, whereas if it is not quenched its level lies below that of the standard. By this way, it is often possible to fix upper and lower limits to the lowest triplet levels of the compound under study. The method is based on the finding that when the triplet levels of two compounds differ by more than 0.08–0.12 eV, then the triplet energy will be transferred from the compound with the higher triplet level to the compound with the lower triplet level with a rate constant approaching the diffusion-controlled limit [4]. As an example, indigo quenches the triplets of biphenyl (2.84 eV), perylene (1.53 eV), TPP (1.42 eV) and rubrene (1.14 eV). Assuming that these all involve energy transfer and since indigo is known to sensitise single oxygen (0.94 eV), this puts the triplet somewhere above 0.94 but below 1.14 eV, *i.e.*, 1.0 plus or minus 0.1 eV (see Scheme 15.3).



Scheme 15.4 Some of the molecules, described in the text, where the vibronic effect was found and investigated

15.4 The Vibronic Effect

Exceptions to Kasha's rule can not only be found with azulene and other compounds [37], where emission from S_2 is observed (typically because the energetic difference between the S_2 and S_1 states is sufficiently large to reduce the S_2 - S_1 internal conversion to values close to the S_2 - S_0 radiative rate), but also when there is competition between vibrational relaxation and photochemistry, the so-called vibronic effect. This is an important concept that has been recently developed contrasting with the general wisdom in photochemistry, that only very few exceptions to Kasha's rule exist. The foundations of the vibronic effects were found in 1966 when Ralph Becker and Joseph Michl noticed that the fluorescence excitation spectrum of a photochromic compound, 2,2-diethylchromene (see Scheme 15.4), was significantly different from the absorption spectrum [38].

In 1969, a further development of the phenomenon was made [39] in which the relative quantum yields of fluorescence, ϕ_F^{rel} , were obtained for excitation of all the vibronic levels in the first two electronic excited states of 2,2-diethylchromene (I in Scheme 15.4). It was there found that ϕ_F^{rel} showed variation as a function of (a) the electronic state, (b) the vibrational mode and (c) the vibrational level that was being excited. Comparison was made to a molecule of similar structure to 2,2-diethylchromene except the O atom was replaced by $-\text{CH}_2$ (1,2-dihydronaphthalene, II in Scheme 15.4). In this case, excitation over 15 wavelengths, between 296 and 250 nm (first entire transition), did not result in any deviation ($\pm 5\%$) of ϕ_F^{rel} and no photochemistry was observed over irradiation times comparable to that

used for the chromene. Indeed, in that work the ϕ_F^{rel} values for 2,2-diethylchromene changed, within the first absorption band, from ϕ_F^{rel} at 329 nm, to $\phi_F^{\text{rel}} = 0.33$ at 303 nm and in the second electronic absorption band from $\phi_F^{\text{rel}} = 0.51$ at 278 nm, to $\phi_F^{\text{rel}} = 0.10$ at 257 nm [39].

Very surprisingly, these findings had no impact or repercussion during more than 30 years until 1999, when further work with another photochromic compound (Flindersine, III in Scheme 15.4) was published [40]. An improved mechanism was developed to understand the strong dependence of ϕ_F^{rel} on the particular vibronic level excited for molecules that underwent photochromism. It is worth noting that in order to validate this model, and equations, no triplet state can be formed, which was validated on the absence of phosphorescence [41, 42] and triplet transients with chromenes and benzochromenes, except for a small amount ($\sim 0.1\%$) for molecules having a 7,8-benzochromene core. This means that photochemistry should, in these molecules, be considered uniquely in competition with vibrational relaxation at every vibronic level. With this premise, the fraction of molecules that relax from an upper (n) to a lower ($n-1$) vibronic level (within a given mode) is given by [39–41]:

$$k_V / (k_V + k_{\text{PC}}) \quad (15.16)$$

where k_V is the vibrational relaxation constant (in the one of the pioneering works [39] k_V was identified as k_{IC}) and k_{PC} is the photochemistry rate constant. The subsequent model is valid in the absence of vibrational redistribution, as it is implicit in Scheme 15.1 and Eqs. 15.16 through 15.22. Considering n vibronic levels one gets:

$$\phi_F^{\text{rel}}(n) = [k_V / (k_V + k_{\text{PC}})]^n \quad (15.17)$$

Applying logarithms to this equation shows that a plot of $\log \phi_F^{\text{rel}}(n)$ versus n should give a straight line with a slope equal to $\log[k_V / (k_V + k_{\text{PC}})]$ and consequently from this, the ratio of k_V / k_{PC} can be obtained. This, by itself, showed that, for these molecules, the quantum yield was changing with energy, which was in contradiction with the known wisdom, Kasha's–Vavilov's rule.

In order to obtain all the rate constants, and to fully solve the kinetic scheme, one would need to also evaluate the dependence of ϕ_{PC} as a function of n , which was established in the 1999 work where the absolute ϕ_{PC} and ϕ_F values for Flindersine were experimentally determined [40]. This led to improved equations to obtain ϕ_F , particularly because $\phi_F(n)$ was considered as the experimentally absolute quantum yield of fluorescence as a function of the vibronic level (n) and state that is excited and:

$$\phi_F(0) = k_F / [k_F + k_{\text{PC}}(0) + k_{\text{NR}}] \quad (15.18)$$

with $\phi_F(0)$ the quantum yield of fluorescence (from $n = 0$) of S_1 and k_{NR} includes k_{ISC} if any triplet is formed [from $S_1(0)$ to T_n]. Furthermore, an equation for ϕ_{PC}

was given (expansion in series) which allowed the evaluation of $\phi_{PC}(n)$ and its dependence on ϕ_V and the vibronic or state level excited.

$$\phi_{PC}(n) = \phi_{PC}(0)\phi_V^n + \phi_{PC}[1 + \phi_V + \phi_V^2 + \dots + \phi_V^{n-2} + \phi_V^{n-1}] \quad (15.19)$$

with

$$\phi_V = k_V/(k_V + k_{PC}) \quad (15.20)$$

where ϕ_V is the vibrational relaxation quantum yield (in the absence of triplet formation). The ϕ_V can be considered a measure of the efficiency of relaxation from one vibronic level to another, in competition with photochemistry within a given mode. It is worth noting that the concept of a vibrational relaxation quantum yield was new and had never been considered before in photochemistry or photophysics. Note also that such as the fluorescence quantum yield at the zero level (Eq. 15.18) has a different expression relative to $\phi_F^{rel}(n)$ (Eq. 15.17), and the same occurs with the photochemistry quantum yield, $\phi_{PC}(0)$:

$$\phi_{PC}(0) = k_{PC}(0)/[k_{PC}(0) + k_{NR} + k_F] \quad (15.21)$$

where k_{NR} includes k_{ISC} if triplet states are formed and since ϕ_{PC} is given by:

$$\phi_{PC} = k_{PC}/(k_{PC} + k_V) \quad (15.22)$$

this means that for $n = 0$, $\phi_{PC}(0) = k_{PC}(0)/[k_{PC}(0) + k_{NR} + k_F]$, for $n = 1$, $\phi_{PC}(1) = \phi_{PC}(0)\phi_V + \phi_{PC}$ and for $n = 2$, $\phi_{PC}(2) = \phi_{PC}(0)\phi_V^2 + \phi_{PC}(1 + \phi_V)$.

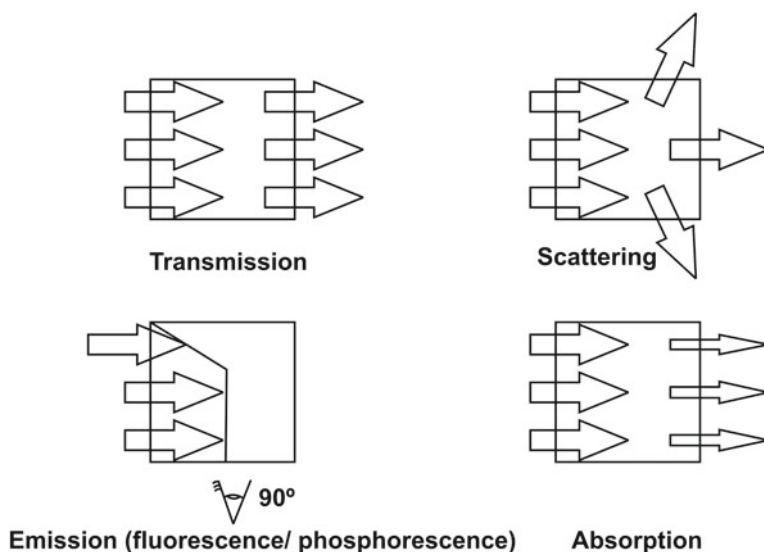


Fig. 15.8 Typical ways light interacts with matter in a cuvette. The eye in the emission represents the detector location

15.5 Absorption and Emission: Avoiding Experimental Pitfalls

The way light interacts with matter and is observed in solution can be summarised in four different manners: absorption, transmission, emission and scattering (Fig. 15.8). The first two are related through the relation of absorbance (A) with transmittance (T) ($A = -\log_{10}T$). Considering as $T = I/I_0$ and $I_{\text{abs}} = I_0 - I$, that is the difference between the incident light (I_0) and the emerging light (I), the intensity of light absorbed is given by $I_{\text{abs}} = I_0 - I = I_0 - I_0T = I_0(1 - 10^{-A})$. This expression can be further developed in terms of series of terms,

$$I_{\text{abs}} = I_0 \left[1 - (1 - 2.303 \times \epsilon cl + (2.303\epsilon cl)^2/2! + \dots) \right] \quad (15.23)$$

which, for sufficiently low values of A , reduces to $I_{\text{abs}} = I_0(1 - 10^{-A}) \cong 2.303I_0\epsilon cl$.

The intensity of emission, I_{em} , is proportional to the number of molecules in solution and therefore $I_{\text{em}} = I_{\text{abs}} \times \phi_{\text{F}}$ and consequently $I_{\text{em}} = I_0[2.303\epsilon cl]\phi_{\text{F}}$ or $I_{\text{em}} = I_0 \times A \times \phi_{\text{F}}$. However, this stands only for diluted solutions, typically with $A \leq 0.01$. When this is not the case, the light that excites the molecules does not reach the centre of the cuvette, where the photomultiplier ‘eye’ is set to observe the emitted light, and in extreme cases no emission is observed even for solutions of a highly fluorescent compound.

When recording the emission spectra of a fluorophore other considerations/observations should be taken into account. The excitation, also known as the Rayleigh, and the Raman peaks is commonly observed in the emission (and excitation) spectra (see Fig. 15.9). For several reasons, people tend to avoid

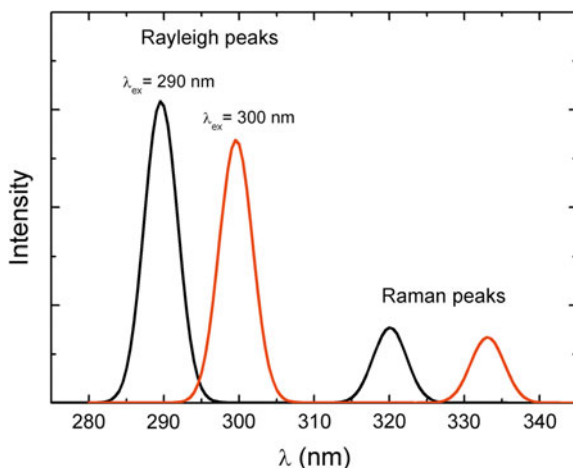


Fig. 15.9 Illustrative representation of the Rayleigh and Raman peaks observed in the fluorescence emission spectrum

collecting the excitation (Rayleigh) peak when acquiring the emission spectra. However, this can be sometimes critical. The so-called scatter peak should be centred at the wavelength of excitation and this gives a good indication of the monochromator position; any departure from this can indicate that the spectrofluorimeter is somehow misaligned.

The intensity of the Rayleigh scattering (I_{RS}) is proportional to the size of the solute particles (r) and to the excitation wavelength (λ_{ex}) through the relationship $I_{RS} \propto r^6/\lambda_{ex}^4$. Moreover, the Raman peak is also present in the emission spectra when the solutions are very dilute or display very low fluorescence quantum yields. Indeed, this transition results from the fact that part of the excitation energy is subtracted by the active vibrational modes of the solvent molecules. For example, with water or other hydroxylic solvents the dominant vibrational mode is the O–H stretching mode at $\sim 3,300\text{ cm}^{-1}$. When collecting an emission spectrum, this Raman peak (λ_{RA}) will be observed at a wavelength that should be energetically lower by $3,300\text{ cm}^{-1}$ than the excitation (Rayleigh peak), $\lambda_{ex}(\lambda_{RS})$; which is easily mirrored from the relationship: $1/\lambda_{RA} = 1/\lambda_{ex} - 0.00033$. Taking into consideration that the usual units when tracing an emission spectrum in a spectrofluorimeter are nm, if one excites with $\lambda_{ex} = 290\text{ nm}$ one gets $\lambda_{RA} = 320.69\text{ nm}$ (a difference of 30.69 nm), whereas when the same solution is excited with $\lambda_{ex} = 300\text{ nm}$ one gets $\lambda_{RA} = 333\text{ nm}$ (a difference of 33 nm). Indeed, this difference should be identical and would constitute a proof that what we are observing is a Raman peak. This, indeed, is true when we considered energetic units: $\lambda_{ex} = 290\text{ nm}$ ($33,482.76\text{ cm}^{-1}$) and $\lambda_{RA} = 320.69\text{ nm}$ ($31,182.76\text{ cm}^{-1}$); $\lambda_{ex} = 300\text{ nm}$ ($33,333.33\text{ cm}^{-1}$) and $\lambda_{RA} = 333\text{ nm}$ ($30,030\text{ cm}^{-1}$); in both situations an identical energetic difference of $3,300\text{ cm}^{-1}$ is obtained.

15.6 Fluorescence Lifetimes. Decay Times. Fluorescence Lifetime Standards in the ns and ps Time Scales

Fluorescence decays are generally measured using the time-correlated single photon counting (TCSPC) technique [43, 44], although the ‘phase-shift’ [45] method has been also used (see Chap. 14). A brief description of TCSPC apparatus with nanosecond and picosecond time resolution is given below in order to illustrate the essential components and requirements for each time resolution.

15.6.1 Fluorescence Decays with Nanosecond Time Resolution

The light source is either a pulsed flash lamp (e.g., the IBH 5000 coaxial flash-lamp, typically filled with N_2 , D_2 , H_2 or mixtures of these gases), or pulsed

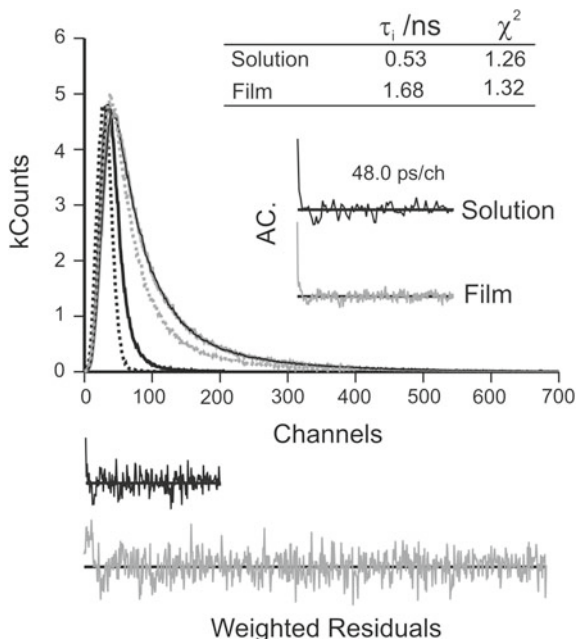
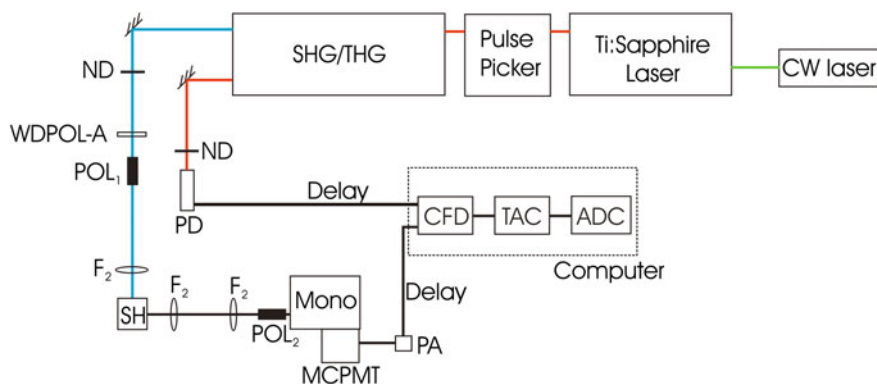


Fig. 15.10 Fluorescence decays for a polythiophene derivative in toluene solution at 293 K and in thin film. The dashed lines in the decays are the pulse instrumental response functions in solution (obtained with a Ludox solution) and in the solid state (obtained with a blank sapphire disc inside the Horiba-Jobin-Yvon integrating sphere). Autocorrelation functions (AC.), weighted residuals and Chi square values (χ^2) are also present as insets. Reproduced with permission from Ref. [49], Copyright 2007, the American Chemical Society

NanoLEDs. The excitation wavelength is selected with interference filters or a monochromator (e.g., a Jobin-Yvon H20, with a UV-blazed grating), and focused on the sample. The sample emission is passed through a second monochromator (Vis-blazed grating) and detected with a high gain photomultiplier, such as the Philips XP2020Q. The electric signals from the light source and from the photomultiplier are supplied to a TCSPC board (Becker & Hickl or PicoQuant) in a computer as start and stop signals. The TCSPC board integrates two discriminators, a time-to-amplitude converter, and a multichannel analyser where the histogram of counts as a function of time is recorded. Since the measurement time can be long, alternate collection of pulse (recorded with a scattering solution) and sample is usually made [46–48]. If the controlling software allows alternate measurements (1,000 counts per cycle) of the pulse and sample profiles to be performed, a typical experiment is made until 5×10^4 to 20×10^4 counts at the maximum intensity are reached.

With this equipment solid-state fluorescence decays can also be measured with samples in a Horiba-Jobin-Yvon integrating sphere [49]. For these experiments the pulse profile, at the excitation wavelength, is obtained by collecting the pulse



Scheme. 15.5 Time-correlated single photon counting experimental setup: SHG/THG, second and third harmonic generator; ND, neutral density filter; WDPOL-A, depolariser; POL₁, vertically aligned polariser; POL₂, polariser at magic angle; F₂, lenses; PD, photodiode; Mono, monochromator; MCPMT, microchannel plate photomultiplier; PA, pre-amplifier; CFD, constant fraction discriminators; TAC, time-to-pulse height converter; ADC, analog-to-digital signal converter

with a sapphire blank disc inside the integrating sphere. In this way, it is possible to produce the pulse profile with the instrumental response function (IRF) as generated within the integrating sphere, that, as seen from Fig. 15.10 is significantly different from the IRF obtained with a scattering Ludox solution. In the case of our laboratories, the fluorescence decays are usually analysed using the modulating functions method to evaluate the decay times [6], which are then optimised [50].

15.6.2 Fluorescence Decays with Picosecond Time Resolution

A TCSPC apparatus with ps-time-resolution requires three changes with respect to the previous equipment: the light source, the emission photomultiplier and several details in the optical path. An example of a simple home-built picosecond TCSPC apparatus is shown in Scheme 15.5 [35, 51]. The excitation source consists of a picosecond mode-locked Ti:Sapphire laser (Tsunami, Spectra Physics, tuning range 700–1,000 nm, 82 MHz), pumped by a diode-pump YAG Laser (Millennia Pro-10s, Spectra Physics). A harmonic generator is used to produce the second and third harmonic from the Ti:Sapphire output. The pulse frequency of the excitation beam is reduced with a pulse-picker unit whenever decays longer than 2 ns are present. Samples are measured using the second (horizontally polarised) or the third (vertically polarised) harmonic output beam from the GWU that is first passed through a depolariser (WDPOL-A) and

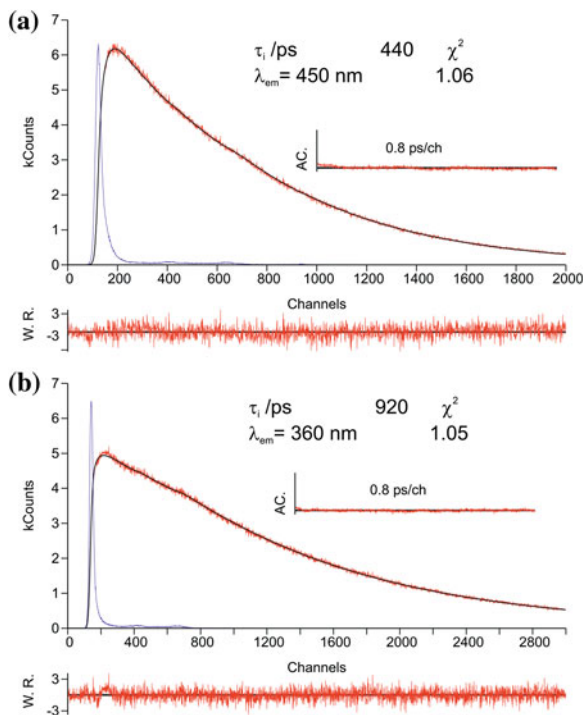


Fig. 15.11 Fluorescence decays showing monoexponential fits of the reference compounds (obtained for the calibration of the ps time-resolution apparatus) **a** 2,2':5',2'':5'',2'''-quaterthiophene in methylcyclohexane ($\lambda_{\text{ex}} = 425 \text{ nm}$) and **b** p-terphenyl in cyclohexane ($\lambda_{\text{ex}} = 296 \text{ nm}$). For better judgment of the quality of the fits, autocorrelation functions (AC), weighted residuals (W.R.) and χ^2 values are also presented as insets. The shorter pulse is the instrumental response

after by a Glan–Thompson polariser (POL_1) with vertical polarisation. Emission at 90° geometry is collected at magic angle polarisation (POL_2) and detected through a double monochromator (Mono) by a microchannel plate photomultiplier (MCPMT, Hamamatsu R3809U-50). Special care with focusing, and keeping the diameter of the emission beam as small as possible is recommended. Signal acquisition and data processing are performed employing a Becker and Hickl SPC-630 TCSPC module. The full width at half maximum (FWHM) of the IRF ranges from 17 to 22 ps and is highly reproducible within identical system setups. Again, deconvolution of the fluorescence decay curves is performed using the method of modulating functions [50].

The verification of good calibration of the ps-TCSPC system is performed, when possible, with standard compounds that are easily obtained/purified and exhibit a single exponential decay independent of excitation and emission wavelength in a solvent of good spectral grade. In general, depending on the excitation wavelength, p-terphenyl (p-terp) in cyclohexane [52] and 2,2':5',2'':5'',2'''-quaterthiophene ($\alpha 4$) in methylcyclohexane are used as standards for calibration of our

Table 15.3 Fluorescence lifetimes for reference compounds obtained with ns and ps time-resolution apparatus. Unless noted the solutions were previously degassed for 20 min and sealed with nitrogen before measuring

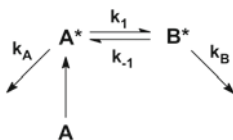
Compound	Solvent	λ_{ex} (nm)	λ_{em} (nm)	Lifetime (this work) $\bar{\tau} \pm s(\text{ns})^{\text{b}}$	Lifetime (literature)(ns)
p-terp	Cyclohexane	282	330	0.98 ± 0.01	0.98 (Ref. [52])
		296	360	0.92 (air saturated) ^a	
PPO	Cyclohexane	311	360	1.34 ± 0.01	1.36 (Ref. [52, 53])
DPA	Cyclohexane	373	430	7.44 ± 0.01	7.50 (Ref. [52])
		392	430	4.59 ± 0.02 (air saturated) ^a	
$\alpha 4$	Methylcyclohexane	373	450	0.46 ± 0.01	0.44 (Ref. [7, 16])
		425	450	0.44 (air saturated) ^a	
C153	Methanol	460	550	4.27 ± 0.02	4.30 (Ref. [52])

p-terp (p-terphenyl), PPO (2,5-diphenyloxazole), DPA (9,10-diphenylanthracene), $\alpha 4$ (2,2':5',2'':5'',2''':5'''-quaterthiophene), C153 (coumarin 153)

^a psTCSPC time resolution

^b $\bar{\tau}$ is the averaged lifetime (resulting from five independent measurements); the s values are the

sample standard deviation that was obtained by applying, $s = \left[(n-1)^{-1} \sum_{n=1}^3 (x - \bar{x})^2 \right]^{1/2}$



Scheme 15.6 Kinetic scheme involving two excited state species (A* and B*) formed at the expense of a single ground-state species (A)

system (see Fig. 15.11 and Table 15.3). However, 2,5-diphenyloxazole (PPO), 9,10-diphenylanthracene (DPA) and coumarin 153 (C153) are also commonly used standards for calibration of pico- and nanosecond TCSPC, see Table 15.3 [52, 53].

15.7 Excited-State Kinetics

15.7.1 Analysis of Two-State Systems

As mentioned before, an electronically excited molecule A* can undergo a number of (intramolecular or intermolecular) reactions, from which another excited molecule B*, emitting (or not) at a different wavelength, results. This may be called a

two-state system, for which, in the most general case, the fluorescence decays of both A^* and B^* follow a sum of two exponential terms.

We will briefly describe the kinetics of the two-state system, and then apply the result to some common examples of inter and/or intramolecular reactions: excimer formation, charge transfer (leading to an exciplex), electron transfer (leading to radical ions), proton transfer or isomerisation. Scheme 15.6 is a condensed representation of the two-state system.

15.7.1.1 Dynamic Approach

The time evolution of the concentrations of A^* and B^* [$\mathbf{A}(t)$ and $\mathbf{B}(t)$] is given by Eq. (15.24), where k_1 , k_{-1} , k_A and k_B represent the rate constants of the four processes involved (Scheme 15.6). $k_X = k_1 + k_A$ is the decay constant of A and $k_Y = k_{-1} + k_B$ is that of B.

$$\frac{d}{dt} \begin{bmatrix} \mathbf{A} \\ \mathbf{B} \end{bmatrix} (t) = \begin{bmatrix} -k_X & k_{-1} \\ k_1 & -k_Y \end{bmatrix} \begin{bmatrix} \mathbf{A} \\ \mathbf{B} \end{bmatrix} (t) \quad (15.24)$$

The solution of Eq. (15.24) predicts double exponential decays for the two species, A and B, (Eq. 15.25),

$$\begin{bmatrix} \mathbf{A} \\ \mathbf{B} \end{bmatrix} (t) = \begin{bmatrix} a_{1,1} & a_{2,2} \\ a_{2,1} & a_{2,2} \end{bmatrix} \begin{bmatrix} e^{-\lambda_1 t} \\ e^{-\lambda_2 t} \end{bmatrix} \quad (15.25)$$

where the reciprocal decay times $\lambda_j = 1/\tau_j$ are the *eigenvalues* of the characteristic polynomial (Eq. 15.26),

$$\begin{vmatrix} \lambda - k_X & k_{-1} \\ k_1 & \lambda - k_Y \end{vmatrix} = 0 \quad (15.26)$$

and the pre-exponential coefficients $a_{i,j}$ are linear combinations of the *eigenvectors* of the rate constants matrix \mathbf{k} that satisfies the initial conditions (see below).

Substitution of Eqs. (15.25) and (15.26) provides an expression of the rate constants matrix \mathbf{k} as a function of the pre-exponential coefficients ($a_{i,j}$) matrix \mathbf{a} and the reciprocal decay time ($\lambda_j = 1/\tau_j$) matrix λ (Eq. 15.27, or abbreviated as $\mathbf{k} = \mathbf{a}\lambda\mathbf{a}^{-1}$).

$$\mathbf{k} = \begin{bmatrix} -k_X & k_{-1} \\ k_1 & -k_Y \end{bmatrix} = \begin{bmatrix} a_{1,1} & a_{1,2} \\ a_{2,1} & a_{2,2} \end{bmatrix} \times \begin{bmatrix} -\lambda_1 & 0 \\ 0 & -\lambda_2 \end{bmatrix} \times \begin{bmatrix} a_{1,1} & a_{1,2} \\ a_{2,1} & a_{2,2} \end{bmatrix}^{-1} \quad (15.27)$$

However, because the pre-exponential coefficients $a_{i,j}$ (concentrations) must be evaluated from the experimental pre-exponential coefficients $A_{i,j}$ (fluorescence intensities at a given wavelength, depending on the experimental setup and number of accumulated counts), it is easier, in the case of the two-state system, to evaluate the rate constants using the procedure first introduced by John Birks [54] to solve

the kinetics of excimer formation (the relation between $a_{i,j}$ and $A_{i,j}$ will be discussed latter for three-state or four-state systems [55]).

In the Birks' method the two reciprocal decay times are expressed as functions of the rate constants by Eq. (15.28) (which also results from Eq. (15.26)).

$$2\lambda_{2,1} = (k_X + k_Y) \pm \sqrt{(k_X + k_Y)^2 + 4k_1k_{-1}} \quad (15.28)$$

The pre-exponential coefficients can also be expressed as functions of the rate constants after definition of the initial conditions. If only A has been excited, then the normalised concentration of A^* at $t = 0$ is unity, *i.e.*, $\mathbf{A}(0) = a_{1,1} + a_{1,2} = 1$ and that of \mathbf{B}^* is equal to zero, *i.e.*, $\mathbf{B}(0) = a_{2,1} + a_{2,2} = 0$. Note that the last equation implies $a_{2,1} = -a_{2,2}$.

$$a_{1,2} = \frac{k_X - \lambda_2}{\lambda_1 - \lambda_2} \quad (15.29)$$

$$a_{1,1} = \frac{\lambda_1 - k_X}{\lambda_1 - \lambda_2} \quad (15.30)$$

$$a_{2,1} = \frac{k_X - \lambda_1}{k_d} \times \frac{k_X - \lambda_2}{\lambda_1 - \lambda_2} \quad (15.31)$$

$$a_{2,2} = \frac{k_X - \lambda_2}{k_d} \times \frac{\lambda_1 - k_X}{\lambda_1 - \lambda_2} \quad (15.32)$$

The problem of relating the pre-exponential coefficients $a_{i,j}$ to the experimental pre-exponential coefficients $A_{i,j}$ is solved here by using the ratios of the coefficients (because $A_{i,j} = S_i a_{i,j}$, being S_i a constant for a given measurement, $a_{i,1}/a_{i,2} = A_{i,1}/A_{i,2}$). However, this solution leaves us with only three experimental values, the two decay times and the $A_{1,1}/A_{1,2}$ ratio (the $A_{2,1}/A_{2,2}$ ratio equals -1 , *i.e.*, Eqs. 15.31 and 15.32 are not independent), for the four unknowns (rate constants). There are several methods to obtain the fourth piece of information, the most common being the measurement of the lifetime of A^* in the absence of reaction ($1/k_A$), when possible. From the $A_{1,1}/A_{1,2}$ ratio one obtains,

$$R = \frac{A_{1,2}}{A_{1,1}} = \frac{\lambda_1 - k_X}{k_X - \lambda_2} \quad (15.33)$$

and from rearrangement of Eq. (15.33) we obtain the value of k_X ,

$$k_X = \frac{\lambda_1 + R\lambda_2}{R + 1} \quad (15.34)$$

¹ As a general rule, the credibility of the results obtained from the analysis of fluorescence decays should be (with few exceptions) assessed, by checking the interconsistency of results obtained under different experimental conditions (temperature, solvent viscosity and/or polarity

which, with the value of τ_A and from $k_X = k_1 + 1/\tau_A$, provides the value for k_1 .

$$k_1 = k_X - k_A \quad (15.35)$$

Because $k_X + k_Y = \lambda_1 + \lambda_2$ (from Eq. 15.28) we obtain the following relationships:

$$k_Y = \lambda_1 + \lambda_2 - k_X \quad (15.36)$$

and

$$k_1 k_{-1} = k_X k_Y - \lambda_1 \lambda_2 \quad (15.37)$$

Simple manipulation of Eqs. (15.36) and (15.37) leads to:

$$k_{-1} = \frac{k_X k_Y - \lambda_1 \lambda_2}{k_1} \quad (15.38)$$

and finally, from $\tau_B = 1/(k_Y - k_{-1})$, we obtain τ_B .

Despite its mathematical simplicity, the foregoing procedure may present some experimental difficulties, which normally result from: (1) small values of some pre-exponential coefficients in the decays of A^* and/or B^* , (2) too close decay times (differing by less than a factor of two) that mix, or (3) insufficient time resolution. In most cases, these difficulties can be overcome by changing the experimental conditions (temperature, solvent viscosity and/or polarity, and concentration among others, e.g. pressure)¹ and/or by coupling the results from time-resolved fluorescence with those obtained from steady-state experiments (Stern–Volmer [1] and/or Stevens–Ban [56] plots).

15.7.1.2 Steady-State Approach

Under steady-state conditions (continuous irradiation), the concentrations of A and B do not change with time,

(Footnote 1 continued)

and concentration, among others, e.g. pressure). Changing temperature provides Arrhenius plots of the rate constants, which should be linear. Otherwise, something is wrong with the experiments, or something interesting/new is happening. Changing solvent viscosity (η) provides log–log plots of diffusion-dependent rate constants *versus* η , which should also be linear (slope = -1) for diffusion-controlled processes (deviations are also interesting) [56–59]. Solvent polarity strongly affects charge and electron transfer processes in a well-known way. For inter-molecular processes, changing the concentration [Q] provides linear plots of the pseudo-unimolecular rate constant $k_1 = k_{\text{bimol}}[Q]$ and an accurate value for the bimolecular rate constant, k_{bimol} .

Finally, coupling results from time-resolved fluorescence with those obtained from steady-state experiments are essential in some cases (complex kinetics or low time resolution), and advisable in most other cases. For example, the rate constants obtained from time-resolved experiments can be used to evaluate Stern–Volmer or Stevens–Ban plots (see below) and compare them to those obtained from steady-state experiments. Agreement tells us that everything is alright, while disagreement means that something else is happening, as for example, undetectable short components in the decays (e.g., *static quenching* and *transient effects*, see below).

$$\frac{d}{dt} \begin{bmatrix} \mathbf{A} \\ \mathbf{B} \end{bmatrix} (t) = 0 \quad (15.39)$$

and, if only A is excited, Eq. (15.24) reads:

$$\begin{bmatrix} I_{ss} \\ 0 \end{bmatrix} + \begin{bmatrix} -k_X & k_{-1} \\ k_1 & -k_Y \end{bmatrix} \begin{bmatrix} \mathbf{A}_{ss} \\ \mathbf{B}_{ss} \end{bmatrix} = 0 \quad (15.40)$$

where I_{ss} is the mole of *quanta* absorbed by A, per litre and per second and \mathbf{A}_{ss} and \mathbf{B}_{ss} are the steady-state concentrations of A and B, respectively. Rearranging Eq. (15.40) [57], one obtains,

$$\begin{bmatrix} \mathbf{A}_{ss} \\ \mathbf{B}_{ss} \end{bmatrix} = \frac{I_{ss}}{\det(\mathbf{k})} \begin{bmatrix} k_Y \\ k_1 \end{bmatrix} = \frac{I_{ss}}{k_X k_Y - k_1 k_{-1}} \begin{bmatrix} k_Y \\ k_1 \end{bmatrix} \quad (15.41)$$

and, because the (wavelength) integrated fluorescence intensities of A and B are proportional to their respective steady-state concentrations and radiative rate constants ($\phi_A = k_{FA} \mathbf{A}_{ss}$ and $\phi_B = k_{FB} \mathbf{B}_{ss}$), the following relationship between the fluorescence intensities and rate constants holds:

$$\begin{bmatrix} \phi_A \\ \phi_B \end{bmatrix} = \frac{I_{ss}}{k_X k_Y - k_1 k_{-1}} \begin{bmatrix} k_{FA} & k_Y \\ k_{FB} & k_1 \end{bmatrix} \quad (15.42)$$

15.7.1.3 Stevens–Ban plots: Determination Of Thermodynamic Parameters Associated with an Excimer Formation Reaction

Equation (15.42) is the basis of Stern–Volmer and Stevens–Ban plots. The Stevens–Ban plot [56] is a representation of $\ln(\phi_B/\phi_A)$, given by Eq. (15.43), *versus* the reciprocal temperature, T^{-1} :

$$\ln(\phi_B/\phi_A) = \ln \frac{k_{FB}}{k_{FA}} + \ln \frac{k_1}{k_{-1} + k_B} \quad (15.43)$$

For exothermic reactions, these plots have a characteristic parabolic like shape (see Fig. 15.12) where two limits are reached: the high (HTL) and the low temperature limits (LTL). In the LTL, $k_{-1} \ll k_B$, while the reverse condition ($k_{-1} \gg k_B$) defines the HTL. In these limits, Eq. (15.43) reads:

$$\ln(\phi_B/\phi_A)_{LTL} = \ln \frac{k_{FB}}{k_{FA}} + \ln \frac{k_1}{k_B} \quad (15.44)$$

$$\ln(\phi_B/\phi_A)_{HTL} = \ln \frac{k_{FB}}{k_{FA}} + \ln \frac{k_1}{k_{-1}} \quad (15.45)$$

Considering that the ratio of the radiative rate constants is approximately independent of temperature (the dependence of the radiative rates on the solvent

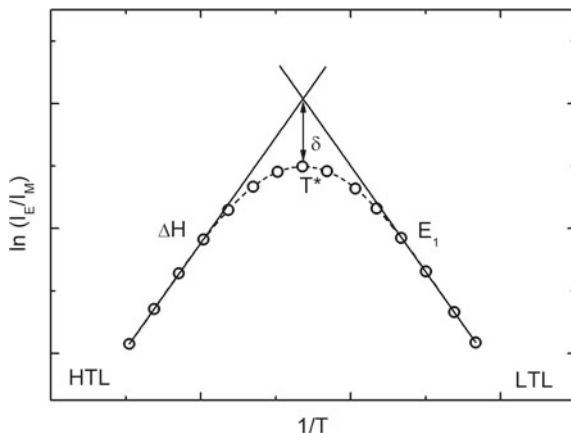


Fig. 15.12 Generic Stevens–Ban plot showing the high (HTL) and low temperature limits (LTL), the transition temperature between these two regimes (T^*), the enthalpy (ΔH) and the activation energy of excimer formation (E_1), together with the δ parameter (see text for further details)

refractive index, which depends on temperature, cancels), and the dependence of k_B on temperature is often weak, the LTL slope of the Stevens–Ban plot (Eq. 15.44) provides an approximate value for the activation energy of the forward reaction (E_1), and the HTL slope (Eq. 15.45) is equal to the reaction enthalpy ($\Delta H^* = E_1 - E_{-1}$).

By comparing Eqs. (15.44) and (15.45), it is seen that the LTL and HTL straight lines cross at a temperature at which $k_{-1} = k_B$ (see Fig. 15.12). At this temperature, the difference δ between the crossing point and the full function (Eq. 15.43) is equal to $\ln 2$.

When the fluorescence intensity of A in the absence of reaction ϕ_A^0 ($\phi_A^0 = k_{\text{FA}}\mathbf{A}_{\text{SS}}^0$, with $\mathbf{A}_{\text{SS}}^0 = I_{\text{SS}}/k_A$) can be measured, the ϕ_A^0/ϕ_A ratio (Eq. 15.46) provides an alternative method to analyse the steady-state data.

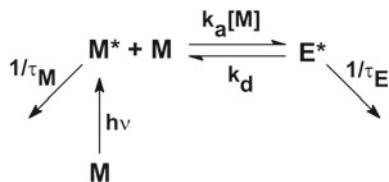
$$\phi_A^0/\phi_A = 1 + \frac{k_1}{k_A} \frac{k_B}{k_{-1} + k_B} \quad (15.46)$$

Classical Stern–Volmer plots are normally used when the back reaction is negligible ($k_{-1} \ll k_B$) and the forward reaction in Scheme 15.6 is bimolecular, and consequently k_1 is a pseudo-first-order rate constant of the form $k_1 = k_q[\text{Q}]$. Under these conditions, the representation of the ϕ_A^0/ϕ_A ratio as a function of $[\text{Q}]$ is linear with intercept = 1, and slope $k_{\text{SV}} = k_1/k_A (= k_q\tau_A)$.

$$\phi_A^0/\phi_A = 1 + k_q\tau_A[\text{Q}] \quad (15.47)$$

However, Eq. (15.46) can be useful in many other ways. For example, the representation of $(\phi_A^0/\phi_A - 1)k_A$ as a function of the reciprocal temperature, T^{-1}

Scheme 15.7 Kinetic scheme for intermolecular excimer formation



provides a modified Stevens–Ban plot, which has, at least, three advantages over the classic Stevens–Ban plot. First, it does not require B to be fluorescent. Second, it avoids the assumption that k_{FB}/k_{FA} is independent of temperature. Third, from the LTL ($k_{-1} \ll k_B$), the value of k_1 is obtained, besides that of E_1 . Finally, when both ϕ_B/ϕ_A and ϕ_A^0/ϕ_A are available the $k_{FB}/k_{FA} = \phi_B/\phi_A - \phi_A^0/\phi_A$ ratio can be obtained (Eqs. 15.43 and 15.46).

As mentioned, the formalism derived here is valid for any excited state system involving two species. We will next describe the required adaptations for the most common reactions.

15.7.1.4 Excimer Formation

Aromatic hydrocarbons such as pyrene, naphthalene, perylene or other related compounds are known to undergo excimer formation reactions in the excited state. For intermolecular excimer formation, the kinetics fall in the category of two-state systems (Scheme 15.7), as well as for the intramolecular case when the interconnecting chain is sufficiently long. With short connecting chains, two excimer conformations may occur, leading to three excited state species (three-state system, see below).

It is worth noting that Scheme 15.6 is equivalent to Scheme 15.7, with $k_1 = k_a[M]$, where k_a is the bimolecular association rate constant (diffusion controlled in most excimer formation reactions) and $[M]$ is the concentration of monomer in the ground state (k_{-1} is the dissociation rate constant, which is usually denoted k_d).

From the above-mentioned aromatic hydrocarbons, pyrene is for sure the most widespread excimer forming fluorescent probe. The fluorescence spectra of pyrene are known to display the characteristic vibronically resolved pyrene band with a maximum at ≈ 375 nm, together with a structureless long-wavelength band (*ca.* 480 nm). Typically, only at concentrations of pyrene above *ca.* 10^{-3} mol dm $^{-3}$, intermolecular excimer formation is clearly observed. For intramolecular excimer formation (concentration independent kinetics) the long-wavelength emission band can be observed for concentrations as low as 10^{-7} mol dm $^{-3}$.

Due to the fact that the two emission bands of pyrene (monomer and excimer) are well separated, the monomer and excimer decays can be measured without mutual interference, and analysed with the two-state model (Eqs. 15.33–15.38). For the intermolecular case, the monomer lifetime is measured with pyrene at very low concentration ($< 10^{-7}$ mol dm $^{-3}$), but for the intramolecular case a model

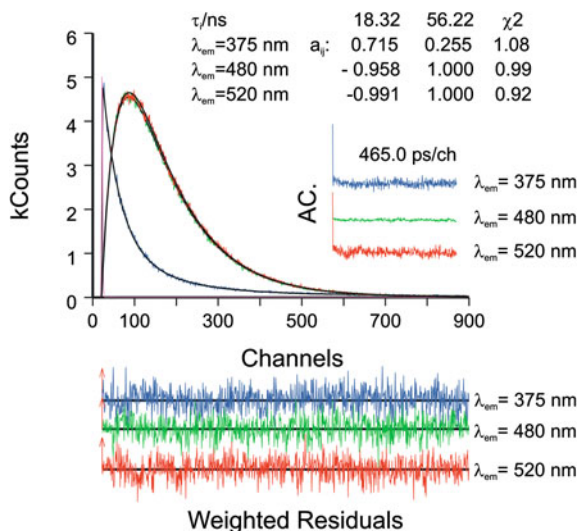
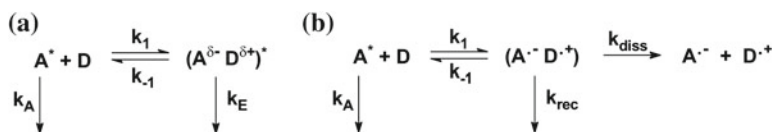


Fig. 15.13 Fluorescence decays of 1Py(10)1Py in *n*-decane at 293 K obtained with $\lambda_{\text{ex}} = 339 \text{ nm}$ and collected at 375 nm (monomer) and 480, 520 nm (excimer). At 375 nm an additional exponential of 259 ns (with a pre-exponential factor of 0.028) is needed to fit the decay. This most likely results from un-reacted pyrene; a similar situation has been reported elsewhere [89, 96] for 1Py(3)1Py. For a better judgment of the quality of the fits, autocorrelation functions (AC), weighted residuals (W.R.) and χ^2 values are also present as insets. The short pulse line in the first channels is the pulse instrumental response

compound (an alkylpyrene) is required [58, 59]. For short interconnecting chains this procedure may also be problematic [60]. Excimer formation with pyrene has also been measured as function of temperature, using both time-resolved and steady-state fluorescence (Stevens–Ban plots), in order to evaluate the energy parameters of the reaction.

In Fig. 15.13, the fluorescence decays of 1,1'-dipyrenyldecane [1Py(10)1Py] in *n*-decane, are presented. In this compound, the two pyrene units are connected by a saturated carbon chain of 10 carbons, in this case only one excimer (more stable and non-parallel conformation) and one monomer exist; this leads to a bi-exponential decay in which the sum of pre-exponential factors at the emission wavelengths of the excimer cancel out.



Scheme. 15.8 **a** exciplex formation and **b** full electron transfer. The excited molecule can be either the electron acceptor A or donor D

15.7.1.5 Charge Transfer and Electron Transfer Exciplexes

There is some parallelism between charge/electron transfer and excimer formation. They both are two-state systems (in the simplest case), and both can occur either intra- or intermolecularly [61–69]. In this case, Scheme 15.6 is slightly modified as for excimer formation (Scheme 15.8). The major difference between charge transfer (Scheme 15.8a) and electron transfer (Scheme 15.8b) reactions lies on the reaction product: an exciplex (more or less fluorescent), resulting from partial charge transfer, and a non-fluorescent, solvent-separated radical-ion pair from (full) electron transfer, respectively.

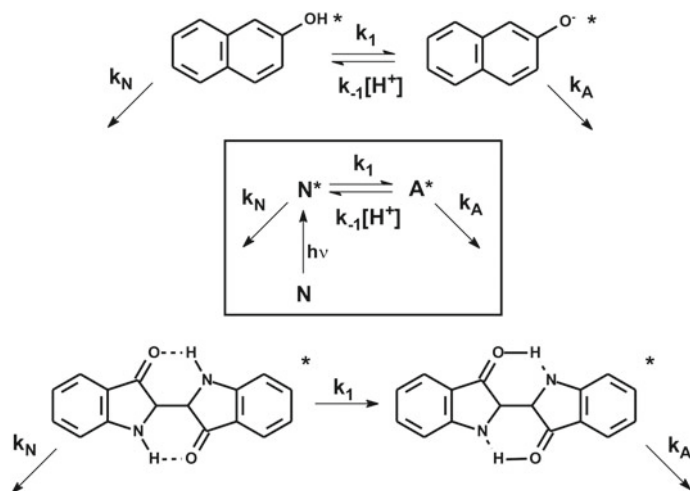
For a given acceptor–donor system, charge transfer can switch to electron transfer by increasing solvent polarity. Potentially, the kinetic analysis of electron transfer can be more complex than charge transfer for a number of reasons. First, the reaction product is non-fluorescent (less information is available from fluorescence techniques). Second, electron transfer can occur at distances larger than the collisional distance, leading to distance-dependent rate ‘constants’, *i.e.*, to non-exponential decays. Third, the geminate radical-ion pair can count as a third species (leading to a three-state system), except when either the dissociation rate constant k_{diss} (leading to the solvent-separated radical-ion pair) or the recombination rate constant k_{rec} (to give the ground states of acceptor and donor) is much larger than recombination to the excited state of either the acceptor or donor (which is frequently true). In this case $k_{-1} = 0$ and thus $a_{1,1} = 0$ (Eq. 15.27), leading to a single exponential decay of the fluorophore. Thus, only the electron transfer rate constant is accessible from fluorescence studies, being the sequent processes accessible only from time-resolved absorption (flash photolysis and/or pump probe). Note that for intramolecular electron transfer, the full dissociation of the geminate radical-ion pair is hindered.

For charge transfer leading to a fluorescent exciplex, all rate constants can be evaluated from the fluorescence decays, but particular attention should be paid to the possibility of occurrence of (1) transient effects, (2) the *harpoon mechanism* [70] (the electron goes first and then the exciplex is formed) and (3) ground-state charge-transfer complexes. All these phenomena lead to deviations from double-exponential decays and/or differences between Stern–Volmer plots obtained from time-resolved (τ_0/τ vs [Q]) and steady-state (I_0/I vs [Q]) measurements.

In conclusion, for the analysis of fluorescence data in systems where charge or electron transfer reactions occur, the availability of both time-resolved and steady-state fluorescence data, as a function of solvent polarity and temperature, has particular importance. Moreover, experimental (or theoretical) oxidation and reduction potentials of A and D are also important to rationalise the results.

15.7.1.6 Proton Transfer

It is well-known that aromatic alcohols become stronger acids in the excited state (less negative charge on the hydroxyl oxygen), while aromatic acids or ketones

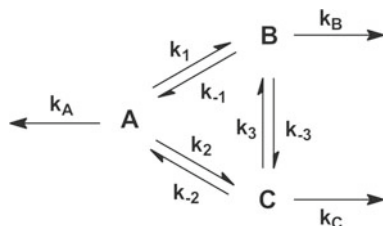


Scheme 15.9 Two examples of proton transfer in the excited state. The *top* (with β -naphthol, [73]) is illustrative of an intermolecular proton transfer (to the solvent) process whereas the *bottom* (with indigo, [22]) is illustrative of an intramolecular proton transfer. In the two cases the kinetic scheme (in the middle) applies with a single ground-state species; however in the case of indigo, the back-proton transfer reaction in the excited state is unlikely

become stronger bases (more negative charge on the carbonyl oxygens) [51, 71–74]. Therefore, electronic excitation triggers a proton transfer reaction (usually to or from water). When an aromatic molecule possesses both acid and base moieties in appropriate locations, intramolecular proton transfer can occur in a few ps or faster as with 3-hydroxyflavothione [75]. A classical example of intermolecular proton transfer to water is β -naphthol shown in Scheme 15.9, where **N** is the neutral (acidic) form, and **A** is the anionic (base) form [73].

Scheme 15.9 is once again similar to Scheme 15.6 except that the protonation back reaction is bimolecular. Thus, the two-state formalism is applicable with some changes concerning the determination of the fourth unknown. Because the lifetime of **N** in the absence of reaction, $\tau_N = 1/k_{FN}$, cannot be reliably measured with **N** even at very low pH values, it has to be obtained with a parent compound, with which the proton transfer reaction does not occur (in this case, 2-methoxynaphthalene). However, the implicit assumption of the procedure, that the lifetime measured with the methoxylated compound would be equal to τ_N , may be dangerous with the strongly hydrogen bonding solvent water (the most common solvent for proton transfer).

Alternatively, τ_A may be evaluated independently at sufficiently high pH values such that **A** is present in the ground state and can be selectively excited. This provides a single exponential decay with the lifetime, τ_A . Another, perhaps safer, solution is to profit from the fact that the back reaction is bimolecular, $k_{-1} =$



Scheme 15.10 Kinetic scheme involving three species

$k_p[\text{H}^+]$ and we can vary $[\text{H}^+]$. Thus, k_p can be obtained, [51, 55], from the slope the plot of $\lambda_1 + \lambda_2 = k_X + k_Y$ as a function of $[\text{H}^+]$, because all the remaining rate constants are pH independent.

15.7.2 Three-State Systems

Excited state processes involving three species (three-state systems) are now commonly observed. These can be found in excimer formation (oligomers and polymers containing pyrene, naphthalene and carbazole), proton transfer [76], charge transfer, etc.

The most general kinetic scheme for a three-state system is the so-called photokinetic triangle (Scheme 15.10), described by Eqs. (15.48–15.50) (these are simple extensions of Eqs. (15.24–15.26)). The decays are sums of three exponential terms (Eq. 15.49), and the kinetics involves nine unknowns (six reaction rate-constants and three reciprocal lifetimes).

$$\frac{d}{dt} \begin{bmatrix} \text{A} \\ \text{B} \\ \text{C} \end{bmatrix} (t) = \begin{bmatrix} -k_X & k_{-1} & k_{-2} \\ k_1 & -k_Y & k_3 \\ k_2 & k_{-3} & -k_Z \end{bmatrix} \begin{bmatrix} \text{A} \\ \text{B} \\ \text{C} \end{bmatrix} (t) \quad (15.48)$$

with $k_X = k_A + k_1 + k_2$, $k_Y = k_B + k_{-1} + k_{-3}$, and $k_Z = k_C + k_{-2} + k_3$.

$$\begin{bmatrix} \text{A} \\ \text{B} \\ \text{C} \end{bmatrix} (t) = \begin{bmatrix} a_{1,1} & a_{1,2} & a_{1,3} \\ a_{2,1} & a_{2,2} & a_{2,3} \\ a_{3,1} & a_{3,2} & a_{3,3} \end{bmatrix} \begin{bmatrix} e^{-\lambda_1 t} \\ e^{-\lambda_2 t} \\ e^{-\lambda_3 t} \end{bmatrix} \quad (15.49)$$

$$\begin{vmatrix} \lambda - k_X & k_{-1} & k_{-2} \\ k_1 & \lambda - k_Y & k_3 \\ k_2 & k_{-3} & \lambda - k_Z \end{vmatrix} = 0 \quad (15.50)$$

In this case the extension of the algebraic analysis of Birks is too complex and the rate constants are better evaluated with Eq. (15.51) (see also Eq. 15.27), which relates the experimental pre-exponential coefficients $A_{i,j}$ to $a_{i,j}$, as previously discussed.

$$k = a \times \lambda \times a^{-1} \quad (15.51)$$

Let us first consider that only the species **A** is excited, and that the fluorescence decays of **A**, **B** and **C** can be measured in independent experiments (the presence of emission overlap will be discussed latter). Then, each of the three rows of the experimental pre-exponentials matrix **A** is affected by a constant depending on: (1) the number of counts accumulated, (2) the fraction of the total emission collected at the measurement wavelength and (3) the instrumental response at that wavelength, *i.e.* $A_{i,j} = S_i a_{i,j}$. The relation between matrixes **A** and **a** is given by Eq. (15.52), and its substitution in Eq. (15.51) yields the explicit relation of the rate constants matrix to the experimental matrixes of rate constants λ and pre-exponential coefficients, **A** (Eq. 15.53).

$$A = \begin{bmatrix} S_1 & 0 & 0 \\ 0 & S_2 & 0 \\ 0 & 0 & S_3 \end{bmatrix} a = S \times a \quad (15.52)$$

$$k = s^{-1} A \lambda A^{-1} S \quad (15.53)$$

This adds three unknowns (S_1 , S_2 and S_3) to the initial nine unknowns giving a total number of 12 unknowns, which are larger than the number of independent equations provided by the three decays (3 reciprocal decay times plus $7 = 3 + 2 + 2$ pre-exponential coefficients). Therefore, the solution of Eq. (15.53) requires additional information.

As discussed for the two-state systems, there are several possibilities, depending on the system, to obtain such information. These are: (1) independent measurement of k_A , k_B or k_C , (2) changing the concentration of quencher (when a bimolecular reaction is involved) and (3) using steady-state fluorescence data (Eqs. 15.55 and 15.56).

Under steady-state conditions, the integrated fluorescence intensities of **A**, **B** and **C** are given by Eq. (15.54) (an extension of Eq. 15.42),

$$\begin{bmatrix} \phi_A \\ \phi_B \\ \phi_C \end{bmatrix} = \frac{I_{ss}}{\det(k)} \begin{bmatrix} k_{FA}(k_Y k_Z - k_3 k_{-3}) \\ k_{FB}(k_1 k_Z - k_2 k_3) \\ k_{FC}(k_1 k_{-3} - k_2 k_Y) \end{bmatrix} \quad (15.54)$$

and the ratios of fluorescence intensities are given by Eqs. (15.55) and (15.56).

$$\frac{\phi_A}{\phi_B} = \frac{k_{FA}}{k_{FB}} \frac{k_Y k_Z - k_3 k_{-3}}{k_1 k_Z - k_2 k_3} \quad (15.55)$$

$$\frac{\phi_C}{\phi_B} = \frac{k_{FC}}{k_{FB}} \frac{k_1 k_{-3} + k_2 k_Y}{k_1 k_Z + k_2 k_3} \quad (15.56)$$

Two examples, illustrating the foregoing possibilities to obtain the additional information will be described below.

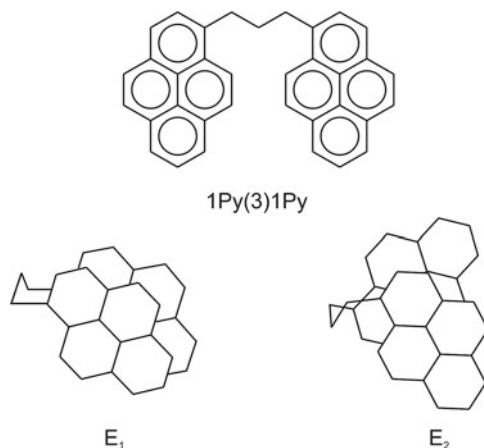
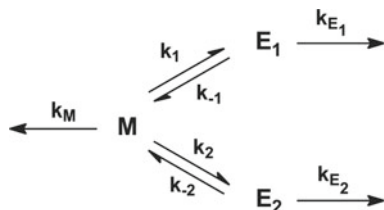


Fig. 15.14 Chemical structure of 1Py(3)1Py, together with the drawings of the two excimers [97] (E_1 and E_2) conformations

15.7.2.1 Excimer Formation

A classic example of a three-state system is the intramolecular excimer formation with 1,1'-dipyrenylpropane [1Py(3)1Py], a dipyrenyl oligomer with three carbon atoms connecting the two pyrenes (see Fig. 15.14). Three species are observed: one monomer and two excimers (sandwich-like and twisted conformations). It is worth noting that in the case of 2,2'-dipyrenylpropane [2Py(3)2Py] only one monomer and one excimer (less stable with a parallel sandwich-like geometry and decay time of 150 ns, [59]) are present, because the C_2 symmetry of the pyrene-chain bond axis allows only one excimer conformation. Also, with the longer (ten carbon atoms chain) of 1,1'-dipyrenyldecane [1Py(10)1Py], see Fig. 15.13 above, only one monomer and one excimer are present, because the longer chain is sufficiently flexible to allow relaxation to the most stable conformation of the excimer (two-state system).

The short propane chain of [1Py(3)1Py] does not allow direct interconversion from E_1 to E_2 or E_2 to E_1 without excimer dissociation, *i.e.*, k_3 and k_{-3} are equal to



Scheme 15.11 Kinetic scheme for the formation of two distinct and non-interconverting excimers E_1 and E_2

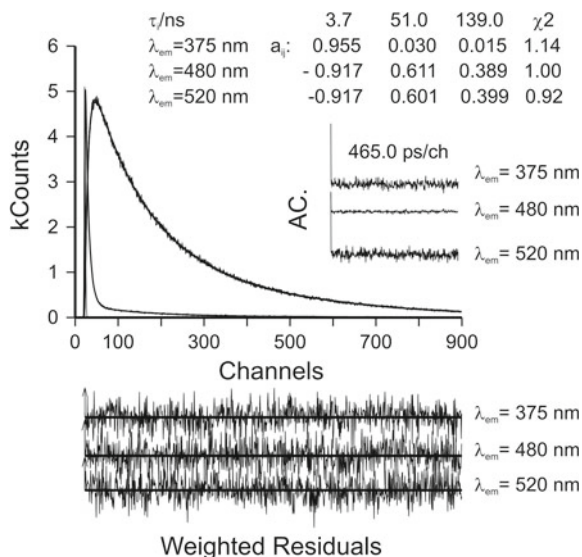


Fig. 15.15 Fluorescence decays of 1Py(3)1Py in *n*-heptane at 313 K obtained with $\lambda_{ex} = 339$ nm and collected at 375 nm (monomer) and 480, 520 nm (excimer). Autocorrelation functions (A.C.), weighted residuals (W.R.) and χ^2 values are also presented as insets

zero (Scheme 15.11), thus reducing the number of unknowns to seven. Additionally, k_M can be measured with a parent compound (e.g., 1-propylpyrene).

Despite the simplification to a number of six unknowns (smaller than the seven equations obtained from the fluorescence decays), there are still problems, because the fluorescence decays of the two excimers cannot be measured independently from each other (due to strong overlap of the emission spectra of \mathbf{E}_1 and \mathbf{E}_2). Thus, the pre-exponential coefficients of the excimer decays are linear combinations of $A_{2,j}$ and $A_{3,j}$, and their splitting implies knowledge of the emission spectra and the radiative rate constants of the two excimers (see below). The splitting is not simple because the emission spectra of \mathbf{E}_1 and \mathbf{E}_2 nearly overlap, and thus the fluorescence decays of [1Py(3)1Py] do not substantially change along the excimer band (see pre-exponential coefficients at 480 and 520 nm in Fig. 15.15).

This limitation leaves us with only five pieces of information from the fluorescence decays (three decay times and two ratios of pre-exponential coefficients from the monomer decay), for the six unknowns.

The kinetics were successfully solved, using an extension of the Birks' method, by measuring the decays as a function of temperature, and globally fitting the data, under a number of reasonable assumptions on the temperature dependence of the rate constants [58].

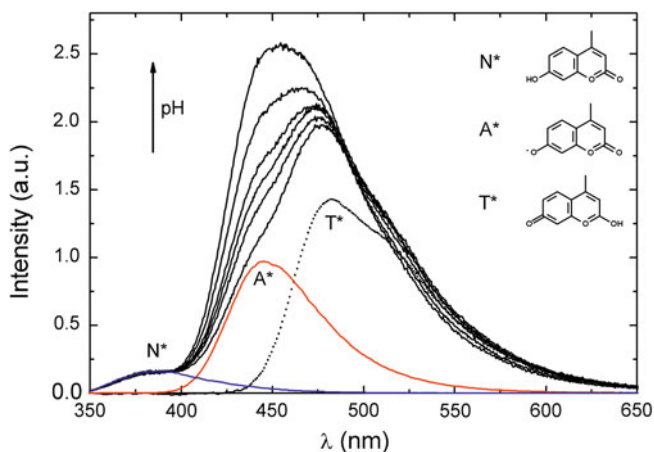


Fig. 15.16 Emission spectra of 7H4MC in water as a function of the pH. The spectra display three bands: N^* (380 nm), A^* (450 nm), T^* (480 nm). The structures of N , A and T are depicted in the picture

15.7.2.2 Proton Transfer and Tautomerisation

Another representative example of a three-state system has been observed with 7-hydroxy-4-methylcoumarin (7H4MC) in water, where three excited species are present: the neutral N^* , anionic A^* and tautomeric T^* forms of 7H4MC (see Fig. 15.16 [77]).

Figure 15.17 illustrates a typical decay at pH = 1.6 (obtained with ps time resolution) and the overall decay time dependence on pH (obtained with ns-time resolution). There is good agreement of the ns and ps data, as attested by the values obtained at $[H^+] = 0.025 \text{ mol dm}^{-3}$ (ps-time resolution) which match the extrapolated values in the left-hand panel obtained with ns time resolution.

The fluorescence decays and steady-state data (see below) indicated that all the prototropic reactions shown in Scheme 15.12 had to be considered (six rate constants plus three reciprocal lifetimes).

An additional difficulty to solving the kinetics results from the fact that the fluorescence decay of A^* cannot be obtained without contribution from those of N^* and T^* , and that of T^* will always have some contribution of A^* (see Fig. 15.16). When the decays of A^* and T^* are measured at 450 and 530 nm, respectively, the equation that relates the pre-exponential matrixes a and A is given by Eq. (15.57),

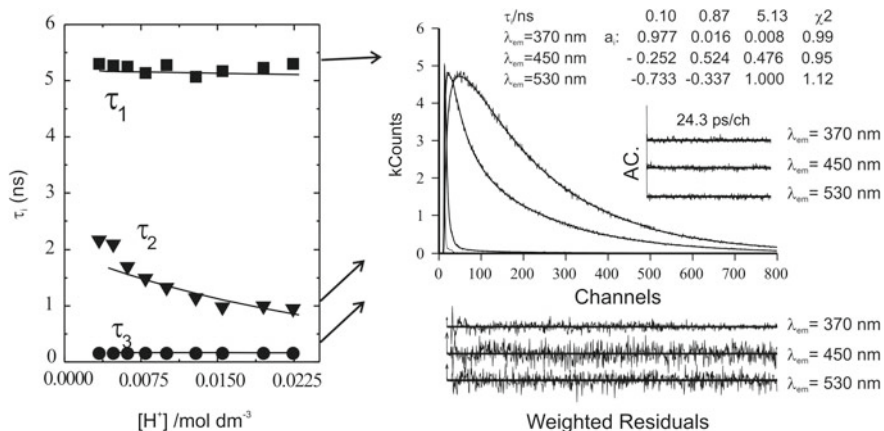
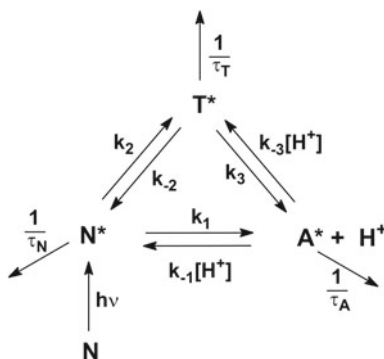


Fig. 15.17 *Left*: decay time values dependence with $[H^+]$, obtained with ns-time resolution, for 7H4MC in a dioxane–water mixture 1:4, [77]. *Right*: fluorescence decays of 7H4MC in a dioxane–water mixture 1:4, $[H^+] = 0.025 \text{ M}$, obtained at 293 K and at three different emission wavelengths: 370 nm (N^*), 450 nm (A^*) and 530 nm (T^*), with ps-time resolution. The *arrows* in the *left*-hand panel indicate the $[H^+]$ value at which the decay times values in the *right* hand panel were obtained

$$A = \begin{bmatrix} S_1 & 0 & 0 \\ \alpha S_2 & S_2 & \beta S_2 \\ 0 & \gamma S_3 & S_3 \end{bmatrix} a \tag{15.57}$$

where $\alpha = \frac{f_N(450)}{f_A(450)}$, $\beta = \frac{f_T(450)}{f_A(450)}$, $\gamma = \frac{f_A(530)}{f_T(530)}$, and $f_i(\lambda) = k_{Fi} \frac{I_i(\lambda)}{\int_0^\infty I_i(\lambda) d\lambda}$ is the fraction of

the fluorescence intensity of the species i ($= N, A$ or T) that is emitted at wavelength λ . Therefore, the determination of the rate constants using Eq. (15.53) involves five additional unknowns (S_1, S_2, α, β and γ), *i.e.*, a total of 14 unknowns



Scheme 15.12 Photokinetic triangle for 7H4MC [77]

for the 10 pieces of information provided by the fluorescence decays (three lifetimes and seven pre-exponential coefficients).

Let us see for this case how the four missing pieces of information can be obtained. First, the fluorescence lifetime and quantum yield of \mathbf{N}^* can be measured with the parent compound 7-methoxy-4-methylcoumarin, thus providing the values of $k_{\mathbf{N}}$ and $k_{\mathbf{FN}}$. The same measurements can be carried out for the anion, by measuring 7H4MC at basic pH, to evaluate the values of $k_{\mathbf{A}}$ and $k_{\mathbf{FA}}$. At this stage, the number of unknown rate constants has been reduced to seven ($k_{\mathbf{N}}$ and $k_{\mathbf{A}}$ are known), and the values of $f_{\mathbf{N}}(\lambda)$ and $f_{\mathbf{A}}(\lambda)$ can be evaluated from the radiative constants and emission spectra (after spectral decomposition, shown in Fig. 15.16), yielding the value of α . Now, by guessing a value for $k_{\mathbf{FT}}$, $f_{\mathbf{T}}(\lambda)$ can also be evaluated to obtain estimated values for β and γ (depending only on the guessed $k_{\mathbf{FT}}$). This reduces the number of the additional unknowns to three (S_1 , S_2 and $k_{\mathbf{FT}}$), *i.e.*, a total number of unknowns ($7 + 3 = 10$) equal to the number of pieces of information provided by the fluorescence decays. However, because of the propagation of the experimental errors in the calculations, this equality is not sufficient.

Let us now analyse the information that can be extracted from steady-state fluorescence data. First we note that the matrix of rate constants \mathbf{k} (Eq. 15.57) contains two pseudo-unimolecular rate constants, $k_{-1}[\mathbf{H}^+]$ and $k_{-3}[\mathbf{H}^+]$ (Eq. 15.58, where $k_{\mathbf{X}} = k_{\mathbf{N}} + k_1 + k_2$, $k_{\mathbf{Y}} = k_{\mathbf{A}} + (k_{-1} + k_{-3})[\mathbf{H}^+]$ and $k_{\mathbf{Z}} = k_{\mathbf{T}} + k_{-2} + k_3$).

$$\mathbf{k} = \begin{bmatrix} -k_{\mathbf{X}} & k_{-1}[\mathbf{H}^+] & k_{-2} \\ k_1 & -k_{\mathbf{Y}} & k_3 \\ k_2 & k_{-3}[\mathbf{H}^+] & -k_{\mathbf{Z}} \end{bmatrix} \quad (15.58)$$

Second, by adapting Eqs. (15.55) and (15.56) (replacing \mathbf{A} , \mathbf{B} and \mathbf{C} with \mathbf{N} , \mathbf{A} and \mathbf{T}) one obtains Eqs. (15.59) and (15.60), which predict that $\phi_{\mathbf{N}}/\phi_{\mathbf{A}}$ and $\phi_{\mathbf{T}}/\phi_{\mathbf{A}}$ are linear functions of $[\mathbf{H}^+]$, a prediction that has been experimentally observed [77].

Thus, the intercepts and slopes of $\phi_{\mathbf{N}}/\phi_{\mathbf{A}}$ and $\phi_{\mathbf{T}}/\phi_{\mathbf{A}}$ versus $[\mathbf{H}^+]$ gives four additional values related to the rate constants, which complete and exceed the required information.

$$\frac{\phi_{\mathbf{N}}}{\phi_{\mathbf{A}}} = \frac{k_{\mathbf{FN}}}{k_{\mathbf{FA}}} \cdot \frac{k_{\mathbf{A}}k_{\mathbf{Z}}}{k_1k_{\mathbf{Z}} + k_2k_3} + \frac{k_{\mathbf{FN}}}{k_{\mathbf{FA}}} \cdot \frac{k_{\mathbf{Z}}(k_{-1} + k_{-3}) - k_3k_{-3}}{k_1k_{\mathbf{Z}} + k_2k_3} \cdot [\mathbf{H}^+] \quad (15.59)$$

$$\frac{\phi_{\mathbf{T}}}{\phi_{\mathbf{A}}} = \frac{k_{\mathbf{FT}}}{k_{\mathbf{FA}}} \cdot \frac{k_1k_{\mathbf{A}}}{k_1k_{\mathbf{Z}} + k_2k_3} + \frac{k_{\mathbf{FT}}}{k_{\mathbf{FA}}} \cdot \frac{k_2(k_{-1} + k_{-3}) - k_1k_{-3}}{k_1k_{\mathbf{Z}} + k_2k_3} \cdot [\mathbf{H}^+] \quad (15.60)$$

The data analysis can be carried out by calculating the matrix of rate constants \mathbf{k} with an initial guess of S_1 , S_2 and $k_{\mathbf{FT}}$ and optimising these values by minimisation of the differences between the experimental and calculated values of $k_{\mathbf{N}}$, $k_{\mathbf{A}}$, which result of intercepts 1 and 2 and slopes 1 and 2 in Eqs. (15.59) and (15.60).

Other examples of three-state systems can be found with the β -carboline harmine [78, 79], poly(acrylic acid) labelled with pyrene [80] or naphthalene [81],

polyphenylsiloxanes [82], poly(N-vinylcarbazole) [83, 84], etc. The solution of a four-state system has also been carried out [55].

15.7.3 Other Models: Lifetime Distributions, Stretched Exponential and Transient Effects

15.7.3.1 Lifetime Distributions

The analysis of time-resolved fluorescence decay curves, using a sum of discrete exponential functions to fit the experimental data, is based on a simple assumption: the number of different exponential terms used has to be equal to the number of kinetically different excited state species present in the molecular system. While this assumption has the advantage of providing a clear physical meaning for the fitting parameters, decay times and pre-exponential coefficients, the identification of the different kinetic species is frequently not evident, particularly in more complex systems like polymers and proteins, and this approach has been questioned [85].

The possibility of using alternative kinetic schemes to rationalise the same fitting parameters, and the fact that in general a distribution of lifetimes can be fitted successfully by a sum of discrete exponential terms are the main reasons against the multi-exponential approach [86]. However, this difficulty can be overcome when narrow and well-separated time distributions can be identified, and

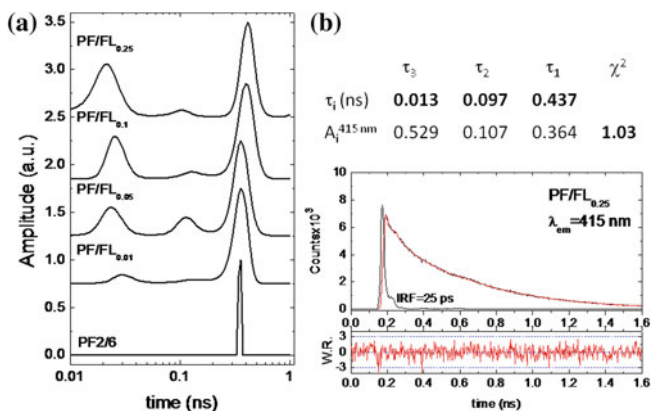


Fig. 15.18 Maximum entropy method (MEM) analysis of PF2/6 and PF/FLx copolymers fluorescence decays **a**, and fluorescence decay of PF/FL_{0.25}, with emission collected at 415 nm, analysed with a sum of three exponential functions, decay times (τ_i), amplitudes ($A_i^{415\text{ nm}}$) and χ^2 are also given in **b**. Reproduced with permission from Ref. [90], Copyright 2006, the American Chemical Society

data obtained from other techniques can be used as a functional block to help on the model selection.

Lifetime distributions can be expected in different situations: molecules incorporated in micelles and cyclodextrins, polymers—in solution and films, solid solutions, complex biological molecules—as for example proteins with several residuals located within different environments, which make impossible the use of the multi-exponential approach [45, 85, 87, 88].

In such cases, the individual pre-exponential amplitudes (a_i) are substituted by distribution functions $a_i(\tau)$, and the intensity decay component, associated with a time constant τ , is given by $I(\tau, t) = a(\tau)e^{-t/\tau}$. The entire decay law will then be described by the sum of the individual decay components, weighted by the amplitudes: $I(t) = \int_0^{\infty} a(\tau)e^{-t/\tau}d\tau$, with $\int_0^{\infty} a(\tau)d\tau = 1$ [45, 85].

In the absence of a physical model, describing the underlying physics that leads to the appearance of a distribution of lifetimes in the molecular system, the best way to analyse the data is to use a method that does not require the assumption of a particular distribution shape to describe the $a(\tau)$ values, as for example the maximum entropy method (MEM) [6].

While still being criticised by some for subjectivity on the specification of the fitting parameters, MEM is thought not to introduce more components than those necessary to fit the data, and has the advantage of giving a smooth $a(\tau)$ plot, that reveals the shape of the distribution. However, the instability of the distribution recovered has been reported for repeated experiments, even under exactly the same experimental conditions [63, 89, 90].

The MEM analysis of time-resolved fluorescence decays of several copolymers is shown in Fig. 15.18a. For the homopolymer PF2/6, only a narrow distribution is observed around 360 ps. However, for copolymers PF/FLx, with different fractions of fluorenone residues, distributed randomly along the polymer chain, the distribution at 360 ps is accompanied by two additional peaks. These are observed around 20 and 100 ps as a result of quenching of polyfluorene emission, due to energy transfer from the fluorene to the fluorenone sinks. Figure 15.18b shows the fluorescence decay of the copolymer labelled with 25 % of fluorenone groups, analysed with a sum of three exponential functions. Note the good agreement between MEM and multiexponential analysis [91].

15.7.3.2 Dipole–Dipole Energy Transfer and Stretched Exponential

Dipole–dipole (Förster) energy transfer depends on the distance and relative orientation of the donor and acceptor dipoles. For the simplest case of transfer from a donor to an isotropic three-dimensional distribution of energy acceptors, the fluorescence decay of the donor is given by Eq. (15.61), where $A = (4/3)\pi^{3/2}R_0^3c_A$ is proportional to the cubic power of the Förster radius R_0 and to the acceptor concentration c_A , and β is equal to 1/2.

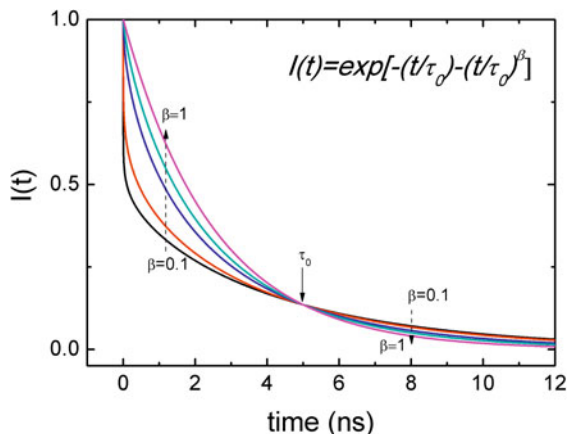


Fig. 15.19 Stretched exponential decay curves for several values of β . For small β values, the curve decays faster for $t < \tau_0$, and is followed by a slower tail afterwards

$$I(t) = I_0 \exp[-t/\tau_0 - A(t/\tau_0)^\beta] \quad (15.61)$$

For other distributions and/or dimensionalities the donor decay becomes more complex with β assuming values equal to $1/6$ and $1/3$ for one and two dimensional systems, respectively [85, 86]. In many cases, such as photon-harvesting polymer systems, where a distribution of relaxation times is expected, due to intrachain donor–acceptor energy transfer steps, either the distributions and/or the dimensionality are difficult to define *a priori*. Thus the use of a stretched exponential (Eq. 15.61, where $0 < \beta < 1$ is an empirical parameter) has been proposed.

Equation 15.61 predicts two time regimes for $0 < \beta < 1$ (see Fig. 15.19, where A was set equal to 1). The non-exponential behaviour is more pronounced for small values of β and becomes almost imperceptible when β approaches unity.

In the particular case of conjugated polymers, the situation can be even more complex due to the presence of both Dexter and Förster energy transfer mechanisms (the former being dominant at short distances), and the possibility of interchain energy transfer steps; these are favoured in polymer solid films due to a closer proximity between chains.

Energy migration is strongly dependent on the number of neighbour chromophores that a given excitation can ‘hop’ to and in conjugated polymers this is particularly evident. These long molecules can be looked as being formed by an array of different chromophores (conjugated segments) of close energy, separated by chemical and conformational defects. Since shorter segments have higher energies than the longer ones, an energy funnelling from shorter to longer segments occurs every time an excitation is created at sufficiently higher energies.

At early times, after an excitation has been created, there are a large number of acceptors available, and migration proceeds in a sub-ps time scale, after some hops, as the excitation moves to lower energy sites, the number of acceptors

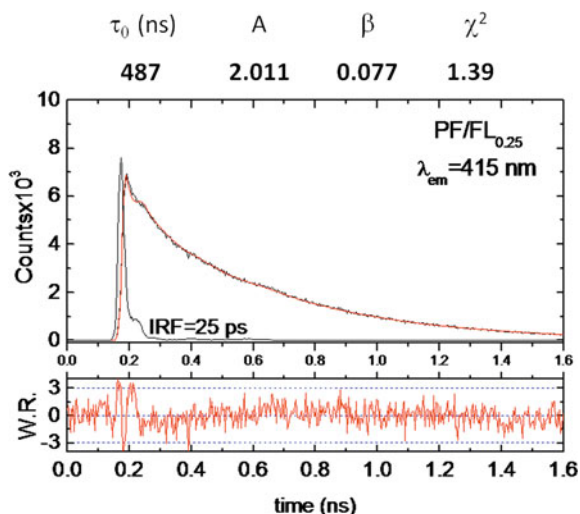


Fig. 15.20 Stretched exponential analysis of PF/FL_{0.25} copolymer fluorescence decay, with emission collected at 415 nm. Reproduced with permission from Ref. [91], Copyright 2006, the American Chemical Society

Table 15.4 Results, fit parameters (τ_0 , A , β) and χ^2 values, obtained from deconvolution with a stretched exponential, of fluorescence decays of PF2/6 and of PF/FLX in toluene solution at 295 K. Reproduced with permission from Ref. [91]., Copyright 2006, the American Chemical Society

Compound	λ_{em} (nm)	τ_0 (ns)	A	β	χ^2
PF2/6	415	0.367	0.048	1.0	1.16
PF/FL _{0.01}	415	0.419	0.324	0.415	1.58
PF/FL _{0.05}	415	0.433	0.801	0.364	1.1
PF/FL _{0.1}	415	0.441	1.379	0.108	1.12
PF/FL _{0.25}	415	0.487	2.011	0.077	1.39

decreases, and the rate of migration slows down. This initial regime of migration is described by a time-dependent rate constant and is referred to as dispersive migration.

After reaching the lower energy sites available in the polymer density of states, energy migration can only proceed *via* dynamical thermal fluctuations of the polymer backbone that dynamically alter the polymer energy landscape. Such fluctuations can break and form new energy sites very close in energy that allows migration to proceed with a constant rate. This regime, occurring in solution on a time window that goes typically up to a hundred of picoseconds, is referred to as non-dispersive migration.

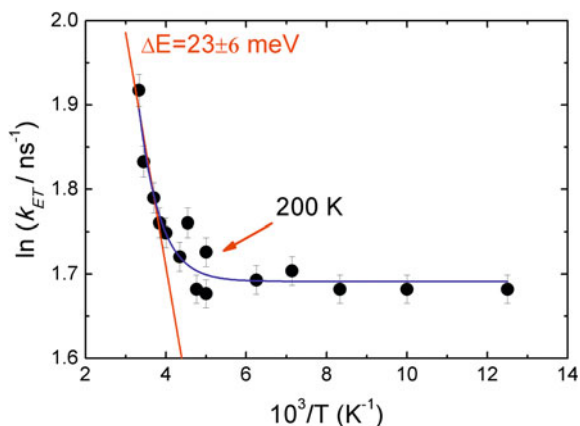


Fig. 15.21 Energy migration rate constant plotted against the reciprocal of temperature, for a fluorene copolymer containing dibenzothiophenedioxide and benzothiadiazole units. Both activated and barrier-less temperature regimes are observed. Reproduced with permission from Ref. [92], Copyright 2009, Wiley–VCH

The analysis with a stretched exponential (Eq. 15.61) of the fluorescence decay of a fluorene copolymer labelled with 25 % of fluorenone groups is shown in Fig. 15.20. Table 15.4 shows the results obtained from the analysis of fluorescence decays of PF2/6 and several PF/FLx copolymers in toluene solution with Eq. (15.61) [91].

Apart from the identification of different physical kinetic species, the picture that emerges from the data analysis with Eq. (15.61) (see Table 15.4) agrees with the interpretation obtained from analysis with a sum of three exponential functions, showing that with the increase on the fluorenone fraction in the copolymer backbone, the decay times associated with the quenching of the copolymer emission are becoming faster, in agreement with a more efficient energy transfer from fluorene to fluorenone moieties [91]. At higher fluorenone fractions the local concentration of acceptors increases, giving larger A values; the importance of the fast component in the overall decay also increases with the fluorenone fraction, giving smaller β values. However, the physical meaning of parameters τ_0 and β is not so clear; actually the former increases with the fluorenone fraction, assuming a value of 487 ps for PF/FL_{0.25}, about 120 ps longer than the polyfluorene lifetime.

However, even in the absence of a physical model, which would justify the use of a particular model, sum of exponentials or stretched exponential functions, relevant information can be obtained from time-resolved fluorescence decays of complex systems. For example, Fig. 15.21 shows the temperature dependence of the migration rate constant (obtained using a sum of exponential functions) in the non-dispersive regime for a polyfluorene copolymer film. At room temperature, the migration shows an activated regime with an energy barrier of 23 meV, turning

over to a non-activated regime below 200 K. Above this temperature transition, migration is a thermally assisted process, with indication that the thermal energy value ($k_B T$) is larger than the average energy difference between two close segments, and both “downhill” and “uphill” exciton jumps in energy are possible. Below 200 K, the thermal energy value, $k_B T$, becomes smaller than the average energy difference between two close segments and thermal assisted around Uphill and downhill with in a non-activated way and at slower rate, since the number of energy acceptors available has also decreased [92]. The behaviour identified in Fig. 15.21 was confirmed by fluorescence steady-state experiments, giving similar energy barrier in the activated region and turn-over temperature.

15.7.3.3 Transient Effects

An additional source of non-exponential emission decays is the transient effect that might appear at short times following excitation. This effect is frequently found in collisional quenching controlled by diffusion. In this situation, the quenching rate depends on the encounter probability between the fluorophore and the quencher, which is obviously also dependent on the diffusion coefficient and on quencher accessibility; at early times, fluorophores that have quenchers located at short distances will react almost ‘immediately’, leaving behind just those that have to diffuse to encounter a quencher centre. The phenomenon is going to be perceived as a quenching rate that is time dependent at early times, and results in a faster decay component of the fluorophore emission [93].

While important, transient effects often pass unnoticed due to limited time resolution of the experimental apparatus or due to the small magnitude of the effect; in fact, the phenomenon is more easily detected on slow diffusion processes in viscous media and long fluorescence lifetimes. The non-exponential intensity decay, resulting from a transient effect is described by Eq. (15.62), where a and b depend on diffusional parameters (diffusion coefficient and collision distance) and quencher concentration.

$$I(t) = I_0 \exp(-at - bt^{1/2}) \quad (15.62)$$

Such decays can also be fitted by an infinite sum of exponential terms, but those components cannot be assigned to different populations of excited state species, *i.e.*, in the case of a transient effect, it is the single fluorophore population that gives origin to a non-exponential decay.

There are thus several different models able to describe time-resolved fluorescence decays, all of them equally valid but giving origin to different physical meanings of the fitting parameters. The choice of an appropriate model is crucial and should rely on our knowledge of the system under investigation and the underlying physical phenomena involved.

15.8 Conclusions

In this chapter, we have described the fundamental parameters that should be obtained when characterising an electronic, singlet or triplet, excited state and how to determine them experimentally including methodologies and required equipment. These characteristics include electronic energy, quantum yields, lifetimes and number and type of species in the excited state. Within this last context, *i.e.*, when excited state reactions give rise to additional species in the excited state we have explored several excited state kinetic schemes, found to be present when excimers, exciplexes are formed and (intra and intermolecular) proton transfer occurs. This includes a complete formalism (with equations) for the steady-state and dynamic approaches for two and three-state systems, from where all the rate constants can be obtained. Additionally, we have explored additional recent developments in photophysics: the competition between vibrational relaxation and photochemistry, and the non-discrete analysis (stretched-exponential) of fluorescence decays.

References

1. Stern O, Volmer M (1919) Über die Abklingzeit der Fluoreszenz. *Physikalische Zeitschrift* 20:183–188
2. Murov S, Chermichael I, Hug GL (1993) *Handbook of photochemistry*. M Dekker Inc, New York
3. Karpovich DS, Blanchard GJ (1995) Relating the polarity-dependent fluorescence response of pyrene to vibronic coupling. Achieving a fundamental understanding of the py polarity scale. *J Phys Chem* 99:3951–3958
4. Bensasson RV, Land EJ, Truscott TG (1993) *Excited states and free radicals in biology and medicine*. Oxford Science Publications, Oxford
5. Rusakowi R, Testa AC (1968) Comparison of quinine bisulfate and 9,10-diphenylanthracene as fluorescence standards. *J Phys Chem* 72:793–796
6. Valeur B (2002) *Molecular fluorescence: principles and applications*. Wiley-VCH, Weinheim
7. Montalti M, Credi A, Prodi L, Gandolfi M (2006) *Handbook of photochemistry*. 3rd edn. CRC Press, Boca Raton
8. Parker CA, (1968) *Photoluminescence of solutions*. Elsevier, Amsterdam
9. deMello JC, Wittmann HF, Friend RH (1997) An improved experimental determination of external photoluminescence quantum efficiency. *Adv Mater* 9:230–233
10. Palsson LO, Monkman AP (2002) Measurement of solid-state photoluminescence quantum yields using a fluorimeter. *Adv Mater* 14:757–758
11. Pina J, Seixas de Melo J, Burrows HD et al (2008) Excited state properties of oligophenyl and oligothiophenyl swivel cruciforms. *J Phys Chem B* 112:1104–1111
12. Pina J, Seixas de Melo J (2009) A comprehensive investigation of the electronic spectral and photophysical properties of conjugated naphthalene–thiophene oligomers. *Phys Chem Chem Phys* 11:8706–8713
13. Kristiansen M, Scurlock RD, Iu KK, Ogilby PR (1991) Charge-transfer state and singlet oxygen ($^1\Delta_g$ O₂) production in photoexcited organic molecule-molecular oxygen complexes. *J Phys Chem* 95:5190–5197

14. Martinez CG, Neumer A, Marti C et al (2003) Effect of the media on the quantum yield of singlet oxygen ($O_2(^1\Delta_g)$) production by 9H-fluoren-9-one: solvents and solvent mixtures. *Helv Chim Acta* 86:384–397
15. Carmichael I, Hug GL (1986) Triplet-triplet absorption spectra of organic molecules in condensed phases. *J Phys Chem Ref Data* 15:1–250
16. Becker RS, Seixas de Melo J, Maçanita AL, Elisei F (1996) Comprehensive evaluation of the absorption, photophysical, energy transfer, structural, and theoretical properties of α -oligothiophenes with one to seven rings. *J Phys Chem* 100:18683–18695
17. Kumar CV, Qin L, Das PK (1984) Aromatic thioketone triplets and their quenching behavior towards oxygen. *J Chem Soc-Faraday Trans II* 80:783–793
18. Seixas de Melo J, Silva LM, Arnaut LG, Becker RS (1999) Singlet and triplet energies of α -oligothiophenes: a spectroscopic, theoretical, and photoacoustic study: extrapolation to polythiophene. *J Chem Phys* 111:5427–5434
19. Pineiro M, Gonsalves A, Pereira MM et al (2002) New halogenated phenylbacteriochlorins and their efficiency in singlet-oxygen sensitization. *J Phys Chem A* 106:3787–3795
20. Seixas de Melo J, Serpa C, Burrows HD, Arnaut LG (2007) The triplet state of indigo. *Angew Chem Int Ed* 46:2094–2096
21. Seixas de Melo J, Moura AP, Melo MJ (2004) Photophysical and spectroscopic studies of indigo derivatives in their keto and leuco forms. *J Phys Chem A* 108:6975–6981
22. Seixas de Melo J, Rondão R, Burrows HD et al (2006) Spectral and photophysical studies of substituted indigo derivatives in their keto forms. *Chem Phys Chem* 7:2303–2311
23. Becker RS (1969) Theory and interpretation of fluorescence and phosphorescence. Wiley-Interscience, New York
24. Land EJ (1968) Extinction coefficients of triplet–triplet transitions. *Proc Royal Soc Lond A* 305:457–471
25. Bensasson R, Land EJ (1971) Triplet-triplet extinction coefficients via energy transfer. *Trans Faraday Soc* 67:1904–1915
26. Keene JP (1964) Pulse radiolysis equipment. *J Sci Instrum* 41:493–496
27. Butler J, Hodgson BW, Hoey BM et al (1989) Experimental studies of some moderately fast processes initiated by radiation. *Radiat Phys Chem* 34:633–646
28. Monkman AP, Burrows HD, Miguel MD et al (2001) Triplet state spectroscopy of conjugated polymers studied by pulse radiolysis. *Synth Met* 116:75–79
29. Cooper R, Thomas JK (1968) Formation of excited states in the nanosecond-pulse radiolysis of solutions of benzene and toluene. *J Chem Phys* 48:5097–6002
30. Candeias LP, Wildeman J, Hadziioannou G, Warman JM (2000) Pulse radiolysis—optical absorption studies on the triplet states of p-phenylenevinylene oligomers in solution. *J Phys Chem B* 104:8366–8371
31. Hoofman R, de Haas MP, Siebbeles LDA, Warman JM (1998) Highly mobile electrons and holes on isolated chains of the semiconducting polymer poly(phenylene vinylene). *Nature* 392:54–56
32. Grozema FC, Siebbeles LDA, Warman JM et al (2002) Hole conduction along molecular wires: σ -bonded silicon versus π -bond-conjugated carbon. *Adv Mater* 14:228–231
33. Burrows HD, Seixas de Melo J, Serpa C et al (2001) $S_1 \sim T_1$ intersystem crossing in π -conjugated organic polymers. *J Chem Phys* 115:9601–9606
34. Monkman AP, Burrows HD, Miguel MD et al (1999) Measurement of the S_0 – T_1 energy gap in poly(2-methoxy,5-(2'-ethyl-hexoxy)-p-phenylenevinylene) by triplet–triplet energy transfer. *Chem Phys Lett* 307:303–309
35. Pina J, Seixas de Melo J, Burrows HD et al (2009) Alternating binaphthyl—thiophene copolymers: synthesis, spectroscopy, and photophysics and their relevance to the question of energy migration versus conformational relaxation. *Macromolecules* 42:1710–1719
36. Fonseca SM, Pina J, Arnaut LG et al (2006) Triplet-state and singlet oxygen formation in fluorene-based alternating copolymers. *J Phys Chem B* 110:8278–8283
37. Maciejewski A, Steer RP (1993) The photophysics, physical photochemistry, and related spectroscopy of thiocarbonyls. *Chem Rev* 93:67–98

38. Becker RS, Michl J (1966) Photochromism of synthetic and naturally occurring 2H-chromenes and 2H-pyrans. *J Am Chem Soc* 88(5931):5933
39. Becker RS, Dolan E, Balke DE (1969) Vibronic effects in photochemistry- competition between internal conversion and photochemistry. *J Chem Phys* 50:239–245
40. Becker RS, Pelliccioli AP, Romani A et al (1999) Vibronic quantum effects in fluorescence and photochemistry. Competition between vibrational relaxation and photochemistry and consequences for photochemical control. *J Am Chem Soc* 121:2104–2109
41. Becker RS, Favaro G, Romani A et al (2005) Vibronic effects in pathways of photochemistry and vibrational relaxation. *Chem Phys* 316:108–116
42. Lenoble C, Becker RS (1986) Photophysics, photochemistry and kinetics of photochromic 2H-pyrans and chromenes. *J Photochem* 33:187–197
43. Demas JN (1983) Excited state lifetime measurements. Academic Press, Inc, London
44. O'Connor DV, Phillips D (1984) Time-correlated single photon counting. Academic Press, London
45. Lakowicz JR (2006) Principles of fluorescence spectroscopy, 3rd edn. Kluwer Academic, New York
46. Zachariasse KA, Busse R, Schrader U et al (1982) Intramolecular siglet and triplet excimers with diphenanthrylpropanes. *Chem Phys Lett* 89:303–308
47. Seixas de Melo J, Fernandes PF (2001) Spectroscopy and photophysics of 4- and 7-hydroxycoumarins and their thione analogs. *J Mol Struct* 565:69–78
48. Maçanita AL, Costa FP, Costa S et al (1989) The 9-anthroate chromophore as a fluorescent probe for water. *J Phys Chem* 93:336–343
49. Pina J, Seixas de Melo J, Burrows HD et al (2007) Spectral and photophysical studies of poly[2,6-(1,5-dioctyl)naphthalene]thiophenes. *J Phys Chem C* 111:7185–7191
50. Striker G, Subramaniam V, Seidel CAM et al (1999) Photochromicity and fluorescence lifetimes of green fluorescent protein. *J Phys Chem B* 103:8612–8617
51. Lima JC, Abreu I, Brouillard R, Maçanita AL (1998) Kinetics of ultra-fast excited state proton transfer from 7-hydroxy-4-methylflavylium chloride to water. *Chem Phys Lett* 298:189–195
52. Boens N, Qin WW, Basaric N et al (2007) Fluorescence lifetime standards for time and frequency domain fluorescence spectroscopy. *Anal Chem* 79:2137–2149
53. Lampert RA, Chewter LA, Phillips D et al (1983) Standards for nanosecond fluorescence decay time measurements. *Anal Chem* 55:68–73
54. Birks JB (1970) Photophysics of aromatic molecules. Wiley, London
55. Freitas AA, Quina FH, Fernandes AC, Maçanita AL (2010) Picosecond dynamics of the prototropic reactions of 7-hydroxyflavylium photoacids anchored at an anionic micellar surface. *J Phys Chem A* 114:4188–4196
56. Stevens B, Ban MI (1964) Spectrophotometric determination of enthalpies and entropies of photoassociation for dissolved aromatic hydrocarbons. *Trans Faraday Soc* 60:1515–1523
57. Boyce WE, DiPrima RC (1986) Elementary differential equations and boundary value problems, 4th edn. Wiley, New York
58. Zachariasse KA, Busse R, Duveneck G, Kühnle W (1985) Intramolecular monomer and excimer fluorescence with dipyrenylpropanes: double-exponential versus triple-exponential decays. *J Photochem* 28:237–253
59. Zachariasse KA, Duveneck G, Kühnle W (1985) Double-exponential decay in intramolecular excimer formation: 1,3-di(2-pyrenyl)propane. *Chem Phys Lett* 113:337–343
60. Zachariasse KA, Maçanita AL, Kühnle W (1999) Chain length dependence of intramolecular excimer formation with 1, n-bis(1-pyrenylcarboxy)alkanes for n = 1–16, 22, and 32. *J Phys Chem B* 103:9356–9365
61. Serpa C, Gomes PJS, Arnaut LG et al (2006) Temperature dependence of ultra-exothermic charge recombinations. *Chem Phys Chem* 7:2533–2539
62. Gordon M, Ware WR (1975) The exciplex. Academic Press, New York
63. Waluk J (2000) Conformational analysis of molecules in excited states. Wiley-VCH, New York

64. Becker HD (1993) Unimolecular photochemistry of anthracenes. *Chem Rev* 93:145–172
65. Chandross EA, Thomas HT (1971) Intramolecular exciplex formation in naphthylalkylamines. *Chem Phys Lett* 9:393–396
66. Hinatu J, Masuhara H, Mataga N et al (1978) Absorption spectra of inter- and intramolecular exciplex systems of pyrene and N, N-dimethylaniline in alcoholic solutions. *Bull Chem Soc Jpn* 51:1032–1036
67. Itoh M, Mimura T, Usui H, Okamoto T (1973) Intramolecular exciplex and charge transfer complex formations in (9,10-dicyanoanthracene)-(trimethylene)-(naphthalene) systems. *J Am Chem Soc* 95:4388–4392
68. Leinhos U, Kühnle W, Zachariasse KA (1991) Intramolecular charge transfer and thermal exciplex dissociation with p-aminobenzonitriles in toluene. *J Phys Chem* 95:2013–2021
69. Swinnen AM, Vanderauweraer M, De Schryver FC et al (1987) Photophysics of the intramolecular exciplex formation in omega-(1-pyrenyl)-alpha-(dimethylamino)alkanes. *J Am Chem Soc* 109(321):330
70. Fajardo ME, Withnall R, Feld J et al (1988) Condensed phase laser induced harpoon reactions. *Laser Chem* 9:1–3
71. Douhal A, Lahmani F, Zewail AH (1996) Proton-transfer reaction dynamics. *Chem Phys* 207:477–498
72. Arnaut LG, Formosinho SJ (1993) Excited-state proton transfer reactions I. Fundamentals and intermolecular reactions. *J Photochem Photobiol A-Chem* 75:1–20
73. Laws WR, Brand L (1979) Analysis of two-state excited-state reactions. The fluorescence decay of 2-naphthol. *J Phys Chem* 83:795–802
74. Nunes RMD, Pineiro M, Arnaut LG (2009) Photoacid for extremely long-lived and reversible pH-jumps. *J Am Chem Soc* 131:9456–9462
75. Aloisi GG, Latterini L, Maçanita AL et al (2003) Singlet and triplet state properties of substituted flavothiones. *Phys Chem Chem Phys* 5:69–3464
76. Costa T, Pina J, de Seixas Melo J (2009) Photophysical processes in polymers and oligomers. *Spec Period Rep Photochem* 37:44–71
77. Seixas de Melo J, Maçanita AL (1993) Three interconverting excited species: experimental study and solution of the general photokinetic triangle by time-resolved fluorescence. *Chem Phys Lett* 204:556–562
78. Dias A, Varela AP, Miguel MD et al (1996) β -Carbolines. 2. Rate constants of proton transfer from multiexponential decays in the lowest singlet excited state of harmine in water as a function of pH. *J Phys Chem* 100:17970–17977
79. Dias A, Varela AP, Miguel MD et al (1992) β -Carboline photosensitizers. 1. Photophysics, kinetics and excited-state equilibria in organic solvents, and theoretical calculations. *J Phys Chem* 96:10290–10296
80. Seixas de Melo J, Costa T, Francisco A et al (2007) Dynamics of short as compared with long poly(acrylic acid) chains hydrophobically modified with pyrene, as followed by fluorescence techniques. *Phys Chem Chem Phys* 9:1370–1385
81. Costa T, Miguel MG, Lindman B et al (2005) Dynamics and energetics of the self-assembly of a hydrophobically modified polyelectrolyte: naphthalene-labeled poly(acrylic acid). *J Phys Chem B* 109:11478–11492
82. Dias FB, Lima JC, Pierola IF et al (2001) Internal dynamics of poly(methylphenylsiloxane) chains as revealed by picosecond time resolved fluorescence. *J Phys Chem A* 105:10286–10295
83. Masuhara H, Tamai N, Mataga N et al (1983) Excimer formation in poly(N-vinylcarbazole) and its model compounds as revealed by picosecond time-resolved absorption spectroscopy. *Chem Phys Lett* 95:471–475
84. Vandendriessche J, Palmans P, Toppet S et al (1984) Configurational and conformational aspects in the excimer formation of bis(carbazoles). *J Am Chem Soc* 106(8057):8064
85. Berberan-Santos MN, Bodunov EN, Valeur B (2005) Mathematical functions for the analysis of luminescence decays with underlying distributions 1. Kohlrausch decay function (stretched exponential). *Chem Phys* 315:171182

86. Webber SE (1990) Photon-harvesting polymers. *Chem Rev* 90:1469–1482
87. Noronha M, Lima JC, Paci E et al (2007) Tracking local conformational changes of ribonuclease A using picosecond time-resolved fluorescence of the six tyrosine residues. *Biophys J* 92:4401–4414
88. Noronha M, Santos R, Paci E et al (2009) Fluorescence lifetimes of tyrosine residues in cytochrome *c''* as local probes to study protein unfolding. *J Phys Chem B* 113:4466–4474
89. Zachariasse KA, Striker G (1988) Three and only three excited-state species (one monomer and two excimers) in 1,3-di(1-pyrenyl)propane. *Chem Phys Lett* 145:251
90. Liu YS, Ware WR (1993) Photophysics of polycyclic aromatic hydrocarbons adsorbed on silica gel surfaces. 1. Fluorescence lifetime distribution analysis: an ill-conditioned problem. *J Phys Chem* 97:5980–5986
91. Dias FB, Knaapila M, Monkman AP, Burrows HD (2006) Fast and slow time regimes of fluorescence quenching in conjugated polyfluorene—fluorenone random copolymers: The role of exciton hopping and Dexter transfer along the polymer backbone. *Macromol* 39:1598–1606
92. Dias FB, Kamtekar KT, Cazati T et al (2009) Exciton diffusion in polyfluorene copolymer thin films: kinetics, energy disorder and thermally assisted hopping. *Chem Phys Chem* 10:2096–2104
93. Lakowicz JR, Johnson ML, Joshi N et al (1986) Transient effects in quenching detected by harmonic-content frequency-domain fluorometry. *Chem Phys Lett* 131:343–348
94. Pina J, Seixas de Melo J, Batista RMF et al (2010) Synthesis and characterization of the ground and excited states of tripod-like oligothiophenyl-imidazoles. *J Phys Chem B* 114:4964–4972
95. Pina J, Seixas de Melo J, Burrows HD et al (2006) Spectral and photophysical studies on cruciform oligothiophenes in solution and the solid state. *J Phys Chem B* 110:15100–15106
96. Zachariasse KA, Kühnle W, Leinhos U et al (1991) Time-resolved monomer and excimer fluorescence of 1,3-di(1-pyrenyl)propane at different temperatures: no evidence for distributions from picosecond laser experiments with nanosecond time resolution. *J Phys Chem* 95:5476–5488
97. Zachariasse KA, Duveneck G, Kühnle W et al (1991) Multicomponent fluorescence decay analysis in intramolecular excimer formation with dipyrenylalkanes. In: Honda K (ed) *Photophysical processes in organized molecular systems*. Elsevier, Amsterdam, pp 83
98. Seixas de Melo J (2005) The influence of oxygen on the lifetime of luminescence probes. A simple device for degassing solutions for fluorescence experiments. *Chem Educ* 10:29–35

Index

A

α -fragmentation, 95
Absorption, 2, 3, 8, 46, 52–53, 56–60, 63–67, 167, 177, 380, 385, 406, 473, 490, 516, 521, 543, 553
Absorption filters, 489, 490
Acceptor, 65, 75, 77, 149, 169, 170, 173, 282, 287, 296, 414, 416, 419, 420, 423
Acid dissociation constant, 410
Acid rain, 241, 242
Actinic flux, 219, 220, 240
Actinometer, 152, 175, 494, 495
Additive colour system, 366
Adiabatic cooling, 224, 225, 239
Advanced oxidation processes (AOP's), 247, 248, 251, 260
Advection, 225, 227
Aerosols, 217, 231, 232, 241
Age-related macular degeneration, 306, 339, 399
Aggregation, 2, 64–66, 337, 420, 472
Airglow, 234
Air mass filter, 484
Alkoxy radicals, 323, 357
Ammonia, 34, 44, 63, 371, 376, 379, 394, 411, 412, 419
Amplification, 353, 369, 374, 382, 386, 398, 428, 446, 447, 486, 497
Analyte, 167, 403–411, 413–422, 426–432
Analytical balance, 473
Angular momentum, 12, 13, 17, 21, 28, 37, 55
Anion, 82, 84, 94, 116, 120, 252, 256, 406, 414, 416, 418, 428, 568, 573, 574
Anisotropy, 407–409, 467
Anthraquinone dyes, 153, 186, 204
Antibody–antigen, 352, 353

Antibonding orbital, 32, 36, 37, 39, 109, 110, 128
Antioxidant, 305–307, 314–318, 320, 322–324
Ascorbic acid, 307, 315, 319, 322
Atmospheric gases, 221
Atomic emission, 158
Atomic orbitals, 31
Azimuthal angle, 219
Azo dyes, 153, 205, 389
AZ-series resists, 444
Azulene, 550

B

β -carotene, 37, 154, 174, 317, 320, 322
Bacterial PDT, 340
Bandgap, 42, 62, 150, 157, 255, 257, 258
Band model, 41, 43, 380
Bandpass, 489, 492
Bandwidth, 6, 59, 69, 480, 484, 487, 490, 492–494, 503, 508, 509, 513
Bathochromic shift, 64
Beer–Lambert law, 58, 59, 409, 472, 473, 493, 504, 507
Benzophenone, 155, 175, 540, 546
Binding, 284, 337, 352, 355, 404, 409, 410, 413, 417, 420, 587
Binding equilibria, 409
Binding mechanisms, 410
Biomimetic water splitting, 296
Biomolecule, 305, 307, 314, 321, 324, 338, 410, 428, 518, 543
Birks' method, 560, 571
Blood diagnostics, 350
Blueprints, 152, 363, 389
Boltzmann distribution equation, 50

- Bond order, 3, 36–39, 68
 Bonding orbital, 32, 36, 37, 120
 Born–Oppenheimer approximation, 48
 Bose–Einstein statistics, 18
 Bosons, 18
 Box model, 243
 Bulk heterojunctions, 267, 281, 284, 286, 287
- C**
 C₆₀, 281, 285, 286
 Calibration, 409, 422, 427–431, 472, 482, 483, 502, 506, 521, 557, 559
 Calotype, 374–376
 Camera-obscura, 370, 272–374
 Carbon prints, 396
 Carbonate radical, 321, 324
 Carotenoid, 154, 174, 289, 307, 317–319, 321, 324
 Carrier, 279–290, 292, 294, 297, 377, 381, 398, 458, 496
 Carrier separation, 284
 Catalytic, 117, 121, 126, 230, 232, 233, 244, 251, 294–296, 384, 386
 Cation, 31, 82, 94, 117–119, 269, 270, 274, 279, 307, 312, 319, 322, 412, 413, 417, 428, 432
 Charge carrier mobilities, 280, 282, 283
 Charge-coupled devices, 497
 Charge-separated state, 114, 269, 280, 285
 Charge separation, 114, 137, 140, 258, 268, 269, 279–281, 284, 285, 287, 295, 298, 471
 Charge transfer, 62, 63, 82, 110, 114–118, 120, 153, 175, 206, 253, 260, 278, 284, 293, 317, 416, 422, 471, 523, 559, 566, 568
 Charge transfer (MLCT and LMCT) transitions, 61, 109, 112, 152
 Charge transfer excited state, 114, 253
 Charge-transfer exciton, 41, 284
 Chemical actinometers, 494, 495
 Chemical binding, 410, 412
 Chemical development, 369, 375, 386, 436
 Chemical lifetime, 229, 235, 236
 Chemical sensitisation, 374, 383, 384, 391
 Chemically amplified photoresists, 445, 446
 Chemically amplified resists, 446
 Chemiluminescence, 166, 234
 Chlorofluorocarbon, 225, 230
 Chlorophenols, 247, 252, 259–261
 Chromaticity, 160, 501, 503
 Chromogenic, 388, 389, 395
 Chromogenic development, 388
 Cibachrome, 389
 CIE (*x*, *y*)-chromaticity diagram, 501
 CIE colour coordinates, 429, 430, 500, 501
 11-*cis*-retinal, 2, 3
Cis-trans isomerisation, 2, 73, 130, 131, 134, 179, 185, 333
 Clusters, 121, 138–141, 227, 252, 381, 383, 386
 CMOS, 455
 CMYK, 368
 CO dissociation, 127, 128, 138
 CO₂ reduction, 116, 137, 268, 288, 289, 297
 Coherence, 6
 Collisional energy transfer quenching, 78
 Colorants, 61, 150, 151, 153–155, 183, 367, 368
 Colorimetric, 155, 405, 411, 410, 413, 429, 431
 Colour, 4, 8, 37, 61–63, 150–154, 159–161, 176–179, 183, 185, 354, 357, 364, 366–369, 387–390, 498, 500, 501
 Colour vision, 366
 Colour-rendering index, 161
 Complex, 11, 12, 34, 40, 46, 55, 59, 61–63, 82, 108, 110–118, 120–123, 128, 152, 153, 181, 184, 227, 230, 238, 242, 244, 252, 275–277, 289, 317, 321, 386, 408–413, 416, 417, 421, 422, 430, 432, 468, 566, 576, 579
 Conduction band, 42, 43, 48, 65, 255, 270–272, 380–382, 384, 385, 391, 392, 496
 Cones, 305, 366, 367
 Confocal fluorescence microscopy, 518
 Conjugated polyelectrolytes, 168, 421
 Conjugated polymers, 41, 43, 68, 84, 155, 165, 168, 281, 282, 287, 420, 421, 577
 Conjugation, 37, 40, 92, 154, 178, 280, 338, 411
 Correction factors, 539
 Correlated colour temperature, 161
 Covalent bonding, 31
 Cross-linking, 389, 396, 428, 439–441, 442, 452, 455, 456
 CRTs, 160
 Cryostats, 522
 Cu₂O, 294
 Curve fitting, 499, 523
 Cut-off wavelength, 65, 471, 504
 Cuvettes, 474, 521, 548, 553
 Cyanine dyes, 154, 384
 J-aggregates, 64, 65, 385, 472
 Cyanotype, 152, 393–395
 Cyanotype process, 152, 393
 Cyclic voltammetry, 45

2+2 cycloaddition (intra- and inter-molecular),
92, 95, 98
Cycolor, 395, 399
Cyliths, 395

D

Daguerreo type, 372–374
DAPI (4'-6-diamidino-2-phenylindole), 414
Data analysis, 499, 523
Data recording, 183, 520
dd-states, 111–113, 116, 127, 136, 137
d-*d* transitions, 55, 61, 152, 153
de Broglie, 13–15, 20, 22, 453
Defects, 48, 62, 158, 283, 282, 369, 398, 577
Degenerate, 24, 27, 29, 30, 35, 39, 49, 50, 316
Delayed fluorescence, 2, 82–84, 157, 166, 169
Depletion region, 291
Deuterium lamps, 481, 482
Developer, 381, 386–391, 395, 443, 451
Device, 9, 10, 41, 43, 162, 164, 168, 185, 268,
272, 273, 275, 287, 369, 370, 425–427,
430–433, 436–438, 445, 447, 484, 494,
497, 520, 524
Dexter energy transfer, 2, 78, 79, 170, 171
Diazonium salt, 394
Diazotype, 394
Dichromate, 395, 396, 398
Dielectric constant, 16, 284, 471, 523
Dielectric filters, 489, 490
Differential kinetic rate, 272
Diffraction, 10, 15, 109, 122, 396, 447–449,
460, 461, 491, 492, 494, 508, 518, 519,
541
Diffraction grating, 396, 491, 492, 494, 504,
508, 541
Diffraction limit, 10, 183, 447, 519
Diffuse reflectance, 8, 503, 504, 522
Diffusion, 77, 91, 127, 170, 171, 178, 227,
250, 260, 273, 274, 279–280, 294, 338,
387, 390, 412, 418, 423, 458, 519, 580
Diffusion-controlled, 77, 127, 471, 550, 561
Digitisation, 498
Dimetallic species, 121, 127
Dipole moment, 54, 55, 60, 64, 65, 75, 422
Displacement assay, 413
Dissociation constant, 409, 410
Dissociative photochemistry, 120, 126
DNA, 168, 233, 306, 313, 322, 341, 354–356,
414
Donor, 65, 74–78, 80, 82, 115, 118, 134, 153,
170, 172, 250, 269, 280–282, 284, 286,
314, 317, 348, 419, 422, 524, 545, 546,
548, 549, 576, 577

Donor levels, 65
Doppler broadening, 63
Dye-sensitised solar cells, 137, 142, 267, 267,
271, 276, 298
Dynamic, 76, 77, 79, 80, 350, 367, 379, 407,
409, 416, 425, 471, 473, 559, 581

E

$\delta\delta^*$ excited state, 122, 125
Einstein coefficient, 52, 60, 61
Electric dipoles, 5, 55–57, 60, 172
Electrocyclic reactions, 92
Electroluminescence, 157, 162–165, 188, 197
Electrolyte, 270, 272–279, 290–294
Electromagnetic radiation (EMR), 4, 6, 12, 15,
52–55, 391
Electron beam lithography, 435–438,
448–457, 462
 beam resists, 450
 conduction, 277
 exchange, 160, 235, 280, 307, 317, 381, 418
 exchange energy transfer, 307, 317, 418
 injection, 271, 272, 276, 278
 interference lithography, 453
 paramagnetic resonance, 118, 308
 transfer, 94, 173, 269, 307, 311, 312,
 319–323, 337, 566
 transfer kinetics, 269, 272
 transfer quenching, 78, 317
 trapping, 126, 239, 273, 282, 383, 384
 tunnelling, 282, 283
 volt, 18
 waves, 20
Electronic coupling, 123, 272, 273, 282
Electron–phonon coupling, 283, 284
Electrophotographic, 364, 368, 377, 393, 397,
399
Electrophotography, 393, 397
Electrostatic, or coulombic force, 16
ELISA, 191, 353
Emulsions, 75, 377, 383, 384, 390
Energy gap law, 72
Energy level diagrams, 45
Energy transfer, 71, 74–76, 78, 84, 91, 150,
157, 161, 170, 305, 307, 309, 312, 316,
317, 334, 412, 578
Erasable memory, 183, 208
Etching, 371–373, 396, 439, 440
Evanescent wave, 9, 426
Excimer, 80, 82, 308, 421, 425, 488, 560,
562–565, 570, 572
Excimer formation, 81, 425, 533, 559,
564–566, 570, 571

Exciplexes, 2, 71, 80, 283, 284, 566, 581
 Excited state, 106–116, 118–125, 127, 128,
 130, 132–134, 136, 137, 139, 141, 142,
 308, 309, 312, 313, 316, 537
 Excited-state atom transfer, 121
 Excited-state kinetics, 558
 Exciton, 41, 77, 157, 280, 282, 286, 420
 Exciton diffusion, 280–282
 Exciton diffusion lengths, 281
 Exciton migration, 41, 77, 157, 280, 421
 Extreme ultraviolet (EUV) lithography, 448
E–Z photoisomerism, 92

F

Fe₂O₃, 152, 241, 255, 292, 293
 Fermi's golden rule, 272
 Fermi-Dirac statistics, 18
*f**f*-transitions, 114
 Fibre optic, 6, 9, 343, 426, 430, 460, 481, 510,
 520
 Fill factor (FF), 276, 277, 282
 Filter solution, 492
 FISH, 355–357
 Fixation, 386, 387
 Flash photolysis, 82, 171, 174, 176, 253, 305,
 307, 308, 309, 316, 512, 545
 Flavonoid, 307, 313, 315, 320
 Fluorescein, 77, 154, 168, 350, 356
 Fluorescence, 71, 192, 350, 352, 528, 536
 anisotropy, 407, 408, 467
 decay rates, 75, 384, 421
 decays, 554, 556, 559, 565, 566, 571–573,
 578, 579
 microscopes, 517
 quantum yield, 2, 64, 73, 111, 133, 137,
 157, 309, 539
 standards, 541
 Fluorimeter, 468, 469, 482, 498, 504–506,
 510, 511, 514, 521
 Fluorophore, 352, 356, 407, 412, 416, 422,
 469, 518, 519, 553
 Fox-Talbot, 373, 374, 395, 396, 399
 Förster distance, 75
 Förster resonance energy transfer (FRET), 2,
 75–77, 168, 171
 Franck-Condon factor, 272, 283
 Free radical, 170, 284, 305–308, 324, 455
 Freeze-pump-thaw cycles, 477
 Frenkel exciton, 41
 Frequency domain, 514, 515

G

GaP, 294
 Gated photochromics, 181
 Gelatin, 377, 379, 381, 383, 389, 395, 490
 Geminate recombination, 284, 286
 Gibbs–Thomson effect, 379, 387
 Glassware, 472, 473
 Glutathione, 306, 307, 319, 320, 322–324
 Grassmanns' laws, 500
 Grotthus–Draper law, 468
 Gurney–Mott, 382

H

Hadley cycles, 225
 H-aggregates, 64, 65
 Halide radical, 311
 Halogenation, 99, 100, 102, 199
 Heavy atom effect, 28, 30, 31, 107, 110, 172,
 418, 547
 Heavy atom halides, 415
 Heliograms, 372
 Henderson–Hasselbalch, 351, 410
 Heterogeneous catalysis, 142, 250
 Heterogeneous photocatalysis, 251, 254, 255,
 259
 Heterosphere, 228
 Highest energy occupied molecular orbital, 40
 History, 5, 277, 363, 364, 369, 370, 376, 383,
 390, 399
 Hole, 42, 164, 170, 255–258, 269, 281,
 380–385
 Hole conduction, 277, 279
 Hole mobility, 279, 282, 286
 Homosphere, 228, 235
 Hopping motion, 283
 Host matrix, 418, 425, 427
 Hot embossing, 454, 455
 HSQ, 451–453
 Hund's rule, 27
 Hydrazides, 391
 Hydrogen, 21, 44, 153, 242, 255, 288
 Hydrogen abstraction, 91, 95–98, 175, 204,
 235, 248, 253, 314, 321, 322
 Hydrogen evolution reaction, 288, 291
 Hydrogen silsesquioxane, 451, 452
 8-Hydroxypyrene-1,3,6-trisulfonic acid, 413
 Hydroxyl radical, 248, 306, 309–311,
 313–315, 320
 Hyperbilirubinemia, 333
 Hypsochromic shift, 64

I

I_3^-/I^- redox pair, 269, 273, 274, 279
Image sharpness, 365
Imaging, 18, 356, 363, 391, 393, 517
Imaging systems, 364–366, 369, 376, 388, 393, 395, 397, 398
Immersion lithography, 447, 449
Immersion well reactors, 484
Immobilisation, 258, 259, 261, 269, 427
Immunoassays, 351, 353
Immunofluorescence, 351–353
Incandescent lamps, 90, 158, 159
Incident photon-to-current conversion efficiency, 276
Indicator, 80, 163, 405, 410–414, 419, 428, 500
Indicator displacement assays, 413
Inert gas purging, 477
Inner filter, 472, 474, 476, 506, 507, 537
Inorganic colloidal nanoparticles, 429
Inorganic colorants, 151
Instrumental response function, 555, 556
Integrating sphere, 8, 491, 503, 522, 539, 541, 555, 556
Interference, 4, 9, 10, 15, 22, 31, 431, 439, 453
Internal conversion, 72–74, 83, 106, 534, 536, 548
Interstitial silver ions, 381, 382
Intersystem crossing, 72–74, 83, 106, 110, 286, 313, 316, 536, 545, 548
Intersystem crossing quantum yield, 545–547
Intra-ligand, 110, 112, 113
Intra-ligand charge-transfer, 82, 113, 432
Intramolecular charge transfer, 423
Ion–electron recombination, 226, 227
Ionic bonding, 31
Ionisation potential, 43, 44, 280
Ionosphere, 220, 226, 227, 234
Ir(III) dopants, 384
Iridium complexes, 121, 296
IrO₂, 296

J

Jablonski diagram, 2, 69, 70, 334, 534, 537
J-aggregates, 64, 65, 384, 385
JJ coupling, 30

K

Karyotyping, 355
Kasha's rule, 72, 106, 137, 139, 207, 550
Kinetic energy, 13, 18, 19, 21, 22, 222–225, 255

Kodachrome, 388
Kubelka-Munk function, 503, 504, 506

L

Label, 11, 192, 407, 419
Lamp, 30, 90, 91, 100, 102, 158, 469, 479, 481, 483, 502
Lanthanides, 160, 172, 392, 503
Laser, 167, 207, 343, 485, 486, 488, 520, 524
Laser dyes, 155, 168, 167, 187, 525
Laser flash photolysis, 174, 253, 305, 307–309, 316, 323, 324, 544
Laser lithotripsy, 343
Laser power, 462, 487, 495
Latent image, 374, 381, 383–388, 391, 392, 399
Latensification, 375, 387
Laurdan, 422, 423
LCDs, 162, 201
LED, 163, 164, 198, 427, 469, 484, 485
Lifetime, 4, 70, 74–81, 83, 91, 110, 113–115, 123–125, 127, 150, 157, 167, 170, 173–175, 185, 195, 205, 229, 235, 286, 338, 351, 356, 406–408, 471, 514, 518, 535–537, 554, 558, 575, 576
Lifetime distributions, 575, 576
Ligand-dissociation, 126
Ligand to ligand charge transfer (LLCT), 117
Ligand to metal charge transfer (LMCT), 61, 116, 260
Light-emitting diodes, 84, 134, 161, 163, 165, 426, 469, 484
Light irradiation, 259, 294, 340, 481
Light management, 468
Light scattering, 474, 365, 398, 469, 472
Light sources, 6, 149, 159, 161, 163, 165, 166, 177, 480
Linkage isomerism, 132–134
Lippert–Mataga theory, 422
Long-lived excited state, 66, 71, 112, 113, 486
Lowest energy unoccupied molecular orbital, 40
Low-lying excited states, 120, 139
Low temperature phosphorescence, 169, 478
Luminance, 364, 365, 500
Luminous efficacy, 161, 163, 165

M

Magnetic dipole, 6, 172
Manganese, 151, 152, 281, 296
Maximum entropy method, 575, 576
MEH-PPV, 188, 189, 281, 282

- Mercury, 75, 90, 159–161, 202, 373, 374, 376, 413, 439, 441, 180, 181, 483–485, 517, 525, 523
- Mercury lamps, 90, 159, 439, 481, 483, 523
- Mesosphere, 223, 226, 227, 229, 233, 234
- Meta benzene-alkene cycloaddition, 94
- Metal carbonyls, 107, 126–129
- Metal cation recognition, 412
- Metal-centred, 61, 110, 114, 152
- Metal-enhanced fluorescence, 429
- Metal-metal bonds, 122, 138
- Metal ligand complexes, 351
- Metal to ligand charge transfer (MLCT), 61, 109, 115–116
- Metal to metal charge transfer (MMCT), 61
- Microchannel plate, 556, 557
- Micro electro mechanical systems (MEMS), 440, 441, 443–445
- Microenvironment, 422, 423, 518
- Microreactor, 91, 92
- Model, 20, 21, 26, 34, 41, 43, 79, 112, 114, 115, 189, 206, 231, 236, 237, 242–245, 260, 285, 287, 344, 379, 380, 407, 423, 469, 472, 517, 523, 534, 551, 564, 575, 576, 579
- Molar absorption, 58–62, 70, 114, 115, 118, 154, 160, 172, 173, 176, 185, 277, 280, 282, 309, 336, 473–475, 503, 543, 544, 545
- Molecular logic, 184, 418
- Molecular modelling, 26, 273, 523
- Molecular orbitals, 1, 22, 31–33, 35, 36, 38–40, 61, 65, 154, 284, 523
- Molecular rotors, 423
- Monochromators, 469, 492–494, 505, 508, 510, 521
- Morphology, 275, 279, 377, 378, 461
- N**
- $n \rightarrow \pi^*$, 62, 91, 110
- Nanoimprint lithography, 436, 438, 444, 446, 448, 449, 454, 455, 459
- NanoLED, 555
- Nanomedicine, 349, 357, 359
- Nanosecond time resolution, 308, 554
- Nanosurgery, 344, 345
- Nanowire, 278, 279
- Natural photosynthesis, 288–290, 289
- Nd/YAG laser, 157, 513
- Negative, 5, 11, 16, 22, 31, 32, 43, 115, 176, 269, 271, 272, 281, 292, 294, 297, 312, 315, 354, 368, 369, 373–375, 381, 386, 388, 389, 396, 422, 436, 437, 439–441, 443, 453, 500, 535, 566, 567
- Negative photoresist, 437, 439, 440
- Negative-positive, 369
- Negative tone resists, 440, 443
- Neutral density (ND) filters, 489, 490, 556
- Niepce, 370–373, 376
- Nile red, 206, 422
- Nitrate, 19, 239, 319, 320, 370, 371, 373–375, 378
- Non-bonding, 32, 34, 35, 68, 110, 111
- Novalaks, 442
- NO_x, 319
- n*-type semiconductor, 202, 290, 293
- O**
- OLEDs, 134, 163–165, 186–191, 195–197, 203
- Open circuit voltage, 281, 287
- Ophthalmic lenses, 176, 178, 182
- Optical anisotropy, 183
- Optical brighteners, 67, 87
- Optical cells, 474
- Optical fibre, 9, 204, 426, 460, 461, 519
- Optical response, 404, 405, 414, 428, 430
- Optodes, 426
- Optoelectronic noses, 431
- Orbital angular momentum quantum number, 23, 31
- Orbital hybridisation, 34
- Orbital magnetic quantum number, 24
- Orbital momentum selection rule, 56
- Organic colorants, 151, 153
- Organic glass, 427, 476
- Organic photovoltaic, 188, 280, 298
- Ormosils, 427
- Oscillator strength, 60, 71, 523
- Oswald ripening, 379, 392, 393
- (oxa)-di- π -methane rearrangement, 92, 93
- Oxidative addition, 123, 124, 135
- Oxide pigments, 152
- Oxidising agent, 251, 260, 296, 320, 323
- Oxygen, 3, 4, 34, 38, 39, 81, 83, 91, 99, 117, 123, 133, 150, 153, 159, 170, 173–175, 181, 185, 187, 191, 192, 194, 195, 197, 205, 217, 234, 248, 250–254, 256, 268, 288, 295, 305, 307, 314–320, 322, 324, 334, 341, 370, 418, 429, 431, 453, 461, 477, 478, 510, 533, 537, 538
- Oxygen evolution reaction, 288, 291

- Oxygen evolving complex (OEC), 289, 295, 296
- Ozone, 217, 218, 226, 228–233, 236–241, 243, 244, 251, 260, 319, 332, 481–483
- Ozone depletion, 217, 231
- Ozone distribution, 243
- Ozone hole, 232, 233, 244
- P**
- $\pi \rightarrow \pi^*$, 62, 110
- P3HT, 190, 282, 287
- Panchromatic, 175, 198, 278, 387
- Parity, 23, 24, 38, 39, 55, 59
- Parity selection rule, 55
- Particle waves, 12, 14
- Passive absorbers, 150
- Paternò-Büchi reaction, 95
- Pattern recognition, 431
- Pauli exclusion principle, 26, 30
- PDMS, 457, 458
- PEBBLE, 428
- Peroxyacetyl nitrate, 239
- Peroxyl radical, 305, 307, 314, 315, 317, 318, 322–324
- Perturbation quenching, 78, 415
- Pesticides, 247–249, 252, 254, 258, 259, 261
- pH, 84, 113, 120, 131, 155, 182, 184, 192, 194, 204–206, 252, 255, 292, 293, 307, 313, 319, 321, 323, 350, 351, 405, 407, 410, 411, 519, 572
- Phase modulated, 514
- Phenoxyl radical, 323
- phosphorescence, 31, 53, 70, 71, 79, 82, 117, 124, 157, 166, 169, 186, 192, 195, 197, 201, 207, 415, 418, 471, 476, 477, 509, 533–535, 540–542, 547, 551
- Phosphorescence quantum yields, 540, 541
- Phosphorimeter, 509, 540
- Phosphors, 32, 114, 157, 159, 160, 163, 172, 187, 199, 203, 392
- Photoacoustic calorimetry, 546, 547
- Photoactivation, 132, 133, 135, 335, 359
- Photoanode, 270, 290–292, 295
- Photocatalysis, 141, 143, 175, 250, 258, 259, 261, 250
- Photocatalyst, 122, 252, 253, 256, 258, 259, 295
- Photocatalytic water splitting (PC), 294
- Photochemical CO₂ reduction, 297
- Photochemical materials, 185, 186, 210
- Photochemical oxidation, 237, 241
- Photochemical synthesis, 89–91, 139, 140, 192, 468
- Photochemical tissue bonding, 331, 333, 341, 342
- Photochemistry, 3, 5, 15, 89, 126, 139, 141, 226, 228, 233, 235, 245, 357, 435, 468, 494, 523, 525, 526, 528–530
- Photochromic glasses, 177, 381
- Photochromism, 153, 176, 177, 179–182, 184, 185, 364, 381, 393, 551
- Photoconductive, 380
- Photocrystallography, 132
- Photocyclisation, 102, 180, 181
- Photocycloaddition, 97
- Photo-decarbonylation, 96
- Photodegradation, 173, 188, 205, 407, 481, 484, 488, 499, 512, 513
- Photodiodes, 496, 510
- Photodissociation, 73, 107, 111, 178, 223
- Photodynamic therapy, 185, 196, 206, 331, 332, 359
- Photoelectrochemical cells, 291, 298
- Photoelectrochemical water splitting (PEC), 289, 290, 292–295
- Photoelectron, 43, 44, 46, 256, 383, 391, 392, 398, 496, 497
- Photo-Fenton, 250, 251, 254, 260, 261
- Photofrin, 194, 335–337
- Photograms, 370–372, 376
- Photography, 191, 208, 363–365, 368–370, 372–377, 380, 381, 383–385, 396, 398, 399, 436, 517
- Photoinduced electron transfer (PET), 76, 94, 115, 282, 406, 412, 415
- Photoinduced linkage isomerism, 132
- Photoionisation, 226, 249, 321
- Photoisomerisation, 92, 129–131, 134, 153, 179, 333
- Photolabilisation, 111, 130
- Photolithography, 10, 372, 376, 435–440, 447, 449, 461, 462, 482
- Photoluminescence, 32, 46, 157, 165, 203, 405, 407, 478, 488, 501, 504, 508
- Photolysis, 73, 82, 97, 111, 115, 127, 129, 130, 221, 251, 307, 377, 511, 512
- Photomedicine, 331, 332
- Photomultiplier tubes, 496, 497
- Photon, 15, 16, 19, 53, 67, 181, 343, 505, 514, 529
- Photooxidation, 98, 123, 153, 247, 253
- Photopolymerisation, 176, 185, 364, 393
- Photoracemisation, 111

- Photo-rearrangements, 92
 Photoreceptors, 2, 397
 Photoresists, 372, 435–443
 Photosensitisation, 250, 305, 334, 345
 Photosensitiser, 194, 197, 205, 206, 249, 259, 260, 289, 296, 297, 305, 316, 317, 332, 334–339, 345
 Photosensitivity, 337, 338, 371
 Photosubstitution, 110, 111, 127
 Photosynthesis, 141, 288–290
 Photosystems I and II, 289
 Phototautomerisation, 181
 Phototherapy, 67, 333
 Photothermolysis, 343
 Phototoxicity, 155, 334
 Physical binding, 410, 413, 414
 Physical development, 386, 387
 Picosecond laser pulse excitation, 384
 Piezochromic, 424
 Pigments, 150–154, 162, 182, 398
 Plasmas, 159, 162, 448
 Platinum(II) octethylporphyrin (PtOEP), 418
 PLED, 165, 188, 190, 198
 PMMA, 451–453
 Polariser, 162, 489, 505, 514, 556
 Polarity, 62, 115, 119, 175, 421–423, 471, 519, 566
 Polaroid, 390, 395
 Polar stratospheric ice clouds, 232, 244
 Pollutant, 217, 239, 247–249, 252, 257, 258, 260, 261, 319, 322
 Pollution. *See* Pollutant, 239
 Poly(methyl methacrylate), 451, 522
 Poly(vinyl cinnamate), 440, 441
 Polydimethylsiloxane, 457
 Polyenes, 92, 154, 179
 Polymer hole-transporting materials, 279
 Polymers, 41, 43, 84, 125, 155, 164, 287, 279, 398, 427, 436, 438, 442, 548
 Polyoxometalate, 251–253
 Polyphenol, 307, 314, 321
 Polypyridylruthenium, 275
 Polypyridyl sensitisers, 273
 Polythiophene, 286, 555
 Populated rotational states, 51
 Population inversion, 52, 71, 81, 157, 167, 486
 Porphyria, 338
 Porphyrins, 110, 169, 171, 249, 259, 278, 338
 Positive photoresist, 444–445
 Potential energy (PE) curves, 46, 222
 Preparative photochemical reactions, 90
 Pressure, 44, 63, 90, 156, 159, 160, 221, 223, 242, 244, 429, 481, 483, 484, 524
 Pressure-sensitive paint, 429
 Primary, 79, 91, 138, 199, 218, 253, 313, 515, 353, 354, 392, 468
 Primary colours, 367, 500
 Principal quantum number, 23, 24, 27
 Print-out, 375, 381
 Probe, 24, 57, 108, 167, 245, 271, 313, 355, 357, 404, 407–414, 422, 428, 461, 478, 535
 Probe-analyte complex, 407, 408
 Prodan, 422, 423
 Proton transfer, 2, 84, 153, 155, 297, 324, 533, 559, 566–568
 Proximity effect, 450, 451
 (PSI) (PSII), 289
 ps-time-resolution, 556
 p-type, 201, 202, 290, 293
 p-type semiconductors, 293, 294, 297
 Pulsed diode lasers, 485
 Pulsed LEDs, 469, 485, 514
 Pulsed xenon lamp, 511, 540
 Pulse radiolysis, 84, 253, 305, 307–309, 314–316, 318–320, 322, 324, 548
 Pump probe absorption spectroscopy, 516
 Purification, 255, 258, 287, 527
 PUA therapy, 333, 342
 PVC, 395, 419
 Pyrene, 80, 169, 186, 535–537, 565, 568, 570, 571
- Q**
 Quantum counter, 191, 521
 Quantum dot, 62, 66, 155, 156, 278, 357, 359
 Quantum number, 11, 17, 18, 20, 23, 24, 26, 28, 56, 173
 ‘Quantum’, or ‘wave’, mechanics, 4, 17, 24, 54, 283, 527
 Quantum yield, 2, 64, 74–77, 111, 112, 117, 124, 127, 129, 134, 136, 157, 167, 171, 185, 220, 253, 256, 295, 309, 337, 384, 413, 418, 423, 446, 472, 479, 483, 495, 521, 534, 537, 574
 Quartz Dewar, 476, 522
 Quencher, 74, 169
 Quenching, 537
- R**
 Radiative lifetime, 71, 74, 75, 77–80, 149, 150, 167, 170, 174, 176, 316, 407, 415, 420, 477, 569, 580
 Radical anions, 82, 94, 118, 312, 314, 315, 322

- Radical cations, 82, 118, 119, 307, 312, 319, 322, 324
- Radical initiators, 175, 176, 248, 395
- Radicals, 73, 91, 95, 150, 169, 170, 175, 237, 248, 260, 306–309, 315, 322, 324, 439
- Radioluminescence, 67, 157, 165, 166
- Radiometer, 494, 500
- Raman, 57, 108, 121, 140, 308, 520, 553, 555
- Raman lines, 506
- Raman peak, 554
- Rayleigh, 54, 57, 218, 461, 506, 539, 553–555
- Rayleigh band, 506
- Rayleigh scattering, 54, 554
- Re and Ru complexes, 123, 172, 278
- Reactive oxygen species, 305, 307, 313, 315, 324, 334
- Reagent-mediated, 405, 406
- Rearrangement, 3, 78, 92, 98, 134, 135, 171, 319, 442, 443
- Receptor, 184, 338, 410, 413, 416, 417, 432
- Reciprocity failure, 383, 384
- Recognition probe, 412, 413
- Redox buffers, 387
- Redox couple, 114, 269, 270, 275, 277, 279, 291, 295
- Redox potential, 1, 43–45, 175, 252, 274, 294, 417
- Redox sensitisers, 175
- Reduction, 43, 45, 68, 77, 79, 115, 116, 118, 123, 137, 152, 248, 252, 260, 268, 273, 292, 297, 320, 323, 370
- Reduction sensitising, 374
- Reductive elimination, 135
- Reference materials, 521, 525
- Refractive index, 7, 10, 11, 59, 75, 151, 179, 184, 403, 457, 447, 537
- Reichardt's dye, 206, 421
- Reichardt $E_T(30)$ scale, 471
- Residence time, 218, 220, 221, 235, 236
- Resonance, 109, 121, 140, 346, 359, 413, 486, 520
- Resonance energy transfer, 2, 75, 168, 418, 419
- Response mechanism, 403, 404, 408, 414, 418, 421
- Response signal, 405
- Reversal, 223, 379, 388, 391
- RGB, 160, 367, 368
- Roll-to-roll, 459
- Rose bengal, 77, 99, 191, 192, 242, 249, 316, 541
- Rose oxide, 99
- Rotational energy, 46–49, 63, 64
- $[\text{Ru}(\text{bpy})_3]^{2+}$, 45, 115, 197, 296, 297
- Russell–Saunders coupling, 30, 31
- Ruthenium complexes, 135, 139, 278
- Ruthenium dimer, 296
- S**
- Saccharide, 410, 412
- Saccharide probes, 412
- Safety, 429, 469, 477, 523, 524
- Sample concentrations, 474, 498, 507
- Scanning near-field optical microscope, 11, 460
- Scanning probe nanolithography, 460
- Scattering, 15, 54, 57, 151, 155, 218, 225, 242, 275, 335, 344, 396, 405, 427, 428, 450, 469, 491, 521, 522, 554–556
- Scheele, 370, 371, 376
- Schrödinger wave equation, 21, 22, 46
- Schulze, 370
- Schumann–Runge, 219, 222, 228
- SCIL, 457, 458
- Screen, 162, 275, 364, 365, 367, 392, 396
- Second order transmission, 508
- Self-absorption, 507, 508
- Self absorption effects, 506
- Self-assembled monolayers, 461
- Self-quenching, 74, 472
- Semiconductor(s), 3, 42, 48, 62, 65, 66, 71, 151, 155, 200, 254, 255, 258, 259, 270–272, 275, 279, 282, 287, 290, 293, 379, 437–441, 446, 454, 457, 498, 774–776
- Semiconductor photoanode, 291
- Semiconductor photocathode, 293–295, 495, 497
- Sensitiser dye, 207, 269, 270, 272, 275, 277, 279
- Sensitisers, 92, 149, 170, 171, 175, 185, 197, 206, 275, 278, 295, 296, 316, 339, 344, 349
- Sensitivity, 108, 166, 168, 184, 218, 276, 350, 351, 356, 357, 378, 383, 405, 411, 415, 419, 431, 436, 495, 503, 521
- Sensor, 80, 168, 184, 196, 198, 350, 403–405, 412, 413, 416, 420, 422, 425–433
- Sensor array, 430, 431
- Sharpness, 365, 368, 369
- Short circuit current, 279
- Sigma bond to ligand charge transfer, 120
- Signal-to-noise, 498, 511
- Signal-to-noise-ratio, 8, 428, 478, 482, 493
- Silver, 175, 177, 178, 364, 365, 371, 377, 380, 389, 393
- Silver halides, 175, 177, 370, 379–381, 398

- Silver halides photolysis, 364, 369, 377, 378, 379
- Silver nitrate, 370, 371, 373, 374, 378
- Singlet, 4, 28–31, 39, 43, 46, 56, 69, 75, 83, 99, 123–125, 171, 173, 234, 236, 249, 280, 286, 306, 312, 316, 334, 337, 341, 395, 407, 418, 423, 510, 514, 534
- Singlet depletion method, 543
- Singlet oxygen, 39, 83, 99, 150, 173–175, 205, 206, 234, 250, 251, 305, 306, 316, 317, 335, 337, 340, 471, 510, 514, 531, 541
- Singlet oxygen phosphorescence, 541
- Singlet oxygen quantum yields, 337
- Singlet oxygen. *See* oxygen, 39, 99, 172, 305–307, 316, 317, 334, 515
- Singlet-oxygen formation quantum yields, 541
- Singlet-triplet splitting, 83, 286
- Smog, 217, 244
- Smoluchowski equation, 77
- $S_{\text{N}}1$ reaction, 94
- $S_{\text{RN}}1$ reaction, 94
- Snell's law, 7
- SNOM, 11, 460–462, 519
- Snomipede, 462
- Soft stamp imprint, 456, 459
- Solar cell, 42, 43, 66, 74, 137, 142, 168, 175, 190, 202, 267, 269, 275, 280, 284, 295
- Solar energy, 137, 175, 206, 248, 249, 257, 268, 277, 288, 289, 297
- Solar fuels, 268, 288
- Solar heating, 224, 225, 239
- Solar radiation, 66, 218, 225, 226, 228, 234, 242, 282
- Solar spectrum, 218, 219, 233, 244, 274–277, 280, 482
- Solvatochromic, 118, 206, 422, 432, 471
- Solvent, 82, 112, 181, 470, 471, 478, 506, 558
- Solvent deuteration, 175
- Solvent polarity, 175, 176, 186, 206, 421, 422, 471, 566
- Solvent viscosity, 66, 471, 561
- Spectral sensitisation, 175, 383–385, 399
- Spectrograph, 494, 502, 510
- Spectroscopic ruler, 424
- Specular reflection, 8
- Spin angular momentum, 17, 18, 26, 28, 29, 40, 53, 56, 72, 173
- Spin multiplicity, 28, 38, 39, 71, 72, 306, 316
- Spin quantum number, 16–18
- Spin selection rule, 31, 56, 57, 59, 71, 106
- Spin-orbit coupling, 30, 31, 56, 59, 78, 106, 107, 115, 157, 169, 172, 207
- Spiropyrans, 178, 208
- Spontaneous emission, 52, 53, 61, 70, 71, 519
- $S_{\text{RN}}1$ reaction, 95, 95
- SrTiO_3 , 294
- Stain, 192, 205, 206, 355
- Standing waves, 11–12
- Static, 76, 77, 80, 407, 561
- Static or dynamic quenching, 407
- Static quenching, 77, 80, 561
- Steady-state approach, 563
- Step and flash imprint lithography, 456
- Stern–Volmer equation, 2, 79, 407, 536
- Stern–Volmer plot, 80, 407
- Stern–Volmer relationship, 79
- Stevens–Ban plots, 561, 562, 565
- Stimulated emission, 2, 52, 70, 71, 81, 486, 519
- Stokes' shift, 191, 507
- Stratosphere, 220–231, 233, 234, 239, 241, 243
- Stretched exponential, 575–579, 581
- SU-8, 439, 443–445
- SU-8 resist, 443, 444
- Subtractive, 367, 368
- Substrate conformal imprint lithography, 458
- Sulfochlorination, 100, 102
- Sulfonation, 100
- Sulfur radicals, 321
- Sunscreens, 84, 150, 155, 185, 201, 204
- Superadditivity, 386, 387
- Superoxide anion, 205, 256, 334
- Surface plasmon resonance, 426
- Surfactants, 100, 102, 151, 252, 258, 543
- Symmetry, 22–24, 26, 32, 37–40, 46, 47, 49, 55–57, 59, 61, 62, 111, 124, 186, 518, 570
- Symmetry labels, 37, 39
- Synthesis
- carbonyl, 90, 126, 139
 - cycloaddition, 90, 93, 94, 97–99
 - electrocyclic reactions, 92
 - electrophilic attack, 91
 - fragmentation, 95, 96, 199, 452
 - hydrogen abstraction, 91, 95, 97, 175
 - substitution, 94
 - sulfonation, 99
 - unimolecular, 92
- T**
- Tandem cell, 295
- Tanning, 388, 389, 394
- Tanning development, 388, 394
- Tautomerisation, 533, 572

- Technicolor, 389, 390
Temperature, 66, 423, 424, 521, 522, 539
Term symbols, 1, 28, 30, 37
Thermochromic, 424
Thermoluminescence, 67, 157, 158
Thermosphere, 223, 225, 226, 234
Thiosulphate, 376
Three-state systems, 568, 574, 581
Ti:Sapphire laser, 516, 556
Time, 554, 556
Time correlated single photon counting, 485, 514, 526, 554, 556
Time-resolved, 74, 108, 109
Time-resolved infrared, 108, 116, 125, 129, 130
Time-resolved infrared spectroscopy, 116, 125, 129
TiO₂, 151, 201, 252, 255–259, 261, 294, 296, 428
Tissue optical window, 344
Tissue therapeutic window, 335
Tocopherol, 307, 322–324
Toner, 398
Transient absorption, 108, 134, 167, 174, 277, 293, 308, 309, 490, 511, 543, 545, 548
Transient effect, 580
Transient species, 3, 80, 109, 138, 307, 308, 478, 513
Transient two-dimensional infrared spectroscopy, 108
Transitions, 62, 110
Transition dipole moment, 55, 60
Transition metal complexes, 55, 61, 106, 110, 112, 113, 120, 132, 135, 137, 297, 418
Transition probabilities, 2, 70
Translational, 48, 49, 425, 519
Trap, 91, 109, 150, 170, 176, 200, 230, 255, 283, 374, 382, 384, 391, 428
Tribocharging, 398
Triplet, 167, 169, 171, 286, 543, 547–549
Triplet energy, 549
Triplet excitons, 280, 286
Triplet sensitizers, 171, 186, 194, 316, 548
Triplet state, 29, 30, 39, 71, 83, 121, 172–174, 280, 544, 546–548, 551
Triplet–triplet annihilation, 83, 84, 169, 207, 423, 472, 511, 543
Triplet–triplet energy transfer, 418, 547–549
Triplet–triplet transient absorption, 543
Tristimulus values, 500, 501
Troposphere, 217, 220, 222, 223, 225, 227, 230, 231, 235–237, 245
T-type, 176, 178, 179, 182, 193, 208
Tungsten halogen lamps, 479
Two-photon, 67, 181–183, 339, 343, 344, 462, 518
Two-photon excitation, 518
Two-photon excited photodynamic therapy, 344, 399
Two-state systems, 52, 558, 564, 566, 569
Type I mechanism, 305, 334, 340
Type II mechanism, 305, 334, 342
- U**
Ultrafast, 106–108, 114, 122, 125–127, 133, 135, 139, 487, 516, 517, 520, 526
Unimolecular chemical reactions, 72
Uranyl ion, 117
UV/Vis spectrophotometer, 502
- V**
Vacancies, 201, 381
Valence band, 42, 62, 65, 66, 188, 255, 271, 279, 292, 293, 358, 379–381, 496
Vascular targeting, 339
Vertical transitions, 68, 69
Vibrational energy, 4, 46–49, 51, 69, 107, 108, 142, 506
Vibrational relaxation, 72, 107, 108, 534, 550–552, 581
Vibrational relaxation quantum yield, 552
Vibrational spectroscopy, 108
Vibrational state, 49, 50, 57
Vibronic coupling, 57
Vibronic effect, 534, 550
Viscosity, 77, 170, 171, 186, 423–424, 437, 440, 455, 456, 459, 471, 519
Vision, 3, 6, 73, 162, 339, 343, 359, 366
Vitamin D, 92, 332
Vitamin D synthesis, 332–333
- W**
Wannier–Mott, 41
Water, 137, 187, 189, 190, 205, 247, 258, 260, 290, 296, 309, 335, 471, 524
Water oxidation, 290–293, 295–297
Water purification, 258
Water splitting, 137, 141, 268, 288, 290–296
Wavefunction, 12, 22, 24, 25, 37–39, 54, 55
Wavelength-ratiometric, 410
WO₃, 258, 259, 292, 293, 295
Work function, 42, 281, 285

X

Xe flash lamps, [485](#)

Xenon lamps, [481](#), [511](#)

Xerox, [397](#)

X-ray, [43](#), [109](#), [122](#), [132](#), [133](#), [136](#), [201](#), [204](#),
[391](#), [392](#), [398](#)

Y

Yalow–Berson method, [353](#), [354](#)